Universidade de Lisboa
Faculdade de Farmácia

Iminoboronates as useful scaffolds for tumor-targeting

Fábio Miguel Figueiredo Santos

Orientadores: Prof. Doutor Pedro M. P. Góis
Prof. Doutor João M. B. Gonçalves

Tese especialmente elaborada para obtenção do grau de Doutor em Farmácia, especialidade em Química Farmacêutica e Terapêutica

2018

Universidade de Lisboa
Faculdade de Farmácia

Iminoboronates as useful scaffolds for tumor-targeting

Fábio Miguel Figueiredo Santos

Orientadores: Prof. Doutor Pedro M. P. Góis
Prof. Doutor João M. B. Gonçalves

Tese especialmente elaborada para obtenção do grau de Doutor em Farmácia, especialidade em Química Farmacêutica e Terapêutica

Júri:

Presidente: Doutor António José Leitão das Neves Almeida, Professor Catedrático e Presidente do Conselho Científico da Faculdade de Farmácia da Universidade de Lisboa.

Vogais:

- Doutor Uwe Pischel, *Professor Titular de Universidad Universidad de Huelva,* Espanha;
- Doutor Eurico José da Silva Cabrita, Professor Associado com Agregação Faculdade de Ciências e Tecnologia da Universidade Nova de Lisboa;
- Doutor Artur Manuel Soares da Silva, Professor Catedrático Departamento de Química da Universidade de Aveiro;
- Doutor Rudi Micael Santiago de Oliveira, *Chemist* Hovione FarmaCiência, SA, especialista de reconhecimento mérito;
- Doutor Rui Ferreira Alves Moreira, Professor Catedrático Faculdade de Farmácia da Universidade de Lisboa;
- Doutor Pedro Miguel Pimenta Góis, Professor Auxiliar com Agregação Faculdade de Farmácia da Universidade de Lisboa, Orientador;

FCT - Fundação para a Ciência e a Tecnologia, *SFRH/BD/94779/2013*

2018

O presente trabalho foi desenvolvido sob orientação do Professor Doutor Pedro M. P. Góis e co-orientação do Professor Doutor João M. B. Gonçalves, ambos do iMed.ULisboa (Instituto de Investigação do Medicamento) da Faculdade de Farmácia da Universidade de Lisboa. Este trabalho foi financiado pela Fundação para a Ciência e Tecnologia através da bolsa de doutoramento SFRH/BD/94779/2013.

This work was developed under scientific supervision of Professor Dr. Pedro M. P. Góis and co-supervision of Professor Dr. João M. B. Gonçalves, both from iMed.ULisboa (Instituto de Investigação do Medicamento), Faculty of Pharmacy, University of Lisbon. This work was financially supported by Fundação para a Ciência e Tecnologia, through the doctoral grant SFRH/BD/94779/2013.

List of Publications and Awards

Papers in International Scientific Periodicals with Referees:

- **Fábio M. F. Santos**, Ana I. Matos, Ana E. Ventura, João Gonçalves, Luís F. Veiros, Helena Florindo and Pedro M. P. Gois "Modular Assembly of Reversible Multivalent Targeting Drug Conjugates", *Angew.Chem. Int.Ed.*, **2017**, *56 (32)*, 9346-50 (doi: 10.1002/anie.201703492).
- **[Very important paper] Fábio M. F. Santos**, João N. Rosa, Nuno R. Candeias, Cátia Parente Carvalho, Ana I. Matos, Ana E. Ventura, Helena F. Florindo, Liana C. Silva, Uwe Pischel and Pedro M. P. Gois "A Three-Component Assembly Promoted by Boronic Acids Delivers a Modular Fluorophore Platform (BASHY Dyes)", *Chem. Eur. J.*, **2016**, *22*,1631-37 (doi: 10.1002/chem.201503943); **[Cover Picture]** A Three-Component Assembly Promoted by Boronic Acids Delivers a Modular Fluorophore Platform (BASHY Dyes) (Chem. Eur. J. 5/2016) (doi: 10.1002/chem.201680501).
- **Fábio M. F. Santos**, Zoe Domínguez, María M. Alcaide, Ana I. Matos, Helena F. Florindo, Nuno R. Candeias, Pedro M. P. Gois and Uwe Pischel "Highly Efficient Energy Transfer Cassettes by Assembly of Boronic Acid Derived Salicylidenehydrazone Complexes", *ChemPhotoChem* **2018** (doi: 10.1002/cptc.201800150)
- María M. Alcaide, **Fábio M. F. Santos**, Vânia F. Pais, Joana Inês Carvalho, Daniel Collado, Ezequiel Pérez-Inestrosa, Jesús F. Arteaga, Francisco Boscá, Pedro M. P. Gois and Uwe Pischel "Electronic and Functional Scope of Boronic Acid Derived Salicylidenehydrazone (BASHY) Complexes as Fluorescent Dyes", *J. Org. Chem.*, **2017**, *82 (14)*, 7151-58 (doi: 10.1021/acs.joc.7b00601).
- Pedro M. S. D. Cal, Florian Sieglitz, **Fábio M. F. Santos**, Cátia Parente Carvalho, Ana Guerreiro, Jean B. Bertoldo, Uwe Pischel, Pedro M. P. Gois* and Gonçalo J. L. Bernardes "Site-selective installation of BASHY fluorescent dyes to Annexin V for targeted detection of apoptotic cells", *Chem. Commun.*, **2017**, *53*, 368-71 (doi: 10.1039/C6CC08671C).

Book Chapter:

- João P. M. Antonio, Gonçalo D. V. Farias, **Fábio M. F. Santos**, Rudi Oliveira, Pedro M. S. D. Cal and Pedro M. P. Gois. Non-covalent Interactions in the Synthesis and Design of New Compounds; "Boron-Nitrogen bond: A useful molecular construction tool", Ed. Prof. Armando Pombeiro, *Wiley* **2016**, ISBN: 978-1-119-10989-1.

Patent Submission:

- **Fábio M. F. Santos**, Pedro M. P. Gois, Hovione SA, "Boronated Multifunctional Targeting Drug Conjugate", **PCT/GB2018/050534; PT109941.**

Oral Communications in Scientific Conferences:

- **Fábio M. F. Santos**, Ana I. Matos, Ana E. Ventura, João Gonçalves, Luís F. Veiros, Helena Florindo and Pedro M. P. Gois "Boron-promoted Modular Assembly of Reversible and Multivalent Tumor-Targeting Drug Conjugates", 2nd Encontro do Colégio de Química da ULisboa, held in Lisbon, December 2017.
- **Fábio M. F. Santos**, Ana I. Matos, Ana E. Ventura, João Gonçalves, Luís F. Veiros, Helena Florindo and Pedro M. P. Gois "Modular Assembly of Reversible Multivalent Targeting Drug Conjugates", 4th EFMC Young Medicinal Chemist Symposium, held in Vienna, September 2017 (Selected by "Divisão de Química Terapêutica da SPQ" as the portuguese representative).
- **Fábio M. F. Santos**, João N. Rosa, Nuno R. Candeias, C. Parente Carvalho, Dr. U. Pischel and Pedro M. P. Gois, " A Three-Component Assembly Promoted by Boronic Acids Delivers a Modular Fluorophore Platform (BASHY Dyes)" 8th Postgraduate iMed.ULisboa Students Meeting, held in Lisbon, in July 2016.

Poster Communications in Scientific Conferences:

- **Fábio M. F. Santos**, Ana I. Matos, Ana E. Ventura, João Gonçalves, Luís F. Veiros, Helena Florindo and Pedro M. P. Gois "Boron-promoted Modular Assembly of Multivalent and Reversible Tumor-Targeting Drug Conjugates", 12th National Organic Chemistry Meeting (12ENQO) and 5th National Medicinal Chemistry (5ENQT), held in Coimbra, in January 2018.

- **Fábio M. F. Santos**, Ana I. Matos, Ana E. Ventura, João Gonçalves, Luís F. Veiros, Helena Florindo and Pedro M. P. Gois “Modular Construction of Reversible Multivalent Targeting Drug Conjugates”, XXV Encontro Nacional da SPQ, held in Lisbon, in July 2017.
- **Fábio M. F. Santos**, Ana I. Matos, Ana E. Ventura, João Gonçalves, Luís F. Veiros, Helena Florindo and Pedro M. P. Gois “Modular Assemblage of Reversible Targeting Drug Conjugates”, 9th Postgraduate iMed.ULisboa Students Meeting, held in Lisbon, in July 2017.
- **Fábio M. F. Santos**, João N. Rosa, Nuno R. Candeias, C. Parente Carvalho, Dr. U. Pischel and Pedro M. P. Gois, " Three-Component Assembly Promoted by Boronic Acids Delivers a Modular Fluorophore Platform (BASHY Dyes)” 6th EuCheMS in Life Sciences, held in Lisbon, in July 2016.
- **Fábio M. F. Santos**, João N. Rosa, Nuno R. Candeias, C. Parente Carvalho, Dr. U. Pischel and Pedro M. P. Gois, "Bashy complexes: Construction and characterization of boronic acid based fluorescent dyes” 19th European Symposium of Organic Chemistry, held in Lisbon, in July 2015.
- **Fábio M. F. Santos** and Pedro M. P. Gois, "A novel approach for tumor targeted therapy based on iminoboronate constructs" 1st EFMC Young Medicinal Chemist Symposium, held in Lisbon, in September 2014.
- **Fábio M. F. Santos** and Pedro M. P. Gois, "Iminoboronates, an exciting approach for tumor-targeting of cytotoxic boronic acids" XXIII International Symposium on Medicinal Chemistry, held in Lisbon, in September 2014.

News Article:

- **Fábio M. F. Santos**, Ana I. Matos, Ana E. Ventura, João Gonçalves, Luís F. Veiros, Helena Florindo and Pedro M. P. Gois “Construção modular de bioconjugados citotóxicos com seletividade para células cancerígenas”, *Associação Portuguesa de Investigação em Cancro* (ASPIC), 02.10.2017.

Award:

- Best poster “Boron-promoted Modular Assembly of Multivalent and Reversible Tumor-Targeting Drug Conjugates” in medicinal chemistry, presented at the 12th National Organic Chemistry Meeting (12ENQO) and 5th National Medicinal Chemistry (5ENQT) in Coimbra, in January 2018.

Agradecimentos

A elaboração e realização da tese de doutoramento que aqui vos apresento só foi possível, graças a um conjunto notável de pessoas, por quem tenho o maior respeito e admiração. Não querendo esquecer ninguém, a todos, o meu sincero agradecimento. Dentro deste ilustre grupo, existem pessoas a quem devo um especial reconhecimento.

Ao meu orientador, Professor Dr. **Pedro M. P. Gois**, por ter apostado em mim e por me ter dado a possibilidade de fazer investigação numa área tão fascinante. O seu constante apoio e motivação, quer a nível profissional, quer a nível pessoal, foram determinantes para o sucesso deste projecto e para o meu desenvolvimento como investigador e pessoa.

Ao meu co-orientador Professor Dr. **João M. B. Gonçalves**, pela pela sua orientação nesta tese de doutoramento, quer ao nível da transmissão de conhecimentos teóricos, quer ao nível das sugestões elaboradas ao longo desta dissertação.

Ao professor Dr. **Uwe Pischel**, pela sua dedicação e interesse demonstrados ao longo da nossa colaboração no projecto BASHY.

A todos os colaboradores que estiveram directamente envolvidos no desenvolvimento deste projecto de doutoramento, **Ana I. Matos** (Ensaios de citoxicidade, BASHY-nanoparticulas e bioimagem), **Ana E. Ventura** (BASHY-nanoparticulas e bioimagem), **Luís F. Veiros** e **Nuno R. Candeias** (Cálculos DFT), **João N. Rosa**, **Joana Inês Carvalho** e **Jesús F. Arteaga** (Síntese de BASHYs), **Cátia Parente Carvalho** (Avaliação fotofísica), **María M. Alcaide** e **Vânia F. Pais** (Síntese de BASHYs e avaliação fotofisica), **Francisco Boscá** (Caracterização dos BASHY *via* “laser-flash photolysis”), **Daniel Collado** e **Ezequiel Pérez-Inestrosa** (Avaliação fotofísica de dois fotões), **Zoe Domínguez** (Avaliação fotofísica BASHY ETC), **Pedro M. S. D. Cal** (Bioconjugação Anexina V-BASHY e Anexina V-FITC), **Ana Guerreiro** (Ensaios de viabilidade celular do BASHY **89**), **Jean Bertolo** (Análise estrutural da Anexina V e bioconjugados) e **Florian Sieglitz** (Bioimagem dos bioconjugados Anexina V), pela grande dedicação, ajuda e profissionalismo.

A todos os meus **colegas de investigação**, quer na discussão cientifica ao longo do doutoramento, quer pelo fantástico ambiente dentro e fora do laboratório.

Aos meus **pais**, pela educação que me incutiram e por me terem proporcionado excelentes condições para evoluir quer a nivel pessoal quer a nivel académico.

Às minhas meninas lá de casa, **Ana Catarina Tavares** e **Matilde Santos**, pelo excelente ambiente familiar, que foi fundamental de modo a manter uma saniedade mental estável ao longo desta jornada.

Table of Contents

Figure Index

Chart Index

Table Index

Scheme Index

Abbreviations and Symbols

- **2PE** – Two-photon excitation
- **ADC(s)** – Antibody drug conjugate(s)
- **Ab** – Antibody
- **Arom** – Aromatic
- **BASHY** – Boronic acid salicylidenehydrazone
- **Bn** – Benzyl
- **^{11}B-NMR** – ^{11}Boron Nuclear magnetic resonance
- **BMDC** – Bone marrow dendritic cells
- **BNCT** – Boron Neutron Capture Therapy
- **BODIPY** – Boron-dipyrromethene
- **B-complex(es)** – Boronate-complex(es)
- **Btz** – Bortezomib
- **CD** – Circular dichroism
- **Cy** – Cyclohexyl
- **DBCO** – Dibenzocyclooctyne
- **DFT** – Density functional theory
- **DMF** – Dimethylformamide
- **DMSO** – Dimethyl sulfoxide
- **E.A** – Elemental analysis
- **ETC** – energy-transfer cassettes
- **equiv.** – Equivalents
- **ESI-MS** – Electrospray ionization mass spectrometry
- **FA** – Folic acid
- **FAB** – Fragment antigen-binding
- **FDA** – Food and Drug Administration
- **FPLC** – Fast protein liquid chromatography
- **FR(s)** – Folate receptor(s)
- **FRET** – Förster resonance energy transfer
- **FTIR** – Fourier-transform infrared spectroscopy
- **GSH** – Reduced glutathione
- **HNE** – Human neutrophile elastase
- **HPLC** – High-performance liquid chromatography
- **HRMS** – High resolution mass spectrometry

- ***iBu*** – isobutyl
- **ICT** – Intramolecular charge-transfer
- **IPTG** – Isopropyl β-D-1-thiogalactopyranoside
- **LB** – Lysogeny broth
- **LC-MS** – Liquid-chromatography mass spectrometry
- **LRMS** – Low resolution mass spectrometry
- **mal-DBCO** – Dibenzocyclooctyne-maleimide
- **MFI** – Median fluorescence intensity
- **MM** – Human multiple myeloma
- **mp** – Melting point
- **MTS** – 3-(4,5-dimethylthiazol-2-yl)-5-(3-carboxymethoxyphenyl)-2-(4-sulfophenyl)--2H-tetrazolium
- **NCI** – National Cancer Institute
- **NBD** – 7-nitrobenzooxadiazole
- **NP(s)** – Nanoparticle(s)
- **OD** – Optical density
- **PBS** – Phosphate buffer saline
- **PDI** – Polydispersity index
- **PEG** – Polyethylene glycol
- **Ph** – Phenyl
- **PI** – Propidium iodide
- **PLGA** – Poly(lactide-co-glycolide)
- **PM** – Plasmatic membrane
- **PVA** – Poly(vinyl alcohol)
- **ROS** – Reactive oxygen species
- **RPMI** – Roswell Park Memorial Institute
- **RT** – Room temperature
- **SD** – Standard deviation
- **SDS-PAGE** – Sodium dodecyl sulfate polyacrylamide gel electrophoresis
- **SI** – Supporting information
- **SMDC(s)** – Small-molecule drug conjugate(s)
- **SPAAC** – Strain-promoted alkyne–azide cycloaddition
- **TBET** – Through-bond energy transfer
- **TBTU** – O-(Benzotriazol-1-yl)-N,N,N′,N′-tetramethyluronium tetrafluoroborate
- ***t*-Bu** – *tert*-butyl

- **TDC** – Targeting drug conjugates
- **ZP** – Zeta potential
- $\mathbf{E_p^{red}}$ – Peak reduction potential
- $\boldsymbol{E_{exc}}$ – Excitation energies
- $\lambda_{\mathbf{abs}}$ – Longest-wavelength absorption maximum
- $\lambda_{\mathbf{fluo}}$ – Fluorescence maximum
- $\Phi_{\mathbf{fluo}}$ – Fluorescence quantum yield
- $\tau_{\mathbf{fluo}}$ – Fluorescence lifetime

Abstract

Boron has an unique set of chemical and physical properties, since it lies on the borderline between non-metals and metals and is also next to carbon in the periodic table. Boronic acids are trivalent boron compounds with a strong Lewis acid character, therefore they are able to chelate with Lewis base donors through dynamic covalent bonds. These bonds are the ideal tools to construct reversible multicomponent systems, since these ligations can be stable as covalent bonds or reversible as non-covalent bonds, depending on the stimulus applied.

Carcinogenesis is classified as a multifaceted biological process and recent therapies are focus in interrupting one or more of these stages by the use of selective multivalent conjugates. Herein, a novel modular platform for the construction of cancer-cell-targeting drug conjugates is described and is based on multifunctional and reversible boronate complexes (B-complexes), which were designed to accommodate bortezomib (**Btz**), polyethylene glycol (PEG) chains and folate targeting units. These B-complexes revealed to be stable under biocompatible conditions (e.g. $t_{1/2}$ (**72**) in human plasma = 60 h), and were hydrolyzed in the presence of glutathione (GSH), leading to intracellular cargo delivery in cancer cells. Small-molecule drug conjugates (SMDCs) **63** and **67** demonstrated a high selectivity for folate-positive MDA-MB-231 cancer cell line and IC_{50} values in the low nanomolar range.

This modular technology was also employed in the construction of responsive and electronically tunable fluorescent boronic acid salicylidenehydrazone (BASHY) complexes, which revealed to have suitable structural and photophysical properties for live cell bioimaging applications. This modular approach enabled the straightforward synthesis (yields up to 99 %) of structurally diverse and photostable intramolecular charge-transfer (ICT) dyes, including energy-transfer cassettes (ETCs), that exhibit a polarity-sensitive emission, high quantum yields of up to 0.68 in nonpolar environments, high brightness (up to 121000 $M^{-1}.cm^{-1}$) and a two-photon-absorption behavior. In terms of bioimaging applications, BASHYs **81a,e** were applied in the selective staining of lipid droplets in HeLa cells. Dyes **81a,e** and ECT **85** were used to prepare non-cytotoxic and highly fluorescent poly(lactide-co-glycolide) (PLGA) nanoparticles (NPs), which were effectively internalized by bone marrow dendritic cells (BMDC). BASHY-azide **89** was used for the site-selective labelling of Annexin V, which is an apoptosis biomarker. Annexin V-BASHY **92** successfully targeted and detected apoptotic cells maintaining high levels of specific activity.

Keywords: Boron; Modular; Reversible; Tumor-targeting; Bioimaging

Resumo

O elemento boro tem propriedades físico-químicas únicas, visto que na tabela periódica se encontra na fronteira entre o grupo dos não-metais e metais e também porque se localiza na posição adjacente ao carbono. Estas propriedades únicas do boro, despertaram o interesse da comunidade científica no desenvolvimento de novas moléculas com este elemento, a fim de ser usadas numa vasta gama de aplicações, tais como medicina, síntese de complexos dinâmicos, entre outras.

Os ácidos borónicos são compostos trivalentes de boro com dois grupos hidroxilo e uma unidade alquílica ou arílica. São classificados como ácidos de *Lewis* fortes, tendo assim a capacidade de formar ligações covalentes dinâmicas com bases de *Lewis*, que contêm na sua estrutura, álcoois e aminas numa correlação vicinal (1,2) ou hominal (1,3).

As ligações covalentes dinâmicas são ideais para a construção de sistemas multivalentes reversíveis, uma vez que as mesmas podem ser estáveis como ligações covalentes ou reversíveis como ligações não covalentes, dependendo do estímulo aplicado. Os sistemas multivalentes dinâmicos podem ser aplicados em diferentes áreas, tais como bioimagem, bioconjugação, terapia do cancro, entre outras.

As células cancerígenas emergem a partir de células saudáveis que adquiriram mutações no ADN que não foram reparadas. Esta transformação é atualmente classificada como um processo biológico multifacetado e complexo, e por consequência, as terapias mais recentes para o tratamento do cancro, visam a interrupção do processo de carcinogénese através do uso de conjugados multifuncionais e específicos.

Nesta tese de doutoramento é apresentada uma nova abordagem modular para a construção de conjugados multivalentes terapêuticos direcionados para as células cancerígenas. Estes conjugados são baseados em complexos de boro, mantidos por ligações covalentes reversíveis e contêm um agente citotóxico (*bortezomib*), uma cadeia hidrofílica (polietilenoglicol) e uma unidade de reconhecimento das células cancerígenas (ácido fólico).

Estes complexos de boro demonstraram serem estáveis em condições biocompatíveis (ex: tempo de semi-vida do composto **72** em plasma humano = 60 h), no entanto são hidrolisados na presença da glutationa. A distribuição seletiva e libertação dos componentes destes complexos de boro nas células cancerígenas foram comprovadas através de microscopia de fluorescência confocal e foi também proposto um mecanismo para a hidrólise destes complexos de boro induzida pela glutationa com base em dados recolhidos por espectrometria de massa e cálculos teóricos.

Esta nova abordagem modular permitiu a construção de conjugados multivalentes **63** e **67**, que têm uma elevada seletividade para células cancerígenas MDA-MB-231 (sobre-expressão de receptores para o ácido fólico) com valores de IC_{50} na região do baixo nanomolar.

Esta tecnologia modular foi também utilizada nesta tese de doutoramento na síntese de complexos de boro fluorescentes (BASHYs) com elevada sensibilidade e adaptabilidade em termos das suas propriedades fotofísicas. Os BASHYs foram preparados através da assemblagem modular entre ácidos borónicos e ligandos *Schiff-base* e revelaram possuir propriedades estruturais e fotofísicas adequadas à aplicação na área da bioimagem em células.

Esta metodologia sintética modular permitiu a síntese (rendimentos até 99 %) de diversos BASHYs fotoestáveis que têm uma fluorescência dependente da polaridade, com bons rendimentos quânticos (até 0,68 em ambientes não polares), que possuem um elevado brilho (até 121000 $M^{-1}.cm^{-1}$) e cujas propriedades fotofísicas permitem a absorção de dois fotões.

Relativamente às aplicações de bioimagem em células, BASHYs **81a,e** foram utilizados para corar seletivamente gotículas lipídicas nas células HeLa. Sondas fluorescentes **81a,e** e **85** foram usadas na preparação de nanopartículas não citotóxicas e fluorescentes que foram efetivamente internalizadas por células dendríticas da medula óssea.

BASHY-azida **89** foi utilizada na conjugação com a Anexina V e o conjugado daí resultante (Anexina V-BASHY **92**) foi usado com sucesso na marcação seletiva por fluorescência de células apoptóticas.

Palavras-chave: Boro; Modular; Reversível; Terapia do cancro; Bioimagem

Chapter I

State of Art (B-Complexes)

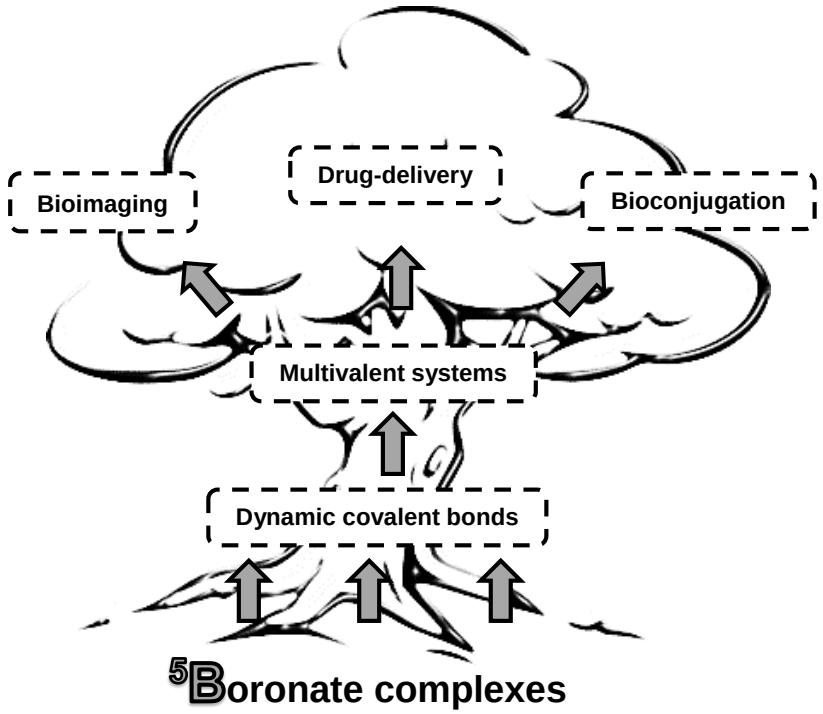

Abstract

Boron has an unique set of chemical and physical properties, since it lies on the borderline between non-metals and metals and is also next to carbon in the periodic table. Consequently, the scientific community has become more interested in the development of novel boron-containing compounds in order to be applied on a wide range of subjects, such as medicine or molecular design.

Boronic acids are trivalent boron compounds with two hydroxyl groups and an alkyl or aryl moiety. With a strong Lewis acid character, boronic acids have the ability to form dynamic covalent bonds with Lewis base donors, which contain in their structure, alcohols and amines in a vicinal (1,2) or hominal (1,3) correlation.

Dynamic covalent bonds are the ideal tools for synthesis of multicomponent systems since these ligations can be stable as covalent bonds or reversible as non-covalent bonds, depending on the stimulus applied. These dynamic systems can be applied in different fields, such as bioimaging, bioconjugation, drug delivery, among others.

I.1. Boron

Boron is a hybrid element in the periodic table, since it lies on the borderline between non-metals and metals, thus it shares both properties. This atom is also next to carbon, therefore they are structurally very similar. For instance, in an aromatic moiety, B-O and B-N bonds are isoelectronic, isovalent and isosteric to C=N and C=C bonds, respectively. Therefore, boron has a remarkable set of chemical and physical properties, which have been gathering the interest of the scientific community in the discovery of novel boron-containing compounds to be applied on a wide range of subjects, such as medicine, molecular design, among others (**Figure 1**).[1–4]

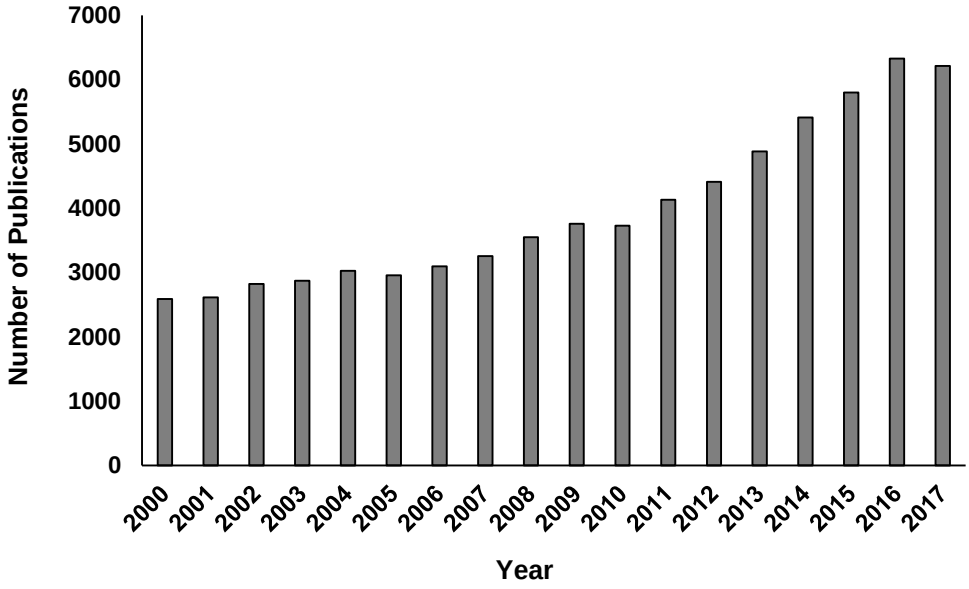

Figure 1 – Number of publications focusing on boron in Web of Science between 2001-2017.

The boron atom can adopt two different geometric configurations, tri-coordinated (sp^2) and tetra-coordinated (sp^3). In the trigonal planar geometry, boron is an electrophile that is able to accept a pair of electrons from a nucleophile in its vacant *p* orbital, switching its configuration to tetrahedral (**Scheme 1**).[5,6]

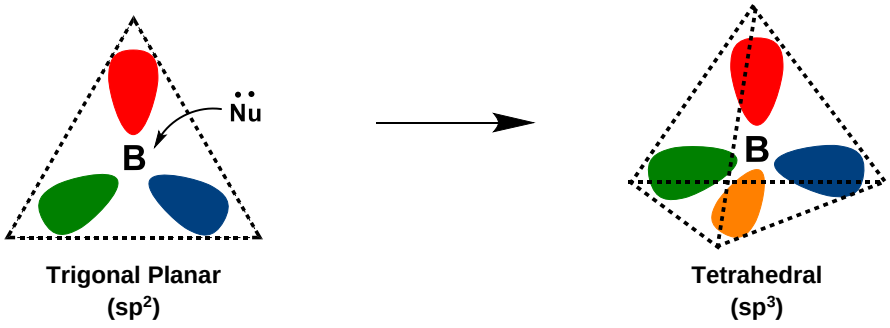

Scheme 1 – Geometric configurations of the boron atom.

Boron is mostly found in nature in the form of boric acid, which is an important plant nutrient. To date, several boron-containing natural products (*e.g*. boromycin, tartrolon B, borophycin and AI-2) with important biological properties (*e.g*. antibiotic, anti-HIV, anticancer, antimicrobial, antibacterial, antihepatitis) have been discovered, reinforcing the important role of boron in nature (**Figure 2**).[7,8] The number of boronated natural products already discovered could be higher, however the labile nature of boron complexation to these natural skeletons leads to their disassembly in the processes of extraction and purification from the natural source.

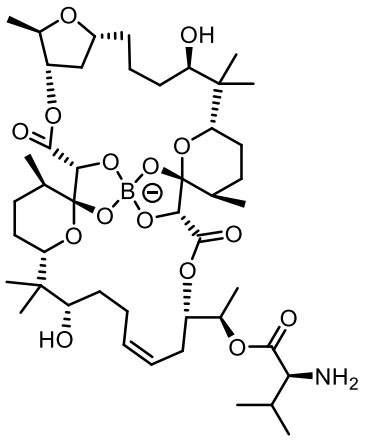

Boromycin
(Antibiotic and anti-HIV)

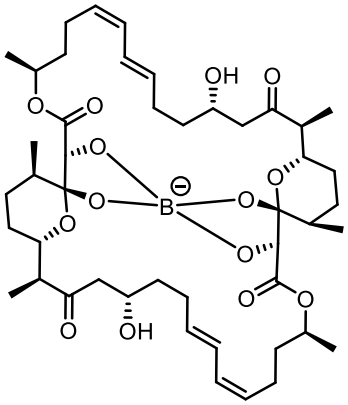

Tartrolon B
(Anticancer, antibacterial and antihepatitis)

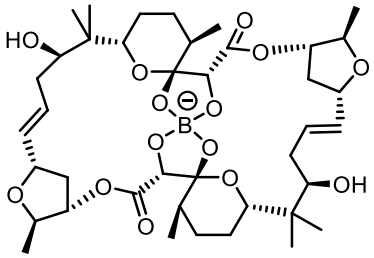

Borophycin
(Anticancer and antimicrobial)

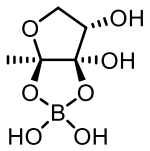

AI-2
(Antimicrobial)

Figure 2 – Selected examples of natural boronated compounds and their biological properties.

Throughout the years, several families of boronate compounds (e.g: boronic acids, boranes, boroxines, diazoborines, boroles, BODIPYs) have been discovered and described in the literature with a vast range of applications (e.g: antiseptic, anticancer, antibacterial, antifungal, catalysis, supramolecular, hydrogen storage, bioimaging) (**Figure 3**). Among these boron-containing families, no evidence of severe toxicity associated with the boron moiety was ever observed in mammals.[5,9,10] For a better understanding of this thesis, boronic acids and derivatives will be further addressed in higher detail.

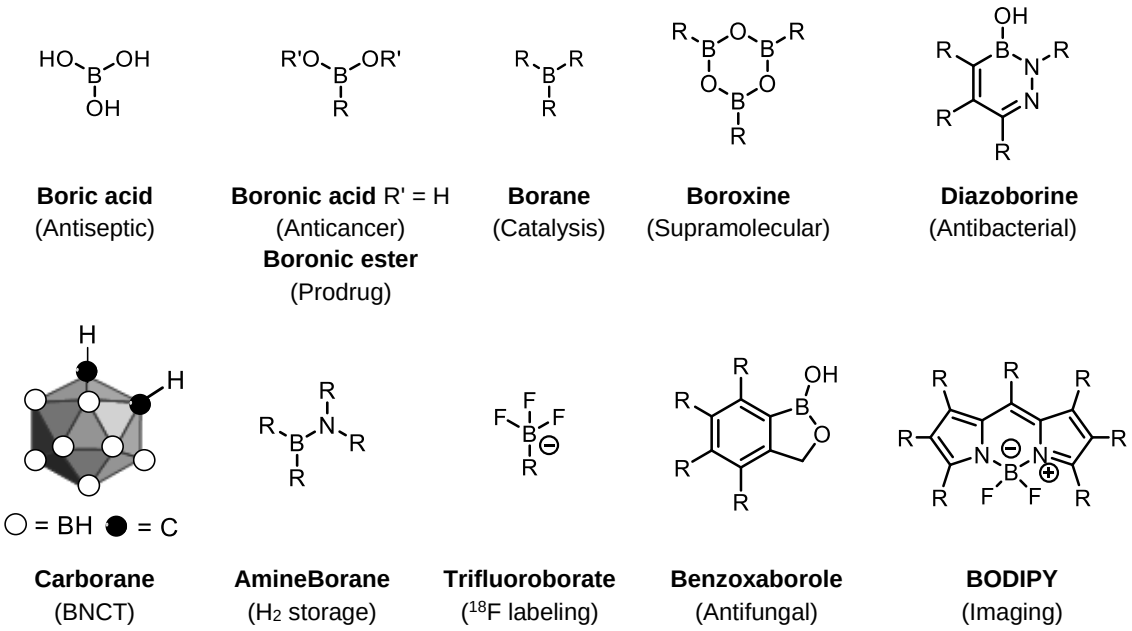

Figure 3 – Selection of different families of boron compounds and some examples of their applications. BNCT stands for Boron Neutron Capture Therapy.

I.2. Boronic acids

In 1860, Frankland and Duppa reported for the first time the isolation of a boronic acid. Since this family of boron compounds is not found in nature, the discovery of hydroboration in 1956 was a turning point, as it made organoborons like boronic acids more available.[11–13]

Boronic acids are trivalent boron compounds with two hydroxyl groups and an alkyl or aryl moiety. With a strong Lewis acid character, boronic acids have the ability to form dynamic covalent bonds with Lewis base donors, which contain in their structure, alcohols and amines in a vicinal (1,2) or hominal (1,3) correlation. Dynamic covalent bonds are the ideal tools for synthesis of multicomponent systems, since these ligations can be stable as covalent bonds or reversible as non-covalent bonds, depending on the stimulus applied.[14,15]

In tri-coordinated complexes (**Scheme 2A**), the boron atom has only 6 valence electrons, therefore it can do another bond in order to fulfil the octet rule. In some cases, boron octet can be completed *via* a dative B-N bond, giving rise to a stable tetra-coordinated boron construct (**Scheme 2B**).[12,14,16]

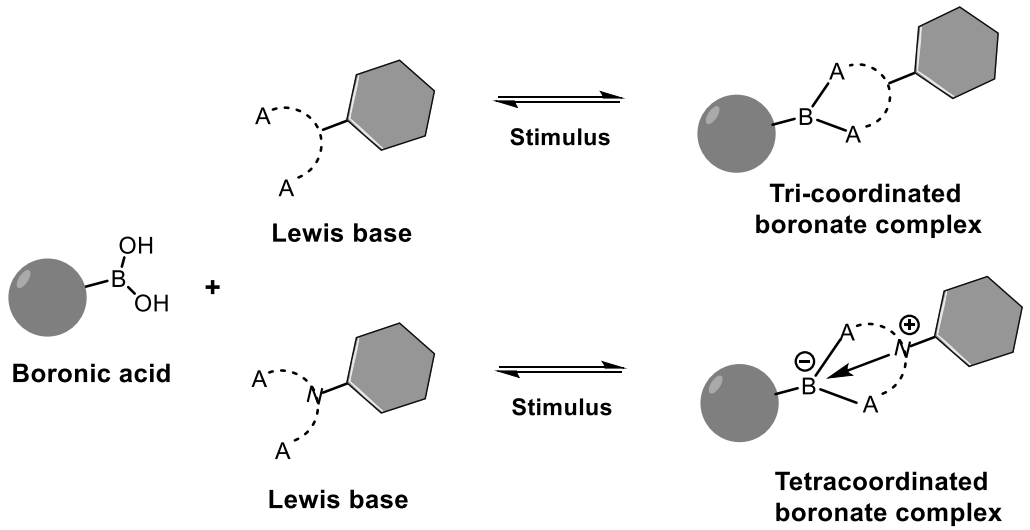

Scheme 2 – Top: Formation of a reversible tri-coordinated boronate complex; Bottom: Construction of a reversible tetra-coordinated boronate complex. A= O or NH.

Bortezomib (**Btz**; Velcade®) was the first boronic acid to be approved by Food and Drug Administration (FDA) in 2003 as a proteasome inhibitor for the treatment of mantle cell lymphoma and multiple myeloma. However, due to the unspecific reactivity of boronic acids with Lewis bases (*e.g:* sugars and proteins in the bloodstream), **Btz** have been revealing an unfavorable pharmacokinetic profile and off-target toxicity.[17,18]

Several studies have been done in the past years to solve the aforementioned problem, in order to make the therapy with **Btz** more efficient and safer.[19–24] In one of these studies, Bilciger and co-workers tested the stability at physiological pH of several B-complexes **1** – **5**, using isobutylboronic acid as a simplified model of **Btz**. This evaluation was done to choose the best complex for the construction of liposome-Btz nanoparticles. B-complex **1**, in which the boron atom is in a tetrahedral configuration, proved to be the most stable ($t_{1/2}$= 190 min; **Figure 4B**). The ligand used in complex **1** was further applied in the complexation of **Btz** to liposomes, giving rise to construct **6**. Liposome-Btz **6** was then evaluated in two cancer cell lines and the IC_{50}'s obtained (MM.1S – 25 nM; NCI-H929 – 45 nM; **Figure 4C**) were in the same range as **Btz** alone (**Figure 4A**).[18]

A

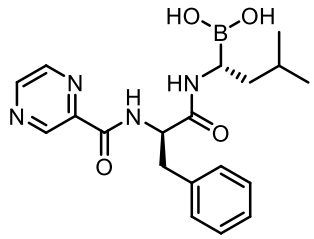

Bortezomib

IC_{50} – MM.1S (17 nM); NCI-H929 (20 nM)

B

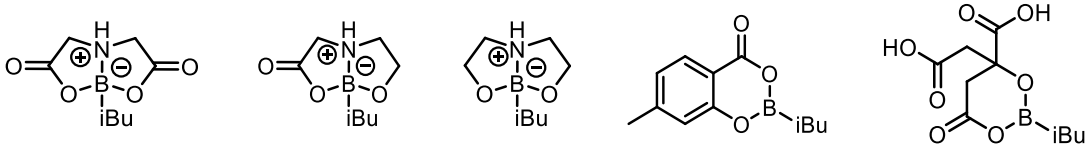

1	**2**	**3**	**4**	**5**
$t_{1/2}$ = 190 min	$t_{1/2}$ = 8.8 min	$t_{1/2}$ = 1.6 min	$t_{1/2}$ = 10 min	$t_{1/2}$ = 1.6 min

C

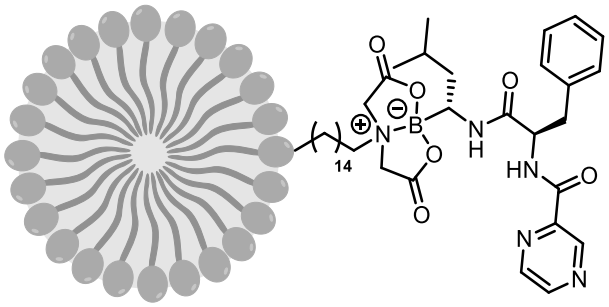

6

IC_{50} – MM.1S (25 nM); NCI-H929 (45 nM)

Figure 4 – A: Btz with the IC_{50}'s obtained in MM.1S and NCI-H929 cancer cell lines; **B:** Half-lives obtained in PBS (pH 7.4) for the different boronated complexes **1 – 5**, using isobutylboronic acid as a model for Btz; **C:** Liposome-Btz **6** with IC_{50} obtained in MM.1S and NCI-H929 cancer cell lines.

In recent years, several boronic acid derivatives, besides **Btz** (Velcade® 2003), have been shown to possess relevant biological activities and were approved by FDA: AN2690 (Kerydin® 2014; antifungal agent for the treatment of onychomycosis);[25] Ixazomib (Ninlaro® 2015; proteasome inhibitor for the treatment of multiple myeloma);[26] AN2728 (Eucrisa® 2016; anti-inflammatory non-steroidal agent for mild to moderate eczema).[27] Moreover, further boronic acids with therapeutic potential have been developed and some of them are currently being evaluated in clinical trials (**Figure 5**).[5,16,28,29]

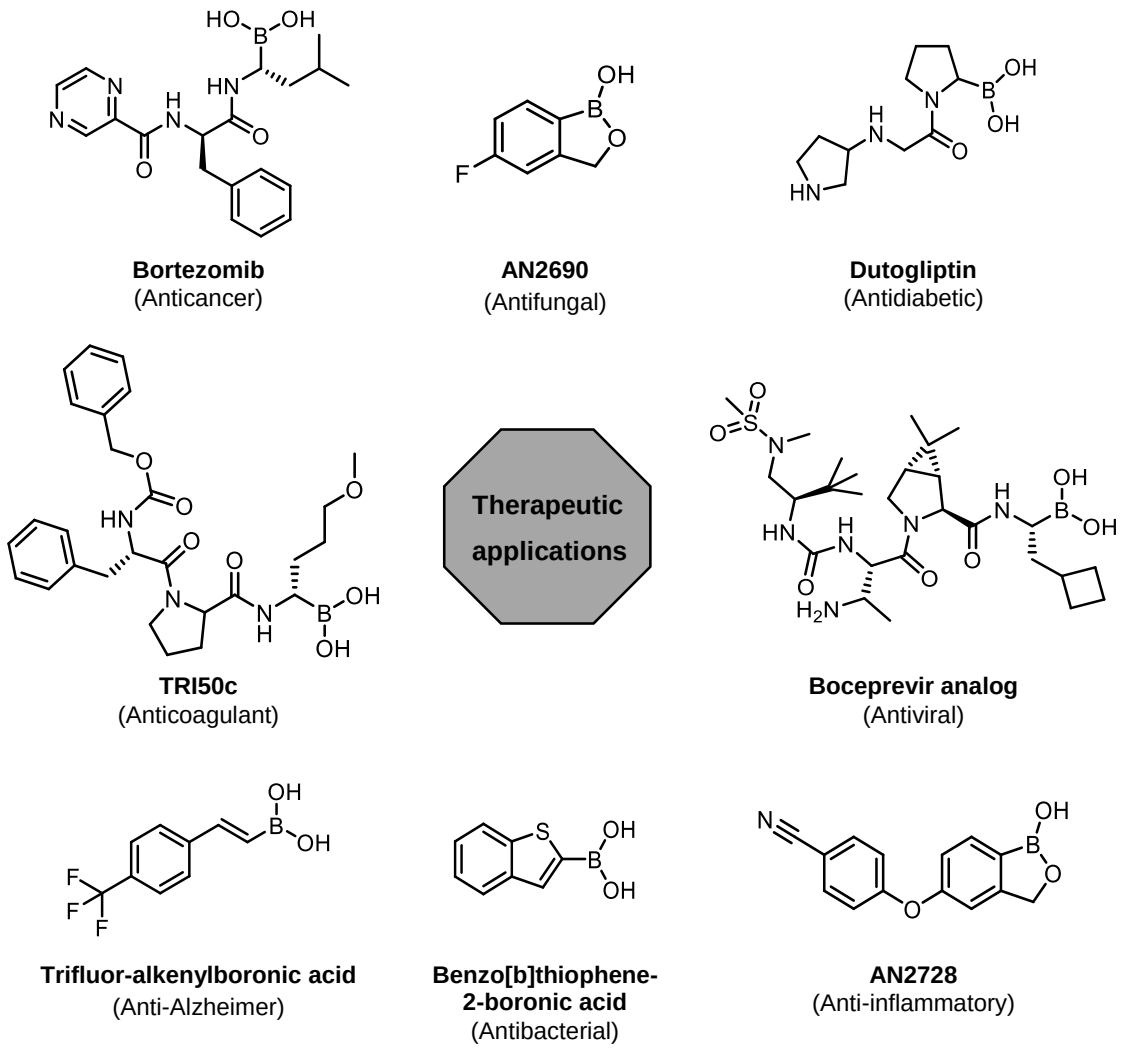

Figure 5 – Examples of boronic acid derivatives with therapeutic applications.

Due to their unique set of chemical and physical properties, boronic acids have been showing a great versatility, therefore they are not only restricted to therapeutic applications, being also very useful in a vast range of applications, including modular synthesis, biological labelling, sensing, electrophoresis, protein immobilization, bioconjugation, among others (**Figure 6**).[30–35]

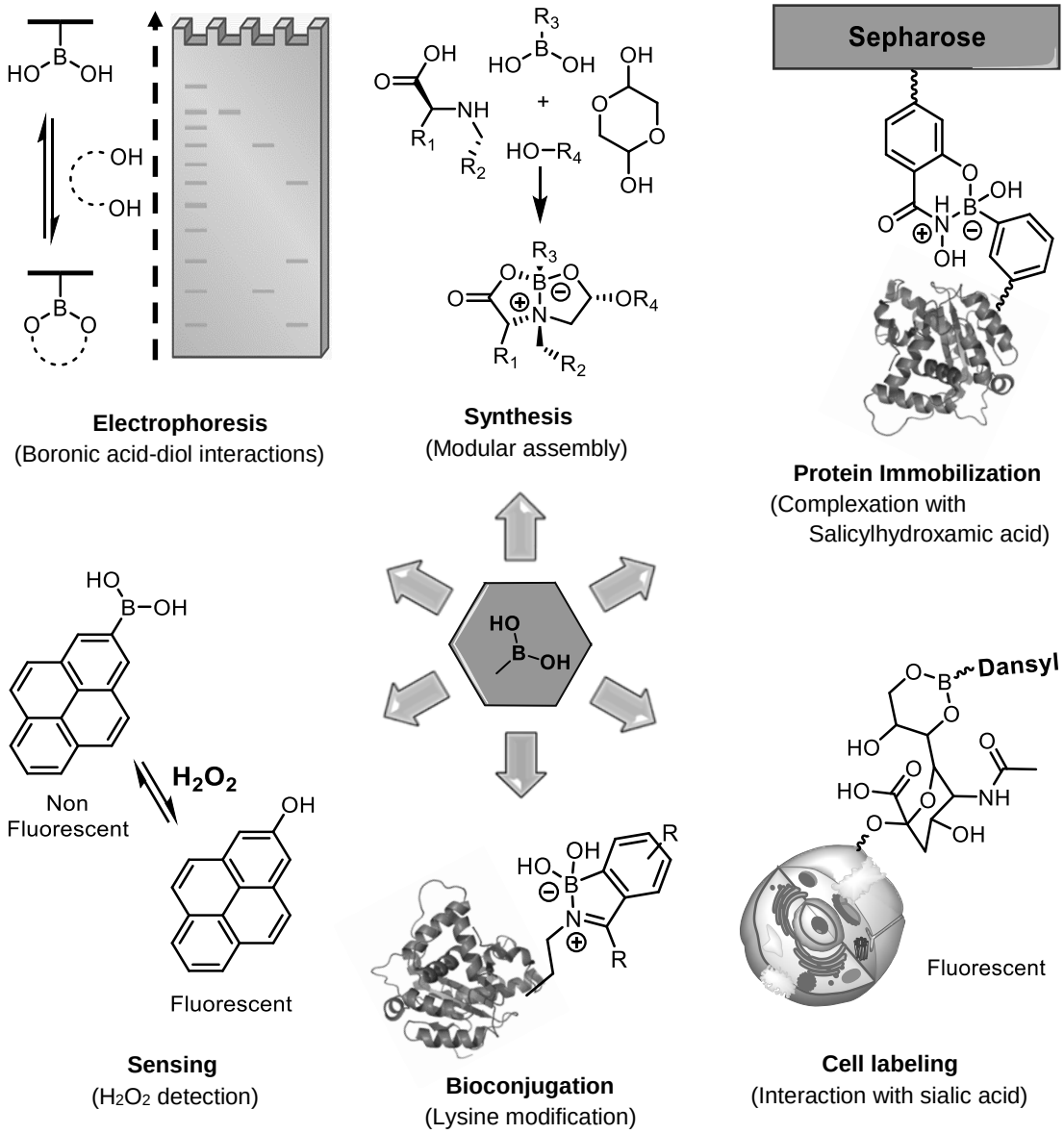

Figure 6 – Boronic acid's role in different applications.

The main focus on this PhD project will be in the modular synthesis of multivalent constructs, in which the boronic acid moiety will have an instrumental role in the assembly and reversibility of these dynamic multicomponent structures. In the context of this thesis, imino- and hydrazono-boronate complexes will be further discussed (**Figure 7**).

Figure 7 – Generic structures of imino- and hydrazono- boronate complexes.

I.3. B-complexes

I.3.1 Iminoboronates

Barba and co-workers were one of the first research groups to demonstrate interest in the modular construction of iminoboronates. In one of their works, three different iminoboronates **9a-c** were prepared from the condensation of Schiff base ligands **7a-c** with boronic acid **8** (**Scheme 3**) in order to assess how strong the assemblage was. This evaluation was done by ^{11}B-NMR and the obtained chemical shifts of boron, indicated that the assemblage in the iminoboronate **9b** (δ = 5 ppm) was slightly stronger than in **9c** (δ = 6 ppm) and **9a** (δ = 8 ppm). This statement may be explained by the fact that a boron shift in a higher field of the ^{11}B-NMR spectra indicates that B-N bond is stronger, as the boron atom is more shielded by the electronic donation of nitrogen.[36]

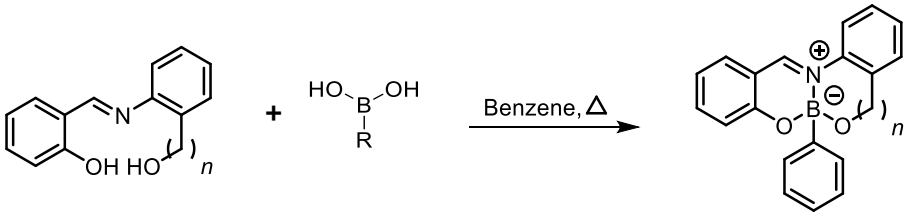

7a (n = 0)
7b (n = 1)
7c (n = 2)

8
(R= Ph)

9a (n = 0)
9b (n = 1)
9c (n = 2)

Scheme 3 – Synthesis of iminoboronates **9a–c**.

The skeleton of iminoboronate **9a** was then found to be further modified *via* acetolysis, Grignard or Diels-Alder chemistry, by exploring the reactivity of the imine function. Farfan research group took advantage of this reactivity in order to improve the complexity of B-complexes structure, as shown in the iminoboronates **10**–**13** (**Scheme 4**).[37–40]

The scaffold of multicomponent iminoboronates could also be achieved in one-pot four-component reaction, revealing the versatility of the boronic acid moiety in the modular assembly of dynamic complexes. Zhu and co-workers prepared a small library of iminoboronates **17** from the condensation of isatoic anhydride **16** with derivatives of 2-hydroxybenzaldehyde **14**, boronic acid **8** and benzylamine **15** (**Scheme 5**).[41]

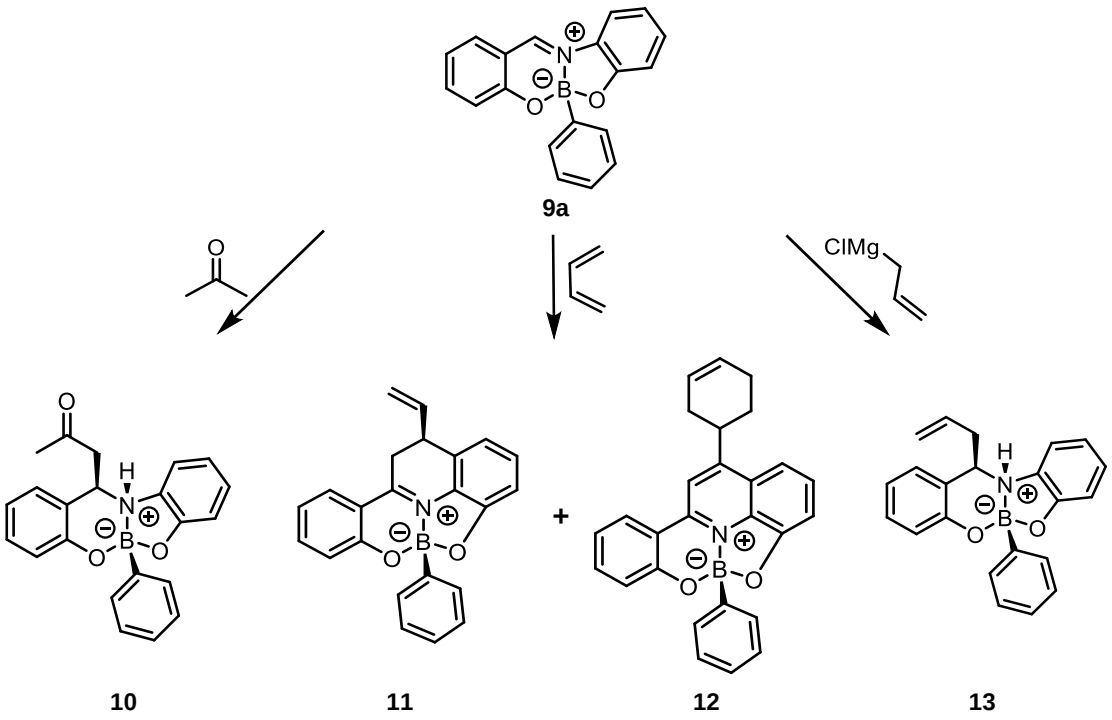

Scheme 4 – Construction of iminoboronates **10–13** *via* acetolysis, Grignard and Diels-alder chemistry.

The planar and rigid structure of this class of iminoboronates was further explored by the Nakatani research group in order to create π-conjugated donor-acceptor systems. The push and pull boronates **18**–**21** revealed to have non-linear optical properties, which can be used in photonic and opto-electronic applications, such as image processing, computing, data storage, among others (**Figure 8**).[42–47]

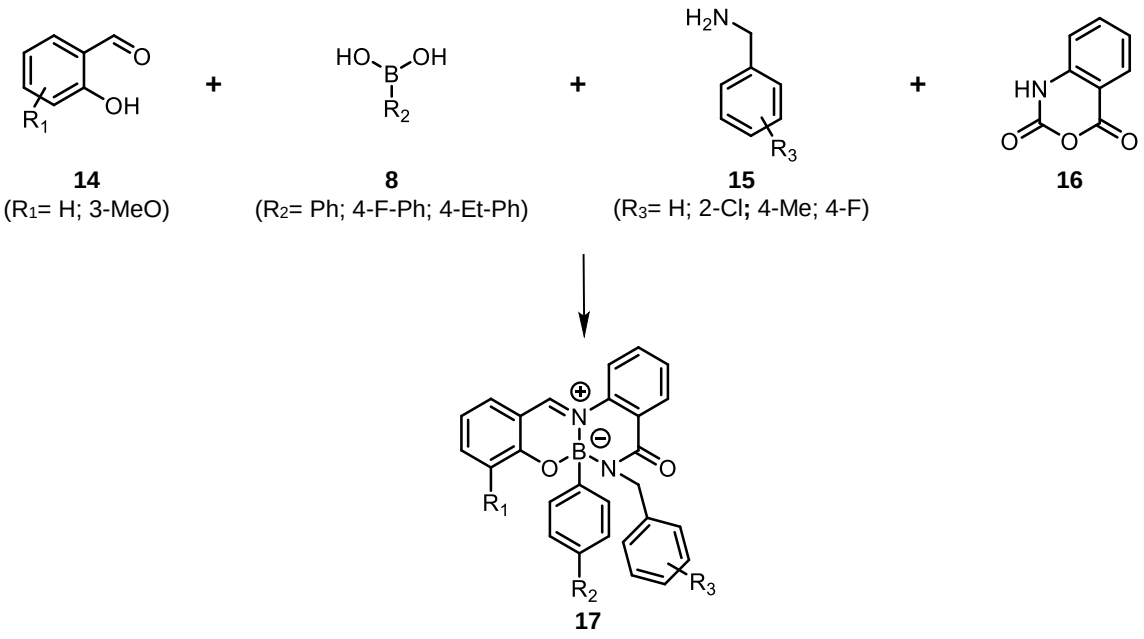

Scheme 5 – Four-component synthesis of iminoboronates **17**.

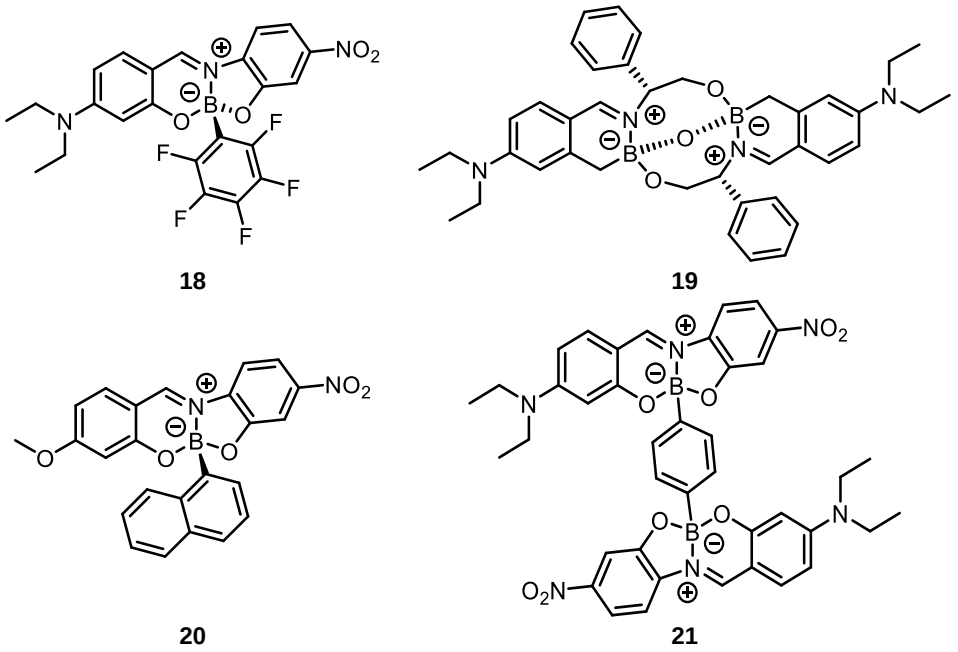

Figure 8 – Selected examples of iminoboronates **18–21** with non-linear properties.

A *tert*-butyl derivative **23** of bis-iminoboronate **21** was prepared by Jiménez-Pérez and co-workers and revealed to be a fluorescent molecular rotor with different quantum yields depending on the system's viscosity (**Scheme 6**). It was observed that the higher the viscosity, the lower the rotation of **23** and therefore the quantum yield increases. This correlation between quantum yield and viscosity can be very useful in the study of cellular mechanisms, since viscosity plays a key role at the cellular level.[48]

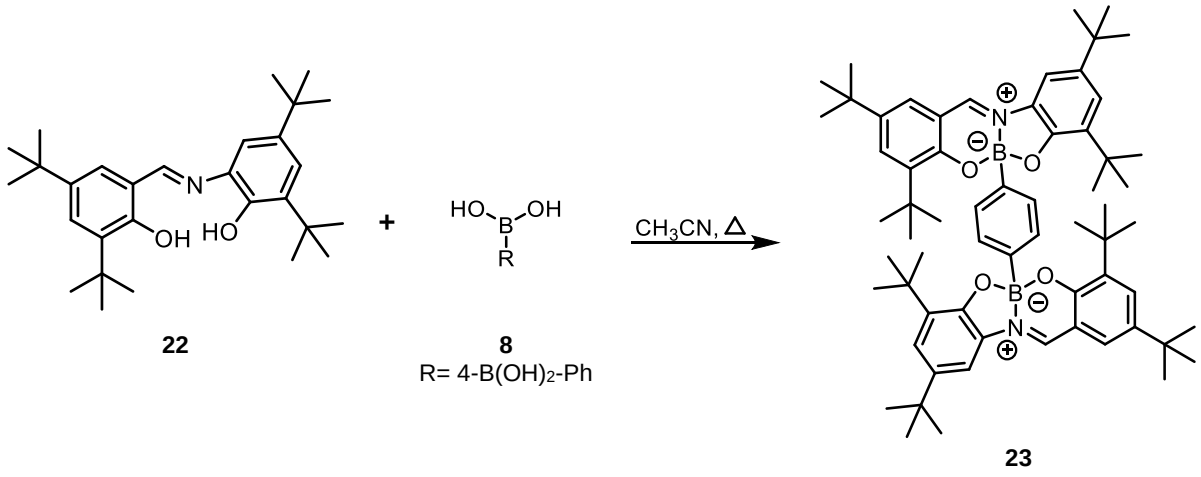

Scheme 6 – Synthesis of a boronate fluorescent molecular rotor **23**.

Kirihata research group developed a bioimaging system to detect boronated pharmaceuticals **8** (*e.g*: **Btz** and *p*-boronophenylalanine) in tumor cells. They have prepared a boronic acid sensor **24**, which after chelation with a boronate drug **8**, gave rise to fluorescent iminoboronate **25**, which can be detected inside the cells (**Scheme 7**). This technology is promising, since the number of boronate pharmaceuticals is increasing, consequently there is a need to understand the biological targets of these boronate drugs.[49,50]

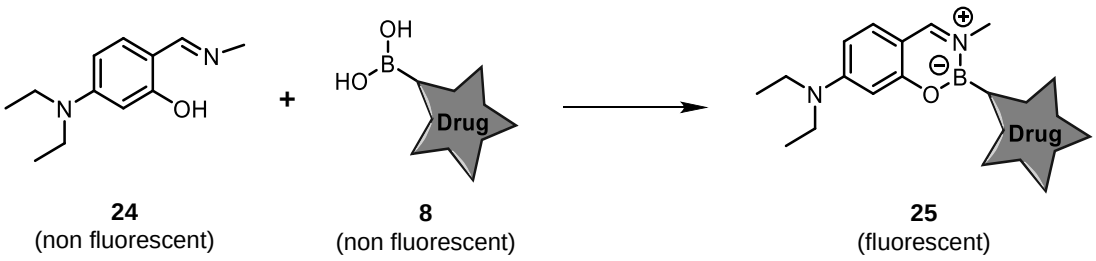

24
(non fluorescent)

8
(non fluorescent)

25
(fluorescent)

Scheme 7 – Bio-imaging system for detection of boronate drugs **8** in tumor cells.

On a different research area, our research group reported for the first time that a multicomponent assemblage between salicylaldehydes **14**, amino acids **26** and boronic acids **8** could be used in the preparation of several iminoboronates **27**. These three dimensional B-complexes were shown to interact with specific recognition moieties in certain enzymes (*e.g.* human neutrophile elastase (HNE) and phenylalanine hydroxylase) in order to inhibit or modulate their activity (**Scheme 8**).[51–53]

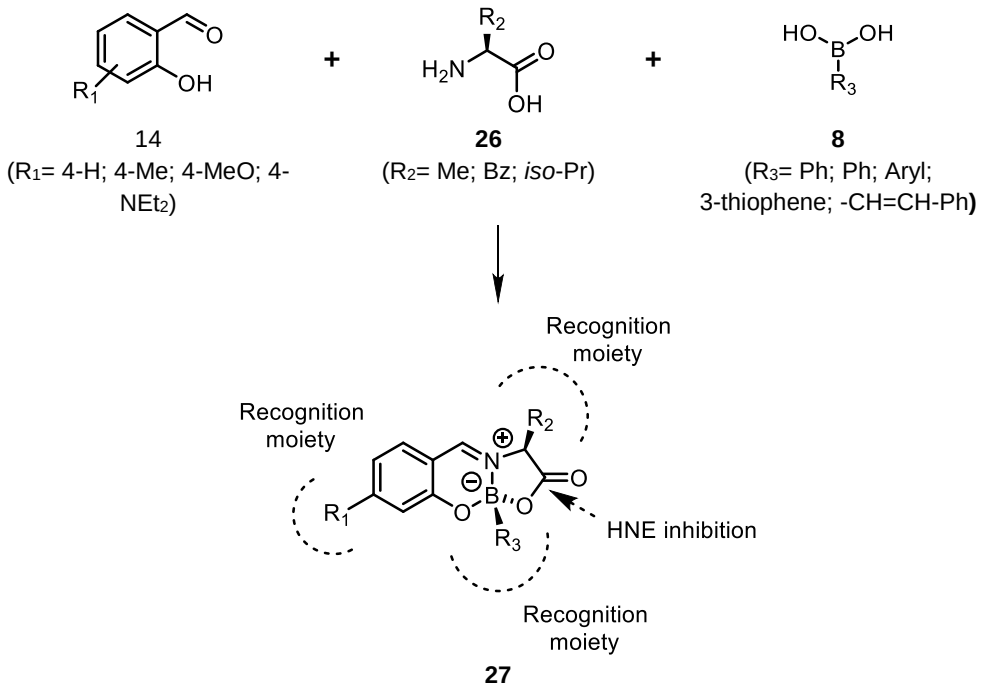

14
(R_1= 4-H; 4-Me; 4-MeO; 4-NEt_2)

26
(R_2= Me; Bz; *iso*-Pr)

8
(R_3= Ph; Ph; Aryl; 3-thiophene; -CH=CH-Ph**)**

27

Scheme 8 – Modular construction of iminoboronates **27**, as inhibitors or modulators of enzymes.

Our research group was also involved in the use of iminoboronates **28** and **29a** as a tool for reversible bioconjugation in different residues, such as lysines/protein's *N*-terminal (**Scheme 9A**) or *N*-terminal cysteines (**Scheme 9B**). Both modifications revealed to be fast and stable under physiological conditions, being hydrolyzed in presence of certain stimuli.[35,54]

Bioconjugation on the lysine's residue (**Scheme 9A**) was used to introduce a fluorescein tag and a sugar moiety in lysozyme, and a PEG chain in insulin. This methodology was also employed in drug delivery with the modification of a terminal amine in the *N*-(2-aminoethyl) folic acid with fluorescent motifs and a cytotoxic drug (paclitaxel).[55,56]

In the *N*-terminal cysteine functionalization, the iminoboronate **29a** acts as an intermediate for thiazolidine **29b** formation (**Scheme 9B**). This powerful reversible bioconjugation tool allowed the dual functionalization of different cysteine residues, since it was highly selective for *N*-terminal cysteine, allowing the modification of other cysteine residues *via* maleimide chemistry.[54]

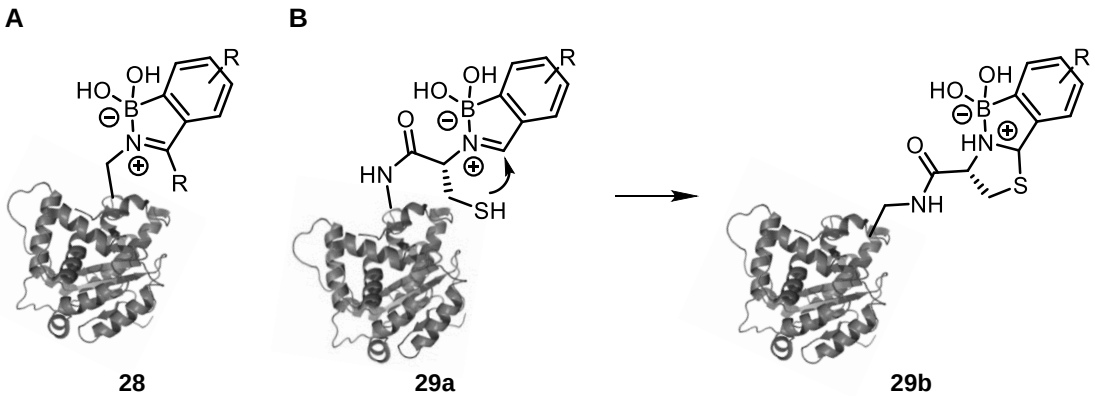

Scheme 9 – Iminoboronates **28** and **29a** as powerful tools for reversible protein/peptide modification in lysine/protein's *N*-terminal **(A)** or *N*-terminal cysteine residues **(B)**.

Concomitantly, Gao´s research team reported a related work on the bioconjugation of *N*-terminal cysteine residues *via* an iminoboronate intermediate.[57] This research group also demonstrated the versatility of the iminoboronate chemistry, as a tool for:

- Cyclization of peptides, which can be used in the synthesis of therapeutic cyclic peptides **30** (**Scheme 10A**).[58,59]
- Labelling of lipids, which can be applied on important membrane lipids **31**, which have a key role on the regulation of several mechanisms in the cell machinery (**Scheme 10B**).[60]
- Cysteine-responsive peptides **32a** as fluorescence sensor of cysteine (**Scheme 10C**).[61]

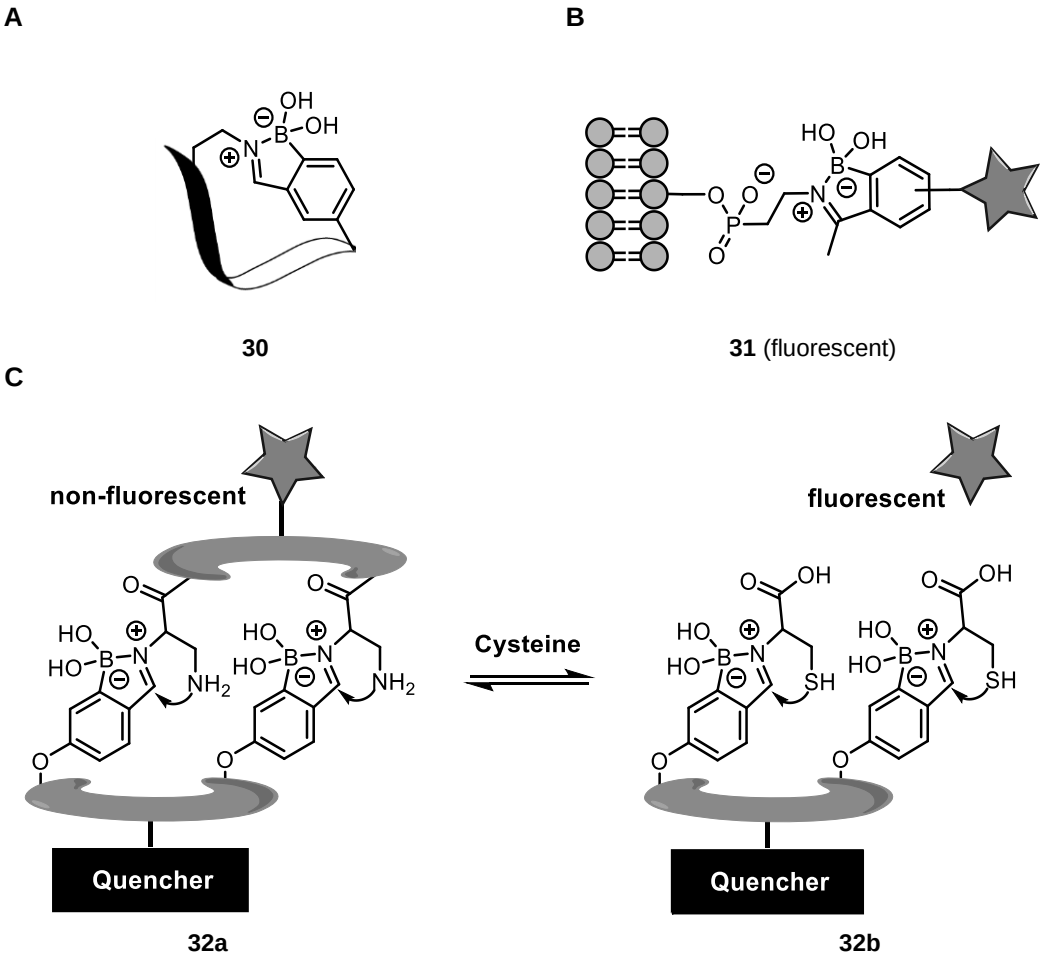

Scheme 10 – Iminoboronates as a tool for: **A-** Cyclization of peptides **30**; **B-** Labeling of lipids **31**; **C-** Cysteine-responsive peptides **32a**.

I.3.2 Hydrazonoboronates

Diazoborines are one of the most representative groups of hydrazonoboronate complexes and have been mainly described in the literature as antibacterial agents *via* inhibition of Enoyl-ACP reductase, which is a well-known molecular target of several successful antibiotics (**Scheme 11**).[62–64] Recent reports also classify diazoborines as antifungal agents[65] and as inhibitors of eukaryotic biogenesis of ribosomes.[66]

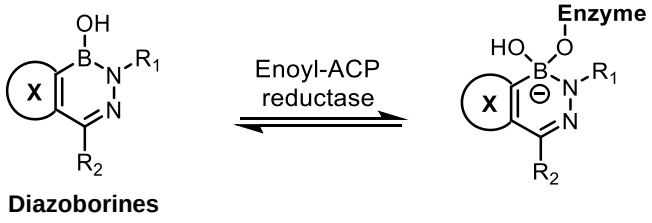

Scheme 11 – Inhibition mechanism of Enoyl-ACP reductase by diazoborines.

Due to the benzodiazoborines planar and aromatic skeleton, Gillingham and co-workers hypothesized that this conjugated system could be extended and modified in order to create a donor-acceptor system. With this idea in mind, two different series of hydrazonoboronates **36** and **37** were prepared (**Scheme 12A,B**) from the condensation of 2-formyl- or 2-acetyl-phenylboronic acids **33a,b** with phenylhydrazines **34** and **35** in pH 7.2 phosphate buffer. Compounds **37** proved to be more fluorescent than **36**, since the free hydroxyl can act as a fluorescence quencher.[67,68]

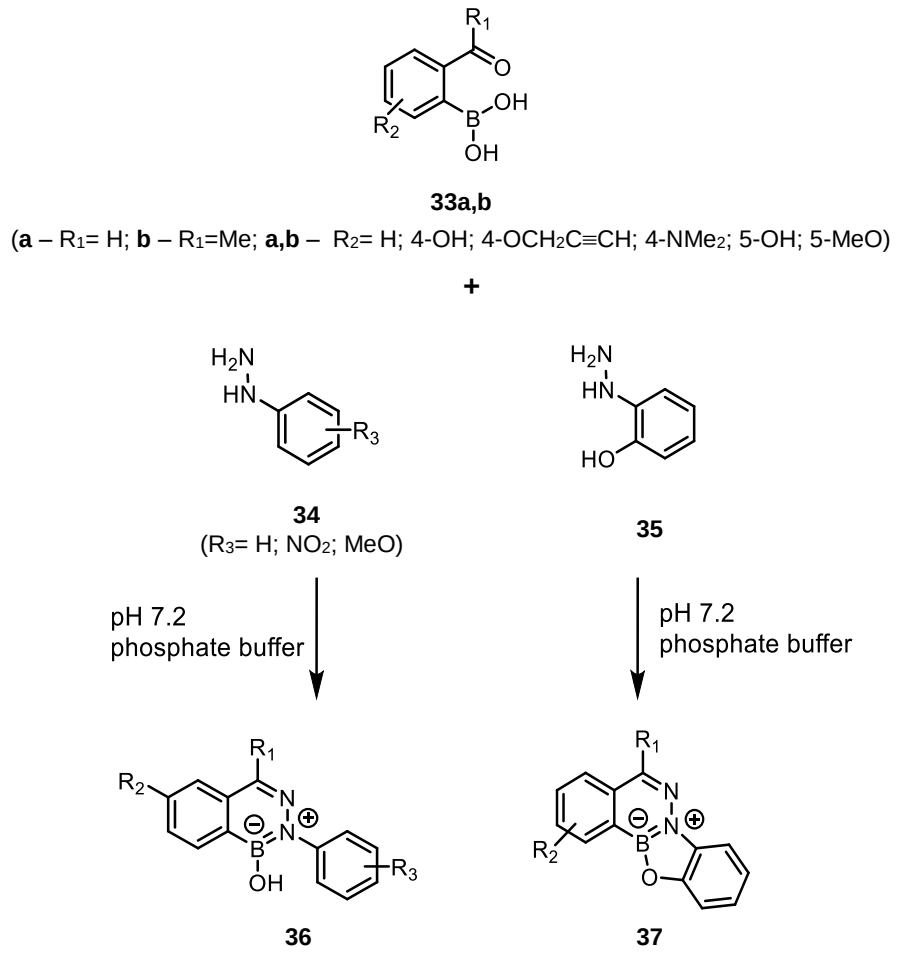

Scheme 12 – Struture of fluorescent benzodiazoborines **36** and **37**.

A similar class of hydrazonoboronates **39a-c** was also prepared by Olmstead's research group *via* condensation of 2-formylphenylboronic acid **33a** with salicyloyl or anthraniloyl hydrazides **38** (**Scheme 13**). It was observed that compound **39a** had a slim fluorescence in solution under long-wavelength (365 nm) and its naphthalene derivative **39c** was slightly more fluorescent. Boronate **39b** was not fluorescent at all due to the lack of solubility in common organic solvents.[69]

33a (R_1=R_2= H)

38 (R_3= 2-OH-Ph; 2-NH_2-Ph; 2-OH-Naphthalene

39a (A= O)
39b (A= NH)

39c (A= O)

Scheme 13 – Synthesis of hydrazonoboronates **39a-c**.

Since the formation of diazoborines can generate fluorescence, Bane and co-workers hypothesized that with the right tuning, the construction of diazoborines could become a click reaction and thus diazoborines could be used as a turn-on fluorogenic bioconjugation tool. Therefore, diazoborine **40** was prepared from condensation of 2-formylphenylboronic acid **33a** with a phenylhydrazine derivative **34** and it was observed that the reaction had enhanced kinetics (10^3 $M^{-1}.s^{-1}$) under physiological condition (**Scheme 14**).[70]

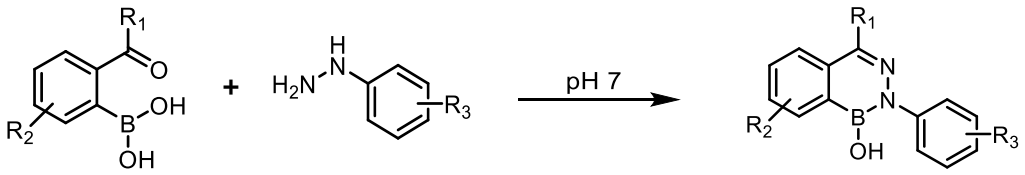

33a (R_1=R_2= H)

34 (R_3= COOH)

40

Scheme 14 – Click synthesis of diazoborine **40** under physiological pH.

This technology was further explored by this research group in the bioconjugation of fluorescent 2-formylphenylboronic acid-coumarin **41** with hydrazine-containing bovine serum albumin (BSA) **42a** or α-amino carbohydrazide-containing BSA **42b**. Both BSA-coumarins **43a,b** revealed to be fluorescent at physiological pH and stable under sodium dodecyl sulfate polyacrylamide gel electrophoresis (SDS-PAGE) analysis (**Scheme 15**).[70,71]

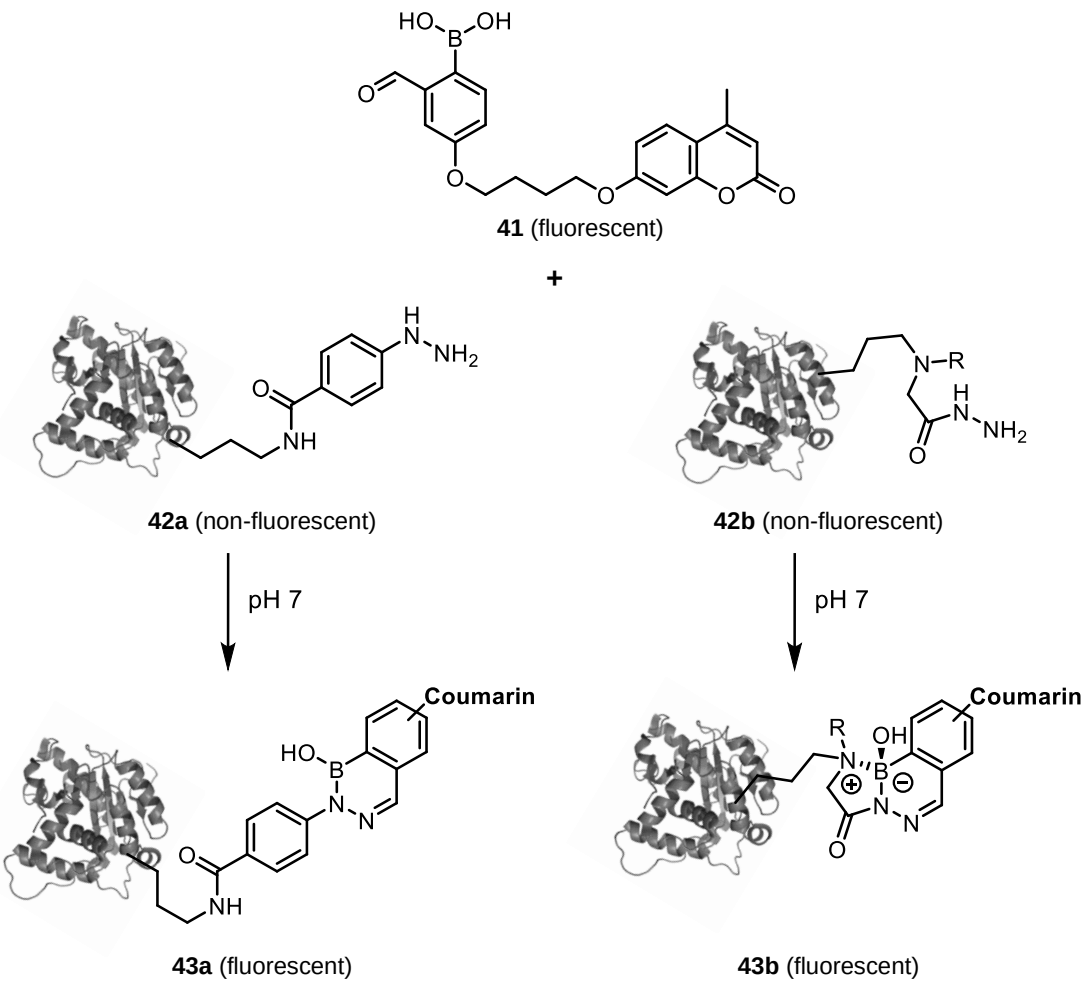

Scheme 15 – BSA-coumarin **43a,b** from the conjugation of 2-formylboronic acid-coumarin **41** with hydrazine-containing BSA **42a** or α-amino carbohydrazide-containing BSA **42b.**

In the sequence of Bane investigation, Gao and co-workers also observed that the synthesis of diazoborines from semicarbazide and 2-acetylphenyl boronic acid had a similar kinetic constant (10^3 $M^{-1}.s^{-1}$) under physiological conditions. This methodology was then used for visualization of bacteria **44** modified with semicarbazide-amino acid (D-DAP-SBC) *via* conjugation with non-fluorescent 2-acetylphenyl boronic acid-coumarins, given rise to fluorogenic diazoborines **45** (**Scheme 16**).[72,73]

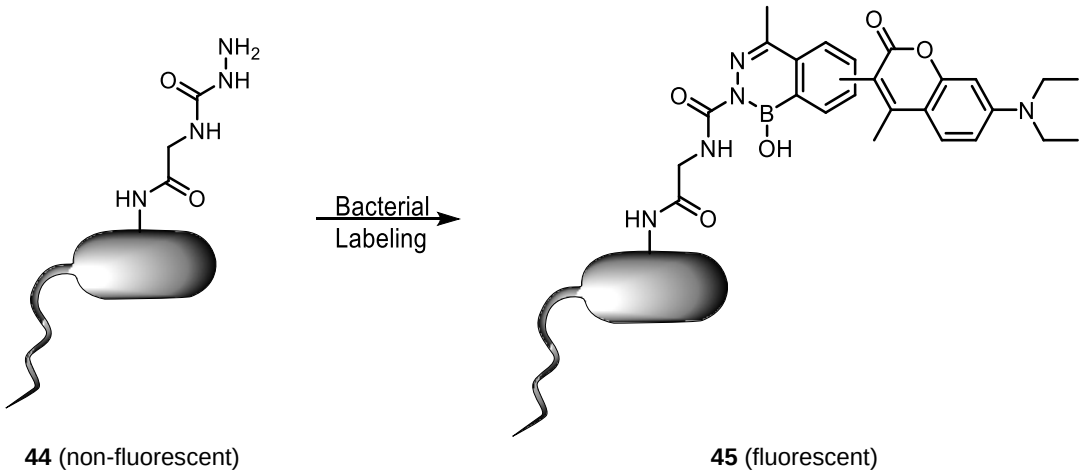

44 (non-fluorescent) **45** (fluorescent)

Scheme 16 – Bacterial labeling *via* click formation of fluorogenic diazoborines.

Waksman's group prepared a different family of hydrazonoboronates **46** *via* condensation of salicylaldehydes **14**, hydrazides **38** and phenylboronic acid **8**. Although B-complexes **46** revealed fluorescence properties, the quantum yields obtained were very low, mainly due to strong internal conversion (**Scheme 17**).[74]

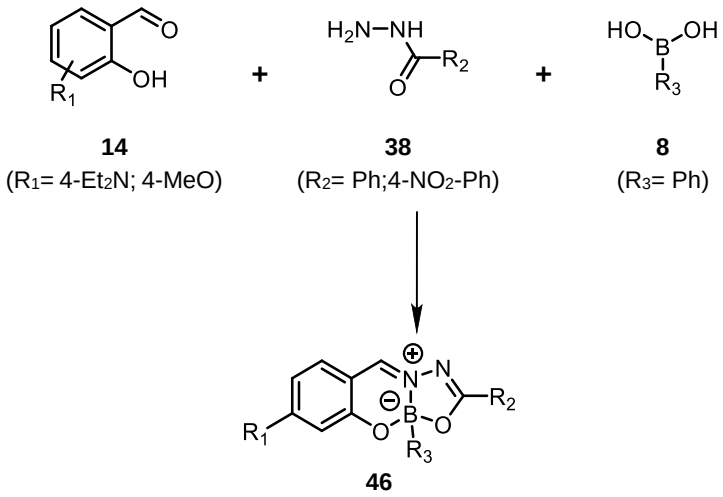

14 (R_1= 4-Et_2N; 4-MeO) **38** (R_2= Ph;4-NO_2-Ph) **8** (R_3= Ph)

46

Scheme 17 – Synthesis of fluorescent tetrahedral boron complexes **46.**

The multicomponent construction of hydrazonoboronates was also explored by Joule and co-workers in order to discover novel and promising bioactive scaffolds for pharmaceutical applications. B-complexes **48** were assembled between dehydroacetic acid **47**, hydrazide derivatives **38** and boric acid **8** in the presence of acetic anhydride (**Scheme 18**).[75] Hydrazonoboronates **50** were synthesized by condensation of *β*-keto acid **49**, hydrazide derivatives **38** and boronic acids **8** (**Scheme 19**).[76,77]

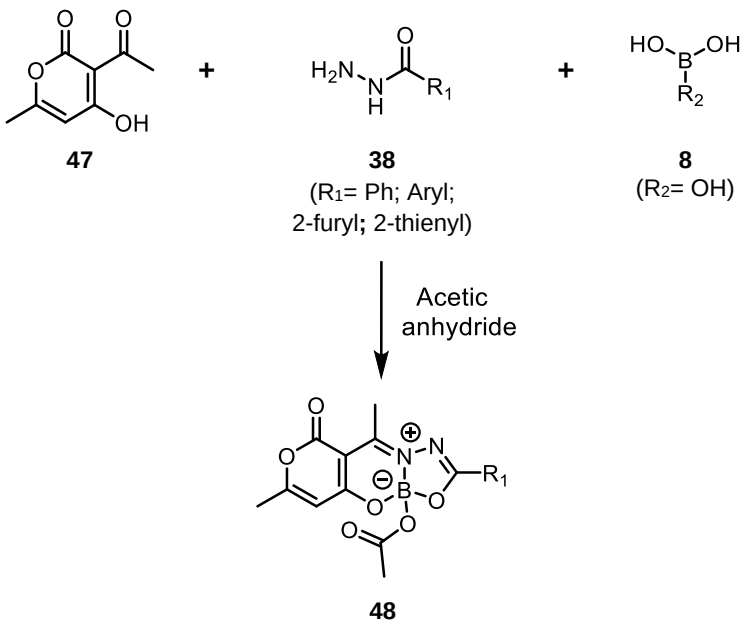

Scheme 18 – Three component construction of boron complexes **48.**

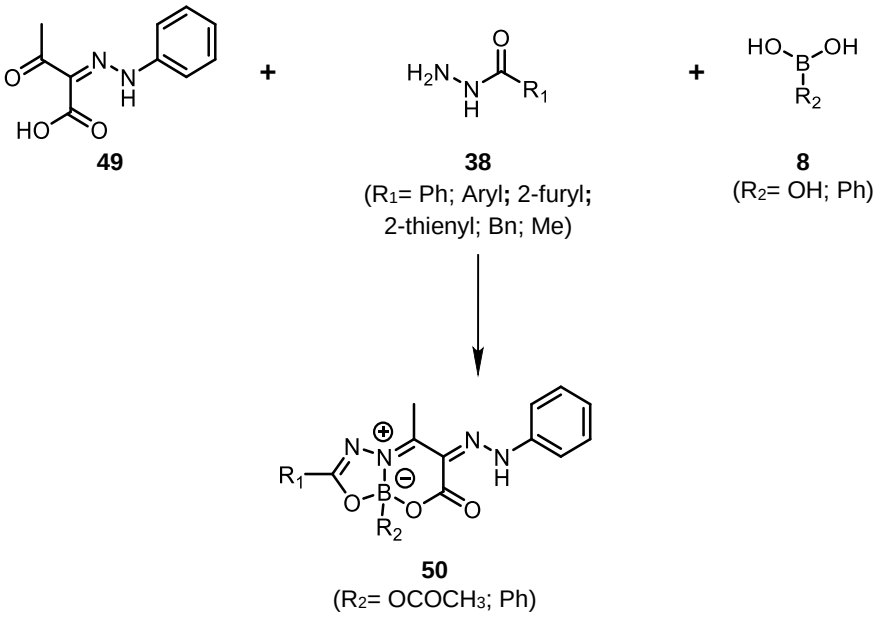

Scheme 19 – Tripodal assembly of hydrazonoboronates **50.**

The hydrazonoboronate framework was also reached *via* a four component reaction. Nielsen's research team prepared a diverse library of enantio- and diastereomerically dioxadiazaborocines **53** with multiple stereocenters (see selected examples in **Scheme 20**) from the condensation of hydrazides **51**, two different boronic acids **8** and **8'** (one acts as a nucleophile and the other one as an electrophile) and protected *α*-hydroxy aldehydes **52** (**Scheme 20**).[78]

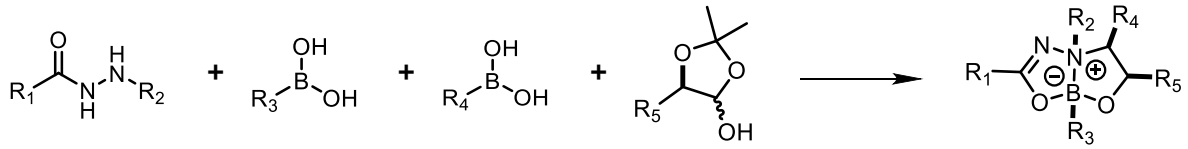

51 **8** **8'** **52** **53**

Selected examples of dioxadiazaborocines **53a-e:**

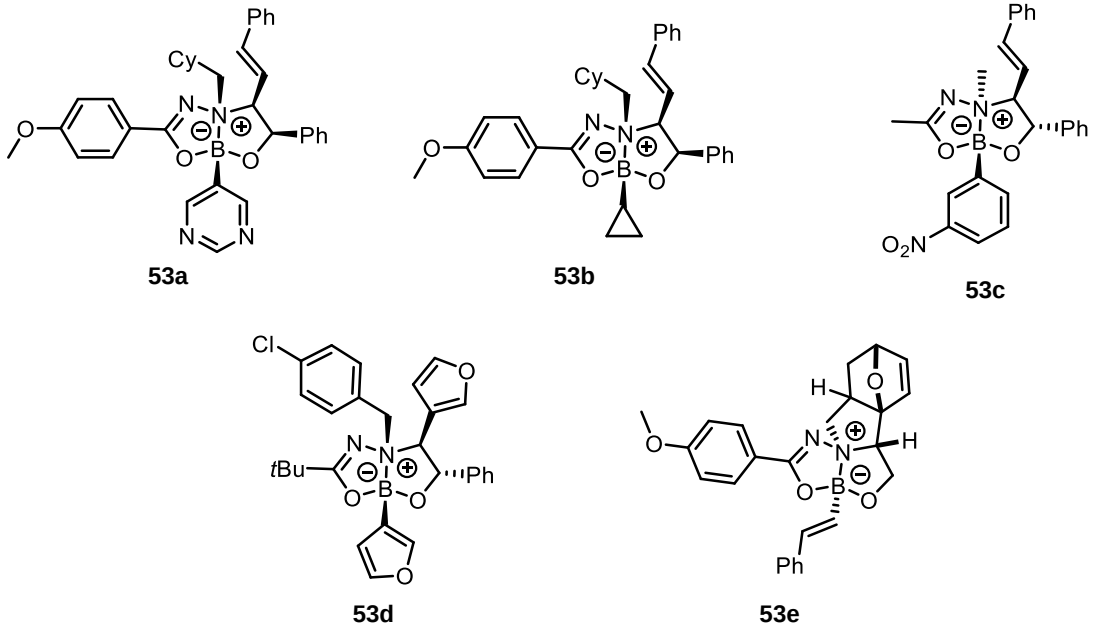

53a **53b** **53c** **53d** **53e**

Scheme 20 – Top: Four component construction of dioxadiazaborocines **53; Bottom:** Selected examples of **53a-e.**

It was concluded that the boronic acid moiety plays a key role in the modular assembly of a wide variety of reversible B-complexes, which have been very useful among different fields, such as drug-delivery, bioimaging, electronic, bioconjugation and medicinal chemistry. This modular technology was then explored in this work in the construction of multivalent and reversible iminoboronates for selective tumor therapy and for the development of a fluorophore platform (BASHY).

Chapter II

Multivalent and reversible iminoboronates for selective tumor therapy

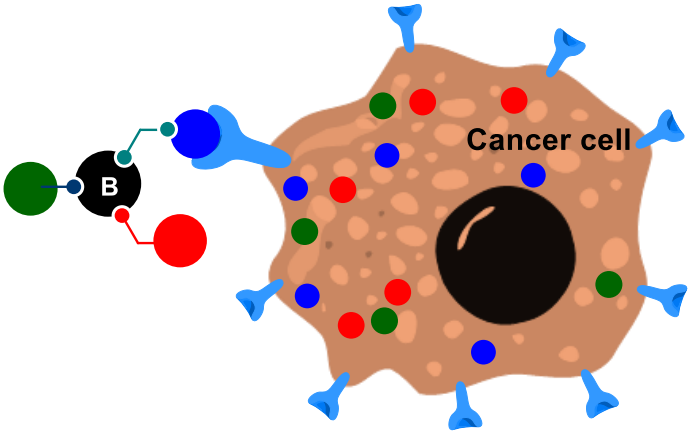

Abstract

Cancer cells emerge from healthy cells with unrepaired DNA mutations and this transformation is currently classified as a multifaceted and intricate biological process. Consequently, the most recent therapies to treat cancer aim at interrupting one or more of these stages by the use of selective multivalent conjugates.

In this chapter is described a new modular platform for the construction of cancer-cell-targeting drug conjugates based on tripodal B-complexes featuring reversible covalent bonds to accommodate a cytotoxic drug (**Btz**), PEG chains, and folate targeting units.

The B-complex core was assembled in a single step, proved to be stable under biocompatible conditions, namely, in human plasma (half-life up to 60 h), and underwent disassembly in the presence of GSH. Stimulus-responsive intracellular payload delivery was confirmed by confocal fluorescence microscopy, and a mechanism for GSH-induced B-complex hydrolysis was proposed on the basis of mass spectrometry and density functional theory (DFT) calculations. This novel technology enabled the modular construction of multivalent boronate SMDCs **63** and **67** with high selectivity for folate-positive MDA-MB-231 cancer cells and IC_{50} values in the low nanomolar range.

A grateful acknowledgement to all collaborators involved in this chapter:

Ana I. Matos (Cytotoxicity assays and bioimaging)

Ana E. Ventura (Bioimaging)

Luís F. Veiros (DFT calculations)

II.1 Rationale and Goals

Cancer is nowadays the second leading cause of death globally and its occurrence is expected to rise 70 % in the next 2 decades. Tumor cells emerge from healthy cells with unrepaired DNA mutations and this transformation is currently classified as a multifaceted biological process, in which healthy cells acquire the capability of sustaining proliferative signaling, resisting cell death, evading growth suppressors, inducing angiogenesis, enabling replicative immortality, activating invasion, and metastasis.[79,80]

Consequently, the most recent therapies to treat cancer aim at interrupting one or more of these stages by the use of multivalent conjugates, in which the biological activity of the building blocks is preserved and tuned depending on the construct structure. Despite conceptual simplicity, the construction of multifunctional conjugates is often hampered by the complexity of the synthetic methodology.[81–87]

Targeting drug conjugates (TDC), such as antibody or small-molecule drug conjugates (ADCs and SMDCs, respectively), are multivalent conjugates that combine, *via* a linker, the lethality of potent cytotoxic drugs with the targeting skills of specific biomolecules with a high affinity for overexpressed receptors located in cancer cells.[88–90]

The linker technology used in TDCs, contributes decisively to the therapeutic potential of these constructs, since it enables the functionalization of the targeting biomolecule without altering its pharmacokinetic profile; confers stability to the conjugate in circulation; and promotes the release of the active drug only upon reaching the desired target.

Given these requirements, the construction of these linkers often involves the insertion of reactive handles to selectively attach the therapeutic cargo and the targeting unit; moieties that may regulate the construct physicochemical properties (*e.g.* PEG chains); cleavable units that modulate the stimulus-responsive (*e.g.* enzymes, pH, GSH) release of the therapeutic cargo at the target.

Therefore, linkers often exhibit structures with a high functional density, and their preparation involves a series of complex and costly synthetic steps that are unsuitable for straightforward structural diversification (*e.g.* Vintafolide depicted in **Figure 9**). [84,86,87,91–93]

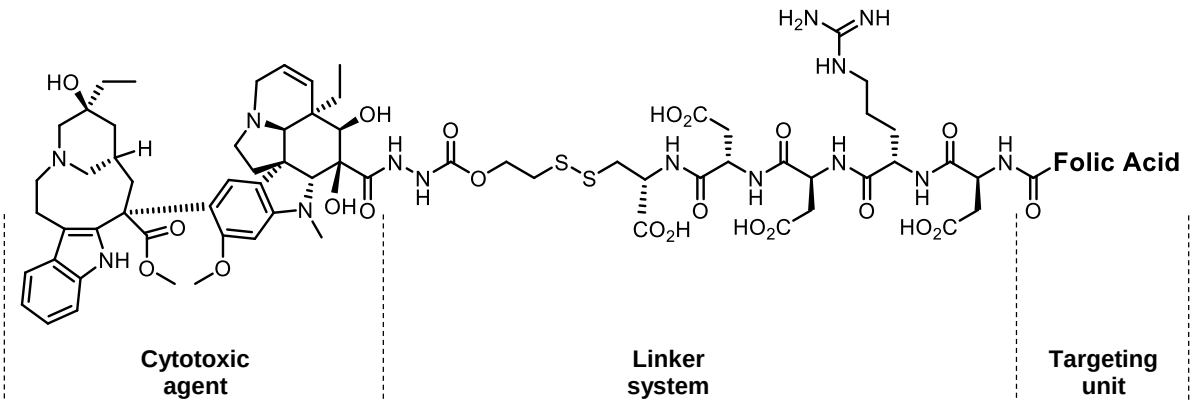

Figure 9 – Structure of SMDC Vintafolide.

Consequently, the synthesis of composite multivalent constructs that enable the tuning of the conjugate properties by direct modification of the building blocks individual properties is highly desirable for the discovery of novel TDCs with therapeutic potential. Boronic acids, as previously described, readily form reversible covalent bonds with Schiff base ligands to yield B-complexes featuring a reversible and modular tripodal framework. With this idea in mind, it was envisioned that if B-complexes displayed suitable stability and controlled reversibility in biological conditions, they could be used as a novel platform for the design of multivalent conjugates to selectively target and deliver a therapeutic payload to cancer cells (**Scheme 21**).

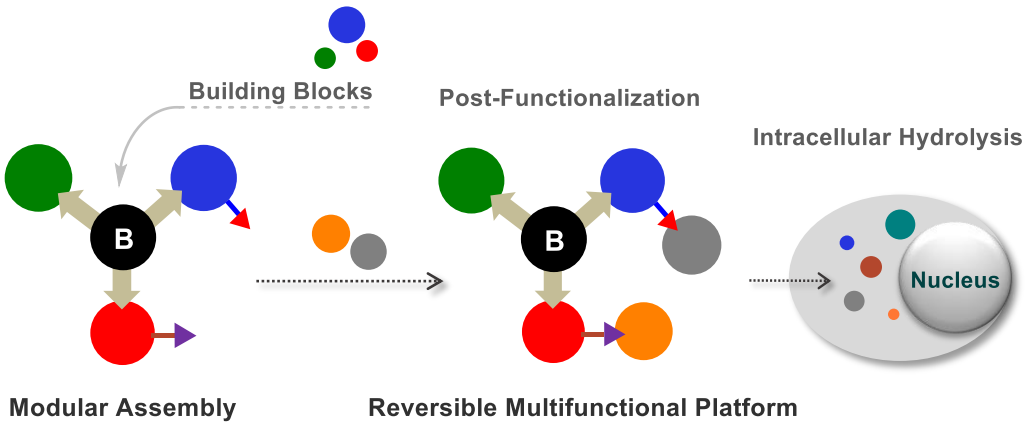

Scheme 21 – Modular assembly of reversible multifunctional TDCs promoted by boron and their intracellular hydrolysis in target cells.

II.2 Results and Discussion

II.2.1 Synthesis and stability evaluation of core iminoboronates

In order to prove the feasibility of this novel platform for the construction of multivalent TDCs, several core B-complexes were prepared from a three-component one-pot reaction, in which salicylaldehyde **14** and phenylboronic acid **8** were treated with amino acid **26**, anthranilic acid **55**, or 2-aminophenol **56** in equimolar amounts. This simple protocol allowed the straightforward synthesis of the corresponding B-complexes **27a**; **57** and **58a** in yields up to 90 % (**Scheme 22**; see also **section IV.1.1**).

The stability of constructs **27a, 57** and **58a** at physiological pH 7.4 was then evaluated by high-performance liquid chromatography (HPLC), following the disappearing of B-complexes over time. Each hydrolysis process followed pseudo first-order kinetic, and the pseudo first-order rate constant (k_{obs}) was determined from the slopes of ln (concentration) vs time plots (**Equation 1** see also **section IV.1.2**). Then, the k_{obs} obtained was used to calculate the half-life ($t_{1/2}$), as indicated in the **Equation 2**.

$$\textbf{Equation 1: } \mathbf{Ln}\,[\,] = -\boldsymbol{k}_{\mathbf{obs}} \times \mathbf{time} + [\,]_{\mathbf{0}};$$

$$\textbf{Equation 2: } \mathbf{t_{1/2}} = \frac{\mathbf{Ln}\,(2)}{\boldsymbol{k}_{\mathbf{obs}}}$$

B-complexes **27a, 57** and **58a** displayed, at pH 7.4, half-lives lower than 2 h (**Scheme 22**; see also **section IV.1.2**). The poor stability observed for these molecules could be explained by the fast addition of water to the electrophilic imine carbon atom, which promoted a rapid hydrolysis of these constructs.[52] To reduce this reactivity, analogous B-complexes **27b** and **58b** from salicylketone **54** were synthesized (**Scheme 22**; see also **section IV.1.1)**. These transformations proved to be slightly more challenging, and despite many attempts, the B-complex from the condensation of salicylketone **54**, anthranilic acid **55** and phenylboronic acid **8** was never formed.

The stability of these constructs **27b** and **58b** at pH 7.4 was then evaluated as aforementioned and the presence of a methyl substituent on the imine carbon atom of these B-complexes considerably improved their stability under these conditions. Both B-complexes displayed half-lives higher than 30 h, but due to the low yield (γ = 10 %) obtained in the preparation of B-complex **27b**, it was decided to move forward with the stability evaluation only with construct **58b** (**Scheme 22**; see also **section IV.1.2**).

B-complex **58b** maintained the same robustness at pH 7.4 ($t_{1/2}$ = 39.8 h) in other biomimetic conditions, such as at lysosomal pH 4.8 ($t_{1/2}$ = 38 h) and in human plasma ($t_{1/2}$ = 39.6 h) (**Scheme 22**; see also **section IV.1.2**).

After stability evaluation of these B-complexes under different biological conditions, the stimulus-responsive hydrolysis of **58b** in the presence of GSH was then evaluated. Cancer cells typically exhibit an increased concentration (millimolar range) of GSH in the cytoplasm, and for that reason, GSH has been extensively targeted to promote dissociation of therapeutic conjugates upon internalization.[94]

B-complex **58b** was then incubated at pH 7.4 in the presence of GSH (10 equiv.) and, as expected, the presence of GSH compromised the structural integrity of this construct, since its half-life decreased 7 h under these conditions (**Scheme 22**; see also **section IV.1.2**). The hydrolysis mechanism will be further discussed in section **II.2.4**.

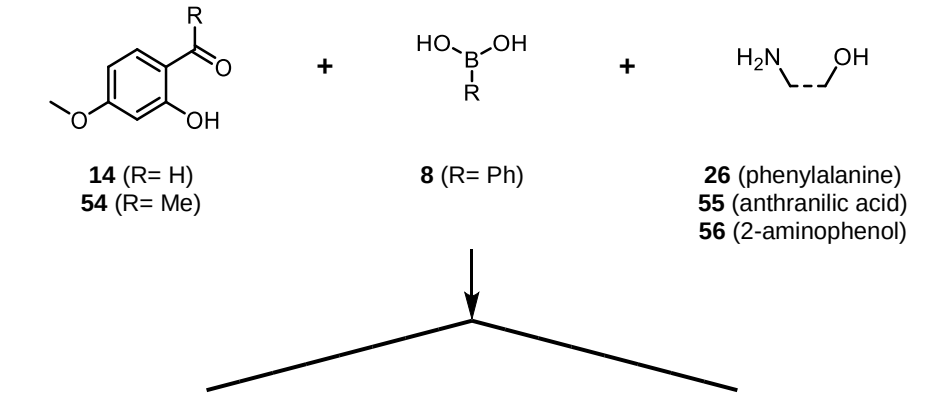

14 (R= H)
54 (R= Me)

8 (R= Ph)

26 (phenylalanine)
55 (anthranilic acid)
56 (2-aminophenol)

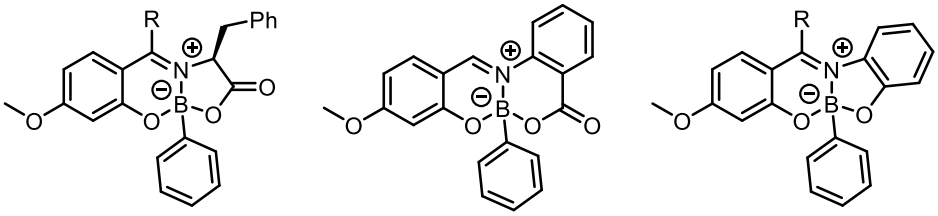

27a
(R = H); γ = 87 %;
$t_{1/2}$ (pH 7.4) = 1.7 h

27b
(R = Me); γ = 10 %;
$t_{1/2}$ (pH 7.4) = 32.2 h

57
γ = 90 %;
$t_{1/2}$ (pH 7.4) = 31.4 min

58a
(R = H); γ = 90 %;
$t_{1/2}$ (pH 7.4) = 17.6 min)

58b
(R = Me); γ = 85 %;
$t_{1/2}$ (pH 7.4) = 39.8 h;
$t_{1/2}$ (pH 4.8) = 38 h;
$t_{1/2}$ (human plasma)= 39.6 h;
$t_{1/2}$ (pH 7.4; GSH)= 32.8 h

Scheme 22 – One-pot synthesis of B-complexes (**27a,b**, **57** and **58a,b**) and evaluation of their stability at pH 7.4 (all complexes), at pH 4.8, and in human plasma (B-complex **58b**).

II.2.2 Construction and cytotoxic evaluation of multifunctional boronate SMDCs

After evaluation of B-complex **58b** stability and the controlled reversibility of its formation, we selected aminophenol and salicylketone moieties as the model components for the assemblage of a multivalent SMDC featuring a cytotoxic drug, a small hydrophilic PEG chain and a targeting unit.

Btz was chosen as the cytotoxic component, since it has a boronic acid moiety, which is essential for the generation of the B-complex, and also because **Btz** would benefit from an improved selectivity to cancer cells promoted by the B-complex.

The targeting unit chosen to direct the boronate SMDCs to cancer cells was folic acid, which is an essential vitamin for cell functioning and is commonly used as a targeting moiety, since due to their fast cell division and growth, many cancer cell lines overexpress receptors that recognize this molecule.[95–97]

Folic acid is composed by a glutamic acid residue linked to a pteroic acid moiety and in 2014 the alpha folate receptor (α-FR) was isolated and crystallized providing a key information on the interaction between the receptor and folates. Pterin moiety docks to the receptor pocket, being stabilized by numerous hydrogen bridges and hydrophobic interactions. Glutamate residue is stabilized by six hydrogen bonds, four of them in the α-carboxylic acid. These observations clearly show that the modification of the γ-carboxylic acid of folic acid is more promising than α modification, since it should retain most of the affinity toward the FR receptor. Based on this information, the folate-cyclooctyne **61** was prepared by the insertion of a cyclooctyne moiety in the γ-carboxylic acid (**Scheme 23)**.[98]

Construction of the remaining components of the boronate SMDC was done by following reported methodologies, in which the hydroxyacetophenone moiety was modified to incorporate a small PEG chain (**59a**) and the aminophenol component was modified with an azide function (**60**) for post-functionalization with folate-cyclooctyne **61** (**Scheme 23,** see also **section IV.1.1**).

The assembly reaction was attempted with the components **Btz**, **59a**, and **60**, but the desired B-complex was never formed. It was hypothesized that this lack of reactivity might be due to a combination of steric constraints imposed by the **Btz** structure and the PEG chain in *para* position on **59a** (see DFT calculations in **section IV.1.6**).

Building blocks

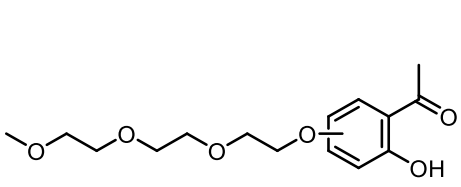

59a (4'-PEG chain)
59b (5'-PEG chain)

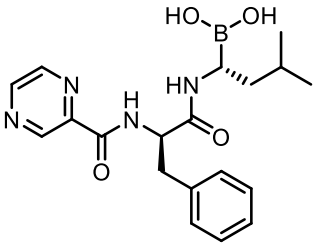

Btz

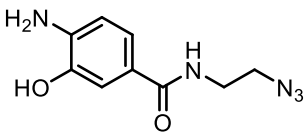

60

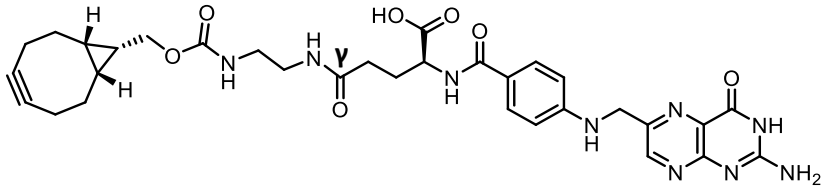

61

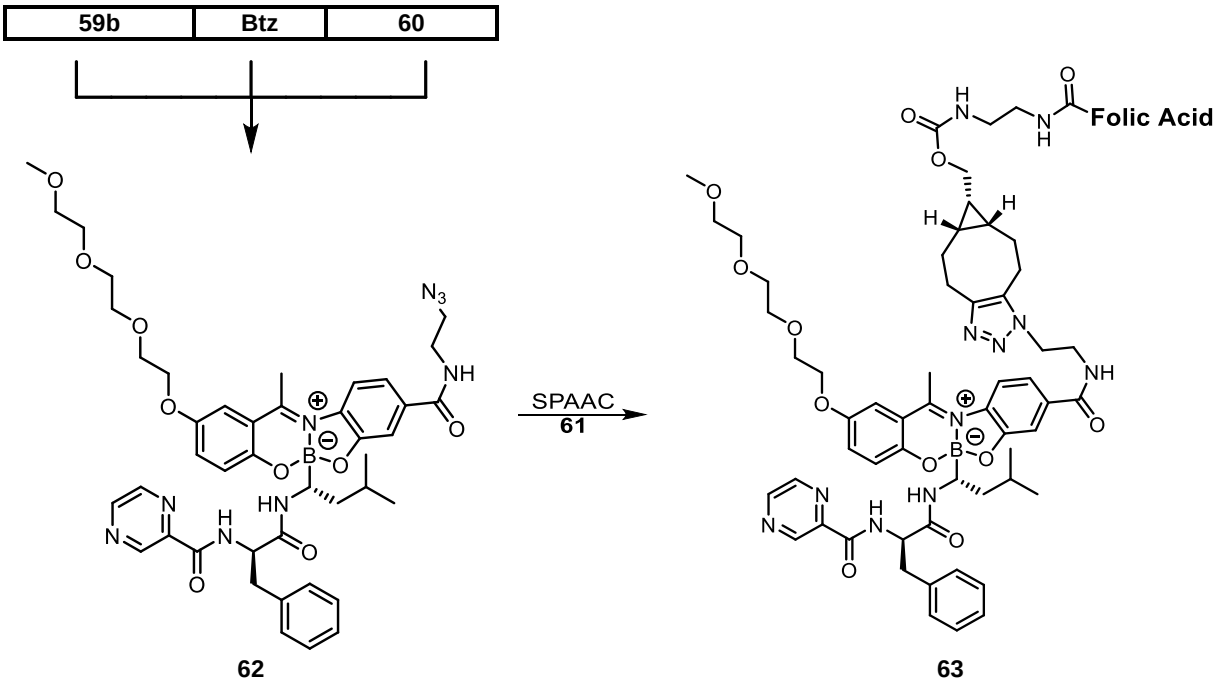

62 **63**

Scheme 23 – Top: Building blocks (**Btz**, **59a,b**; **60** and **61**);
Bottom: Assembly of B-complex **62** (CH_3CN, 75 ºC, 18 h, 25 %) and subsequent folate functionalization by SPAAC (DMSO, 25 ºC, 17 h, 85 %) to yield boronate SMDC **63**.

In order to solve this problem, 5-substituted salicylketone **59b** was prepared and incubated with **60** and **Btz** in acetonitrile (75 ºC; 18 h). Pleasingly, these building blocks readily afforded B-complex **62**, which was isolated in 25 % yield. Then, the installation of the targeting unit was achieved *via* a strain-promoted alkyne–azide cycloaddition (SPAAC) with folate-cyclooctyne **61**. The reaction proceeded smoothly in dimethyl sulfoxide (25 ºC; 17 h) and boronate SMDC **63** was afforded in 85 % yield (**Scheme 23**; see also **section IV.1.1**).

Inspired by the design of ADCs, in which the antibody (Ab) moiety features bivalent fragments for antigen-binding (Fab) regions that are responsible for the high specificity and affinity of the Ab for a particular epitope,[99] we envisioned that the B-complex could also be modified with a bivalent folate-recognition moiety.[84,100–102] In order to achieve that, salicylketone and aminophenol moieties needed to be modified with small PEG chains and azide groups.

With this idea in mind, salicylketone-azide **64** and aminophenol-azide **65** were readily prepared and incubated with **Btz** in acetonitrile, 75 ºC, 18 h in order to assemble B-complex **66**, which was isolated in 8 % yield. The post-functionalization of **66** with the folate–cyclooctyne **61** was done in DMSO, 25 ºC, 17 h, affording difolic SMDC **67** in 99 % yield (**Scheme 24**; see also **section IV.1.1**).

Cytotoxicity evaluation of boronate SMDCs **63** and **67** was then performed against MDA-MB-231 human breast cell line (overexpression of FRs) and 4T1 mouse breast carcinoma cell line (low expression of FRs), using a 3-(4,5-dimethylthiazol-2-yl)-5-(3--carboxymethoxyphenyl)-2-(4-sulfophenyl)-2H-tetrazolium (MTS) cell-proliferation assay (see **section IV.1.3**).

This study was initiated with the cytotoxic evaluation of the free drug **Btz** in MDA-MB-231 cancer cells, which was shown to be quite cytotoxic (IC_{50}: 14.2 nM). In the same conditions non-folate B-complexes **62** and **66** revealed to be inactive up to a concentration of 100 nM, whereas monofolate SMDC **63** and difolate SMDC **67**, exhibited improved potency in the same nanomolar range (IC_{50} (**63**): 67.5 nM and IC_{50} (**67**): 62 nM). It was also observed that folate-cyclooctyne **61** was non cytotoxic against MDA-MB-231 cancer cells, therefore the observed activity of boronate SMDCs **63** and **67** clearly points out that folic acid mediates the internalization of these SMDCs into the cancer cells, where after disassembly, the therapeutic cargo **Btz** is released (**Chart 1**).

In order to evaluate the selectivity induced by the presence of the folic acid targeting unit, we tested boronate SMDCs **63** and **67** against a 4T1 mouse breast carcinoma cell line, which exhibits a low expression of FRs. Unlike the free drug **Btz**, which proved to be highly cytotoxic against this cell line (IC_{50}: 22.8 nM), neither SMDCs **63** and **67** perturbed the viability of these cancer cells up to a concentration of 100 nM (see **section IV.1.3**). The two constructs **63** and **67** were only cytotoxic at micromolar range (1 – 100 µM; **Chart 2**).

These data indicates that boronate SMDCs **63** and **67** are somewhat less potent than free **Btz**, however they exhibited improved selectivity towards FR-overexpressing cancer cell lines.

Building blocks

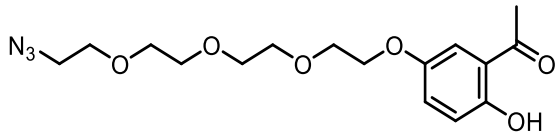

64

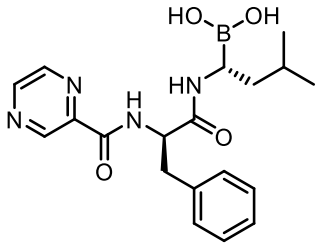

Btz

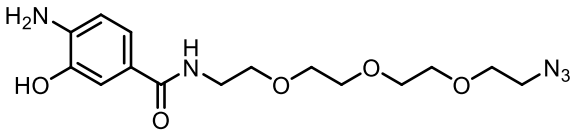

65

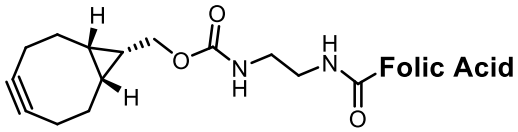

61

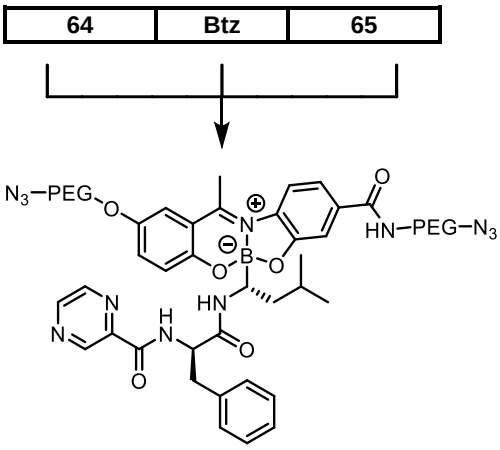

66

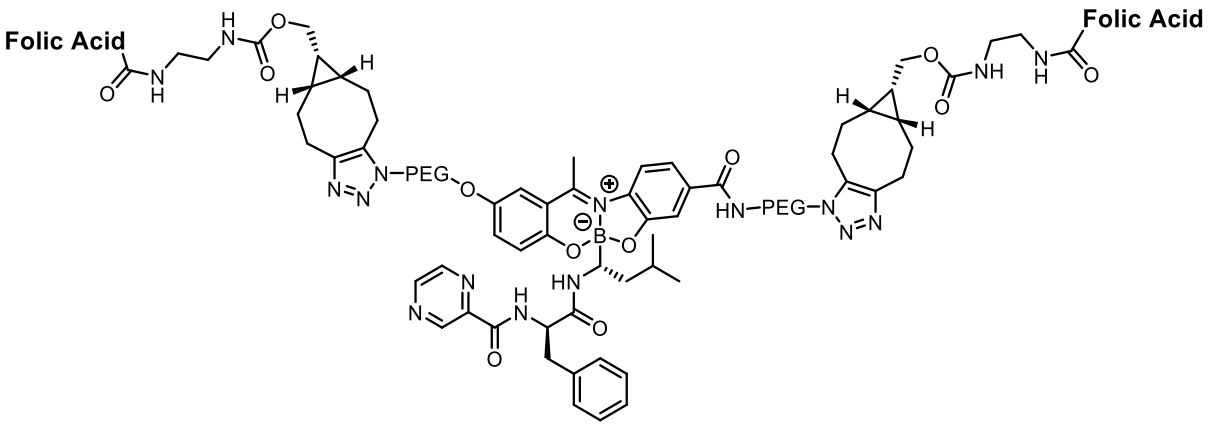

67

Scheme 24 – Top: Building blocks (**Btz**, **61**, **64** and **65**);
Bottom: Construction of B-complex **66** (CH_3CN, 75 ºC, 18 h, 8 %) and folate functionalization by SPAAC (DMSO, 25 ºC, 17 h, 99 %) to yield difolate SMDC **67**.

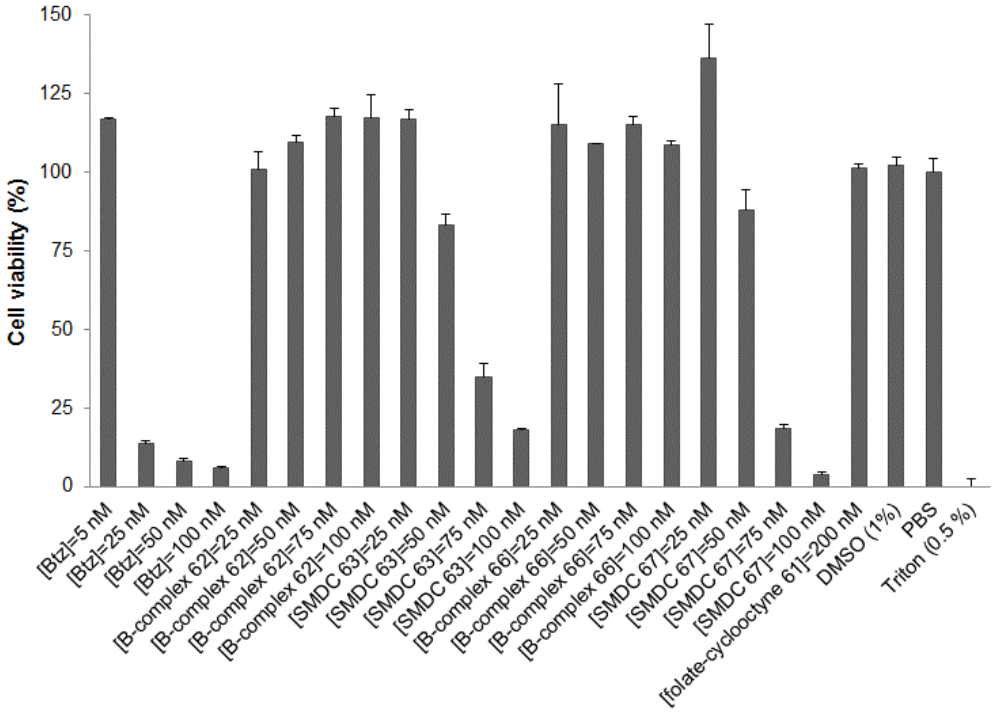

Chart 1 – Cell viability determined by MTS assay 48 h after incubation of MDA-MB-231 (ATCC® HTB-26™) with **Btz** (5-100 nM); B-complexes **62** and **66** (25-100 nM); SMDCs **63** and **67** (25-100 nM) and folate-cyclooctyne **61** (200 nM). Mean ± standard deviation (SD); n=3. Phosphate-buffered saline (PBS) and Triton X-100 were used as controls

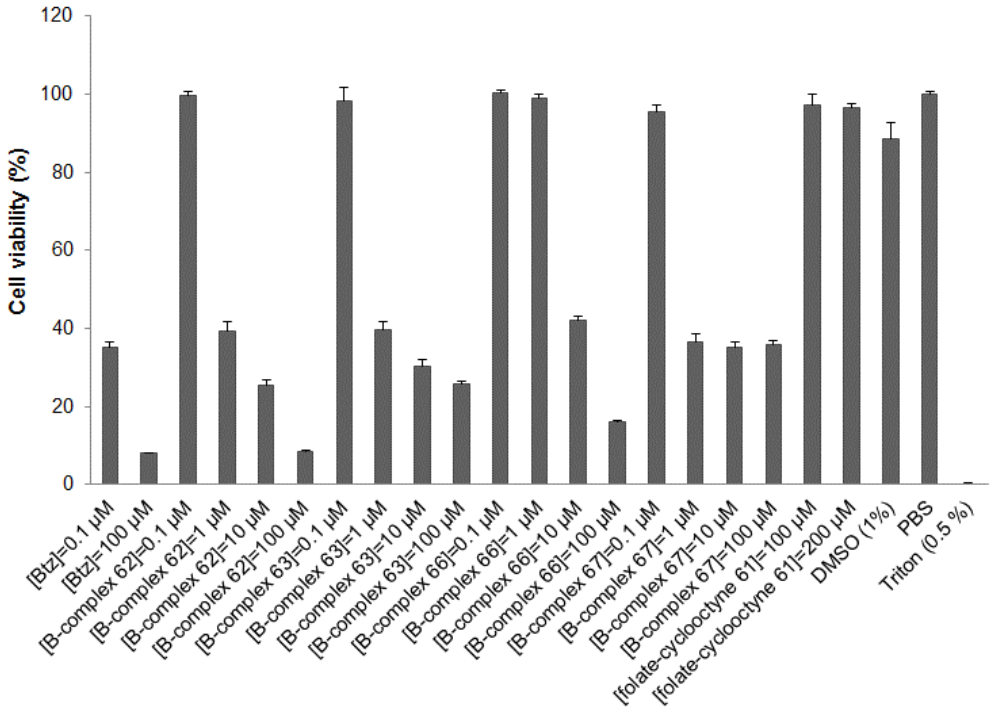

Chart 2 – Cell viability determined by MTS assay 48 h after incubation of 4T1 (ATCC® CRL-2539™) with **Btz** (0.1, 100 µM); B-complexes **62** and **66** (0.1 – 100 µM); SMDCs **63** and **67** (0.1 – 100 µM) and folate-cyclooctyne **61** (100 – 200 µM). Mean ± standard deviation (SD); n=3. Phosphate-buffered saline (PBS) and Triton X-100 were used as control

II.2.3 Internalization and cargo release from boronate SMDC

Having established the potential of this modular approach for an effective targeted delivery of **Btz**, we decided to evaluate the drug-delivery mechanism. For this purpose, and based on the previous synthetic methodologies, a folate-conjugate **68** featuring a non-fluorescent boronate-coumarin was prepared. Compound **68** was designed to signal the hydrolysis of the boronic acid derivative **69** through its oxidation to phenol **70**, since it is well-established that boronic acids readily undergo oxidative boronate cleavage in the presence of intracellular reactive oxygen species (ROS), namely, at the cytoplasm of cancer cells.[103,104] Further oxidation of phenol **70** will generate a quinone methide and the fluorescent coumarin probe **71** (**Scheme 25**, see also **section IV.1.1**).

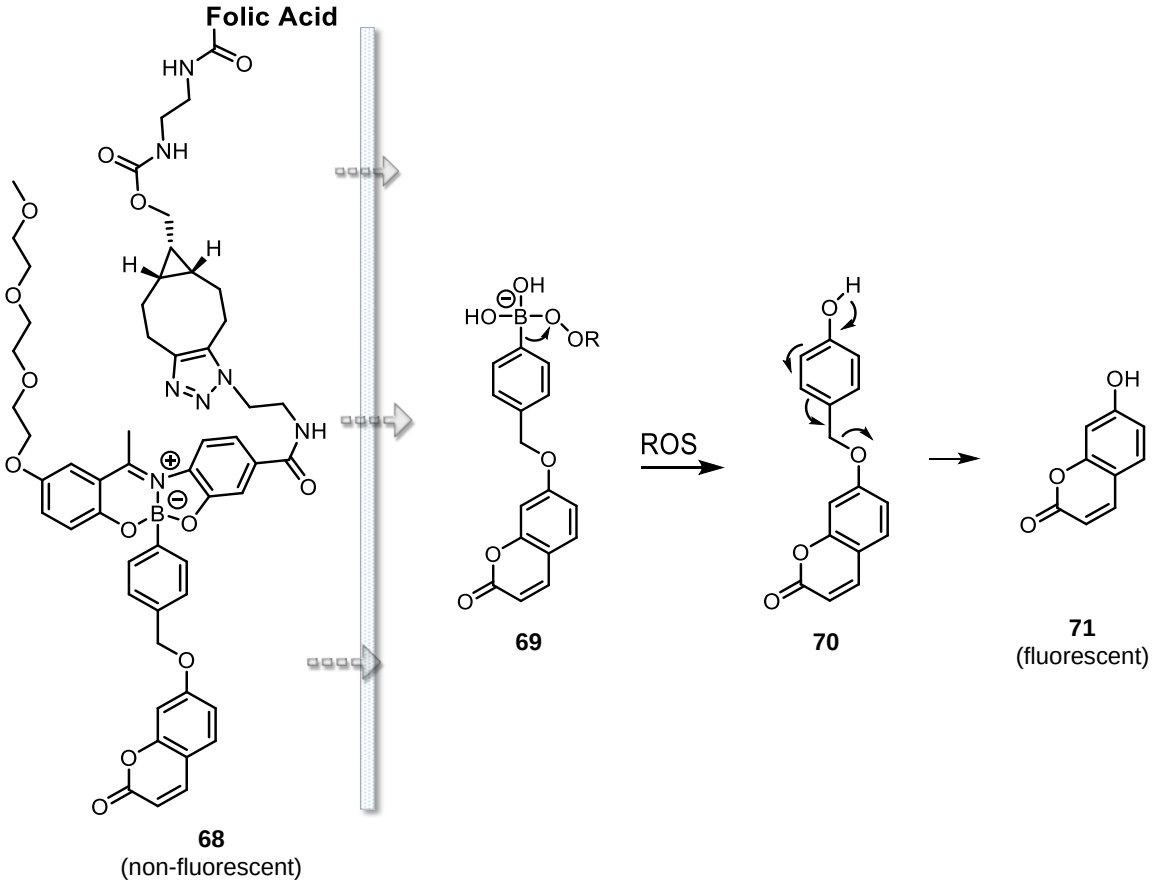

Scheme 25 – Intracellular hydrolysis of conjugate **68** mediated by ROS species in order to release and generate a fluorescent coumarin **71**.

To test this hypothesis, conjugate **68** (1 mM) was incubated in MDA-MB-231 and 4T1 cells at 10, 30, and 180 min. Images obtained by confocal microscopy clearly showed that the fluorescent coumarin probe **71** was only distributed throughout the cell cytoplasm of MDA-MB-231 cancer cells. This data confirmed the successful entry of conjugate **68** into the cells as well as the hydrolysis of the boronic acid component at the first time point recorded (10 min). An analogous internalization pattern was not observed in the incubation of **68** in 4T1 cancer cells (**Figure 10)**. The statistical analysis also corroborates the observation that the fluorescent coumarin **71** was only observed inside the FR^+ cancer cell line MDA-MB-231 (**Chart 3** and **4**, see also **section IV.1.4**).

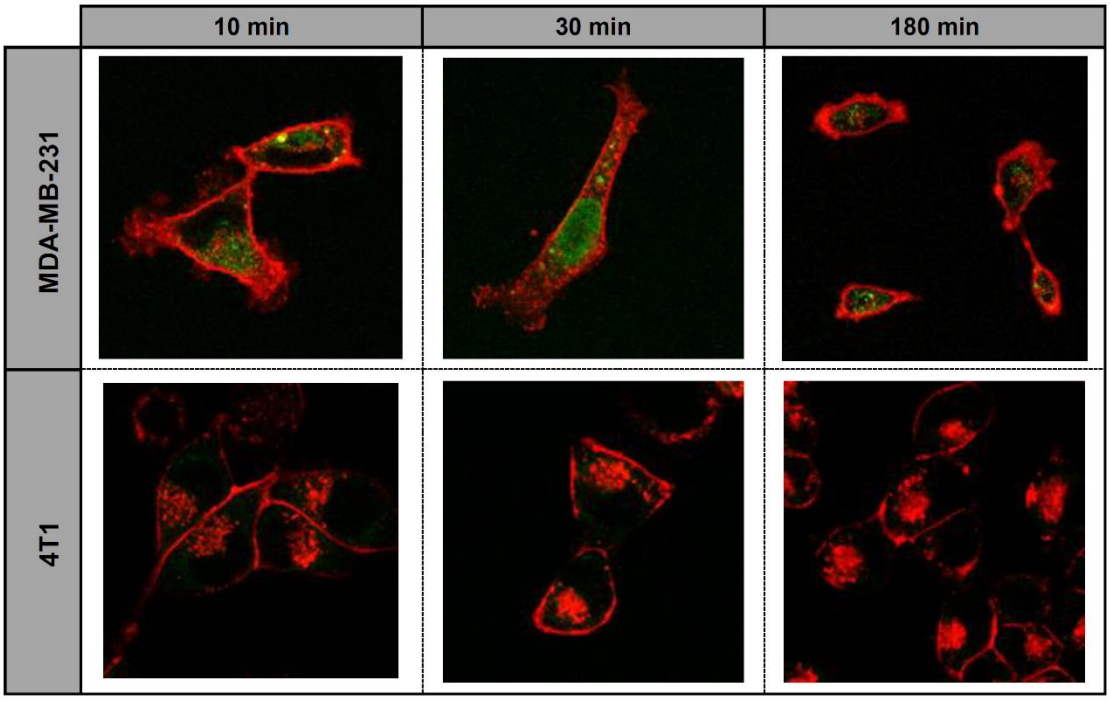

Figure 10 – Confocal fluorescence microscopy analysis at different times of MDA-MB-231 and 4T1 cancer cell lines incubated with B-complex **68**. The plasma membrane was labeled with WGA-Alexa Fluor 594 (red) and coumarin **71** is green.

In order to prove that the internalization of conjugate **68** in MDA-MB-231 cells was mediated by the folic acid moiety, B-complex **68'**, which is the non-folate version of conjugate **68** (see **section IV.1.1**), was also incubated with this cancer cell line in the same conditions. Results obtained from statistical analysis revealed that the fluorescent coumarin **71** was not present in the cytoplasm of MDA-MB-231 cell line, therefore we can conclude that the folic acid has an instrumental role in the internalization of conjugate **68** (**Chart 3**, see also **section IV.1.4**).

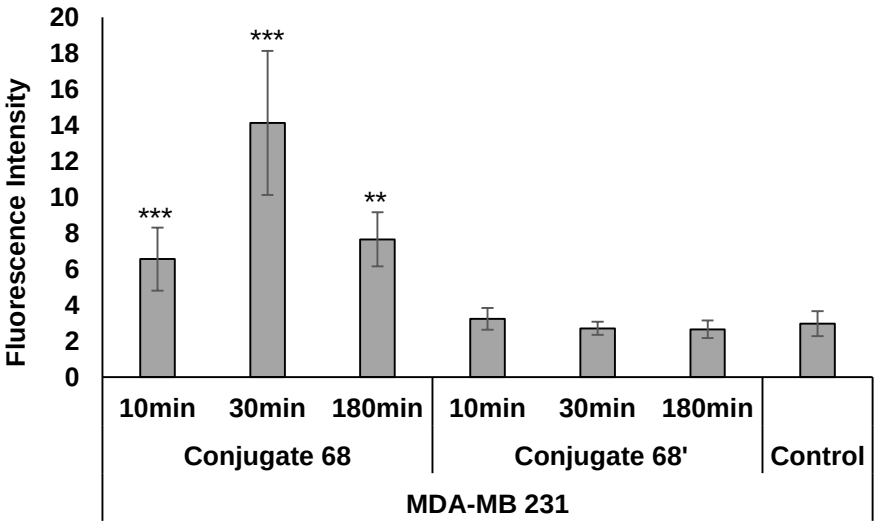

Chart 3 – Fluorescence intensities obtained after incubation of folate-conjugate **68** and non-folate **68'** in MDA-MB-231 cancer cell lines at 10, 30 and 180 min. Statistical significance was determined by a t-test and significant differences were only observed in the incubation of conjugate **68** in this cell line, **p*<0.01; ***p*<0.001; ****p*<0.0001 versus control (cellular autofluorescence).

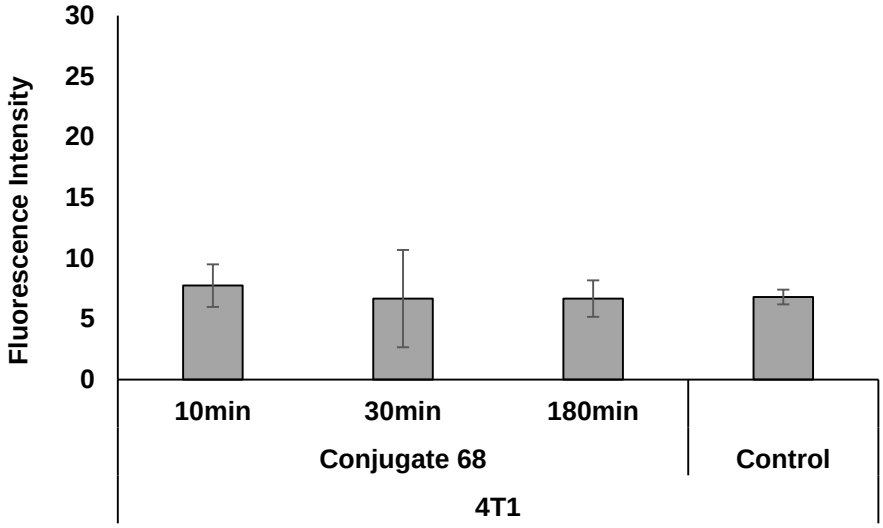

Chart 4 – Fluorescence intensities obtained after incubation of conjugate **68** in 4T1 cancer cell lines at 10, 30 and 180 min. Statistical significance was determined by a t-test and no significant differences versus control (cellular autofluorescence) were observed in the incubation of conjugate **68** in this cell line.

II.2.4 Hydrolysis mechanism of iminoboronate core by GSH

After establishing that the boronic acid cargo was released inside the cancer cells, it was decided to evaluate GSH as a promoter of B-complex hydrolysis. With this idea in mind, B-complex **72**, featuring **Btz**, was prepared (**Scheme 26,** see also **section IV.1.1**) and evaluated in human plasma. This B-complex proved to be more stable than analogue **58b** constructed with phenylboronic acid, and exhibited a half-life of 60 h under these conditions (see **section IV.1.2**).

Afterwards, B-complex **72** was incubated with 10 equivalents of GSH in ammonium acetate solution (pH 7.4) at 37 ºC, and the reaction was examined by electrospray ionization mass spectrometry (ESI-MS) over 72 h. Analysis of the reaction mixture immediately points out to an adduct combining the masses of **72** and GSH (m/z 913). It was also observed in the course of the assay, the formation of other m/z signals (367, 489, and 258), which were assigned to **Btz**, **74** and **75**, respectively (**Scheme 26**, **Figure 11,** see also **section IV.1.5**).

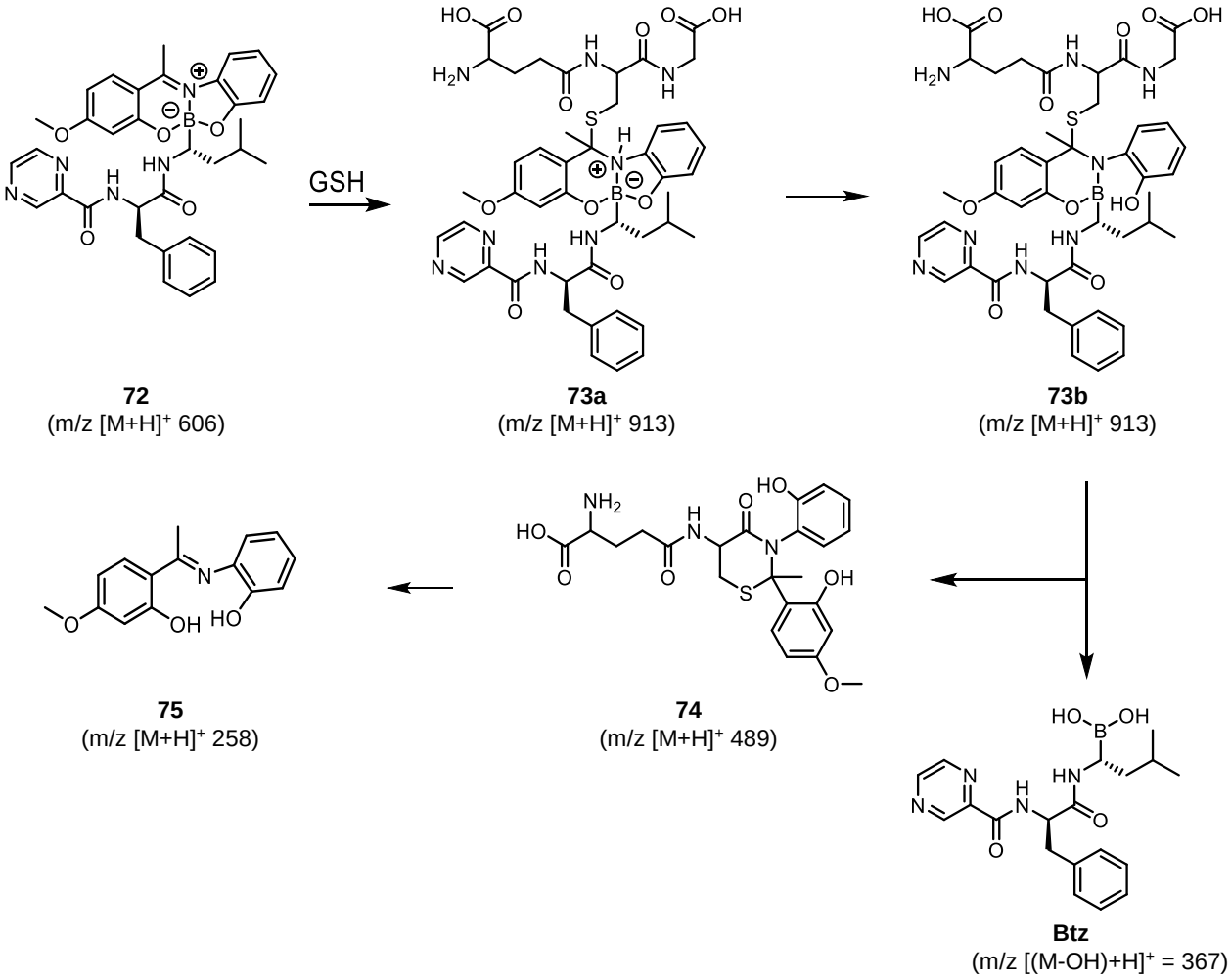

Scheme 26 – B-complex **72** disassembly promoted by GSH. See below **Figure 11**.

The compilation and analysis of these data, allowed us to propose a hydrolysis mechanism of the B-complex, in which the boronated payload is released after the addition of the GSH thiol group to the electrophilic imine carbon center of compound **72** to form intermediate **73a** (m/z 913). DFT calculations performed on a simplified model[105] suggest that thiol addition destabilizes the B-complex structure by increasing the electronic density on the boron atom, thus weakening the B-O bond to the aminophenol component (**Scheme 26**, **Figure 11**, see also **sections IV.1.5** and **IV.1.6**).

This process promotes the opening of the five membered ring, giving rise to intermediate **73b**, in which **Btz** (m/z 367) is more solvent-exposed and consequently more susceptible to release. Intermediary **73b** proved to be the less stable structure along the path, 15 kcal.mol^{-1} above the reagents. The hydrolysis mechanism proposed is also supported by the presence of compound **74** (m/z 489), which is probably derived from intramolecular addition of the amino group to the GSH amide and the consequent release of a glycine residue. Further hydrolysis of **74** gives rise to schiff base **75**, which is also present in the reaction mixture (m/z 258). The free energy balance calculated for the entire process indicates a fairly exergonic reaction with ΔG = - 6 kcal.mol^{-1} (**Scheme 26**, **Figure 11**, see also **section IV.1.5**).

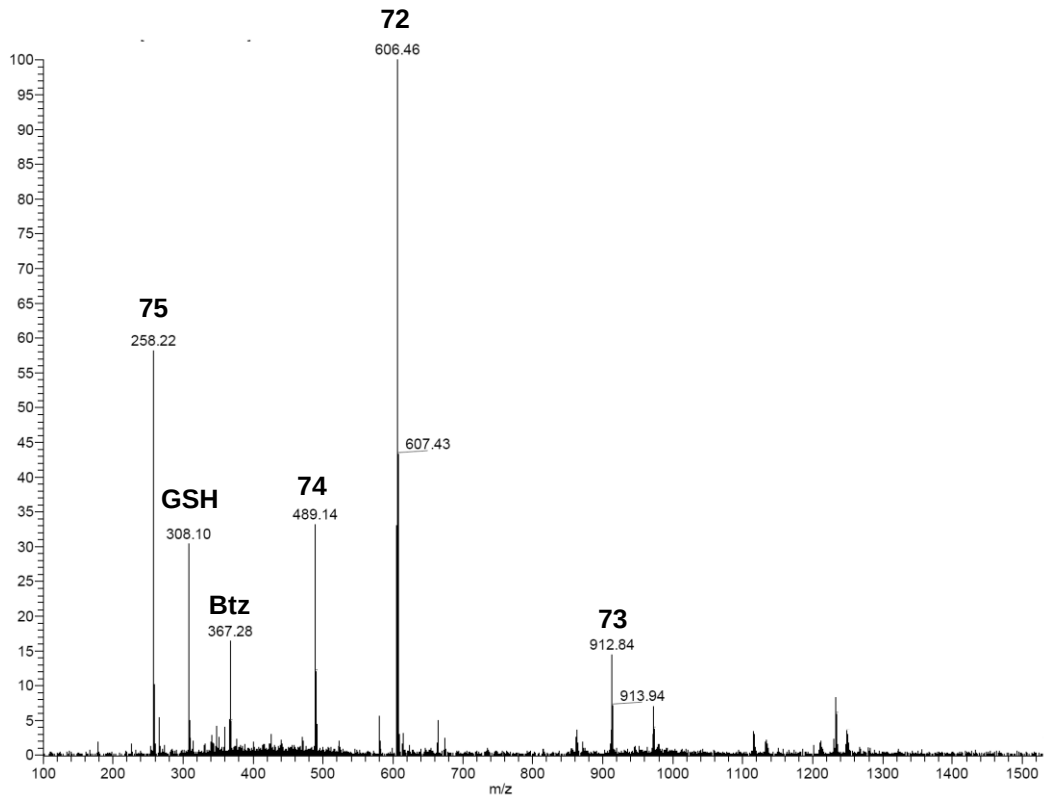

Figure 11 – ESI-MS analysis of B-complex **72** disassembly promoted by GSH, after 1 h of incubation.

II.3 Conclusions

Herein was presented a novel modular platform to construct cancer-cell-targeting drug conjugates, in which the boronic acid moiety promoted the assembly of functional building blocks featuring a cytotoxic drug (**Btz**), hydrophilic units (PEG chain), and azide handles for post-functionalization via click chemistry with a targeting unit (folic acid).

The multivalent boronate core was assembled in a single step (yields up to 25 %), and the azide moiety was effectively post-functionalized with folate targeting units *via* SPAAC reaction (yields up to 99 %). The boronate core was shown to be quite stable in human plasma (half-life up to 60 h), and hydrolyzed in the presence of GSH.

This modular architecture afforded boronate SMDCs **63** and **67** with high selectivity against FR^+ cancer cell line MDA-MB-231 and the IC_{50} values obtained were in the low nanomolar range.

The intracellular delivery of the cargo attached to the boronic acid component was confirmed by confocal fluorescence microscopy assay via the incubation of B-complex **68** with the MDA-MB-231 cell line**.** This B-complex was then hydrolyzed by ROS, giving rise to a fluorescent coumarin probe **71**.

Based on mass spectrometry assays and DFT calculations, a reaction mechanism for the GSH-induced hydrolysis of a model B-complex **72** was proposed, which involves the addition of the GSH thiol to the electrophilic imine carbon atom.

Considering the straightforward modularity and tunable reversibility of the boronated core, its stability in biomimetic conditions, its stimulus responsiveness, and the availability of cytotoxic drugs that may be readily borylated (*e.g.* SN38), this platform exhibits unique properties for the development of multivalent conjugates with therapeutic usefulness.

Chapter III

Modular Fluorophore Platform (BASHY)

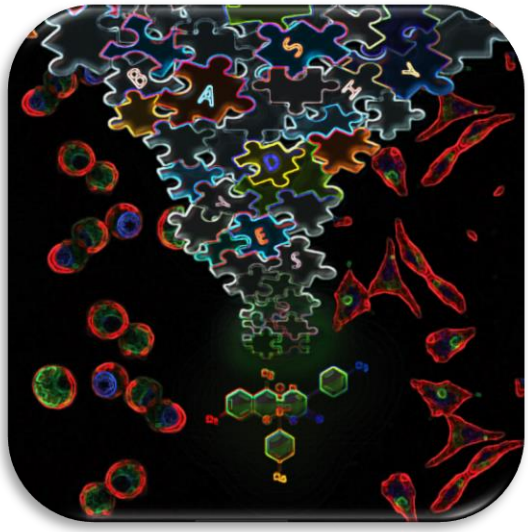

Abstract

The pursue for modular approaches that allow the construction of electronically tunable and responsive fluorophore platforms has become vital for the development of functional dyes for sensing, bioimaging and probing applications. Taking advantage of the multicomponent methodology addressed in **Chapter II**, herein is described the modular assembly of boronic acids with Schiff-base ligands in order to construct fluorescent dyes (BASHY) with suitable structural and photophysical properties for live cell bioimaging applications.

This modular approach enabled the straightforward synthesis (yields up to 99 %) of structurally diverse and photostable dyes, including ETCs, that exhibit a polarity-sensitive emission with high quantum yields of up to 0.68 in nonpolar media. BASHYs also displayed a high brightness (up to 121000 $M^{-1}.cm^{-1}$) and a two-photon--absorption behavior. The promising structural and fluorescence properties of BASHY promoted the preparation of non-cytotoxic and highly fluorescent NPs that were effectively internalized by BMDCs. BASHYs **81a,e** proved to selectively stain lipid droplets in HeLa cells, without any appreciable cytotoxicity. BASHY-azide **89** was used to label Annexin V and the fluorescent conjugate Annexin V-BASHY **92** revealed to be able to target and detect apoptotic cells maintaining high levels of specific activity.

A grateful acknowledgement to all collaborators involved in this chapter:

João N. Rosa (BASHY synthesis)

Joana Inês Carvalho (BASHY synthesis)

Jesús F. Arteaga (BASHY synthesis)

Cátia Parente Carvalho (Photophysical evaluation)

María M. Alcaide (BASHY synthesis and photophysical evaluation)

Vânia F. Pais (BASHY synthesis and photophysical evaluation)

Nuno R. Candeias (DFT calculations)

Francisco Boscá (Laser-flash photolysis characterization of BASHY)

Daniel Collado (Two-photon absorption measurements of BASHY)

Ezequiel Pérez-Inestrosa (Two-photon absorption measurements of BASHY)

Zoe Domínguez (BASHY energy-transfer cassette photophysical evaluation)

Ana I. Matos (BASHY-nanoparticles and cellular imaging)

Ana E. Ventura (BASHY-nanoparticles and cellular imaging)

Pedro M. S. D. Cal (Bioconjugation Annexin V-BASHY and Annexin V-FITC)

Ana Guerreiro (Cell viability assays of BASHY **89**)

Jean Bertolo (Structural analysis of Annexin V and bioconjugates)

Florian Sieglitz (Cellular imaging of Annexin V bioconjugates)

III.1 Rationale and Goals

The pursuit for modular approaches that enable the preparation of electronically tunable and responsive fluorophore platforms has become essential for the development of functional dyes for a wide range of applications, such as, sensing, bioimaging, probing applications, among others.[106–110] Along these lines, several highly fluorescent probes, such as rhodamines,[111,112] fluoresceins,[108,113] phenoxazines,[108] coumarins,[108] cyanines[114,115] and boron dipyrromethenes (BODIPYs)[116–120] have been extensively explored.

For instance, BODIPY derivatives have become an important family of dyes with a wide range of applications due to a combination of remarkable photophysical properties, including high molar absorption coefficients, high quantum yields and narrow absorption/emission bands. The success of this family triggered the interest in the construction of fluorescent molecules featuring a central boron(III) atom coordinated to a bidentate ligand, usually with N,N or N,O charged sites, and two anions, typically F^- or $Arom^-$ (**Scheme 27**).[121]

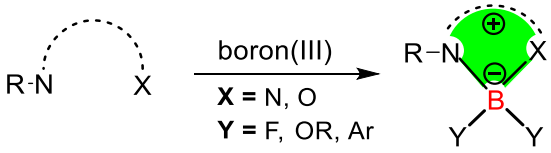

Scheme 27 – Boron(III) based fluorescent dyes.

Four-coordinate organoboron N,C chelates have also been intensively studied and some of them revealed to be highly fluorescent, consequently they are suitable for applications in organic light-emitting materials.[122] In many of these scaffolds, the boron atom assumes an important role, due to stabilization of the ligand and in this way enhancing the planarity, conjugation, and charge transfer throughout the π system on the dye.[121] Thus, it is quite surprising that boronic acids, which are widely available and structurally diverse, have been generally disregard as useful building blocks for the assemblage of fluorescent probes.

The oversight of boronic acids as conformational blocks, may suggest some issues in the modular construction of fluorescent probes based on this function. Boronic acids are known to generate fluorescent complexes after chelation with bidentate ligands[123–126], however since the chelation process is reversible, the constructed B-complexes often lack the long-term stability required for their application as functional

dyes (**Scheme 28**). Otherwise, the chelation of boronic acids with tridentate ligands generates more stable B-complexes but at the cost of its fluorescent nature since the central boron atom adopts an out-of-plane tetrahedral geometry (**Scheme 28**).[74]

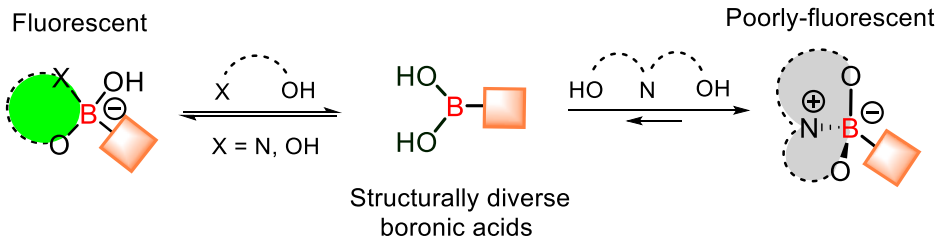

Scheme 28 – B-complexes based on bi and tridentate ligands.

The properties of boronic acids offer novel opportunities in the discovery of new fluorescent supramolecular architectures, since this function may be used to rigidify unreported structures of tridentate π-conjugated ligands. With this idea in mind, we envisioned that Schiff base ligands could be used as a platform to build fluorescent B-complexes, since the modular structure of these ligands can be tuned in order to chelate boronic acids, giving rise to a conformationally stable π-conjugated B-complex.[42,44,45,47,127,128]

Based on the multicomponent approach described in **Chapter II**, a novel modular fluorophore platform (BASHY) is presented on this chapter (**Scheme 29**).

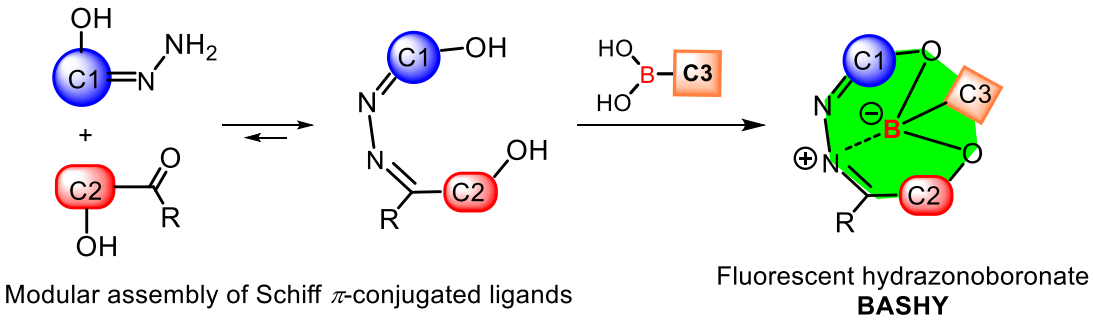

Scheme 29 – BASHY discovery: Boronic acids as configurational locks for Schiff based ligands.

III.2 Results and Discussion

III.2.1 BASHY discovery (Synthesis and photophysical evaluation)

In the course of the project previously described in **Chapter II**, our research group observed that boronate **27a** (**Scheme 30;** see also **section IV.1.1**) displayed fluorescence properties, although the quantum yield obtained was very low (λ_{fluo} = 456 nm, Φ_{fluo} = 0.03 in acetonitrile; **Table 2**). This observation led us to engage in the discovery of a modular fluorophore platform based on boronic acids.

With this idea in mind, the fluorescence properties of B-complex **57** (**Scheme 30**; see also **section IV.1.1**) were evaluated, since in comparison to **27a**, B-complex **57** has a more conjugated π-system framework, enhanced ligand planarity and greater rigidity. In general, these attributes are fundamental for the observation of significant and bathochromically shifted fluorescence. To our disappointment, B-complex **57** proved to be also very poorly fluorescent (Φ_{fluo} < 0.01 in acetonitrile; **Table 2**) in spite of the bathochromically shifted emission ($\Delta\lambda$ = 42 nm) in comparison to compound **27a**.

Subsequently, we anticipated that the installation of a hydrazone bridge between the donor and acceptor moieties could enhance the π-system conjugation along the main axis of the ligand and contribute to improved dye fluorescence properties. In order to achieve this new family of B-complexes, salicylhydrazone **76a**, phenylglyoxylic acid **77**, and phenylboronic acid **8** were mixture in acetonitrile at 80 ºC for 2 h (**Scheme 30**, see also **section IV.2.1**). The only product observed on this reaction was BASHY **78a**, which proved to be significantly more fluorescent than B-complexes **27a** and **57**. Dye **78a** also displayed a further bathochromic shift of the emission band (λ_{fluo}= 506 nm, Φ_{fluo}= 0.17 in acetonitrile; **Table 2**).

Encouraged by this result, several BASHYs were constructed following the multicomponent methodology described in **Chapter II**. As shown in **Scheme 30**, dyes **78b,c** were readily obtained in 99 % yield and interestingly, the insertion of a methyl group in the imine function of BASHY **78b** or a PEG functionality in BASHY **78c** did not quench the fluorescence properties (**Chart 5** and **Table 2**).

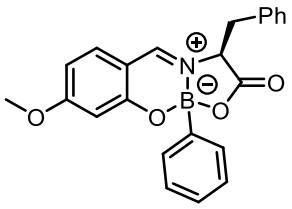

27a

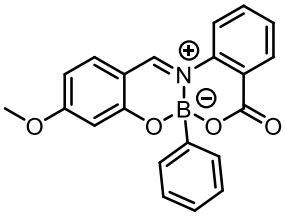

57

BASHY synthesis

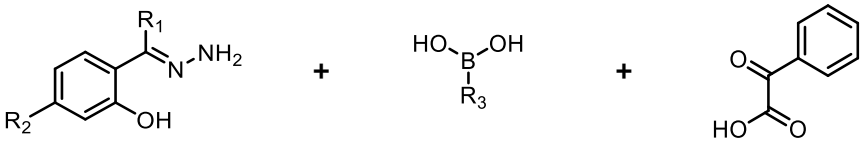

76a (R_1 = H, Me; R_2 = MeO)
76b (R_1 = Me, Me; R_2 = MeO)
76c (R_1 = Me; R_2 = -O(-CH_2)$_2$-O-)$_3$-Me)

8 (R_3 = Ph)

77

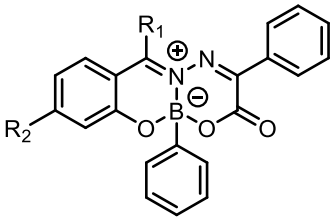

78a (R_1 = H; R_2 = MeO); γ = 99 %
78b (R_1 = Me; R_2 = MeO); γ = 99 %
78c (R_1 = Me; R_2 = -O(-CH_2)$_2$-O-)$_3$-Me); γ = 99 %

Scheme 30 – Top: Structures of B-complexes **27a** and **57**; Bottom: One-pot modular construction of BASHY **78a-c** (CH_3CN, 80 ºC, 2h).

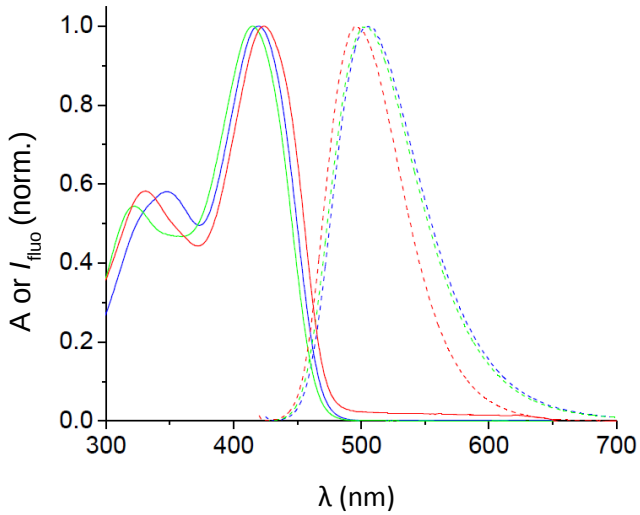

Chart 5 – UV/vis absorption (solid lines) and fluorescence spectra (dashed lines) of **78a** (blue), **78b** (green) and **78c** (red) in acetonitrile.

The incorporation of a stronger electron-donating *N,N*-diethylamino substituent on BASHYs revealed to be slightly more challenging due to the undesired formation of a symmetric azine product in the reaction between hydrazine and 4-diethylamino derivative of salicylaldehyde **14**. Therefore, in order to overcome this problem, a new synthetic approach, involving the formation of hydrazones **79a,b** from phenylglyoxylic acid derivatives **77** was developed (**Scheme 31,** also **section IV.2.1**).

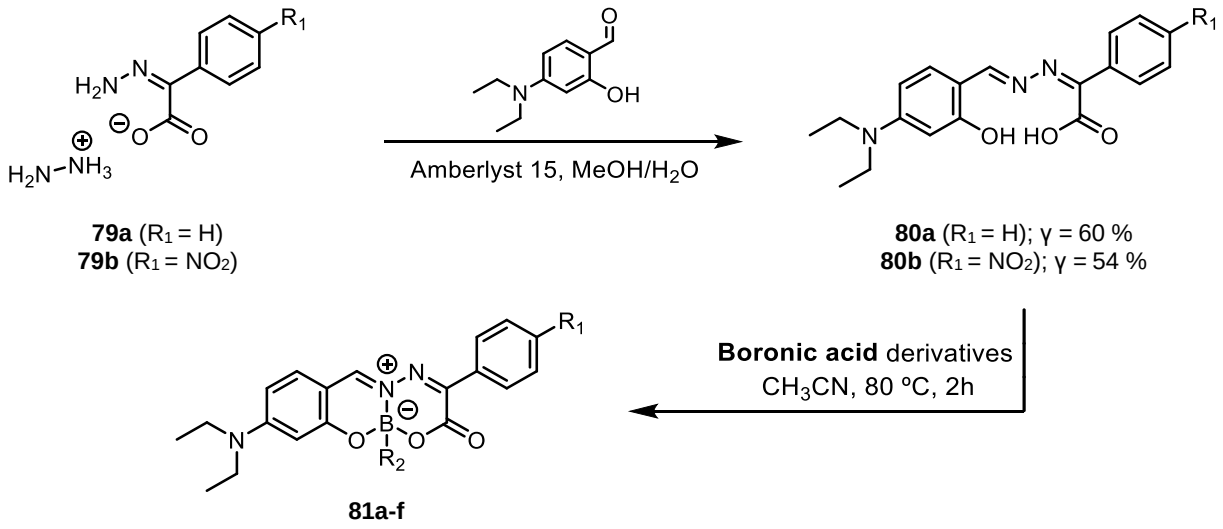

79a (R_1 = H)
79b (R_1 = NO_2)

80a (R_1 = H); γ = 60 %
80b (R_1 = NO_2); γ = 54 %

81a-f

Structures of BASHYs **81a-f**

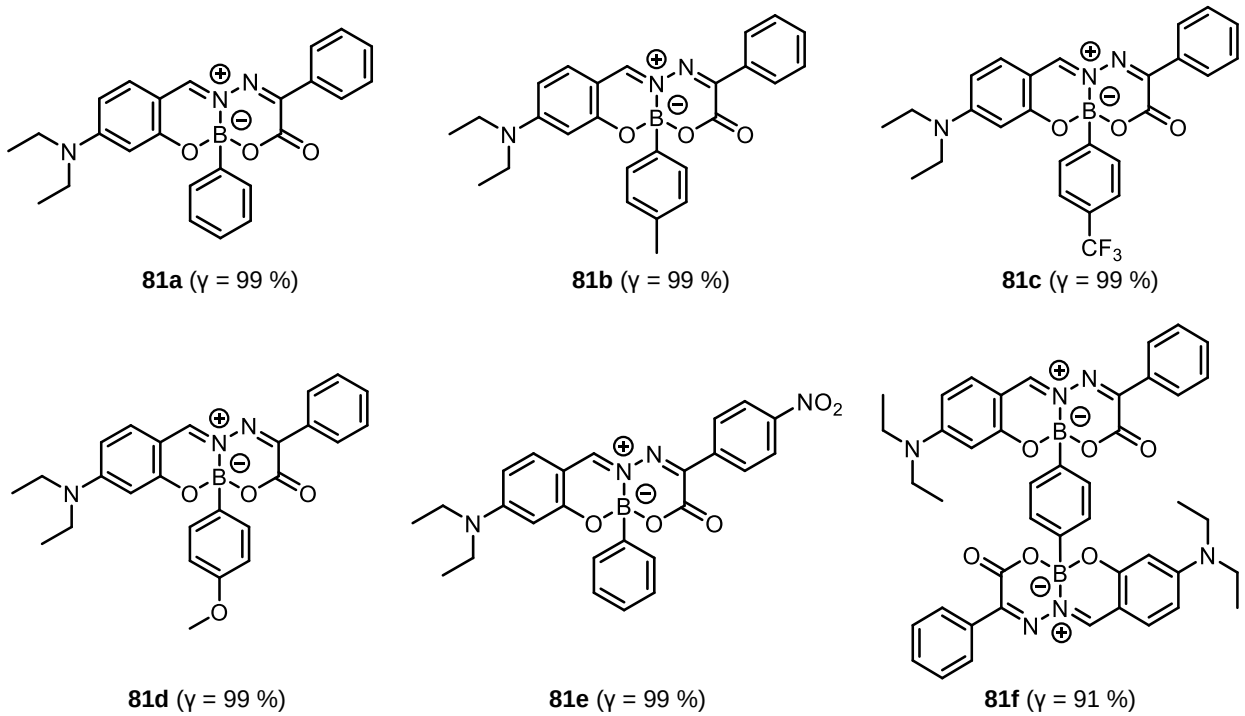

81a (γ = 99 %)
81b (γ = 99 %)
81c (γ = 99 %)
81d (γ = 99 %)
81e (γ = 99 %)
81f (γ = 91 %)

Scheme 31 – Different approach for the construction of BASHYs **81a-f** featuring an *N,N*-diethylamino substituent.

Hydrazones **79a,b** were then used in the preparation of Schiff base ligands **80a,b**, which are able to chelate with different boronic acid derivatives in CH_3CN, 80 ºC, 2 h, giving rise to BASHYs **81a-f** in excellent to almost quantitative yields (up to 99 %) (**Scheme 31**, see also **section IV.2.1**). The straightforwardness of this methodology allows BASHY dyes to be readily obtained in high purity, without the need of laborious chromatographic steps.

The key role of the boronic acid component in the generation of fluorescence from a nonfluorescent ligand was confirmed in a control experiment with ligand **80b**. Upon addition of three equivalents of phenylboronic acid **8** to this ligand (leading to the slow formation of dye **81e**), the buildup of the typical fluorescence band (enhancement factor of ca. 150 within 95 h) was observed (**Chart 6**).

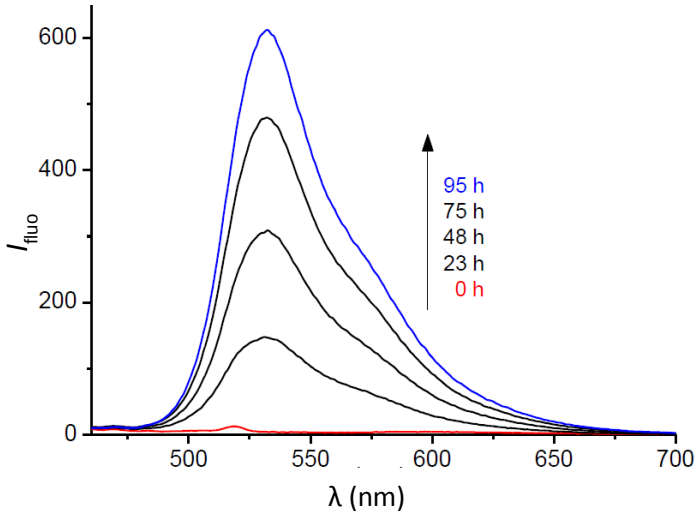

Chart 6 – Development of the fluorescence spectra of **81e** (λ_{exc} = 450 nm) from the addition of addition of 3 equivalents of phenylboronic acid to ligand **80b** (5 µM in toluene).

Taking the photophysical properties of BASHY **78a** as a starting point, an extensive investigation of some of the newly prepared BASHYs was performed. This data is compiled in **Table 2** and representative UV/Vis absorption and fluorescence spectra are represented in **Chart 7A,B**. BASHY **81a**, which contains *N,N*-diethylamino as an electron-donating group, exhibited a further bathochromic shift (by ca. 40 nm) in polar solvents, such as acetonitrile (λ_{fluo} = 540 nm, Φ_{fluo} = 0.08; **Chart 7A**), relative to those of methoxy-substituted **78a,b**. However, in nonpolar solvents, the emission maximum of **81a** was displaced hypsochromically (λ_{fluo} = 508 nm in toluene and 517 nm in chloroform; **Chart 7B** and **Table 2**).

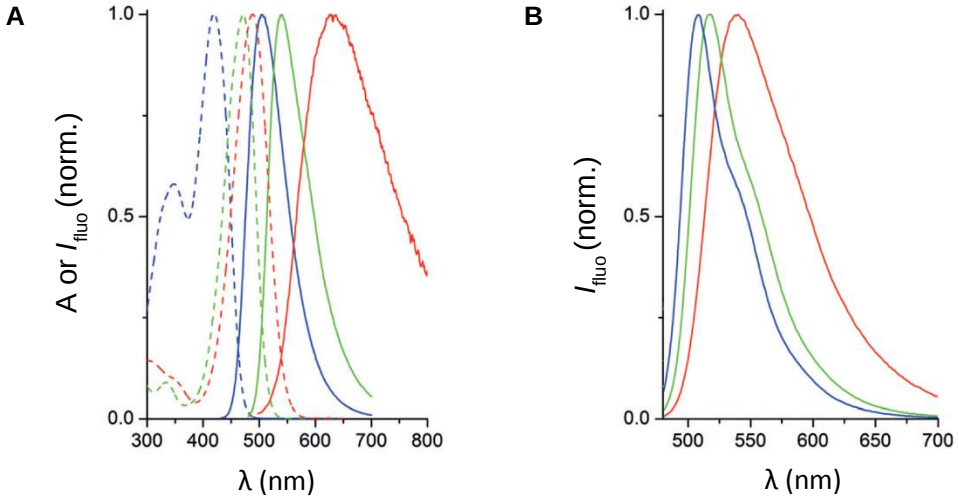

Chart 7 – A) UV/Vis absorption (dashed lines) and fluorescence spectra (solid lines) of dyes **78a** (blue), **81a** (green), and **81e** (red) in acetonitrile; B) Fluorescence spectra of **81a** in toluene (blue), chloroform (green), and acetonitrile (red).

The photophysical properties of BASHY dyes, such as the broad emission bands, pronounced Stokes shifts (70 – 80 nm) and the influence of the solvent's polarity and the donor substituent in the spectral position of the emission bands led us to categorize BASHYs as ICT fluorophores.[129]

The observed Stokes shifts in BASHYs enables their excitation far from the spectral window of emission observation, avoiding potential complications in fluorescence microscopy, such as the reabsorption of emitted photons or stray-light detection. These issues are often encountered for BODIPY dyes and require alternative photophysical designs, such as ETCs.[118,130]

The ICT character of the BASHY dyes was further supported by time-dependent DFT calculations[131] at the CAM-B3LYP/6-31G** level of theory (see **section IV.2.3.1**). The calculations were performed for the representative dyes **78a** and **81a,e**. DFT calculations clearly demonstrated that the strongest transition (S_0 → S_1) is manly represented by HOMO → LUMO transition. The excitation energies (E_{exc}) calculated are in accordance with the observed experimental E_{exc}, although the absolute values appear to be slightly overestimated by the method (by ca. 0.4 – 0.5 eV) (**Table 1**).

Table 1 – Selected time-dependent DFT-calculated parameters (CAM-B3LYP/6-31G**) for the vertical excitation of BASHYs **78a** and **81a,e** in acetonitrile.

	Electronic transition [a]	E_{exc} (eV) [b]	Orbitals	CI [c]
78a	$S_0 \rightarrow S_1$	3.36 [2.95]	HOMO → LUMO	0.67896 (92 %)
81a	$S_0 \rightarrow S_1$	3.18 [2.63]	HOMO → LUMO	0.65914 (87 %)
			HOMO-1 → LUMO	0.16522 (6 %)
81e	$S_0 \rightarrow S_1$	3.09 [2.54]	HOMO → LUMO	0.60451 (73 %)
			HOMO → LUMO+1	0.26906 (14 %)
			HOMO-2 → LUMO	0.16488 (5 %)
			HOMO-1 → LUMO	0.14670 (4 %)
			HOMO-4 → LUMO	0.12003 (3 %)

[a] Only the strongest transition is considered. **[b]** Excitation energy. The experimental value, corresponding to the UV/vis absorption maximum, is shown in square bracket. **[c]** Absolute CI coefficient of the wavefunction for each excitation. In parenthesis the percentage contribution to the excitation is indicated.

The depiction of HOMO and LUMO orbitals of representative BASHYs **78a** and **81a,e** (**Figure 12**), reveals that the HOMO orbitals are mainly located on donor moiety of these dyes (**78a** – MeO; **81a,e** – NEt_2) while the corresponding LUMO orbitals are distributed along the main axis of the π-conjugated framework with significant contributions from the oxadiazaborinine ring. In the case of BASHY **81e**, the LUMO orbital is manly located in the nitro acceptor moiety. These observations support the experimentally well manifested ICT character of BASHY dyes.

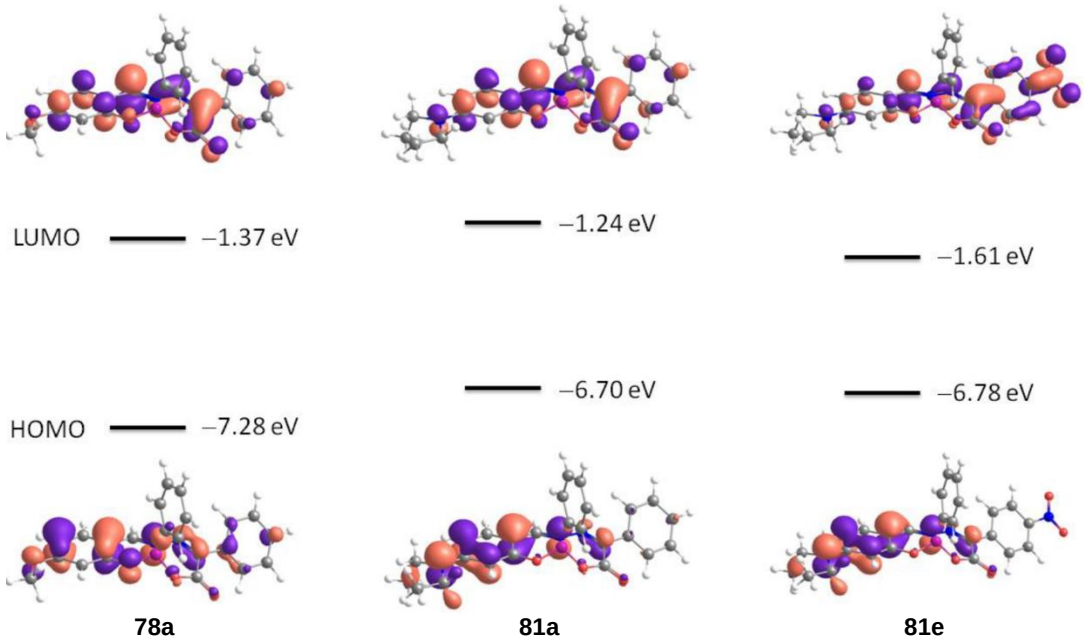

Figure 12 – Isosurface plots for BASHYs **78a**, **81a,e**; isosurface value: 0.04.

Energetically low-lying ICT states often deactivate through competitive nonradioactive channels. This is a direct consequence of the phenomenon known as the energy gap law and explains the relatively low quantum yields of BASHY dyes in polar solvents, which stabilize the ICT state.[129] However, this also means that in nonpolar solvents the fluorescence quantum yields should increase significantly, which indeed was verified by values as high as 0.60 – 0.62 (**Table 2**).

Evaluation of this series of BASHYs **81a-f** clearly points out that the emission properties of this family of dyes remains unaltered despite the modifications on the phenylboronic acid moiety (**Table 2**). This is an important observation, that enables the electronical modification of these dyes and even the preparation of dimers, such as BASHY **81f**, in which both halves are electronically non-communicating as demonstrated by DFT calculations (**Figure 13**, see also **section IV.2.3**).[44]

Hence, dimeric BASHY **81f** maintains the fluorescence properties of **81a** (**Table 2**), and as expected nearly doubles the molar absorption coefficient (60000 $M^{-1}.cm^{-1}$ for **81a** versus 103900 $M^{-1}.cm^{-1}$ for **81f** in acetonitrile; see also in **section IV.2.2**, **Chart 38**)

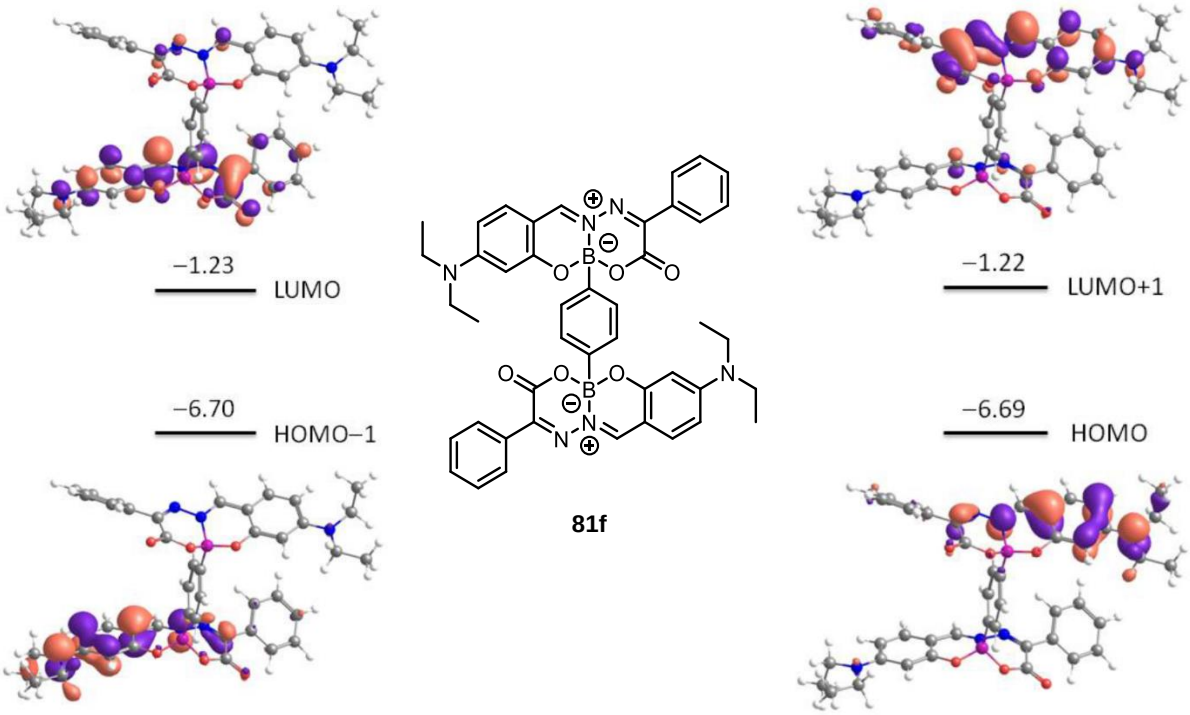

Figure 13 – Isosurface plots for dimeric BASHY **81f**; isosurface value: 0.04.

The amplification of the electron-accepting properties on BASHY **81e** due to the nitro substituent, led to a shift in the emission maximum further to λ = 632 nm in acetonitrile (**Chart 7A**), but at the cost of its fluorescent nature (Φ_{fluo} < 0.01). Again, the energy-gap law is behind these observations. As expected for a push–pull dye with strong ICT character, it was observed for BASHY **81e**, a strong solvatochromic effect and an effective hypsochromic shift of the fluorescence emission in nonpolar solvents (λ_{fluo} = 535 nm in toluene and 555 nm in chloroform; **Table 2**, see also in **section IV.2.2**, **Chart 39**). Again, this was accompanied by fluorescence light-up behavior in nonpolar media (Φ_{fluo} = 0.55 and 0.48 in toluene and chloroform, respectively; **Table 2**).

Table 2 – Photophysical properties of BASHY dyes in air-equilibrated solution.

	Solvent [a]	λ_{abs} **(nm)** [a]	λ_{fluo} **(nm)** [b]	Φ_{fluo} [c]	τ_{fluo} **(ns)** [d]
27a	acetonitrile	363	456	0.03	0.49
57	acetonitrile	401	498	< 0.01	-- [e]
78a	acetonitrile	420	506	0.17	1.59
78b	acetonitrile	415	503	0.16	1.45
78c	acetonitrile	415	497	0.15	1.39
78c	toluene	424	494	0.13	1.07
78c	toluene	424	500	0.10	0.86
81a	methanol	473	544	< 0.01	-- [e]
81a	acetonitrile	471	540	0.08	0.43
81a	chloroform	477	517	0.62	2.70
81a	toluene	471	508	0.60	2.38
81b	acetonitrile	472	540	0.09	0.59
81c	acetonitrile	471	542	0.06	0.36
81d	acetonitrile	471	540	0.09	0.52
81e	methanol	487	592	< 0.01	-- [e]
81e	acetonitrile	488	632	< 0.01	-- [e]
81e	chloroform	496	555	0.48	2.85
81e	toluene	489	535	0.55	2.64
81f	acetonitrile	463	534	0.06	0.65
81f	chloroform	472	520	0.53	3.47

[a] Longest-wavelength absorption maximum; **[b]** Fluorescence maximum; **[c]** Fluorescence quantum yield; **[d]** Fluorescence lifetime; **[e]** Not determined because of the low emission intensity.

The brightness ($\varepsilon \times \Phi_{fluo}$) of BASHYs **81a,e,f** in nonpolar solvents was evaluated for the excitation at their maximum absorption wavelength, which in the case of these dyes matched quite well with the output lines of the Argon ion laser (λ = 488, 476 nm), frequently used in confocal fluorescence microscopy. The results obtained demonstrated that BASHY dyes have brightness values (**81a** – 37000, **81e** – 28000 and **81f** – 54000 $M^{-1}.cm^{-1}$, in nonpolar media (*e.g*. chloroform), comparable to those of other well-performing fluorescent dyes, such as, carbofluorescein (67000 $M^{-1}.cm^{-1}$), phenoxazine dyes (*e.g.* resorufin, 41000 $M^{-1}.cm^{-1}$), tetramethylrhodamines (35000 $M^{-1}.cm^{-1}$) or cyanine dyes (*e.g.* Cy3, 18000 $M^{-1}.cm^{-1}$).[108]

The brightness and hydrophobic asymmetric 3D structure of BASHY dyes may be explored for applications in bioimaging. These dyes were then evaluated in **section III.2.4**, as stains for nonpolar, hydrophobic intracellular environments, such as lipid droplets[132], since they can be an interesting alternative for commonly employed Nile red.[133,134] Another approach explored by us, was their entrapment in the hydrophobic environment of polymeric nanoparticles (NPs) to tag these promising drug-delivery vehicles (see **section III.2.5.1**)

BASHY photostability was then evaluated. As shown in **Table 3**, photostability of BASHYs **81a,e,f** in acetonitrile and chloroform is comparable to Nile red, with less than 15 % decomposition (as rated by the intensity of the fluorescence signal) after irradiation for 3 h with a 150 W xenon lamp and a λ= 455 nm cutoff filter (see in **section IV.2.2**, **Chart 40**). As observed for other ICT dyes, the excited ICT state serves as an energy sink, thereby protecting the fluorophores from major photodecomposition.[135]

Table 3 – Photostability of selected BASHY **81a,e,f** in air-equilibrated solution.

	Solvent	I_{fluo} / I_0 **x 100 %** [a]
81a	CH_3CN	90
	$CHCl_3$	90
81e	CH_3CN	-- [b]
	$CHCl_3$	96
81f	CH_3CN	92
	$CHCl_3$	87
Nile Red	CH_3CN	81
	$CHCl_3$	93

[a] After irradiation for 3 h with a 150 W xenon lamp equipped with a λ= 455 nm cutoff filter; followed by fluorescence; **[b]** Not determined because of low fluorescence; the UV/Vis absorption spectrum indicates no photodecomposition.

III.2.2 Fluorescence and functional fine-tuning of BASHY dyes

Encouraged by the fact that BASHY dyes display remarkable photophysical properties and their modular construction is so straightforward, we decided to expand the scope of these dyes through electronic and functional fine-tuning (**Figure 14**). Electronic modifications on the ligand backbone of BASHYs will promote changes in the photophysical parameters such as emission color, Stokes shift and two-photon-absorption (2PA) cross section. Functional alterations at the level of the boronic acid moeity will broaden the spectrum of BASHY applications, ranging from biorelevant contexts to optoelectronic materials.

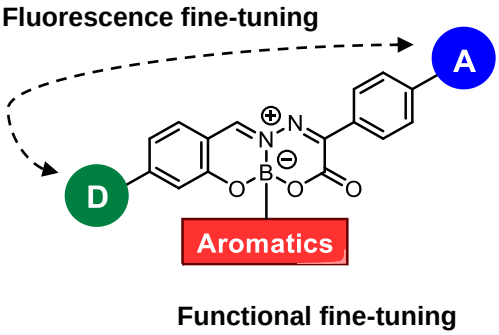

Figure 14 – Fluorescence and functional fine-tuning of BASHY dyes.

The functional diversity of the BASHY platform *via* changes on the boronic acid moiety is shown in **Figure 15** (see also the synthetic approach in **Scheme 31** and **section IV.2.1**). The triphenylamine moiety, installed in **82a**, is a known strong electron donor and the opposite electronic situation is found on dye **82g**, which contains a strong electron-accepting pentafluorophenyl residue, also known for its importance as a fluorous tag. BASHY **82e** features a phenylsulfonamide, which is a key structural motif of carbonic anhydrase inhibitors. Nitrogen-containing heterocyclic moieties such as 4-isoquinolinyl (dye **82d**) or 4-pyridyl (dye **82f**) were chosen for their possible implication in metal−ligand chelation. BASHYs **82c,h** feature a fluorene moiety, which is a prominent chromophore in organic light-emitting diodes.

Installation of these various motifs was done in moderate to excellent yields and in general, as recently reported in a theoretical study of BASHY complexes,[136] does not alter the photophysical properties of BASHYs, since the electronic properties of the boronic acid-derived aromatic moiety only have a minor influence. Gratifyingly, this allows the orthogonal assembly of BASHY dyes, where the photophysical properties are practically only determined by the electronic properties of the ligand backbone. Rare exceptions to

this generalization occur in the presence of redox-active residues, such a triphenylamine (**82a**) or pyrene (**82b**).

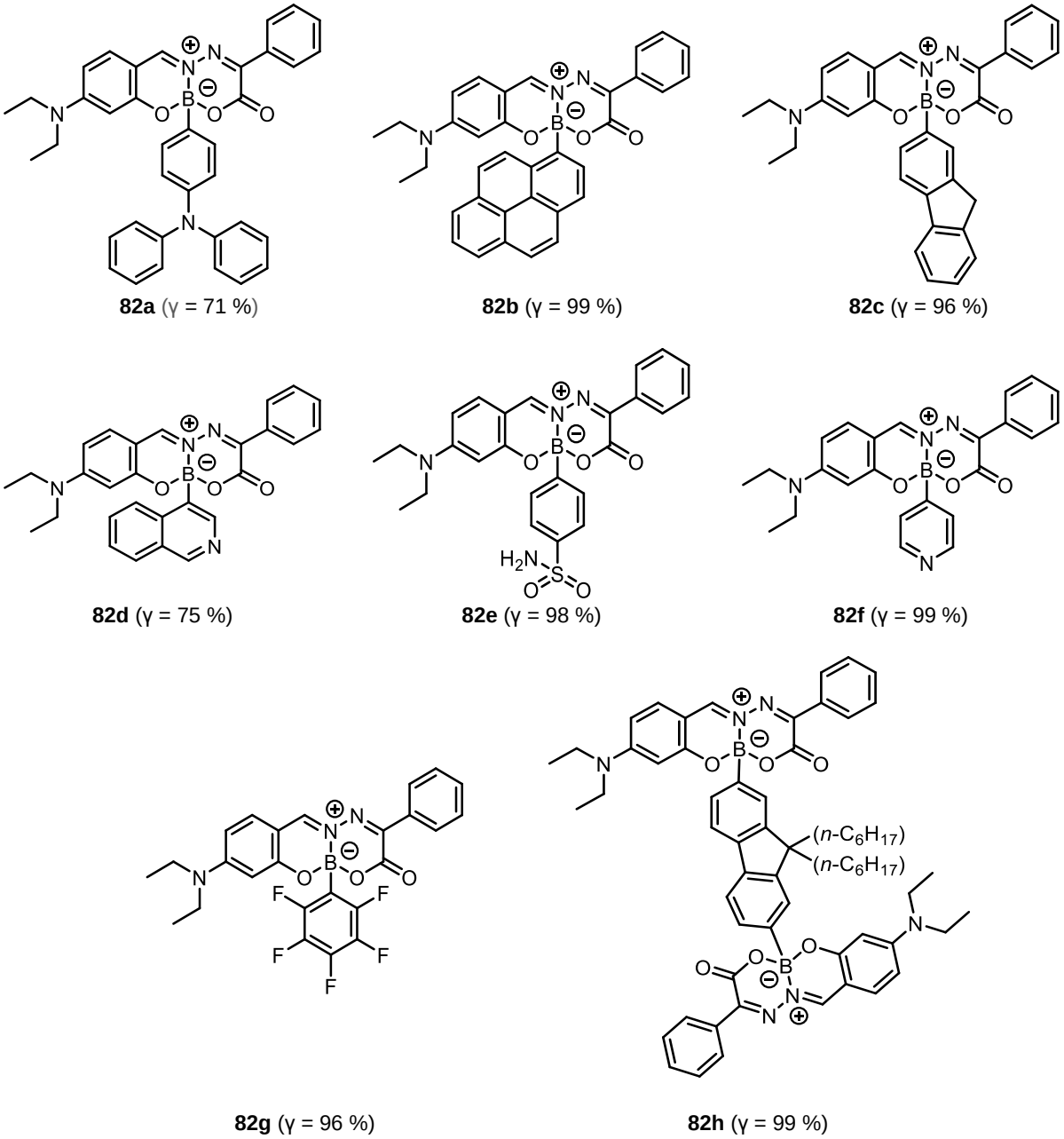

Figure 15 – Structures of BASHYs **82a-h**.

Electronic variations on the ligand backbone of the BASHY platform were also made, by changing the R_1 group (H, NO_2, CF_3 and CN; **Scheme 32**). These modifications provide a way to control the photophysical properties of BASHYs by means of the degree of ICT along the ligand backbone.[136]

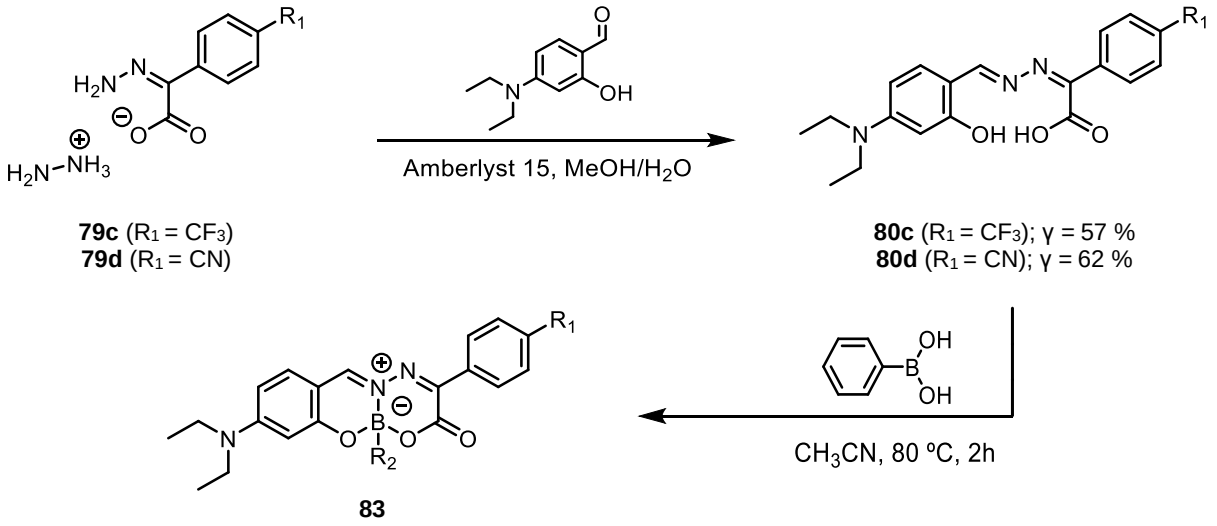

79c ($R_1 = CF_3$)
79d ($R_1 = CN$)

80c ($R_1 = CF_3$); γ = 57 %
80d ($R_1 = CN$); γ = 62 %

83

Structures of BASHYs **83a,b**

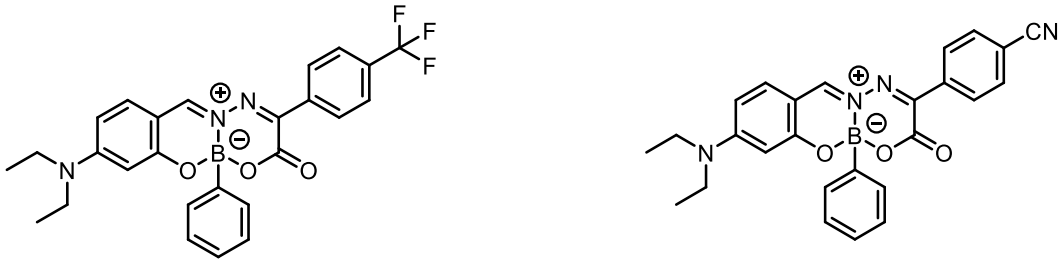

83a (γ = 99 %)

83b (γ = 99 %)

NOTE: BASHY **81a** (R_1= H) and **81e** (R_1= NO_2) and described in **Scheme 31.**

Scheme 32 – Construction of BASHYs **83a,b** featuring different moieties (CF_3 and CN, respectively) in R_1 group.

The photophysical data of these novel dyes **82a-h** and **83a,b** in air-equilibrated toluene and acetonitrile solutions are described in **Table 4**. BASHYs **82c-h** have similar wavelength of maximum absorbance, ranging from 465 to 475 nm and high molar absorption coefficients (generally 50000 – 60000 $M^{-1}.cm^{-1}$; except for the dimeric BASHY **82h**, for which values as high as 121000 $M^{-1}.cm^{-1}$ were observed) both in toluene and acetonitrile.

The fluorescence emission maximum is located at 505 − 510 nm in toluene and at 540 − 545 nm in acetonitrile. The bathochromic shift of the emission, observed for acetonitrile, corroborates with the partial involvement of ICT in the excited state, as has been suggested recently by quantum chemical calculations of BASHY dyes.[136]

Also the emission quantum yields and lifetimes show parallel trends in dependence on the solvent. For a polar solvent such as acetonitrile, low quantum yields of 0.05 – 0.12 were observed, while in a non-polar solvent (toluene), an increase to 0.5 – 0.7

was noted. The fluorescence of BASHY dyes is not quenched by oxygen, as shown in quantum yield measurements with nitrogen-purged solutions of the representative BASHYs **81a** and **82b,e** (quantum yields remain the same within an error margin of 10 %).

The fluorescence lifetimes are situated at ca. 0.3 − 0.5 ns in acetonitrile and significantly longer in toluene (ca. 2.4 − 3.0 ns). The proportionality between Φ_{fluo} and τ_{fluo} points to a rather solvent-independent radiative rate constant ($k_r = \Phi_{fluo} / \tau_{fluo}$), being generally in the order of 10^8 s^{-1} for the investigated series. Still, the nonradiative deactivation [$k_{nr} = (1 - \Phi_{fluo} / \tau_{fluo}$] is by one order of magnitude faster in acetonitrile as compared to toluene (ca. 10^9 s^{-1} versus 10^8 s^{-1}; **Table 4**). This may be reasoned with the energy-gap law, predicting a faster $S_1 - S_0$ deactivation for energetically lower lying excited singlet states.

The invariability of the electronic structure of the BASHY backbone was confirmed by electrochemical measurements. The reduction of the BASHY core proceeded at peak potentials (E_p^{red}) that are located for most of the dyes at ca. − 1.1 V (in dichloromethane) (**Figure 16**).

	E_p^{red} (V)
82a	- 1.12
82b	- 1.12
82c	- 1.12
82d	- 1.06
82e	- 1.16, -0.88
82f	- 1.07
82g	- 1.07
82h	- 1.11
81a	- 1.12
83a	- 1.12
83b	- 1.00
81a	- 1.26

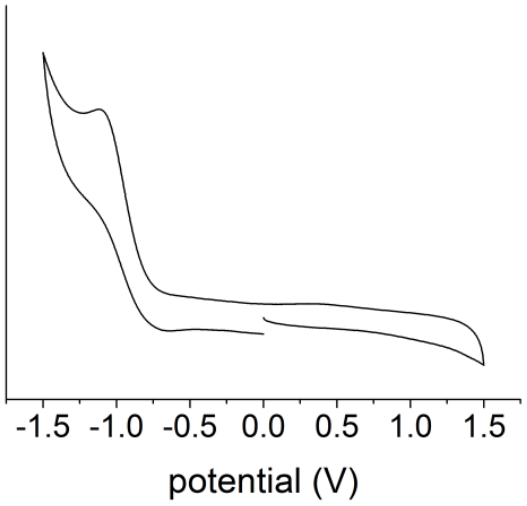

Figure 16 – Left: Peak reduction potentials of BASHYs (**81a,e; 82a-f; 83a,b**) in dichloromethane; Right: Representative cyclovoltammogram of BASHY **81a.**

Table 4 – Photophysical data of BASHYs (**81a,e**; **82a-f**; **83a,b**) in air-equilibrated toluene and acetonitrile.

	Solvent	$\lambda_{abs,max}$ (nm) [ε ($M^{-1}.cm^{-1}$)]	$\lambda_{fluo\ abs,max}$ (nm)	Φ_{fluo}	τ_{fluo} (ns)	k_r (s^{-1})	k_{nr} (s^{-1})
82a	toluene	305 [28000] [a]	376				
		471 [42000]	501	0.01 [b]	-- [c]		
	acetonitrile	300 [27000] [a]	401				
		470 [40000]	534	< 0.01 [b]	-- [c]		
82b	toluene	346 [47000] [a]	381				
		471 [57000]	520	0.02 [b],d	2.62	7.6×10^6	3.7×10^8
	acetonitrile	343 [47000] [a]	377				
		471 [56000]	562	<0.01 [b]	-- [c]		
82c	toluene	471 [54000]	510	0.54	2.67	2.0×10^8	1.7×10^8
	acetonitrile	471 [51000]	540	0.12	0.48	2.5×10^8	1.8×10^9
82d	toluene	471 [47000]	506	0.66	2.80	2.4×10^8	1.2×10^8
	acetonitrile	469 [56000]	540	0.06	0.32	1.9×10^8	2.9×10^9
82e	toluene	474 [47000]	509	0.70 [d]	2.80	2.5×10^8	1.1×10^8
	acetonitrile	472 [54000]	542	0.06 [d]	0.42	1.4×10^8	2.2×10^9
82f	toluene	473 [56000]	509	0.66	2.44	2.7×10^8	1.4×10^8
	acetonitrile	472 [57000]	541	0.06	0.28	2.1×10^8	3.4×10^9
82g	toluene	467 [58000]	504	0.51	3.01	1.7×10^8	1.6×10^8
	acetonitrile	465 [52000]	545	0.05	0.37	1.4×10^8	2.6×10^9
82h	toluene	471 [121000]	509	0.63	4.96	1.3×10^8	7.5×10^7
	acetonitrile	471 [118000]	536	0.08	1.04	7.7×10^7	8.8×10^8
81a	toluene	471 [63000]	508	0.60 [d]	2.38	2.5×10^8	1.7×10^8
	acetonitrile	471 [61000]	540	0.08	0.43	1.9×10^8	2.1×10^9
83a	toluene	478 [63000]	516	0.65	2.83	2.3×10^8	1.2×10^8
	acetonitrile	476 [56000]	559	0.05	0.26	1.9×10^8	3.7×10^9
83b	toluene	484 [62000]	525	0.57	2.51	2.3×10^8	1.7×10^8
	acetonitrile	482 [67000]	577	0.05	0.29	1.7×10^8	3.3×10^9
81e	toluene	489 [55000]	535	0.55	2.64	2.1×10^8	1.7×10^8
	acetonitrile	488 [54000]	632	<0.01	-- [c]		

[a] On excitation at the short-wavelength maximum two emission bands with the indicated maxima are observed. However, on excitation at the long-wavelength maximum only the more red-shifted emission is seen. **[b]** Fluorescence quantum yield on excitation in the long-wavelength absorption band. **[c]** Not determined due to the weak fluorescence. **[d]** For a nitrogen-purged solution the quantum yield for excitation in the long-wavelength absorption band remains nearly unchanged within an error margin of 10 %. No quenching by oxygen is observed.

The brightness ($\varepsilon \times \Phi_{fluo}$) of these novel BASHYs is as expected more pronounced in nonpolar media, reaching values of up to 37000 $M^{-1}.cm^{-1}$ for dye **82f**, or even 76000 $M^{-1}.cm^{-1}$ for the dimeric BASHY dye **82h** in toluene. These values are comparable to or even larger than those of bright-emitting traditional dyes, such as fluoresceins, rhodamines, cyanines, BODIPY or 7-nitrobenzooxadiazole (NBD) ICT dyes (**Table 5**).[108]

Table 5 – Comparison of the photophysical properties of representative BASHY dyes (**81a,e** and **83a,b**) with those of a typical solvatochromic dye N,N-diethylamino-NBD and BODIPY.

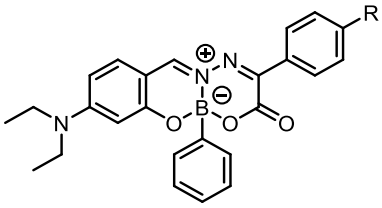

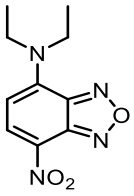

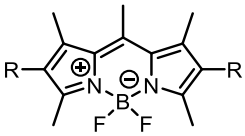

	BASHYs (81a,e and 83a,b) [a]	**NBD-DEA [b]**	**BODIPY (R = H; SO_3Na) [c]**
$\lambda_{abs,max}$ (nm)	470 – 490	468	493
ε ($M^{-1}.cm^{-1}$)	*ca*. 60000	*ca*. 18000 [d]	*ca*. 80000
$\lambda_{fluo\ abs,max}$	510 – 535	525	519
Φ_{fluo}	0.55 – 0.65	0.55	0.99
Brightness ($\varepsilon \times \Phi_{fluo}$)	*ca*. 35000 – 40000	*ca*. 10000	*ca*. 80000
Solvatochromism ($\nu_{tol} - \nu_{CH3CN}$)/ cm^{-1}	1200 – 1900	600	-- [e]
Stokes shift ($\nu_{abs} - \nu_{fluo}$)/ cm^{-1}	1500 – 1800	2300	1000
σ_2/ GM	120 – 300 (>900 nm)	< 1 [f]	10 – 20 [g]

[a] Data for a typical BASHY dye in a nonpolar solvent (e.g., toluene), as reflected in this work. **[b]** Data for *N,N*-diethylamino-NBD in toluene.[137] **[c]** Data for BODIPY with R= H in ethanol.[118] **[d]** In cyclohexane. **[e]** BODIPY dyes are known to show only very weak solvatochromism. **[f]** In dichloromethane.[138] [**g]** Data for BODIPY with R = SO_3Na in water.[139]

However, there are exceptions which are reflected in the observations that were made for the dyes **82a,b**. These dyes show very low fluorescence quantum yields in toluene (≤ 0.02) and are essentially nonfluorescent in acetonitrile (**Table 4**). It is proposed that photoinduced electron transfer interferes, either in the excited singlet or triplet state.

Photostability of solvatochromic dyes is in general considerably reduced in nonpolar solvents, implying triplet state formation and thereby photooxidations.[140] For this reason we evaluated some selected BASHY dyes in long-term irradiations of air--equilibrated toluene solutions with a 150 W Xe-lamp, exciting at > 455 nm. As judged from

the changes in the UV−vis absorption spectrum, the dyes **81a,e**, **82a,c** and **83b** showed very minor decomposition (6 % for **82a**, 8 % for **82c**, and 3 % for **81a,e** and **83b**) after 1 h of irradiation under comparable conditions. This reduced photoreactivity is in accordance with the high fluorescence quantum yield in toluene. As an exception, BASHY **82b** showed a pronounced tendency to photodecompose in air-equilibrated solution (61 % after 1 h of irradiation, **Chart 8**).

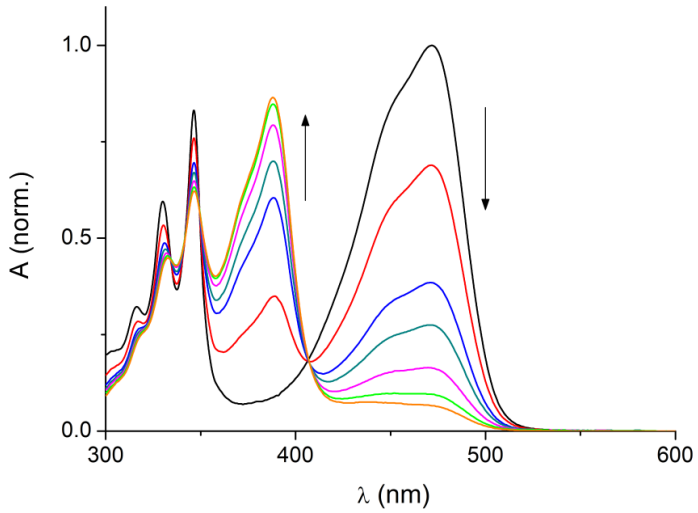

Chart 8 – Irradiation (λ > 455 nm) of BASHY **82b** in air-equilibrated toluene solution. The spectra were taken after 0 (black line), 30 (red line), 60 (blue line), 90 (cyan line), 120 (pink line), 150 (green line), and 180 (orange line) minutes.

One- and two- photon absorption properties of BASHYs **81a,e** and **83a,b** were then evaluated since these dyes maintain a common donor moiety (-NEt_2), while each one has a different electron-accepting group. It was observed that the increase of electron-acceptor strength in this BASHY series [Hammett constants σ_{para}: 0 (H; **81a**), 0.54 (CF_3; **83a**), 0.66 (CN; **83b**), 0.78 (NO_2; **81e**)][141] leads to bigger bathochromic shifts of the absorption spectrum which is even more pronounced for the fluorescence spectrum (**Chart 9**).

Thus, on moving from dye **81a** (weakest electron-withdrawing substituent) to **81e** (strongest electron-withdrawing group), a bathochromic shift of the emission band by 27 nm (toluene) and by 92 nm (acetonitrile) was noted. Again, this solvent dependence is in line with the proposed ICT character of the emissive state.[136]

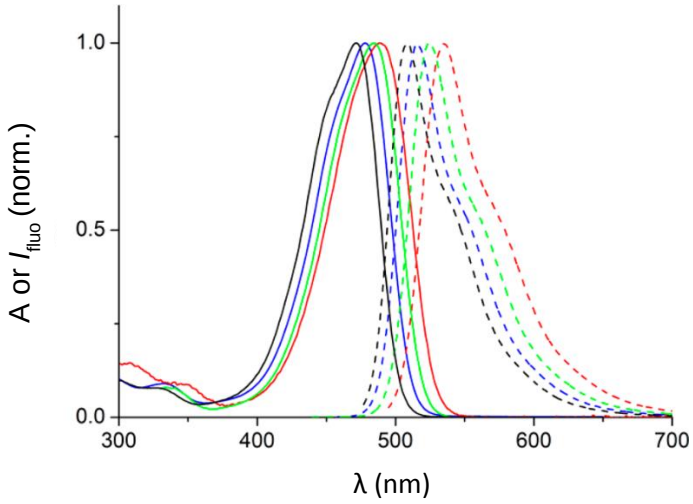

Chart 9 – Normalized UV−vis absorption (solid lines) and fluorescence spectra (dashed lines) of dye **81a** (black), **83a** (blue), **83b** (green), and **81e** (red) in air-equilibrated toluene.

The quantum yields of this BASHY series (**81a,e** and **83a,b**), as shown in **Table 4**, remain high for toluene (Φ_{fluo} ca. 0.55 − 0.65), becoming lower in polar solvents such as acetonitrile (Φ_{fluo} ca. 0.05 − 0.08 for **81a** and **83a,b** and < 0.01 for **81e**). This is in accordance with the observations made for previous BASHY dyes **82c-h** (**Table 4**).

With the intention to evaluate the solvatochromic character[140] of BASHYs, the fluorescence of **81e** and **83a,b** was investigated in a series of solvents (toluene, chloroform, tetrahydrofuran, ethyl acetate, acetone, acetonitrile, and dimethylformamide) (**Table 6**, see also **section IV.2.2**, **Chart 41**). BASHYs **81e**, **83a,b** showed gradual bathochromic shifts of the emission spectrum and a decrease of the emission quantum yield upon increasing the solvent polarity. The corresponding Lippert−Mataga plots[142–144] confirm the increasing push−pull character in the order **83a** < **83b** < **81e** (**Chart 10**).

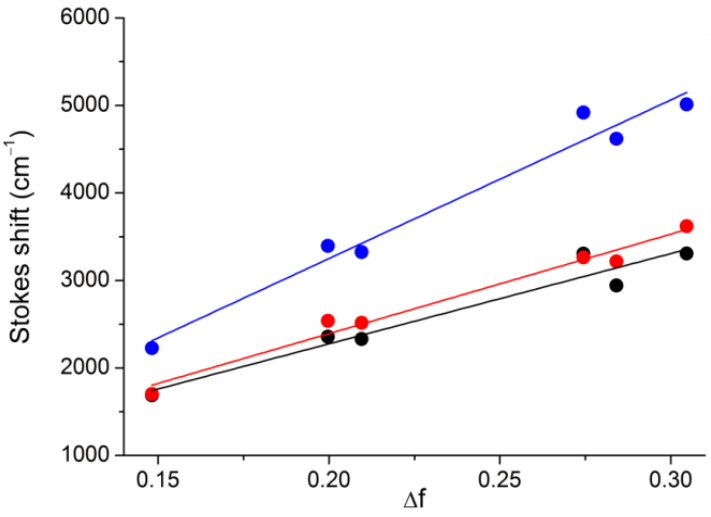

Chart 10 – Lippert-Mataga plots for dyes **83a** (black points), **83b** (red points) and **81e** (blue points). Data points from left to right corresponds to chloroform, ethyl acetate, THF, DMF, acetone, acetonitrile.

Table 6 – Optical properties of **81e**, **83a,b** in various solvents with different polarities.

	Solvent	$\lambda_{abs,max}$ (nm)	$\lambda_{fluo,max}$ (nm)	Φ_{fluo}
BASHY 81e	toluene	489	535	0.55
	chloroform	496	555	0.47
	ethyl acetate	486	577	0.16
	tetrahydrofuran	489	579	0.23
	acetone	488	622	<0.01
	acetonitrile	488	632	<0.01
	dimethylformamide	494	636	<0.01
BASHY 83a	toluene	478	516	0.65
	chloroform	484	525	0.68
	ethyl acetate	475	534	0.27
	tetrahydrofuran	478	537	0.30
	acetone	477	552	0.09
	acetonitrile	476	559	0.05
	dimethylformamide	481	566	0.08
BASHY 83b	toluene	484	525	0.57
	chloroform	492	537	0.56
	ethyl acetate	481	546	0.25
	tetrahydrofuran	483	549	0.28
	acetone	483	567	0.09
	acetonitrile	482	577	0.05
	dimethylformamide	482	567	0.07

Based on the Donor–πbridge−Acceptor framework of BASHY dyes (**Figure 14**), it was expected the observation of significant two-photon-absorption phenomena.[135,145–148] Hence, the two-photon-absorption spectra and cross sections (σ_2) for dyes **81a,e** and **83a,b** were measured (**Chart 11A** and **Table 7**). Strong two-photon-absorption bands with maxima between ca. 900 and 1000 nm were observed and two-photon-absorption cross sections reached values of almost 300 GM for dye **81e** and ca. 200 GM for the other three BASHYs (**81a** and **83a,b**). These values are larger than observed for comparable push−pull dyes such as NBD fluorophores,[138] which absorb and emit in the same spectral region as BASHYs (**Table 5**).

The two-photon excitation (2PE) led to the population of the lowest excited singlet state, resulting in the observation of the same fluorescence as observed in conventional one-photon spectroscopy (**Chart 11B** and **Table 7**)

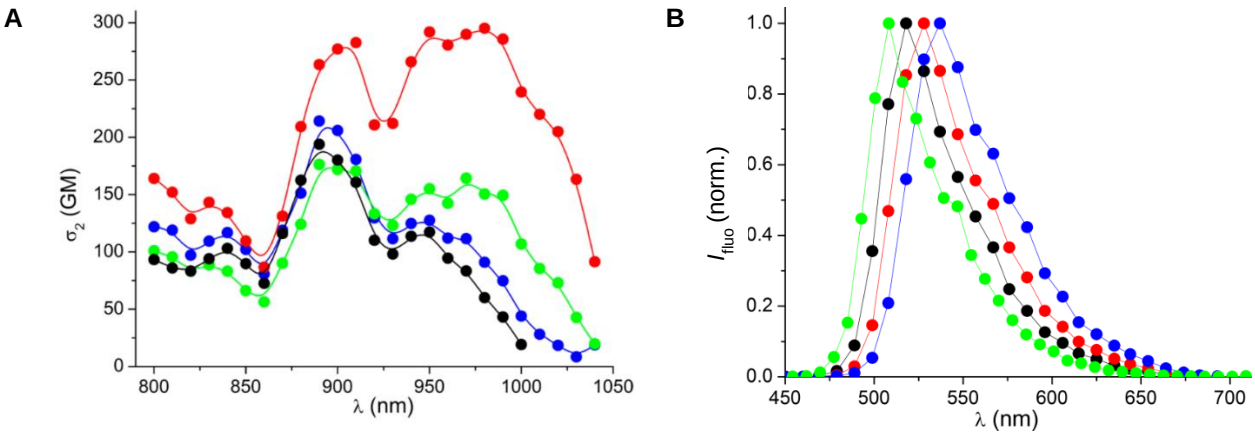

Chart 11 – A: Two-photon absorption spectra of the dyes **81a** (black), **83a** (blue), **83b** (green), and **81e** (red) in air-equilibrated toluene; B: Fluorescence spectra of **81a** (green), **83a** (black), **83b** (red), **81e** (blue) upon two-photon excitation at 960 nm in toluene.

Table 7 – Photophysical Data Related to Two-Photon Absorption of **81a,e** and **83a,b** in toluene.

	Two-photon process	
	σ_2 (GM)	**λ_{fluo}^{2PE} (nm)**
BASHY 81a	890 nm (194), 950 nm (117)	508
BASHY 83a	890 nm (214), 950 nm (128)	518
BASHY 83b	890 nm (176), 970 nm (164)	528
BASHY 81e	910 nm (283), 980 nm (295)	537

III.2.3 Highly efficient ETCs based on the BASHY platform

ETCs take advantage of the photophysical properties of donor and acceptor dyes to allow an efficient energy-transfer communication between both entities through-bound and/or through-space mechanisms. This approach promotes the photophysical improvement of dyes, such as increased pseudo Stokes shifts and efficient light absorption/emission (*e.g.* high brightness).[130,149–153] The enhancement of these characteristics is important for the successful application of dyes in bio-relevant contexts,[108] therefore, ETCs have found extensive use for sensing,[130,153,154] in fluorescence microscopy,[153,155–157] for lasing applications,[158,159] in multicolor labeling[160] and for theranostic logic devices.[161,162]

In general, the assembly between donor and acceptor linkage is made *via* metal-catalyzed coupling reactions (*e.g.* Pd-catalyzed Sonogashira coupling, Cu-catalyzed click reaction). However, these methodologies require laborious purification protocols, since traces of the metal catalyst in the final product may cause undesired fluorescence quenching. Hence, the development of a metal-free and straightforward approach for the construction of ETCs continues to be a goal for the scientific community, since it will expand the scope of ETCs.

Therefore, it was envisioned that the modular synthesis applied for the construction of BASHYs could be used in the development of novel highly efficient ETCs. With this idea in mind a novel ETC BASHY-BODIPY **85** was prepared from the condensation of Schiff base ligand **80a** with a boronate-BODIPY **84** (**Scheme 33**, see also **section IV.2.1**).

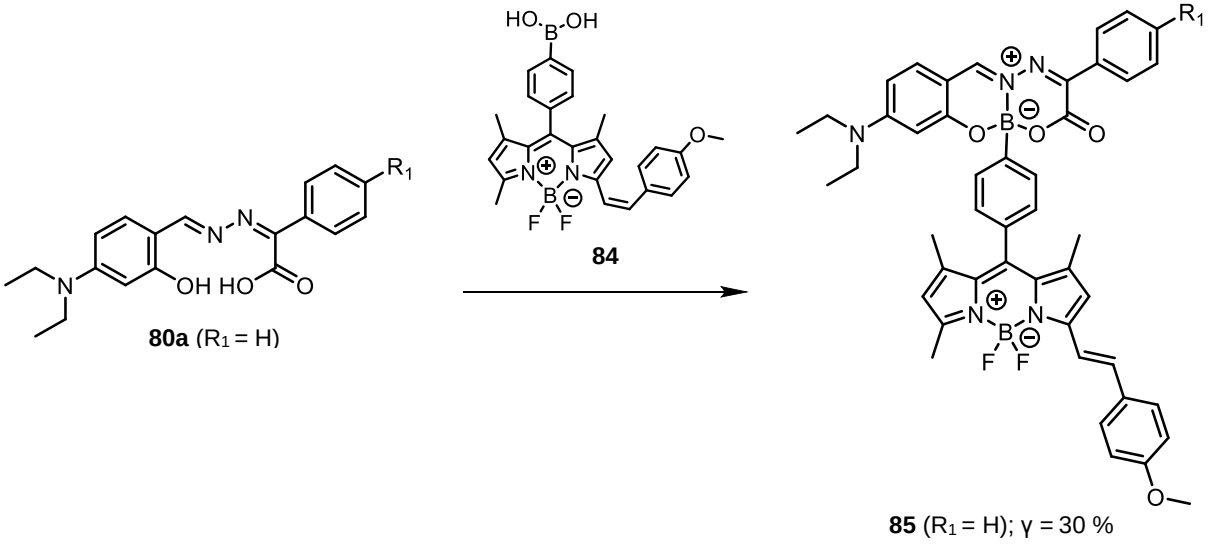

80a (R_1 = H) **84** **85** (R_1 = H); γ = 30 %

Scheme 33 – Synthesis of ETC BASHY-BODIPY **85** (CH_3CN, 80 ºC, 2 h, 30 %).

BASHY-BODIPY **85** has a UV/vis absorption spectrum with a broad band at 473 nm (ε = 52000 $M^{-1}.cm^{-1}$) corresponding to the BASHY skeleton and a more narrow peak at 572 nm (ε = 74000 $M^{-1}.cm^{-1}$), which is characteristic for the styryl-BODIPY chromophore[117] (**Chart 12A,B**; BASHY **81a** and pinacolate derivative of bodipy **84**, were used as models). The presence of both chromophores UV/vis bands, clearly indicates that the different dyes are non-conjugated. The selective excitation of each chromophore in ETC **85** is possible since the absorption spectra of the BASHY moiety only overlaps with the one from stryryl-BODIPY between 410 – 490 nm, in which the absorbance of the bodipy chromophore is ≤ 5 % of the maximum (572 nm) (**Chart 12B,** see also **section IV.2.2**).

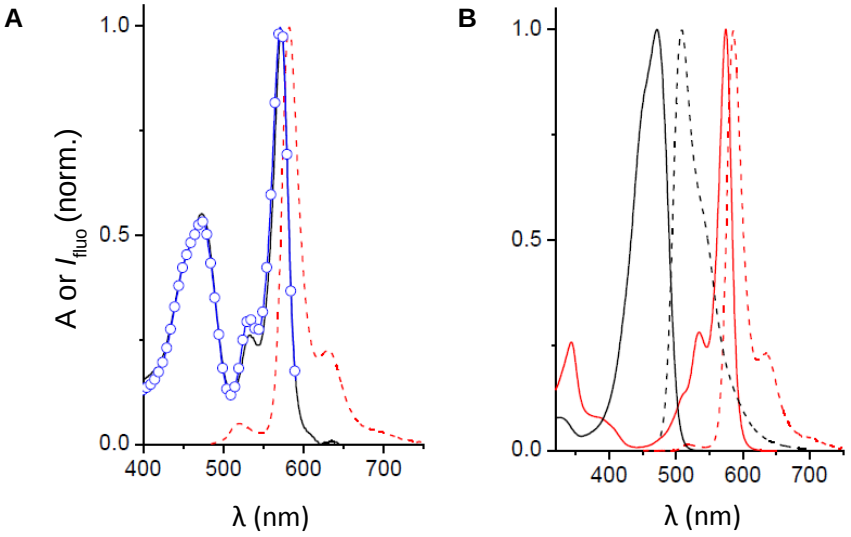

Chart 12 – (A) UV/vis-absorption spectrum (black solid line) and corrected fluorescence spectrum (red dashed line; excitation at 473 nm) of ETC **85** in air-equilibrated toluene. In blue the corrected excitation spectrum, monitoring the BODIPY emission (at 615 nm), is shown. (B) UV/vis-absorption (solid lines) and corrected fluorescence spectra (dashed lines) of the model chromophores used (pinacolate derivative of **84** (red) and BASHY **81a** (black) in air-equilibrated toluene.

The selective excitation of ECT **85** into the BODIPY absorption band (λ_{exc} > 520 nm) promoted the typical orange emission of this chromophore at a maximum of 582 nm with a high quantum yield of Φ_{fluo}= 0.76. Since this value is similar with the one of the individual Bodipy chromophore (pinacolate derivative of **84**, Φ_{fluo}= 0.78), it was concluded that there was no significant through-space fluorescence quenching of the Bodipy chromophore by the BASHY moiety. Moreover, the selective excitation of the BASHY chromophore at 473 nm yielded a low BASHY fluorescence (at a maximum around 508 nm), though it was observed a very dominant Bodipy emission (ratio I_{582} / I_{508} ca. 20) (**Chart 12A**). The strong quenching of the BASHY fluorescence (model chromophore **81a**,

Φ_{fluo} = 0.60) suggests a virtually quantitative energy transfer (Φ_{ET} > 95 %) from the chromophore BASHY to BODIPY fluorophore (**Scheme 34)**.

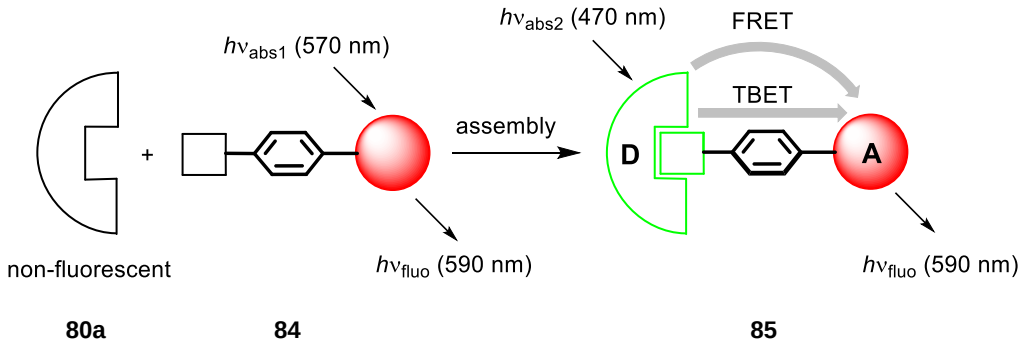

Scheme 34 – Assembly of ETC **85** and the energy transfer mechanisms (TBET and FRET) involved.

Due to the non-planarity and rigidity of the ETC **85** (see an optimized structure in **Figure 17,** see also **section IV.2.3.2**) and the proximity of both chromophores that are linked by a phenylene spacer, the operation of through-bond energy transfer (TBET) was proposed (**Scheme 34)**. TBET is generally observed for ETC architectures, in which donor and acceptor are connected by an unsaturated linker and the whole system is non-planar due to steric hindrance.[149,154] However, it was observed in the DFT calculations that the orbital overlap at the chromophore-linker connection is close to zero, due to the perpendicular orientation assumed by the linker in comparison with both chromophore planes (**Figure 17**). This observation excludes Dexter exchange energy transfer[163,164] as discussed for a series of ETC with similar geometrical conditions.[150,165] Nevertheless, TBET should not be excluded since nowadays it is known that Dexter exchange energy transfer is not the only contributor for TBET mechanism.

It was also hypothesized that Förster resonance energy transfer (FRET)[164,166] could be operating in parallel with TBET[154] (**Scheme 34**) due to several factors, such as the considerable spectral overlap between the efficient donor emission and the strong acceptor absorption (see **Chart 12B**, dashed black and solid red spectra), the non-perpendicular orientation of the donor and acceptor transition dipole moments, and the short distance between both chromophores.

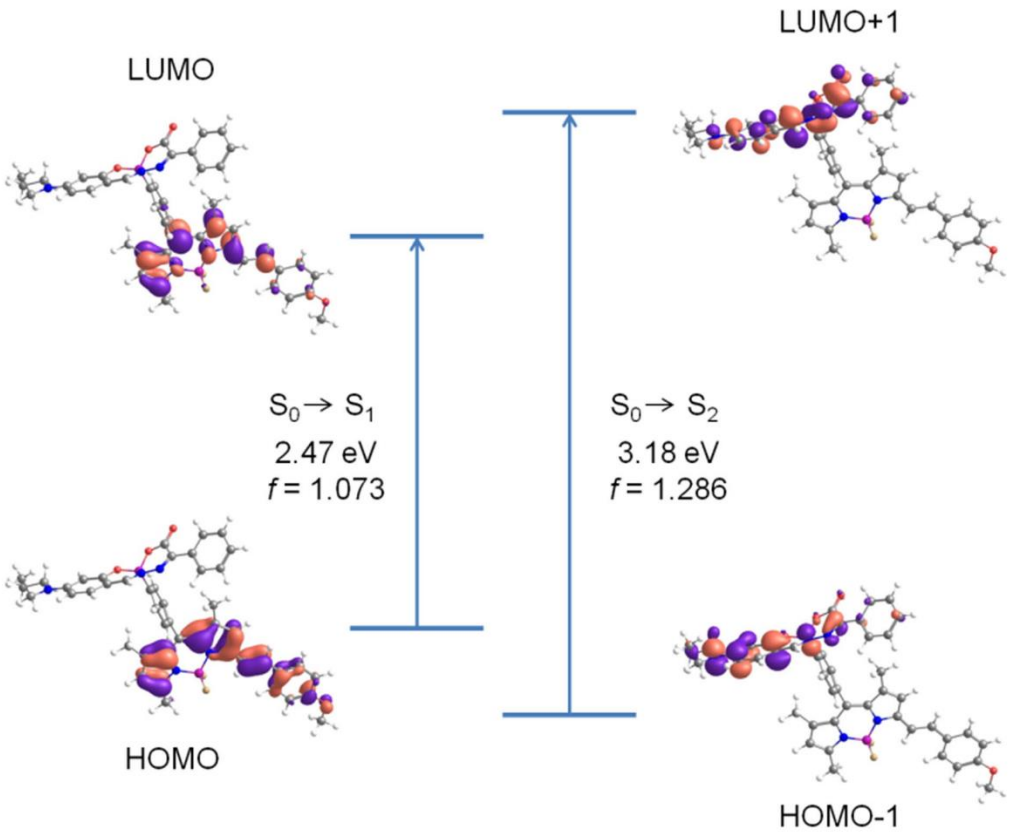

Figure 17 – Frontier orbitals that are involved in the first two electronic transitions in ECT **85**.

As a consequence of being incorporated in the ETC **85**, both chromophores have in general their photophysical properties improved. Excitation of BODIPY chromophore can now be achieved between 410 – 490 nm, taking advantage of BASHY moiety as an antenna, the pseudo Stokes shift have increased from 10 nm to ca. 120 nm (in absolute energy units: 330 cm^{-1} to 3990 cm^{-1}) and the fluorescence signal, obtained on excitation of BASHY, can be further red-shifted in comparison to the individual BASHY chromophore. The usefulness of BASHY-BODIPY **85** in bioimaging applications was then evaluated as described in **section III.2.5.2**.

The next step was the construction of another ETC, in which the BASHY chromophore would play the acceptor role, showing this way the photophysical flexibility of our approach. With this idea in mind, ECT BASHY-coumarin **87** was proposed based on photophysical rationales and previous reports of other coumarin-containing ETC architectures.[159,167–169] The construction of ETC **87** was achieved in an analogous way as **85**, by condensation of Schiff base ligand **80a** with a boronate-coumarin **86**. The preparation of BASHY-coumarin **87** allowed a compact assembly between both fluorophores, which are just separated by a single σ-bond (**Scheme 35,** see also **section IV.2.1**).

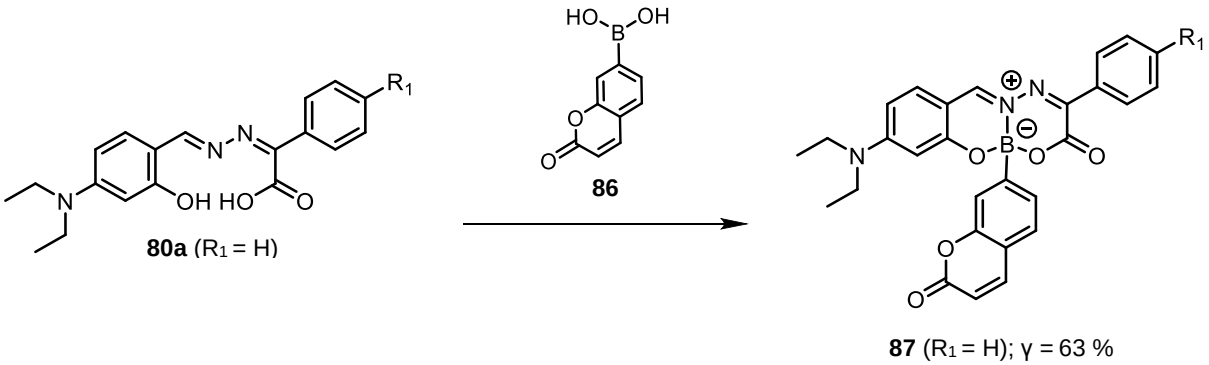

Scheme 35 – Construction of ETC BASHY-coumarin **87** (CH_3CN, 80 ºC, 2 h, 63 %).

The photophysical properties of ECT **87** were then evaluated in chloroform, due to solubility issues. UV/vis-absorption spectrum of the ETC **87** features both chromophores absorptions bands, coumarin with a maximum at 282 nm and 320 nm (ε = 20600 $M^{-1}cm^{-1}$ and 13700 $M^{-1}cm^{-1}$, respectively) and BASHY with a band at 479 nm (ε = 71000 $M^{-1}cm^{-1}$). The selective excitation of ETC **87** into the BASHY absorption band promoted the characteristic strong green fluorescence ($\Phi_{fluo,max}$ = 519 nm in chloroform) of this chromophore with a quantum yield of 0.69. On excitation into the coumarin band at 320 nm, where both chromophores absorb, only BASHY fluorescence was observed (Φ_{fluo} = 0.74). This observation suggests a practically quantitative energy-transfer process (Φ_{ET} > 95 %) from the chromophore coumarin to BASHY fluorophore (**Chart 13**).

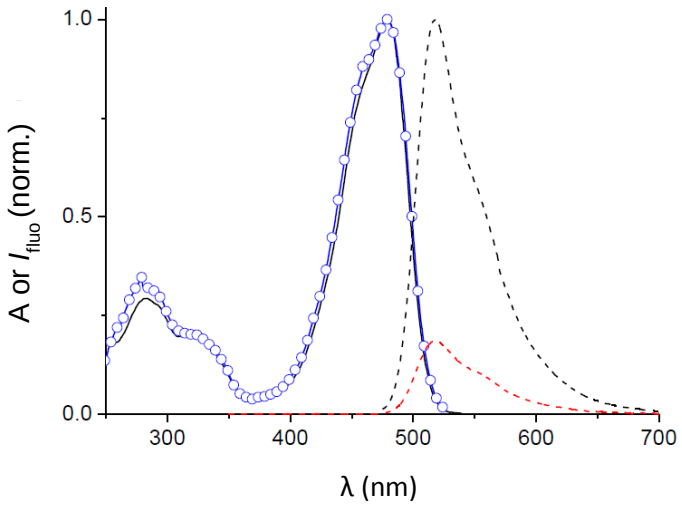

Chart 13 – UV/vis-absorption (black solid line) and corrected fluorescence spectra for excitation at 320 nm (red dashed line) and 470 nm (black dashed line) of ETC **87** in air-equilibrated chloroform. Note that the red emission spectrum is less intense due to the smaller light absorption at 320 nm as compared to 470 nm. The blue spectrum corresponds to the corrected excitation spectrum, monitoring the BASHY emission at 550 nm.

The presence of the coumarin antenna in ETC **87** (**Scheme 36**) leads to an increased pseudo Stokes shift of ca. 200 nm versus ca. 50 nm for the direct excitation into the BASHY chromophore absorption band (11980 cm^{-1} versus 1870 cm^{-1} in absolute energy).

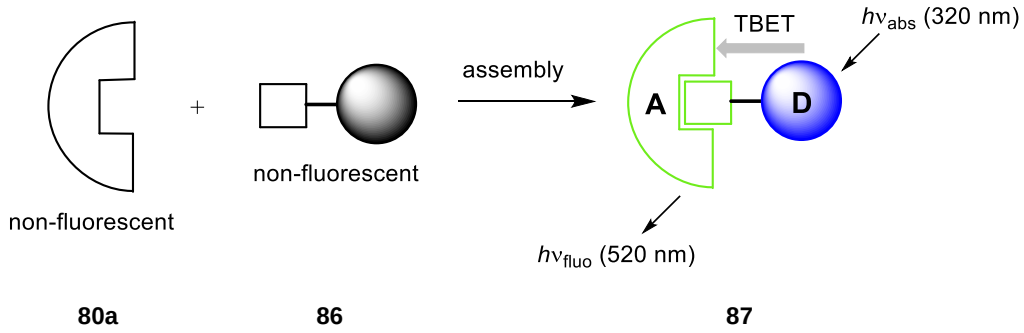

Scheme 36 – Assembly of ETC **87** and the energy transfer mechanism (TBET) involved.

Regarding the energy transfer mechanisms involved in ETC **87**, FRET in principle could be excluded due to observation that boronate-coumarin **86** was not fluorescent,[170] however the formation of **87** triggers the umpolung of the electron-accepting $B(OH)_2$ into an electron-donating $B^{-}O_2N$, thereby possibly activating the fluorescence of the coumarin itself. In any case, given the non-fluorescent nature of the model boronate-coumarin **86**, the FRET mechanism cannot be conclusively discussed.

Therefore, it is reasonable to propose that TBET mechanism is involved in ETC **87**, since both chromophores are at a minimal distance of one single bond (**Scheme 36**). It should be noted that contrary to FRET the TBET mechanism does not require spectral overlap.[149,154]

III.2.4 Selective lipid droplet staining by BASHY dyes

Due to the hydrophobic asymmetric 3D structure of BASHYs and their strong fluorescence in nonpolar environments, it was anticipated that these dyes could be used as selective lysochromic stains for lipid droplets. These lipophilic reservoirs have been recognized as dynamic cellular organelles with a key role in lipid and membrane homeostasis. Anomalous lipid droplet dynamics are in general associated with the pathogenesis of many metabolic disorders, such as diabetes, obesity, atherosclerosis, fatty liver and cancer. Therefore, their labeling became fundamental in order to assess their role on these metabolic disorders.[132,171]

BASHYs **81a,e** were then selected to be incubated in HeLa cells (**Figure 18B**) and to contrast the localization of these dyes, DNA-binding Hoechst 33342 and plasmatic membrane (PM)-selective WGA-Alexa Fluor 633 were employed in a co-staining protocol (**Figure 18A**). It was observed that under the chosen experimental conditions, BASHYs **81a,e** did not compromise the viability of the HeLa cells (**Chart 14,** see also **section IV.2.4.1**).

BASHY dyes **81a,e** were readily internalized by HeLa cells and accumulated at intracellular structures of variable sizes and cellular distribution (**Figure 18B**). Remarkably, these dyes did not partition into structures that displayed a tighter lipid packing, such as the plasmatic membrane,[172] hence they could be used to differentiate between membrane regions with variable packing properties.

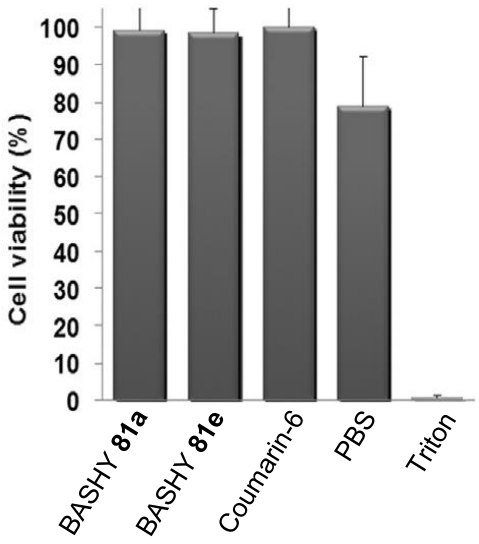

Chart 14 – Cell viability determined by alamarBlue assay 24 h after incubation of HeLa cells with 5 mg.mL^{-1} of dye (**81a,e** or coumarin-6); mean±standard deviation (SD); n=6. PBS and Triton were used as controls.

To confirm the selective staining of lipid droplets by these dyes, BASHYs **81a**,**e** were used in dual color experiments with the archetypal lipid droplet stain Nile red (**Figure 18C,D**).[133,134] The colocalization analysis and determination of Pearson's correlation coefficient (R_r = 0.85 and 0.94 for colocalization between Nile red and dyes **81a**,**e** respectively) revealed the potential of BASHYs as selective lipid droplet labeling agents.

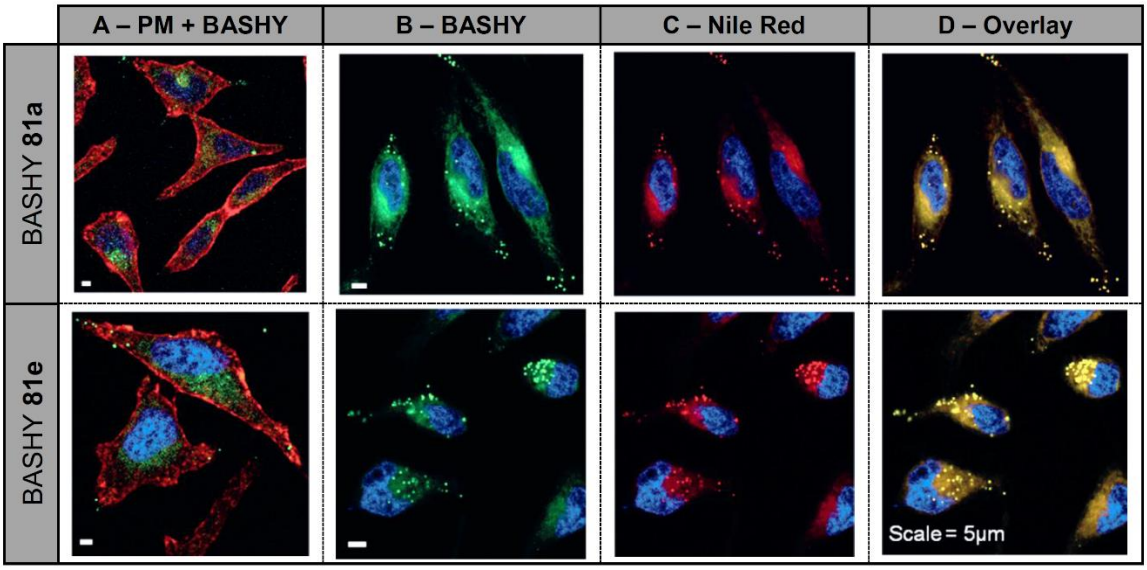

Figure 18 – Confocal fluorescence microscopy images of HeLa cells. A) and B) Labeled with BASHYs **81a,e** (2.5 mgmL^{-1}; green), and A) additionally with WGA-Alexa Fluor 633 (5 mgmL^{-1}; red) as the PM stain, after 10 min of incubation; C) Labeled with Nile red (1 mgmL^{-1}) for lipid droplet staining (red), during 10 min. D) Overlay images of B) and C). Hoechst 33342 (1 mgmL^{-1}) was used for nucleus labeling (blue) in all images.

III.2.5 BASHY-labeled NPs

Polymeric NPs have been recently classified as promising drug-delivery vehicles and its labeling with fluorescent moieties became fundamental in the evaluation of their biophysical properties at the cellular level in confocal microscopy studies. These conjugates may improve our knowledge in the recognition and uptake mechanisms by target cells, and also provide a tool to assess undesired side effects, such as cytotoxicity, bioaccumulation and the triggering of unwanted cellular responses.[173–179]

III.2.5.1 BASHYs 81a,e NPs

The encapsulation of BASHY in the nonpolar environment of PLGA NPs provides additional protection of these dyes from slow hydrolytic degradation, which was observed for free dyes (*e.g.* $t_{1/2}$ ca. 3 h for BASHY **78b** at pH 4.5). For instance, in toluene, BASHYs (*e.g.* **81a**) show practically no degradation over 12 h, so it is expected an analogous stability level for BASHYs, entrapped inside PLGA-NPs.[180,181]

BASHYs **81a,e** and coumarin-6, which is widely used in NPs labeling, were then encapsulated in PLGA-NPs *via* a double emulsion–solvent evaporation methodology (see **section IV.2.4.2**). BASHYs **81a,e** revealed a quantitative entrapment in the NPs, however for coumarin-6, it was observed 10 % of non-entrapped dye (**Chart 15**).

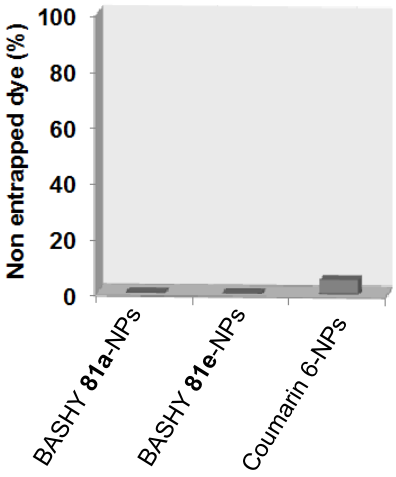

Chart 15 – Amount of dye (**81a,e** or coumarin-6) non-entrapped from (1 mg.mL^{-1}) NP incubation in RPMI cell culture media at 37 °C for 24 h.

Physicochemical properties of BASHY **81a,e**-labeled NPs remain identical to those of unlabeled NPs or coumarin-6 NPs (see **section IV.2.4.2**). BASHY **81a,e**-NPs reveal a

mean diameter ranging from 182 ± 3 to 189 ± 8 nm, which is similar to the mean diameter of 185 ± 7 nm for unloaded PLGA NPs. The narrow particle size distribution (polydispersity index (PdI) obtained for BASHY **81a,e**-labeled NPs ranges from 0.050 ± 0.022 to 0.088 ± 0.034, which is also analogous with the PdI of 0.054 ± 0.018 obtained for unloaded NPs. Another parameter that remains parallel for unloaded and BASHY **81a,e**-NPs is the zeta potential (ZP), which was close to neutrality at pH 7.4 (**Table 8)**.

Table 8 – Physicochemical properties of non-labeled and dye-labeled PLGA NPs. Nanoparticle size (Z-Ave), PdI, and surface charge (ZP), mean ± SD; n=3.

	Z-Ave (nm)	PdI	ZP (mV)
BASHY 81a-NP	182 ± 3	0.088 ± 0.034	- 3.51 ± 0.36
BASHY 81e-NP	182 ± 7	0.072 ± 0.034	- 1.64 ± 0.39
Coumarin-6 NP	189 ± 8	0.050 ± 0.022	- 2.65 ± 0.51
Non-labeled NP	185 ± 7	0.054 ± 0.018	- 1.71 ± 0.51

BASHY **81a,e**-labeled NPs were then compared with coumarin 6-labeled NPs in terms of their leaching from the nanoparticulate polymer matrix in RPMI (Roswell Park Memorial Institute) cell culture media over a period of 24 h at 37 ºC (see **section IV.2.4.2**). The results clearly indicated that there was no undesired leaching from BASHY **81a,e**-labeled NPs, however in the same conditions it was observed the leak of around 30 % of coumarin 6 from the NPs (**Chart 16**).

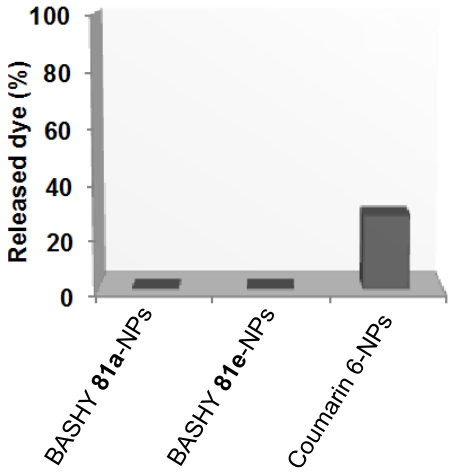

Chart 16 – Amount of dye (**81a,e** or coumarin-6) released from (1 mg.mL^{-1}) NP incubation in RPMI cell culture media at 37 °C for 24 h.

Due to the polarity-dependent fluorescence of BASHYs, the nonpolar microenvironment provided by the polymer matrix makes these BASHY **81a,e**-NPs rather brightly fluorescent (**Figure 19B**). These dye-labeled NPs have lost their environmental polarity sensitivity, but can now be explored as fluorescent tags in confocal microscopy. BMDCs were then selected by us as biological models, due to their potential in the development of prophylactic and therapeutic vaccines.[182]

BASHY **81a,e**-labeled NPs were successfully internalized on BMDCs after 18 h of incubation time and the internalization process for both dye-labeled NPs was unequivocally demonstrated by Z-stack confocal microscopy images, which clearly provided evidence of intracellular localization and excluded external adsorption onto the plasmatic membrane (**Figure 19C**, see also **section IV.2.4.2**)

The microscopic images of the BMDCs incubated with the unsupported BASHYs **81a,e** showed qualitatively the same fluorescence patterns (**Figure 19A**). Also relevant is the fact that BASHY **81a,e**-NPs revealed low levels of cytotoxicity, as shown by the cell viability (> 90 %), even 24 h after incubation (see in **section IV.2.4.2**, **Chart 44**).

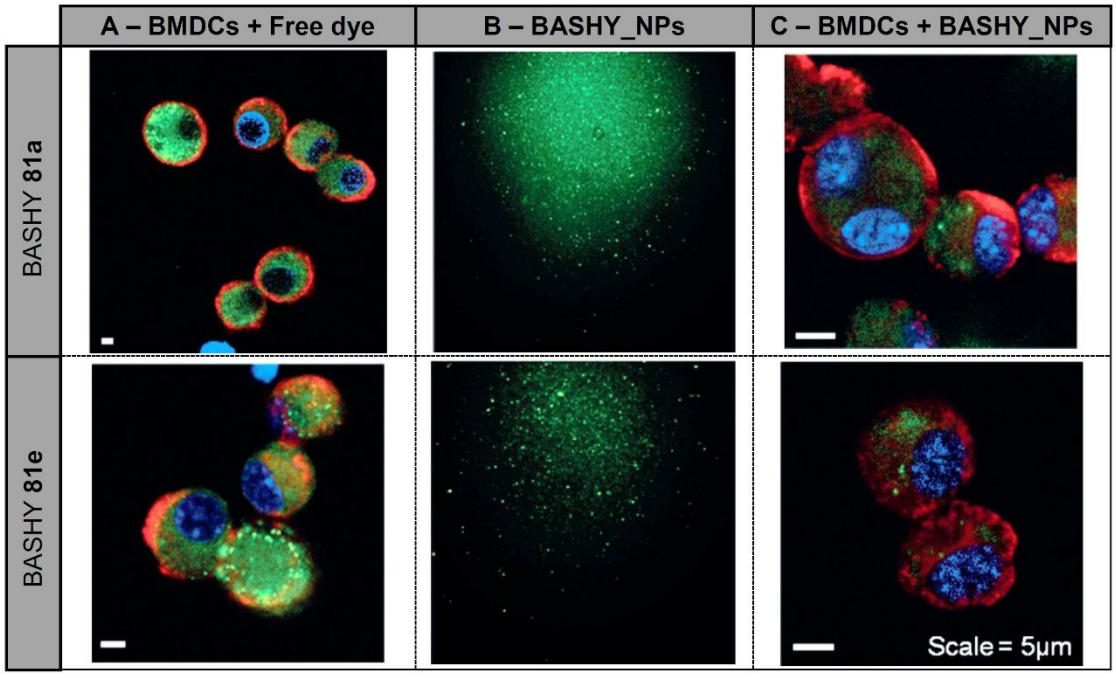

Figure 19 – A) Confocal microscopy images obtained after incubation of BMDCs with BASHYs **81a,e** (2.5 mg.mL^{-1}; green) and C) BASHY-labeled PLGA NPs (0.5 mg.mL^{-1}; green), for 10 min and 18 h, respectively. The plasma membrane (PM) was stained with WGA Alexa Fluor 633 (5 mg.mL^{-1}; red), whereas Hoechst 33342 (1 mg.mL^{-1}) was used for nucleus labeling (blue), after 10 min of incubation. B) Fluorescence microscopy images of BASHY-labeled PLGA NPs.

III.2.5.2 ETC BASHY-BODIPY 85 NPs

Looking on the literature, we observed that ETCs have been useful for bioimaging applications,[155,156,183] therefore we decided to encapsulate ETC **85** in the hydrophobic environment of polymeric PLGA/PVA [poly(lactide-co-glycolide)/poly(vinyl alcohol)] NPs, by using a double emulsion solvent evaporation method (see **section IV.2.4.3**).[184] Physicochemical properties of ECT **85**-labeled NPs revealed a mean size of 219 ± 4 nm, a PdI of 0.112 ± 0.005 and a ZP of - 0.88 ± 0.15.

ETC **85**-NPs were then incubated with BMDCs, for 1, 3, and 18 h in order to evaluate their internalization and their impact on cell viability by flow cytometry. At 1 and 3 h, the internalization of ETC **85**-NPs in BMDCs was 63 and 88 %, being lower than observed for the free ETC **85**. However at the maximum time of incubation (18 h), the internalization of ETC **85**-NPs in BMDCs was almost quantitative (98 – 100 %), being similar to the value obtained for the free ETC **85** (**Chart 17A**). This time-dependent internalization profile was expected for dye-labeled NPs, due to the nanoparticulate nature of this carrier versus the molecular structure of the free dye. In fact, median fluorescence intensity (MFI) values evidence that ETC **85**-NPs were internalized at higher extent than the free ETC **85** (**Chart 17B,** see also **section IV.2.4.3**).

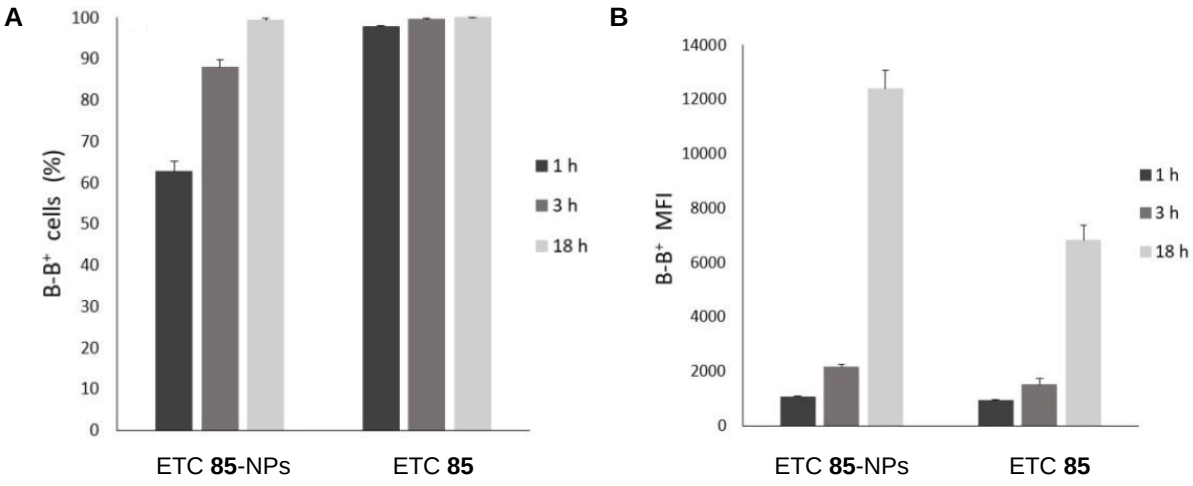

Chart 17 – Internalization of free ETC **85** (2.5 µg.mL^{-1}) and ETC **85**-NPs (0.5 mg.mL^{-1}) by BMDCs, after 1, 3 and 18 h of incubation, expressed by (A) percentage and (B) MFI of positive cells in the population sorted by the flow cytometer (mean ± SD; N = 3; n = 2).

Also relevant is the fact that both free ETC **85** and ETC **85**-loaded NPs did not have a negative impact on the viability of BMDCs up to 18 h of incubation, as determined by the propidium iodide (PI) assay (**Chart 18**, see also **section IV.2.4.3**).

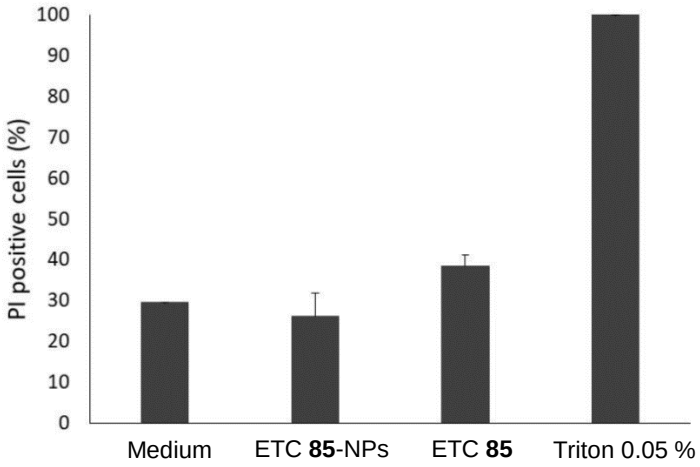

Chart 18 – Impact of free ETC **85** and ETC **85**-NPs on BMDCs viability. Dead cells were determined with the PI assay, after 18 h of incubation with ETC **85** (2.5 µg.mL^{-1}) and ETC **85**-NPs (0.5 mg.mL^{-1}), being expressed as PI positive cells (%) in the population sorted by flow cytometry (mean ± SD; N = 3; n = 2).

Moreover, confocal fluorescence microscopy analysis also corroborates the successful internalization of ETC **85**-labeled NPs by BMDCs after 2, 4 and 10 h of incubation. ETC **85**-loaded NPs were selectively excited at 488 nm (Argon ion laser) and a bright fluorescence signal was detected at 580 nm (**Figure 20,** see **section IV.2.4.3**).

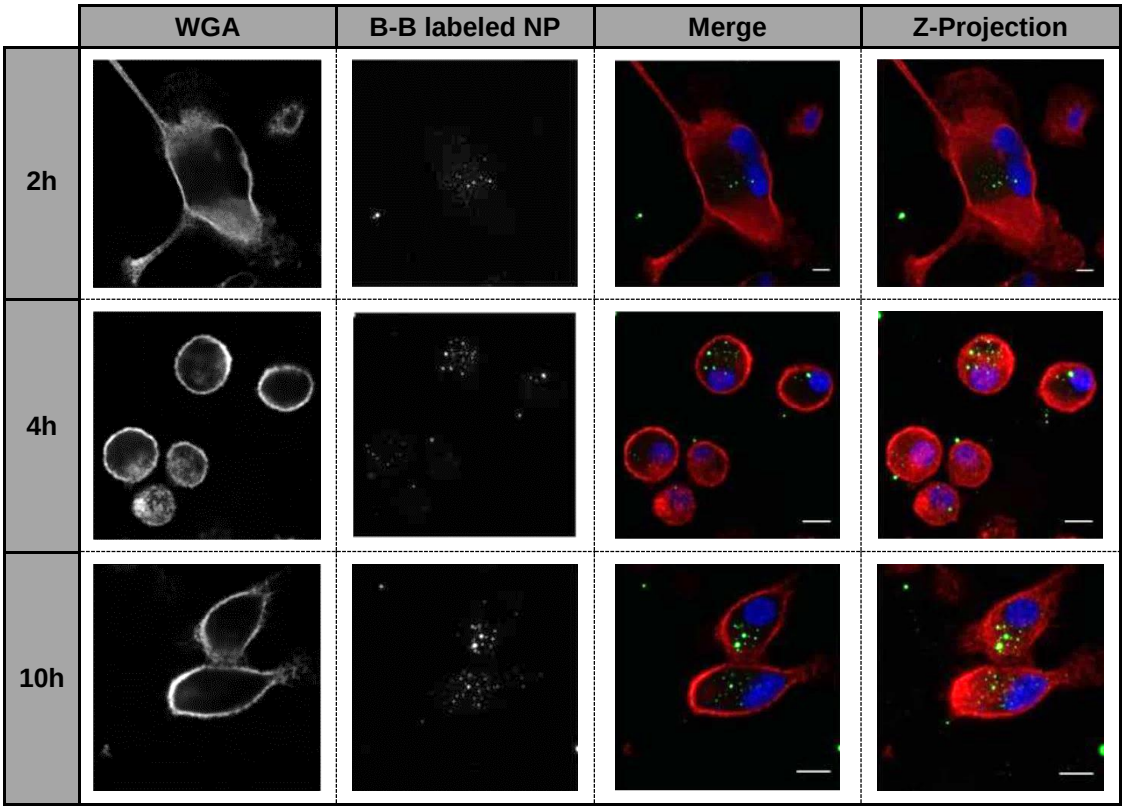

Figure 20 – Confocal microscopy images obtained after incubation of BMDCs with ETC **85**-NPs (0.5 mg.mL^{-1}, green), for 2, 4 and 10 hours. Nuclei and plasma membrane were stained with Hoechst®33342 (2 µg.mL^{-1}, blue) and WGA-Alexa Fluor®633 (5 µg mL^{-1}, red), respectively. Representative images of two independent experiments are shown. Scale bars = 10 µm.

III.2.6 Bioconjugation of Annexin V with BASHY for targeted detection of apoptotic cells

The design of functionalized dyes for site-selective protein modification approaches is of paramount importance, since it will allow the scientific community to gain more knowledge on several important biological processes (*e.g.* apoptosis). However, the construction of such fluorescent bioconjugates is an intricate process due to fluorescence quenching and/or loss of biomolecule's specific activity.

As observed in **section III.2.2**, the photophysical properties of BASHY dyes are in general only determined by the electronic properties of the ligand backbone and the boronic acid-derived aromatic moiety only has a minor influence. Consequently, it was envisioned that the modular construction of BASHY dyes could be easily fine-tuned for site-selective bioconjugation with Annexin V without compromising either the protein's function or the fluorescent properties of these dyes.

Annexin V is a protein used as an early marker of the apoptotic process, since it binds to a phospholipid membrane component (phosphatidylserine), which is translocated from the inner to the outer layer of the plasmatic membrane during apoptosis.[185–187] There are already on the market, kits with heterogeneous mixtures of labelled dye-Annexin V for detection of apoptosis, however the non-site-specific incorporation of fluorescent dyes into protein biomarkers can lead to a significant reduction in the protein's binding ability.

Herein is proposed the construction of a homogenous fluorescent Annexin V-BASHY **92** *via* a SPAAC reaction between BASHY-azide **89** and dibenzocyclooctyne (DBCO)-tagged Annexin V **91** (**Scheme 37** and **Scheme 38**).

This quest started with the synthesis of BASHY **88** which has a carboxylic acid function and was prepared from ligand **80a** in 97 % isolated yield. This complex **88** smoothly underwent *O*-(Benzotriazol-1-yl)-*N,N,N′,N′*-tetramethyluronium tetrafluoroborate (TBTU)-mediated amidation with 2-azidoethylamine to afford BASHY-azide **89** in excellent yield (95 %). Remarkably, the functionalized dyes **88** and **89** retained the photophysical properties of unmodified model BASHY **81a,** including high quantum yields, narrow absorption and emission bands, and high molar absorption coefficients (**Table 9**, see also **section IV.2.1**).

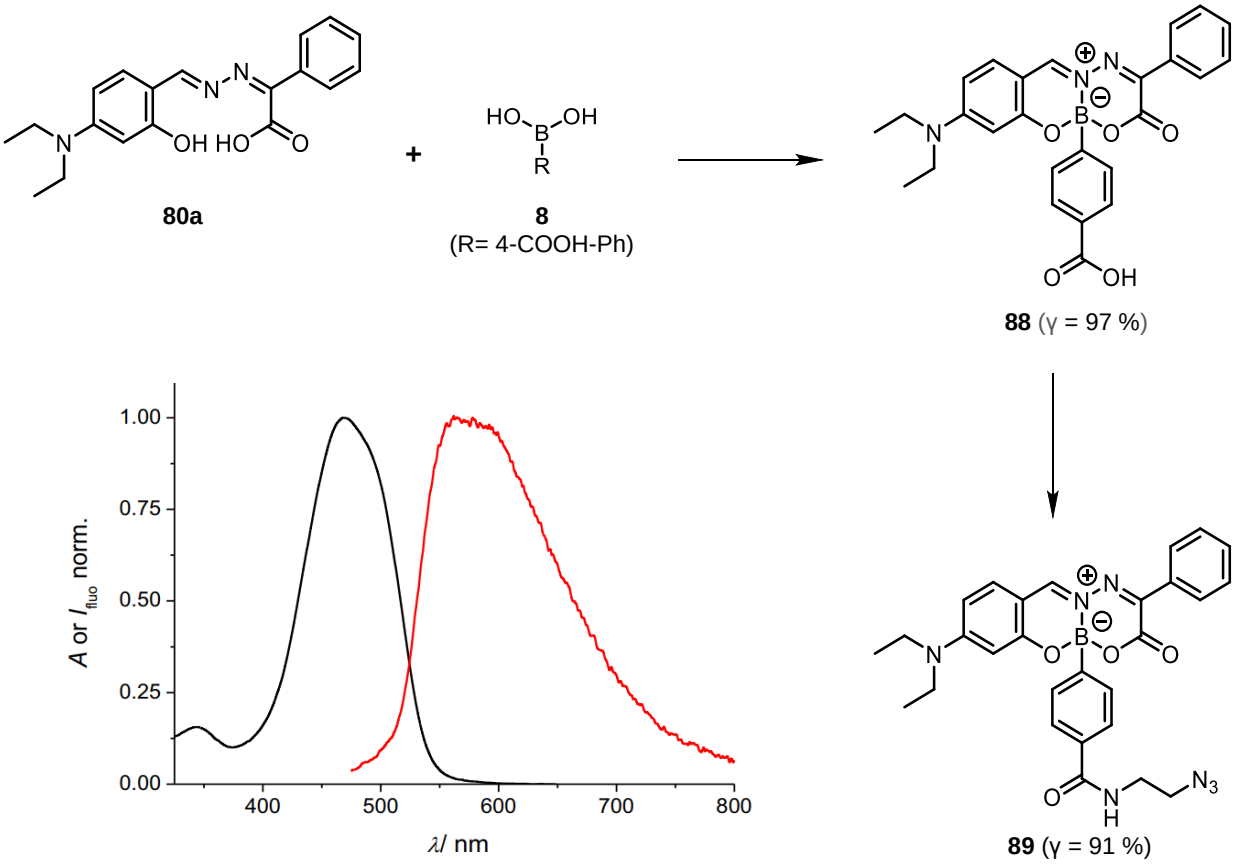

Scheme 37 – One pot-assembly of BASHY **88** (CH_3CN, 80 ºC, 2 h, 97 %) and post-functionalization with a bioorthogonal azide handle to prepare BASHY **89** (**(**ET_3N, TBTU, DMF, RT, 18 h, 91 %); Normalized UV/Vis absorption (black) and fluorescence (grey) spectra of BASHY **89** in 5 % DMSO / NaPi (50 mM, pH 6)

Table 9 – Photophysical data of BASHY dyes **88** and **89** in air-equilibrated solution.

	Solvent	λ_{abs} (nm) [a]	λ_{fluo} (nm) [b]	Φ_{fluo} [c]	τ_{fluo} (ns) [d]	$\varepsilon_{abs,max}$ ($M^{-1}.cm^{-1}$) [e]
BASHY **88**	CH_3CN	471	537	0.06	0.36	58600
	$CHCl_3$	477	516	0.58	2.92	61200
BASHY **89**	CH_3CN	471	541	0.07	0.58	58500
	$CHCl_3$	478	519	0.60	3.39	56500

[a] Longest-wavelength absorption maximum; **[b]** Fluorescence maximum;
[c] Fluorescence quantum yield; **[d]** Fluorescence lifetime; **[e]** Molar extinction coefficient

The cytotoxicity of BASHY-azide **89** was then evaluated against HeLa and HEK 293T cell lines at different concentrations 1, 5 and 10 µg/mL. Similar to what was previously observed for BASHYs **81a**,**e** (**Chart 14**), the viability of the cell lines tested was not compromised after 24 h of incubation at 37 ºC (**Chart 19**, see also **section IV.2.4.4**).

Then, with the BASHY-azide **89** in hand, it was necessary to install a strained alkyne counterpart in Annexin V. This protein displays a free, hindered cysteine at position 316, which has been shown to be reactive towards a variety of different alkylating and Michael acceptor reagents including maleimides,[188–190] so a commercially available dibenzocyclooctyne-maleimide (mal-DBCO, **90**) that contains a reactive maleimide and a strained-cyclooctyne ring, was used to construct DBCO-tagged Annexin V **91**. Full conversion into **91** was observed when using 25 equivalents of **90** in buffer (TrisHCl, 20 mM. pH 8) for 5 days at RT (**Scheme 38**, see also **section IV.2.1**).

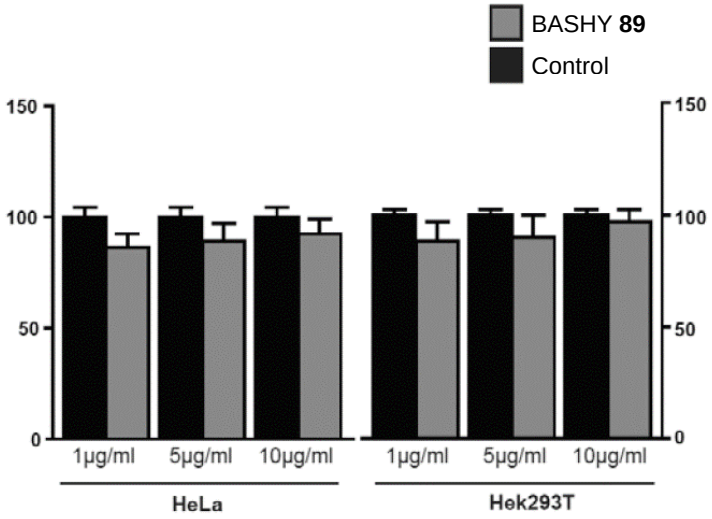

Chart 19 – HeLa and Hek293T cells viability after treatment with 1 µg/mL, 5 µg/mL and 10 µg/mL of BASHY **89** for 24 h compared with the control treatment (medium + vehicle (DMF)). The results correspond to 3 biological replicates (each with 3 technical replicates) and are shown as percentage of control (mean + SD). Differences were tested with a Mann-Whitney test that indicated no significant differences between cells treated with BASHY **89** and the control.

Size-exclusion chromatography was then used to purify the DBCO-tagged Annexin V **91** and a single protein adduct was detected using liquid-chromatography mass spectrometry (LC-MS) analysis. Upon tryptic digestion and analysis using LC-MS/MS, it was confirmed that Cys316 is the primary site of modification (**Scheme 38,** see also **section IV.2.1**).

Afterwards, SPAAC reaction between DBCO-Annexin V **91** and BASHY-azide **89** was achieved in sodium phosphate buffer (NaPi, 50 mM, pH 6), 6 h at RT. Pleasantly, after purification, a homogenous construct Annexin V-BASHY **92** was identified by LC-MS analysis (**Scheme 38,** see also **section IV.2.1**). The secondary structure protein content of the conjugates Annexin V **91** and **92** was analyzed by circular dichroism (CD) showing no significant differences from naked Annexin V (**Chart 20**, see also **section IV.2.1**).

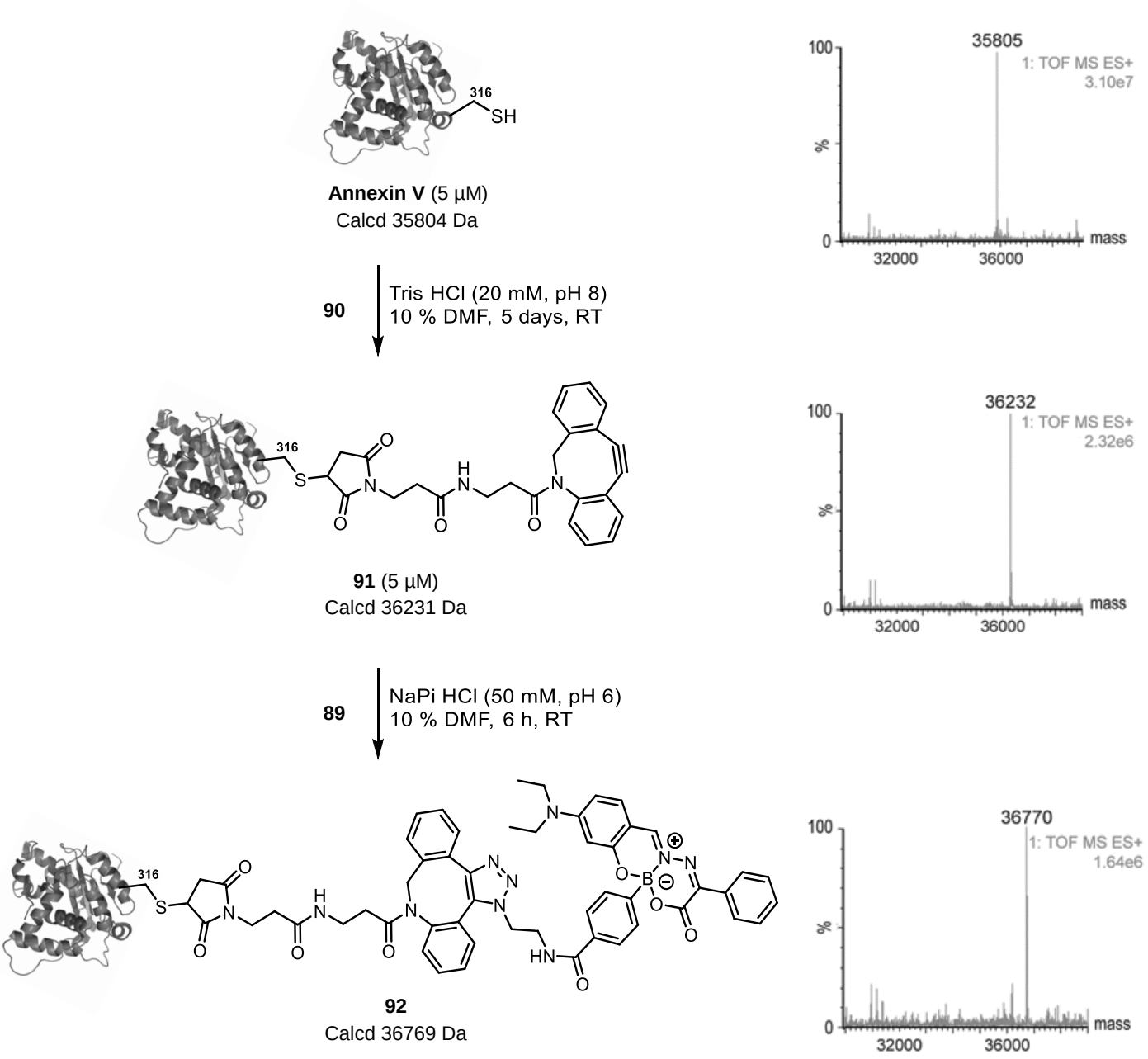

Scheme 38 – LEFT: Reaction of Annexin V (5.0 µM) with 25 equivalents of mal-DBCO **90** in TrisHCl buffer (20 mM, pH 8) and 10 % DMF, during five days at RT. Reaction of purified DBCO-Annexin V **91** with 5 equiv. of BASHY **89** in NaPi buffer (50 mM, pH 6) and 10 % DMF during 6 h at RT to construct Annexin V-BASHY **92**; RIGHT: Deconvoluted mass spectra of each conjugate.

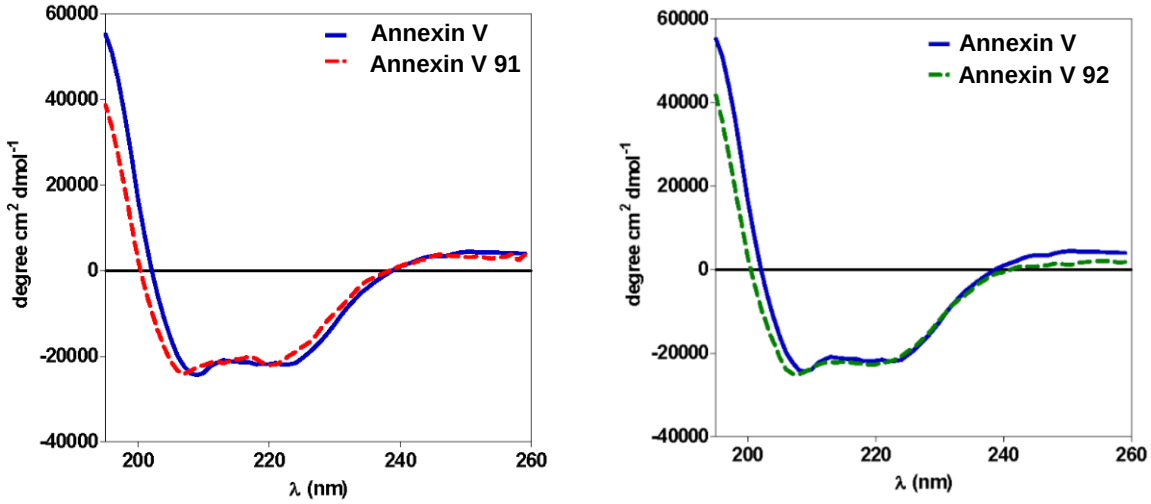

Chart 20 – CD spectra of Annexin V, Annexin V-mal-DBCO **91** and Annexin V-BASHY **92** (0.5 µM) in buffer (20 mM NaPi, pH 7.4).

In order to have a basis of comparison, Annexin V was also labelled at cysteine 316 with sulfo-cyanine5 dye (Annexin V-Cy5 **93**), since this conjugate is routinely used for biological imaging of apoptosis.[191–193] This conjugate **93** was used as a specific positive control, since the labeling of Annexin V with sulfo-cyanine5 is usually *via* a non-selective lysine bioconjugation. The non-selective bioconjugation of Annexin V was also covered with the preparation of a heterogeneous Annexin V-FITC conjugate **94** (**Figure 21**, see also **section IV.2.1**).[187]

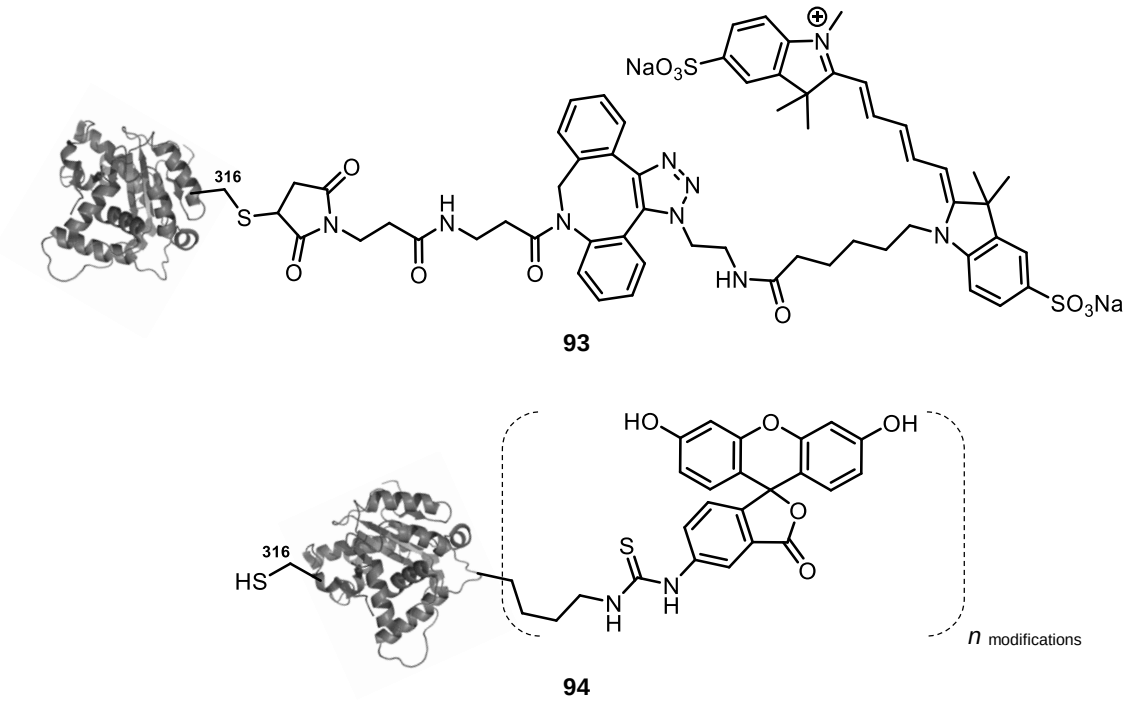

93

94

Figure 21 – Structures of homogenous Annexin V-Cy5 **93** and heterogeneous Annexin V-FITC **94**.

Annexin V fluorescent conjugates **92** – **94** were then evaluated in the bioimaging of apoptotic cells using confocal microscopy.[191] HeLa cells were incubated with either actinomycin D (apoptosis inducer) or DMSO (negative control)[187] for 6 h followed by incubation with Annexin V-BASHY **92** for 20 minutes. Finally, cells were fixed and the nuclei was stained with Hoechst 33342 (**Figure 22,** see also **section IV.2.4.4**). Following the same methodology, homogenous Annexin V-Cy5 **93** and the heterogenous Annexin V-FITC **94** were also evaluated in separate assays for their specificity to bind phosphatidylserine in apoptotic cells (see **section IV.2.4.4**, **Figure 36** and **Figure 37**).

Pleasingly, Annexin V-BASHY **92** was successfully able to target apoptotic cells (**Figure 22**) with a similar labeling efficiency of homogeneous Annexin V-Cy5 **93** (**Chart 21**). Moreover, in a blocking experiment where cells were incubated with non-fluorescent DBCO-Annexin V **91** before addition of Annexin V-BASHY **92**, we observed a significant decrease in fluorescence, which demonstrates the specificity of the BASHY-tagged biomarker (see **section IV.2.4.4**, **Figure 35**).

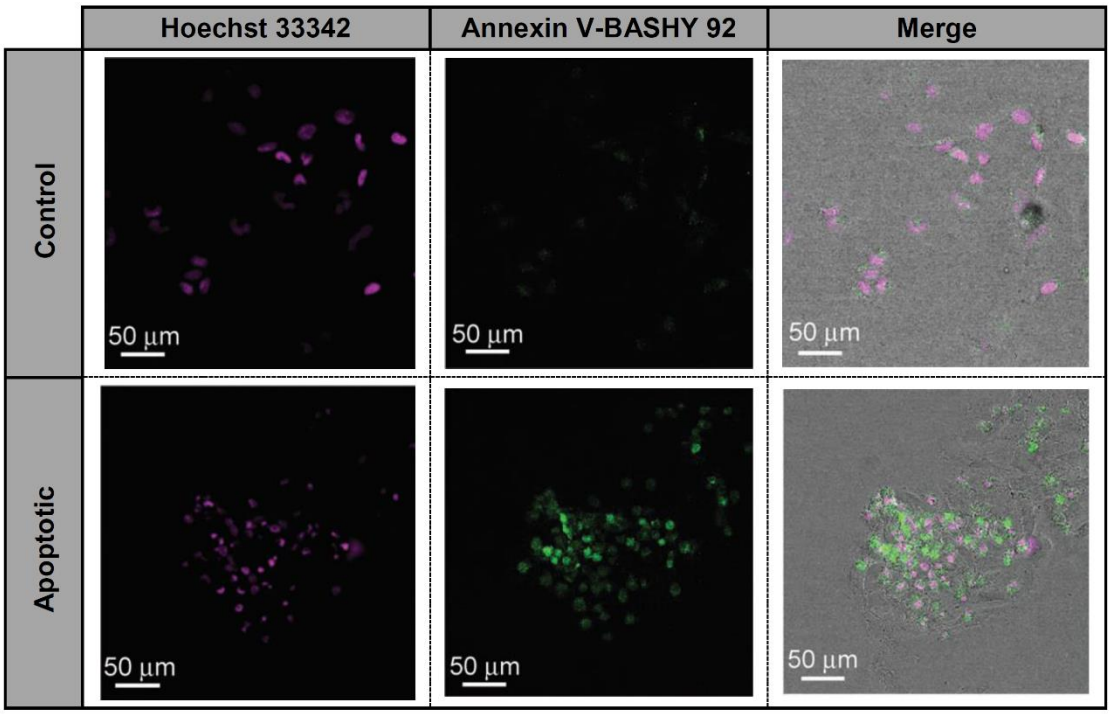

Figure 22 – Confocal microscopy images of HeLa cells treated with 1 mM actinomycin D for 6 h to induce apoptosis or the vehicle control (0.1 % DMSO) followed by incubation with 1 µg.ml^{-1} of Annexin V-BASHY **92** for 20 min. Annexin V-BASHY **92** (green), nuclear Hoechst staining (purple).

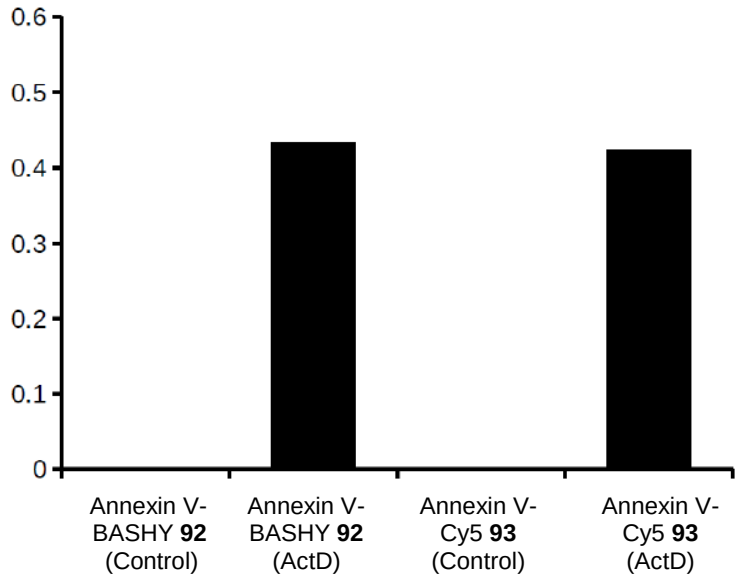

Chart 21 – Labelling efficiencies for both site-selective Annexin V constructs **92** and **93**. Ratio of labelled cells vs total cells of Annexin V-BASHY **92** and Annexin V-Cy5 **93** in the absence (Control – 0.1 % DMSO) or presence of the apoptotic inducer (actinomycin D – ActD).

These data clearly demonstrates the utility of site-selective BASHY-protein conjugates for bioimaging applications due to their stability and non-detectable quenching or photobleaching. These properties lead to low levels of unselective fluorescence background and high signal-to-noise ratio, as demonstrated for the detection of apoptotic cells through confocal microscopy.

III.3 Conclusions

For the first time, it was shown that boronic acids are valuable building blocks for the multicomponent assembly of a functionally and structurally versatile fluorescent dye platform. This novel straightforward protocol afforded BASHYs in high yields without the need for laborious chromatographic steps and the modularity of the synthetic approach allows the integration of virtually any functionality, without compromising the photophysical properties.

The resulting photostable fluorescent dyes show polarity-sensitive green-to-yellow emission with quantum yields of up to 0.68 in nonpolar environments and a brightness value comparable with the widely commercialized ICT fluorescence imaging dyes.

The electronic fine-tuning along the ligand backbone of BASHYs opens possibilities to construct Donor−πbridge−Acceptor systems with tailored emission properties as well as significant solvatochromic and two-photon-absorption behavior.

The modular construction applied to the synthesis of BASHYs was also used in the preparation of highly efficient energy-transfer cassettes, which revealed to have practically quantitative energy-transfer efficiency with variable donor/acceptor scenarios, supporting the photophysical flexibility of the BASHY platform.

In terms of bioimaging applications, BASHYs **81a,e** were successfully used as lipid droplets staining agents, due to their hydrophobic asymmetric 3D structure and strong fluorescence in nonpolar environments. Dyes **81a,e** and ECT **85** were efficiently entrapped in NPs and these stable and highly fluorescent conjugates were shown to be readily internalized by BMDCs cells.

BASHY-azide **95** was used for the site-selective labelling of Annexin V, which is an apoptosis biomarker. Notably, the fluorescence of BASHY was retained after protein labelling and the conjugate Annexin V-BASHY **92** successfully targeted and detected apoptotic cells maintaining high levels of specific activity.

The development of new live-cell imaging methodologies is vital to foster new research in cell biology. Therefore, it is envisioned that this BASHY modular platform, featuring dyes with remarkable photophysical properties, low toxicity, amenability for NP labeling, selectivity towards subcellular structures and precise bioconjugation of biomarkers will emerge as a powerful tool for the tailored design of fluorescent dyes for advanced bioimaging applications.

Chapter IV

Supporting Information

IV.1 Experimental section of Chapter II

IV.1.1 Synthesis and structural characterization

Dry reaction solvents, as dichloromethane and acetonitrile were dried over calcium hydride under nitrogen or argon atmosphere. Tetrahydrofuran was dried in a mixture of metallic sodium and benzophenone under nitrogen or argon atmosphere. DMSO and dimethylformamide (DMF) were purchased from Acros (Extra Dry over Molecular Sieve, AcroSeal®). Other reaction solvents were used without any purification. Phenylboronic acid, 2-hydroxy-4-methoxyacetophenone, anthranilic acid, L-phenylalanine, 2-aminophenol, (1R,8S,9s)-Bicyclo[6.1.0]non-4-yn-9-ylmethyl-*N*-succinimidyl carbonate, umbelliferone and 4-(Hydroxymethyl)phenylboronic acid pinacol ester were purchased from Aldrich. 4-methoxysalicylaldehyde, 2,5-dihydroxyacetophenone, 2,4-dihydroxyacetophenone, cesium carbonate and benzeneboronic acid polymersupported (2.6-3.2 mmol/g) were bought from Alfa Aesar. Btz was acquired from eNovation Chemicals, methanesulfonyl chloride (MsCl) and *N,N*-diisopropylethylamine (DIPEA) were bought from Fluka, 4-amino-3-hydroxybenzoic acid was obtained from Acros and TBTU was bought from Apollo.

Thin layer chromatography was performed using Merck silica gel 60F254 aluminium plates and visualized using UV light and in a phosphomolybdic acid solution. In column chromatography it was silica gel 60 M purchased from MN (Ref. 815381).

NMR spectra were recorded in a Bruker Advance III 600, Bruker AMX 400 and in a Bruker Fourier 300 using $CDCl_3$ and $(CD_3)_2SO$ as deuterated solvents. All coupling constants are expressed in Hz and chemical shifts (δ) in ppm. Multiplicities are given as: s (singlet), d (doublet), dd (double doublet), t (triplet), q (quartet), and m (multiplet). Fourier transform infrared spectroscopy (FTIR) was done in Perkin Spectrum Two. UV spectra were traced in Thermo Scientific Evolution 201 UV-visible spectrophotometer. Low resolution mass spectrometry (LRMS) was performed in a mass spectrometer (Micromass Quattro Micro API, Waters, Ireland) with a Triple Quadrupole (TQ) and with an electrospray ion source (ESI) operating in positive mode. It was also used an ion trap mass analyser (Thermo Scientific LCQ Fleet Ion Trap LC/MS) equipped with an electrospray interface. High resolution mass spectrometry (HRMS) was performed in a mass spectometer (LTQ Orbitrap XL) using an ESI source operating in positive mode. Elemental analysis (E.A) was made in a Flash 2000 CHNS-O analyzer (ThermoScientific, UK).

- **B-complexes 27a,b**

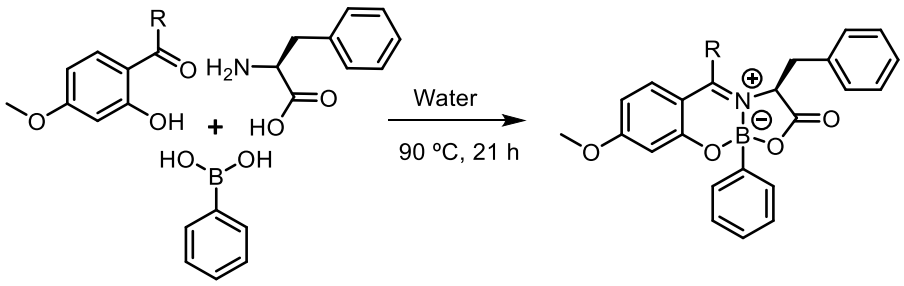

27a (R = H); γ = 87 %
27b (R = Me); γ = 10 %

Scheme 39 – Synthetic methodology to prepare B-complexes **27a,b**.

Assembly of B-complexes **27a,b** was accomplished by following a reported literature procedure,[52] in which, a round bottomed flask was charged with 4-methoxysalicylaldehyde or 2-hydroxy-4-methoxyacetophenone (0.62 mmol), L-phenylalanine (0.82 mmol) and 2 mL of distilled water. This suspension was stirred at 90 ºC for 1 h after which the phenylboronic acid (0.41 mmol) was added. The mixture was then stirred at 90 ºC for 20 h. The reaction mixture was filtered and the solid obtained was washed with water (1 mL) followed by hexane (1 mL). B-complexes **27a,b** were obtained as white solids in 87 % and 10 % yield, respectively.

B-complex **27a –** White solid; Yield 87 %; **^{1}H NMR** (400 MHz, $CDCl_3$) δ 7.50 – 7.42 (m, 2H, CH_{Arom}), 7.36 – 7.28 (m, 6H, CH_{Arom}), 7.04 – 6.93 (m, 4H, CH_{Arom}), 6.49 – 6.46 (s, 1H, CH_{imine}), 6.44 (d, *J* = 9.2 Hz, 1H, CH_{Arom}), 4.27 (dd, *J* = 12.0, 2.4 Hz, 1H, -C$\underline{H_2}$CH-), 3.82 (s, 3H, -OC$\underline{H_3}$), 3.36 (dd, *J* = 12.0, 2.4 Hz, 1H, -C$\underline{H_2}$CH-), 2.67 (t, *J* = 12.0 Hz, 1H, -CH_2C$\underline{H}$-); **^{13}C NMR** (101 MHz, $CDCl_3$) δ 170.99, 168.92, 162.79, 159.10, 135.60, 132.98, 130.86, 130.69, 129.56, 129.35, 129.20, 128.52, 128.41, 127.98, 127.90, 127.75, 111.61, 110.21, 102.75, 66.67, 55.97, 37.92; **LRMS** calcd m/z ($[M+H]^+$): 386, found m/z ($[M+H]^+$): 386; **E.A** calcd (%) for $C_{23}H_{20}BNO_4.\frac{1}{4}H_2O$: C 70.88, H 5.3, N 3.59, found (%): C 71.01, H 5.03, N 3.66.

B-complex **27b –** White solid; Yield 10 %; **^{1}H NMR** (400 MHz, $CDCl_3$) δ 7.49 – 7.42 (m, 2H, CH_{Arom}), 7.31 – 7.26 (m, 6H, CH_{Arom}), 7.23 (d, *J* = 9.2 Hz, 1H, CH_{Arom}), 7.01 – 6.93 (m, 2H, CH_{Arom}), 6.46 (dd, *J* = 9.2, 2.4 Hz, 1H, CH_{Arom}), 6.42 (d, *J* = 2.4 Hz, 1H, CH_{Arom}), 4.47 (dd, *J* = 12.0, 3.2 Hz, 1H, -C$\underline{H_2}$CH-), 3.77 (s, 3H, -OC$\underline{H_3}$), 3.32 (dd, *J* = 13.4, 3.2 Hz, 1H, -C$\underline{H_2}$CH-), 2.73 (dd, *J* = 13.4, 12.0 Hz, 1H, -CH_2C$\underline{H}$-), 1.52 (s, 3H, -(C$\underline{H_3}$)C=N-); **^{13}C NMR** (101 MHz, $CDCl_3$) δ 171.72, 169.22, 167.57, 161.20, 136.42, 130.74, 130.30, 129.59, 129.31, 128.27, 127.91, 127.73, 112.94, 109.50, 102.97, 65.39,

55.78, 38.41, 16.72; **LRMS** calcd m/z ([M+H]$^+$): 400, found m/z ([M+H]$^+$): 400; **E.A** calcd (%) for $C_{24}H_{22}BNO_4.\frac{1}{3}H_2O$: C 71.13, H 5.64, N 3.46, found (%): C 71.46, H 5.88, N 3.25.

- **B-complex 57**

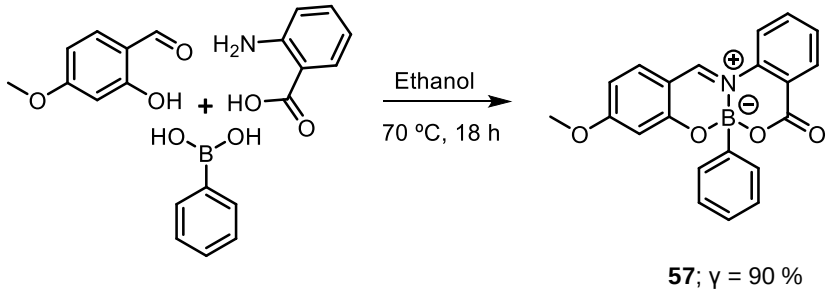

Scheme 40 – Synthetic methodology to construct B-complex **57.**

Construction of B-complex **57** was achieved by adapting a reported literature procedure.[194] Equimolar amounts (0.3 mmol) of 4-methoxysalicylaldehyde, anthranilic acid and phenylboronic acid were added to a round bottomed flask and were dissolved in 2 mL of ethanol. This mixture reacted at 70 ºC for 18 h. Then, the reaction content was filtered and the solid obtained was washed with 1 mL of ethanol. B-complex **57** was obtained as a yellow solid in a 90 % yield.

B-complex **57 –** Yellow solid; Yield 90 %; **^{1}H NMR** (400 MHz, $(CD_3)_2SO$) δ 9.42 (s, 1H, CH_{imine}), 8.05 (d, *J* = 8.0 Hz, 1H, CH_{Arom}), 8.01 (dd, *J* = 7.6, 0.8 Hz, 1H, CH_{Arom}), 7.82 – 7.75 (m, 1H, CH_{Arom}), 7.70 (d, *J* = 8.8 Hz, 1H, CH_{Arom}), 7.53 – 7.47 (m, 1H, CH_{Arom}), 7.19 – 7.12 (m, 2H, CH_{Arom}), 7.12 – 7.06 (m, 3H, CH_{Arom}), 6.68 (dd, *J* = 8.8, 2.0 Hz, 1H, CH_{Arom}), 6.59 (d, *J* = 1.6 Hz, 1H, Arom), 3.87 (s, 3H, -OC$\underline{H}_3$); **^{13}C NMR** (101 MHz, $(CD_3)_2SO$) δ 169.47, 161.54, 161.52, 159.41, 140.11, 135.61, 134.52, 130.56, 130.09, 128.56, 127.40, 123.27, 118.96, 110.45, 110.07, 101.57, 56.24; **LRMS** calcd m/z ([M+H]$^+$): 358, found m/z ([M+H]$^+$): 358; **E.A** calcd (%) for $C_{21}H_{16}BNO_4.H_2O$: C 67.23, H 4.84, N 3.73, found (%): C 66.93, H 4.35, N 3.76.

- **B-complexes 58a,b**

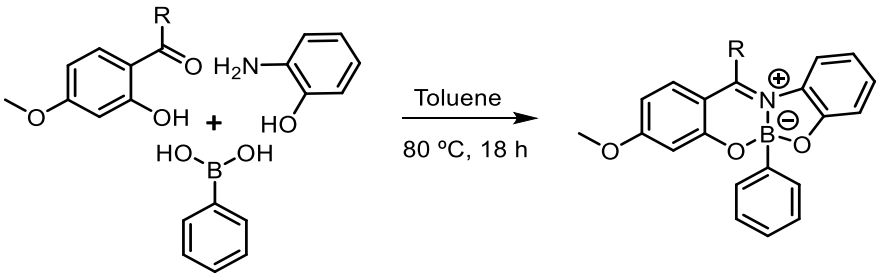

58a (R = H); γ = 90 %
58b (R = Me); γ = 85 %

Scheme 41 – Synthetic methodology to prepare B-complexes **58a,b**.

Synthesis of B-complexes **58a,b** was accomplished by following a reported literature procedure,[36] in which, to a round bottomed flask was added equimolar amounts (0.3 mmol) of 4-methoxysalicylaldehyde or 2-hydroxy-4-methoxyacetophenone, 2-aminophenol and phenylboronic acid. Then 2 mL of toluene were added and the reactional mixture reacted at 80 ºC for 18 h. After evaporation of volatiles, the crude mixture was redissolved in dichloromethane and passed through a plug of silica, using dichloromethane as eluent. After evaporation of dichloromethane under reduced pressure, B-complexes **58a,b** were both obtained as yellow solids in 90 % and 85 % yield, respectively.

B-complex **58a –** Yellow solid; Yield 90 %; **^{1}H NMR** (400 MHz, $CDCl_3$): δ 8.22 (s, 1H, CH_{imine}), 7.42 – 7.32 (m, 3H, CH_{Arom}), 7.32 – 7.24 (m, 2H, CH_{Arom}), 7.21 – 7.12 (m, 3H, CH_{Arom}), 7.08 (d, *J* = 8.4 Hz, 1H, CH_{Arom}), 6.92 – 6.82 (m, 1H, CH_{Arom}), 6.67 (d, *J* = 2 Hz, 1H, CH_{Arom}), 6.52 (dd, *J* = 8.4, 2 Hz, 1H, CH_{Arom}), 3.87 (s, 3H, -OC$\underline{H_3}$); **^{13}C NMR** (101 MHz, $CDCl_3$): δ 168.26, 160.49, 158.17, 148.07, 132.89, 131.34, 131.26, 127.86, 127.53, 119.26, 114.94, 114.54, 110.14, 102.98, 55.94; **LRMS** calcd m/z ($[M+Na]^+$): 352, found m/z ($[M+Na]^+$): 352; **E.A** calcd (%) for $C_{20}H_{16}BNO_3$: C 72.98, H 4.9, N 4.26, found (%): C 73.03, H 4.9, N 4.13.

B-complex **58b –** Yellow solid; Yield 85 %; **^{1}H NMR** (400 MHz, $CDCl_3$): δ 7.54 – 7.40 (m, 2H, CH_{Arom}), 7.35 – 7.23 (m, 3H, CH_{Arom}), 7.16 – 7.07 (m, 4H, CH_{Arom}), 6.93 – 6.83 (m, 1H, CH_{Arom}), 6.70 – 6.65 (m, 1H, CH_{Arom}), 6.52 (d, *J* = 8.8 Hz, 1H, CH_{Arom}), 3.87 (s, 3H, -OC$\underline{H_3}$), 2.71 (s, 3H, -(C$\underline{H_3}$)C=N-); **^{13}C NMR** (101 MHz, $CDCl_3$): δ 167.39, 160.67, 159.92, 158.92, 132.03, 131.36, 130.79, 130.32, 127.57, 127.40, 119.76, 118.67, 115.17, 114.70, 109.61, 103.07, 55.85, 18.18; **LRMS** calcd m/z ($[M+H]^+$): 344, found m/z ($[M+H]^+$): 344; **E.A** calcd (%) for $C_{21}H_{18}BNO_3$: C 73.5, H 5.29, N 4.08, found (%): C 73.36, H 5.30, N 3.93.

- **Building blocks 59a,b**

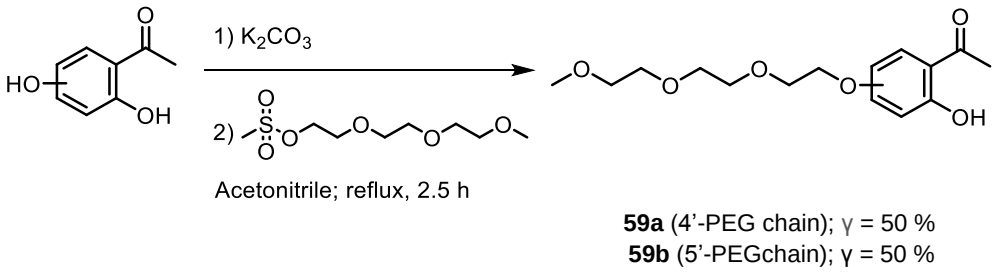

Scheme 42 – Synthetic methodology to construct building blocks **59a,b**.

Preparation of building blocks **59a,b** was performed by adapting a reported literature procedure.[195] 2′,4′-dihydroxyacetophenone or 2′,5′-dihydroxyacetophenone (0.66 mmol) were refluxed in 9 mL of acetonitrile in the presence of K_2CO_3 (0.79 mmol) over 30 minutes. Immediately after, a 1 mL solution of 2-(2-(2-methoxyethoxy)ethoxy)ethyl methanesulfonate[196] (0.79 mmol) in acetonitrile was slowly added to the reaction mixture for 10 minutes. The reaction was left in reflux for 2 h and then it was left to cool down. Volatiles were evaporated under reduced pressure and the crude mixture was redissolved in 50 ml of dichloromethane and washed with a solution NaOH 5 % (20 mL) followed by water (20 mL). The obtained organic phase was dried with sodium sulphate anhydrous, followed by evaporation of dichloromethane. The crude mixture was purified by a column chromatography using ethyl acetate 1:2 hexane as eluent. Building blocks **59a,b** were both obtained as yellow oils in 50 % yield.

Building block **59a –** Yellow oil; Yield 50 %; **^{1}H NMR** (400 MHz, $CDCl_3$) δ 12.71 (s, 1H, -OH), 7.62 (d, *J* = 8.8 Hz, 1H, CH_{Arom}), 6.46 (dd, *J* = 8.8, 2.4 Hz, 1H, CH_{Arom}), 6.41 (d, *J* = 2.4 Hz, 1H, CH_{Arom}), 4.15 (t, *J* = 4.8 Hz, 2H, PEG CH_2), 3.86 (t, *J* = 4.8 Hz, 2H, PEG CH_2), 3.75 – 3.71 (m, 2H, PEG CH_2), 3.69 – 3.63 (m, 4H, PEG CH_2CH_2), 3.58 – 3.52 (m, 2H, Peg CH_2), 3.37 (s, 3H, -OCH_3), 2.55 (s, 3H, -$COCH_3$); **^{13}C NMR** (101 MHz, $CDCl_3$) δ 202.71, 165.38, 165.23, 132.39, 114.07, 108.13, 101.53, 72.02, 70.98, 70.75, 70.70, 69.47, 67.79, 59.17, 26.37; **LRMS** calcd m/z ($[M+H]^+$): 299, found m/z ($[M+H]^+$): 299; **E.A** calcd (%) for $C_{15}H_{22}O_6.\frac{1}{3}H_2O$: C 59.2, H 7.51, found (%): C 59.32, H 7.51.

Building block **59b –** Yellow oil; Yield 50 %; **^{1}H NMR** (300 MHz, $CDCl_3$) δ 11.84 (s, 1H, -OH), 7.23 (d, *J* = 3.0 Hz, 1H, CH_{Arom}), 7.13 (dd, *J* = 9.0, 3.0 Hz, 1H, CH_{Arom}), 6.90 (d,*J* = 9.0 Hz, 1H, CH_{Arom}), 4.14 – 4.07 (m, 2H, PEG CH_2), 3.87 – 3.81 (m, 2H, PEG CH_2), 3.77– 3.71 (m, 2H, PEG CH_2), 3.71 – 3.66 (m, 2H, PEG CH_2), 3.66 – 3.62 (m, 2H, PEG CH_2), 3.56 – 3.51 (m, 2H, PEG CH_2), 3.36 (s, 3H, -OCH_3), 2.60 (s, 3H, -$COCH_3$);

^{13}C NMR (75 MHz, $CDCl_3$) δ 204.19, 157.01, 151.00, 125.00, 119.35, 119.25, 115.19, 72.04, 70.94, 70.77, 70.68, 69.95, 68.65, 59.15, 26.89; **LRMS** calcd m/z ($[M+H]^+$): 299 and ($[M+Na^+]$): 321, found m/z ($[M+H]^+$): 299 and ($[M+Na^+]$): 321; **E.A** calcd (%) for $C_{15}H_{22}O_6.\frac{1}{2}H_2O$: C 58.62, H 7.54, found (%): C 58.71, H 7.53.

- **Building block 60**

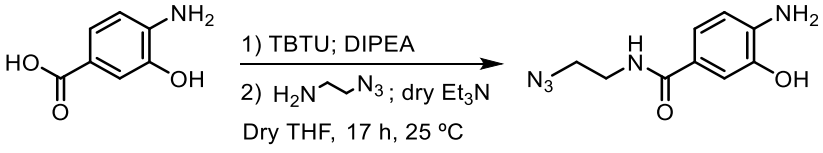

60; γ = 74 %

Scheme 43 – Methodology to synthesize building block **60**.

Construction of building block **60** was performed by adapting a reported literature procedure.[197] A round bottomed flask was flame dried and maintained under argon. Then 4-amino-3-hydroxybenzoic acid (0.45 mmol) was dissolved in 3 mL of dry tetrahydrofuran and it was added DIPEA (0.48 mmol). The mixture was left to react at RT for 10 minutes. Afterwards, TBTU (0.48 mmol) was added and the reaction was stirred for another 30 minutes. Then, a solution of 2-azidoethylamine[198] (0.9 mmol) in 1 mL of dry tetrahydrofuran, and dry triethylamine (1.85 mmol) were added to the reactional mixture. The reaction was stirred for 17 h. The volatiles were then evaporated under reduced pressure and it was performed a column chromatography using a gradient from ethyl acetate 3:1 hexane to ethyl acetate 95:5 methanol. Building block **60** was obtained as a pale yellow oil in a 74 % yield.

Building block **60 –** Pale yellow oil; Yield 74 %; **^{1}H NMR** (400 MHz, $(CD_3)_2SO$) δ 9.25 (s, 1H, -OH), 8.28 – 8.09 (m, 1H, -CONH-), 7.19 (d, *J* = 1.6 Hz, 1H, CH_{Arom}), 7.13 (dd, *J* = 8.0, 1.6 Hz, 1H, CH_{Arom}), 6.55 (d, *J* = 8.0 Hz, 1H, CH_{Arom}), 5.14 – 4.96 (m, 2H, -NH_2), 3.41 – 3.37 (m, 4H, -CH_2CH_2-); **^{13}C NMR** (101 MHz, $(CD_3)_2SO$) δ 166.87, 143.05, 140.38, 121.82, 119.46, 113.75, 112.58, 50.04, 38.89; **LRMS** calcd m/z ($[M+H]^+$): 222, found m/z ($[M+H]^+$): 222.

- **B-complex 62**

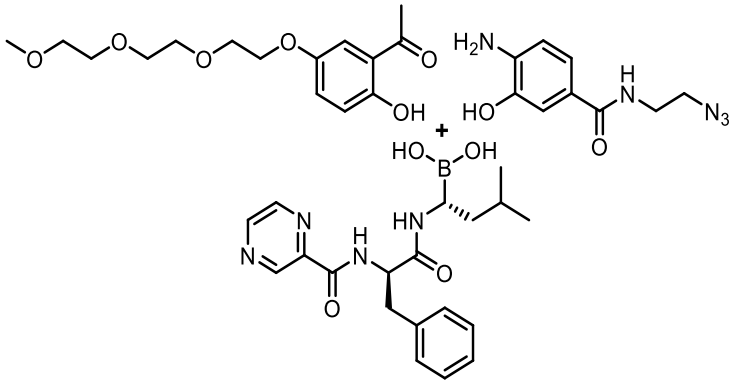

59b **Btz** **60**

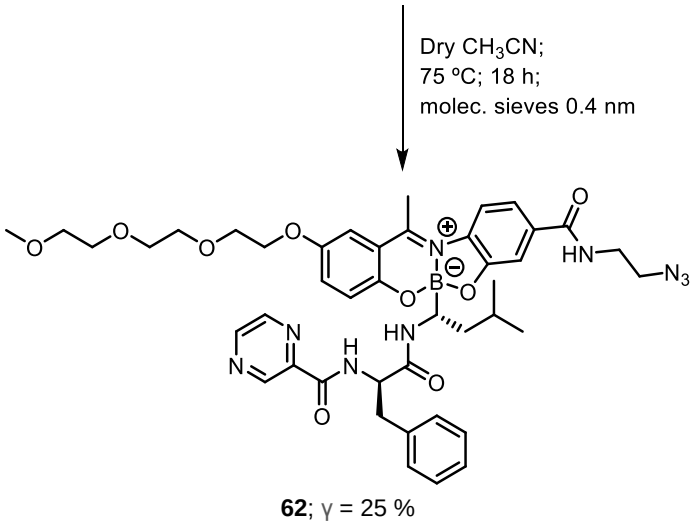

62; γ = 25 %

Scheme 44 – Modular methodology to assemble B-complex **62**.

A round bottomed flask was flame dried and maintained under argon with molecular sieves 0.4 nm. Equimolar amounts (0.2 mmol) of **59b**, **Btz** and **60** were added to the round bottomed flask and dissolved in 1.5 mL of dry acetonitrile. The reactional mixture was stirred for 18 h at 75 ºC. Afterwards, molecular sieves were removed by filtration and the acetonitrile was evaporated under reduced pressure. The crude mixture was redissolved in dichloromethane and purified via preparative thin-layer chromatography using butanone 3:1 hexane as eluent. B-complex **62** was obtained as a red/orange solid with 25 % yield.

B-complex **62 –** Red/orange solid; Yield 25 %; **^{1}H NMR** (300 MHz, $(CD_3)_2SO$) δ 9.15 – 9.10 (m, 1H), 8.90 – 8.83 (m, 1H), 8.75 – 8.70 (m, 1H), 8.68 – 8.60 (m, 1H), 7.74 – 7.62 (m, 1H), 7.54 – 6.85 (m, 12H), 4.83 – 4.65 (m, 1H), 4.26 – 3.96 (m, 2H), 3.74 – 3.39 (m, 14H), 3.30 – 3.10 (m, 6H), 3.13 – 2.98 (m, 2H), 2.70 – 2.56 (m, 1H),

1.55 – 1.36 (m, 2H), 1.27 – 1.20 (m, 1H), 0.95 – 0.63 (m, 6H); **^{13}C NMR** (75 MHz, $(CD_3)_2SO$) δ 203.99, 172.17, 162.19, 155.00, 151.63, 150.72, 147.73, 144.16, 143.39, 137.49, 129.20, 128.87, 128.08, 127.80, 126.37, 124.35, 120.16, 118.50, 114.83, 71.27, 69.93, 69.81, 69.76, 69.60, 69.02, 68.27, 67.90, 63.18, 58.04, 53.70, 49.91, 49.68, 37.46, 36.81, 27.90, 24.36, 23.72, 22.32, 21.36, 20.68; **FTIR** (v cm^{-1}): 3343 (-NH-), 2955-2874 ($C\text{-}H_{alkane}$), 2101 ($-N_3$), 1656 ($C{=}N_{imine}$, $C{=}O_{amide}$); 1517 ($C{=}C_{aromatic}$); **UV** (λ nm): 270 (max), 360, 460; **LRMS** calcd m/z ($[M+H]^+$): 850, found m/z ($[M+H]^+$): 850; **HRMS:** m/z ($[M+H]^+$) calcd = 850.40874, found m/z ($[M+H^+]$) = 850.40630.

- **SMDC 63**

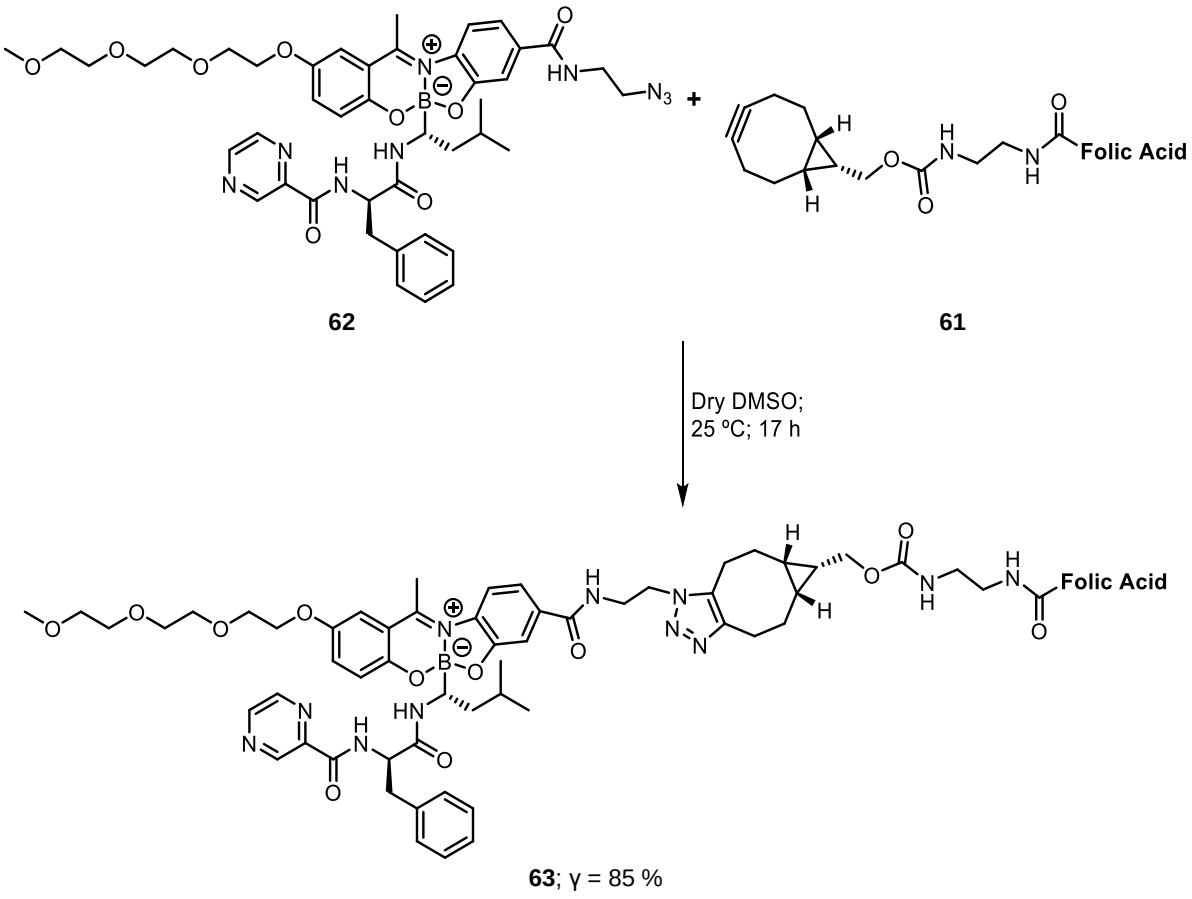

Scheme 45 – Synthetic methodology to prepare SMDC **63**.

In a 2 mL eppendorf, compounds **61** (6.63×10^{-6} mol) and **62** (7.29×10^{-6} mol) were dissolved in 650 µL of dry DMSO. Reaction was placed on the thermomixer at 25 ºC, with 700 rpm for 17 h. Then, the reactional mixture was dropwise into a mixture of 4 mL of cold diethyl ether with 10 % of acetone. It was observed the formation of an orange precipitate, and the mixture was centrifuged in an IKA mini G for 1 minute. The supernatant was

discarded, and the orange solid was then sequentially washed and centrifuged with 4 mL of cold diethyl ether with 10 % of acetone, 4 mL of cold acetone and 4 mL of cold diethyl ether. SMDC **63** was obtained as an orange solid with 85 % yield.

SMDC **63 –** Orange solid; Yield 85 %; **^{1}H NMR** (600 MHz, $(CD_3)_2SO$) δ 11.88 – 11.19 (m, 1H), 9.24 – 8.47 (m, 5H), 8.19 – 8.15 (m, 1H), 7.90 – 7.85 (m, 2H), 7.68 – 7.65 (m, 2H), 7.51 – 6.50 (m, 19H), 4.63 – 4.40 (m, 5H), 4.32 – 4.25 (m, 1H), 4.18 – 3.96 (m, 4H), 3.82 – 3.41 (m, 12H), 3.26 – 3.21 (m, 3H), 3.13 – 2.87 (m, 9H), 2.57 – 2.53 (m, 1H), 2.38 – 1.75 (m, 10H), 1.61 – 1.32 (m, 5H), 1.11 – 1.07 (m, 1H), 1.00 – 0.60 (m, 8H); **FTIR** (v cm^{-1}): 3319 (-NH-), 2940 (C-H_{alkane}), 1695-1603 (C=N_{imine}, C=O_{amide}, C=$O_{carboxylic\ acid}$); 1512 (C=$C_{aromatic}$); **UV** (λ nm): 285 (max), 360; **LRMS** calcd m/z ($[M+2H]^{2+}$): 756 and m/z ($[M+H]^+$): 1509, found m/z ($[M+2H]^{2+}$): 756 and m/z ($[M+H]^+$): 1509; **HRMS:** m/z ($[M+Na]^+$) calcd = 1531.66947, found m/z ($[M+Na]^+$) = 1531.70434.

- **Building block 64**

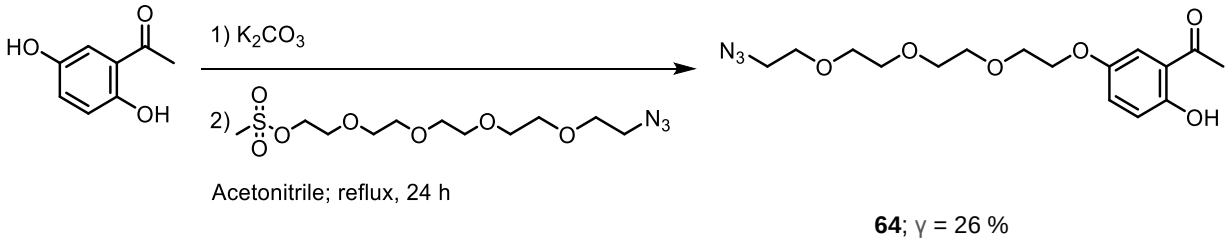

64; γ = 26 %

Scheme 46 – Synthetic methodology to construct building block **64**.

Synthesis of building block **64** was achieved by adapting a reported literature procedure.[195] 2′,5′-dihydroxyacetophenone (1 mmol) was refluxed in 1.8 mL of acetonitrile in the presence of K_2CO_3 (1.2 mmol) over 1 h. Immediately after, a 200 µL solution of 14-azido-3,6,9,12-tetraoxatetradecyl methanesulfonate[199] (1.2 mmol) in acetonitrile was slowly added to the reaction mixture for 10 minutes. The reaction was left in reflux for 23 h. Then the reaction was cooled down, and the volatiles were evaporated under reduced pressure. The crude mixture was then purified by a column chromatography using ethyl acetate 1:1 hexane as eluent. Building block **64** was obtained as a green oil in 26 % yield.

Building block **64** – Green oil; Yield 26 %; **^{1}H NMR** (300 MHz, $CDCl_3$) δ 11.85 (s, 1H, -Ph-O<u>H</u>), 7.24 (d, *J* = 3.0 Hz, 1H, CH_{Arom}), 7.14 (dd, *J* = 9.0, 3.0 Hz, 1H, CH_{Arom}), 6.91 (d, *J* = 9.0 Hz, 1H, CH_{Arom}), 4.14 – 4.09 (m, 2H, PEG C<u>H</u>$_2$), 3.88 – 3.83 (m, 2H, PEG C<u>H</u>$_2$), 3.73 – 3.64 (m, 10H, PEG C<u>H</u>$_2$'s), 3.38 (t, *J* = 4.8 Hz, 2H, PEG C<u>H</u>$_2$), 2.61 (s, 3H, -COC<u>H</u>$_3$);

^{13}C NMR (75 MHz, $CDCl_3$) δ 204.22, 157.01, 151.03, 124.99, 119.36, 119.27, 115.16, 70.95, 70.84, 70.78, 70.18, 69.96, 68.63, 50.80, 26.92; **LRMS** calcd m/z ($[M+Na]^+$): 376, found m/z ($[M+Na]^+$): 376.

- **Building block 65**

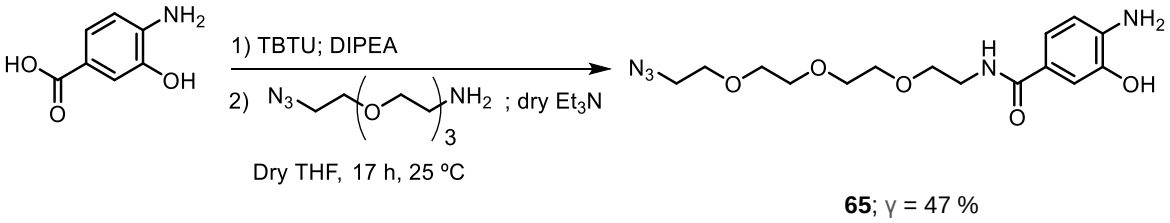

Scheme 47 – Synthetic methodology to prepare building block **65**.

Construction of building block **65** was done by adapting a reported literature procedure.[197] A round bottomed flask was flame dried and maintained under argon. Then 4-amino-3-hydroxybenzoic acid (0.99 mmol) was dissolved in 10 mL of dry tetrahydrofuran and it was added DIPEA (1.04 mmol). The mixture was left to react at RT for 10 minutes. Afterwards, TBTU (1.04 mmol) was added and the reaction was stirred for another 30 minutes. Then, a solution of 2-(2-(2-(2-azidoethoxy)ethoxy)ethoxy)ethan-1-amine[200] (1.2 mmol) in 1 mL of dry tetrahydrofuran and dry triethylamine (2.4 mmol) were added to the reactional mixture. The reaction was stirred for 17 h. The volatiles were evaporated under reduce pressure and it was performed a column chromatography using a gradient from ethyl acetate to ethyl acetate 90:10 methanol. Building block **65** was obtained as a brown oil in a 47 % yield.

Building block **65** – Brown oil; Yield 47 %; **^{1}H NMR** (300 MHz, $CDCl_3$) δ 7.46 (d, *J* = 2.1 Hz, 1H, CH_{Arom}), 7.22 (dd, *J* = 8.1, 2.1 Hz, 1H, CH_{Arom}), 6.77 (t, *J* = 4.2 Hz, 1H, -CONH-), 6.67 (d, *J* = 8.1 Hz, 1H, CH_{Arom}), 3.71 – 3.62 (m, 14H, PEG CH_2's), 3.38 (d, *J* = 5.1 Hz, 2H, PEG CH_2); **^{13}C NMR** (75 MHz, $CDCl_3$) δ 168.17, 143.89, 139.18, 123.80, 119.92, 114.46, 114.32, 70.69, 70.61, 70.53, 70.27, 70.05, 69.94, 50.71, 39.81, 38.75; **LRMS** calcd m/z ($[M+H]^+$): 354, found m/z ($[M+H]^+$): 354.

- **B-complex 66**

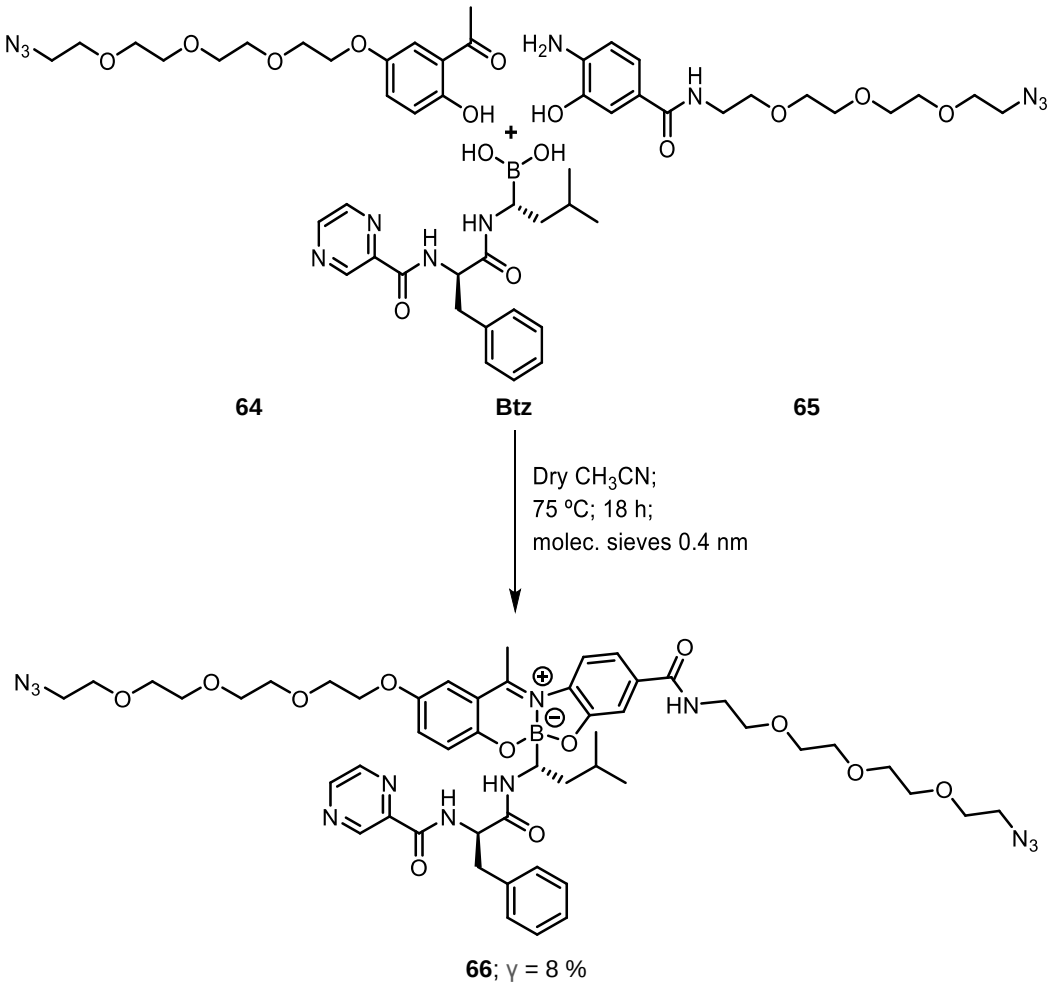

Scheme 48 – Modular methodology to construct B-complex **66.**

A round bottomed flask was flame dried and maintained under argon with molecular sieves 0.4 nm. Equimolar amounts (0.074 mmol) of **64**, **Btz** and **65** were added to the round bottomed flask and dissolved in 1.5 mL of dry acetonitrile. The reactional mixture was stirred for 18 h at 75 ºC. The molecular sieves were removed by filtration and then the acetonitrile was evaporated under reduced pressure. The crude mixture was dissolved in dichloromethane and purified via preparative thin-layer chromatography using ethyl acetate as eluent. B-complex **66** was obtained as an orange solid with 8 % yield.

B-complex **66 –** Orange solid; Yield 8 %; **^{1}H NMR** (300 MHz, $(CD_3)_2SO$) δ 9.18 – 8.32 (m, 5H), 7.99 – 6.49 (m, 12H), 5.13 – 4.89 (m, 1H), 4.29 – 4.02 (m, 2H), 3.88 – 3.35 (m, 30H), 3.35 – 3.29 (m, 3H), 3.24 – 2.97 (m, 2H), 2.88 – 2.78 (m, 1H), 1.5 – 1.22 (m, 3H), 1.10 – 0.46 (m, 6H); **FTIR** (v cm^{-1}): 3376 (-NH-), 2960-2869 ($C\text{-}H_{alkane}$), 2107 (-

N_3), 1656 (C=N_{imine}, C=O_{amide}); 1517 (C=$C_{aromatic}$); **UV** (λ nm): 273 (max), 412; **HRMS:** m/z ($[M+H]^+$) calcd = 1037.50108, found m/z ($[M+H]^+$) = 1037.49992.

- **SMDC 67**

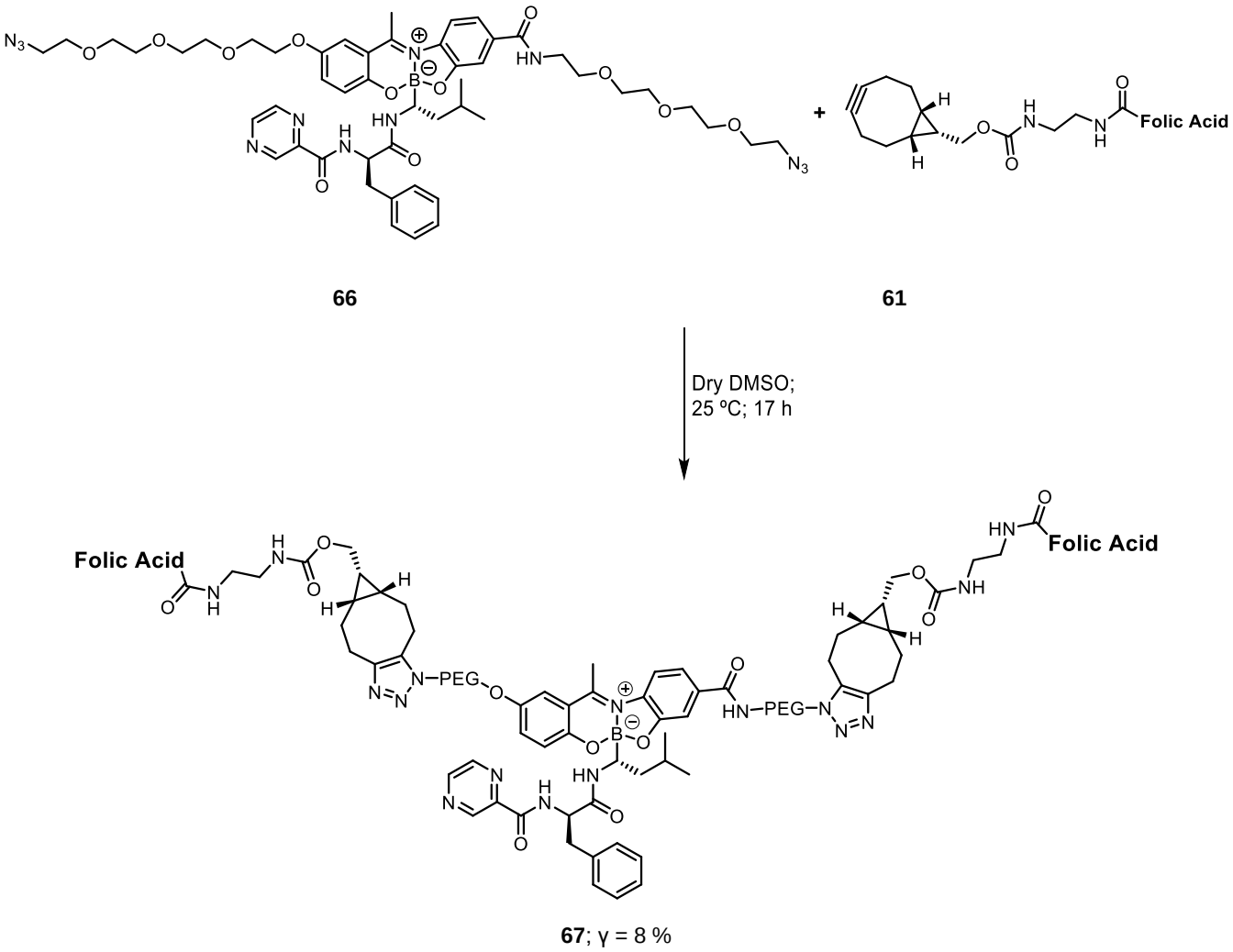

66 **61**

67; γ = 8 %

Scheme 49 – Synthetic methodology to prepare SMDC **67**.

In a 2 mL eppendorf, compounds **61** (4.1 x 10^{-6} mol) and **66** (2.05 x 10^{-6} mol) were dissolved in 205 µL of dry DMSO. Reaction was placed on the thermomixer at 25 ºC, with 700 rpm for 17 h. Then, the reactional mixture was dropwise into mixture of 1.5 mL of cold diethyl ether with 10 % of acetone. It was observed the formation of an orange precipitate, and the mixture was centrifuged in an IKA mini G for 1 minute. The supernatant was discard, and the orange solid was then sequentially washed and centrifuged with 1.5 mL of cold diethyl ether with 10 % of acetone, 1.5 mL of cold acetone and 1.5 mL of cold diethyl ether. SMDC **67** was obtained as an orange solid with 99 % yield.

SMDC **67 –** Orange solid; Yield 99 %; **^{1}H NMR** (600 MHz, $(CD_3)_2SO$) δ 11.58 – 11.36 (m, 2H), 9.06 – 8.45 (m, 7H), 8.28 – 7.72 (m, 8H), 7.69 – 7.61 (m, 4H), 7.45 – 6.83 (m, 24H), 6.67 – 6.59 (m, 4H), 4.51 – 4.44 (m, 4H), 4.41 – 4.26 (m, 7H), 4.07 – 3.97 (m, 4H), 3.79 – 3.36 (m, 32H), 3.31 – 3.25 (m, 3H), 3.09 – 2.93 (m, 10H), 2.54 – 2.54 (m, 1H), 2.51 – 1.80 (m, 20H), 1.55 – 1.14 (m, 9H), 0.97 – 0.51 (m, 10H); **FTIR** (ν cm^{-1}): 3324 (-NH-), 2931-2874 (C-H_{alkane}), 1704-1608 (C=N_{imine}, C=O_{amide}, C=$O_{carboxylic\ acid}$); 1517 (C=$C_{aromatic}$); **UV** (λ nm): 294 (max), 360; **HRMS:** m/z ([M-H_2O]) calcd = 2338.04699, found m/z ([M-H_2O]) = 2338.12592.

- **Conjugate 68**

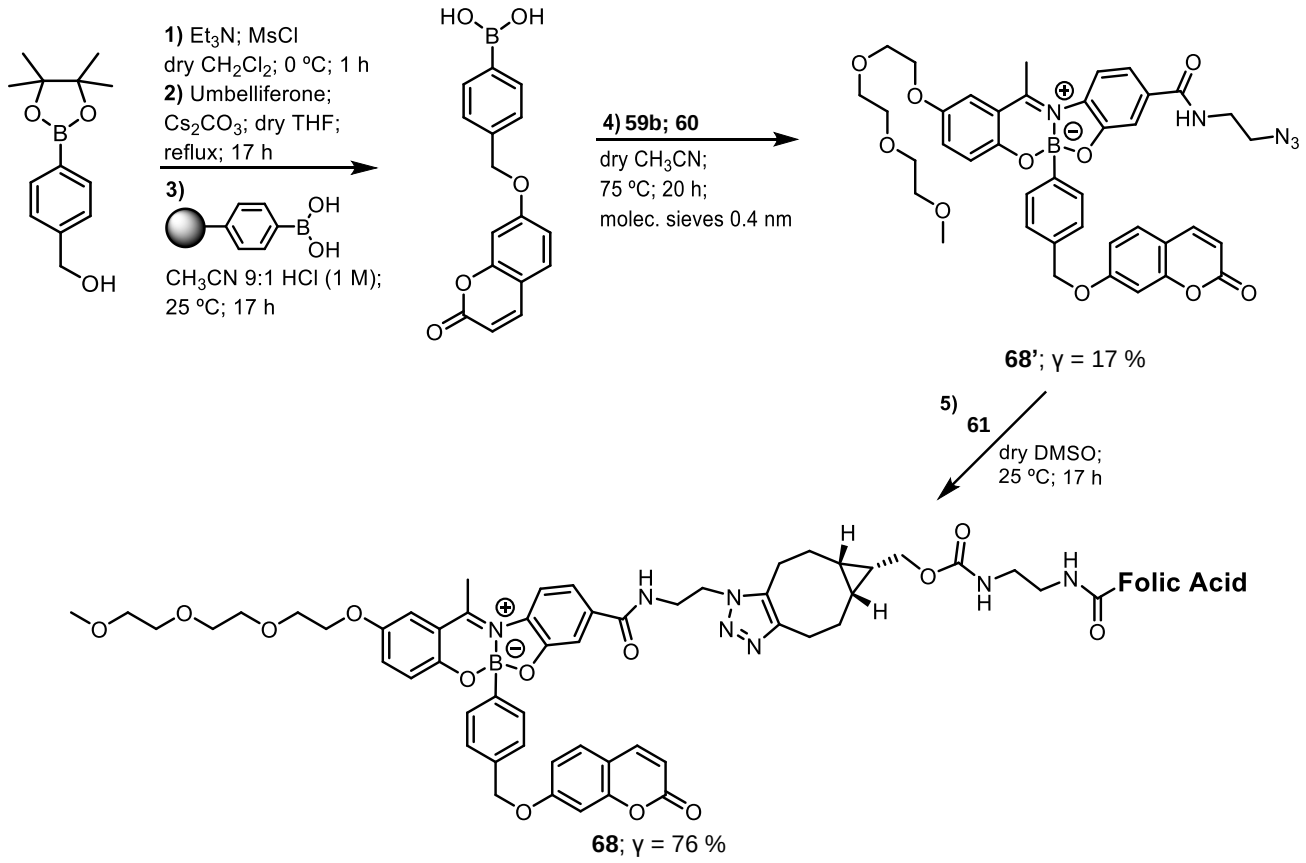

Scheme 50 – Synthetic methodology to prepare conjugate **68**.

Step 1) Mesylation of 4-(Hydroxymethyl)phenylboronic acid pinacol ester was achieved by adapting a reported literature procedure.[201] 4-(Hydroxymethyl)phenylboronic acid pinacol ester (0.43 mmol) was added into a flame dried round bottomed flask and dissolved in 3 ml of dry dichloromethane. The solution was cooled down to 0 ºC and then Et_3N (0.64 mmol) and methanesulfonyl chloride (0.51 mmol) were added. The reaction

stayed at 0 ºC, under stirring for 1 h. The crude mixture was then washed twice with 2 mL of water. The organic phase was dried with sodium sulphate anhydrous and the volatiles were evaporated. Then, it was re-dissolved in 1 mL of dry THF in order to be added in the next step.

Step 2) The coupling with umbelliferone was done by adapting a reported literature procedure.[201] A round bottomed flask was flame dried and then it was added umbelliferone (0.43 mmol) and Cs_2CO_3 (0.85 mmol) which were dissolved in 4 mL of dry tetrahydrofuran. Then, a solution from **step 1** was added and the reactional mixture was refluxed for 18 h. After that, the reaction was filtrated and the volatiles were evaporated under reduced pressure. Afterwards, the yellow solid obtained was washed four times with 1 mL of cold dichloromethane in order to extract the coupling product from the free umbelliferone. Dichloromethane was evaporated and the desired intermediate was obtained as a yellow solid in 58 % yield and was confirmed by LRMS (calcd m/z ($[M+H]^+$): 379, found m/z ($[M+H]^+$): 379). Boronate ester of coumarin was then used in the next reaction step without further purification steps.

Step 3) The conversion of boronate ester into boronic acid was performed using a reported literature procedure.[55] Boronate ester of coumarin from **step 2** (0.053 mmol) was dissolved in a round bottomed flask with 10 mL of a mixture (CH_3CN 9 : 1 HCl (1M)) and benzeneboronic acid polymer-supported (0.26 mmol) was added. The mixture was stirred for 18 h at 25 º C. Then, it was filtrated, and the volatiles were evaporated under reduced pressure. The yellowish solid obtained was washed twice with 1 ml of cold diethyl ether and boronic acid-coumarin was obtained as a white solid in 40 % yield and was used in the next reaction without further purification steps.

Step 4) A round bottomed flask was flame dried and maintained under argon with molecular sieves 0.4 nm. Equimolar amounts (0.053 mmol) of **59a**, **60** and boronic acid-coumarin were added to the round bottom flask and dissolved in 1.5 mL of dry acetonitrile. The reactional mixture was stirred for 18 h at 75 ºC. Then, the molecular sieves were removed by filtration and the volatiles were evaporated. The crude mixture was dissolved in dichloromethane and purified via preparative thin-layer chromatography using butanone 2:1 hexane. B-complex **68'** was obtained as a dark orange solid in a 17 % yield.

Step 5) In a 1.5 mL eppendorf, compounds **61** (1.2×10^{-6} mol) and **68'** (1.2×10^{-6} mol) were dissolved in 120 µL of dry DMSO. Reaction was placed on the thermomixer at 25 ºC, with 700 rpm for 17 h. Then, the reactional mixture was dropwise into mixture of 1 mL of cold diethyl ether with 10 % of acetone. It was observed the

formation of dark brown precipitate, and the mixture was centrifuged in an IKA mini G for 1 minute. The supernatant was discard, and the solid was then sequentially washed and centrifuged with 1 mL of cold diethyl ether with 10 % of acetone, 1 mL of cold acetone and 1 mL of cold diethyl ether. Conjugate **68** was obtained as a dark brown solid in a 76 % yield.

B-complex **68'–** Dark orange solid; Yield 17 %; **^{1}H NMR** (300 MHz, $CDCl_3$) δ 7.59 (d, *J* = 9.7 Hz, 1H, -C<u>H</u>=CH-), 7.54 (s, 1H, CH_{Arom}), 7.42 – 7.28 (m, 4H, CH_{Arom}), 7.25 – 7.20 (m, 3H, CH_{Arom}), 7.18 – 7.11 (m, 3H, CH_{Arom}), 7.07 – 7.02 (m, 1H, CH_{Arom}), 6.85 – 6.75 (m, 2H, CH_{Arom}), 6.58 (t, *J* = 4.8 Hz, 1H, -N<u>H</u>-), 6.21 (d, *J* = 9.7 Hz, 1H, -CH=C<u>H</u>-), 4.97 (s, 2H, -OC<u>H_2</u>Ph-), 4.15 – 4.07 (m, 2H, PEG C<u>H_2</u>), 3.91 – 3.80 (m, 2H, PEG C<u>H_2</u>), 3.78 – 3.71 (m, 2H, PEG C<u>H_2</u>), 3.71 – 3.60 (m, 6H, PEG C<u>H_2</u>), 3.60 – 3.50 (m, 4H, -NHC<u>H_2</u>C<u>H_2</u>N_3), 3.37 (s, 3H, -OC<u>H_3</u>), 2.79 (s, 3H, -(C<u>H_3</u>)C=N-); **^{13}C NMR** (75 MHz, $CDCl_3$) δ 167.12, 162.99, 162.05, 161.45, 159.27, 155.79, 152.27, 151.72, 143.63, 136.89, 134.97, 134.11, 131.85, 128.82, 126.74, 126.66, 121.54, 121.20, 120.29, 118.55, 113.34, 113.06, 112.71, 112.63, 112.57, 101.92, 71.99, 70.89, 70.72, 70.63, 69.85, 68.38, 59.14, 50.82, 39.66, 18.65; **FTIR** (v cm^{-1}): 3415 (-NH-), 2921-2869 (C-H_{alkane}), 2102 (-N_3), 1728-1613 (C=O_{ester}; C=N_{imine}; C=O_{amide}); 1546 (C=$C_{aromatic}$); **UV** (λ nm): 306 (max), 377; 446; **LRMS** calcd m/z ($[M+H]^+$): 762, found m/z ($[M+H]^+$): 762; **E.A** calcd (%) for $C_{40}H_{40}BN_5O_{10}.2H_2O$: C 60.23, H 5.56, N 8.78, found (%): C 60.51, H 5.38, N 8.35.

Conjugate **68 –** Dark brown solid**;** Yield 76 %; **^{1}H NMR** (600 MHz, $(CD_3)_2SO$) δ 8.64 (s, 2H), 8.36 – 8.25 (m, 2H), 8.20 – 8.09 (m, 2H), 8.00 – 7.85 (m, 3H), 7.77 (d, *J* = 9.0 Hz, 1H), 7.69 – 7.62 (m, 2H), 7.44 – 6.87 (m, 11H), 6.78 – 6.71 (m, 2H), 6.66 – 6.60 (m, 2H), 6.56 – 6.51 (m, 1H), 6.25 (d, *J* = 9.0 Hz, 1H), 5.03 (s, 2H), 4.52 – 4.44 (m, 2H), 4.44 – 4.36 (m, 2H), 4.33 (s, 3H), 4.12 – 3.94 (m, 4H), 3.75 – 3.36 (m, 10H), 3.21 (s, 3H), 3.13 – 2.89 (m, 7H), 2.24 – 1.81 (m, 10H), 1.55 – 1.48 (m, 2H), 1.20 – 1.13 (m, 1H), 0.93 – 0.84 (m, 2H); **FTIR** (v cm^{-1}): 3425 (-NH-), 2921 (C-H_{alkane}), 1695-1613 (C=N_{imine}, C=O_{amide}, C=$O_{carboxylic\ acid}$); 1512 (C=$C_{aromatic}$); **UV** (λ nm): 281 (max), 360; **HRMS:** m/z ($[M+H]^+$) calcd = 1421.57569, found m/z ($[M+H]^+$) = 1421.57639.

- **B-complex 72**

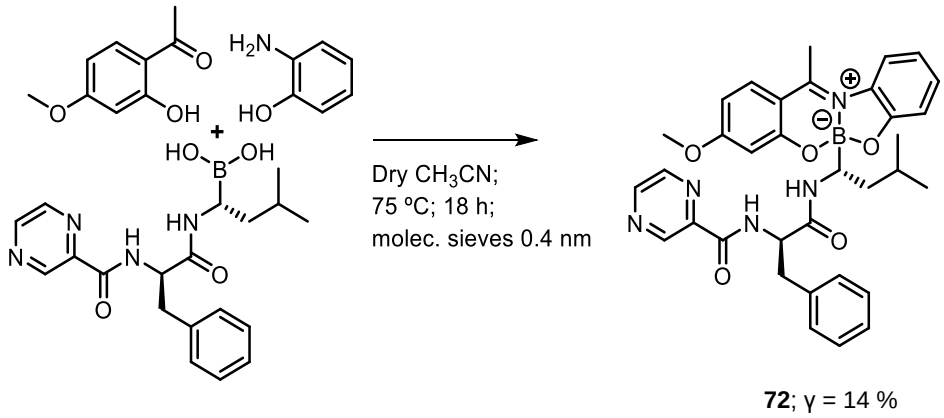

72; γ = 14 %

Scheme 51 – Synthetic methodology to assemble B-complex **72**.

A round bottomed flask was flame dried and maintained under argon with molecular sieves 0.4 nm. Equimolar amounts (0.2 mmol) of 2-hydroxy-4-methoxyacetophenone, 2-aminophenol and **Btz** were added to the round bottom flask and dissolved in 1.5 mL of dry acetonitrile. The reactional mixture was stirred for 18 h at 75 ºC. The molecular sieves were removed by filtration and then the acetonitrile was evaporated under reduced pressure. The crude mixture was dissolved in dichloromethane and purified via column chromatography using the following gradient (ethyl acetate 1:1 hexane → ethyl acetate). B-complex **72** was obtained as a mixture of diastereoisomers in 14 % yield.

B-complex **72** – Yellow solid; Yield 14 %; **^{1}H NMR** (300 MHz, $CDCl_3$) δ 9.42 – 9.13 (m, 1H), 8.85 – 8.63 (m, 1H), 8.56 – 8.39 (m, 1H), 8.14 – 7.79 (m, 1H), 7.65 – 7.33 (m, 2H), 7.28 – 7.17 (m, 5H), 7.04 – 6.84 (m, 2H), 6.76 – 6.51 (m, 2H), 6.43 – 6.22 (m, 1H), 5.58 – 5.31 (m, 1H), 4.71 – 4.25 (m, 1H), 3.90 – 3.74 (m, 3H), 3.50 – 3.20 (m, 1H), 3.18 – 2.76 (m, 2H), 2.71 – 2.59 (m, 3H), 1.39 – 1.31 (m, 1H), 1.24 – 1.11 (m, 2H), 0.78 – 0.59 (m, 6H); **^{13}C NMR** (75 MHz, $CDCl_3$) δ 169.54, 169.15, 167.23, 162.74, 161.62, 159.64, 158.03, 147.41, 144.39, 144.16, 142.75, 136.88, 132.03, 130.74, 130.24, 129.64, 129.33, 128.60, 126.89, 120.11, 118.94, 114.71, 114.34, 109.45, 109.18, 102.96, 55.78, 54.38, 39.95, 38.23, 29.80, 25.31, 23.77, 23.65, 21.93, 18.28, 17.88; **LRMS** calcd m/z ($[M+H]^+$): 606, m/z ($[M+Na]^+$): 628 and m/z ($[M+K]^+$): 644 found m/z ($[M+H]^+$): 606, m/z ($[M+Na]^+$): 628 and m/z ($[M+K]^+$): 644; **HRMS** m/z ($[M+H]^+$) calculated = 606.28095, found m/z ($[M+H]^+$) = 606.28597.

IV.1.2 HPLC stability assays

The stability of B-complexes in the different media was analyzed using a HPLC (Pump – LC-20AT; Detector – 655A Variable Wavelenght UV monitor (254 nm); Column – Gemini NX 5µ C18 110 A 250 x 4.6 mm).

HPLC gradient used was (acetonitrile 5 % → 95 %; Water 95 % → 5 %, time = 30 minutes), with the exception on the assay with B-complex **72** in which the run time was only 20 minutes.

Buffer pH 7.4, ionic strength 150 mM was prepared by dissolving 2.9 g of ammonium acetate in 250 mL of water and the pH was adjusted with diluted ammonia.

Buffer pH 4.8, ionic strength 125 mM was prepared with the dissolution of 300 mg of ammonium acetate in 50 mL of water and the pH was adjust with acetic acid.

Human plasma was collected from several healthy donors in sodium heparinate, and store at -70 ºC until required.

GSH was purchased from alfa aesar. Depending on the solubility of B-complexes in aqueous media, different percentages of DMSO were used in the stability assays.

- **Stability of B-complex 27a at pH 7.4**

Assay: 300 µL of 10^{-2} M solution of B-complex **27a** in DMSO was dissolved in a mixture of 1500 µL of buffer pH 7.4 and 1200 µL of DMSO at 37 ºC. Aliquots of 200 µL were taken from the assay and analyzed on the HPLC.

Table 10 – Data collected from HPLC in the stability assay of B-complex **27a** at pH 7.4.

Time (min)	HPLC peak area	Factor (Area → [ ])	Concentration [ ] (M)	Ln [ ]
0	293386	7×10^8	4.19×10^{-4}	- 7.78
70	241239		3.45×10^{-4}	- 7.97
240	52919		7.56×10^{-5}	- 9.49
290	46957		6.71×10^{-5}	- 9.61

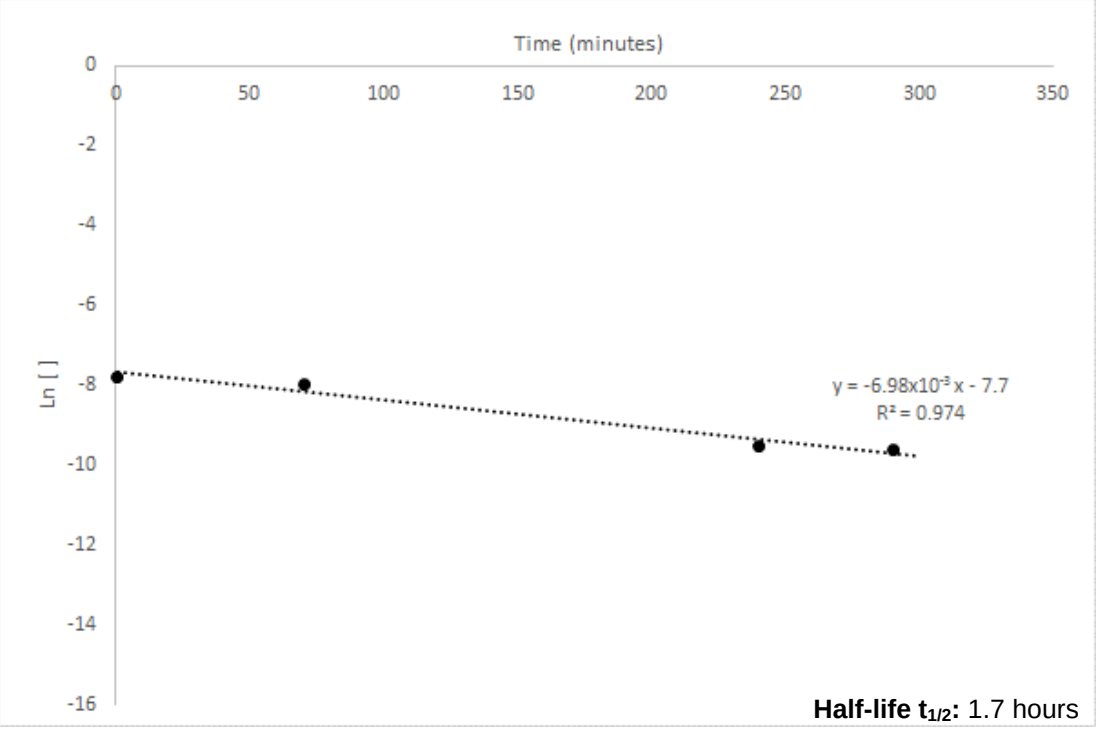

Chart 22 – Chart of Ln [ ] of B-complex **27a** over time at pH 7.4 and half-life obtained.

- **Stability of B-complex 27b at pH 7.4**

Assay: 300 µL of 10^{-2} M solution of B-complex **27b** in DMSO was dissolved in a mixture of 1800 µL of buffer pH 7.4 and 900 µL of DMSO at 37 ºC. Aliquots of 200 µL were taken from the assay and analyzed on the HPLC.

Table 11 – Data collected from HPLC in the stability assay of B-complex **27b** at pH 7.4.

Time (min)	HPLC peak area	Factor (Area → [ ])	Concentration [ ] (M)	Ln [ ]
0	1452107	7×10^{8}	2.07×10^{-3}	- 6.18
45	1408920		2.01×10^{-3}	- 6.21
370	1297294		1.85×10^{-3}	- 6.29
2870	456459		6.52×10^{-4}	- 7.34
4620	221841		3.17×10^{-4}	- 8.06
5930	202376		2.89×10^{-4}	- 8.15

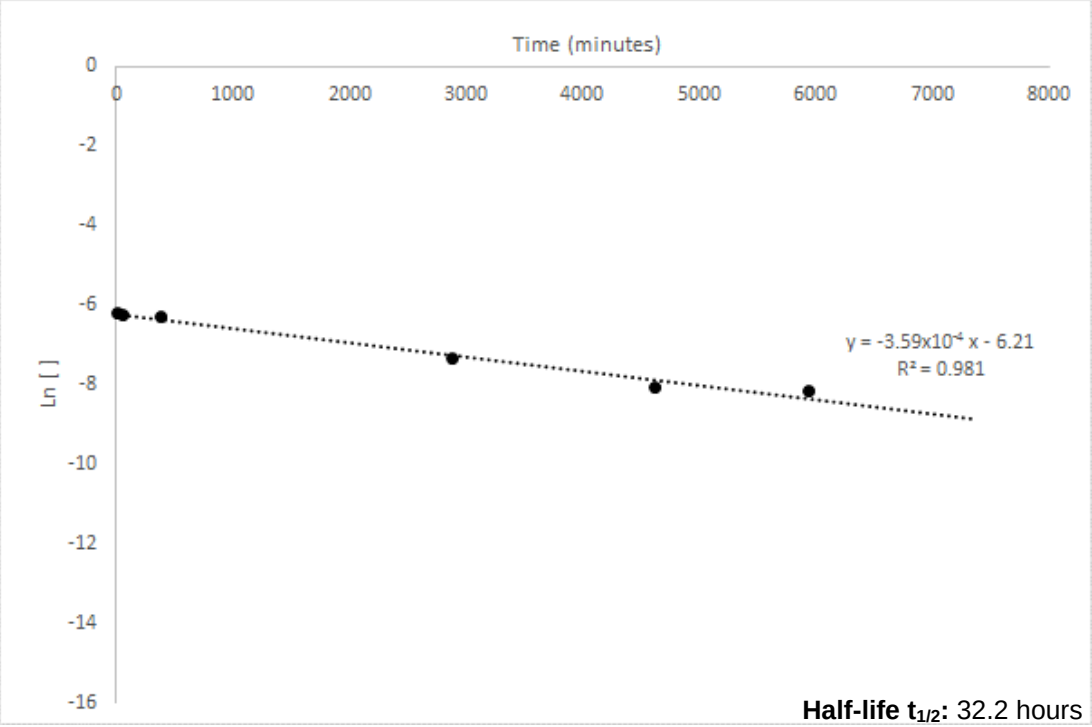

Chart 23 – Chart of Ln [ ] of B-complex **27b** over time at pH 7.4 and half-life obtained.

- **Stability of B-complex 57 at pH 7.4**

Assay: 300 µL of 10^{-2} M solution of B-complex **57** in DMSO was dissolved in a mixture of 1800 µL of buffer pH 7.4 and 900 µL of DMSO at 37 ºC. Aliquots of 200 µL were taken from the assay and analyzed on the HPLC.

Table 12 – Data collected from HPLC in the stability assay of B-complex **57** at pH 7.4.

Time (min)	HPLC peak area	Factor (Area → [ ])	Concentration [ ] (M)	Ln [ ]
0	1010352	7×10^8	1.44×10^{-3}	- 6.54
45	334631		4.78×10^{-4}	- 7.65
85	154967		2.21×10^{-4}	- 8.42

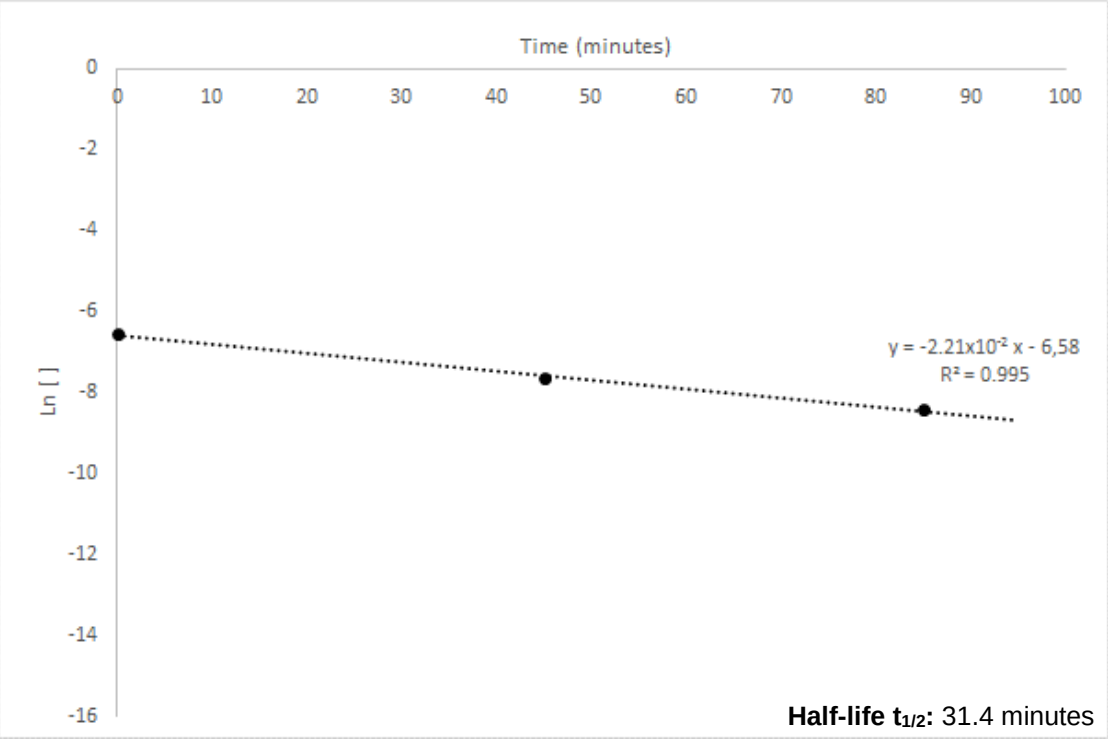

Chart 24 – Chart of Ln [ ] of B-complex **57** over time at pH 7.4 and half-life obtained.

- **Stability of B-complex 58a at pH 7.4**

Assay: 300 µL of 10^{-2} M solution of B-complex **58a** in DMSO was dissolved in a mixture of 1800 µL of buffer pH 7.4 and 900 µL of DMSO at 37 ºC. Aliquots of 200 µL were taken from the assay and analyzed on the HPLC.

Table 13 – Data collected from HPLC in the stability assay of B-complex **58a** at pH 7.4.

Time (min)	HPLC peak area	Factor (Area → [ ])	Concentration [ ] (M)	Ln [ ]
0	1774871	7×10^{8}	2.54×10^{-3}	- 5.98
42	289801		4.14×10^{-4}	- 7.79
85	62476		8.93×10^{-4}	- 9.32

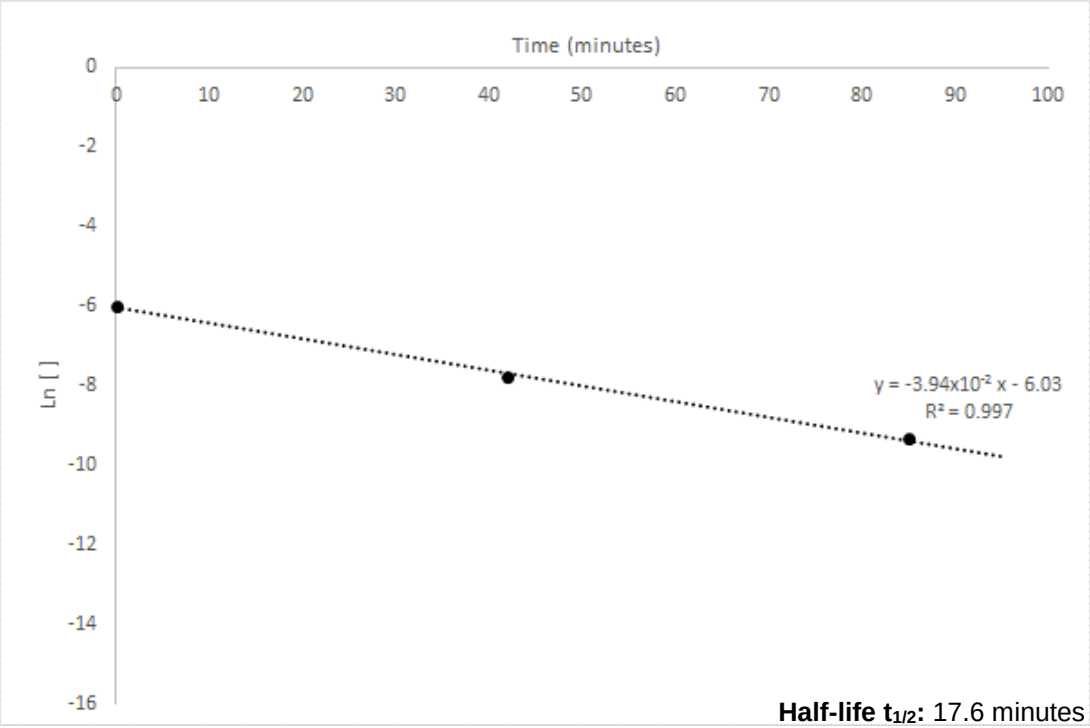

Chart 25 – Chart of Ln [ ] of B-complex **58a** over time at pH 7.4 and half-life obtained.

- **Stability of B-complex 58b at pH 7.4**

Assay: 300 µL of 10^{-2} M solution of B-complex **58b** in DMSO was dissolved in a mixture of 1500 µL of buffer pH 7.4 and 1200 µL of DMSO at 37 ºC. Aliquots of 200 µL were taken from the assay and analyzed on the HPLC.

Table 14 – Data collected from HPLC in the stability assay of B-complex 58b at pH 7.4.

Time (min)	HPLC peak area	Factor (Area → [ ])	Concentration [ ] (M)	Ln [ ]
0	1544175	9×10^8	1.72×10^{-3}	- 6.37
45	1411175		1.57×10^{-3}	- 6.46
410	1117487		1.24×10^{-3}	- 6.69
3330	397850		4.42×10^{-4}	- 7.72
4670	351094		3.90×10^{-4}	- 7.85
5950	280623		3.12×10^{-4}	- 8.07

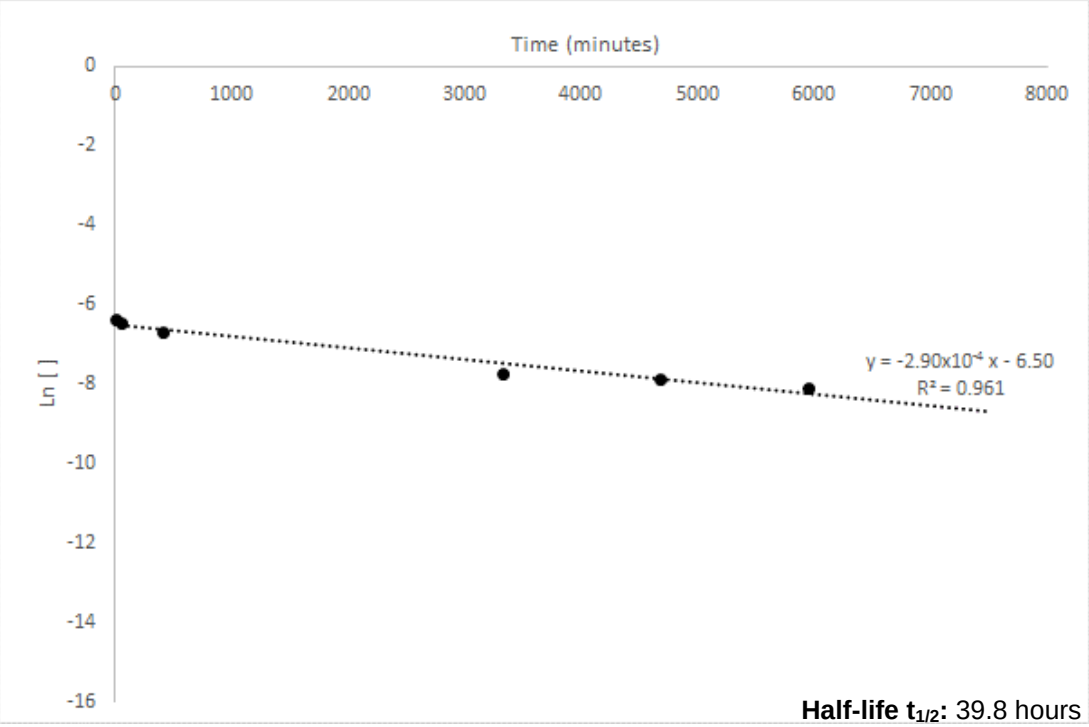

Chart 26 – Chart of Ln [ ] of B-complex **58b** over time at pH 7.4 and half-life obtained.

- **Stability of B-complex 58b at pH 4.8**

Assay: 300 µL of 10^{-2} M solution of B-complex **58b** in DMSO was dissolved in a mixture of 1500 µL of buffer pH 4.8 and 1200 µL of DMSO at 37 ºC. Aliquots of 200 µL were taken from the assay and analyzed on the HPLC.

Table 15 – Data collected from HPLC in the stability assay of B-complex **58b** at pH 4.8.

Time (min)	HPLC peak area	Factor (Area → [ ])	Concentration [ ] (M)	Ln [ ]
0	1596064	9×10^8	1.77×10^{-3}	- 6.33
45	1395279		1.55×10^{-3}	- 6.47
4110	289253		3.21×10^{-4}	- 8.04
5640	332673		3.70×10^{-4}	- 7.90

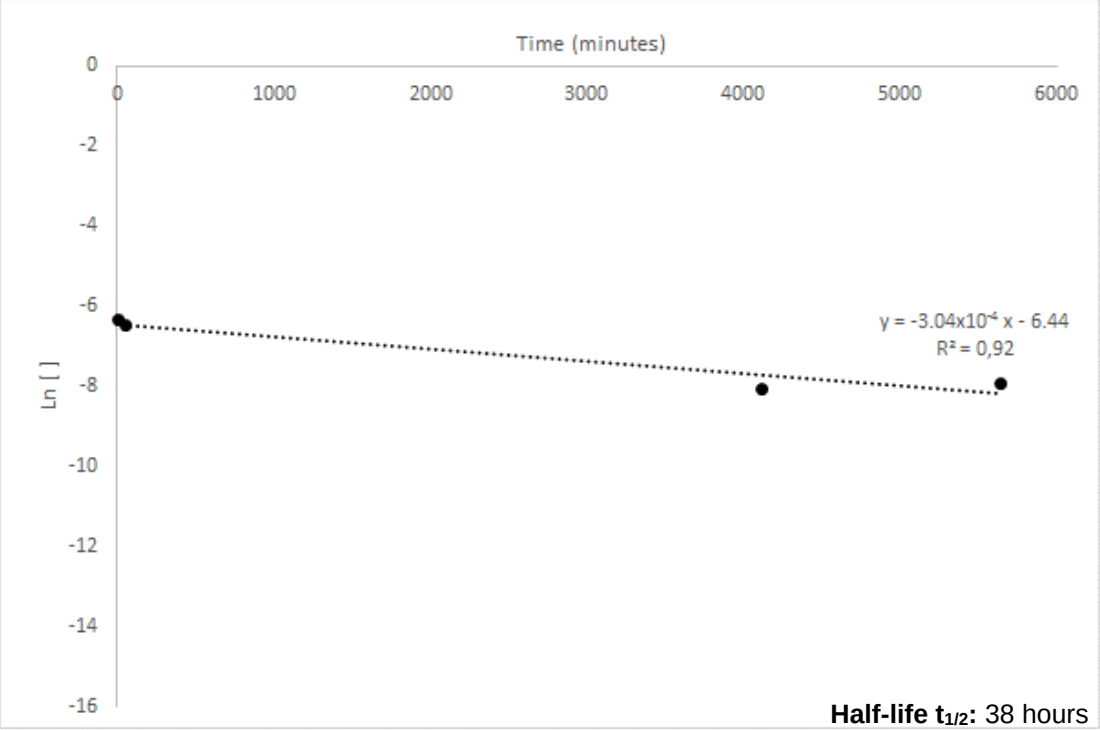

Chart 27 – Chart of Ln [ ] of B-complex **58b** over time at pH 4.8 and half-life obtained.

- **Stability of B-complex 58b in human plasma**

Assay: 300 µL of 10^{-2} M solution of B-complex **58b** in DMSO was dissolved in a mixture of 2000 µL of human plasma and 700 µL of buffer pH 7.4 at 37 ºC. Aliquots of 200 µL were taken from the assay and analyzed on the HPLC.

Table 16 – Data collected from HPLC in the stability assay of B-complex **58b** in human plasma.

Time (min)	HPLC peak area	Factor (Area → [ ])	Concentration [ ] (M)	Ln [ ]
0	2075258	9×10^8	2.31×10^{-3}	- 6.07
40	1691357		1.88×10^{-3}	- 6.28
390	1066896		1.19×10^{-3}	- 6.74
1490	754608		8.38×10^{-4}	- 7.08
1680	729677		8.11×10^{-4}	- 7.12
2880	833364		9.26×10^{-4}	- 6.98
9060	108453		1.21×10^{-4}	- 9.02

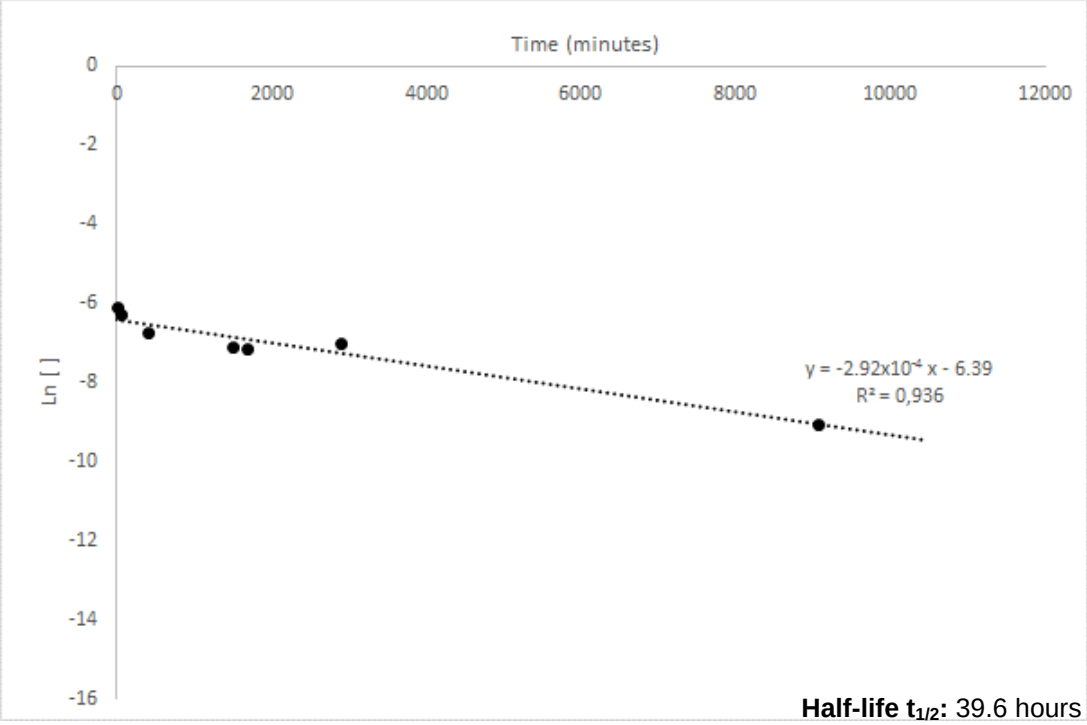

Chart 28 – Chart of Ln [ ] of B-complex **58b** over time at pH 4.8 and half-life obtained.

- **Stability of B-complex 72 in human plasma**

Assay: 300 µL of 10 $^{-2}$ M solution of B-complex **72** in DMSO was dissolved in a mixture of 2000 µL of human plasma and 700 µL of buffer pH 7.4 at 37 ºC. Aliquots of 200 µL were taken from the assay, centrifuged 1 minute in IKA mini G and analyzed on the HPLC.

Table 17 – Data collected from HPLC in the stability assay of B-complex **72** in human plasma.

Time (min)	HPLC peak area	Factor (Area → [ ])	Concentration [ ] (M)	Ln [ ]
0	2042394	1 x 10^{9}	2.04 x 10^{-3}	- 6.19
30	2067122		2.07 x 10^{-3}	- 6.18
60	2096632		2.10 x 10^{-3}	- 6.17
300	1831948		1.83 x 10^{-3}	- 6.30
1320	1679121		1.68 x 10^{-3}	- 6.39
1680	1472912		1.47 x 10^{-3}	- 6.52
3060	1138904		1.14 x 10^{-3}	- 6.78
4320	900498		1.14 x 10^{-4}	- 7.01

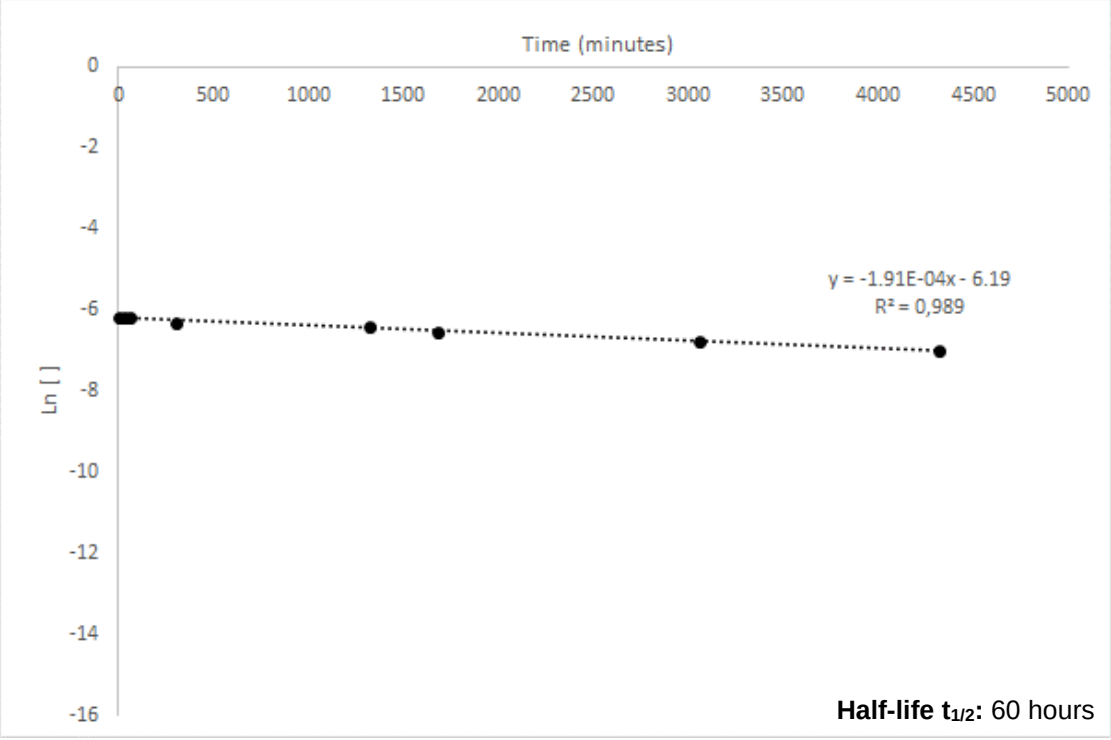

Chart 29 – Chart of Ln [ ] of B-complex **72** over time in human plasma and half-life obtained.

- **Stability of B-complex 58b in the presence of 10 equivalents of GSH**

Assay: 300 µL of 10^{-2} M solution of B-complex **58b** in DMSO was dissolved in a mixture of 1500 µL of buffer pH 7.4, 1200 µL of DMSO and 9 mg of GSH at 37 ºC. Aliquots of 200 µL were taken from the assay and analyzed on the HPLC.

Table 18 – HPLC data in the stability assay of B-complex **58b** in the presence of 10 equiv. of GSH.

Time (min)	HPLC peak area	Factor (Area → [ ])	Concentration [ ] (M)	Ln [ ]
0	1598799	9×10^8	1.78×10^{-3}	- 6.33
45	1494001		1.66×10^{-3}	- 6.40
2720	510313		5.67×10^{-4}	- 7.48
2940	550564		6.12×10^{-4}	- 7.40
4150	375982		4.18×10^{-4}	- 7.78
4355	337980		3.76×10^{-4}	- 7.89
5450	225294		2.50×10^{-4}	- 8.29

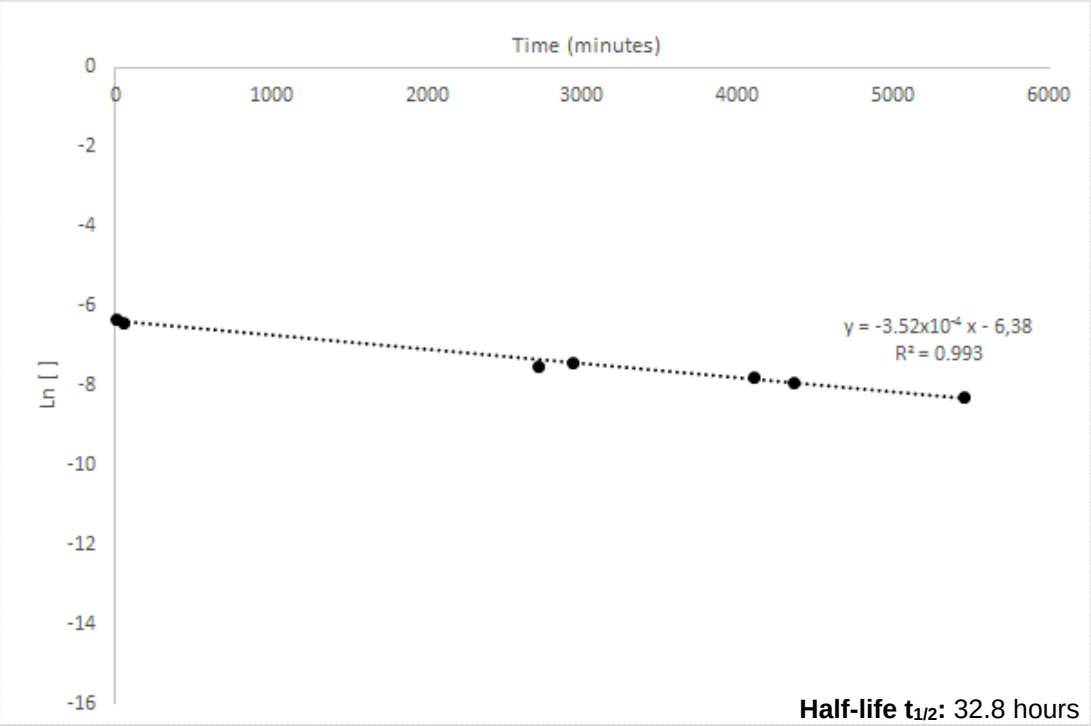

Chart 30 – Chart of Ln [ ] of B-complex **58b** over time in the presence of 10 equiv. of GSH and half-life obtained.

- **Calibration curves**

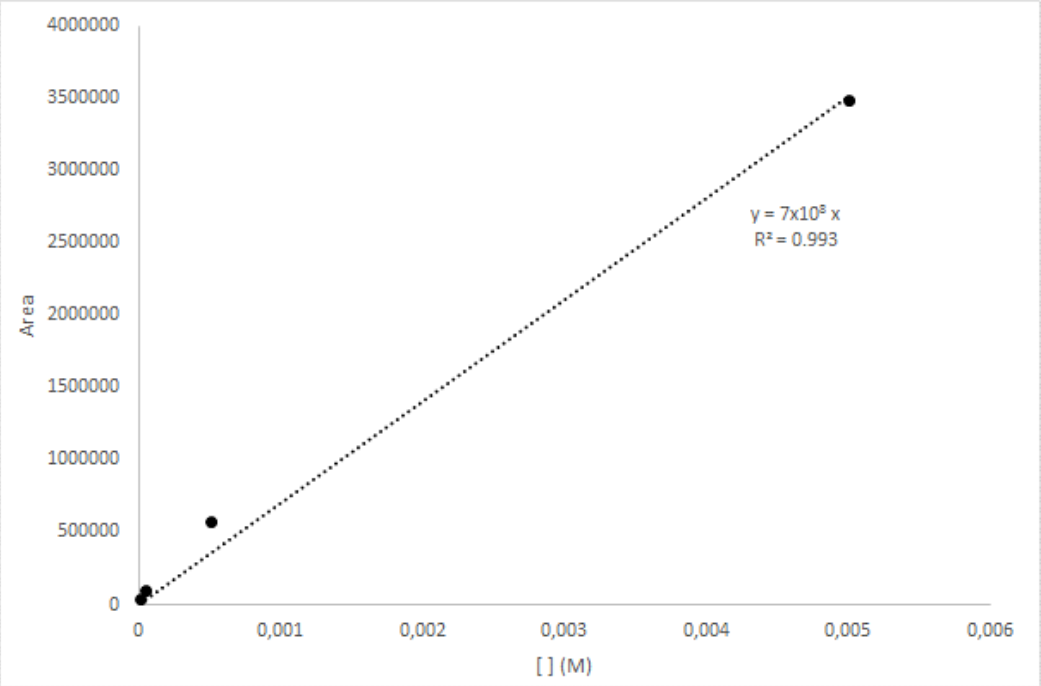

Chart 31 – Calibration curve of B-complex **27a**.

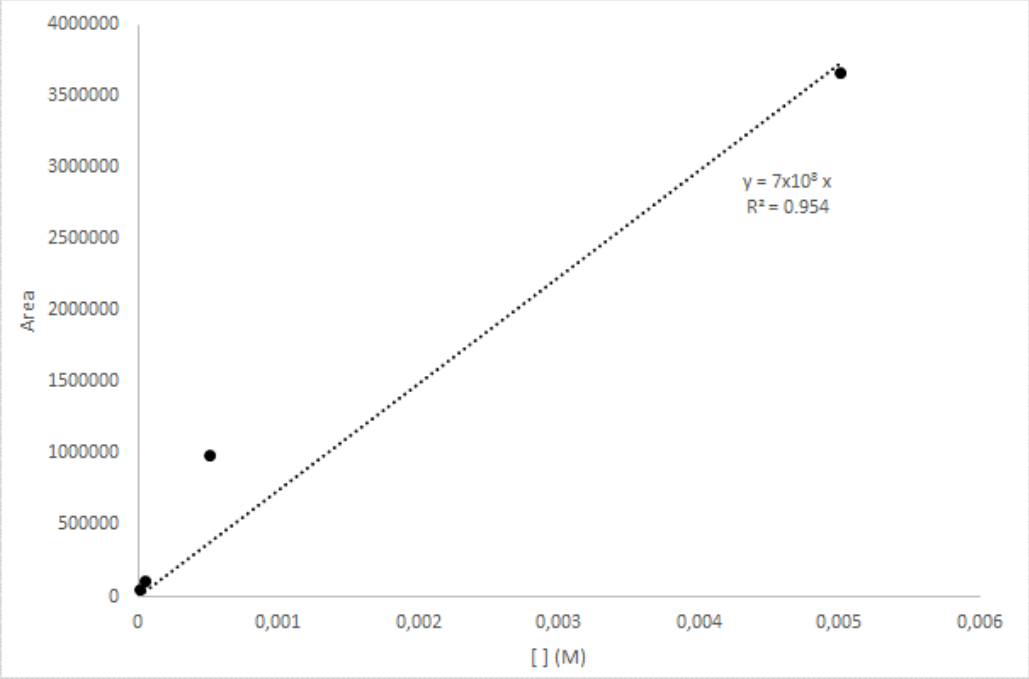

Chart 32 – Calibration curve of B-complex **27b**.

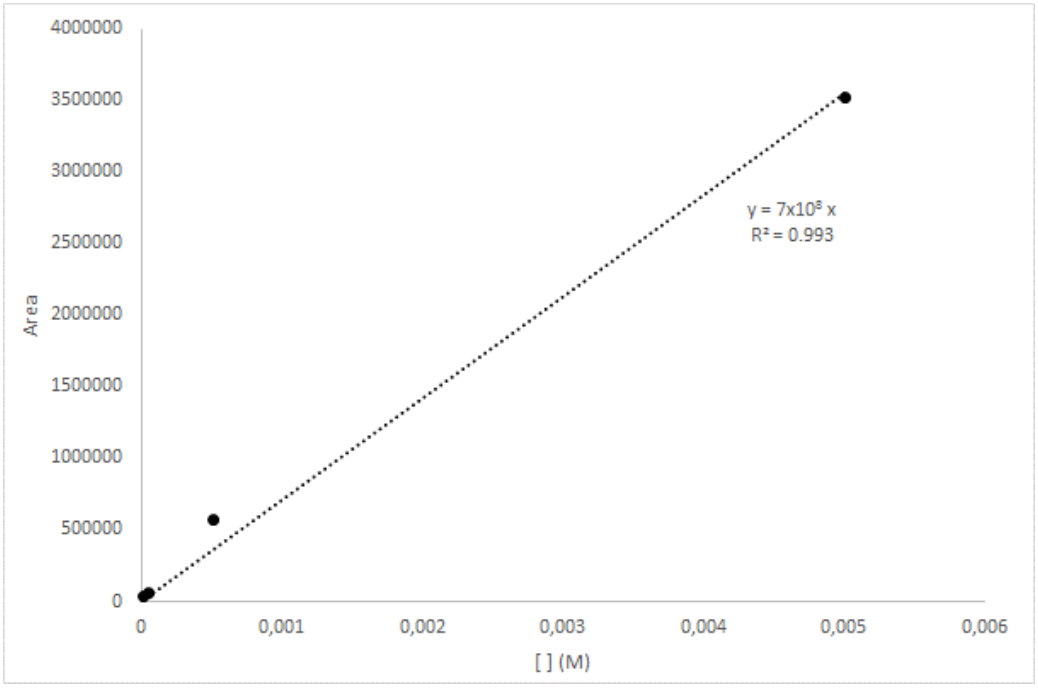

Chart 33 – Calibration curve of B-complex **57.**

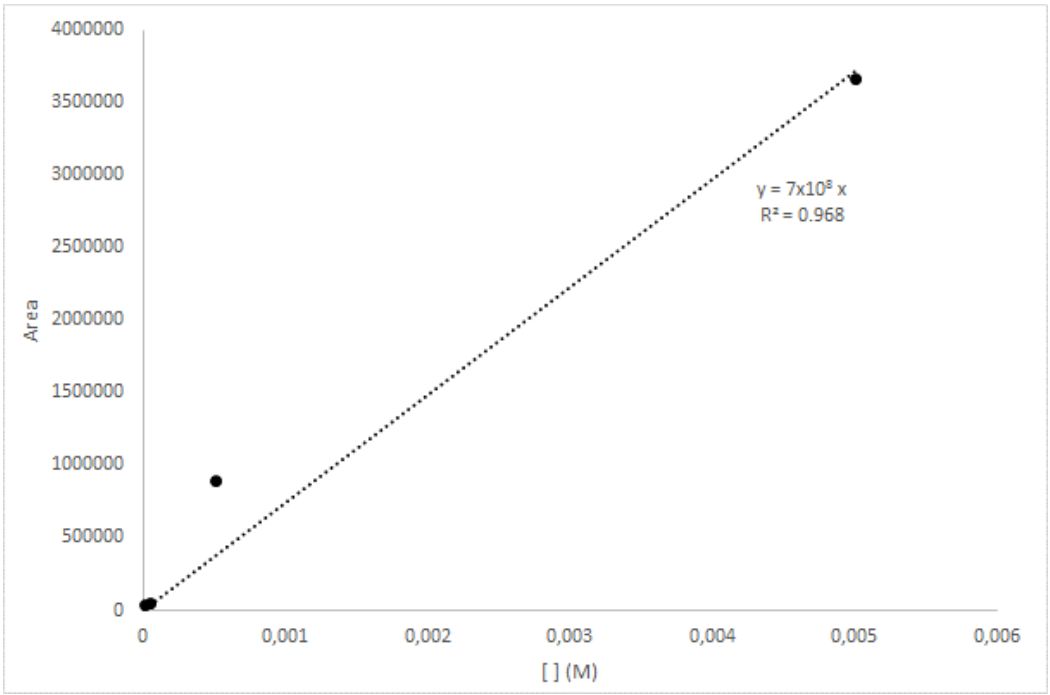

Chart 34 – Calibration curve of B-complex **58a.**

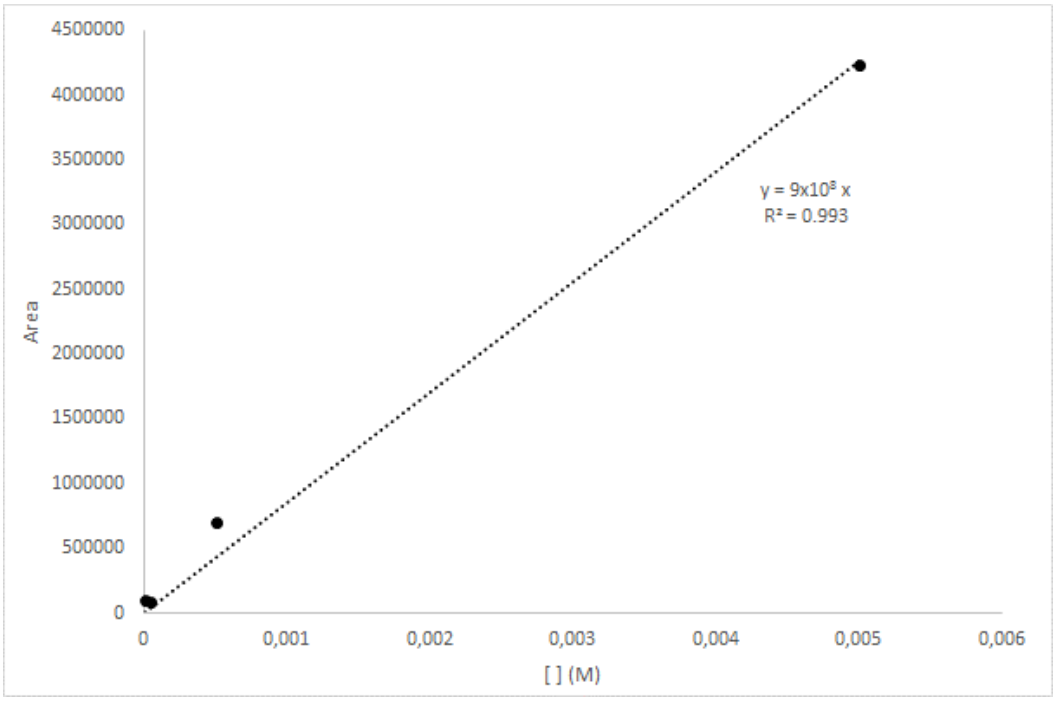

Chart 35 – Calibration curve of B-complex **58b.**

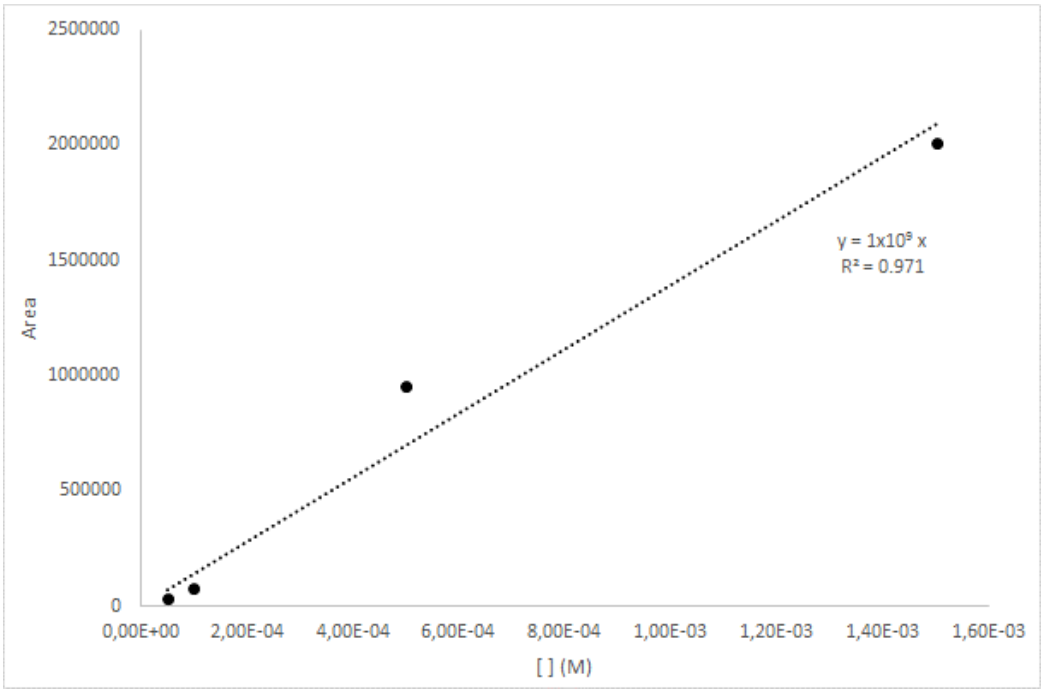

Chart 36 – Calibration curve of B-complex **72**.

IV.1.3 MTS cell proliferation assays

Human MDA-MB-231 and mouse 4T1 breast carcinoma cells were propagated in Dulbecco's Modified Eagle Medium + D-glucose + L-glutamine + pyruvate supplemented with 10 % (v/v) fetal bovine serum, 1 % (v/v) penicillin/streptomycin, and 1 % (v/v) non-essential amino acids.

Cell viability of human MDA-MB-231 (ATCC® HTB-26TM) and mouse 4T1 (ATCC® CRL-2539™) breast carcinoma cell lines incubated with **Btz**, B-complexes **62**, **66**, SMDCs **63**, **67** and folic acid-cyclooctyne **61** was quantified by MTS assay. Cells were seeded at a density of $1x10^4$ cells/well in 96-well plates, incubated for 6 – 8 h and treated with different concentrations of **Btz**, B-complexes **62**, **66**, SMDCs **63**, **67** and folic acid-cyclooctyne **61.** After 48 h of incubation time, the medium was removed and replaced by 100 µL of culture medium. Subsequently, MTS reagent was added at 20 % (v/v) and incubated for 3 h. PBS and DMSO 1 % (v/v), and 0.5 % (v/v) Triton X-100 were used as negative and positive controls, respectively. Absorbance values were measured at 490 nm (MTS reduced form, brown; MTS oxidized form, yellow), using a microplate reader (Biotek, ELx800, USA). Subtraction of the blank (culture medium and MTS, without cells) at 490 nm was carried out to yield corrected absorbances. Absorbance values were normalized for PBS control.

The cell viability was evaluated by determining the percentage of viable cells for each drug concentration. IC_{50} (drug concentration that kills 50 % of cells) was determined by linear interpolation between X_1 and X_2 according to the following equation:[202]

$$\mathbf{Log\ IC_{50}} = \mathbf{Log\ X_1} + \{[(\mathbf{Y_1} - (\mathbf{Y_0})/\mathbf{2})]/(\mathbf{Y_1} - \mathbf{Y_2})\} \times (\mathbf{Log\ X_2} - \mathbf{Log\ X_1})$$

$Y_0/2$ - half cell density in negative control

Y_1 - cell density above $Y_0/2$

X_1 – concentration corresponding to Y_1

Y_2 - cell density bellow $Y_0/2$

X_2 – concentration corresponding to Y_2

- **4T1 MTS assay (nanomolar range)**

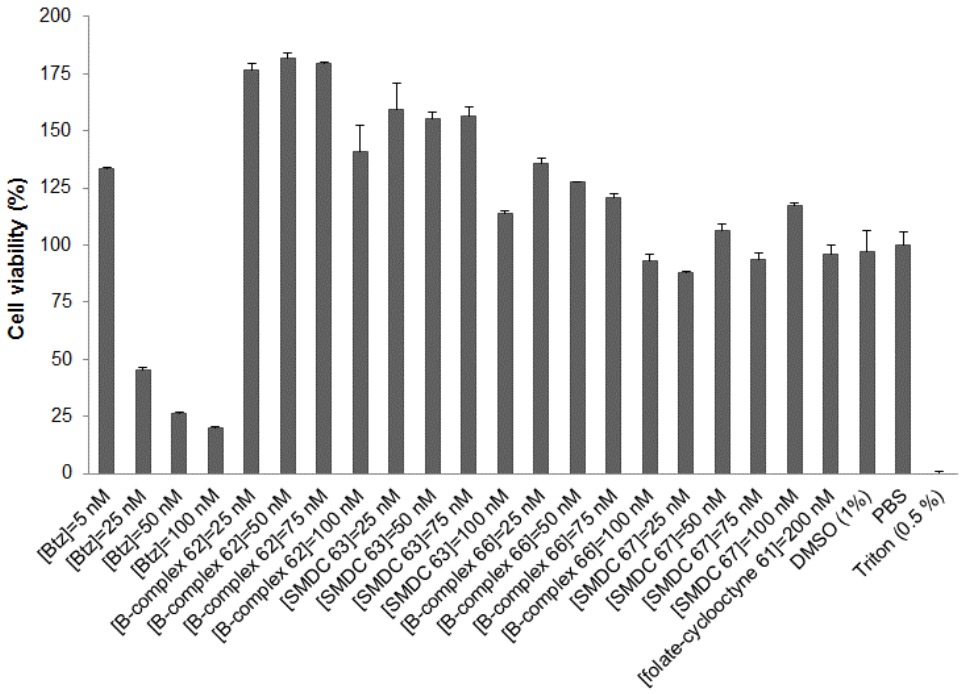

Chart 37 – Cell viability determined by MTS assay 48 h after incubation of 4T1 (ATCC® CRL-2539™) with **Btz** (5-100 nM); B-complexes **62,66** (25-100 nM); SMDCs **63**,**67** (25-100 nM) and folic acid-cyclooctyne **61** (200 nM). Mean ± standard deviation; n=3. PBS and Triton X-100 were used as controls; IC_{50} (Btz)= 22.8 nM

IV.1.4 Confocal fluorescence microscopy experiment

MDA-MB-231 and 4T1 cells (6 × 10^4 cells/200 µl/well) were seeded in 8-well Ibidi Treat® µ-Slide microscopy and incubated in a humidified incubator with 5 % CO_2, at 37 °C, allowing the cells to become adherent. The cells were incubated in different assays for 10, 30 and 180 min with 1 µM of (B-complex **68'** or conjugate **68**) and stained with WGA-Alexa Fluor® 594 plasma membrane for 10 minutes. The cells were then washed with sterile PBS pH 7.4 or DMEM (Dubelco's Modified Eagle Medium, supplemented with 10 % fetal calf serum, 100 IU mL^{-1} penicillin, and 100 µg mL^{-1} streptomycin) without phenol red and the images were obtained by confocal microscopy using a Leica TCS SP5 (Leica Microsystems CMS GmbH, Mannheim, Germany) inverted microscope (DMI6000) with a 63×water (1.2 numerical aperture) apochromatic objective.

The excitation of WGA-Alexa Fluor® 514 was performed at 514 nm. The emission was detected at 600 - 750 nm. The excitation wavelength of the probe was set to 780 nm using a titanium-sapphire laser for two-photon excitation. The emission was detected at 390 – 500 nm. The images were analyzed using S59 ImageJ Software and statistical analysis was done in Microsoft excel.

- **Statistical analysis of cellular uptake in MDA-MB-231**

Table 19 – *p*-values obtained in the t-test analysis of **68** and **68'** against the control experiment (cellular autofluorescence) at 10, 30 and 180 min.

	10 min	**30 min**	**180 min**
Conjugate 68	8.36×10^{-5}	2.19×10^{-7}	2.25×10^{-4}
B-complex 68'	4.82×10^{-1}	4.62×10^{-1}	3.98×10^{-1}

- **Statistical analysis of cellular uptake in 4T1**

Table 20 – *p*-values obtained in the t-test analysis of conjugate **68** against the control experiment (cellular autofluorescence) at 10, 30 and 180 min.

	10 min	**30 min**	180 min
Conjugate 68	2.68×10^{-2}	$8.26 \times 10^{--1}$	7.07×10^{-1}

IV.1.5 ESI-MS analysis on the B-complex 72 disassembly promoted by GSH

In a 2 mL eppendorf, B-complex **72** (10^{-6} mol; 1 equiv.) and GSH (10^{-5} mol; 10 equiv.) were dissolved in a mixture of 500 µL of buffer (ammonium acetate pH 7.4, ionic strength 150 mM) and 500 µL of acetonitrile. Reaction was placed on the thermomixer at 37 ºC, with 700 rpm for 72 h. Aliquots of 30 µL were taken at 1 h, 24 h and 72 h, diluted in 270 µL of acetonitrile: water: formic acid (45:45:10) and analyzed on the ion trap mass analyzer (Thermo Scientific LCQ Fleet Ion Trap LC/MS) equipped with an electrospray interface.

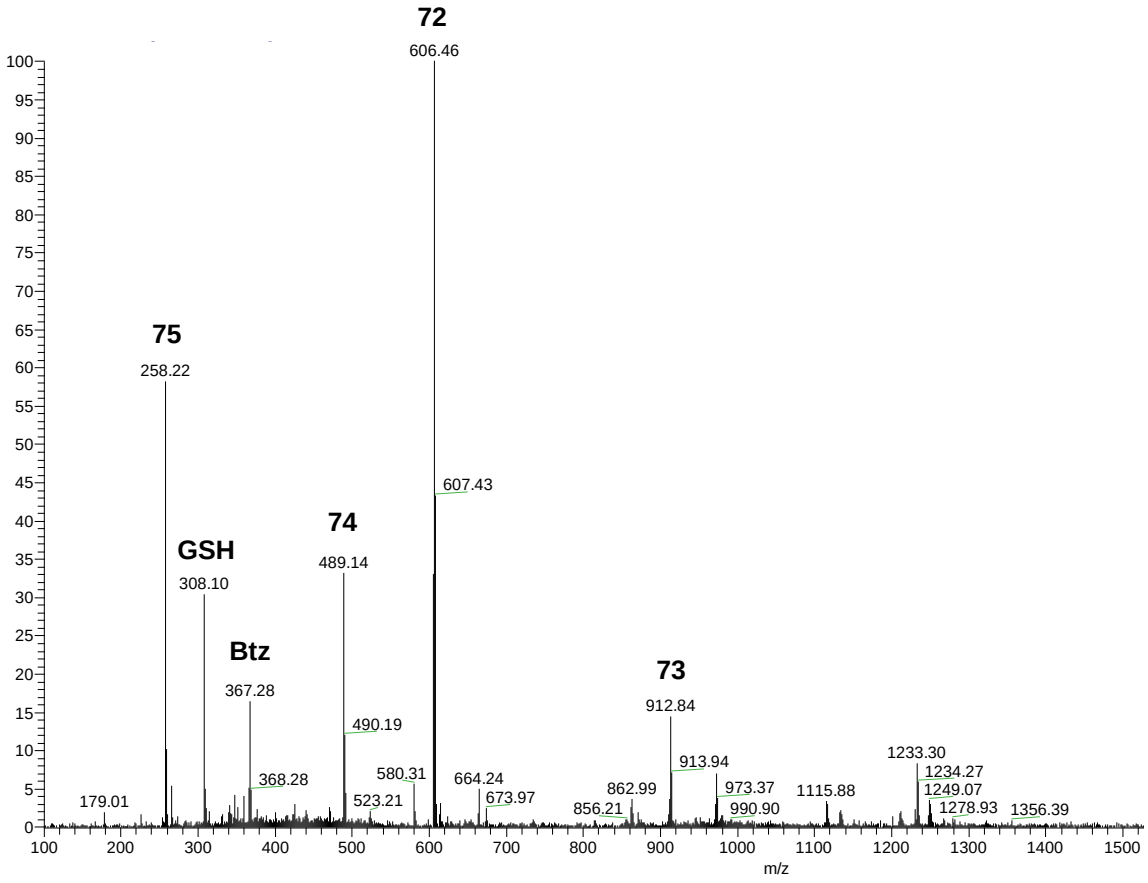

Figure 23 – ESI spectra from the reaction between B-complex **72** and GSH after 1 h.

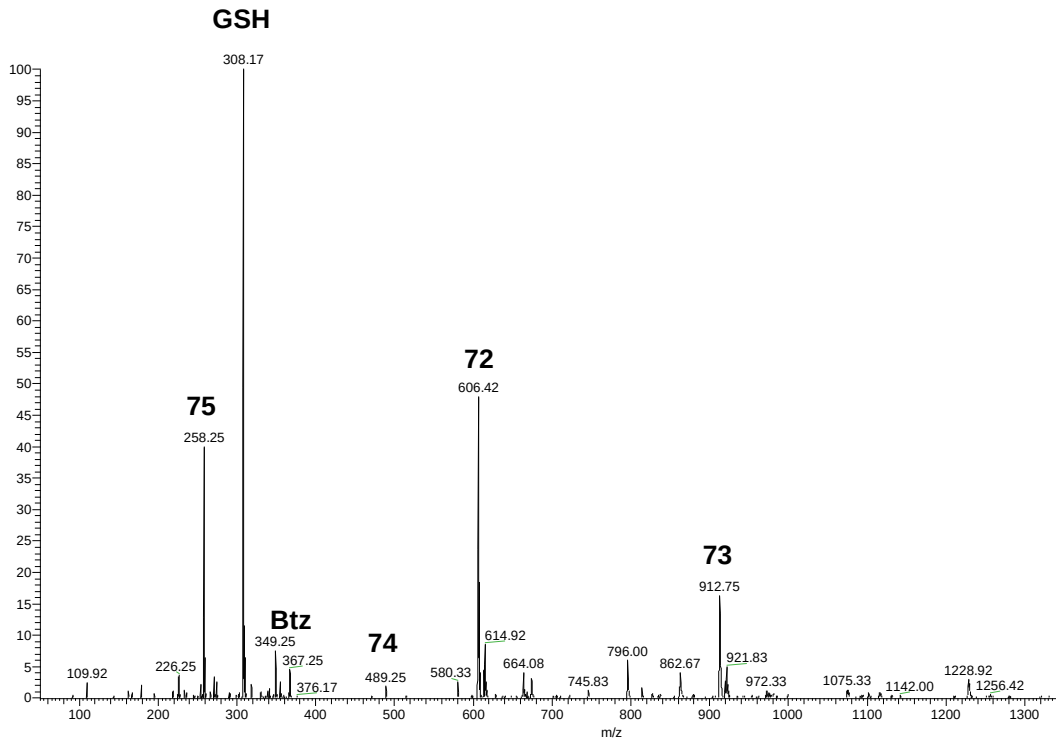

Figure 24 – ESI spectra from the reaction between B-complex **72** and GSH after 24 h.

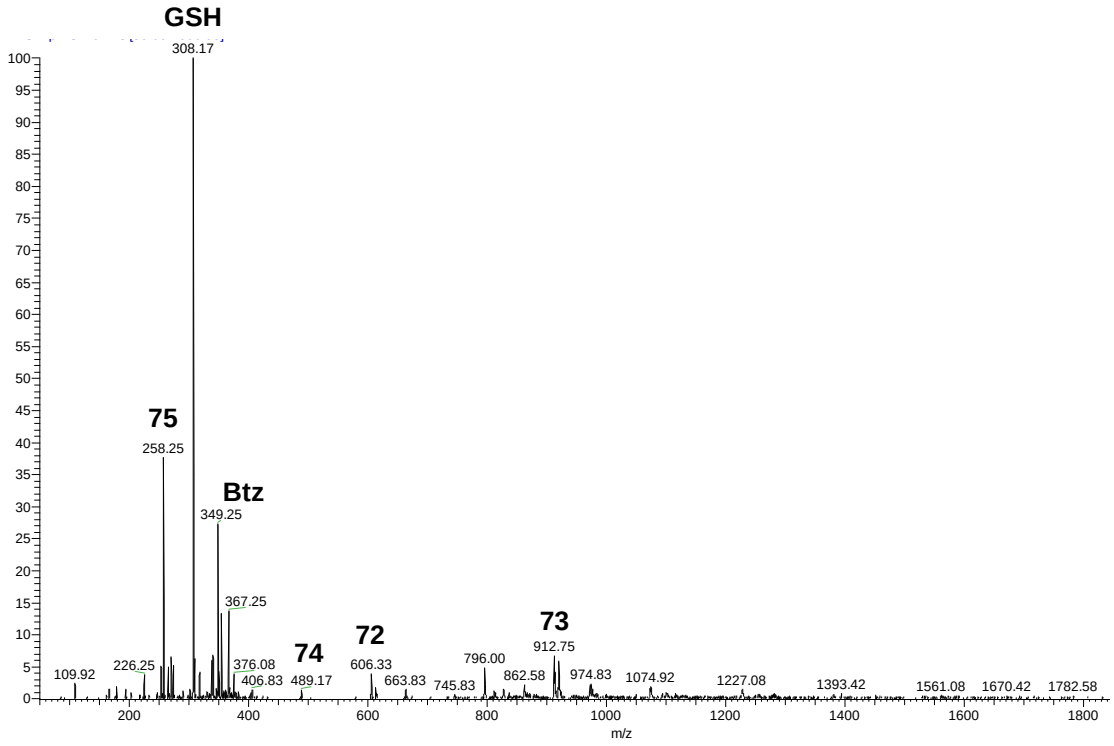

Figure 25 – ESI spectra from the reaction between B-complex **72** and GSH after 72 h.

IV.1.6 DFT calculations

All calculations were performed using the GAUSSIAN 09 software package,[203] and the M06-2X functional, without symmetry constraints. That is a hybrid meta-GGA functional developed by Truhlar and Zhao,[204] and it was shown to perform very well for main-group kinetics, providing a good description of long range effects such as Van der Waals interactions or π-π stacking.[205,206]

The optimized geometries were obtained with a standard 6-31G(d,p)[207–211] basis set. The electronic energies obtained at that level (Eb1) were converted to free energy at 298.15 K and 1 atm (Gb1) by using zero point energy and thermal energy corrections based on structural and vibration frequency data calculated at the same level.

Single point energy calculations were performed on the geometries obtained at the M06-2X/6-31G(d,p) level using the same functional and a 6-311++G(d,p) basis set.[212–220] Solvent effects (water) were accounted for in all calculations (including geometry optimizations) by means of the Polarisable Continuum Model initially devised by Tomasi and coworkers[221–224] with radii and non-electrostatic terms of the SMD solvation model, developed by Truhlar *et al*..[225]

The free energy values presented (Gb2) were derived from the electronic energy values obtained at the M06-2X/6-311++G(d,p)//M06-2X/6-31G(d,p) level (Eb2), according to the following expression: Gb2 = Eb2 + Gb1 – Eb1.

- **Failed assemblage between building blocks Btz, 59a, and 60**

DFT calculations on simple models of the B-complexes (**Scheme 52**) allow the separation of steric and electronic effects on their stability. Here, the large PEG chain was replaced by a MeO group and NHCOMe replaces the complex diamide arm with benzyl and pyrazine substituents present in Btz. Thus, stereochemical constraints are severely reduced in those models.

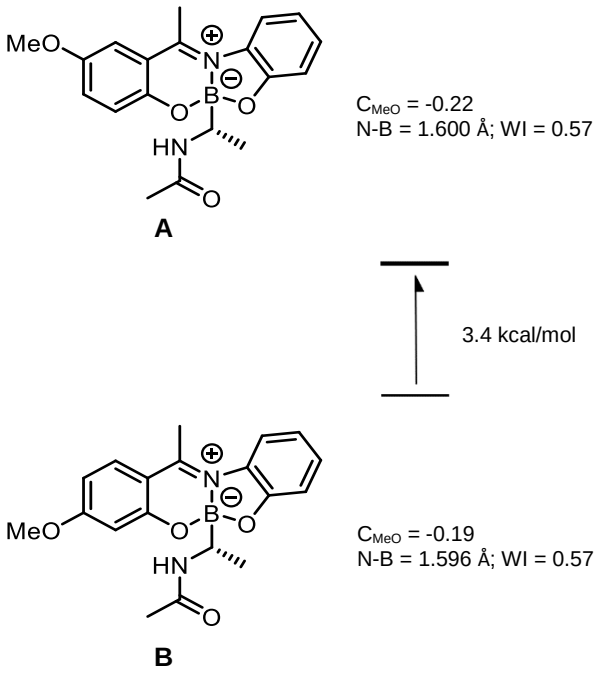

Scheme 52 – Free energy balance (kcal/mol) calculated on a simple model for isomer A and B. Bond B-N distances are indicated (Å).

The results indicate that in the isomer **B** where MeO is *para* with respect to the imine, the MeO group is a better electron donor (with a charge of C = – 0.19) than in the other case (**A**) were it is more negative and, hence, a poor donor (C = – 0.22). This reflected in a slightly stronger B–N bond in **B** (1.596 Å, WI = 0.58) than corresponding one in **A** (dB–N = 1.600 Å, WI = 0.57). As a consequence, the isomer **B** is clearly the most stable (ΔG = 3.4 kcal/mol).

Thus, from the electronic point of view, the most stable boronate complex is the one with the ether chain in *para* with respect to the imine group and this corresponds to the theoretical complex from the building block **59a**. The fact that such complex was not formed but, instead, the B-complex **62** with the PEG chain *meta* to the imine, derived from **59b**, was, is most probably related to greater stereochemical repulsion between the PEG chain and **Btz.**

Atomic coordinates of the optimized species (Isomer **A** and **B**):

Isomer A

C	-3.289255	0.081530	0.999179
C	-3.361324	-1.189317	0.403644
C	-2.306755	-1.679433	-0.340202
C	-1.142516	-0.918187	-0.509880
C	-1.088346	0.379312	0.037889
C	-2.165845	0.866499	0.806028
O	-0.128013	-1.447238	-1.225435
B	1.210713	-0.928654	-0.979930
N	1.092045	0.656146	-0.791773
C	0.034683	1.244621	-0.315667
O	2.055137	-0.990407	-2.199686
C	2.726487	0.180740	-2.285894
C	2.217178	1.199119	-1.456373
C	3.821061	0.418106	-3.104654
C	4.412953	1.681423	-3.057030
C	3.932262	2.679013	-2.208634
C	2.823539	2.448719	-1.392418
C	-0.069870	2.730958	-0.243579
C	1.989287	-1.595092	0.279529
C	2.514454	-2.999715	-0.026449
N	1.185076	-1.527756	1.515089
C	0.164782	-2.334983	1.842839
O	-0.142138	-3.352492	1.201660
C	-0.632448	-1.932931	3.061322
O	-4.377574	0.453105	1.738868
C	-4.333327	1.737166	2.344640
H	-4.258315	-1.782239	0.552612
H	-2.347353	-2.668415	-0.783346
H	-2.095084	1.852204	1.248228
H	4.199956	-0.367516	-3.748708
H	5.274441	1.884999	-3.684889
H	4.426541	3.643238	-2.172427
H	2.472263	3.217648	-0.716413
H	0.534863	3.113270	0.584894
H	-1.100385	3.051078	-0.107894
H	0.313550	3.167290	-1.170487
H	2.864137	-0.968208	0.495985
H	2.897307	-3.489195	0.874643
H	3.336546	-2.919384	-0.742577
H	1.749399	-3.643413	-0.464319
H	1.286928	-0.685524	2.065398
H	-1.653806	-1.711274	2.735854
H	-0.224892	-1.064367	3.580699
H	-0.679053	-2.781193	3.747800
H	-5.273975	1.850993	2.882458
H	-4.245251	2.526730	1.590564
H	-3.497663	1.810635	3.049141

Isomer B

C	-2.756836	0.180516	1.005776
C	-2.842714	-1.089098	0.409941
C	-1.779568	-1.601495	-0.334443
C	-0.613146	-0.863335	-0.489010
C	-0.523359	0.445958	0.062100
C	-1.609464	0.927239	0.809609
O	0.393743	-1.409181	-1.192989
B	1.743497	-0.901954	-0.965542
N	1.653194	0.679799	-0.784359
C	0.615379	1.283110	-0.275591
O	2.574476	-0.991566	-2.190290
C	3.260967	0.169829	-2.296048
C	2.776436	1.203033	-1.468641
C	4.345833	0.381032	-3.133812
C	4.954221	1.637341	-3.115075
C	4.495977	2.652244	-2.275969
C	3.397618	2.447032	-1.438307
C	0.570376	2.769283	-0.149593
C	2.516368	-1.574819	0.295230
C	3.032622	-2.983568	-0.006058
N	1.708112	-1.497384	1.527449
C	0.686520	-2.301993	1.858740
O	0.384879	-3.327878	1.228743
C	-0.117996	-1.886340	3.067855
O	-3.922044	-1.898319	0.516629
H	-3.567159	0.581922	1.599718
C	-5.007333	-1.457301	1.327938
H	-1.847321	-2.595048	-0.762607
H	-1.550615	1.911144	1.261499
H	4.703342	-0.419010	-3.772404
H	5.807956	1.821326	-3.759360
H	4.998820	3.612700	-2.263908
H	3.065879	3.235272	-0.775348
H	1.275134	3.103754	0.617404
H	-0.425287	3.125038	0.102164
H	0.870389	3.219527	-1.101112
H	3.395346	-0.954002	0.512620
H	3.407755	-3.474709	0.897394
H	3.858894	-2.909436	-0.718043
H	2.265728	-3.622722	-0.447256
H	1.804170	-0.647771	2.067511
H	-1.137604	-1.668408	2.734029
H	0.286021	-1.011583	3.579593
H	-0.168294	-2.726653	3.763750
H	-5.746445	-2.256582	1.296256
H	-5.445821	-0.536845	0.931698
H	-4.682543	-1.297999	2.360616

- **Hydrolysis of B-complex 72 promoted by GSH**

The calculations were performed with a simplified model with Btz replaced by $CH_3CONHCH(CH_3)B(OH)_2$ (Btz', **Scheme 53**) and GSH replaced by CH_3SH. Two explicit water molecules were considered, providing H-bond stabilization of the intermediates and the reactants to the hydrolysis of he two B–O bonds of the B-complex.

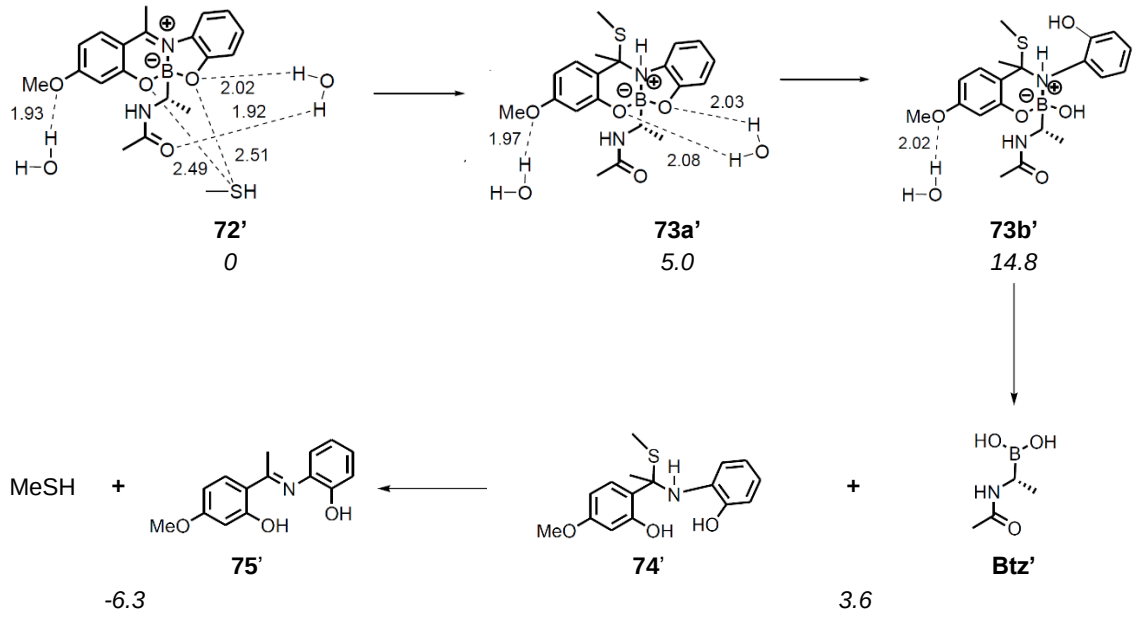

Scheme 53 – Free energy balance (kcal/mol, *italics*) calculated for the reaction of the B-complex **72** disassembly with thiol, including the main intermediates. H-bond distances are indicated (Å).

Atomic coordinates of the optimized species:

72'

C	-4.268966	2.071152	2.638910
O	-1.671237	-1.984159	-2.391694
O	-5.004588	-2.505586	3.282960
C	-4.654689	0.801742	2.182019
H	-5.370853	-1.646018	3.023020
H	-0.967711	-1.321107	-2.330592
C	-3.864359	0.089630	1.279514
H	-1.556584	-2.450567	-1.547000
H	-4.889454	-2.969244	2.444486
C	-2.672217	0.638052	0.825260
C	-2.272359	1.933977	1.252426
C	-3.095369	2.621710	2.156123
O	-1.925719	-0.062725	-0.047302
B	-0.487748	0.145787	0.108683
N	-0.243149	1.728272	0.100338
C	-1.098208	2.545263	0.646652
O	0.243854	-0.239178	-1.122687
C	1.053957	0.779319	-1.491065
C	0.826788	1.977287	-0.787114
C	2.027666	0.701698	-2.474599
C	2.789823	1.842876	-2.731154
C	2.589442	3.023756	-2.016395
C	1.604244	3.105866	-1.029320
C	-0.928488	4.024604	0.571010
C	0.089921	-0.495565	1.501663
C	1.561560	-0.899375	1.409135
N	-0.757574	-1.594940	1.987389
C	-1.122593	-2.631535	1.229017
O	-0.642162	-2.823892	0.094332
C	-2.136162	-3.583848	1.808208
H	-4.873287	2.621228	3.347961
O	-5.792201	0.179054	2.578157
H	-4.165504	-0.900167	0.951983
H	-2.799427	3.604989	2.506129
H	2.183769	-0.225760	-3.014375
H	3.560117	1.803231	-3.494651
H	3.207662	3.890816	-2.220235
H	1.476063	4.020752	-0.465917
H	-0.730790	4.306942	-0.468808
H	-0.072592	4.341262	1.174639
H	-1.820240	4.547567	0.908086
H	0.000329	0.273352	2.277604
H	1.940602	-1.265759	2.367670
H	2.165166	-0.033387	1.115353
H	1.706993	-1.678559	0.656367
H	-1.223248	-1.479448	2.877259
H	-2.937026	-3.715848	1.075672
H	-2.560664	-3.233966	2.749415
H	-1.662416	-4.557385	1.958909
S	-2.144570	2.042407	-2.896930
C	-0.722045	2.445046	-3.964647
H	-1.067554	3.202832	-4.669283
H	-0.397581	1.568611	-4.525538
H	0.106429	2.852035	-3.382941
H	-1.625363	0.957132	-2.295565
C	-6.589940	0.802752	3.585559
H	-7.406317	0.109747	3.782763
H	-6.990592	1.753967	3.225845
H	-6.007738	0.960205	4.497601

73a'

O	-0.800799	-2.090339	-3.258307
H	-1.292237	-1.801939	-2.475903
H	0.094878	-1.818677	-3.005942
C	-3.445763	1.265790	1.496885
C	-3.715794	-0.098925	1.394442
C	-2.844951	-0.946368	0.708499
C	-1.695719	-0.424519	0.135643
C	-1.405303	0.949296	0.209419
C	-2.293193	1.771226	0.896358
O	-0.843052	-1.260834	-0.513396
B	0.581187	-1.104052	-0.256161
N	0.955799	0.499715	-0.067423
C	-0.161212	1.451320	-0.495076
O	1.365038	-1.453721	-1.469959
C	2.345575	-0.536453	-1.623126
C	2.200988	0.592870	-0.817100
C	3.449571	-0.665460	-2.456912
C	4.411820	0.345683	-2.426406
C	4.293579	1.443080	-1.571668
C	3.176283	1.572114	-0.741610
C	0.213185	2.873503	-0.117888
C	1.069970	-1.951829	1.036520
C	0.273972	-1.703044	2.321541
N	2.528522	-1.845666	1.250394
C	3.170762	-0.791312	1.763453
O	2.585269	0.219168	2.202500
C	4.676839	-0.853078	1.744839
O	-4.801557	-0.709483	1.955358
S	-0.480942	1.277992	-2.307908
C	0.604278	2.505740	-3.089740
C	-5.683367	0.099205	2.730071
H	-4.108211	1.935163	2.030505
H	-3.047164	-2.010566	0.650753
H	-2.098215	2.835083	0.975573
H	1.159314	0.678833	0.929700
H	3.557887	-1.539009	-3.090246
H	5.283909	0.261494	-3.067069
H	5.074463	2.194648	-1.541164
H	3.083718	2.401024	-0.047681
H	1.126347	3.188589	-0.622584
H	0.367387	2.938073	0.963899
H	-0.583296	3.562340	-0.406036
H	0.919612	-3.002456	0.761185
H	0.747708	-2.199483	3.174353
H	-0.735728	-2.110196	2.216984
H	0.178122	-0.640128	2.562343
H	3.101858	-2.581410	0.859996
H	5.025215	-0.240823	0.905439
H	5.058237	-1.867945	1.624698
H	5.064178	-0.416913	2.666507
H	1.659291	2.304498	-2.896925
H	0.346504	3.523579	-2.795031
H	0.416815	2.397095	-4.160694
H	-6.443774	-0.576551	3.118772
H	-6.152907	0.865489	2.106342
H	-5.151056	0.571575	3.560964
O	-3.205211	-2.663646	3.401744
H	-3.893025	-2.108151	3.002760
H	-2.995162	-3.296456	2.703841

73b'

C	-3.979847	1.163888	1.462632
O	-3.333307	-1.943957	4.097984
C	-4.216931	-0.207549	1.559129
H	-4.130860	-1.692985	3.607321
C	-3.341480	-1.124144	0.978102
H	-3.024605	-2.732458	3.634417
C	-2.209263	-0.667648	0.315405
C	-1.946346	0.709205	0.201770
C	-2.846530	1.601896	0.779319
O	-1.376406	-1.559968	-0.253281
B	0.084281	-1.451716	-0.161373
N	0.429158	0.273866	-0.051577
C	-0.725680	1.136797	-0.573643
O	1.996620	2.162428	1.449760
C	2.469744	1.663316	0.267470
C	1.745721	0.737629	-0.510680
C	3.688437	2.154351	-0.202952
C	4.187728	1.761210	-1.437936
C	3.464860	0.863397	-2.216170
C	2.252340	0.359632	-1.754909
C	-0.430928	2.622803	-0.428540
C	0.617705	-2.200296	1.188429
C	-0.321326	-2.112298	2.396719
N	2.024777	-1.918822	1.529374
C	2.441358	-0.879267	2.233104
O	1.630622	-0.028945	2.693025
C	3.915593	-0.731939	2.479980
H	-4.651578	1.887144	1.906413
O	-5.273844	-0.756162	2.230660
H	-3.527151	-2.189426	1.067132
H	-2.675337	2.670077	0.704480
H	4.221286	2.862022	0.423690
H	5.134769	2.157058	-1.789542
H	3.835617	0.550082	-3.185773
H	1.702791	-0.335950	-2.369974
H	0.483934	2.889180	-0.959018
H	-0.336348	2.900336	0.624418
H	-1.250294	3.191994	-0.873664
H	0.636739	-3.254437	0.889535
H	0.149480	-2.522513	3.295903
H	-1.214237	-2.705220	2.180562
H	-0.645259	-1.092311	2.616470
H	2.728681	-2.551643	1.171767
H	4.232383	0.250689	2.118183
H	4.504369	-1.508987	1.992234
H	4.091107	-0.760813	3.558167
S	-0.894739	0.753562	-2.397955
C	-2.648297	1.144299	-2.638364
H	-2.879150	2.145547	-2.268225
H	-3.290764	0.405723	-2.156645
H	-2.815266	1.121813	-3.716947
H	0.412846	0.435035	0.965362
C	-6.156796	0.137896	2.902388
H	-6.915426	-0.487425	3.371128
H	-6.631937	0.822336	2.193652
H	-5.624706	0.709611	3.669068
O	0.675675	-2.023725	-1.316935
H	0.161559	-1.759235	-2.093146
H	1.859058	1.404519	2.087197

Btz'

B	-1.525711	-0.336460	-0.914199
O	-0.900642	-0.477020	-2.115672
C	-0.851598	-0.889961	0.432255
H	-0.052617	-0.949496	-1.984780
C	-1.644323	-0.578703	1.695619
N	0.521983	-0.378591	0.599317
C	1.553227	-0.779855	-0.146703
O	1.403450	-1.534228	-1.131922
C	2.921757	-0.301112	0.253230
H	-0.766857	-1.980883	0.325430
H	-1.155596	-0.989330	2.583561
H	-2.642998	-1.019316	1.628193
H	-1.757401	0.502035	1.835011
H	0.707159	0.218217	1.396213
H	3.523879	-1.173783	0.518675
H	2.899954	0.391483	1.095083
H	3.392174	0.180089	-0.606658
O	-2.745754	0.279188	-0.937402
H	-3.141486	0.366026	-0.061452

74'

C	-2.462753	0.093640	2.196730
C	-2.967431	-1.057903	1.596429
C	-2.321069	-1.606603	0.487161
C	-1.165292	-1.023481	-0.011466
C	-0.608244	0.127056	0.594993
C	-1.297217	0.660413	1.682989
O	-0.615125	-1.625080	-1.113301
H	1.753225	-1.782291	-1.256824
N	1.732967	-0.353476	0.312742
C	0.716737	0.715581	0.131228
O	2.483035	-1.721382	-1.902896
C	3.384446	-0.850004	-1.364664
C	3.050860	-0.125011	-0.209195
C	4.636007	-0.703762	-1.958381
C	5.574316	0.142491	-1.374682
C	5.277338	0.825775	-0.196236
C	4.017611	0.687173	0.382896
C	1.092218	2.006284	0.855037
H	-2.949249	0.549180	3.049366
O	-4.091429	-1.710444	2.005323
H	-2.730858	-2.485093	0.000736
H	-0.915733	1.549092	2.171865
H	4.864836	-1.268958	-2.855658
H	6.550989	0.253475	-1.834951
H	6.020648	1.463317	0.270005
H	3.778115	1.203833	1.307572
H	2.020080	2.401711	0.439931
H	1.241497	1.811849	1.922269
H	0.317207	2.769088	0.746658
S	0.670317	1.086104	-1.704506
C	-0.902561	1.984746	-1.810063
H	-0.913504	2.831910	-1.122369
H	-1.750024	1.326600	-1.611883
H	-0.971463	2.361470	-2.832017
H	1.784279	-0.519397	1.317280
C	-4.793132	-1.164981	3.115516
H	-5.654082	-1.813880	3.273293
H	-5.135458	-0.147270	2.902937
H	-4.168942	-1.162203	4.014678
H	-0.107763	-0.951169	-1.612140

75'

C	-3.082138	1.242854	1.037763
C	-2.911143	0.353694	2.108037
C	-1.779642	-0.455698	2.180489
C	-0.806606	-0.393589	1.188436
C	-0.957144	0.489582	0.083975
C	-2.108280	1.290662	0.052917
O	0.269207	-1.197361	1.317358
H	1.428205	-2.313993	-1.147009

N	1.131289	-0.140230	-0.828809
C	0.062585	0.577922	-0.973608
O	2.225243	-2.514352	-1.662596
C	2.802003	-1.339573	-2.054248
C	2.240245	-0.101813	-1.695442
C	3.958021	-1.392134	-2.826775
C	4.576603	-0.211466	-3.228092
C	4.044437	1.022376	-2.858098
C	2.883967	1.073713	-2.091262
C	-0.206313	1.464217	-2.157488
H	-3.949569	1.886028	0.968870
O	-3.799490	0.215979	3.125920
H	-1.651850	-1.138156	3.013372
H	-2.247943	1.987581	-0.766318
H	4.360410	-2.362988	-3.096744
H	5.480855	-0.257977	-3.825997
H	4.535218	1.942772	-3.155229
H	2.476987	2.027402	-1.769166
H	0.484877	1.252235	-2.972066
H	-0.108783	2.518659	-1.881053
H	-1.227255	1.305921	-2.510409
C	-4.962126	1.037749	3.098725
H	-5.533364	0.779033	3.989208
H	-5.563930	0.836549	2.207247
H	-4.694325	2.098161	3.130248
H	0.872250	-0.962758	0.545345

MeSH

H	0.917202	-1.202456	-0.918720
S	1.240056	-0.337424	0.055412
C	-0.380376	0.488974	0.163989
H	-0.281534	1.277401	0.910814
H	-1.152306	-0.209371	0.486557
H	-0.654643	0.938076	-0.790153

IV.2 Experimental section of Chapter III

IV.2.1 Synthesis and structural characterization

The solvents acetonitrile, ethanol, and methanol were used without further purification. Dichloromethane was dried over calcium hydride under nitrogen atmosphere and DMF was dried over molecular sieve and distilled under reduced pressure. The boronic acid derivatives, 2-hydroxy-4-methoxysalicylaldehyde, 2-hydroxy-4-methoxyacetophenone, hydrazine hydrate and amberlyst 15 were purchased from Aldrich and used without further purification. Phenylglyoxylic acid was purchased from Fluka and 4-nitrophenylglyoxylic acid was bought from Alfa-Aesar and they were used as received. F_3C- and NC-phenylglyoxylic acids were prepared via basic hydrolysis of the corresponding ethyl ester.[226,227] Boronate-BODIPY **84** and boronate-coumarin **86** were prepared according to reported methodologies.[228,229]

Thin layer chromatography was performed using Merck silica gel 60 F254 aluminum plates and visualized by UV light or with phosphomolybdic acid solution. For column chromatography silica gel 60 M (Macherey-Nagel) was used.

The NMR spectra (δ values in ppm) were recorded on standard instrumentation, operated at 400 or 300 MHz (^{1}H), 100 or 75 MHz (^{13}C), and 128 MHz (^{11}B), using $CDCl_3$ or $(CD_3)_2SO$ as deuterated solvents. All coupling constants (*J*) are expressed in Hz. Multiplicities are given as: s (singlet), d (doublet), dd (double doublet), t (triplet), q (quartet), and m (multiplet). LRMS analysis were done on a Micromass Quattro Micro API mass spectrometer (Waters, Ireland), equipped with a triple quadrupole and an electrospray ion source (ESI) operating in positive mode. HRMS were done on a triple quadrupole/linear ion trap mass spectrometer, using electrospray ionization. Infrared spectra of samples dispersed in KBr disks were recorded on a Fourier transform spectrometer with ceramic infrared light source and a deuterated L-alanine doped triglycine sulfate detector. Elemental analysis was performed with a Flash 2000 CHNS-O analyzer (ThermoScientific, UK).

Reagents and solvents used for Annexin V conjugations were obtained from Sigma- Aldrich and used without any prior purification. Sulfo-cyanine5 azide (Cy5-N_3) was bought from Lumiprobe and used without any prior purification. Dibenzocyclooctyne--maleimide **90** was purchased from Sigma-aldrich. Mass spectra were acquired on a high-mass Q-TOF-type instrument Xevo G2-S (Waters, Manchester, UK). Mass spectrometry experiments were performed at a capillary voltage of 1990 V, cone voltage of 80 V and source offset voltage of 80 V. Spectra were processed using MassLynx V4.1 (Waters).

- **BASHYs 78a-c and their salicylhydrazones precursors 76a-c**

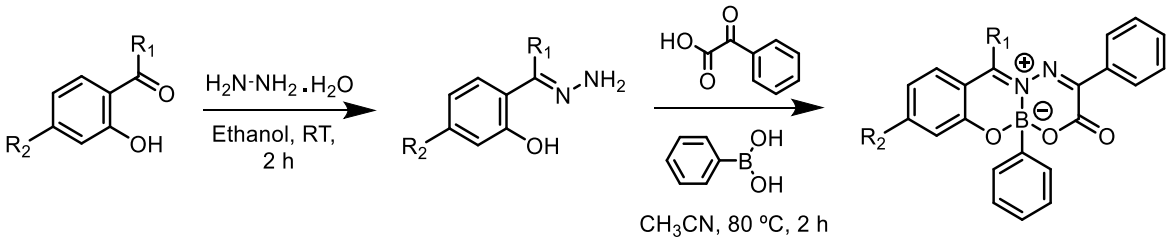

76a (R_1 = H; R_2 = MeO);
76b (R_1 = Me; R_2 = MeO);
76c (R_1 = Me; R_2 = -O(-CH_2)$_2$-O-)$_3$-Me

78a (R_1 = H; R_2 = MeO);
78b (R_1 = Me; R_2 = MeO);
78c (R_1 = Me; R_2 = -O(-CH_2)$_2$-O-)$_3$-Me

Scheme 54 – Methodology to prepare BASHYs **78a-c** and their salicylhydrazones precursors **76a-c**.

The synthesis of salicylhydrazones **76a-c** was done by adapting a reported literature procedure.[230] Therefore, in order to prepare salicylhydrazones **76a-c**, an excess of hydrazine hydrate (2 mmol) was added into a round bottom flask and dissolved in 250 µL of ethanol. Then, a solution of aldehyde or ketone (0.3 mmol) in 250 µL of ethanol was dropwised into the hydrazine solution over a period of 30 min. The reaction mixture was then stirred for 1.5 h at RT. Afterwards, volatiles were evaporated and compounds **76b,c** were obtained with high purity in near quantitative yield. Compound **76a** was obtained after evaporation of volatiles and washing the solid obtained with 1.5 mL of cold ethanol, being the desired compound in the ethanolic solution. Volatiles were evaporated and compound **76a** was obtained in 81 % yield.

Compound **76a –** Yellow solid; Yield 91 %; **^{1}H NMR** (300 MHz, $CDCl_3$) δ 11.29 (s, 1H, -OH), 7.83 (s, 1H, CH_{imine}), 7.00 (d, *J* = 8.4 Hz, 1H, CH_{Arom}), 6.48 (d, *J* = 2.4 Hz, 1H, CH_{Arom}), 6.43 (dd, *J* = 8.4, 2.4 Hz, 1H, CH_{Arom}), 5.28 (s, 2H, -NH_2), 3.79 (s, 3H, -OCH_3); **^{13}C NMR** (75 MHz, $CDCl_3$) δ 161.47, 159.58, 147.33, 130.42, 112.07, 106.26, 101.41, 55.44; **LRMS** calcd m/z ($[M+H]^+$): 167, found m/z ($[M+H]^+$): 167;

Compound **76b –** Yellow solid; Yield 99 %; **^{1}H NMR** (300 MHz, $CDCl_3$) δ 13.04 (s, 1H, -OH), 7.28 (d, *J* = 8.7 Hz, 1H, CH_{Arom}), 6.48 (d, *J* = 2.4 Hz, 1H, CH_{Arom}), 6.41 (dd, *J* = 8.7, 2.4 Hz, 1H, CH_{Arom}), 5.13 (s, 2H, NH_2), 3.79 (s, 3H, -OCH_3), 2.18 (s, 3H, -(CH_3)C=N-); **^{13}C NMR** (75 MHz, $CDCl_3$) δ 161.17, 160.53, 153.37, 127.80, 113.58, 105.58, 101.78, 55.38, 11.03; **LRMS** calcd m/z ($[M+H]^+$): 181, found m/z ($[M+H]^+$): 181; **E.A** calcd (%) for $C_9H_{12}N_2O_2$: C 59.99, H 6.71, N 15.55, found (%): C 59.88, H 6.87, N 15.44.

Compound **76c –** Yellow oil; Yield 99 %; **^{1}H NMR** (300 MHz, $CDCl_3$) δ 13.03 (s, 1H, -OH), 7.26 (d, *J* = 8.7 Hz, 1H, CH_{Arom}), 6.46 (d, *J* = 2.4 Hz, 1H, CH_{Arom}), 6.43 (dd, *J* = 8.7, 2.4 Hz, 1H, CH_{Arom}), 5.13 (s, 2H, -NH_2), 4.19 – 4.06 (m, 2H, PEG CH_2), 3.90 – 3.80 (m, 2H, PEG CH_2), 3.76 – 3.71 (m, 2H, PEG CH_2), 3.71 – 3.62 (m, 4H, PEG CH_2's), 3.58 – 3.51 (m, 2H, PEG CH_2), 3.37 (s, 3H, -OCH_3), 2.18 (s, 3H, -(CH_3)C=N-); **^{13}C NMR** (75 MHz, $CDCl_3$) δ 160.44, 160.32, 153.33, 127.77, 113.69, 106.14, 102.43, 72.04, 70.94, 70.76, 70.68, 69.74, 67.44, 59.16, 11.05; **LRMS** calcd m/z ($[M+H]^+$): 313, found m/z ($[M+H]^+$): 313.

BASHYs **78a-c** were then assembled, using equimolar amounts (0.16 mmol) of the corresponding salicylhydrazones **76a-c** precursor, phenylglyoxylic acid and phenylboronic acid. These 3 components were added to a round bottom flask, dissolved in 1 mL of acetonitrile and stirred at 80 ºC for 2 h. Volatiles were evaporated and BASHYs **78a-c** were obtained with high purity in near quantitative yield.

BASHY **78a –** Yellow solid; Yield 99 %; **^{1}H NMR** (300 MHz, $(CD_3)_2SO$) δ 9.30 (s, 1H, CH_{imine}), 7.89 (d, *J* = 7.2 Hz, 2H, Arom), 7.75 (d, *J* = 8.7 Hz, 1H, Arom), 7.63 – 7.42 (m, 3H, Arom), 7.27 – 7.15 (m, 5H, Arom), 6.74 (dd, *J* = 8.7, 2.1 Hz, 1H, Arom), 6.70 (m, 1H, Arom), 3.90 (s, 3H, -OCH_3); **^{13}C NMR** (101 MHz, $(CD_3)_2SO$) δ 169.96, 161.29, 159.17, 156.64, 154.41, 135.71, 134.06, 131.73, 130.17, 129.27, 128.51, 128.05, 127.73, 127.34, 110.78, 109.29, 101.85, 56.41; **LRMS** calcd m/z ($[M+H]^+$): 385, found m/z ($[M+H]^+$): 385; **E.A** calcd (%) for $C_{22}H_{17}BN_2O_4$: C 68.78, H 4.46, N 7.29, found (%): C 68.63, H 4.38, N 7.29.

BASHY **78b –** Yellow solid; Yield 99 %; **^{1}H NMR** (400 MHz, $(CD_3)_2SO$) δ 7.98 (d, *J* = 9.2 Hz, 1H, Arom), 7.93 (d, *J* = 7.6 Hz, 2H, Arom), 7.66 – 7.53 (m, 1H, Arom), 7.53 – 7.43 (m, 2H, Arom), 7.24 – 7.13 (m, 5H, Arom), 6.70 (dd, *J* = 8.8, 1.6 Hz, 1H, Arom), 6.67 – 6.59 (m, 1H, Arom), 3.88 (s, 3H, -OCH_3), 2.96 (s, 3H, -(CH_3)C=N-); **^{13}C NMR** (101 MHz, $(CD_3)_2SO$) δ 169.46, 168.57, 160.25, 155.50, 154.66, 132.85, 131.92, 131.74, 130.31, 129.38, 128.50, 127.81, 127.63, 110.13, 109.98, 102.05, 56.21, 14.11; **LRMS** calcd m/z ($[M+H]^+$): 399, found m/z ($[M+H]^+$): 399; **E.A** calcd (%) for $C_{23}H_{19}BN_2O_4$: C 69.37, H 4.81, N 7.03, found (%): C 69.15, H 4.77, N 6.95.

BASHY **78c –** Yellow solid; Yield 99 %; **^{1}H NMR** (300 MHz, $CDCl_3$) δ 8.09 – 7.99 (m, 2H, Arom), 7.60 (d, *J* = 9.0 Hz, 1H, Arom), 7.53 – 7.39 (m, 3H, Arom), 7.33 – 7.27 (m, 2H, Arom), 7.23 – 7.14 (m, 3H, Arom), 6.61 (dd, *J* = 9.0, 2.4 Hz, 1H, Arom), 6.53 (d, *J* = 2.4 Hz, 1H, Arom), 4.18 (d, *J* = 4.5 Hz, 2H, PEG CH_2), 3.87 (d, *J* = 4.5 Hz, 2H,

PEG C$\underline{H_2}$), 3.76 – 3.70 (m, 2H, Peg C$\underline{H_2}$), 3.70 – 3.62 (m, 4H, PEG C$\underline{H_2}$'s), 3.59 – 3.52 (m, 2H, PEG C$\underline{H_2}$), 3.38 (s, 3H, OC$\underline{H_3}$), 2.90 (s, 3H, -(C$\underline{H_3}$)C=N-); **^{13}C NMR** (75 MHz, $CDCl_3$) δ 168.30, 167.62, 161.53, 156.49, 155.30, 132.27, 131.88, 131.14, 130.86, 129.94, 128.49, 128.16, 127.79, 111.43, 110.32, 103.09, 72.03, 71.00, 70.75, 70.71, 69.32, 68.26, 59.18, 14.07; **LRMS** calcd m/z ($[M+H]^+$): 531, found m/z ($[M+H]^+$): 531; **E.A** calcd (%) for $C_{29}H_{31}BN_2O_7$: C 65.67, H 5.89, N 5.28, found (%): C 65.37, H 5.96, N 5.38.

- **Schiff base ligands 80a-d and their precursors 79a-d**

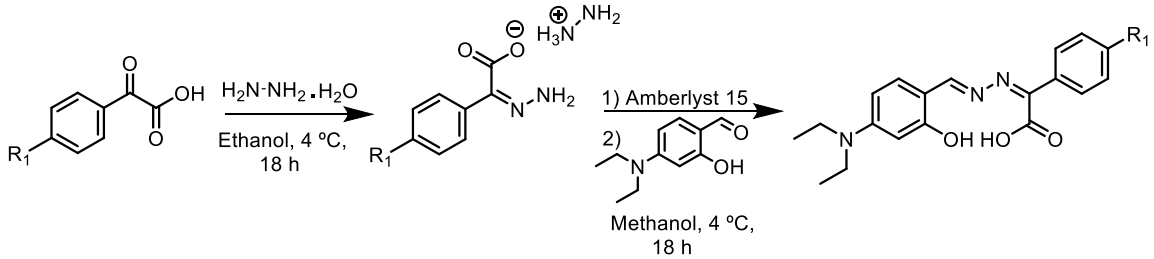

79a – R_1 = H
79b – R_1 = NO_2
79c – R_1 = CF_3
79d – R_1 = CN

80a – R_1 = H
80b – R_1 = NO_2
80c – R_1 = CF_3
80d – R_1 = CN

Scheme 55 – Synthetic methodology to construct Schiff base ligands **80a-d** and their precursors **79a-d.**

Preparation of hydrazonophenylacetates **79a-d** was achieved by adapting a reported literature procedure.[231] In order to synthesize hydrazonophenylacetates **79a-d**, hydrazine hydrate (30 mmol) and the corresponding phenylglyoxylic acid derivative (10 mmol) were each dissolved in a separate portion of ethanol (5 mL). Then, the two solutions were mixed into a round bottomed flask and the reaction continued for 18 h at 4 °C. The reaction mixture was then filtered and the solid obtained was washed with 2 mL of cold ethanol. Hydrazonophenylacetates were all obtained as solids in moderate to good yields (**79a –** white solid, 70 %; **79b –** yellow solid, 66 %; **79c –** yellow solid, 40 %; **79d –** yellow solid, 50 %) and used immediately in the preparation of the corresponding Schiff base ligand **80a-d** without further purification or characterization.

Construction of Schiff base ligands **80a-d** was performed by adapting a reported literature procedure.[232] Synthesis of each Schiff base ligands **80a-d** started with the dissolution of the corresponding hydrazonophenylacetates **79a-d** in 5 mL of water and then 45 mL of methanol were added. This solution was slowly passed through a column packed with amberlyst 15 (3 ml of dry resin wetted with methanol) into a round bottomed flask containing a 5 mL methanolic solution of 4-diethylaminosalicylaldehyde (2.5 mmol). The resulting mixture was stirred for 2 h at RT and then it was left at 4 °C for 18 h.

Afterwards, the reaction mixture was filtered and the solid obtained was washed with 2 mL of cold methanol and 2 mL of cold dichloromethane. Schiff base ligands **80a-d** were obtained as solids in high purity and in moderate to good yields.

Schiff base ligand **80a –** Orange solid; Yield 60 %; **^{1}H NMR** (300 MHz, $CDCl_3$) δ 8.14 (s, 1H, CH_{imine}), 8.05 – 8.00 (m, 2H, CH_{Arom}), 7.69 (d, *J* = 1.8 Hz, 1H, CH_{Arom}), 7.42 – 7.36 (m, 3H, CH_{Arom}), 7.17 (d, *J* = 9.3 Hz, 1H, CH_{Arom}), 6.33 (dd, *J* = 9.3, 2.4 Hz, 1H, CH_{Arom}), 3.56 (q, *J* = 6.9 Hz, 4H, -N($C\underline{H}_2$)$_2$(CH_3)$_2$), 1.29 (t, *J* = 6.9 Hz, 6H, -N(CH_2)$_2$($C\underline{H}_3$)$_2$); **^{13}C NMR** (75 MHz, $(CD_3)_2SO$) δ 166.84, 164.47, 161.37, 159.07, 151.94, 134.28, 131.50, 131.34, 129.26, 129.18, 127.51, 126.87, 106.08, 104.52, 96.86, 44.03, 12.56; **LRMS** calcd m/z ([M+H]$^+$): 340, found m/z ([M+H]$^+$): 340; **E.A** calcd (%) for $C_{19}H_{21}N_3O_3.\frac{3}{5}H_2O$: C 65.16, H 6.39, N 12.00, found (%): C 65.54, H 6.08, N 11.61.

Schiff base ligand **80b –** Orange solid; Yield 54 %; **^{1}H NMR** (300 MHz, $(CD_3)_2SO$) δ 8.78 (s, 1H, CH_{imine}), 8.35 (d, *J* = 9.0 Hz, 2H, CH_{Arom}), 7.99 (d, *J* = 9.0 Hz, 2H, CH_{Arom}), 7.41 – 7.32 (m, 1H, CH_{Arom}), 6.37 (dd, *J* = 9.0, 2.1 Hz, 1H, CH_{Arom}), 6.11 (d, *J* = 2.1 Hz, 1H, CH_{Arom}), 3.40 (q, *J* = 6.9 Hz, 4H, -N($C\underline{H}_2$)$_2$(CH_3)$_2$), 1.12 (t, *J* = 6.9 Hz, 6H, -N(CH_2)$_2$($C\underline{H}_3$)$_2$); **LRMS** calcd m/z ([M+H]$^+$): 385, found m/z ([M+H]$^+$): 385; **E.A** calcd (%) for $C_{19}H_{20}N_4O_5$: C 59.37, H 5.24, N 14.58, found (%): C 59.48, H 5.55, N 14.25; **Note:** ^{13}C NMR was not possible due to solubility problems.

Schiff base ligand **80c –** Orange solid; Yield 57 %; **^{1}H NMR** (300 MHz, $(CD_3)_2SO$) δ 8.77 (s, 1H, CH_{imine}), 7.96 (d, *J* = 8.7 Hz, 2H, CH_{Arom}), 7.89 (d, *J* = 8.7 Hz, 2H, CH_{Arom}), 7.38 (d, *J* = 9.0 Hz, 1H, CH_{Arom}), 6.37 (dd, *J* = 9.0, 2.1 Hz, 1H, CH_{Arom}), 6.11 (d, *J* = 2.1 Hz, 1H, CH_{Arom}), 3.41 (q, *J* = 6.9 Hz, 4H, -N($C\underline{H}_2$)$_2$(CH_3)$_2$), 1.12 (t, *J* = 6.9 Hz, 6H, -N(CH_2)$_2$($C\underline{H}_3$)$_2$); **^{13}C NMR** (75 MHz, $(CD_3)_2SO$) δ 166.27, 165.28, 161.61, 157.35, 152.31, 135.50, 134.46, 127.53, 126.19 ($\underline{C}F_3$), 126.14 ($\underline{C}F_3$), 126.09 ($\underline{C}F_3$), 126.04 ($\underline{C}F_3$), 106.02, 104.75, 96.80, 44.06, 12.55; **LRMS** calcd m/z ([M+H]$^+$): 408, found m/z ([M+H]$^+$): 408; **E.A** calcd (%) for $C_{20}H_{20}F_3N_3O_3$: C 58.97, H 4.95, N 10.31, found (%): C 58.63, H 4.88, N 10.19.

Schiff base ligand **80d –** Orange solid; Yield 62 %; **^{1}H NMR** (300 MHz, $(CD_3)_2SO$) δ 8.77 (s, 1H, CH_{imine}), 7.98 (d, *J* = 8.7 Hz, 2H, CH_{Arom}), 7.90 (d, *J* = 8.7 Hz, 2H, CH_{Arom}), 7.38 (d, *J* = 9.0 Hz, 1H, CH_{Arom}), 6.38 (dd, *J* = 9.0, 2.1 Hz, 1H, CH_{Arom}), 6.11 (d, *J* = 2.1 Hz, 1H, CH_{Arom}), 3.41 (q, *J* = 6.9 Hz, 4H, -N($C\underline{H}_2$)$_2$(CH_3)$_2$), 1.12 (t, *J* = 6.9 Hz, 6H, -N(CH_2)$_2$($C\underline{H}_3$)$_2$); **^{13}C NMR** (75 MHz, $(CD_3)_2SO$) δ 166.13, 165.37, 161.69, 157.13, 152.41, 135.89, 134.50, 133.08, 127.40, 118.45, 113.04, 106.05, 104.83, 96.78, 44.08, 12.56;

LRMS calcd m/z ([M+H]$^+$): 365, found m/z ([M+H]$^+$): 365; **E.A** calcd (%) for $C_{20}H_{20}N_4O_3$: C 65.92, H 5.53, N 15.38, found (%): C 65.95, H 5.53, N 15.04.

- **BASHYs (81a-e, 82a-g, 83a-b, 85**, **87 and 88) and dimeric BASHYs (81f and 82h)**

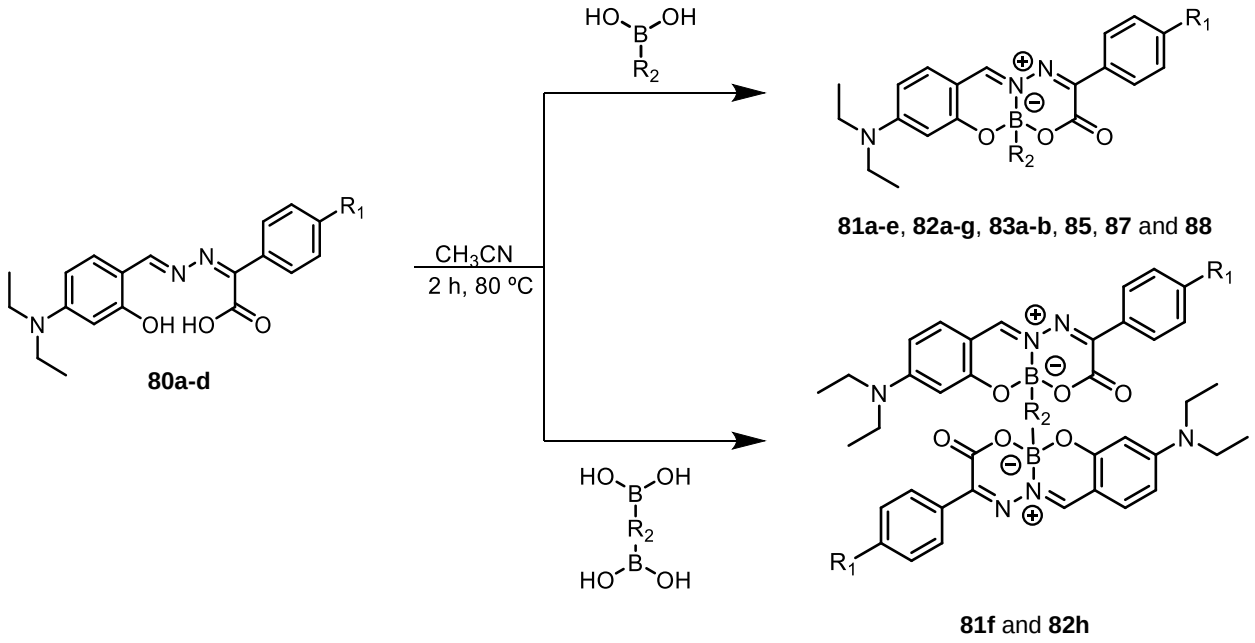

Scheme 56 – Synthetic methodology to assemble monomeric BASHYs **(81a-e, 82a-g, 83a-b** and **88)** and dimeric BASHYs **(81f** and **82h).**

In order to assemble the monomeric BASHY complexes (**81a-e**, **82a-g**, **83a-b**, **85**, **87** and **88)**, equimolar amounts of the corresponding Schiff base ligand and phenylboronic acid derivative (0.1 mmol) were added to a round bottomed flask, dissolved in 1 mL of acetonitrile and stirred at 80 ºC for 2 h. Then the volatiles were evaporated.

In the case of BASHYs **81a-e**, **82b,c,e-g** and **83a,b**, this procedure yielded high purity products in near quantitative yield without the need for further purification. Eventual trace impurities, that were observed in the synthesis of BASHY **88**, can be removed by washing the solid obtained with a small amount (0.5 mL) of cold methanol. Exceptions from this very direct and straightforward procedure were BASHYs **82a,d**, **85** and **87**, for which additional purification was required [BASHY **82a** – preparative thin-layer chromatography using dichloromethane as eluent; BASHY **82d** – flash column chromatography using hexane / dichloromethane (1 : 9) as eluent; BASHY **85** – flash column chromatography using hexane / ethylacetate (1 : 1) as eluent; BASHY **87** – filtration through a plug of silica, using ethyl acetate as eluent.

Dimeric BASHYs **81f** and **82h** were prepare, using 2 equivalents of the corresponding Schiff base ligand (0.2 mmol) and 1 equivalent of diboronic acid derivative (0.1 mmol). These two components were dissolved in 1 mL of acetonitrile and stirred at 80 ºC for 2 h. After evaporation of volatiles, BASHY **82h** was obtained as a solid in near quantitative yield. For BASHY **81f**, the solid obtained was washed with 0.5 mL of cold methanol in order to remove minor impurities.

BASHY **81a** (R_1 = H; R_2 = Ph) – Orange solid; Yield 99 %; **^{1}H NMR** (300 MHz, $CDCl_3$) δ 8.29 (s, 1H, CH_{imine}), 8.00 (dd, *J* = 8.1, 1.5 Hz, 2H, CH_{Arom}), 7.45 – 7.35 (m, 5H, CH_{Arom}), 7.24 – 7.18 (m, 4H, CH_{Arom}), 6.37 (dd, *J* = 9.0, 2.4 Hz, 1H, CH_{Arom}), 6.22 (d, *J* = 2.1 Hz, 1H, CH_{Arom}), 3.52 – 3.39 (m, 4H, -N($C\underline{H_2}$)$_2$(CH_3)$_2$), 1.24 (t, *J* = 7.2 Hz, 6H, -N(CH_2)$_2$($C\underline{H_3}$)$_2$); **^{13}C NMR** (75 MHz, $CDCl_3$) δ 161.67, 157.38, 155.90, 154.03, 153.68, 134.70, 132.77, 130.93, 130.85, 129.56, 128.29, 127.92, 127.70, 107.80, 106.49, 98.74, 45.46, 12.83; **LRMS** calcd m/z ($[M+H]^+$): 426, found m/z ($[M+H]^+$): 426; **E.A** calcd (%) for $C_{25}H_{24}BN_3O_3$: C 70.6, H 5.69, N 9.88, found (%): C 70.8, H 5.98, N 9.89.

BASHY **81b** (R_1 = H; R_2 = 4-MePh) – Orange solid; Yield 99 %; **^{1}H NMR** (300 MHz, $CDCl_3$) δ 8.28 (s, 1H, CH_{imine}), 8.02 – 7.97 (m, 2H, CH_{Arom}), 7.44 – 7.35 (m, 3H, CH_{Arom}), 7.29 (d, *J* = 7.8 Hz, 2H, CH_{Arom}), 7.21 (d, *J* = 9.3 Hz, 1H, CH_{Arom}), 7.02 (d, *J* = 7.6 Hz, 2H, CH_{Arom}), 6.36 (dd, *J* = 9.3, 2.4 Hz, 1H, CH_{Arom}), 6.20 (d, *J* = 2.4 Hz, 1H, CH_{Arom}), 3.50 – 3.38 (m, 4H, -N($C\underline{H_2}$)$_2$(CH_3)$_2$), 2.24 (s, 3H, Ph-$C\underline{H_3}$), 1.24 (t, *J* = 7.0 Hz, 6H, -N(CH_2)$_2$($C\underline{H_3}$)$_2$); **^{13}C NMR** (75 MHz, $CDCl_3$) δ 161.74, 157.35, 155.94, 154.12, 153.65, 137.48, 134.65, 132.81, 130.91, 129.59, 128.50, 128.29, 107.72, 106.54, 98.83, 45.47, 21.44, 12.86; **LRMS** calcd m/z ($[M+H]^+$): 440, found m/z ($[M+H]^+$): 440; **E.A** calcd (%) for $C_{26}H_{26}BN_3O_3$: C 71.08, H 5.97, N 9.56, found (%): C 70.93, H 6.18, N 9.51.

BASHY **81c** (R_1 = H; R_2 = 4-CF_3Ph) – Orange solid; Yield 99 %; **^{1}H NMR** (300 MHz, $CDCl_3$) δ 8.33 (s, 1H, CH_{imine}), 8.01 – 7.95 (m, 2H, CH_{Arom}), 7.51 – 7.37 (m, 7H, CH_{Arom}), 7.24 (d, *J* = 9.3 Hz, 1H, CH_{Arom}), 6.39 (dd, *J* = 9.3, 2.4 Hz, 1H, CH_{Arom}), 6.20 (d, *J* = 2.4 Hz, 1H, CH_{Arom}), 3.55 – 3.37 (m, 4H, -N($C\underline{H_2}$)$_2$(CH_3)$_2$), 1.24 (t, *J* = 7.2 Hz, 6H, -N(CH_2)$_2$($C\underline{H_3}$)$_2$); **^{13}C NMR** (75 MHz, $CDCl_3$) δ 161.45, 157.59, 155.64, 154.01, 153.72, 134.80, 132.55, 131.15, 131.08, 129.55, 128.40, 124.49 (CF_3), 124.44 (CF_3), 124.39 (CF_3), 124.34 (CF_3), 108.12, 106.44, 98.74, 45.57, 12.84; **LRMS** calcd m/z ($[M+H]^+$): 494, found m/z ($[M+H]^+$): 494; **E.A** calcd (%) for $C_{26}H_{23}BF_3N_3O_3$: C 63.31, H 4.7, N 8.52, found (%): C 63.22, H 4.9, N 8.7.

BASHY **81d** (R_1 = H; R_2 = 4-MeOPh) – Orange solid; Yield 99 %; **^{1}H NMR** (300 MHz, $CDCl_3$) δ 8.27 (s, 1H, CH_{imine}), 8.02 – 7.97 (m, 2H, CH_{Arom}), 7.47 – 7.36 (m, 3H, CH_{Arom}), 7.31 (d, *J* = 8.4 Hz, 2H, CH_{Arom}), 7.21 (d, *J* = 9.3 Hz, 1H, CH_{Arom}), 6.78 – 6.72 (m,

2H, CH_{Arom}), 6.36 (dd, *J* = 9.3, 2.1 Hz, 1H, CH_{Arom}), 6.21 (d, *J* = 2.1 Hz, 1H, CH_{Arom}), 3.72 (s, 3H, -OC$\underline{H_3}$), 3.54 – 3.36 (m, 4H, -N(C$\underline{H_2}$)$_{\underline{2}}$$(CH_3)_2$), 1.23 (t, *J* = 7.1 Hz, 6H, -N$(CH_2)_2$(C$\underline{H_3}$)$_{\underline{2}}$); **^{13}C NMR** (75 MHz, $CDCl_3$) δ 161.71, 159.54, 157.35, 155.99, 154.11, 153.59, 134.65, 132.80, 132.17, 130.94, 129.57, 128.31, 113.26, 107.74, 106.48, 98.78, 55.06, 45.47, 12.85; **LRMS** calcd m/z ($[M+H]^+$): 456, found m/z ($[M+H]^+$): 456; **E.A** calcd (%) for $C_{26}H_{26}BN_3O_4$: C 68.59, H 5.76, N 9.23, found (%): C 68.24, H 5.87, N 9.26.

BASHY **81e** (R_1 = NO_2; R_2 = Ph) – Red solid; Yield 99 %; **^{1}H NMR** (300 MHz, $CDCl_3$) δ 8.30 (s, 1H, CH_{imine}), 8.26 – 8.14 (m, 4H, CH_{Arom}), 7.40 – 7.32 (m, 2H, CH_{Arom}), 7.25 – 7.16 (m, 4H, CH_{Arom}), 6.40 (dd, *J* = 9.2, 2.1 Hz, 1H, CH_{Arom}), 6.20 (d, *J* = 2.1 Hz, 1H, CH_{Arom}), 3.56 – 3.40 (m, 4H, -N(C$\underline{H_2}$)$_{\underline{2}}$$(CH_3)_2$), 1.26 (t, *J* = 7.1 Hz, 6H, -N$(CH_2)_2$(C$\underline{H_3}$)$_{\underline{2}}$); **^{13}C NMR** (75 MHz, $CDCl_3$) δ 162.05, 157.99, 155.54, 153.85, 150.70, 148.69, 138.72, 135.10, 130.76, 130.39, 128.13, 127.81, 123.30, 108.59, 107.07, 98.73, 45.66, 12.85; **LRMS** calcd m/z ($[M+H]^+$): 471, found m/z ($[M+H]^+$): 471; **E.A** calcd (%) for $C_{25}H_{23}BN_4O_5$: C 63.85, H 4.93, N 11.91, found (%): C 64.04, H 5.16, N 11.62.

Dimeric BASHY **81f** (R_1 = H; R_2 = Ph) – Orange solid; Yield 91 %; **^{1}H NMR** (300 MHz, $(CD_3)_2SO$) δ 8.79 (s, 2H, 2x(CH_{imine})), 7.80 (d, *J* = 7.5 Hz, 4H, CH_{Arom}), 7.53 – 7.37 (m, 9H, CH_{Arom}), 7.08 – 7.00 (m, 3H, CH_{Arom}), 6.59 – 6.49 (m, 2H, CH_{Arom}), 6.19 – 6.11 (m, 2H, CH_{Arom}), 3.58 – 3.41 (m, 8H, 2x(-N(C$\underline{H_2}$)$_{\underline{2}}$$(CH_3)_2$)), 1.11 (t, *J* = 6.3 Hz, 12H, 2x(-N$(CH_2)_2$(C$\underline{H_3}$)$_{\underline{2}}$)); **^{13}C NMR** (75 MHz, $(CD_3)_2SO$) δ 160.70, 157.08, 155.21, 154.85, 152.10, 135.48, 132.46, 130.68, 129.61, 128.92, 128.24, 128.09, 108.03, 106.03, 97.40, 44.73, 12.59; **LRMS** calcd m/z ($[M+H]^+$): 773, found m/z ($[M+H]^+$): 773; **E.A** calcd (%) for $C_{44}H_{42}B_2N_6O_6$: C 68.41, H 5.48, N 10.88, found (%): C 67.91, H 5.66, N 10.9.

BASHY **82a** (R_1 = H; R_2 = triphenylamine) – Orange solid; Yield 71 %; **^{1}H NMR** (400 MHz, $CDCl_3$): δ 8.17 (s, 1H, CH_{imine}), 7.94 (d, *J* = 7.9, 2H, CH_{Arom}), 7.41 – 7.29 (m, 3H, CH_{Arom}), 7.26 – 6.78 (m, 15H, CH_{Arom}), 6.28 (d, *J* = 7.6 Hz, 1H, CH_{Arom}), 6.16 (d, *J* = 1.6 Hz, 1H, CH_{Arom}), 3.47 – 3.28 (m, 4H, -N(C$\underline{H_2}$)$_{\underline{2}}$$(CH_3)_2$), 1.16 (t, *J* = 7.0 Hz, 6H, -N$(CH_2)_2$(C$\underline{H_3}$)$_{\underline{2}}$); **^{13}C NMR** (100 MHz, $CDCl_3$): δ 161.73, 157.37, 155.95, 154.10, 153.59, 147.98, 147.45, 134.68, 132.84, 131.80, 130.97, 129.59, 129.31, 129.14, 128.35, 124.30, 123.25, 122.50, 107.75, 106.44, 98.74, 45.48, 12.87; **^{11}B NMR** (128 MHz, $CDCl_3$): δ 4.3 ppm; **FTIR** (KBr, cm^{-1}): 2973, 2925, 2870, 2360, 1771, 1760, 1749, 1733, 1703, 1621, 1590, 1524, 1505, 1474, 1455, 1440, 1384, 1351, 1260, 1226, 1189, 1164, 1143, 1074, 1026, 971, 942, 828, 800, 789, 753, 715, 693, 420; **HRMS** m/z ($[M+H]^+$) calcd = 593.2718, found m/z ($[M+H]^+$) = 593.2707.

BASHY **82b** (R_1 = H; R_2 = 1-pyrene) – Orange solid; Yield 99 %; **mp** 255 − 258 °C; **^{1}H NMR** (300 MHz, $CDCl_3$): δ 9.08 (d, *J* = 9.0 Hz, 1H, CH_{Arom}), 8.53 (s,

1H, CH_{imine}), 8.24 – 8.13 (m, 2H, CH_{Arom}), 8.13 – 8.05 (m, 1H, CH_{Arom}), 8.02 – 7.85 (m, 6H, CH_{Arom}), 7.72 – 7.56 (m, 1H, CH_{Arom}), 7.43 – 7.31 (m, 3H, CH_{Arom}), 7.23 – 7.13 (m, 1H, CH_{Arom}), 6.28 (d, *J* = 8.1 Hz, 1H, CH_{Arom}), 6.19 – 5.99 (m, 1H, CH_{Arom}), 3.47 – 3.19 (m, 4H,-$N(C\underline{H_2})_2(CH_3)_2$), 1.11 (m, 6H, -$N(CH_2)_2(C\underline{H_3})_2$); **^{13}C NMR** (75 MHz, $CDCl_3$):δ 161.58, 157.32, 155.71, 154.00, 153.74, 134.62, 134.27, 132.70, 131.39, 131.18, 130.92, 129.59, 129.34, 129.14, 128.26, 127.52, 127.12, 126.53, 125.55, 125.32, 125.18, 124.66, 124.31, 123.83, 108.04, 106.80, 98.76, 45.30, 12.73; **^{11}B NMR** (128 MHz, $CDCl_3$): δ 6.1 ppm; **FTIR** (KBr, cm^{-1}): 2975, 2927, 2870, 2360, 1771, 1760, 1749, 1733, 1703, 1621, 1590, 1524, 1506, 1473, 1455, 1440, 1396, 1351, 1259, 1224, 1188, 1166, 1145, 1075, 1025, 974, 940, 829, 801, 793, 755, 714, 691, 420; **LRMS** calcd m/z ($[M+H]^+$): 550, found m/z ($[M+H]^+$): 550; **E.A** calcd (%) for $C_{35}H_{28}BN_3O_3$: C 76.51, H 5.14, N 7.65, found (%) C 76.21, H 5.07, N 7.60.

BASHY **82c** (R_1 = H; R_2 = 2-fluorene) – Orange solid; Yield 96 %; **mp** 235 − 238 °C; **^{1}H NMR** (400 MHz, $CDCl_3$): δ 8.34 (s, 1H, CH_{imine}), 7.99 (d, *J* = 7.0 Hz, 2H, CH_{Arom}), 7.69 (d, *J* = 7.6 Hz, 1H, CH_{Arom}), 7.63 (d, *J* = 7.7 Hz, 1H, CH_{Arom}), 7.59 (s, 1H, CH_{Arom}), 7.49 – 7.20 (m, 8H, CH_{Arom}), 6.38 (d, *J* = 8.9 Hz, 1H, CH_{Arom}), 6.22 (s, 1H, CH_{Arom}), 3.77 (s, 2H, $C\underline{H_2}$), 3.51 – 3.38 (m, 4H, -$N(C\underline{H_2})_2(CH_3)_2$), 1.24 (t, *J* = 6.9 Hz, 6H, -$N(CH_2)_2(C\underline{H_3})_2$); **^{13}C NMR** (100 MHz, $CDCl_3$): δ 161.67, 157.40, 156.01, 154.31, 153.68, 143.52, 142.71, 142.11, 141.51, 134.69, 132.78, 130.97, 129.55, 129.35, 128.32, 127.49, 126.58, 126.42, 125.02, 199.82, 119.25, 107.79, 106.53, 98.86, 45.50, 36.98, 12.88; **^{11}B NMR** (128 MHz, $CDCl_3$): δ 4.1 ppm; **FTIR** (KBr, cm^{-1}): 2974, 2927, 2870, 2360, 1771, 1760, 1749, 1733, 1703, 1623, 1591, 1526, 1505, 1472, 1455, 1440, 1383, 1352, 1260, 1226, 1210, 1189, 1166, 1146, 1077, 1025, 976, 947, 918, 828, 800, 768, 712, 691, 419; **HRMS** m/z ($[M+H]^+$) calcd = 514.2296, found m/z ($[M+H]^+$) = 514.2290.

BASHY **82d** (R_1 = H; R_2 = 4-Isoquinoline) – Orange solid; Yield 75 %; **^{1}H NMR** (400 MHz, $CDCl_3$): δ 9.06 (s, 1H, CH_{Arom}) 8.74 (d, *J* = 8.2 Hz, 1H, CH_{Arom}), 8.47 (s, 1H, CH_{imine}), 8.08 (s, 1H, CH_{Arom}), 7.98 (d, *J* = 8.8 Hz, 2H, CH_{Arom}), 7.88 (d, *J* = 8.0 Hz, 1H, CH_{Arom}), 7.75 (dt, J = 7.0, 1.3 Hz, 1H, CH_{Arom}), 7.56 (t, *J* = 7.0 Hz, 1H, CH_{Arom}), 7.45 – 7.33 (m, 3H, CH_{Arom}), 7.23 (s, 1H, CH_{Arom}), 6.34 (dd, *J* = 9.2 Hz, 2.3 Hz, 1H, CH_{Arom}), 6.03 (d, *J* = 2.2 Hz, 1H, CH_{Arom}), 3.42 – 3.33 (m, 4H, -$N(C\underline{H_2})_2(CH_3)_2$), 1.18 (t, *J* = 7.1 Hz, 6H, -$N(CH_2)_2(C\underline{H_3})_2$); **^{13}C NMR** (100 MHz, $CDCl_3$): δ 161.38, 157.49, 155.46, 154.13, 153.42, 152.93, 144.78, 138.74, 134.88, 132.54, 131.06, 129.96, 129.66, 128.71, 128.29, 128.07, 126.62, 108.24, 106.77, 98.72, 45.45, 12.83; **^{11}B NMR** (128 MHz, $CDCl_3$): δ 5.5 ppm; **FTIR** (KBr, cm^{-1}): 2973, 2924, 2870, 2360, 1771, 1760, 1749, 1733, 1622, 1592, 1526, 1504, 1475, 1455, 1441, 1383, 1350, 1261, 1223, 1189, 1166, 1146, 1077, 1054, 1025, 977,

826, 799, 782, 754, 714, 691, 420; **HRMS** m/z ($[M+H]^+$) calcd = 477.2092, found m/z ($[M+H]^+$) = 477.2089.

BASHY **82e** (R_1 = H; R_2 = phenylsulfonamide) – Orange solid; Yield 98 %; **^{1}H NMR** (400 MHz, $CDCl_3$): δ 8.33 (s, 1H, CH_{imine}), 7.97 (d, *J* = 8.5 Hz, 2H, CH_{Arom}), 7.73 (d, *J* = 8.4 Hz, 2H, CH_{Arom}), 7.51 (d, *J* = 8.3 Hz, 2H, CH_{Arom}), 7.46 – 7.37 (m, 3H, CH_{Arom}), 7.24 (s, 1H, CH_{Arom}), 6.40 (dd, *J* = 9.1, 2.4 Hz, 1H, CH_{Arom}), 6.20 (s, 1H, CH_{Arom}), 4.68 (s, 2H, $N\underline{H_2}$), 3.50 – 3.40 (m, 4H, -$N(C\underline{H_2})_2(CH_3)_2$), 1.24 (t, *J* = 7.1 Hz, 6H, -$N(CH_2)_2(C\underline{H_3})_2$); **^{13}C NMR** (100 MHz, $CDCl_3$): δ 161.38, 157.67, 155.54, 153.95, 153.72, 141.01, 134.83, 132.49, 131.62, 131.23, 129.56, 128.43, 125.59, 108.26, 106.48, 98.80, 45.64, 12.88; **^{11}B NMR** (128 MHz, $(CD_3)_2SO$): δ 0.2 ppm; **FTIR** (KBr, cm_{-1}): 2975, 2929, 2870, 2360, 1771, 1760, 1749, 1733, 1705, 1621, 1589, 1530, 1503, 1473, 1456, 1443, 1385, 1348, 1261, 1223, 1187, 1165, 1144, 1075, 1025, 975, 943, 828, 802, 759, 724, 713, 690, 420; **HRMS** m/z ($[M+Na]^+$) calcd = 527.1531, found m/z ($[M+Na]^+$) = 527.1523.

BASHY **82f** (R_1 = H; R_2 = 4-pyridine) – Orange solid; Yield 99 %; **mp** 246 − 248 °C; **^{1}H NMR** (300 MHz, $CDCl_3$): δ 8.42 (d, *J* = 5.7 Hz, 2H, CH_{Arom}), 8.32 (s, 1H, CH_{imine}),7.98 (d, *J* = 6.9 Hz, 2H, CH_{Arom}), 7.46 – 7.38 (m, 3H, CH_{Arom}), 7.29 – 7.21 (m, 3H, CH_{Arom}), 6.40 (dd, *J* = 9.3, 2.0 Hz, 1H, CH_{Arom}), 6.21 (d, *J* = 2.0 Hz, 1H, CH_{Arom}), 3.54 – 3.40 (m, 4H, -$N(C\underline{H_2})_2(CH_3)_2$), 1.26 (t, *J* = 6.9 Hz, 6H, -$N(CH_2)_2(C\underline{H_3})_2$); **^{13}C NMR** (75 MHz, $CDCl_3$): δ 161.31, 157.68, 155.42, 153.83, 153.74, 148.44, 134.89, 132.44, 131.20, 129.52, 128.41, 126.11, 108.29, 106.39, 98.71, 45.61, 12.83; **^{11}B NMR** (128 MHz, $CDCl_3$): δ 3.5 ppm; **FTIR** (KBr, cm^{-1}): 2973, 2933, 2870, 2360, 1771, 1760, 1749, 1733, 1712, 1626, 1592, 1527, 1506, 1472, 1456, 1441, 1386, 1353, 1263, 1220, 1187, 1170, 1145, 1079, 826, 798, 754, 714, 691, 420; **LRMS** calcd m/z ($[M+H]^+$): 427, found m/z ($[M+H]^+$): 427; **E.A** calcd (%) for $C_{24}H_{23}BN_4O_3$ C 67.62, H 5.44, N 13.14, found C 67.17, H 5.38, N 12.85.

BASHY **82g** (R_1 = H; R_2 = pentafluorophenyl) – Orange solid; Yield 96 %; **mp** 235 − 237 °C; **^{1}H NMR** (400 MHz, $CDCl_3$): δ 8.23 (s, 1H, CH_{imine}), 8.02 (d, *J* = 7.2 Hz, 2H, CH_{Arom}), 7.49 – 7.37 (m, 3H, CH_{Arom}), 7.25 (s, 1H, CH_{Arom}), 6.44 (d, *J* = 9.0 Hz,1H, CH_{Arom}), 6.21 (s, 1H, CH_{Arom}), 3.48 (m, 4H, -$N(C\underline{H_2})_2(CH_3)_2$), 1.27 (t, *J* = 7.0 Hz, 6H, -$N(CH_2)_2(C\underline{H_3})_2$); **^{13}C NMR** (100 MHz, $CDCl_3$): δ 160.92, 157.70, 155.09, 154.64, 153.34, 134.71, 132.15, 131.32, 129.55, 128.47, 108.36, 106.25, 98.42, 45.64, 12.96; **^{11}B NMR** (128 MHz, $CDCl_3$): δ 2.2 ppm; **FTIR** (KBr, cm^{-1}): 2979, 2932, 2875, 2360, 1771, 1760, 1749, 1733, 1714, 1625, 1594, 1527, 1508, 1458, 1384, 1353, 1289, 1262, 1220, 1189, 1168, 1147, 1025, 969, 927, 829, 801, 759, 745, 715, 692, 420; **HRMS** m/z ($[M+Na]^+$) calcd = 538.1332, found m/z ($[M+Na]^+$) = 538.1331.

Dimeric BASHY **82h** (R_1 = H; R_2 = fluorine derivative) – Orange solid, Yield 99 %; **^{1}H NMR** (300 MHz,$CDCl_3$) δ 8.24 (s, 2H, 2x(CH_{imine})), 7.94 (d, J = 8.2 Hz, 4H, CH_{Arom}), 7.41 − 7.18 (m, 14H, CH_{Arom}), 6.35 (dd, *J* = 9.1, 2.2 Hz, 2H, CH_{Arom}), 6.24 (d, *J* = 2.0 Hz, 2H, CH_{Arom}), 3.47 − 3.39 (m, 8H, CH_{Arom}), 1.80 − 1.64 (m, 4H, 2x(-N($C\underline{H}_2$)$_2$(CH_3)$_2$)), 1.22 (t, J = 7.0 Hz, 12H, 2x(-N(CH_2)$_2$($C\underline{H}_3$)$_2$)), 1.17 − 0.23 (m, 30H, Alkylic chain); **^{13}C NMR** (75 MHz, $CDCl_3$) δ 161.8, 157.2, 156.2, 154.5,153.5, 150.0, 141.1, 134.6, 132.7, 130.9, 129.4, 129.1, 128.3, 125.4, 118.9, 107.7, 106.4, 98.8, 54.7, 45.5, 40.3, 31.9, 30.3, 29.5, 29.4, 24.0, 22.8, 14.3, 12.8 ppm; **^{11}B NMR** (128 MHz, $CDCl_3$): δ 4.2 ppm; **FTIR** (KBr, cm^{-1}): 2925, 2851, 2870, 1705, 1622, 1592, 1526, 1502, 1472, 1441, 1383, 1350, 1259, 1188, 1164, 1144, 1075, 1024, 971, 944, 923, 826, 801, 787, 753, 713, 691, 429; **LRMS** calcd m/z ($[M+H]^+$): 1085, found m/z ($[M+H]^+$): 1085; **E.A** calcd (%) for $C_{67}H_{78}B_2N_6O_6$ C 74.17, H 7.25, N 7.75, found C 73.72, H 7.42, N 7.50.

BASHY **83a** (R_1 = CF_3; R_2 = Ph) – Red solid; Yield 99 %; **mp** 228 − 230 °C; **^{1}H NMR** (300 MHz, $CDCl_3$): δ 8.30 (s, 1H, CH_{imine}), 8.12 (d, *J* = 8.1 Hz, 2H, CH_{Arom}), 7.64 (d, *J* = 8.1 Hz, 2H, CH_{Arom}), 7.41 – 7.34 (m, 2H, CH_{Arom}), 7.25 – 7.18 (m, 4H, CH_{Arom}), 6.39 (dd, *J* = 9.0, 2.1 Hz, 1H, CH_{Arom}), 6.20 (d, *J* = 2.1 Hz, 1H, CH_{Arom}), 3.52 – 3.39 (m, 4H, -N($C\underline{H}_2$)$_2$(CH_3)$_2$), 1.24 (t, *J* = 7.2 Hz, 6H, -N(CH_2)$_2$($C\underline{H}_3$)$_2$); **^{13}C NMR** (75 MHz, $CDCl_3$): δ 161.94, 157.75, 155.70, 153.87, 152.10, 136.17, 134.95, 132.40, 131.97, 130.80, 129.86, 128.08, 127.78, 125.81, 125.16 (q, CF_3), 108.31, 106.83, 98.79, 45.61, 12.85; **^{11}B NMR** (128 MHz, $CDCl_3$) δ 4.2 ppm; **FTIR** (KBr, cm^{-1}): 2981, 2931, 2870, 2360, 2330, 1771, 1760, 1749, 1733, 1699, 1623, 1590, 1527, 1504 1475, 1455, 1440, 1407, 1382, 1354, 1322, 1262, 1227, 1188, 1169, 1149, 1129, 1070, 1018, 977, 944, 853, 843, 822, 795, 714, 699, 420; **LRMS** calcd m/z ($[M+H]^+$): 494, found m/z ($[M+H]^+$): 494; **E.A** calcd (%) for $C_{26}H_{23}BF_3N_3O_3$ C 63.31, H 4.70, N 8.52, found C 63.72, H 4.87, N 8.47.

BASHY **83b** (R_1 = CN; R_2 = Ph) – Red solid, Yield 99 %; **mp** 287−289 °C; **^{1}H NMR** (300 MHz, $CDCl_3$) δ 8.29 (s, 1H, CH_{imine}), 8.13 (d, *J* = 9.0 Hz, 2H, CH_{Arom}), 7.66 (d, *J* = 9.0 Hz, 2H, CH_{Arom}), 7.37 − 7.34 (m, 2H, CH_{Arom}), 7.24 − 7.19 (m, 4H, CH_{Arom}), 6.40 (dd, *J* = 9.0, 2.1 Hz, 1H, CH_{Arom}), 6.20 (d, *J* = 2.1 Hz, 1H, CH_{Arom}), 3.52 − 3.43 (m, 4H, -N($C\underline{H}_2$)$_2$(CH_3)$_2$), 1.25 (t, *J* = 7.2 Hz, 6H, -N(CH_2)$_2$($C\underline{H}_3$)$_2$); **^{13}C NMR** (75 MHz, $CDCl_3$) δ 162.0, 157.9, 155.5, 153.8, 151.1, 137.0, 135.1, 131.9, 130.8, 130.0, 128.1, 127.8, 118.6, 113.8, 108.5, 107.0, 98.7, 45.7, 12.9; **^{11}B NMR** (128 MHz, $CDCl_3$) δ 4.2 ppm; **FTIR** (KBr, cm^{-1}): 2983, 2931, 2870, 2360, 2227, 1771, 1760, 1749, 1733, 1703, 1624, 1588, 1525, 1506, 1472, 1434, 1379, 1263, 1224, 1188, 1166, 1148, 1114, 1096, 1077, 1020, 974, 944, 823, 420; **LRMS** calcd m/z ($[M+H]^+$): 451, found m/z ($[M+H]^+$): 451; **E.A** calcd (%) for $C_{26}H_{23}BN_4O_3$ C 69.35, H 5.22, N 12.21, found C 69.43, H 5.22, N 12.21.

ECT **85** (R_1 = H; R_2 = BODIPY derivative) **–** Brownish-red amorphous solid, Yield 30 %; **^{1}H NMR** (300 MHz, $CDCl_3$) δ 8.32 (s, 1H, CH_{imine}), 7.96 – 7.86 (m, 2H), 7.55 – 7.35 (m, 8H), 7.29 – 7.24 (m, 1H), 7.22 – 7.16 (m, 1H), 7.12 – 7.08 (m, 2H), 6.90 – 6.86 (m, 2H), 6.50 (s, 1H), 6.42 (dd, *J* = 9.3, 2.4 Hz, 1H), 6.27 (d, *J* = 2.4 Hz, 1H), 5.91 (s, 1H), 3.83 (s, 3H, -O-C$\underline{H}_3$), 3.54 – 3.44 (m, 4H, -N(C$\underline{H}_2$)$_2$(CH$_3$)$_2$), 2.55 (s, 3H, -C$\underline{H}_3$), 1.27 (s, 3H, -C$\underline{H}_3$), 1.27 – 1.24 (m, 6H, -N(CH$_2$)$_2$(C$\underline{H}_3$)$_2$), 1.21 (s, 3H, -C$\underline{H}_3$); **^{13}C NMR** (75 MHz, $CDCl_3$) δ 161.5, 160.4, 157.5, 156.1, 154.8, 154.4, 153.6, 153.1, 142.9, 135.8, 134.8, 134.4, 132.6, 131.6, 131.1, 129.7, 129.5, 129.4, 129.1, 128.4, 127.2, 121.0, 117.3, 117.2, 114.3, 107.9, 106.1, 98.7, 55.5, 45.6, 29.8, 25.0, 14.6, 14.4, 12.9; **HRMS** calcd m/z ([M+Na]$^+$): 812.3361, found m/z ([M+Na]$^+$): 812.3364.

ECT **87** (R_1 = H; R_2 = coumarin) **–** Orange amorphous solid, Yield 63 %; **^{1}H NMR** (300 MHz, $CDCl_3$) δ 8.31 (s, 1H, CH_{imine}), 8.04 – 7.96 (m, 2H, CH_{arom}), 7.55 (d, *J* = 9.3 Hz, 1H, CH_{vinyl}), 7.46 – 7.30 (m, 6H, CH_{arom}), 7.25 – 7.21 (m, 1H, CH_{arom}), 6.34 (dd, *J* = 9.0, 2.1 Hz, 1H, CH_{vinyl}), 6.24 (d, *J* = 9.3 Hz, 1H, CH_{arom}), 6.15 (d, *J* = 2.1 Hz, 1H, CH_{arom}), 3.58 – 3.38 (m, 4H, N(C$\underline{H}_2$)$_2$(CH$_3$)$_2$), 1.19 (t, *J* = 7.5 Hz, 6H, -N(CH$_2$)$_2$(C$\underline{H}_3$)$_2$); **^{13}C NMR** (75 MHz, $CDCl_3$) δ 161.4, 157.6, 155.4, 153.7, 153.6, 143.7, 134.8, 132.4, 131.1, 129.43, 128.3, 127.1, 126.9, 118.7, 118.3, 115.9, 108.2, 106.3, 98.6, 45.5, 12.7; **HRMS** calcd m/z ([M+Na]$^+$): 516.1701, found m/z ([M+Na]$^+$): 516.1688.

BASHY **88** (R_1 = H; R_2 = 4-COOH-Ph) – Orange solid, Yield 97 %; **^{1}H NMR** (300 MHz, (CD$_3$)$_2$SO) δ 12.76 (s, 1H, -COO$\underline{H}$), 8.93 (s, 1H, CH_{imine}), 7.88 – 7.81 (m, 2H, CH_{Arom}), 7.78 (d, *J* = 8.1 Hz, 2H, CH_{Arom}), 7.56 – 7.40 (m, 4H, CH_{Arom}), 7.35 (d, *J* = 8.4 Hz, 2H, CH_{Arom}), 6.61 (dd, *J* = 9.0, 2.1 Hz, 1H, CH_{Arom}), 6.25 (d, *J* = 2.1 Hz, 1H, CH_{Arom}), 3.64 – 3.41 (m, 4H, -N(C$\underline{H}_2$)$_2$(CH$_3$)$_2$), 1.13 (t, *J* = 6.9 Hz, 6H, -N(CH$_2$)$_2$(C$\underline{H}_3$)$_2$); **^{13}C NMR** (75 MHz, (CD$_3$)$_2$SO) δ 167.47, 160.51, 157.27, 155.14, 152.19, 135.67, 132.42, 130.81, 130.43, 130.05, 128.95, 128.54, 128.32, 108.34, 106.02, 97.53, 44.82, 12.62; **LRMS** calcd m/z ([M+H]$^+$): 470, found m/z ([M+H]$^+$): 470; **E.A** calcd (%) for $C_{26}H_{24}BN_3O_5$: C 66.54, H 5.15, N 8.95, found (%): C 66.17, H 5.40, N 9.14.

- **BASHY 89**

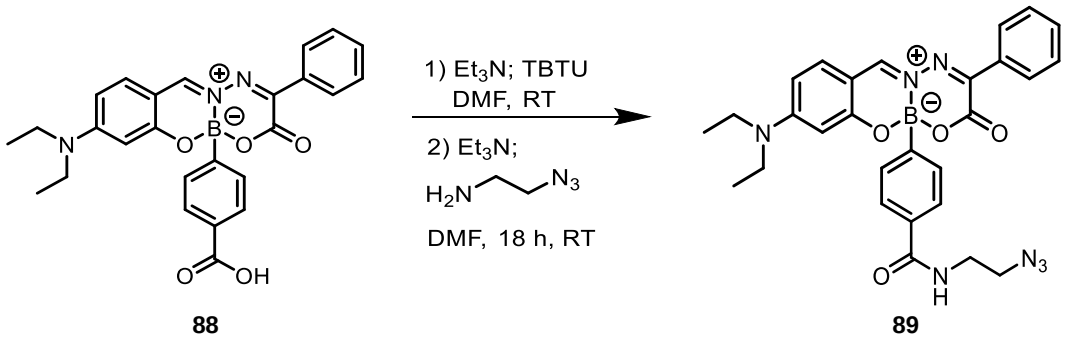

Scheme 57 – Synthetic methodology to construct BASHY **89.**

BASHY **88** (0.181 mmol) was dissolved in 2 mL of dry DMF and then triethylamine (0.217 mmol) was added. The mixture was stirred at RT for 10 min and then TBTU (0.217 mmol) was added. After 30 min, triethylamine (0.235 mmol) and the 2-azidoethanamine[198] (0.217 mmol) were added and the reaction mixture was left to react over 18 h at RT. DMF was evaporated under reduced pressure and 20 mL of ethyl acetate was added to dissolve the crude mixture. Organic phase was washed with water (2 x 20 mL), dried with anhydrous sodium sulfate, filtered and the volatiles were evaporated under reduced pressure. The solid obtained was washed with cold MeOH (2 x 0.75 mL) affording BASHY **89** with 91 % yield.

BASHY **89 –** Orange solid; Yield 91 %; **^{1}H NMR** (300 MHz, $CDCl_3$): δ 8.31 (s, 1H, CH_{imine}), 8.03 – 7.89 (m, 2H, CH_{Arom}), 7.59 (d, *J* = 8.1 Hz, 2H, CH_{Arom}), 7.48 – 7.32 (m, 5H, CH_{Arom}), 7.23 (d, *J* = 9.3 Hz, 1H, CH_{Arom}), 6.52 (t, *J* = 5.4 Hz, 1H, -N<u>H</u>-), 6.37 (dd, *J* = 9.3, 2.1 Hz, 1H, CH_{Arom}), 6.17 (d, *J* = 2.1 Hz, 1H, CH_{Arom}), 3.58 – 3.35 (m, 8H, 4 x C<u>H</u>$_2$), 1.22 (t, *J* = 7.2 Hz, 6H, -N$(CH_2)_2$($C\underline{H}_3$)$_2$); **^{13}C NMR** (75 MHz, $CDCl_3$) δ 168.31, 161.46, 157.56, 155.82, 153.89, 153.73, 134.82, 133.41, 132.58, 131.13, 131.07, 129.50, 128.35, 126.24, 108.09, 106.47, 98.72, 51.00, 45.54, 39.39, 12.83; **LRMS** calcd m/z ($[M+H]^+$): 538, found m/z ($[M+H]^+$): 538; **E.A** calcd (%) for $C_{28}H_{28}BN_7O_4$: C 62.58, H 5.25, N 18.25, found (%): C 62.67, H 5.39, N 18.11.

- **Annexin V expression and purification**

A colony of E. coli C41 (DE3) pLysS harboring the plasmid pET12a-PAPI_annexin was selected to inoculation of 100 mL lysogeny broth medium (LB) containing ampicillin (100 µg/mL). The pre-culture was further incubated over night at 37 °C and 180 rpm. Aliquots of the overnight culture were stored in a 15 % glycerol LB media at - 20 °C. 20 mL of the overnight culture were used to inoculate 400 mL of LB medium containing ampicillin (100 µg/mL). Bacteria were grown to optical density (OD) 0.6 (37 °C, 180 rpm) where upon expression was induced by 1 mM of isopropyl β-D-1-thiogalactopyranoside (IPTG, invitrogen). Expression of Annexin V was allowed for 4 h until cell culture was harvested by centrifugation at 4 °C and 7500 x g for 10 min. Supernatant was inactivated and discarded and the cells were resuspended in 50 mM Tris-HCl (pH 7.2) containing 1 mM β-mercaptoethanol and 10 mM $CaCl_2$. Cells were then lysed using a sonicator (Sonics Vibra-Cell, pulse on 30 s, pulse off 40 s, 2.5 min) and fragments were spinned down at 4 °C and 17000 x g for 45 min. Cell fragments were further resuspended in 50 mM Tris HCl (pH 7.2) containing 1 mM β-mercaptoethanol and 20 mM EDTA and spinned down once more at 4 °C and 17000 x g for 20 min. The supernatant was collected and the protein was purified by fast protein liquid chromatography (FPLC, AKTA basic, GE Healthcare) using a size exclusion column (SepFast GF-HS M 16/60, Generon). The mobile phase was 20 mM Tris HCl (pH 8.0), flow rate 1 mL/min and fractions of 2 mL were collected and analysed by sodium dodecyl sulfate polyacrylamide gel electrophoresis (SDS-PAGE). A second round of purification was done with an anion exchange column (HighRes15 Q, Generon). The column was equilibrated with 20 mM Tris HCl (pH 8.0) at a flow rate of 1 mL/min. After loading the concentrated protein sample, the column was washed with 3 column volumes with the same buffer. A buffer gradient of 0 – 100 % 1 M NaCl in 20 mM Tris HCl eluted the protein and fractions of 1 mL were collected. The fractions were analysed by SDS-PAGE and combined. Protein concentration was determined with a UV spectrometer at wavelength 280 nm.

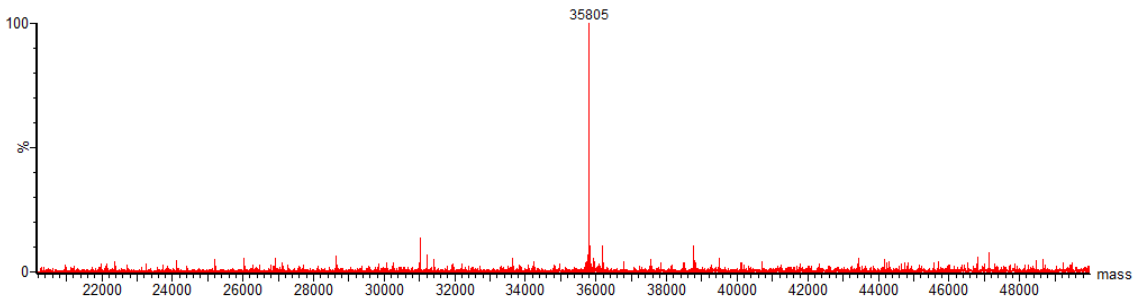

Figure 26 – ESI–MS spectrum of Annexin V in TrisHCl (20 mM, pH 8).

- **Annexin V-mal-DBCO 91**

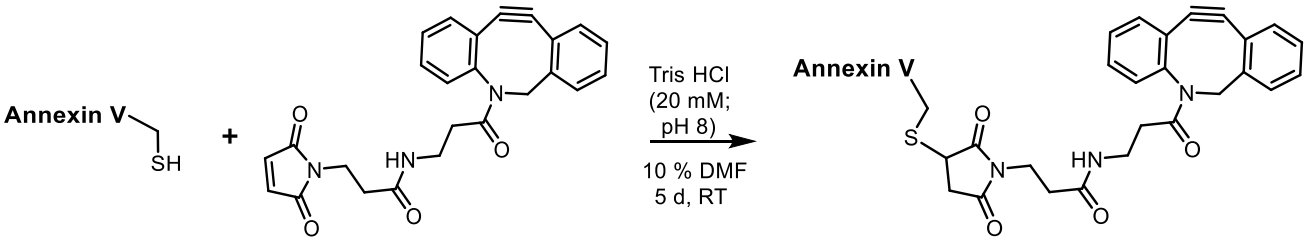

35806 g/mol **90** (427.4 g/mol) **91** (36233 g/mol)

Scheme 58 – Synthetic methodology to prepare Annexin V-mal-DBCO **91.**

In a 0.5 mL eppendorf, 8 µL of a 25 µM solution of Annexin V was added to a solution of 28 µL of TrisHCl (20 mM, pH 8) and 3.5 µL of DMF. After that, 0.5 µL of a solution of 10 mM mal-DBCO **90** (in DMF) was added and the reaction was left stirring at RT for 5 days. Then, Zeba spin desalting column was used to purify the product, which was then concentrated using a vivaspin 500 (MWCO 5 kDa). Annexin V-mal-DBCO **91** was confirmed by LC-MS (**Figure 27**). Optimization of the reaction was made according to the conditions depicted in **Table 21**.

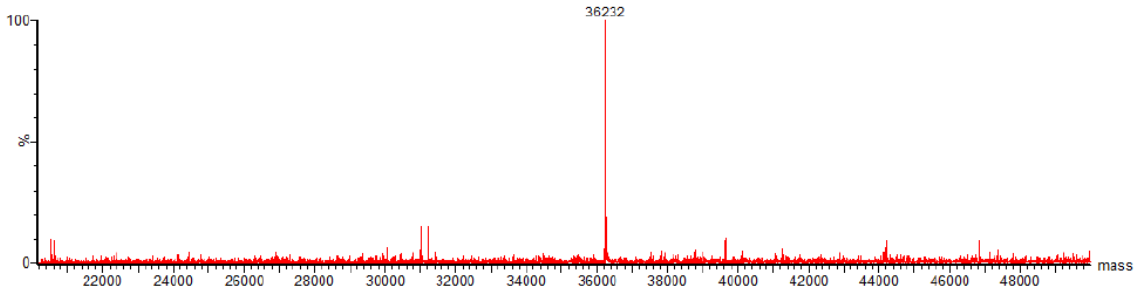

Figure 27 – ESI–MS spectrum of the product **91** from the reaction of Annexin V in TrisHCl (20 mM, pH 8) with 25 equivalents of mal-DBCO **90** for 5 d at RT.

Table 21 – Conditions used to modify 5 μM Annexin V in Tris HCl with DBCO-maleimide **90** at RT.

Attempt	pH	90 (equiv.)	DMF (%)	Time of evaluation (h)
1	7.0	25	1.0	6, 24 and 50
2	7.0	200	4.0	6 and 28
3	8.0	10	5.0	6 and 28
4	8.0	25	1.0	6 and 11
5	8.0	50	2.5	6 and 11
6	6.0	100	5.0	7, 24 and 32
7	6.0	200	10.0	7, 24 and 32
8	8.0	25	10.0	12 and 34
9	7.0	100	5.0	6 and 11
10	8.0	25	10.0	100 and 120

10 μM solution of the purified Annexin V-mal-DBCO **91** sample was digested overnight with trypsin. No reduction/alkylation step was performed. All LC-MS/MS experiments were performed using a nanoAcquity UPLC (Waters Corp., Milford, MA) system and an LTQ Orbitrap Velos hybrid ion trap mass spectrometer (Thermo Scientific, Waltham, MA). Separation of peptides was performed by reverse phase chromatography using a Waters reverse-phase nano column (BEH C18, 75 μm i.d. x 250 mm, 1.7 μm particle size) at flow rate of 300 nL/min. Peptides were initially loaded onto a pre-column (Waters UPLC Trap Symmetry C18, 180 μm i.d x 20mm, 5 μm particle size) from the nanoAcquity sample manager with 0.1 % formic acid for 3 minutes at a flow rate of 10 μL/min. After this period, the column valve was switched to allow the elution of peptides from the pre-column onto the analytical column. Solvent A was water + 0.1 % formic acid and solvent B was acetonitrile + 0.1 % formic acid. The linear gradient employed was 5 – 40 % B in 60 minutes. The LC eluant was sprayed into the mass spectrometer by means of a New Objective nanospray source. All m/z values of eluting ions were measured in the Orbitrap Velos mass analyzer, set at a resolution of 30000. Data dependent scans (Top 20) were employed to automatically isolate and generate fragment ions by collision-induced dissociation in the linear ion trap, resulting in the generation of MS/MS spectra. Ions with charge states of 2+ and above were selected for fragmentation. Postrun, the data was processed using Protein Discoverer (version 1.4., ThermoFisher). Briefly, all MS/MS data were converted to mgf files and these were submitted to the Mascot

search algorithm (Matrix Science, London UK) and searched against a custom database containing the annexin V protein sequence and common contaminant sequences and applying variable modifications of oxidation (M), deamidation (NQ) and a custom modification of mal-DBCO **90**, using a peptide tolerance of 25 ppm (MS) and 0.8 Da (MS/MS).

Peptide identifications were accepted if they could be established at greater than 95 % probability. Significant hits which suggested that **90** was bound to peptides were then verified by manual inspection of the MS/MS data. Mascot search showed that ALLLL**C**GEDD was detected with the expected modification on cysteine. The MS/MS spectrum is depicted in the following figure with the majority of the sequence ions assigned (**Figure 28**).

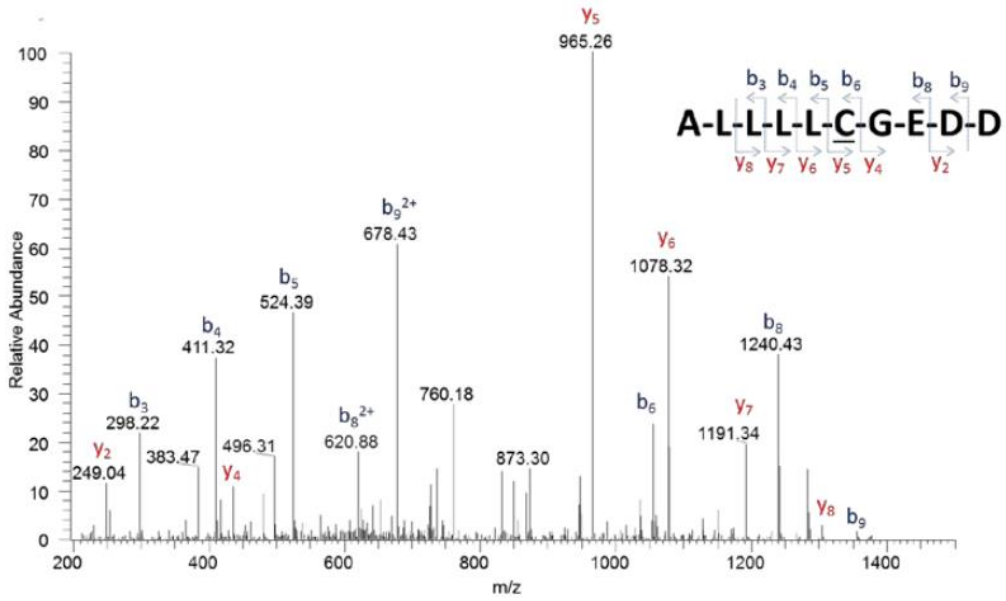

Figure 28 – MS spectrum of the peptide ALLLL**C**GEDD obtained after tryptic digestion of the purified Annexin V-mal-DBCO **91**, containing the modification at cysteine 315. m/z value of the doubly charged peptide = 744.84.

- **Annexin V-BASHY 92**

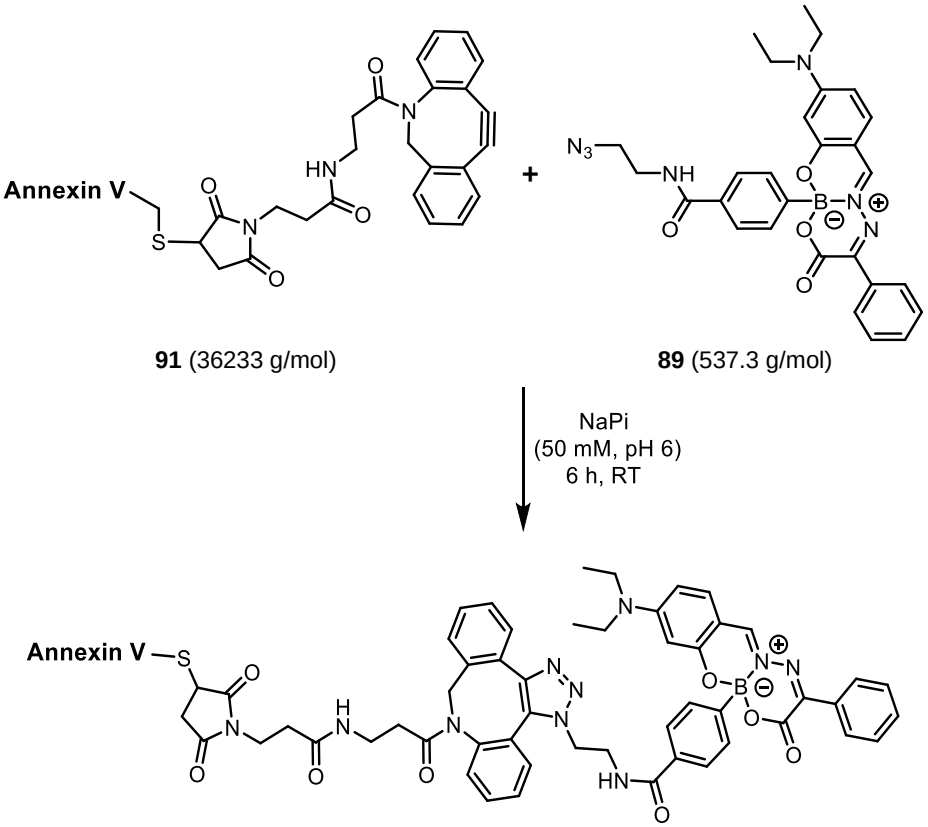

Scheme 59 – Synthetic methodology to construct Annexin V-BASHY **92.**

In a 0.5 mL eppendorf, 20 µL of a 5 µM solution of **91** in NaPi (50 mM, pH 6) were mixed with 1.0 µL of a DMF solution (525 µM) of BASHY **89** and the reaction was left stirring at RT for 6 h. After that, a ZebaTM spin desalting column was used to purify Annexin V-BASHY into NaPi (50 mM, pH 6), which was evaluated by LC-MS (**Figure 29**).

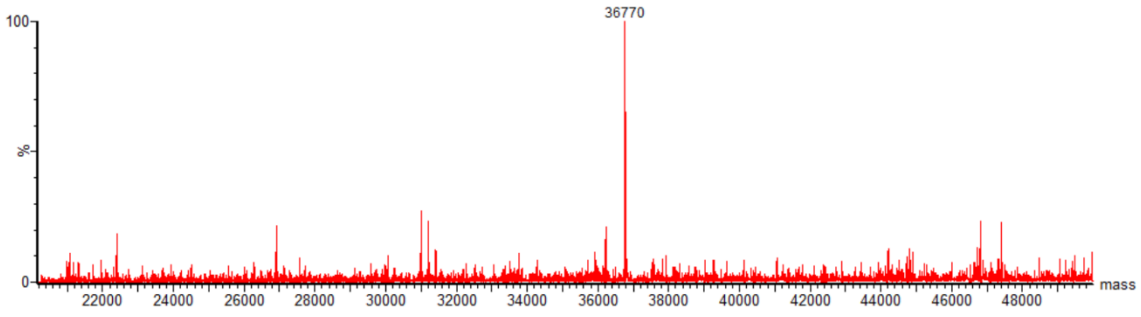

Figure 29 – ESI–MS spectrum of the product **92** from the reaction of **91** in NaPi (50 mM, pH 6) with 25 equiv. of **89** for 6 h at RT.

- **Structural analysis of Annexin V, Annexin V-mal-DBCO 91 and Annexin V-BASHY 92**

Annexin V, Annexin V-mal-DBCO **91** and Annexin V-BASHY **92** were concentrated to 0.5 µM in buffer (20 mM NaPi, pH 7.4) and assessed by CD.[233] The CD measurements were recorded using a Chirascan Spectropolarimeter (Applied Photophysics) equipped with a Quantum TC125 temperature control unit (25 °C). The data was acquired in a 0.1 cm pathlength with a response time of 1 s, a per-point acquisition delay of 5 ms and a pre and post-scan delay of 50 ms. Spectra were averaged over three scans in a wavelength range from 190 nm to 260 nm and deconvoluted according to the equation.

$$[\theta] = (\theta_{[222]} \times 100 \times M) / (C \times l \times n)$$

where θ is the ellipticity in degrees, *l* is the optical path length in cm, C is the concentration of sample in mg/mL, M is the molecular mass and n is the number of residues in the protein.

- **Annexin V-Cy5 96**

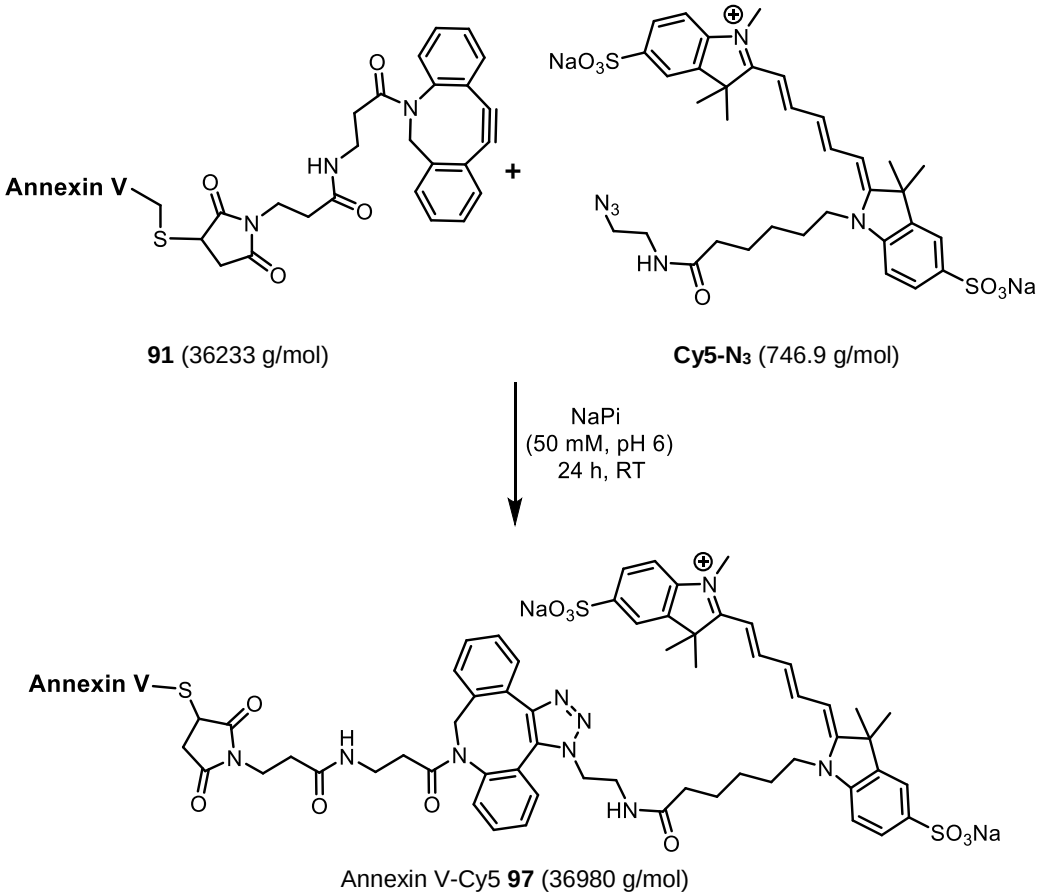

91 (36233 g/mol) **Cy5-N₃** (746.9 g/mol)

Annexin V-Cy5 **97** (36980 g/mol)

Scheme 60 – Synthetic methodology to prepare Annexin V-Cy5 **98**.

In a 0.5 mL eppendorf, 25 µL of a 2.5 µM solution of purified **91** in NaPi (50 mM, pH 6) were mixed with 0.5 µL of a DMF solution (13.4 mM) of Cy5-N_3. The reaction was left stirring at RT for 24 h. After that, a Zeba™ spin desalting column was used to purify Annexin V-Cy5 **99** into NaPi (50 mM, pH 6). The obtained product was evaluated by SDS-Page.

In the gel electrophoresis, proteins were mixed with SDS sample buffer with 200 mM DTT (reducing buffer), heated for five minutes to 95 °C and separated on a 12 % Tris glycine buffered SDS-PAGE gel. After electrophoresis, BASHY and Cy5 labelled proteins were detected using the ChemiDoc XRS+ system with the 520DF30 emission filter, followed by standard Coomassie G250 staining (**Figure 30**).

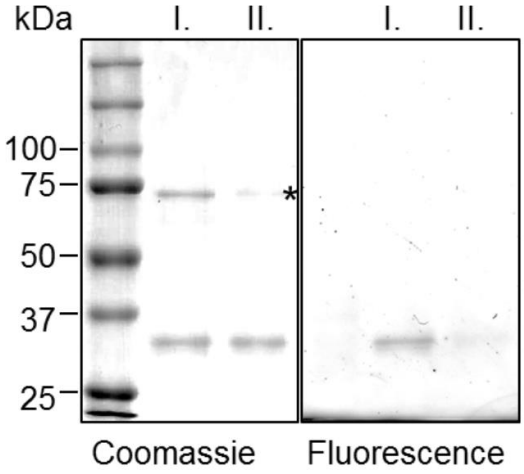

Figure 30 – BASHY and Cy5 labelled AnnexinV were separated by SDS PAGE in reducing conditions (lanes I. and II.). Loading: 350 ng. BASHY fluorescence was detected prior to Coomassie staining using a ChemiDoc XRS+ system. * dimers

- **Annexin V-FITC 94**

Following a described protocol to label annexin V (wild type) with FITC [187] and subsequent imaging of early and late apoptotic cells, a purified sample of Annexin V-FITC **94** was isolated. Taking into account that this heterogenous lysine modification of Annexin V is already reported, only a gel electrophoresis was performed to characterize this construct.

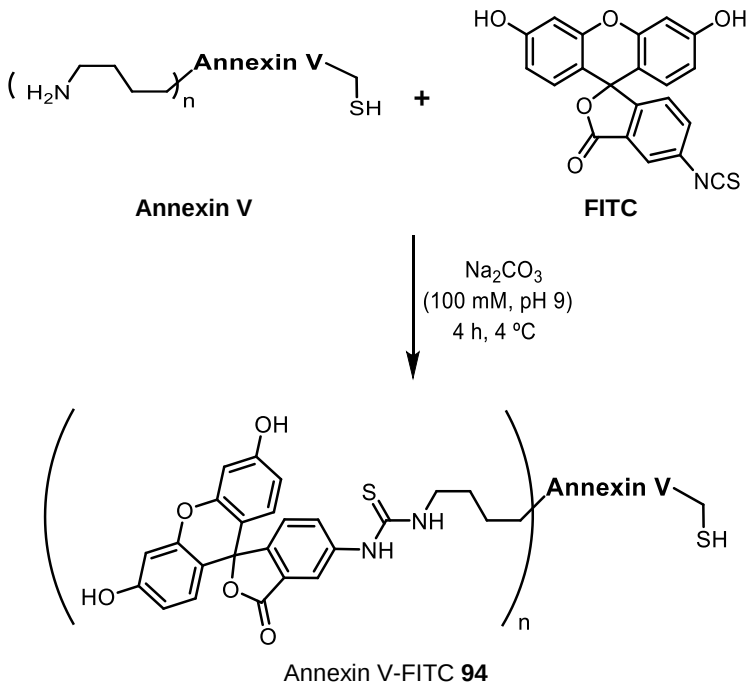

Scheme 61 – Synthetic methodology to construct Annexin V-FITC **94.**

In the gel electrophoresis, proteins were mixed with SDS sample buffer with 200 mM DTT (reducing buffer), heated for five minutes to 95 °C and separated on a 12 % Tris glycine buffered SDS-PAGE gel. After electrophoresis, FITC labelled proteins were detected using the ChemiDoc XRS+ system with the 520DF30 emission filter, followed by standard Coomassie G250 staining (**Figure 31**).

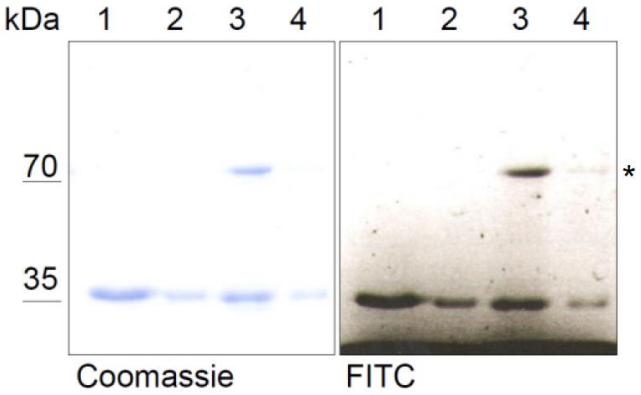

Figure 31 – FITC labelled AnnexinV was separated by SDS PAGE in reducing (lanes 1 and 2) and non-reducing conditions (lanes 3 and 4). Loading: 1 µg (lanes 1 and 3), 200 ng (lanes 2 and 4). FITC fluorescence was detected prior to Coomassie staining using a ChemiDoc XRS+ system. * dimers

IV.2.2 Photophysical measurements and additional photophysical data

The UV/vis absorption and fluorescence measurements were done on optically diluted (optical density ca. 0.1 – 0.2) air-equilibrated solutions at RT. Absorption spectra were recorded on a UV-1603 spectrometer from Shimadzu and corrected steadystate fluorescence spectra were measured with a Varian Cary Eclipse fluorimeter. Time-resolved fluorescence measurements were performed with a FLS 920 time-correlated single-photon-counting setup from Edinburgh Instruments. The fluorescence quantum yields were measured relative to N-propyl-4-amino-1,8-naphthalimide (Φ_{fluo}= 0.48 in aerated acetonitrile), rhodamine B (Φ_{fluo}= 0.95 in ethanol) or quinine sulfate in 0.05 M sulfuric acid; Φ_{fluo}= 0.55) and corrected for the refractive indices of the employed solvents.[234,235]

The lifetime measurements were done with the time-correlated single photon counting technique. For this purpose a picosecond pulsed diode laser (λ= 442 nm, pulse width fwhm 78.3 ps) was used as excitation source. The detector was a multichannel photomultiplier, and the time response of the system was < 50 picoseconds.

Electrochemical measurements were done in dichloromethane containing 0.1 M Bu_4NPF_6 and at a scan rate of 100 mVs^{-1}. The potentials are reported versus aqueous Ag/AgCl electrode and are not corrected for the junction potential. The E_o' value for the ferrocenium/ferrocene couple used in this study was 0.46 V for dichloromethane solutions; glassy carbon electrode.

The two-photon cross section (σ_2) was determined by using the two-photon-induced fluorescence method with femtosecond pulsed excitation.[236,237] BASHYs **81a,e** and **83a,b** were dissolved in toluene (50 µM), and the two-photon-induced fluorescence intensity was measured at 800 − 1040 nm, using rhodamine B (56.0 µM in MeOH) as reference[238] and assuming that the fluorescence quantum yield remains the same regardless whether two-photon or one-photon excitation is used.[239]

- **Additional photophysical data**

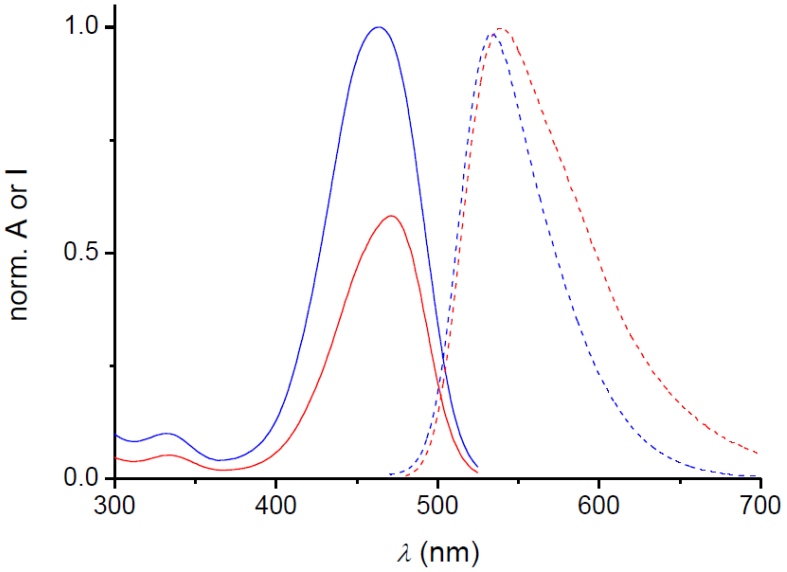

Chart 38 – UV/vis absorption (solid lines) and fluorescence spectra (dashed lines) of **81a** (red) and **81f** (blue) in acetonitrile. The absorption spectra are normalized according to the relative molar absorption coefficients of the two dyes. The fluorescence spectra show the relative difference in the fluorescence quantum yields of the dyes.

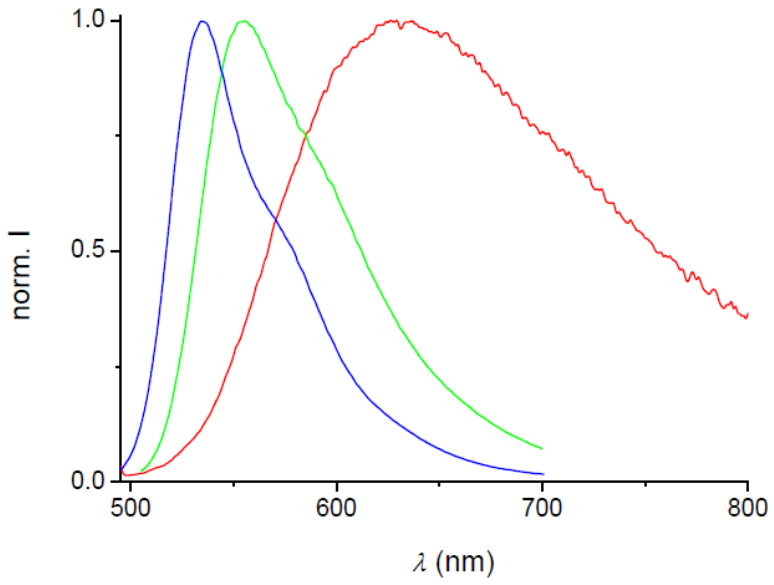

Chart 39 – Fluorescence spectra of **81e** in toluene (blue), chloroform (green), and acetonitrile (red).

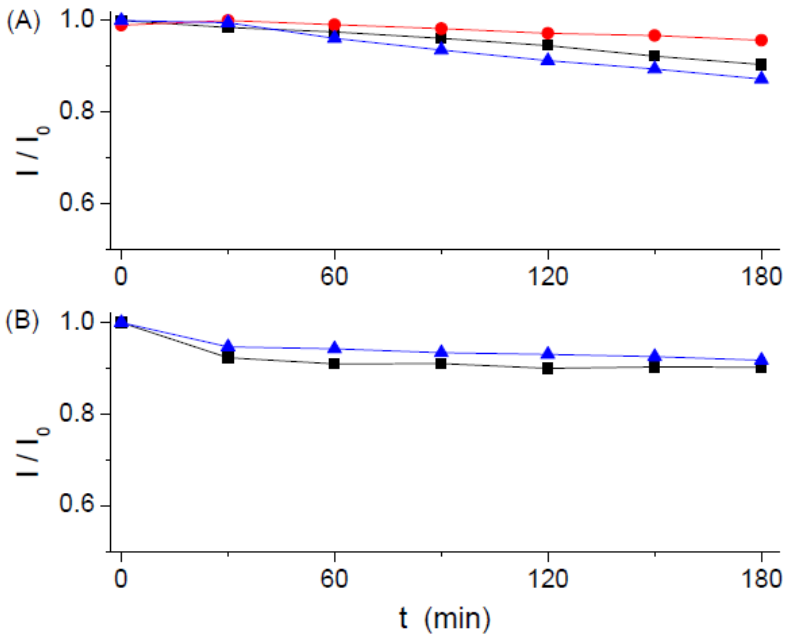

Chart 40 – Photostability of the dyes **81a** (black), **81e** (red), and **81f** (blue) in (A) chloroform and (B) acetonitrile on irradiation at $\lambda > 455$ nm. The irradiations were followed by fluorescence. The normalized fluorescence intensity (versus t = 0) at the maximum is shown. No data are presented for **81e** in acetonitrile due to its low fluorescence.

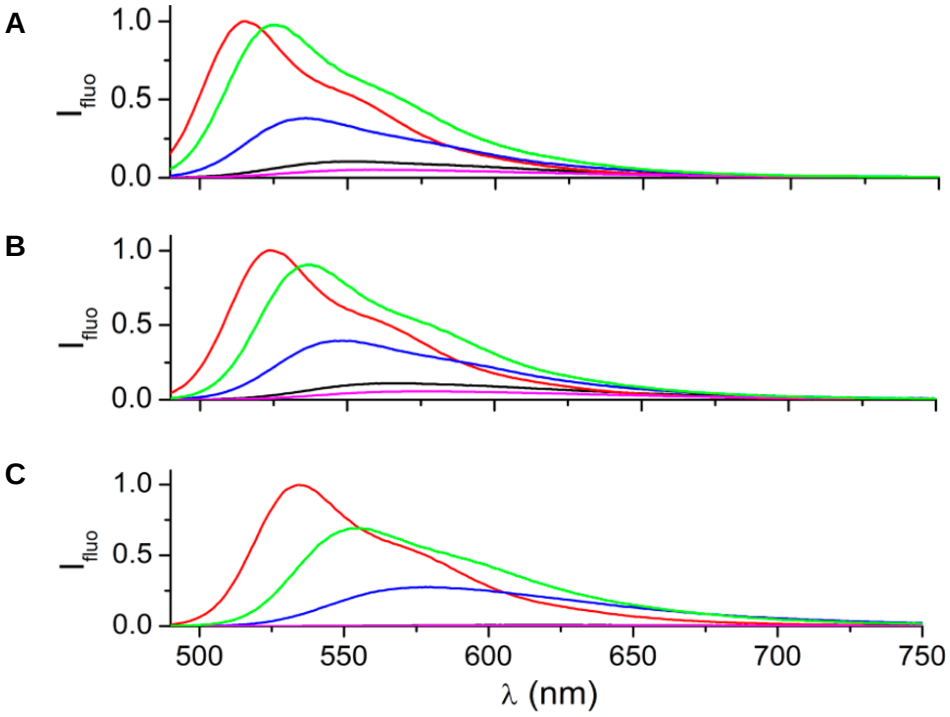

Chart 41 – Fluorescence spectra of (A) **83a**, (B) **83b**, and (C) **81e** in toluene (red), chloroform (green), tetrahydrofuran (blue), acetone (black), and CH_3CN (pink).

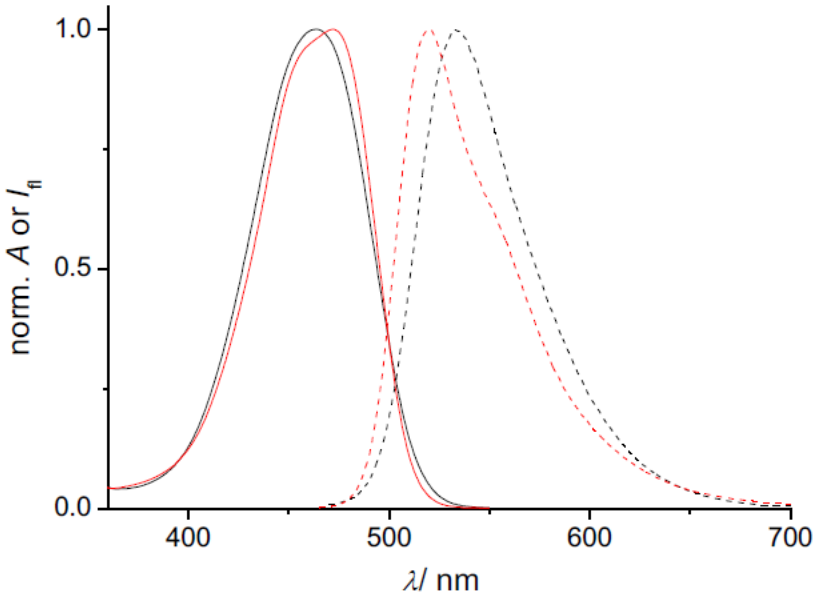

Chart 42 – UV/vis absorption (solid lines) and fluorescence spectra (dashed lines) of BASHY **88** in acetonitrile (black) and in chloroform (red).

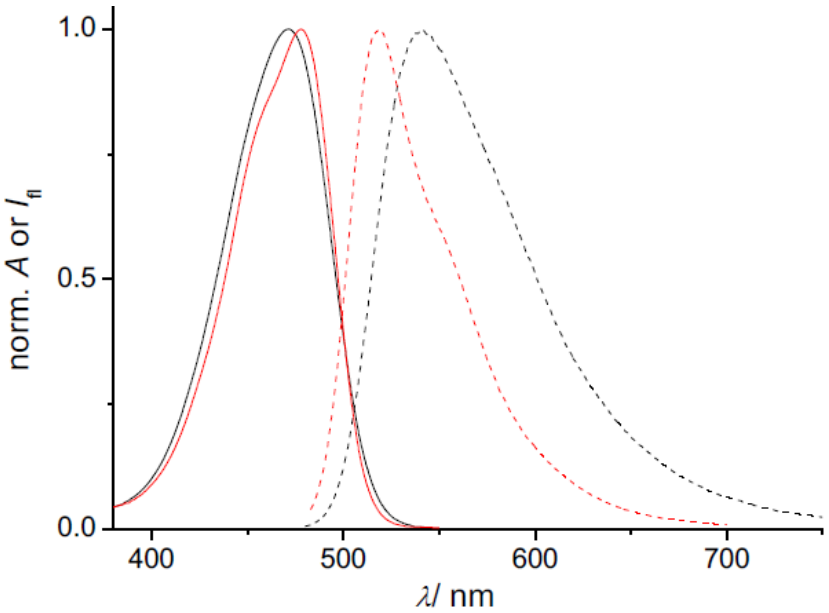

Chart 43 – UV/vis absorption (solid lines) and fluorescence spectra (dashed lines) of BASHY **88** in acetonitrile (black) and in chloroform (red).

IV.2.3 DFT calculations

In order to shine additional light on the nature of the photophysical phenomena,[240][241][242] density-functional-theory calculations (DFT) at the CAM-B3LYP/6-31G** level of theory[243] were performed on the geometry-optimized structures in the electronic ground state using the Gaussian09 program.[203]

No symmetry constraints were applied in the geometry optimizations and local energy minima were confirmed by the absence of imaginary frequencies. The vertical excitations of the optimized ground-state geometry were calculated with the time-dependent DFT (TDDFT) method and the linear-response PCM to determine the first six transitions.

The influence of the solvent (acetonitrile or toluene) was taken into account by the application of the polarized continuum model (linear-response PCM).[224]

IV.2.3.1 Supplementary data from section III.2.1

Atomic coordinates of the optimized species:

BASHY 78a

6 -2.818591 0.757833 1.177237
6 -3.174237 -0.567412 0.824919
6 -2.240248 -1.447140 0.288980
6 -0.925776 -1.016988 0.102450
6 -0.560109 0.312062 0.440592
6 -1.536726 1.183658 0.975220
8 -4.454871 -0.886275 1.049092
8 -0.048655 -1.859145 -0.422945
5 1.401324 -1.614040 -0.414117
7 1.629912 -0.073023 -0.339319
6 0.739747 0.759120 0.126871
8 1.910017 -2.021288 -1.742234
6 2.993211 -1.478830 -2.250834
6 3.535249 -0.237207 -1.552955
7 2.846516 0.453155 -0.712452
8 3.513760 -1.907982 -3.258681
6 4.892994 0.270278 -1.855048
6 2.156946 -2.390384 0.775398
1 1.025747 1.803658 0.225338
6 5.617321 0.870073 -0.816942
6 6.877504 1.401439 -1.050545
6 7.430250 1.347265 -2.326548
6 6.716126 0.756732 -3.363879
6 5.456799 0.216226 -3.134855
6 2.570346 -3.716538 0.593446
6 3.177820 -4.438288 1.615888
6 3.392025 -3.842368 2.855560
6 2.994265 -2.525302 3.060323
6 2.384837 -1.813804 2.030240
6 -4.911692 -2.192107 0.702777
1 5.188181 0.902889 0.178295
1 7.430289 1.854395 -0.234000
1 8.416111 1.762191 -2.511058
1 -3.580643 1.408031 1.589705
1 -2.495074 -2.462053 0.015758
1 -1.248912 2.200717 1.221899
1 7.139891 0.717596 -4.362163
1 4.906645 -0.242411 -3.944146
1 2.419983 -4.192388 -0.372113
1 3.488843 -5.464856 1.445162
1 3.869773 -4.400147 3.655358
1 3.161794 -2.049694 4.022263
1 2.088967 -0.783717 2.212569
1 -5.972921 -2.209819 0.947863
1 -4.389855 -2.958803 1.282584
1 -4.780882 -2.384313 -0.365957

BASHY 81a

6 -2.787320 0.449423 1.432628
6 -3.130669 -0.911437 1.124524
6 -2.142988 -1.721491 0.518215
6 -0.872138 -1.235502 0.265551
6 -0.538841 0.113677 0.583178
6 -1.541256 0.928886 1.162386
7 -4.361134 -1.406780 1.408960
8 0.017011 -2.033084 -0.317887
5 1.453995 -1.726102 -0.331170
7 1.621454 -0.180138 -0.302873
6 0.710755 0.616684 0.207281
8 1.969473 -2.161302 -1.649144
6 3.024824 -1.591842 -2.186613
6 3.502797 -0.292260 -1.557526
7 2.790295 0.394092 -0.732201
8 3.566249 -2.047489 -3.172986
6 4.822731 0.278978 -1.912114
6 2.251289 -2.435850 0.876626
1 0.956681 1.672382 0.293432
6 5.540551 0.947714 -0.912800
6 6.764339 1.537989 -1.195721
6 7.287609 1.472617 -2.483472
6 6.579961 0.812602 -3.482861
6 5.357193 0.214410 -3.203902
6 2.619298 -3.783858 0.769317
6 3.260597 -4.451278 1.807568
6 3.556080 -3.777750 2.989913
6 3.205979 -2.438162 3.119921
6 2.562602 -1.781373 2.073590
6 -4.683024 -2.778499 0.979957
6 -5.424982 -0.537494 1.914816
1 5.134344 0.989275 0.091818
1 7.312109 2.045205 -0.408100
1 8.244772 1.933141 -2.706885
1 -3.517210 1.114810 1.869262
1 -2.340196 -2.745165 0.237505
1 -1.300475 1.962955 1.389898
1 6.980093 0.764002 -4.490526
1 4.812370 -0.298311 -3.984070
1 2.404865 -4.321557 -0.150890
1 3.534547 -5.496315 1.694623
1 4.059543 -4.293239 3.802267
1 3.436740 -1.902090 4.036030
1 2.304863 -0.732506 2.197065
6 -6.029490 -3.310805 1.438236
1 -3.906084 -3.442649 1.369190
1 -4.625597 -2.833348 -0.114390
1 -6.142159 -1.160108 2.445209
6 -6.133235 0.253373 0.821286
1 -5.006181 0.131772 2.667033
1 -6.124435 -4.335451 1.069468
1 -6.869969 -2.738310 1.039360
1 -6.110325 -3.343610 2.527679
1 -5.439258 0.910789 0.290679
1 -6.922181 0.872377 1.258306
1 -6.592859 -0.416995 0.089354

BASHY 81e

6 -2.760689 0.414092 1.464856
6 -3.110753 -0.937079 1.116719
6 -2.124306 -1.737217 0.493943
6 -0.850698 -1.252376 0.260038
6 -0.510627 0.088682 0.614170
6 -1.512674 0.893962 1.212591
7 -4.344474 -1.430799 1.377995
8 0.036382 -2.036463 -0.343212
5 1.474046 -1.735467 -0.317034
7 1.644158 -0.190258 -0.287938
6 0.733826 0.599014 0.244813
8 2.021481 -2.180453 -1.620198
6 3.078644 -1.609338 -2.148984
6 3.524213 -0.292668 -1.538264
7 2.801219 0.391544 -0.721126
8 3.648665 -2.076403 -3.114067
6 4.828069 0.309717 -1.906816
6 2.230335 -2.446913 0.914847
1 0.980349 1.652797 0.349151
6 5.525823 1.018775 -0.921020
6 6.729579 1.637773 -1.210136
6 7.228101 1.539599 -2.501055
6 6.562610 0.846406 -3.501044
6 5.360106 0.227300 -3.198769
6 2.346861 -3.844230 0.927057
6 2.961244 -4.516723 1.977083
6 3.482944 -3.800176 3.051881
6 3.383169 -2.413830 3.062426
6 2.763351 -1.751373 2.004583
6 -4.671870 -2.789337 0.910365
6 -5.403020 -0.573797 1.916673
1 5.121116 1.073454 0.082408
1 7.277582 2.181749 -0.452283
7 8.499076 2.189546 -2.817456
1 -3.489351 1.071100 1.915904
1 -2.326186 -2.752167 0.186397
1 -1.267325 1.920277 1.468214
1 6.978771 0.798212 -4.498633
1 4.830783 -0.318062 -3.966281
8 8.933997 2.083303 -3.956534
8 9.066341 2.810093 -1.927908
1 1.950725 -4.419158 0.093448
1 3.036802 -5.600133 1.958718
1 3.965507 -4.320605 3.873669
1 3.789305 -1.845479 3.894180
1 2.701303 -0.666412 2.034308
6 -6.033617 -3.317216 1.325813
1 -3.909473 -3.470965 1.298434
1 -4.592519 -2.816156 -0.183329
1 -6.123646 -1.211492 2.423780
6 -6.106498 0.260234 0.852679
1 -4.979452 0.064243 2.692841
1 -6.133807 -4.328776 0.923822
1 -6.857987 -2.721350 0.927507
1 -6.137791 -3.382917 2.411658
1 -5.409537 0.934541 0.347887
1 -6.893496 0.865191 1.312239
1 -6.567683 -0.380815 0.095987

BASHY 81f

6 -3.231519 -0.068968 1.101265
6 -3.323335 -1.439795 0.680355
6 -2.165080 -2.044607 0.140939
6 -0.969588 -1.352982 0.050835
6 -0.888107 0.006188 0.474439
6 -2.058035 0.613865 0.991520
7 -4.483440 -2.133623 0.799232
8 0.086019 -1.959070 -0.482319
5 1.447838 -1.431831 -0.309263
7 1.358605 0.117908 -0.217752
6 0.288406 0.725513 0.241600
8 2.170567 -1.719754 -1.569975
6 3.158089 -0.959757 -1.984549
6 3.338219 0.379421 -1.287059
7 2.443976 0.898826 -0.518528
8 3.867081 -1.282862 -2.915927
6 4.560924 1.187574 -1.503565
6 2.197620 -2.068909 0.964606
1 0.346739 1.800019 0.396821
6 5.046821 1.949326 -0.433503
6 6.163778 2.757891 -0.590233
6 6.810424 2.821324 -1.820789
6 6.333108 2.070232 -2.889864
6 5.218608 1.254497 -2.737137
6 2.539201 -3.430065 0.951781
6 3.152915 -4.037481 2.038520
6 3.468558 -3.319305 3.202063
6 3.131557 -1.964360 3.213417
6 2.510844 -1.354822 2.122845
6 -4.542342 -3.501484 0.256483
6 -5.720676 -1.465412 1.207925
1 4.546481 1.891627 0.526785
1 6.532634 3.335221 0.251391
1 7.685028 3.451926 -1.945263
1 -4.096363 0.442997 1.496186
1 -2.168336 -3.063240 -0.216304
1 -2.008539 1.653847 1.300021
1 6.829664 2.120179 -3.853634
1 4.853299 0.671892 -3.570997
1 2.318948 -4.026492 0.068995
1 3.393306 -5.097093 1.984556
1 3.352348 -1.361362 4.091381
1 2.271369 -0.295647 2.185064
6 -5.829377 -4.260072 0.529551
1 -3.715467 -4.069992 0.691289
1 -4.366529 -3.465601 -0.826087
1 -6.389925 -2.219704 1.615909
6 -6.409291 -0.720536 0.070279
1 -5.501015 -0.790860 2.036001
1 -5.722271 -5.260550 0.102120
1 -6.701931 -3.795467 0.064568
1 -6.020057 -4.376926 1.599409
1 -5.767615 0.064561 -0.338770
1 -7.330561 -0.253680 0.430800
1 -6.669454 -1.404538 -0.742597
6 8.886596 -2.155605 4.955700
6 8.997049 -3.220094 3.996721
6 7.842507 -3.990063 3.726349
6 6.634274 -3.711426 4.341164
6 6.533622 -2.649354 5.287298
6 7.699527 -1.897556 5.571952
7 10.169758 -3.477377 3.366103
6 5.340964 -2.475271 5.996476
8 3.499261 -5.303029 4.819358
6 2.508747 -5.273878 5.680535
6 2.291071 -3.973810 6.438909
7 3.173119 -3.036030 6.491019
8 1.827297 -6.253639 5.905530
6 1.046444 -3.742980 7.208820
1 5.265274 -1.785954 6.834112
6 0.545779 -2.436652 7.277030
6 -0.595063 -2.153327 8.014594
6 -1.252600 -3.170997 8.699055
6 -0.761231 -4.470871 8.639034
6 0.377555 -4.761452 7.897584
6 10.245239 -4.646662 2.473535
6 11.388609 -2.743970 3.712375
1 1.053941 -1.646562 6.735416
1 -0.974138 -1.137096 8.049843
1 -2.145988 -2.951800 9.275247
1 9.748813 -1.559498 5.215188
1 7.859916 -4.816036 3.031312
1 7.635289 -1.100342 6.306465
1 -1.266033 -5.268093 9.175260
1 0.752955 -5.773943 7.853119
6 11.566254 -4.837651 1.749356
1 9.455203 -4.551424 1.722262
1 10.021048 -5.549889 3.054051
1 12.060593 -2.786659 2.857847
6 12.090312 -3.286524 4.951570
1 11.141108 -1.689129 3.837951
1 11.478563 -5.736118 1.132887
1 12.404579 -4.987650 2.433573
1 11.798950 -4.002808 1.083675
1 11.444201 -3.234233 5.832057
1 12.993343 -2.704310 5.157328
1 12.383961 -4.330126 4.807352
8 5.582809 -4.477530 4.070581
5 4.213676 -4.068547 4.415875
7 4.277721 -3.184026 5.692699

IV.2.3.2 Supplementary data from section III.2.3

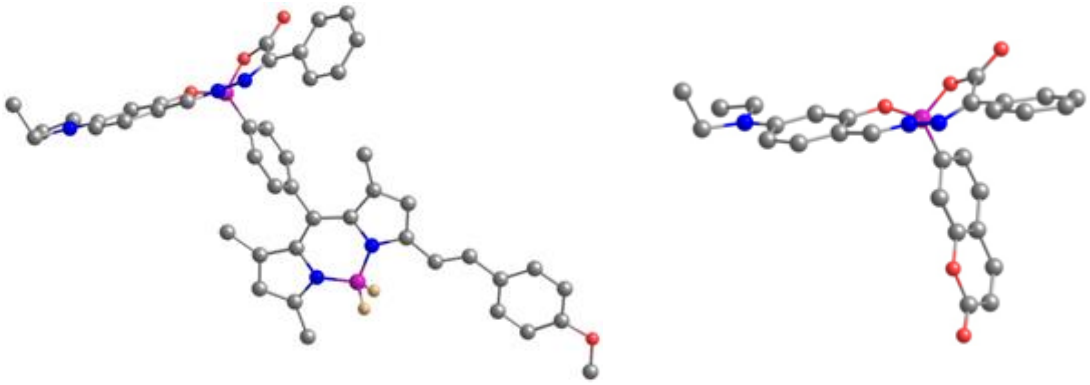

85 **87**

Figure 32 – Optimized ground-state structures of ECTs **85** and **87**.

Selected Angles of the Optimized Structures:

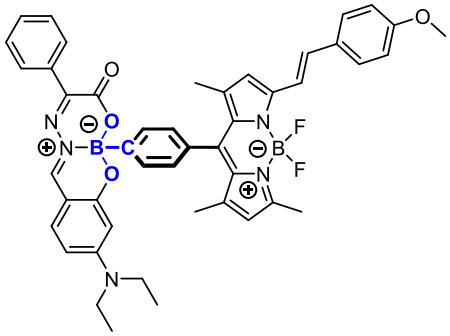	τ_1 = - 34.44 (puckering angle of the boron atom)
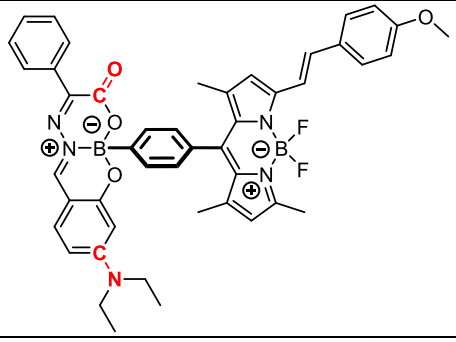	τ_2 = 36.63 (measurement of the BASHY planarity)
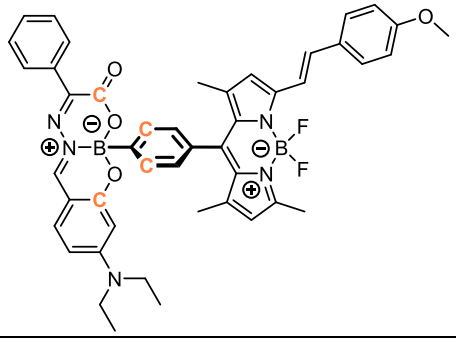	τ_3 = 88.52 (dihedral angle of C-C-C-C; showing the perpendicularity of the phenylene with the BASHY)

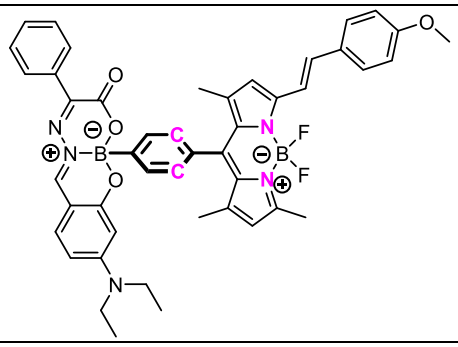	τ_4 = - 91.14 (dihedral angle of C-C-N-N; showing the perpendicularity of the phenylene with the Bodipy)

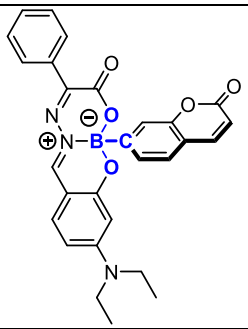	τ_1 = - 34.50 (puckering angle of the boron atom)
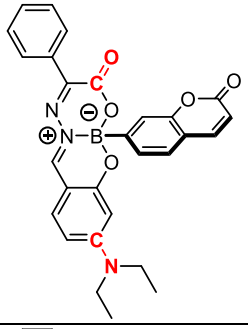	τ_2 = 37.58 (measurement of the BASHY planarity)
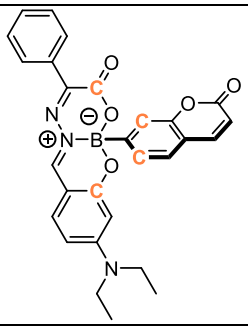	τ_3 = 88.29 (dihedral angle of C-C-C-C; showing the perpendicularity of the coumarin with the BASHY)

- **Frontier Orbitals and Transitions:**

Table 22 – TDDFT data (CAM-B3LYP/6-31G**) for selected first six transitions of ECT **85** in toluene (only transition with f > 0.1 are shown).

Electronic transition	E_{exc} (eV) [a]	f [b]	Orbitals	CI [c]
$S_0 \rightarrow S_1$	2.47	1.073	HOMO → LUMO	0.68689 (94 %)
			HOMO-2 → LUMO	0.11234 (3 %)
$S_0 \rightarrow S_2$	3.18	1.286	HOMO-1 → LUMO+1	0.65848 (87 %)
			HOMO-3 → LUMO+1	0.15594 (5 %)
$S_0 \rightarrow S_4$	3.82	0.253	HOMO-4 → LUMO	0.59005 (70 %)
			HOMO-2 → LUMO	0.29489 (17 %)
			HOMO-7 → LUMO	0.11620 (3 %)
			HOMO → LUMO+3	0.10125 (2 %)
$S_0 \rightarrow S_6$	3.96	0.584	HOMO-2 → LUMO	0.55064 (61 %)
			HOMO-4 → LUMO	0.32486 (21 %)
			HOMO → LUMO+3	0.17475 (6 %)
			HOMO-12 → LUMO	0.11239 (3 %)

[a] Excitation energy. **[b]** Oscillator strength. **[c]** Absolute CI coefficient of the wavefunction for each excitation. In parenthesis the percentage contribution of the configuration to excitation is indicated.

Table 23 – TDDFT data (CAM-B3LYP/6-31G**) for selected first six transitions of ECT **87** in toluene (only transition with f > 0.1 are shown, except $S_0 \rightarrow S_2$).

Electronic transition	E_{exc} (eV) [a]	f [b]	Orbitals	CI [c]
$S_0 \rightarrow S_1$	3.18	1.284	HOMO → LUMO	0.66204 (88 %)
			HOMO-2 → LUMO	0.14334 (4 %)
$S_0 \rightarrow S_2$	3.87	0.080	HOMO-2 → LUMO	0.47633 (45 %)
			HOMO-1 → LUMO	0.27481 (15 %)
			HOMO-6 → LUMO	0.23741 (11 %)
			HOMO-3 → LUMO	0.18269 (7 %)
			HOMO-4 → LUMO	0.17723 (6 %)
			HOMO-6 → LUMO+2	0.13554 (4 %)
			HOMO-2 → LUMO+2	0.1341 (4 %)
$S_0 \rightarrow S_3$	4.05	0.140	HOMO-6 → LUMO	0.46682 (44 %)
			HOMO-1 → LUMO	0.27408 (15 %)
			HOMO-6 → LUMO+2	0.20512 (8 %)
			HOMO-2 → LUMO	0.18398 (7 %)
			HOMO → LUMO	0.12532 (3 %)
			HOMO → LUMO+2	0.11837 (3 %)
			HOMO-4 → LUMO	0.11821 (3 %)
			HOMO-2 → LUMO+2	0.11111 (2 %)
$S_0 \rightarrow S_3$	4.38	0.328	HOMO-1 → LUMO+1	0.56866 (65 %)
			HOMO-1 → LUMO	0.22086 (10 %)
			HOMO-2 → LUMO+1	0.18185 (7 %)
			HOMO-2 → LUMO	0.18071 (7 %)
			HOMO-1 → LUMO+2	0.10291 (2 %)
			HOMO-6 → LUMO	0.10068 (2 %)

[a] Excitation energy. **[b]** Oscillator strength. **[c]** Absolute CI coefficient of the wavefunction for each excitation. In parenthesis the percentage contribution of the configuration to excitation is indicated.

- **Selected frontier orbitals:**

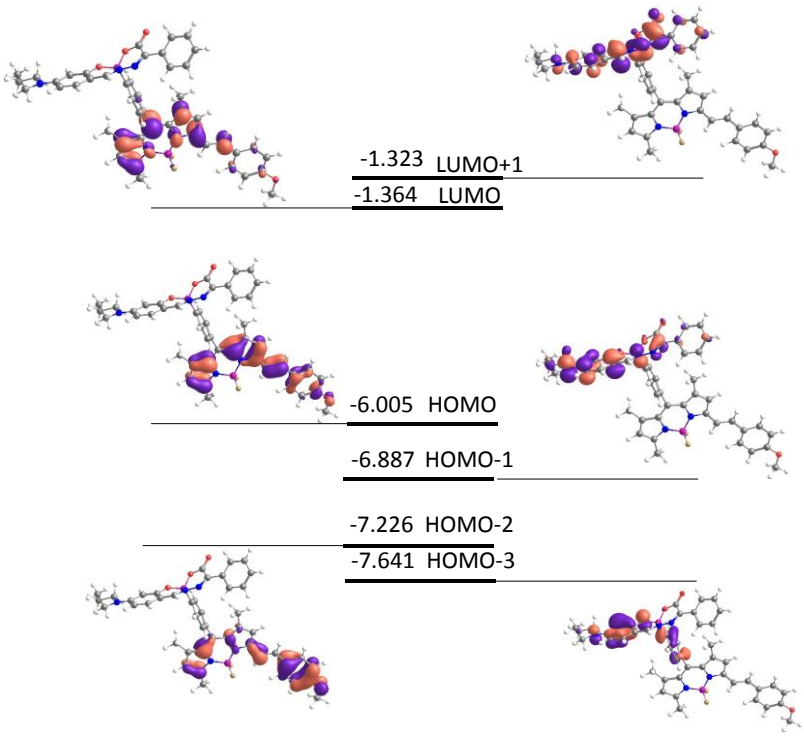

Figure 33 – Selected frontier orbitals of ECT **85**.

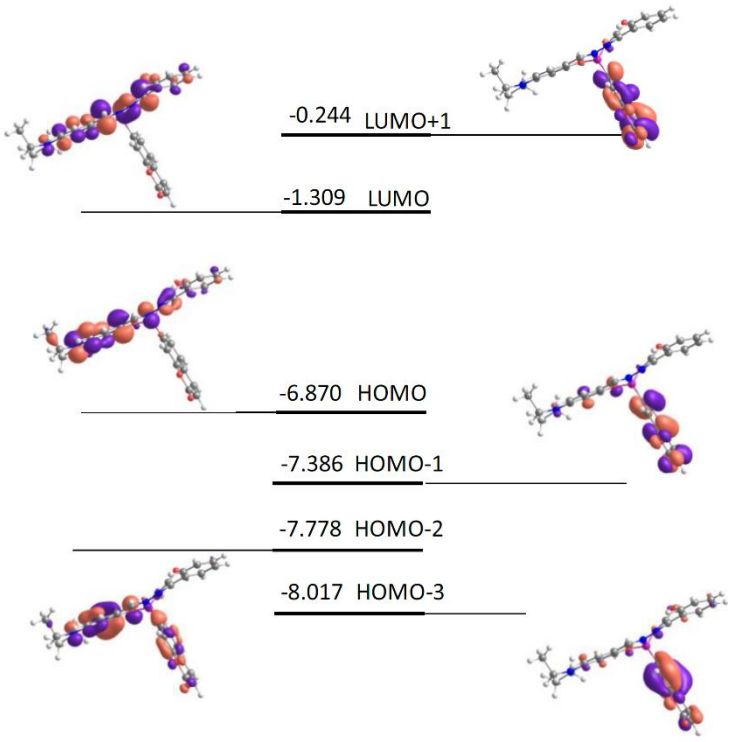

Figure 34 – Selected frontier orbitals of ECT **87**.

Atomic coordinates of the optimized species:

ECT 85

6	7.647034	-1.465871	-1.550784	6	-1.185879	-4.757418	-0.514477
6	7.444977	-2.060222	-0.260310	6	-3.700857	-5.386815	-0.753665
6	6.539439	-1.434874	0.620469	6	1.005900	-3.486360	-0.207617
6	5.829108	-0.305645	0.241999	6	-1.356958	-1.172591	0.033828
6	6.027095	0.267662	-1.046650	6	-2.497178	-0.372576	0.143391
6	6.961487	-0.344603	-1.912765	7	-3.770971	-0.929555	0.035461
7	8.104228	-3.196189	0.100666	6	-4.685995	0.043072	0.208722
8	4.999783	0.249692	1.112351	6	-4.011878	1.265337	0.430415
5	4.003725	1.261714	0.733587	6	-2.654222	1.028919	0.391578
7	4.521695	2.004286	-0.534009	6	-1.609465	2.081105	0.584395
6	5.390547	1.476981	-1.358528	6	-6.108774	-0.221090	0.173596
8	3.991394	2.275783	1.806006	6	-7.038600	0.748854	0.182790
6	3.677838	3.529544	1.565860	6	-8.489070	0.572914	0.159524
6	3.515035	3.929462	0.102942	6	-9.313670	1.707087	0.225987
7	4.000542	3.231986	-0.865987	6	-10.690951	1.603072	0.212343
8	3.576617	4.348209	2.453127	6	-11.295816	0.346222	0.128808
6	2.823920	5.181805	-0.281235	6	-10.497226	-0.797385	0.057521
6	2.542625	0.624879	0.499490	6	-9.115164	-0.675160	0.074094
1	5.615563	2.032089	-2.266181	5	-4.068312	-2.393940	-0.371483
6	2.170820	5.214024	-1.520711	9	-4.950107	-2.977629	0.538699
6	1.532435	6.365427	-1.954594	9	-4.624512	-2.437414	-1.647262
6	1.536885	7.506290	-1.158101	8	-12.650094	0.337315	0.121858
6	2.181053	7.483726	0.073240	6	-13.312352	-0.910132	0.018720
6	2.818328	6.331555	0.516470	1	-0.760247	-5.744051	-0.637124
6	1.794831	0.200722	1.605547	1	-3.339637	-6.395585	-0.958064
6	0.542322	-0.380737	1.461298	1	-4.317111	-5.052369	-1.592789
6	-0.008076	-0.558109	0.190543	1	-4.347079	-5.410625	0.127498
6	0.720150	-0.146600	-0.922949	1	1.439476	-4.488113	-0.252208
6	1.973879	0.435940	-0.762395	1	1.334775	-3.015022	0.721382
6	7.925925	-3.704751	1.468655	1	1.428895	-2.899993	-1.027595
6	9.148694	-3.759932	-0.751964	1	-4.482856	2.219970	0.616034
1	2.162604	4.320377	-2.134148	1	-0.906680	2.118445	-0.251107
1	1.023724	6.370087	-2.913139	1	-1.018734	1.911893	1.487879
1	1.036060	8.408204	-1.495498	1	-2.085926	3.059958	0.672572
1	8.354948	-1.890159	-2.246869	1	-6.393901	-1.266049	0.154323
1	6.358762	-1.807784	1.617033	1	-6.708747	1.785335	0.208609
1	7.134284	0.098440	-2.889156	1	-8.856318	2.690156	0.290675
1	2.190515	8.370677	0.698369	1	-11.322910	2.482712	0.265566
1	3.313119	6.315703	1.476674	1	-10.940369	-1.782623	-0.011300
1	2.197363	0.337784	2.605471	1	-8.517410	-1.578092	0.013617
1	-0.018835	-0.695487	2.336047	1	-14.379850	-0.688555	0.025545
1	0.302267	-0.276252	-1.916701	1	-13.078034	-1.563584	0.866403
1	2.511502	0.756881	-1.650711	1	-13.060254	-1.424664	-0.915120
6	8.565091	-5.052473	1.756927				
1	6.851988	-3.796992	1.654088				
1	8.305857	-2.963800	2.184216				
1	9.251032	-4.814929	-0.505782				
6	10.497668	-3.062754	-0.609961				
1	8.809075	-3.736152	-1.788626				
1	8.323496	-5.324360	2.787714				
1	9.654234	-5.036271	1.671798				
1	8.173091	-5.841530	1.109862				
1	10.431702	-2.004528	-0.875624				
1	11.236975	-3.532324	-1.265549				
1	10.866901	-3.128169	0.417483				
6	-2.555596	-4.458288	-0.544817				
7	-2.718850	-3.141018	-0.352311				
6	-1.464194	-2.550312	-0.198484				
6	-0.483986	-3.579686	-0.299561				

ECT 87

6	-2.472681	2.656615	-2.923035
6	-2.568934	1.250754	-2.653512
6	-1.374393	0.503007	-2.611155
6	-0.139210	1.109563	-2.778507
6	-0.054604	2.507714	-3.034052
6	-1.257448	3.246358	-3.106943
7	-3.776505	0.657552	-2.438874
8	0.953938	0.360566	-2.739564
5	2.295387	0.936535	-2.580910
7	2.289254	2.360817	-3.212991
6	1.196327	3.073710	-3.318383
8	3.213953	0.129767	-3.401918
6	4.286028	0.654204	-3.955000
6	4.449224	2.166283	-3.851973
7	3.472591	2.957719	-3.575982
8	5.081836	-0.007883	-4.582615
6	5.748162	2.789670	-4.185186
6	2.753731	0.965240	-1.033280
1	1.302062	4.099422	-3.663627
6	5.775098	4.106116	-4.659789
6	6.981599	4.731605	-4.932423
6	8.180548	4.055742	-4.724386
6	8.162955	2.750686	-4.247164
6	6.956353	2.115438	-3.982952
6	3.081539	-0.251241	-0.401721
6	3.435130	-0.298901	0.930951
6	3.478633	0.875472	1.697225
6	3.159694	2.080648	1.069539
6	2.802234	2.129014	-0.274000
6	-3.815061	-0.798385	-2.238499
6	-5.021187	1.389483	-2.666471
1	4.839065	4.629759	-4.815686
1	6.987392	5.749267	-5.308922
1	9.125341	4.546183	-4.936056
1	-3.361822	3.264946	-2.993657
1	-1.371236	-0.563013	-2.442616
1	-1.203344	4.310166	-3.318453
1	9.093886	2.219018	-4.079745
1	6.950429	1.096102	-3.621285
1	3.061391	-1.170010	-0.979832
6	3.840281	0.924471	3.090740
8	3.187310	3.262533	1.753876
1	2.572804	3.099077	-0.702943
6	-5.165389	-1.370531	-1.841772
1	-3.101495	-1.044359	-1.446931
1	-3.462173	-1.301896	-3.148168
1	-5.807908	0.902541	-2.093922
6	-5.422918	1.467106	-4.135418
1	-4.928101	2.388587	-2.238120
1	-5.039653	-2.443890	-1.677733
1	-5.926147	-1.247140	-2.616248
1	-5.537786	-0.938359	-0.909225
1	-4.659751	1.972754	-4.732685
1	-6.360577	2.020398	-4.242771
1	-5.569957	0.467759	-4.554980
1	3.686443	-1.243166	1.405187
6	3.524639	3.347026	3.084255
8	3.516639	4.438559	3.600191
6	3.862708	2.095756	3.749756
1	4.093707	-0.002386	3.597304
1	4.128966	2.175454	4.796058

IV.2.4 Bioimaging applications

IV.2.4.1 Additional information from Section III2.4

- **Cell culture conditions**

HeLa cells were cultured in DMEM supplemented with 10 % (v/v) FBS and 1 % (v/v) PEST in a 5 % CO_2 atmosphere at 37 °C

- ***In vitro* cell viability assay**

The effect of unsupported dyes (BASHYs **81a,e** and coumarin-6) on cell viability was quantified with the alamarBlue® assay. HeLa cells seeded at a density of 2 × 10^4 cells/well in 96-well plates were treated overnight with the free dyes (5 µg.mL^{-1}). AlamarBlue® reagent was added at 10 % (v/v). After 24 h of total incubation time, absorbance values were measured at 570 nm (AlamarBlue reduced form, pink) and 600 nm (alamarBlue oxidized form, blue), using a microplate reader (FLUOstar Omega, BMG Labtech, Durham, NY, USA). PBS and 0.5 % (v/v) Triton X-100 were used as positive and negative controls, respectively.

- **Cell staining**

HeLa cells (4 × 10^4 cells/200 µl/well) were seeded in 8-well Ibidi® µ-Slide microscopy chambers previously coated with poly-L-lysine, and incubated for 24 h in a humidified incubator with 5 % CO_2, at 37 °C, allowing the cells to become adherent. HeLa cells were then incubated with **81a,e** (5 µg.mL^{-1}) or 3 µM Nile Red (Life Technologies, Carlsbad, USA) for 10 minutes. The cells were then washed with sterile PBS (pH 7.4) or DMEM supplemented with 10 % fetal calf serum, 100 IU mL^{-1} penicillin, and 100 µg.mL^{-1} streptomycin without phenol red. Images were obtained by confocal microscopy using a Leica TCS SP5 (Leica Microsystems CMS GmbH, Mannheim, Germany) inverted microscope (DMI6000) with a 63 × water (1.2 numerical aperture) apochromatic objective. The excitation of BASHYs **81a,e** and Nile Red was performed using the 476 nm, 488 nm, and 514 nm lines of an Ar+ laser, respectively. The emission was detected at 485 – 600 nm, 500 – 600 nm, and 540 – 610 nm for **81a,e** and Nile Red, respectively. Excitation of WGA-Alexa Fluor® 633 was performed using the 633 nm line from a HeNe laser. The excitation wavelength of Hoechst 33342 was set to 780 nm using a titanium-sapphire laser for two-photon excitation. The images were processed using ImageJ Software.

IV.2.4.2 Additional information from Section III2.5.1

- **Cell culture conditions**

Murine immature bone marrow dendritic cells (JAW SII, ATCC®CRL-11904TM, ATCC, Manassas, VA, USA) were propagated in RPMI 1640 medium and Glutamax™ supplemented with 10 % (v/v) fetal bovine serum (FBS), 1 % (v/v) PEST, 50 µM *β*-mercaptoethanol, 10 mM HEPES, 1 mM sodium pyruvate and 5 ng.mL^{-1} GM-CSF.

- **Preparation of dye-labeled NPs and their physicochemical characterization**

Dye-labeled nanoparticles were prepared using the double emulsion (water-in-oil-inwater (w/o/w)) solvent evaporation method, as reported.[184] PLGA polymer and 10 µg of dye were dissolved in dichloromethane. A 10 % (w/v) poly(vinyl alcohol) (PVA) aqueous solution was added and emulsified with the organic phase under continuous sonication at 70 W for 15 s. A second emulsion was formed when this W/O emulsion was dispersed within a 1.25 % (w/v) PVA aqueous solution under the same conditions. The w/o/w emulsion was added dropwise into a 0.25 % (w/v) PVA aqueous solution, and stirred for 1 h at 37 °C. The dye-labeled NPs were washed with ultrapure water, collected by centrifugation at 14000 × g at 4 °C for 20 min (Beckman Coulter Allegra 64R High Speed Centrifuge), and finally re-suspended in sterile phosphate buffer saline (PBS, pH 7.4).

The mean NP size (Z-Average, Z-Ave) and PdI were determined by Dynamic Light Scattering in combination with cumulative analysis (Malvern Instruments, Worcestershire, UK). The same equipment allowed the determination of NP surface charge (ZP) by Laser Doppler Electrophoresis in combination with Phase Analysis Light Scattering at 25ºC. The NP suspension was diluted in sterile phosphate buffer saline (PBS, pH 7.4).

- **Stability assay of dye-labeled NPs**

The percentage of dye (**81a,e** or coumarin-6) not entrapped during dye-labeled NPs formulation procedure or released from the NP matrix after incubation (1 mg.mL^{-1}) with RPMI 1640 (Roswell Park Memorial Institute) medium in a humidified incubator (5 % CO_2 at 37 °C for 24 h) was indirectly quantified by fluorescence measurements. For this purpose the supernatant was recovered by centrifugation at 14000 × g, 4 °C for 20 min (Beckman Coulter Allegra 64R High Speed Centrifuge). The supernatants were dried and the remaining pellet was re-suspended in ethanol. The fluorescence intensity (excitation at 485 nm) was measured at 520 nm (**81a**, coumarin-6) or 590 nm (**81e**), using a microplate reader (POLARstar OPTIMA, BMG Labtech, Durham, NY, USA). Standard

calibration curves were generated with known dye concentrations in the range of 0 – 5 µg.mL^{-1} in ethanol.

- ***In vitro* cell viability assay of dye-labeled NPs**

The effect of dye-labeled NPs on cell viability was quantified with the alamarBlue® assay. Murine immature bone marrow dendritic cells were seeded at a density of 2 × 10^4 cells/well in 96-well plates, incubated overnight, and treated with dye-labeled NPs (0.5 mg.mL^{-1}). AlamarBlue® reagent was added at 10 % (v/v). After 24 h of total incubation time, absorbance values were measured at 570 nm (AlamarBlue reduced form, pink) and 600 nm (AlamarBlue oxidized form, blue), using a microplate reader (FLUOstar Omega, BMG Labtech, Durham, NY, USA). PBS and 0.5 % (v/v) Triton X-100 were used as positive and negative controls, respectively.

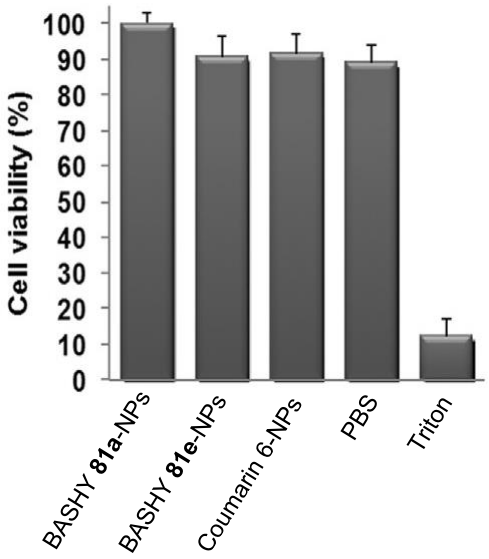

Chart 44 – Cell viability determined by alamarBlue assay 24 h after incubation of BMDCs (JAW SII, ATCC CRL11904TM) with 500 mg.mL^{-1} of dye-labeled NPs (**81a,e** or coumarin-6; mean±standard deviation (SD); n=6. Phosphate-buffered saline (PBS) and Triton were used as controls.

- **Cell staining**

For the qualitative NP uptake study the fluorescent dye-labeled NPs were added to murine immature bone marrow-derived dendritic cells previously seeded in 8-well microscopy chambers at 500 µg.mL^{-1} and incubated for 18 h. The cells were then washed with sterile PBS and stained with WGA-Alexa Fluor® 633 and Hoechst 33342, and the cells were imaged using confocal fluorescence microscopy.

IV.2.4.3 Additional information from Section III2.5.2

- **Preparation of dye-labeled NPs and their physicochemical characterization**

Dye labeled nanoparticles were prepared using a double emulsion (water-in-oil-in-water (w/o/w)) solvent evaporation method, as reported elsewhere with modifications.[184] Poly(lactic-co-glycolic acid) polymer (PLGA, lactide:glycolide 50:50, ester terminated, average molecular weight 7000 – 17000 $g.mol^{-1}$) and 10 µg of ECT **85** were dissolved in dichloromethane. An 8 % (w/v) poly(vinyl alcohol) (PVA; average molecular weight 13000 – 23000 $g.mol^{-1}$) aqueous solution was added and emulsified with the organic phase under continuous sonication at 20 % of amplitude for 15 seconds. A second emulsion was formed when this w/o emulsion was dispersed in a 2.5 % (w/v) PVA aqueous solution under the same conditions. The w/o/w emulsion was poured drop-wise into a 0.25 % (w/v) PVA aqueous solution and stirred for 1 h at RT. The nanoparticles were washed with ultrapure water, collected by centrifugation (17500 rpm, 4 °C, 40 min), and finally re-suspended in sterile phosphate buffer saline (0.01 M, pH 7.4).

The mean nanoparticle size (Z-Average) and polydispersity index (PdI) were determined by dynamic light scattering. The nanoparticle surface charge (zeta potential, ZP) was measured by laser doppler electrophoresis in combination with phase analysis light scattering (PALS), at 25 ºC. The NP suspension (10 $mg.mL^{-1}$) was diluted in 10 mM KCl to a final concentration of 0.6 $mg.mL_{-1}$. All measurements were performed in triplicate.

- **Internalization study and dead cell evaluation**

For the quantitative uptake study, murine immature bone marrow dendritic cells (BMDC; JAW SII, ATCC®CRL-11904TM); 3.5×10^4 cells/190 µL/well) were seeded in 96-well plates, and incubated overnight in a humidified incubator with 5 % CO_2 at 37 °C, allowing the cells to become adherent. The cells were then treated with ECT **85**-NPs (0.5 $mg.mL^{-1}$) for 1, 3, and 18 h. The cells were then washed with sterile phosphate buffer saline (0.01 M, pH 7.4) and labeled with propidium iodide to evaluate the dead cell population. The medium and 0.05 % (v/v) Triton X-100 were used as negative and positive controls, respectively. The fluorescence of 10000 cells was analyzed by flow cytometry.

- **Confocal Fluorescence Microscopy**

Dye-loaded nanoparticles were added to previously seeded BMDCs (6 × 10^4 cells/300 µL/well) and incubated for 2, 4, or 10 hours. The cells were then fixed and co-stained with Hoechst®33258 (nucleus) and WGA-Alexa Fluor® 633 (membrane). The images were obtained by confocal microscopy using an inverted microscope with a 63 × oil (1.4 numerical aperture) plan-apochromat objective. Excitation of the fluorescent nanoparticles was performed using the 488 nm Ar ion laser line and the emission was collected at 550 – 600 nm. Excitation of WGA-Alexa Fluor® 633 was performed using the 633 nm line from a HeNe laser. The excitation wavelength of Hoechst was set to 405 nm using a diode laser. The images were processed using standard software.

IV.2.4.4 Additional information from Section III2.6

- **Cell viability assays of BASHY 89**

Two different cell lines were used for the in vitro studies, namely Hek293T (a human embryonic kidney cell line) and HeLa cells (derived from cervical cancer cells). The cells were maintained in a humidified incubator at 37 ºC under 5 % CO_2 and grown using 1x DMEM with Sodium Pyruvate and without L-Glutamine (Invitrogen, Life Technologies) supplemented with 10 % heat-inactivated fetal bovine serum (FBS) (Gibco, Life Technologies), 1x MEM NEAA (Gibco, Life Technologies) ,1x GlutaMAX (Gibco, Life Technologies), 200 units/mL penicillin and 200 µg/mL streptomycin (Gibco, Life Technologies) and 10 mM HEPES (Gibco, Life Technologies).

Then 10 000 cells/well were seeded in 96 well-plates and were treated with BASHY **89**, 24 h after the seeding, to allow the cells to stabilize. The cells were incubated with 1 µg/mL, 5 µg/mL and 10 µg/mL of **89** for 24 h. After this incubation period, the culture medium was removed and the cells were incubated with CellTiter-Blue (Promega) for 1 h 30 min at 37 ºC. The cells viability was evaluated by measuring the Emission Intensity in RFUs – relative fluorescent Units- with an Infinite M200 plate reader.

- **Apoptosis assay protocol**

HeLa cells were grown to 80 % confluency in DMEM supplemented with 10 % FBS, GlutaMax (Gibco), MEM (Gibco), and 100 U/ml penicillin, 100 mg/ml streptomycin. To induce apoptosis 1 µM actinomycine D in DMSO was added to the medium while 0.1 % DMSO was added to the control.

After 6 h, either 1 µg/mL of either Annexin V-BASHY **92**, Annexin V-Cy5 **93** or Annexin V-FITC **94** was added for 15 min followed by 20 min of 4 % paraformaldehyde fixation, 30 min of 100 µg/mL Hoechst 33342 staining and embedding in Fluoromount-G.

Imaging was done using a Zeiss LSM 710 with identical laser, filter and detector settings for control vs. apoptosis samples.

The blocking experiment followed exactly the same protocol, but using a presaturation of the receptors with a preincubation of non-fluorescent Annexin V-mal-DBCO **91** (1 µg/mL) for 15 min.

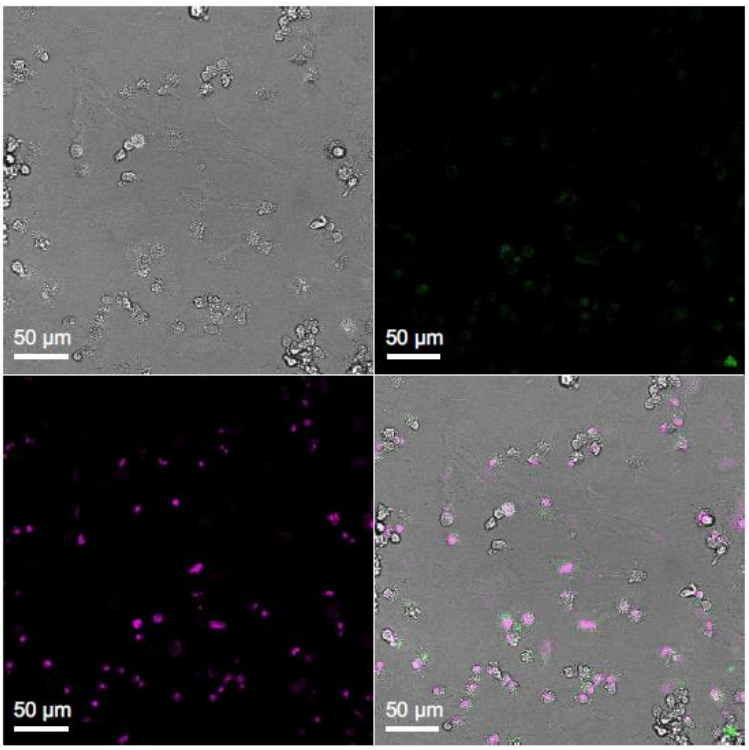

Figure 35 – Blocking experiment. Confocal microscopy images of HeLa cells treated with 1 µM actinomycin D for 6 h to induce apoptosis followed by incubation with 1 µg/mL of Annexin V-mal DBCO **91** for 15 min and subsequent incubation with 1 µg/mL of Annexin V-BASHY **92**. Annexin V-BASHY **92** (green), nuclear Hoechst staining (purple).

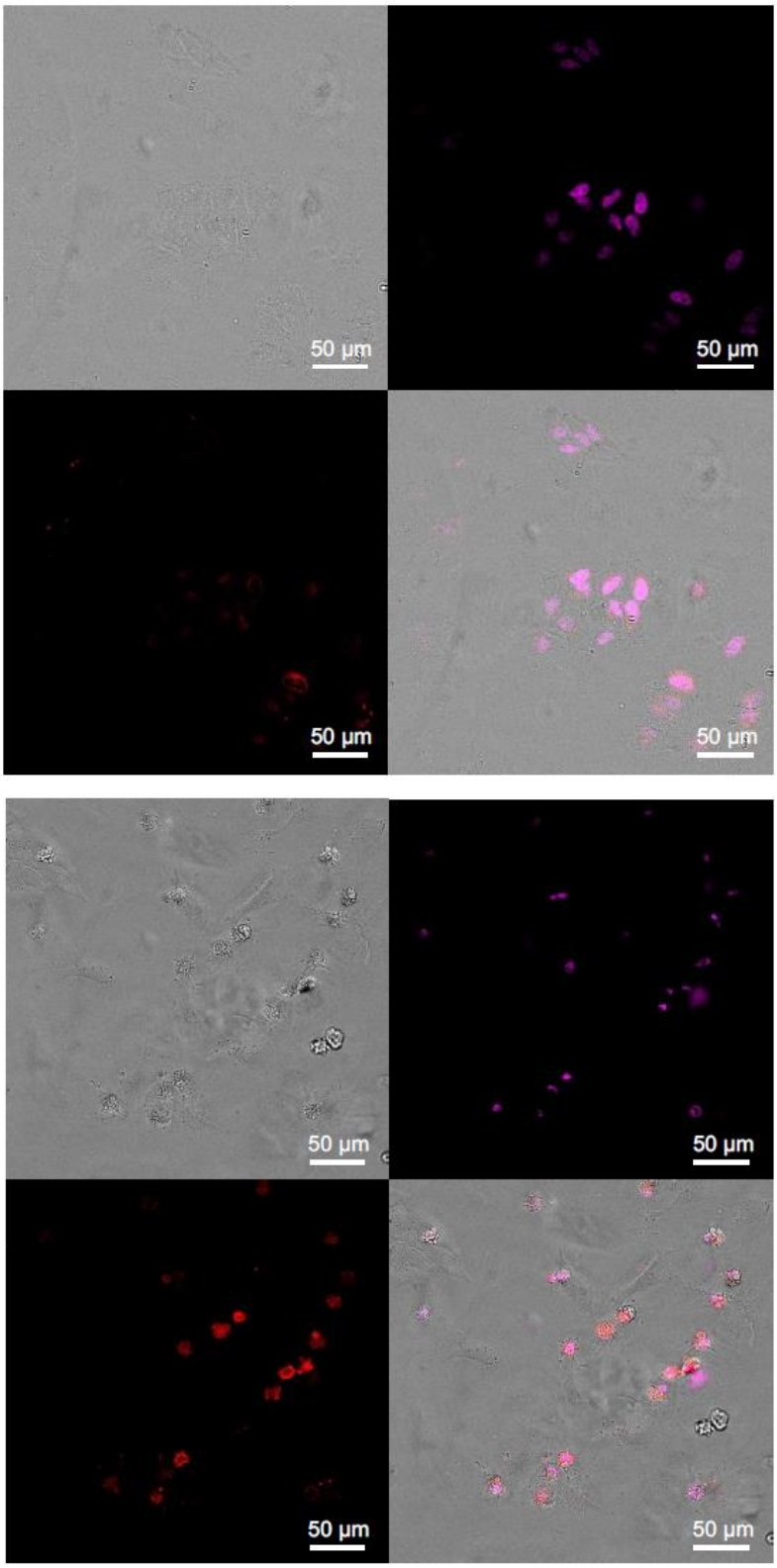

Figure 36 – Top: Confocal microscopy images of HeLa cells treated with the vehicle control (0.1 % DMSO) followed by incubation with 1 µg/mL of Annexin V-Cy5 **93** for 15 min; Bottom: Confocal microscopy images of HeLa cells treated with 1 µM actinomycin D for 6 h to induce apoptosis followed by incubation with 1 µg/mL of Annexin V-Cy5 **93** for 15 min. Annexin V-Cy5 **93** (red), nuclear Hoechst staining (purple).

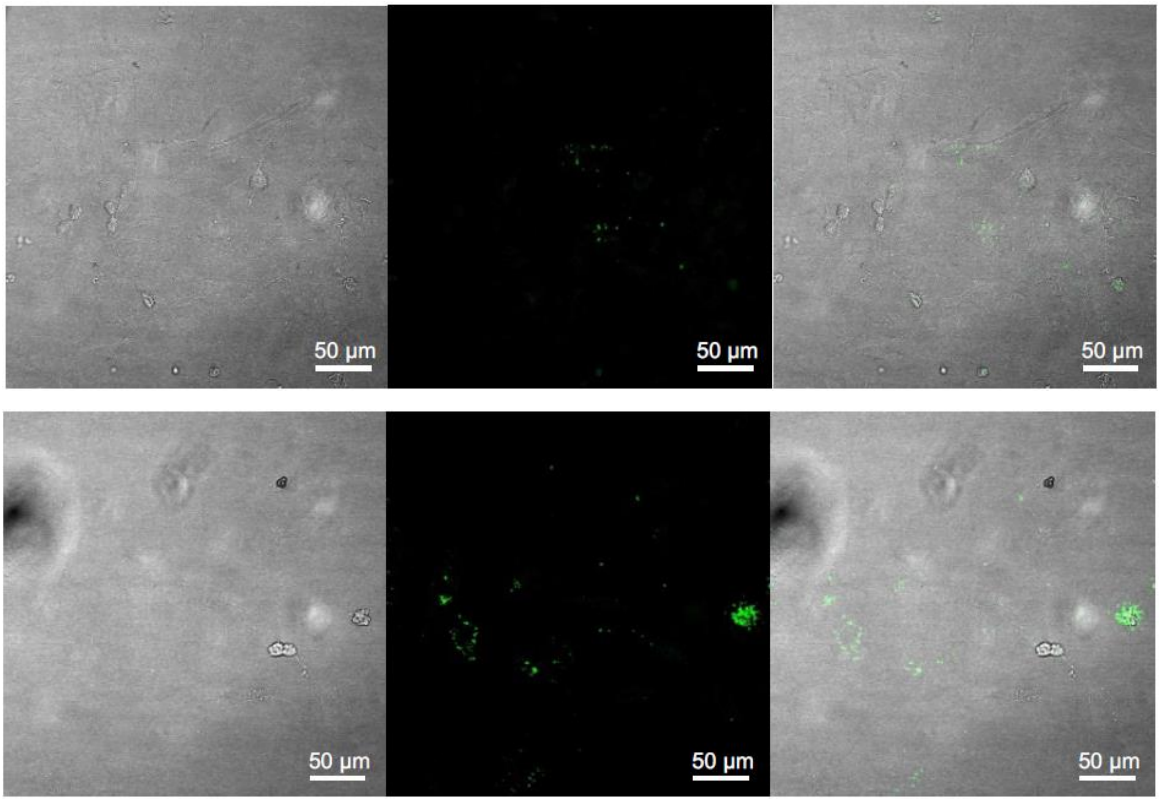

Figure 37 – Top: Confocal microscopy images of HeLa cells treated with the vehicle control (0.1 % DMSO) followed by incubation with 1 µg/mL of Annexin V-FITC **94** for 15 min; Bottom: Confocal microscopy images of HeLa cells treated with 1 µM actinomycin D for 6 h to induce apoptosis followed by incubation with 1 µg/mL of Annexin V-FITC **94** for 15 min. Annexin V-FITC **94** (green).

Bibliographical references

[1] L. Ciani, S. Ristori, *Expert Opin. Drug Discov.* **2012**, *7*, 1017 – 1027.

[2] N. S. Hosmane, *Boron Science: New Technologies and Applications*, Taylor & Francis Group, Boca Raton, **2012**.

[3] D. B. Diaz, A. K. Yudin, *Nat. Chem.* **2017**, *9*, 731 – 742.

[4] W. Yang, X. Gao, B. Wang, *Med. Res. Rev.* **2003**, *23*, 346 – 368.

[5] B. C. Das, P. Thapa, R. Karki, C. Schinke, S. Das, S. Kambhampati, S. K. Banerjee, P. V Veldhuizen, A. Verma, L. M. Weiss, et al., *Future Med. Chem.* **2013**, *5*, 653 – 676.

[6] H. S. Ban, H. Nakamura, *Chem. Rec.* **2015**, *15*, 616 – 635.

[7] S. J. Baker, J. W. Tomsho, S. J. Benkovic, *Chem. Soc. Rev.* **2011**, *40*, 4279 – 4285.

[8] A. R. Martin, J. J. Vasseur, M. Smietana, *Chem. Soc. Rev.* **2013**, *42*, 5684 – 5713.

[9] M. A. Soriano-Ursúa, B. C. Das, J. G. Trujillo-Ferrara, *Expert Opin. Ther. Pat.* **2014**, *24*, 485 – 500.

[10] S. J. Baker, C. Z. Ding, T. Akama, Y.-K. Zhang, V. Hernandez, Y. Xia, *Future Med. Chem.* **2009**, *1*, 1275 – 1288.

[11] E. Frankland, B. F. Duppa, *Justus Liebigs Ann. Chem.* **1860**, *115*, 319 – 322.

[12] D. G. Hall, *Boronic Acids - Preparation and Applications in Organic Synthesis, Medicine and Materials*, Wiley-VCH Verlag & Co. KGaA, Weinheim, **2011**.

[13] P. V. Ramachandran, *Futur. Med. Chem.* **2013**, *5*, 611 – 612.

[14] N. Fujita, S. Shinkai, T. D. James, *Chem. Asian J.* **2008**, *3*, 1076 – 1091.

[15] S. Lascano, K.-D. Zhang, R. Wehlauch, K. Gademann, N. Sakai, S. Matile, *Chem. Sci.* **2016**, *7*, 4720 – 4724.

[16] P. C. Trippier, C. McGuigan, *Med.Chem.Commun* **2010**, *1*, 183 – 198.

[17] R. C. Kane, P. F. Bross, A. T. Farrell, R. Pazdur, *Oncologist* **2003**, *8*, 508 – 513.

[18] J. D. Ashley, J. F. Stefanick, V. A. Schroeder, M. A. Suckow, T. Kiziltepe, B. Bilgicer, *J. Med. Chem.* **2014**, *57*, 5282 – 5292.

[19] E. A. Murphy, B. K. Majeti, R. Mukthavaram, L. M. Acevedo, L. A. Barnes, D. A. Cheresh, *Mol. Cancer Ther.* **2011**, *10*, 972 – 982.

[20] J. Su, F. Chen, V. L. Cryns, P. B. Messersmith, *J. Am. Chem. Soc.* **2011**, *133*, 11850 – 11853.

[21] S. Wu, R. Qi, H. Kuang, Y. Wei, X. Jing, F. Meng, Y. Huang, *Chempluschem* **2013**, *78*, 175 – 184.

[22] G. Pu, C. Ren, D. Li, L. Wang, J. Sun, *RSC Adv.* **2014**, *4*, 50145 – 50147.

[23] S. Shen, X. J. Du, J. Liu, R. Sun, Y. H. Zhu, J. Wang, *J. Control. Release* **2015**, *208*, 14 – 24.

[24] J. Min, H. Moon, H. J. Yang, H. H. Shin, S. Y. Hong, S. Kang, *Macromol. Biosci.* **2014**, *14*, 557 – 564.

[25] N. Sharma, D. Sharma, *J. Pharmacol. Pharmacother.* **2015**, *6*, 236 – 239.

[26] "FDA Approves Ninlaro (Ixazomib) for Multiple Myeloma," can be found under https://www.cancer.org/latest-news/fda-approves-ninlaro-ixazomib-for-multiple-myeloma.html, **2015**.

[27] "Eucrisa (crisaborole) FDA-Approved Patient Labeling," can be found under https://www.pfizermedicalinformation.com/en-us/eucrisa/fda-label, **2016**.

[28] F. Yang, M. Zhu, J. Zhang, H. Zhou, *Medchemcomm* **2018**, *9*, 201 – 211.

[29] S. Thareja, M. Zhu, X. Ji, B. Wang, *Heterocycl. Commun.* **2017**, *23*, 1 – 17.

[30] F. Montalbano, N. R. Candeias, L. F. Veiros, V. André, M. T. Duarte, M. R. Bronze, M. T. Duarte, M. R. Bronze, R. Moreira, P. M. P. Gois, *Org. Lett.* **2012**, *14*, 988 – 991.

[31] K. Lacina, P. Skládal, T. D. James, *Chem. Cent. J.* **2014**, *8*, 1 – 17.

[32] R. Qian, L. Ding, L. Yan, H. Ju, *Anal. Chim. Acta* **2015**, *894*, 85 – 90.

[33] M. L. Stolowitz, C. Ahlem, K. A. Hughes, R. J. Kaiser, E. A. Kesicki, G. Li, K. P. Lund, S. M. Torkelson, J. P. Wiley, A. Se, et al., *Bioconjugate Chem.* **2001**, *12*, 229 – 239.

[34] J. P. Wiley, K. A. Hughes, R. J. Kaiser, E. A. Kesicki, K. P. Lund, M. L. Stolowitz, *Bioconjugate Chem.* **2001**, *12*, 240 – 250.

[35] P. M. S. D. Cal, J. B. Vicente, E. Pires, A. V. Coelho, L. F. Veiros, C. Cordeiro, P. M. P. Gois, *J. Am. Chem. Soc.* **2012**, *134*, 10299 – 10305.

[36] H. Höpfl, M. Sánchez, N. Farfán, V. Barba, *Can. J. Chem.* **1998**, *76*, 1352 – 1360.

[37] V. Barba, D. Cuahutle, R. Santillan, N. Farfán, *Can. J. Chem.* **2001**, *79*, 1229 – 1237.

[38] M. Rodríguez, M. E. Ochoa, R. Santillan, N. Farfán, V. Barba, *J. Organomet. Chem.* 2005, *690*, 2975 – 2988.

[39] M. Rodríguez, M. E. Ochoa, C. Rodríguez, R. Santillan, V. Barba, N. Farfán, *J. Organomet. Chem.* **2007**, *692*, 2425 – 2435.

[40] H. López-Ruiz, I. Mera-Moreno, S. Rojas-Lima, R. Santillán, N. Farfán, *Tetrahedron Lett.* **2008**, *49*, 1674 – 1677.

[41] M. Adib, S. Shabanibalajadeh, E. Sheikhi, M. Rahimi-Nasrabadi, L.-G. Zhu, *Helv. Chim. Acta* **2016**, *99*, 659 – 664.

[42] H. Reyes, B. M. Muñoz, N. Farfán, R. Santillan, S. Rojas-Lima, P. G. Lacroix, K. Nakatani, *J. Mater. Chem.* **2002**, *12*, 2898 – 2903.

[43] H. Reyes, J. M. Rivera, N. Farfán, R. Santillan, P. G. Lacroix, C. Lepetit, K. Nakatani, *J. Organomet. Chem.* **2005**, *690*, 3737 – 3745.

[44] J. F. Lamère, P. G. Lacroix, N. Farfán, J. M. Rivera, R. Santillan, K. Nakatani, *J. Mater. Chem.* **2006**, *16*, 2913 – 2920.

[45] B. M. Muñoz, R. Santillan, M. Rodríguez, J. M. Méndez, M. Romero, N. Farfán, P. G. Lacroix, K. Nakatani, G. Ramos-Ortíz, J. L. Maldonado, *J. Organomet. Chem.* **2008**, *693*, 1321 – 1334.

[46] M. Rodríguez, J. L. Maldonado, G. Ramos-Ortíz, J. F. Lamère, P. G. Lacroix, N. Farfán, M. E. Ochoa, R. Santillan, M. A. Meneses-Nava, O. Barbosa-García, *et al.*, *New J. Chem.* **2009**, *33*, 1693 – 1702.

[47] M. Rodríguez, G. Ramos-Ortíz, M. I. Alcalá-Salas, J. L. Maldonado, K. A. López--Varela, Y. López, O. Domínguez, M. A. Meneses-Nava, O. Barbosa-García, R. Santillan, *et al.*, *Dye. Pigment.* **2010**, *87*, 76 – 83.

[48] M. Ibarra-Rodríguez, B. M. Muñoz-Flores, H. V. R. Dias, M. Sánchez, A. Gomez--Treviño, R. Santillan, N. Farfán, V. M. Jiménez-Pérez, *J. Org. Chem.* **2017**, *82*, 2375 – 2385.

[49] Y. Hattori, M. Ishimura, Y. Ohta, H. Takenaka, T. Watanabe, H. Tanaka, K. Ono, M. Kirihata, *Org. Biomol. Chem.* **2015**, *13*, 6927 – 6930.

[50] Y. Hattori, M. Ishimura, Y. Ohta, H. Takenaka, M. Kirihata, *ACS Sensors* **2016**, *1*, 1394 – 1397.

[51] N. R. Candeias, P. M. S. D. Cal, V. André, M. T. Duarte, L. F. Veiros, P. M. P. Gois, *Tetrahedron* **2010**, *66*, 2736 – 2745.

[52] F. Montalbano, P. M. S. D. Cal, M. A. B. R. Carvalho, L. M. Gonçalves, S. D. Lucas, R. C. Guedes, L. F. Veiros, R. Moreira, P. M. P. Gois, *Org. Biomol. Chem.* **2013**, *11*, 4465 – 4472.

[53] F. Montalbano, J. Leandro, G. D. V. F. Farias, P. R. Lino, R. C. Guedes, J. B. Vicente, P. Leandro, P. M. P. Gois, *RSC Adv.* **2014**, *4*, 61022 – 61027.

[54] H. Faustino, M. J. S. A. Silva, L. F. Veiros, G. J. L. Bernardes, P. M. P. Gois, *Chem. Sci.* **2016**, *7*, 5052 – 5058.

[55] P. M. S. D. Cal, R. F. M. Frade, V. Chudasama, C. Cordeiro, S. Caddick, P. M. P. Gois, *Chem. Commun.* **2014**, *50*, 5261 – 5263.

[56] P. M. S. D. Cal, R. F. M. Frade, C. Cordeiro, P. M. P. Gois, *Chem. Eur. J.* **2015**, *21*, 8182 – 8187.

[57] A. Bandyopadhyay, S. Cambray, J. Gao, *Chem. Sci.* **2016**, *7*, 4589 – 4593.

[58] A. Bandyopadhyay, J. Gao, *J. Am. Chem. Soc.* **2016**, *138*, 2098 – 2101.

[59] K. Li, J. Gao, *Synlett* **2017**, *28*, 1913 – 1916.

[60] A. Bandyopadhyay, K. A. McCarthy, M. A. Kelly, J. Gao, *Nat. Commun.* **2015**, *6*, 1 – 9.

[61] K. Li, C. Weidman, J. Gao, *Org. Lett.* **2018**, *20*, 20 – 23.

[62] L. Roppiyakuda, E. Kosmowska, M. A. Faust, K. P. Tran, F. Chow, E. Buglo, M. P. Groziak, E. A. Sarina, M. M. Olmstead, I. Silva, et al., *Chem. Biodivers.* **2014**, *11*, 1381 – 1397.

[63] C. A. Jordan, B. A. Sandoval, M. V. Serobyan, D. H. Gilling, M. P. Groziak, H. H. Xu, J. L. Vey, *Acta Crystallogr. Sect. Struct. Biol. Commun.* **2015**, *71*, 1521 – 1530.

[64] M. S. Ward, I. Silva, W. Martinez, J. Jefferson, S. Rahman, J. M. Garcia, D. Kanichar, L. Roppiyakuda, E. Kosmowska, M. A. Faust, *et al.*, *Bioorganic Med. Chem.* **2016**, *24*, 3267 – 3275.

[65] J. Yang, B. J. Johnson, A. A. Letourneau, C. M. Vogels, A. Decken, F. J. Baerlocher, S. A. Westcott, *Aust. J. Chem.* **2015**, *68*, 366 – 372.

[66] M. Loibl, I. Klein, M. Prattes, C. Schmidt, L. Kappel, G. Zisser, A. Gungl, E. Krieger, B. Pertschy, H. Bergler, *J. Biol. Chem.* **2014**, *289*, 3913 – 3922.

[67] D. Gillingham, *Org. Biomol. Chem.* **2016**, *14*, 7606 – 7609.

[68] C. J. Stress, P. J. Schmidt, D. G. Gillingham, *Org. Biomol. Chem.* **2016**, *14*, 5529 – 5533.

[69] H. C. Nourie, E. Buglo, M. P. Groziak, E. A. Sarina, M. M. Olmstead, *J. Heterocycl. Chem.* **2017**, *54*, 749 – 752.

[70] O. Dilek, Z. Lei, S. Bane, *Chem. Commun.* **2015**, *51*, 16992 – 16995.

[71] H. Gu, T. I. Chio, Z. Lei, R. J. Staples, J. S. Hirschi, S. Bane, *Org. Biomol. Chem.* **2017**, *15*, 7543 – 7548.

[72] A. Bandyopadhyay, S. Cambray, J. Gao, *J. Am. Chem. Soc.* **2017**, *139*, 871 – 878.

[73] S. Cambray, A. Bandyopadhyay, J. Gao, *Chem. Commun.* **2017**, *53*, 12532 – 12535.

[74] R. Chan-Navarro, V. M. Jiménez-Pérez, B. M. Muñoz-Flores, H. V. R. Dias, I. Moggio, E. Arias, G. Ramos-Ortíz, R. Santillan, C. García, M. E. Ochoa, *et al*., *Dye. Pigment.* **2013**, *99*, 1036 – 1043.

[75] A. Kotali, F. Dimoulaki, E. Kotali, A. Maniadaki, P. A. Harris, E. Rózycka--Sokołowska, P. Bałczewski, J. A. Joule, *Tetrahedron* **2015**, *71*, 7245 – 7249.

[76] A. Kotali, A. Maniadaki, E. Kotali, P. A. Harris, E. Rózycka-Sokołowska, P. Bałczewski, J. A. Joule, *Synthesis* **2016**, *48*, 4117 – 4125.

[77] A. Kotali, A. Maniadaki, E. Kotali, P. A. Harris, E. Różycka-Sokołowska, P. Bałczewski, J. A. Joule, *Tetrahedron Lett.* **2017**, *58*, 512 – 515.

[78] T. Flagstad, M. T. Petersen, T. E. Nielsen, *Angew. Chem. Int. Ed.* **2015**, *54*, 8395 – 8397.

[79] "World Health Organization," can be found under http://www.who.int/cancer/en/, **2018**.

[80] D. Hanahan, R. A. Weinberg, *Cell* **2011**, *144*, 646 – 674.

[81] E. A. Rossi, D. M. Goldenberg, C. H. Chang, *Bioconjugate Chem.* **2012**, *23*, 309 – 323.

[82] C. H. Kim, J. Y. Axup, A. Dubrovska, S. A. Kazane, B. A. Hutchins, E. D. Wold, V. V. Smider, P. G. Schultz, *J. Am. Chem. Soc.* **2012**, *134*, 9918 – 9921.

[83] H. Y. Liu, P. Zrazhevskiy, X. Gao, *Bioconjugate Chem.* **2014**, *25*, 1511 – 1516.

[84] P. J. McEnaney, K. J. Fitzgerald, A. X. Zhang, E. F. Douglass, W. Shan, A. Balog, M. D. Kolesnikova, D. A. Spiegel, *J. Am. Chem. Soc.* **2014**, *136*, 18034 – 18043.

[85] L. N. Anderson, P. K. Koech, A. E. Plymale, E. V. Landorf, A. Konopka, F. R. Collart, M. S. Lipton, M. F. Romine, A. T. Wright, *ACS Chem. Biol.* **2016**, *11*, 345 – 354.

[86] A. Kumar, T. Mastren, B. Wang, J. T. Hsieh, G. Hao, X. Sun, *Bioconjugate Chem.* **2016**, *27*, 1681 – 1689.

[87] J. G. Vineberg, T. Wang, E. S. Zuniga, I. Ojima, *J. Med. Chem.* **2015**, *58*, 2406 – 2416.

[88] G. Casi, D. Neri, *J. Med. Chem.* **2015**, *58*, 8751 – 8761.

[89] S. Cazzamalli, A. Dal Corso, F. Widmayer, D. Neri, *J. Am. Chem. Soc.* **2018**, *140*, 1617 – 1621.

[90] P. Akkapeddi, S.-A. Azizi, A. M. Freedy, P. M. S. D. Cal, P. M. P. Gois, G. J. L. Bernardes, *Chem. Sci.* **2016**, *7*, 2954 – 2963.

[91] K. Tsuchikama, Z. An, *Protein Cell* **2018**, *9*, 33 – 46.

[92] S. Puthenveetil, S. Musto, F. Loganzo, L. N. Tumey, C. J. O'Donnell, E. Graziani, *Bioconjugate Chem.* **2016**, *27*, 1030 – 1039.

[93] M. R. Levengood, X. Zhang, J. H. Hunter, K. K. Emmerton, J. B. Miyamoto, T. S. Lewis, P. D. Senter, *Angew. Chem. Int. Ed.* **2017**, *56*, 733 – 737.

[94] N. Ballatori, S. M. Krance, S. Notenboom, S. Shi, K. Tieu, C. L. Hammond, *Biol. Chem.* **2009**, *390*, 191 – 214.

[95] M. Srinivasarao, C. V. Galliford, P. S. Low, *Nat. Rev. Drug Discov.* **2015**, *14*, 203 – 219.

[96] I. Vergote, C. P. Leamon, *Ther. Adv. Med. Oncol.* **2015**, *7*, 206 – 218.

[97] M. Fernandez, F. Javaid, V. Chudasama, *Chem. Sci.* **2017**, 790 – 810.

[98] A. F. Trindade, R. F. M. Frade, E. M. S. Maçôas, C. Graça, C. A. B. Rodrigues, J. M. G. Martinho, C. A. M. Afonso, *Org. Biomol. Chem.* **2014**, *12*, 3181 – 3190.

[99] R. V. J. Chari, M. L. Miller, W. C. Widdison, *Angew. Chem. Int. Ed.* **2014**, *53*, 3796 – 3827.

[100] C. Rader, *Nature* **2015**, *518*, 38 – 39.

[101] E. D. Wold, J. Y. Axup, B. H. Felding, V. V. Smider, *Bioconjugate Chem.* **2015**, *26*, 2311 – 2314.

[102] H. Khalili, A. Godwin, J. W. Choi, R. Lever, P. T. Khaw, S. Brocchini, *Bioconjugate Chem.* **2013**, *24*, 1870 – 1882.

[103] A. R. Lippert, G. C. Van De Bittner, C. J. Chang, *Acc. Chem. Res.* **2011**, *44*, 793 – 804.

[104] E.-J. Kim, S. Bhuniya, H. Lee, H. M. Kim, C. Cheong, S. Maiti, K. S. Hong, J. Seung, J. S. Kim, *J. Am. Chem. Soc.* **2014**, *136*, 13888 – 13894.

[105] R. G. Parr, W. Yang, *Density-Functional Theory of Atoms and Molecules*, Oxford University Press, New York, **1989**.

[106] A. P. de Silva, H. Q. N. Gunaratne, T. Gunnlaugsson, A. J. M. Huxley, C. P. McCoy, J. T. Rademacher, T. E. Rice, *Chem. Rev.* **1997**, *97*, 1515 – 1566.

[107] R. N. Dsouza, U. Pischel, W. M. Nau, *Chem. Rev.* **2011**, *111*, 7941 – 7980.

[108] L. D. Lavis, R. T. Raines, *ACS Chem. Biol.* **2014**, *9*, 855 – 866.

[109] X. Li, X. Gao, W. Shi, H. Ma, *Chem. Rev.* **2014**, *114*, 590 – 659.

[110] J. Yin, Y. Hu, J. Yoon, *Chem. Soc. Rev.* **2015**, *44*, 4619 – 4644.

[111] M. Beija, C. A. M. Afonso, J. M. G. Martinho, *Chem. Soc. Rev.* **2009**, *38*, 2410 – 2433.

[112] J. B. Grimm, B. P. English, J. Chen, J. P. Slaughter, Z. Zhang, A. Revyakin, R. Patel, J. J. Macklin, D. Normanno, R. H. Singer, et al., *Nat. Methods* **2015**, *12*, 244 – 250.

[113] Y. Kushida, T. Nagano, K. Hanaoka, *Analyst* **2015**, *140*, 685 – 695.

[114] K. Kiyose, H. Kojima, T. Nagano, *Chem. Asian J.* **2008**, *3*, 506 – 515.

[115] E. M. S. Stennett, M. A. Ciuba, M. Levitus, *Chem. Soc. Rev.* **2014**, *43*, 1057 – 1075.

[116] A. Coskun, E. U. Akkaya, *J. Am. Chem. Soc.* **2006**, *128*, 14474 – 14475.

[117] A. Loudet, K. Burgess, *Chem. Rev.* **2007**, *107*, 4891 – 4932.

[118] G. Ulrich, R. Ziessel, A. Harriman, *Angew. Chem. Int. Ed.* **2008**, *47*, 1184 – 1201.

[119] S. Ozlem, E. U. Akkaya, *J. Am. Chem. Soc.* **2009**, *131*, 48 – 49.

[120] S. Kolemen, M. Işlk, G. M. Kim, D. Kim, H. Geng, M. Buyuktemiz, T. Karatas, X. F. Zhang, Y. Dede, J. Yoon, et al., *Angew. Chem. Int. Ed.* **2015**, *54*, 5340 – 5344.

[121] D. Frath, J. Massue, G. Ulrich, R. Ziessel, *Angew. Chem. Int. Ed.* **2014**, *53*, 2290 – 2310.

[122] Y. L. Rao, S. Wang, *Inorg. Chem.* **2011**, *50*, 12263 – 12274.

[123] Y. Kubo, A. Kobayashi, T. Ishida, Y. Misawa, T. D. James, *Chem. Commun.* **2005**, 2846 – 2848.

[124] T. E. Barder, S. L. Buchwald, *Org. Lett.* **2007**, *9*, 137 – 139.

[125] J. W. Tomsho, S. J. Benkovic, *J. Org. Chem.* **2012**, *77*, 2098 – 2106.

[126] M. R. Aronoff, B. Vanveller, R. T. Raines, *Org. Lett.* **2013**, *15*, 5382 – 5385.

[127] V. E. González, F. Medrano, M. Rodríguez, P. G. Lacroix, V. Barba, *Tetrahedron Lett.* **2014**, *55*, 6088 – 6092.

[128] V. E. González, P. Lacroix, V. Barba, *Inorganica Chim. Acta* **2015**, *438*, 23 – 30.

[129] V. F. Pais, H. S. El-Sheshtawy, R. Fernández, J. M. Lassaletta, A. Ros, U. Pischel, *Chem. Eur. J.* **2013**, *19*, 6650 – 6661.

[130] J. Fan, M. Hu, P. Zhan, X. Peng, *Chem. Soc. Rev.* **2013**, *42*, 29 – 43.

[131] M. E. Casida, *Recent Advances in Density Functional Methods*, World Scientific, Singapore, **1995**.

[132] A. R. Thiam, R. V. Farese, T. C. Walther, *Nat. Rev. Mol. Cell Biol.* **2013**, *14*, 775 – 786.

[133] P. Greenspan, S. D. Fowler, *J. Lipid Res.* **1985**, *26*, 781 – 789.

[134] D. L. Sackett, J. Wolff, *Anal. Biochem.* **1987**, *167*, 228 – 234.

[135] V. F. Pais, M. M. Alcaide, R. López-Rodríguez, D. Collado, F. Nájera, E. Pérez-Inestrosa, E. Álvarez, J. M. Lassaletta, R. Fernández, A. Ros, *et al.*, *Chem. Eur. J.* **2015**, *21*, 15369 – 15376.

[136] A. D. Laurent, B. Le, G. Denis, *Theor. Chem. Acc.* **2016**, *135*, 1 – 8.

[137] S. Fery-Forgues, J. P. Fayet, A. Lopez, *J. Photochem. Photobiol. A Chem.* **1993**, *70*, 229 – 243.

[138] P. Subedi, The Two-Photon Excitation Fluorescence (TPEF) Enhancement of Dipolar Organic Chromophores in Y Zeolites, Dalhousie University, **2016**.

[139] W. Denk, J. Strickler, W. Webb, *Science.* **1990**, *248*, 73 – 76.

[140] A. S. Klymchenko, *Acc. Chem. Res.* **2017**, *50*, 366 – 375.

[141] D. H. McDaniel, H. C. Brown, *J. Org. Chem.* **1958**, *23*, 420 – 427.

[142] E. Z. Lippert, *Naturforsch., A Phys. Sci.* **1955**, *10*, 541 – 545.

[143] N. Mataga, Y. Kaifu, M. Koizumi, *Bull. Chem. Soc. Jpn.* **1955**, *28*, 690 – 691.

[144] N. Mataga, Y. Kaifu, M. Koizumi, *Bull. Chem. Soc. Jpn.* **1956**, *29*, 465 – 470.

[145] P. Didier, G. Ulrich, Y. Mély, R. Ziessel, *Org. Biomol. Chem.* **2009**, *7*, 3639 – 3642.

[146] M. Pawlicki, H. A. Collins, R. G. Denning, H. L. Anderson, *Angew. Chem. Int. Ed.* **2009**, *48*, 3244 – 3266.

[147] X. Zhang, Y. Xiao, J. Qi, J. Qu, B. Kim, X. Yue, K. D. Belfield, *J. Org. Chem.* **2013**, *78*, 9153 – 9160.

[148] D. Kim, H. G. Ryu, K. H. Ahn, *Org. Biomol. Chem.* **2014**, *12*, 4550 – 4566.

[149] C.-W. Wan, A. Burghart, J. Chen, F. Bergström, L. B.-Å. Johansson, M. F. Wolford, T. G. Kim, M. R. Topp, R. M. Hochstrasser, K. Burgess, *Chem. Eur. J.* **2003**, *9*, 4430 – 4441.

[150] R. Ziessel, C. Goze, G. Ulrich, M. Césario, P. Retailleau, A. Harriman, J. P. Rostron, *Chem. Eur. J.* **2005**, *11*, 7366 – 7378.

[151] A. Harriman, G. Izzet, R. Ziessel, *J. Am. Chem. Soc.* **2006**, *128*, 10868 – 10875.

[152] O. A. Bozdemir, Y. Cakmak, F. Sozmen, T. Ozdemir, A. Siemiarczuk, E. U. Akkaya, *Chem. Eur. J.* **2010**, *16*, 6346 – 6351.

[153] X. Qu, Q. Liu, X. Ji, H. Chen, Z. Zhou, Z. Shen, *Chem. Commun.* **2012**, *48*, 4600 – 4602.

[154] G.-S. Jiao, L. H. Thoresen, T. G. Kim, W. C. Haaland, F. Gao, M. R. Topp, R. M. Hochstrasser, M. L. Metzker, K. Burgess, *Chem. Eur. J.* **2006**, *12*, 7816 – 7826.

[155] J. Han, A. Loudet, R. Barhoumi, R. C. Burghardt, K. Burgess, *J. Am. Chem. Soc.* **2009**, *131*, 1642 – 1643.

[156] L. Wu, A. Loudet, R. Barhoumi, R. C. Burghardt, K. Burgess, *J. Am. Chem. Soc.* **2009**, *131*, 9156 – 9157.

[157] D. Collado, P. Remón, Y. Vida, F. Najera, P. Sen, U. Pischel, E. Perez-Inestrosa, *Chem. Asian J.* **2014**, *9*, 797 – 804.

[158] Y. Xiao, D. Zhang, X. Qian, A. Costela, I. Garcia-Moreno, V. Martin, M. E. Perez--Ojeda, J. Bañuelos, L. Gartzia, I. L. Arbeloa, *Chem. Commun.* **2011**, *47*, 11513 – 11515.

[159] I. Esnal, G. Duran-Sampedro, A. R. Agarrabeitia, J. Bañuelos, I. García-Moreno, M. A. Macías, E. Peña-Cabrera, I. López-Arbeloa, S. de la Moya, M. J. Ortiz, *Phys. Chem. Chem. Phys.* **2015**, *17*, 8239 – 8247.

[160] X. Zhang, Y. Xiao, L. He, Y. Zhang, *J. Org. Chem.* **2014**, *79*, 6315 – 6320.

[161] S. Erbas-Cakmak, E. U. Akkaya, *Angew. Chem. Int. Ed.* **2013**, *52*, 11364 – 11368.

[162] S. Erbas-Cakmak, O. A. Bozdemir, Y. Cakmak, E. U. Akkaya, *Chem. Sci.* **2013**, *4*, 858 – 862.

[163] D. L. Dexter, *J. Chem. Phys.* **1953**, *21*, 836 – 850.

[164] S. Speiser, *Chem. Rev.* **1996**, *96*, 1953 – 1976.

[165] R. Ziessel, A. Harriman, *Chem. Commun.* **2011**, *47*, 611 – 631.

[166] T. Förster, *Ann. Phys.* **1948**, *437*, 55 – 75.

[167] Y. Zhao, Y. Zhang, X. Lv, Y. Liu, M. Chen, P. Wang, J. Liu, W. Guo, *J. Mater. Chem.* **2011**, *21*, 13168 – 13171.

[168] W. Lin, L. Yuan, Z. Cao, Y. Feng, J. Song, *Angew. Chem. Int. Ed.* **2010**, *49*, 375 – 379.

[169] R. Goel, V. Luxami, K. Paul, *RSC Adv.* **2016**, *6*, 37664 – 37671.

[170] J. Zielonka, A. Sikora, J. Joseph, B. Kalyanaraman, *J. Biol. Chem.* **2010**, *285*, 14210 – 14216.

[171] W. Fei, H. Yang, *Methods Cell Biol* **2012**, *108*, 303 – 316.

[172] D. M. Owen, C. Rentero, A. Magenau, A. Abu-Siniyeh, K. Gaus, *Nat. Protoc.* **2012**, *7*, 24 – 35.

[173] R. Duncan, R. Gaspar, *Mol. Pharm.* **2011**, *8*, 2101 – 2141.

[174] C. J. Cheng, G. T. Tietjen, J. K. Saucier-Sawyer, W. M. Saltzman, *Nat. Rev. Drug Discov.* **2015**, *14*, 239 – 247.

[175] L. Treuel, X. Jiang, G. U. Nienhaus, *J. R. Soc. Interface* **2013**, *10*, 20120939.

[176] I. M. Adjei, B. Sharma, V. Labhasetwar, *Nanoparticles: Cellular Uptake and Cytotoxicity*, Springer, Dordrecht, **2014**.

[177] C. Peetla, S. Vijayaraghavalu, V. Labhasetwar, *Adv. Drug Deliv. Rev.* **2013**, *65*, 1686 – 1698.

[178] S. Tenzer, D. Docter, J. Kuharev, A. Musyanovych, V. Fetz, R. Hecht, F. Schlenk, D. Fischer, K. Kiouptsi, C. Reinhardt, et al., *Nat. Nanotechnol.* **2013**, *8*, 772 – 781.

[179] A. Hafner, J. Lovrić, G. P. Lakoš, I. Pepić, *Int. J. Nanomedicine* **2014**, *9*, 1005 – 1023.

[180] F. Danhier, E. Ansorena, J. M. Silva, R. Coco, A. Le Breton, V. Préat, *J. Control. Release* **2012**, *161*, 505 – 522.

[181] J. M. Silva, M. Videira, R. Gaspar, V. Préat, H. F. Florindo, *J. Control. Release* **2013**, *168*, 179 – 199.

[182] K. Palucka, J. Banchereau, *Nat. Rev. Cancer* **2012**, *12*, 265 – 277.

[183] J. Jose, A. Loudet, Y. Ueno, L. Wu, H.-Y. Chen, D. H. Son, R. Barhoumi, R. Burghardt, K. Burgess, *Org. Biomol. Chem.* **2011**, *9*, 3871 – 3877.

[184] H. F. Florindo, S. Pandit, L. M. D. Gonçalves, M. Videira, O. Alpar, A. J. Almeida, *Biomaterials* **2009**, *30*, 5161 – 5169.

[185] E. A. Schellenberger, A. Bogdanov, A. Petrovsky, V. Ntziachristos, R. Weissleder, L. Josephson, *Neoplasia* **2003**, *5*, 187 – 192.

[186] J. F. Tait, D. F. Gibson, C. Smith, *Anal. Biochem.* **2004**, *329*, 112 – 119.

[187] S. E. Logue, M. Elgendy, S. J. Martin, *Nat. Protoc.* **2009**, *4*, 1383 – 1395.

[188] X. Li, J. M. Link, S. Stekhova, K. J. Yagle, C. Smith, K. A. Krohn, J. F. Tait, *Bioconjugate Chem.* **2008**, *19*, 1684 – 1688.

[189] A. Perreault, J. C. Knight, M. Wang, J. Way, F. Wuest, *Amino Acids* **2016**, *48*, 65 – 74.

[190] P. Yu, I. Strug, T. R. Cafarella, B. A. Seaton, A. Krantz, *Org. Biomol. Chem.* **2012**, *10*, 4500 – 4504.

[191] B. P. Joshi, T. D. Wang, *Cancers (Basel)* **2010**, *2*, 1251 – 1287.

[192] Z. Medarova, S. Bonner-Weir, M. Lipes, A. Moore, *Diabetes* **2005**, *54*, 1780 – 1788.

[193] V. Ntziachristos, E. A. Schellenberger, J. Ripoll, D. Yessayan, E. Graves, A. Bogdanov, L. Josephson, R. Weissleder, *PNAS* **2004**, *101*, 12294 – 12299.

[194] M. Adib, E. Sheikhi, H. R. Bijanzadeh, L.-G. Zhu, *Tetrahedron* **2012**, *68*, 3377 – 3383.

[195] M. G. Gichinga, S. Striegler, *Tetrahedron* **2009**, *65*, 4917 – 4922.

[196] J. M. McFarland, M. B. Francis, *J. Am. Chem. Soc.* **2005**, *127*, 13490 – 13491.

[197] H. S. Jung, M. Park, J. H. Han, J. H. Lee, C. Kang, J. H. Jung, J. S. Kim, *Chem. Commun.* **2012**, *48*, 5082 – 5084.

[198] N. Song, M. Ding, Z. Pan, J. Li, L. Zhou, H. Tan, Q. Fu, *Biomacromolecules* **2013**, *14*, 4407 – 4419.

[199] M. Gonçalves, K. Estieu-Gionnet, T. Berthelot, G. Laïn, M. Bayle, X. Canron, N. Betz, A. Bikfalvi, G. Déléris, *Pharm. Res.* **2005**, *22*, 1411 – 1421.

[200] J. Davila, A. Chassepot, J. Longo, F. Boulmedais, A. Reisch, B. Frisch, F. Meyer, J.-C. Voegel, P. J. Mésini, B. Senger, *et al.*, *J. Am. Chem. Soc.* **2012**, *134*, 83 – 86.

[201] C. Quin, L. Robertson, S. J. McQuaker, N. C. Price, M. D. Brand, R. C. Hartley, *Tetrahedron* **2010**, *66*, 2384 – 2389.

[202] M. Nave, R. E. Castro, C. M. Rodrigues, A. Casini, G. Soveral, M. M. Gaspar, *Nanomedicine* **2016**, *11*, 1817 – 1830.

[203] Gaussian 09, Revision D.01, M. J. Frisch, G. W. Trucks, H. B. Schlegel, G. E. Scuseria, M. A. Robb, J. R. Cheeseman, G. Scalmani, V. Barone, G. A. Petersson, H. Nakatsuji, X. Li, M. Caricato, A. Marenich, J. Bloino, B. G. Janesko, R. Gomperts, B. Mennucci, H. P. Hratchian, J. V. Ortiz, A. F. Izmaylov, J. L. Sonnenberg, D. Williams-Young, F. Ding, F. Lipparini, F. Egidi, J. Goings, B. Peng, A. Petrone, T. Henderson, D. Ranasinghe, V. G. Zakrzewski, J. Gao, N. Rega, G. Zheng, W. Liang, M. Hada, M. Ehara, K. Toyota, R. Fukuda, J. Hasegawa, M. Ishida, T. Nakajima, Y. Honda, O. Kitao, H. Nakai, T. Vreven, K. Throssell, J. A. Montgomery, Jr., J. E. Peralta, F. Ogliaro, M. Bearpark, J. J. Heyd, E. Brothers, K. N. Kudin, V. N. Staroverov, T. Keith, R. Kobayashi, J. Normand, K. Raghavachari, A. Rendell, J. C. Burant, S. S. Iyengar, J. Tomasi, M. Cossi, J. M. Millam, M. Klene, C. Adamo, R. Cammi, J. W. Ochterski, R. L. Martin, K. Morokuma, O. Farkas, J. B. Foresman, and D. J. Fox, Gaussian, Inc., Wallingford CT, **2013**.

[204] Y. Zhao, D. G. Truhlar, *Theor. Chem. Acc.* **2008**, *120*, 215 – 241.

[205] Y. Zhao, D. G. Truhlar, *Acc. Chem. Res.* **2008**, *41*, 157 – 167.

[206] Y. Zhao, D. G. Truhlar, *Chem. Phys. Lett.* **2011**, *502*, 1 – 13.

[207] R. Ditchfield, W. J. Hehre, J. A. Pople, *J. Chem. Phys.* **1971**, *54*, 724 – 728.

[208] W. J. Hehre, R. Ditchfield, J. A. Pople, *J. Chem. Phys.* **1972**, *56*, 2257 – 2261.

[209] P. C. Hariharan, J. A. Pople, *Mol. Phys.* **1974**, *27*, 209 – 214.

[210] M. S. Gordon, *Chem. Phys. Lett.* **1980**, *76*, 163 – 168.

[211] P. C. Hariharan, J. A. Pople, *Theor. Chim. Acta* **1973**, *28*, 213 – 222.

[212] A. D. McLean, G. S. Chandler, *J. Chem. Phys.* **1980**, *72*, 5639 – 5648.

[213] R. Krishnan, J. S. Binkley, R. Seeger, J. A. Pople, *J. Chem. Phys.* **1980**, *72*, 650 – 654.

[214] A. J. H. Wachters, *J. Chem. Phys.* **1970**, *52*, 1033 – 1036.

[215] K. Raghavachari, G. W. Trucks, *J. Chem. Phys.* **1989**, *91*, 1062 – 1065.

[216] P. J. Hay, *J. Chem. Phys.* **1977**, *66*, 4377 – 4384.

[217] R. C. Binning, L. A. Curtiss, *J. Comput. Chem.* **1990**, *11*, 1206 – 1216.

[218] M. P. McGrath, L. Radom, *J. Chem. Phys.* **1991**, *94*, 511 – 516.

[219] T. Clark, J. Chandrasekhar, G. W. Spitznagel, P. V. R. Schleyer, *J. Comput. Chem.* **1983**, *4*, 294 – 301.

[220] M. J. Frisch, J. A. Pople, J. S. Binkley, *J. Chem. Phys.* **1984**, *80*, 3265 – 3269.

[221] E. Cancès, B. Mennucci, J. Tomasi, *J. Chem. Phys.* **1997**, *107*, 3032 – 3041.

[222] M. Cossi, V. Barone, B. Mennucci, J. Tomasi, *Chem. Phys. Lett.* **1998**, *286*, 253 – 260.

[223] B. Mennucci, J. Tomasi, *J. Chem. Phys.* **1997**, *106*, 5151 – 5158.

[224] J. Tomasi, B. Mennucci, R. Cammi, *Chem. Rev.* **2005**, *105*, 2999 – 3094.

[225] A. V. Marenich, C. J. Cramer, D. G. Truhlar, *J. Phys. Chem. B* **2009**, *113*, 6378 – 6396.

[226] J.-Q. Weng, Q.-M. Deng, L. Wu, K. Xu, H. Wu, R.-R. Liu, J.-R. Gao, Y.-X. Jia, *Org. Lett.* **2014**, *16*, 776 – 779.

[227] S. Chiba, L. Zhang, J.-Y. Lee, *J. Am. Chem. Soc.* **2010**, *132*, 7266 – 7267.

[228] J. Zhai, T. Pan, J. Zhu, Y. Xu, J. Chen, Y. Xie, Y. Qin, *Anal. Chem.* **2012**, *84*, 10214 – 10220.

[229] L. Du, M. Li, S. Zheng, B. Wang, *Tetrahedron Lett.* **2008**, *49*, 3045 – 3048.

[230] M. P. Jain, S. Kumar, *Talanta* **1979**, *26*, 909 – 910.

[231] M. Prabhakar, *J. Prakt. Chem.* **1918**, *96*, 273 – 280.

[232] V. H. Neunhoefer, *Liebigs Ann. Chem* **1969**, *722*, 38 – 44.

[233] J. B. Bertoldo, G. Razzera, J. Vernal, F. C. A. Brod, A. C. M. Arisi, H. Terenzi, *Biochim. Biophys. Acta, Proteins Proteomics* **2011**, *1814*, 1120 – 1126.

[234] W. H. Melhuish, *J. Phys. Chem.* **1960**, *64*, 762 – 764.

[235] W. H. Melhuish, *J. Phys. Chem.* **1961**, *65*, 229 – 235.

[236] B. R. Cho, K. H. Son, S. H. Lee, Y.-S. Song, Y.-K. Lee, S.-J. Jeon, J. H. Choi, H. Lee, M. Cho, *J. Am. Chem. Soc.* **2001**, *123*, 10039 – 10045.

[237] M. Rumi, J. W. Perry, *Adv. Opt. Photonics* **2010**, *2*, 451 – 518.

[238] C. Xu, W. W. Webb, *J. Opt. Soc. Am. B Opt. Phys.* **1996**, *13*, 481 – 491.

[239] P.-Y. Gu, C.-J. Lu, Z.-J. Hu, N.-J. Li, T. Zhao, Q.-F. Xu, Q.-H. Xu, J.-D. Zhang, J.-M. Lu, *J. Mater. Chem. C* **2013**, *1*, 2599 – 2606.

[240] D. Jacquemin, E. A. Perpète, I. Ciofini, C. Adamo, *Acc. Chem. Res.* **2009**, *42*, 326 – 334.

[241] L. González, D. Escudero, L. Serrano-Andrés, *ChemPhysChem* **2012**, *13*, 28 – 51.

[242] C. Adamo, D. Jacquemin, *Chem. Soc. Rev.* **2013**, *42*, 845 – 856.

[243] T. Yanai, D. P. Tew, N. C. Handy, *Chem. Phys. Lett.* **2004**, *393*, 51 – 57.

Appendix

- **B-complex 27a**

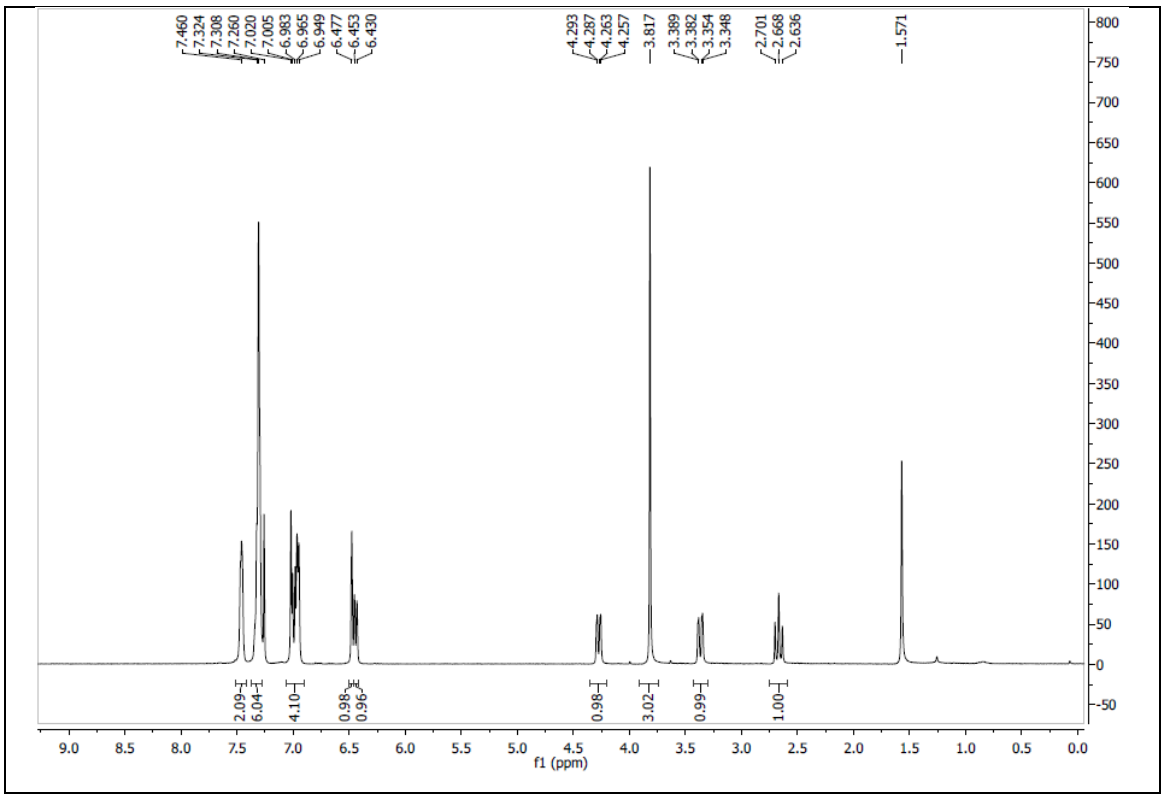

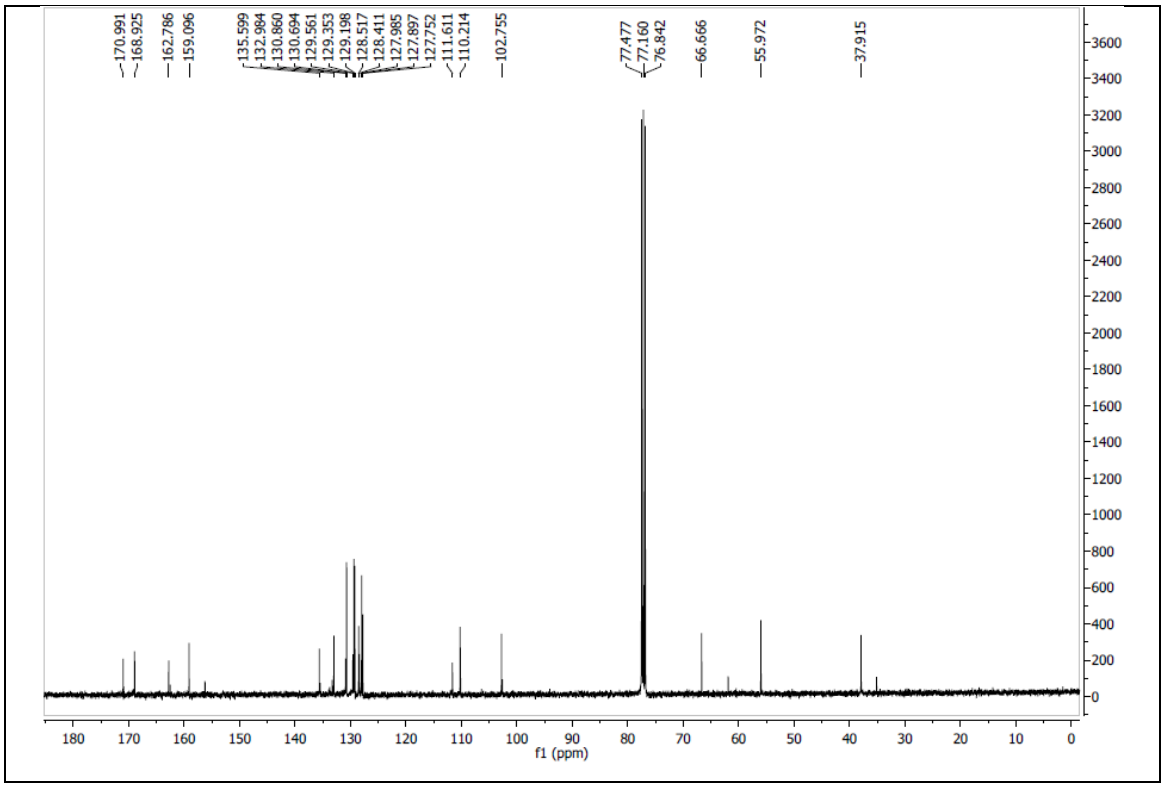

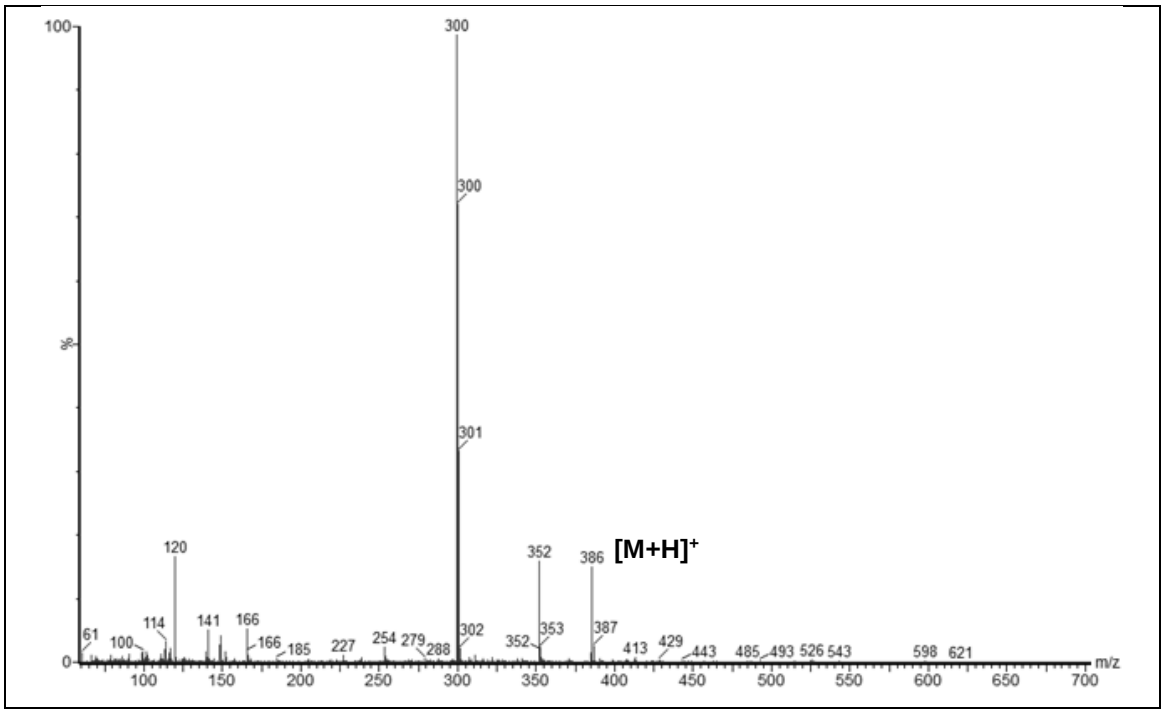

- **B-complex 27b**

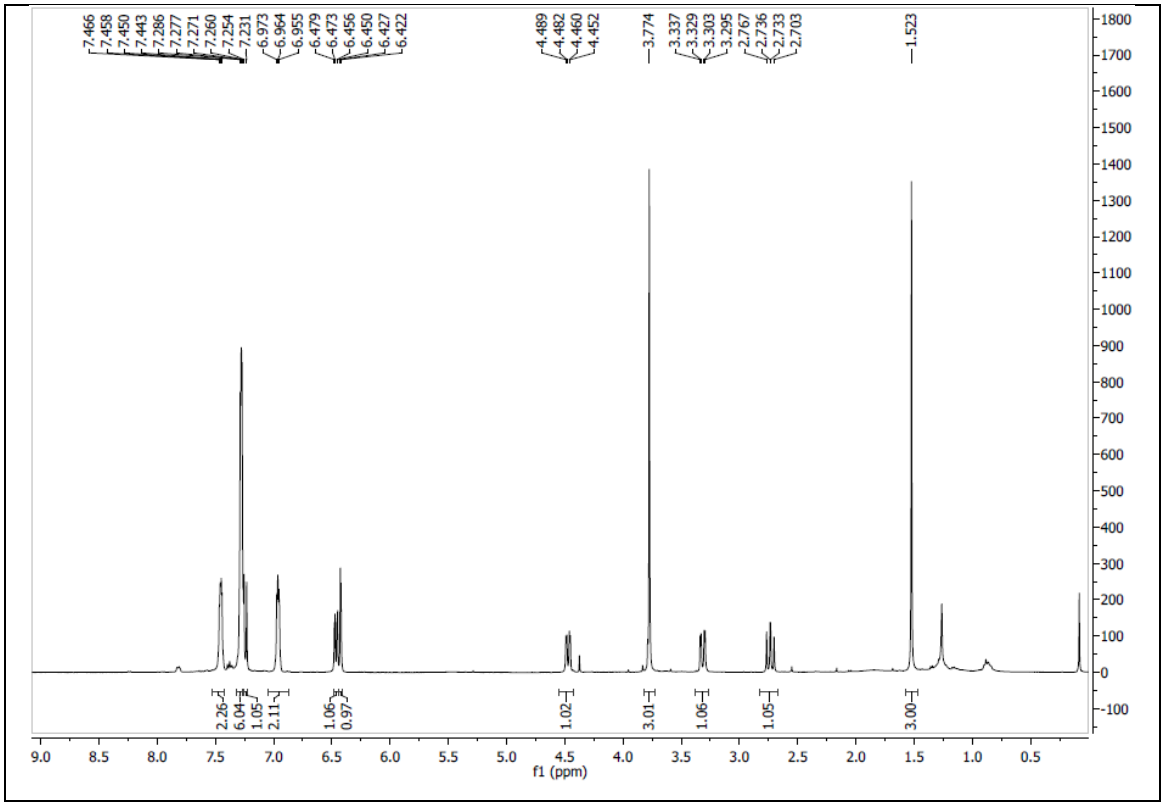

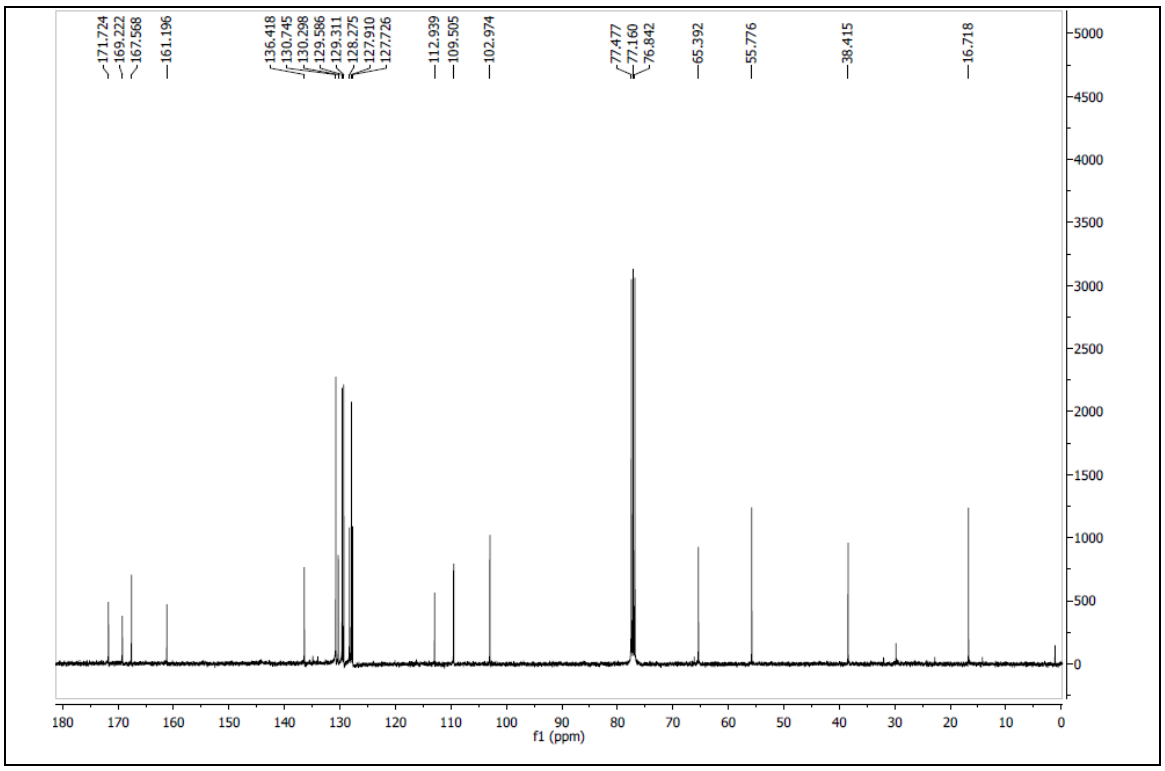
171.724
169.222
167.568
161.196
136.418
130.745
130.298
129.586
129.311
128.275
127.910
127.726
112.939
109.505
102.974
77.477
77.160
76.842
65.392
55.776
38.415
16.718
f1 (ppm)

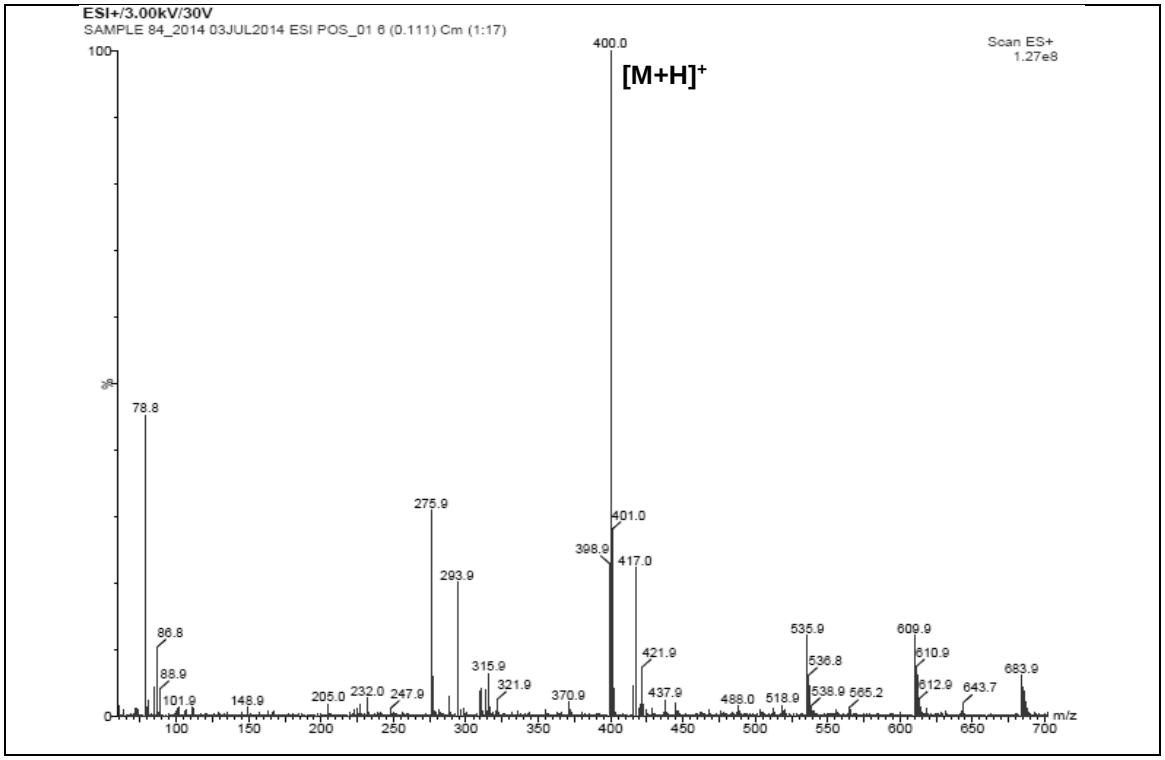
ESI+/3.00kV/30V
SAMPLE 84_2014 03JUL2014 ESI POS_01 6 (0.111) Cm (1:17)
Scan ES+
1.27e8
[M+H]+
400.0
401.0
398.9
417.0
275.9
293.9
78.8
86.8
88.9
101.9
148.9
205.0
232.0
247.9
315.9
321.9
370.9
421.9
437.9
488.0
518.9
535.9
536.8
538.9
565.2
609.9
610.9
612.9
643.7
683.9
%
m/z

- **B-complex 57**

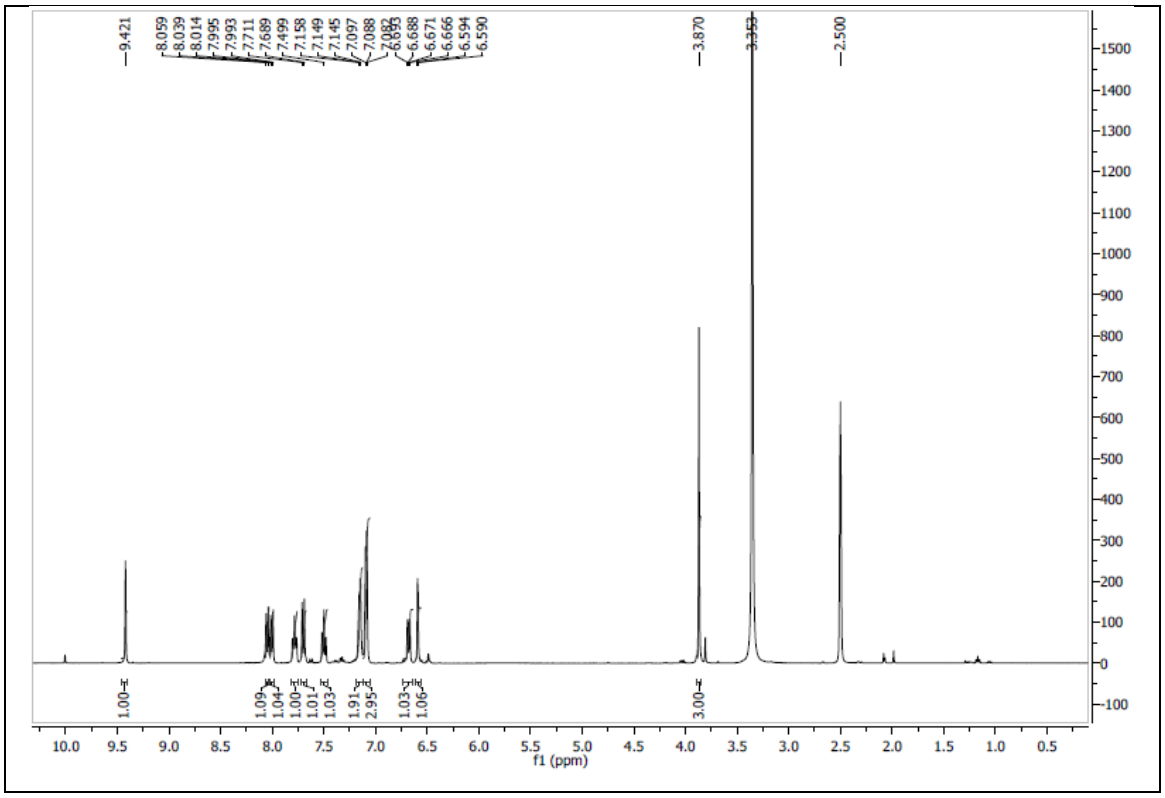
9.421
8.059
8.039
8.014
7.995
7.993
7.711
7.689
7.499
7.158
7.149
7.145
7.097
7.088
6.688
6.671
6.666
6.594
6.590
3.870
3.353
2.500
1.00
1.09
1.04
1.00
1.01
1.03
1.91
2.95
1.03
1.06
3.00
f1 (ppm)

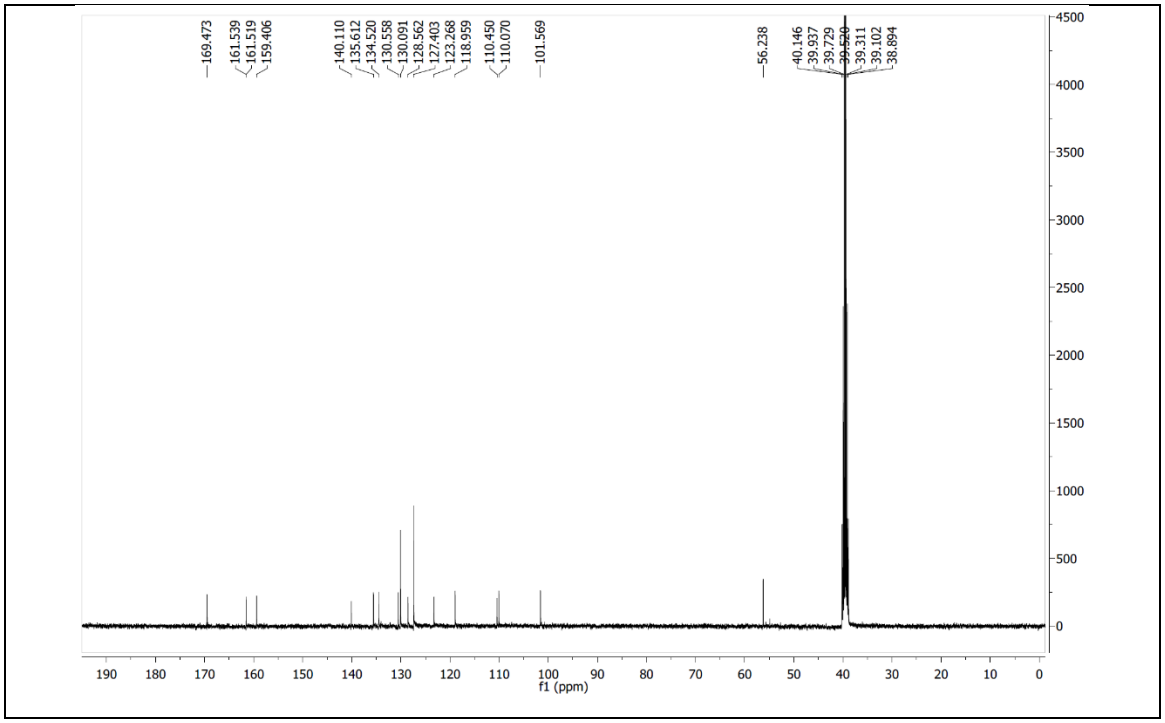
169.473
161.539
161.519
159.406
140.110
135.612
134.520
130.558
130.091
128.562
127.403
123.268
118.959
110.450
110.070
101.569
56.238
40.146
39.937
39.729
39.520
39.311
39.102
38.894
f1 (ppm)

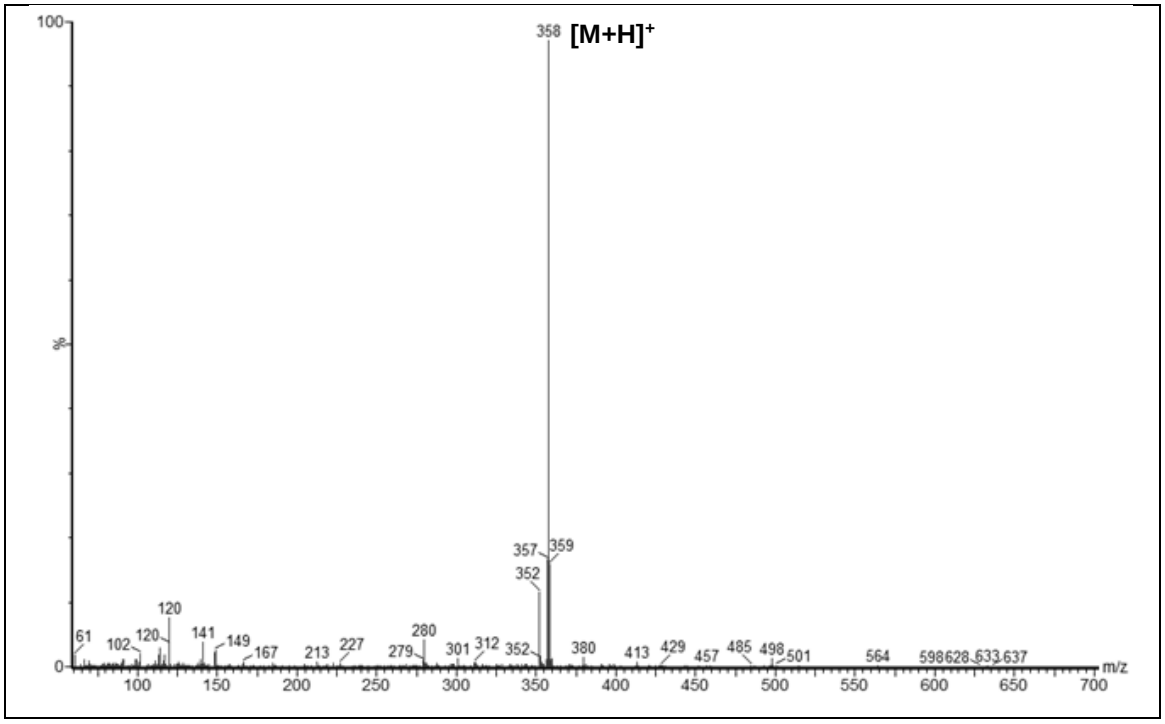

- **B-complex 58a**

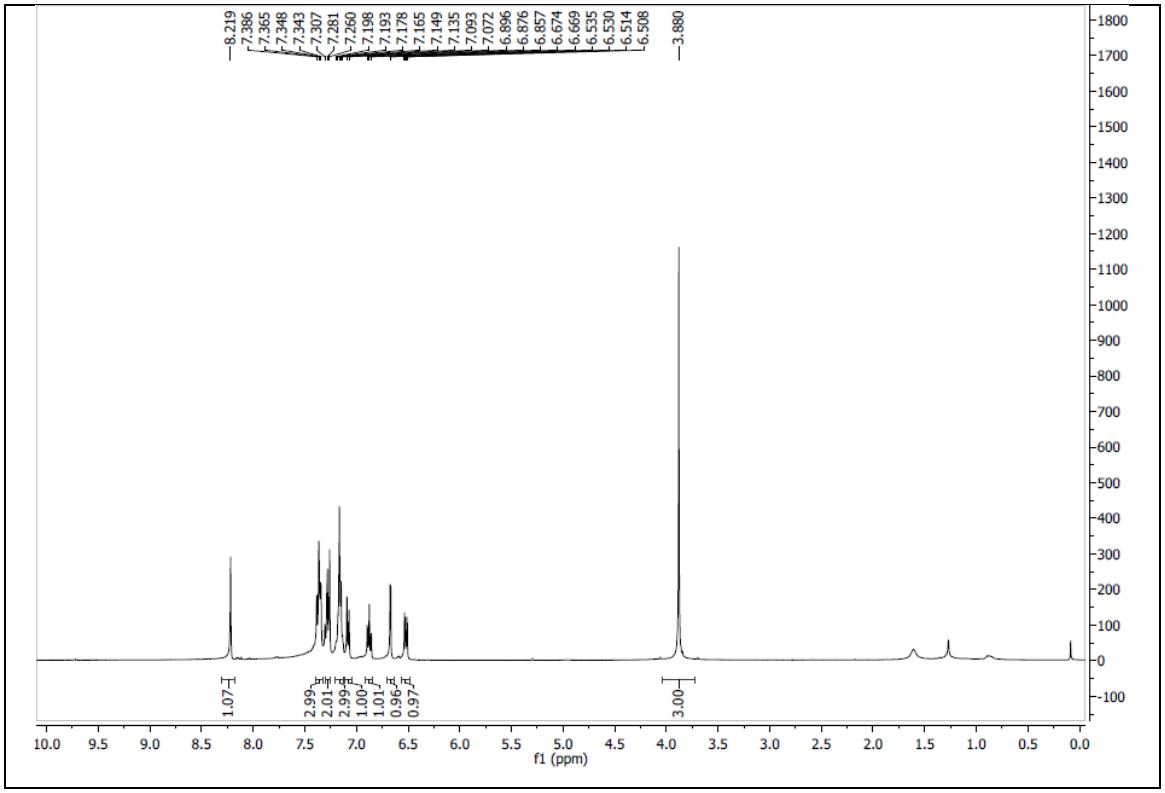

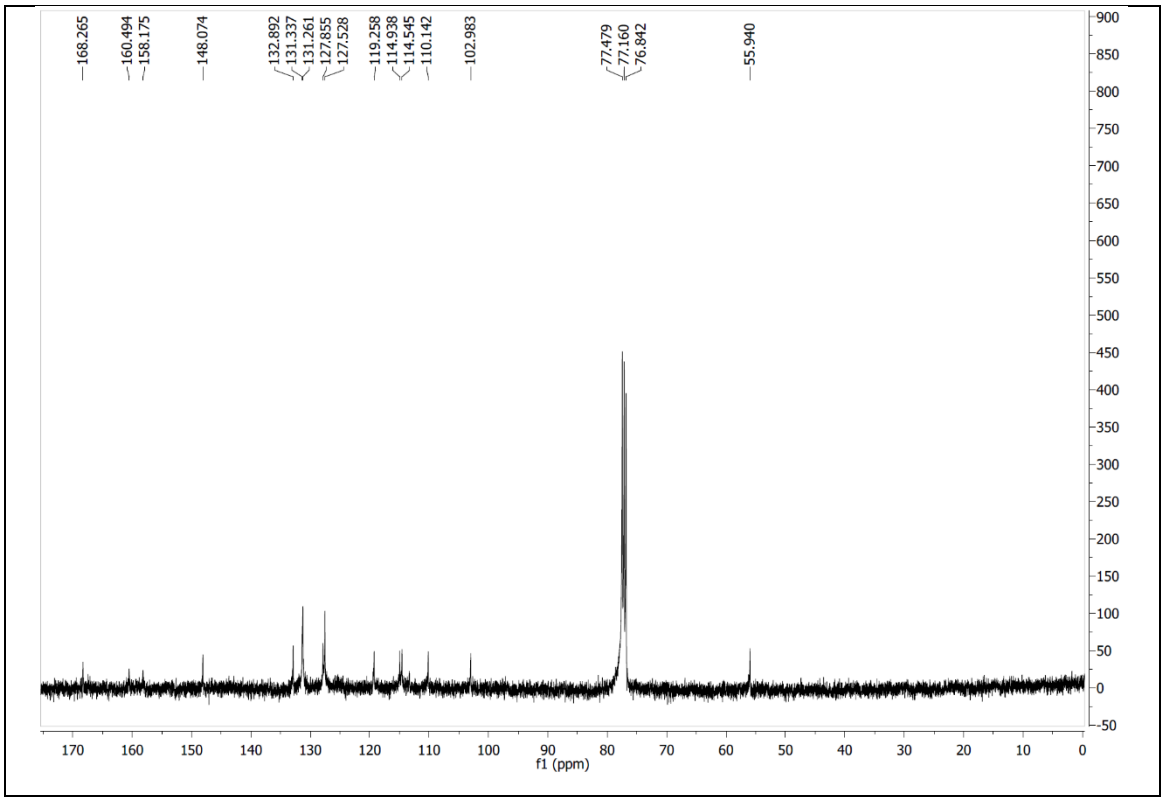
168.265
160.494
158.175
148.074
132.892
131.337
131.261
127.855
127.528
119.258
114.938
114.545
110.142
102.983
77.479
77.160
76.842
55.940
f1 (ppm)

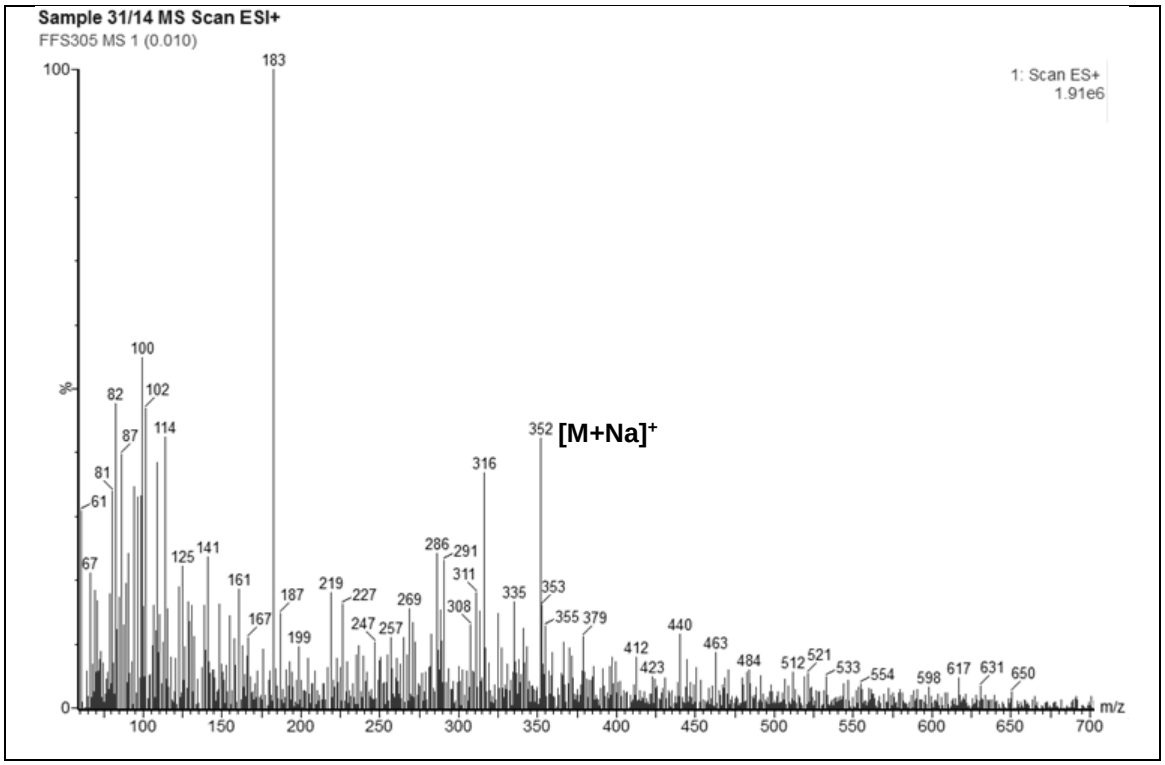
Sample 31/14 MS Scan ESI+
FFS305 MS 1 (0.010)
1: Scan ES+
1.91e6
[M+Na]+
%
m/z

- **B-complex 58b**

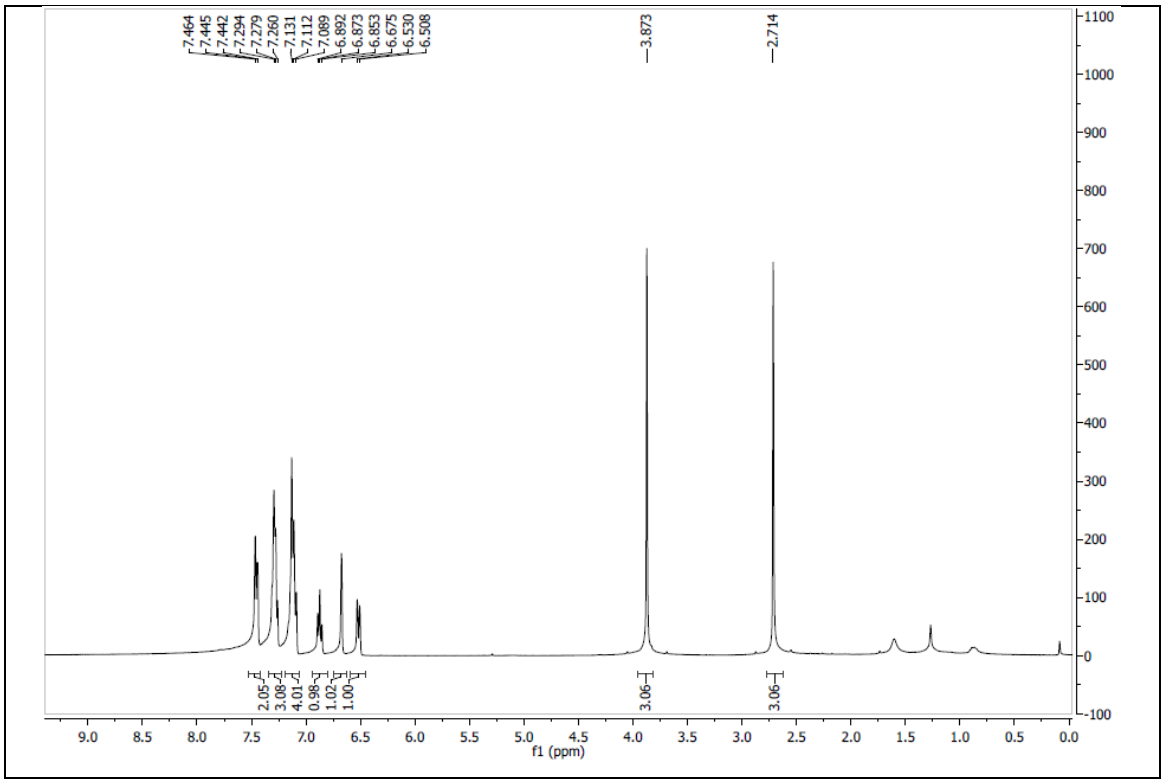

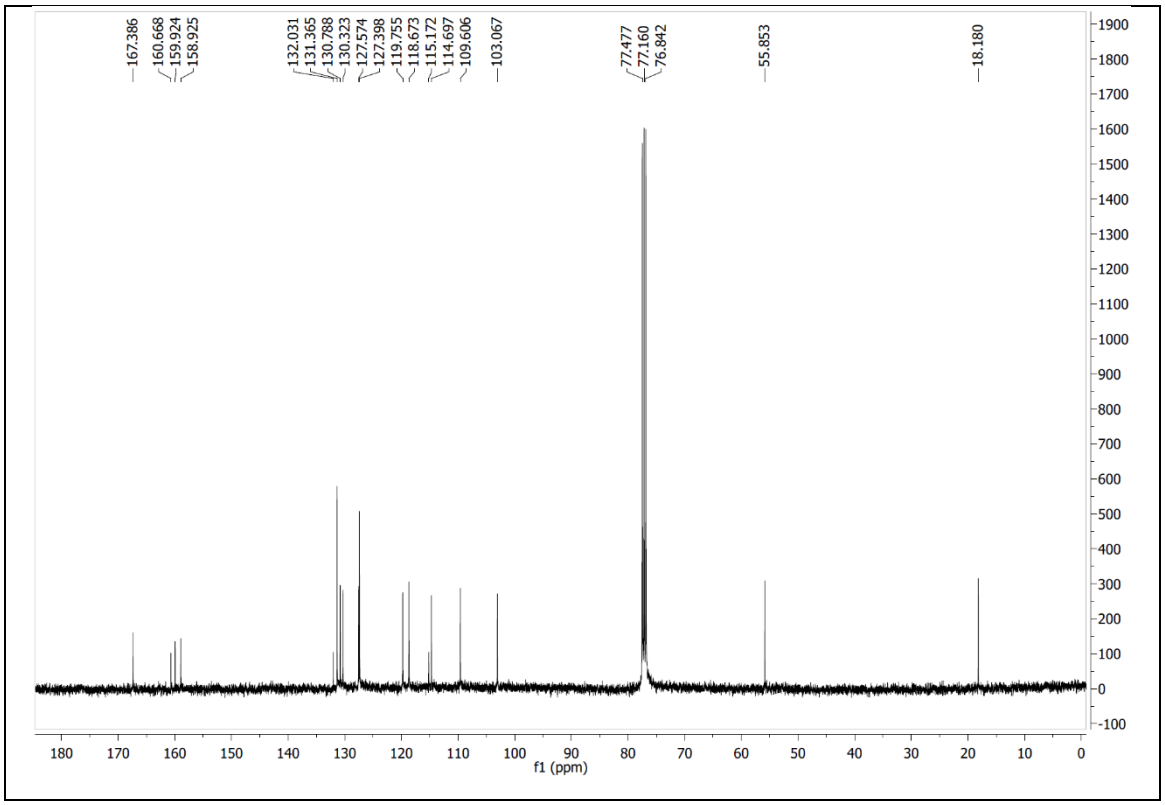

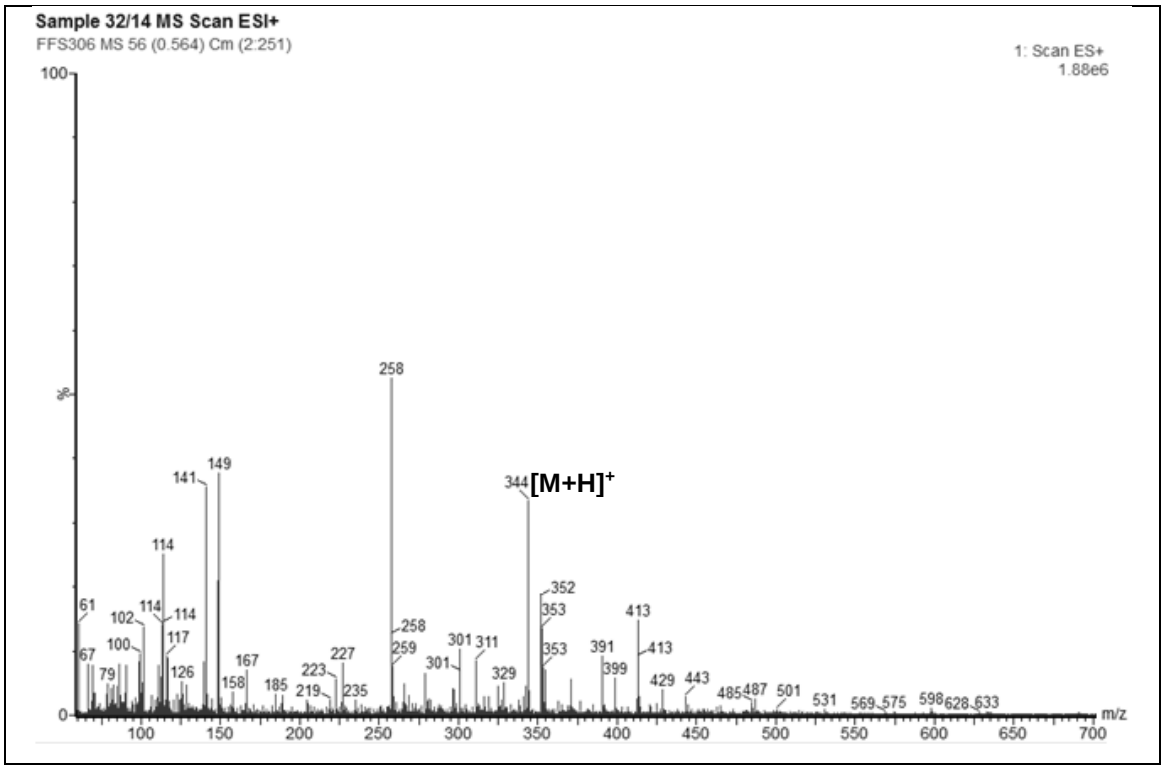

- **Building block 59a**

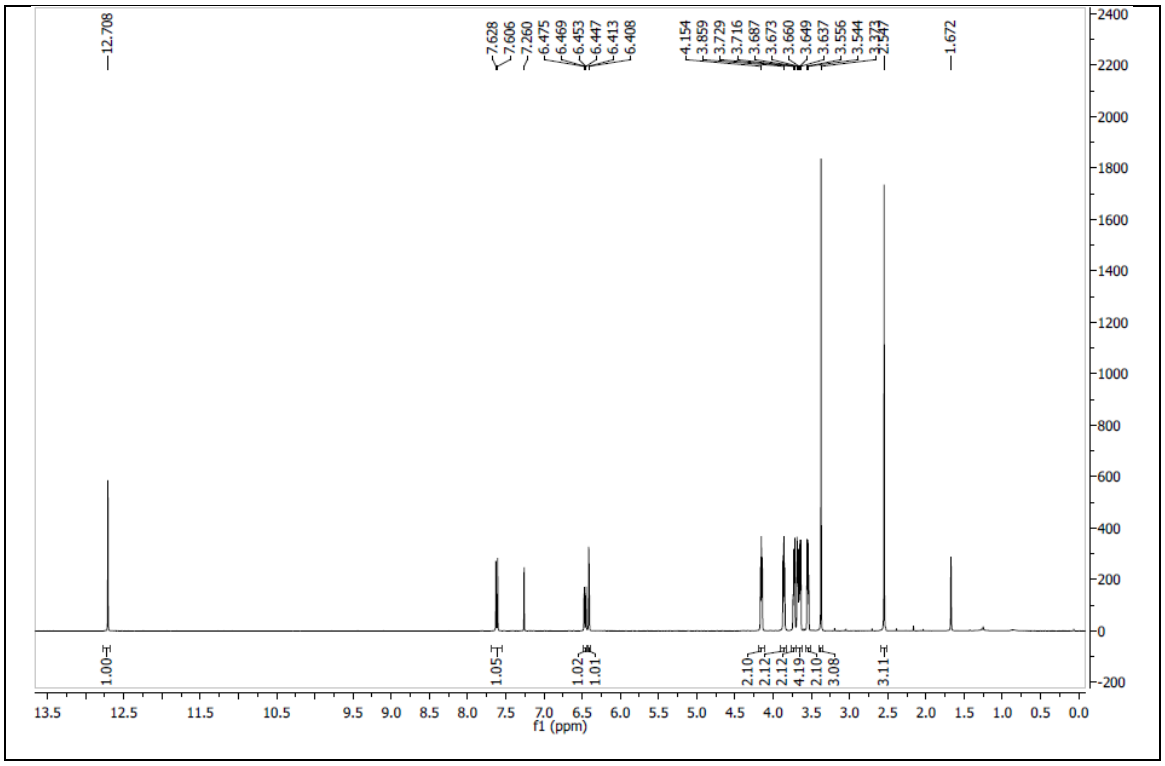

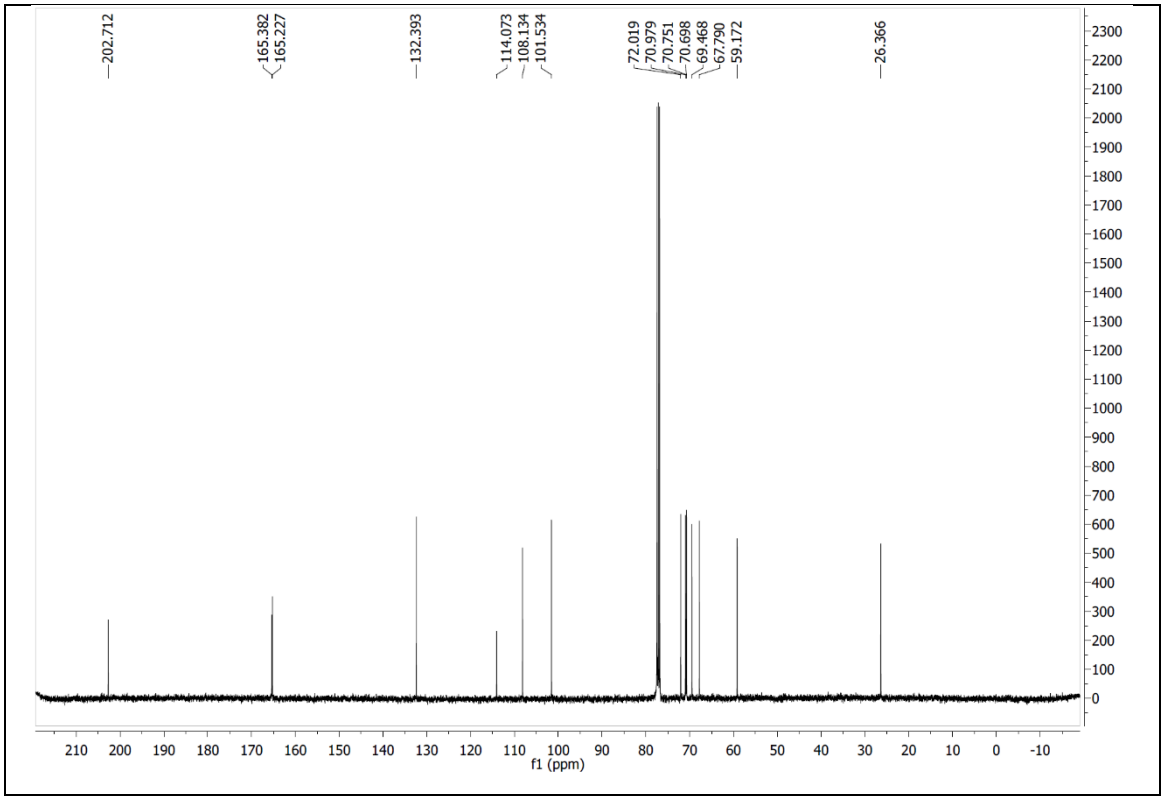
202.712
165.382
165.227
132.393
114.073
108.134
101.534
72.019
70.979
70.751
70.698
69.468
67.790
59.172
26.366
f1 (ppm)

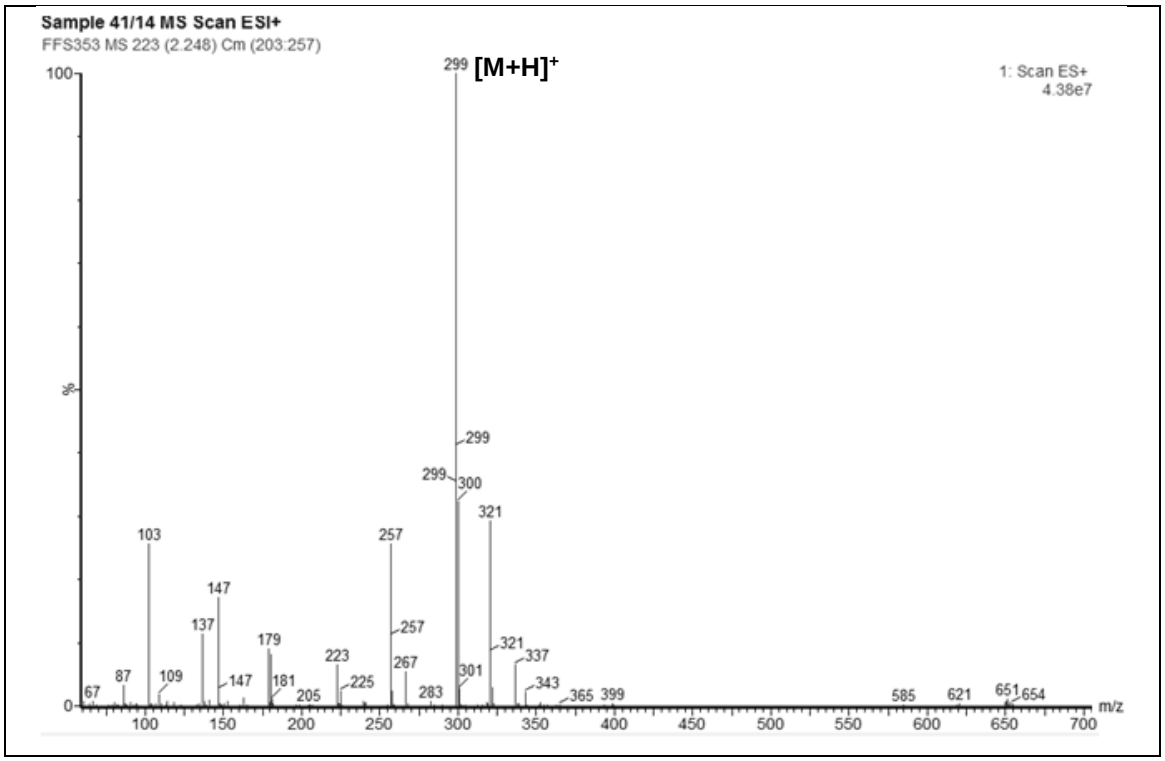
Sample 41/14 MS Scan ESI+
FFS353 MS 223 (2.248) Cm (203:257)
[M+H]+
1: Scan ES+
4.38e7
%
m/z

- **Building block 59b**

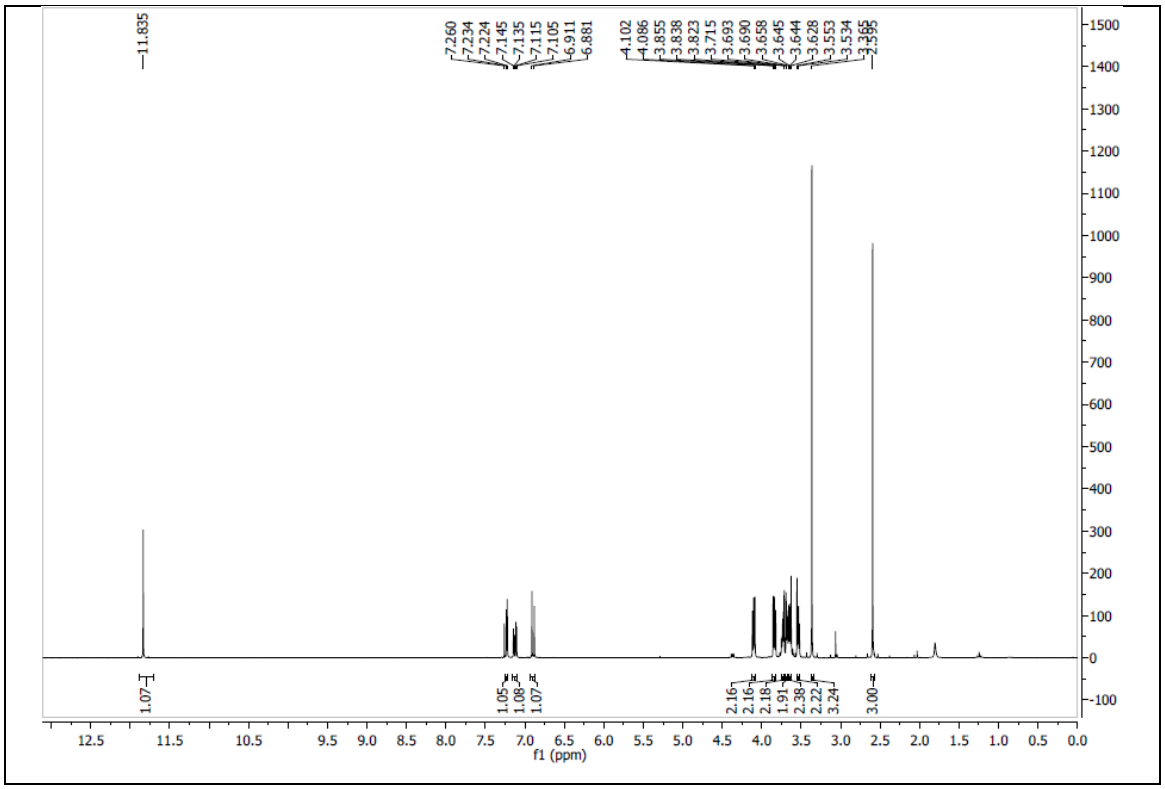

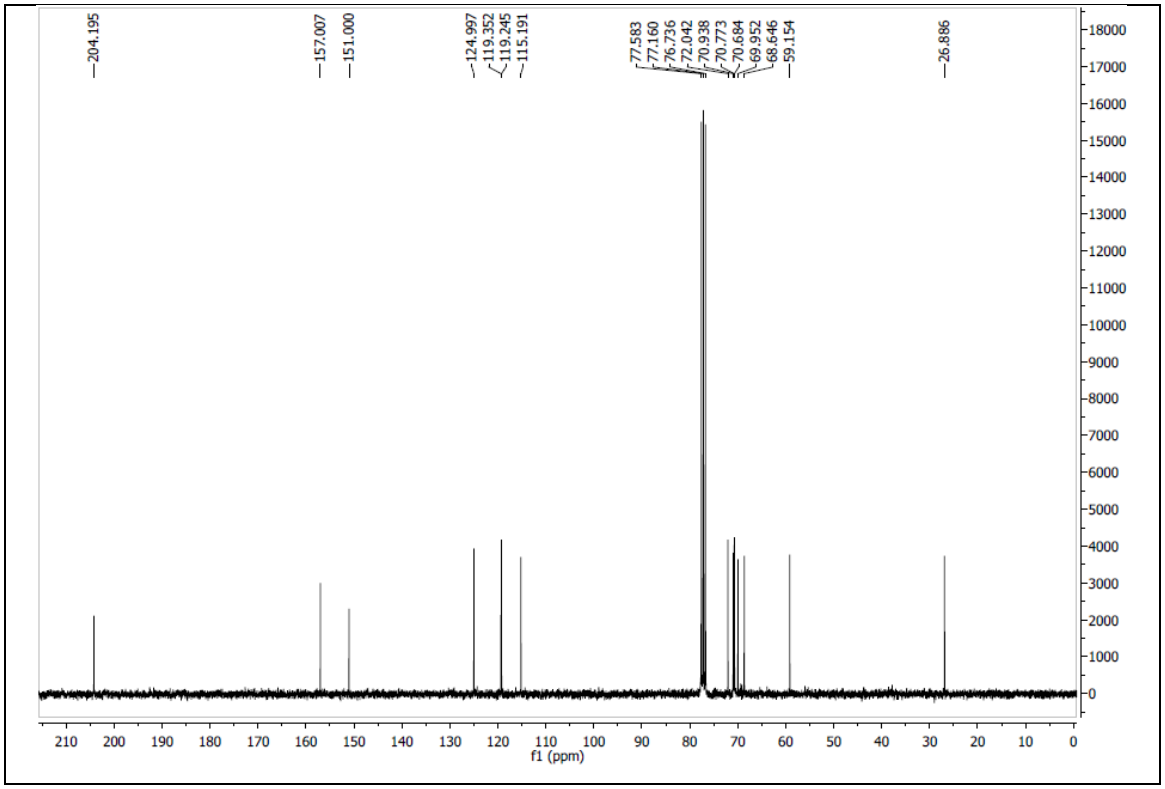

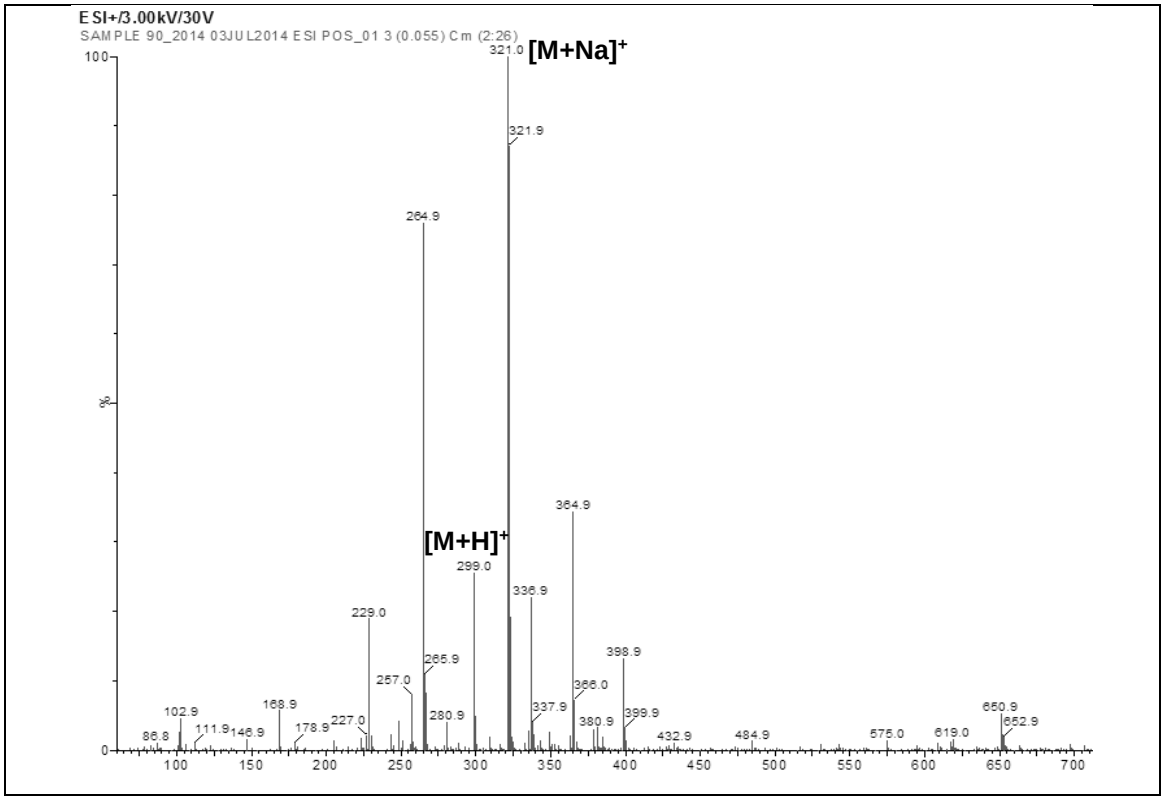

- **Building block 60**

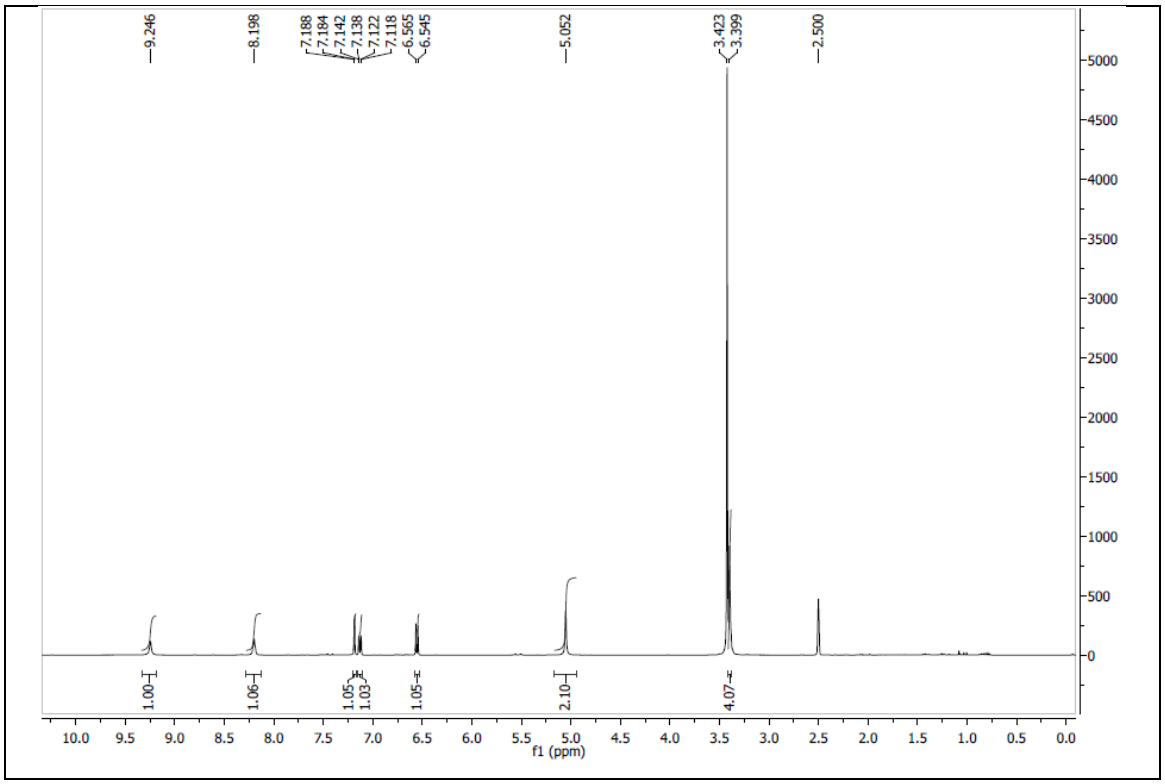

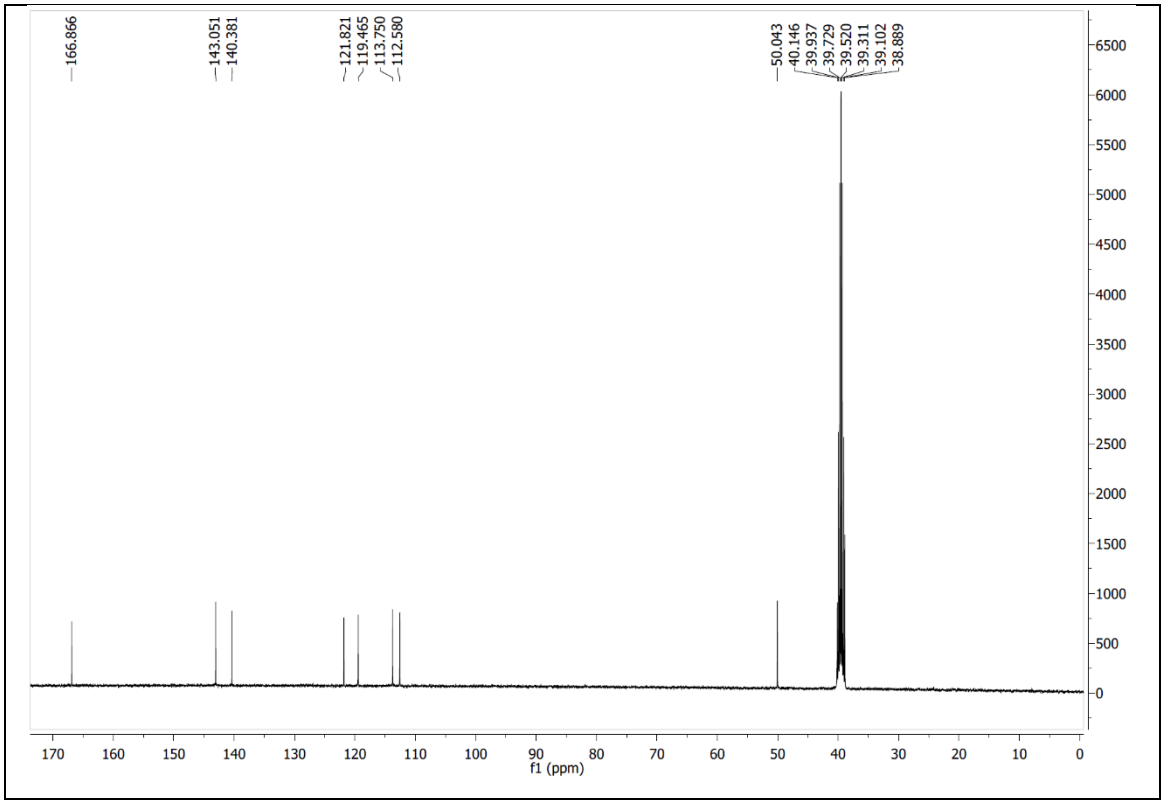
166.866
143.051
140.381
121.821
119.465
113.750
112.580
50.043
40.146
39.937
39.729
39.520
39.311
39.102
38.889
f1 (ppm)

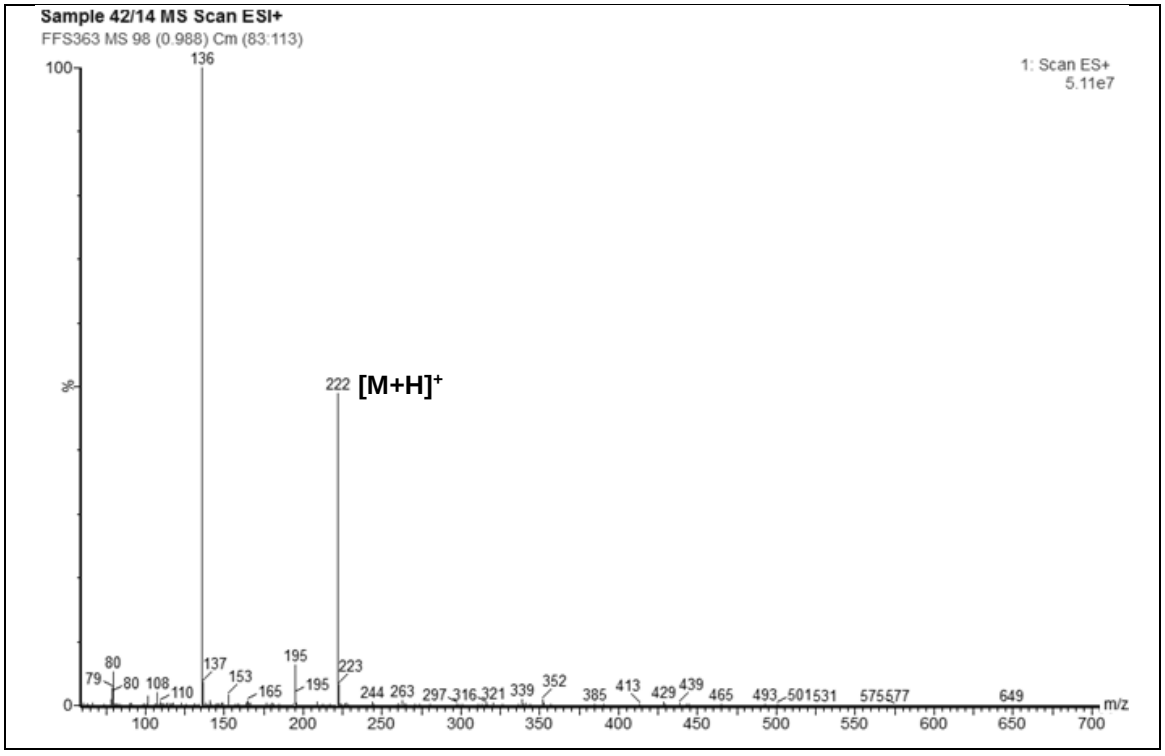
Sample 42/14 MS Scan ESI+
FFS363 MS 98 (0.988) Cm (83:113)
1: Scan ES+
5.11e7
136
222 [M+H]+
m/z

- **B-complex 62**

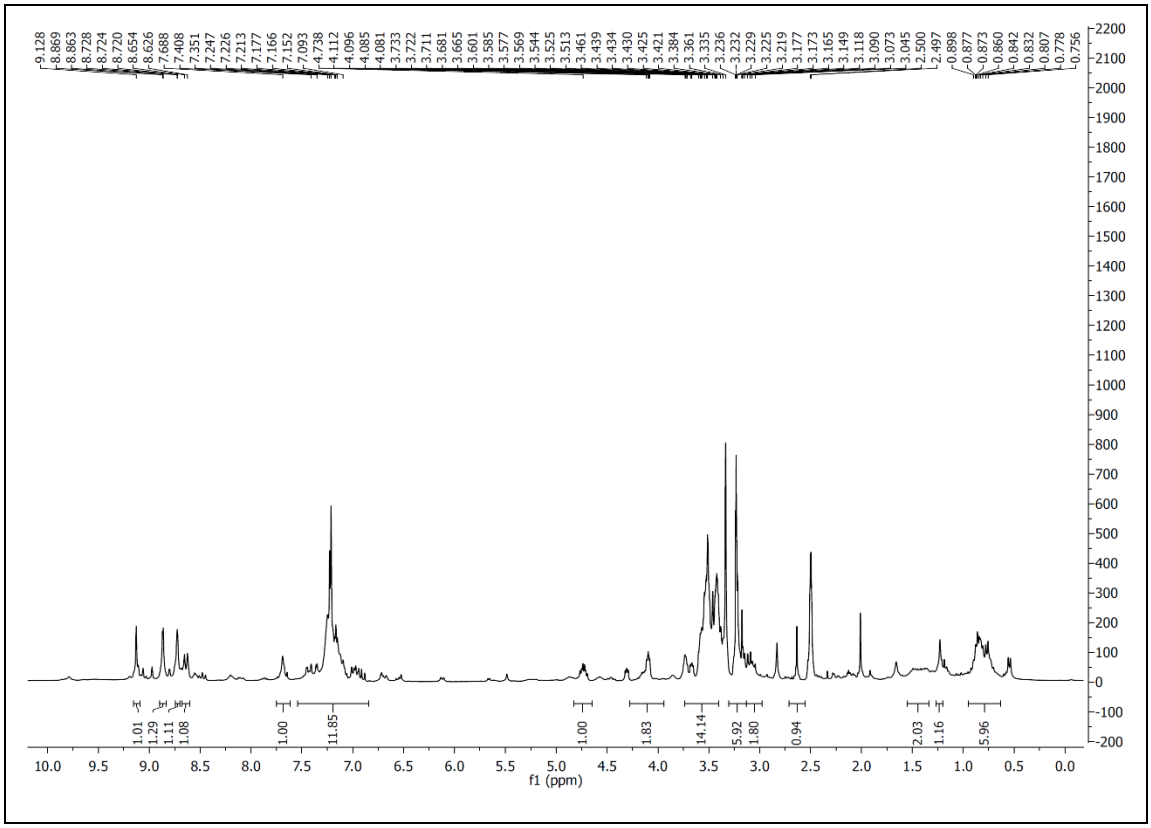

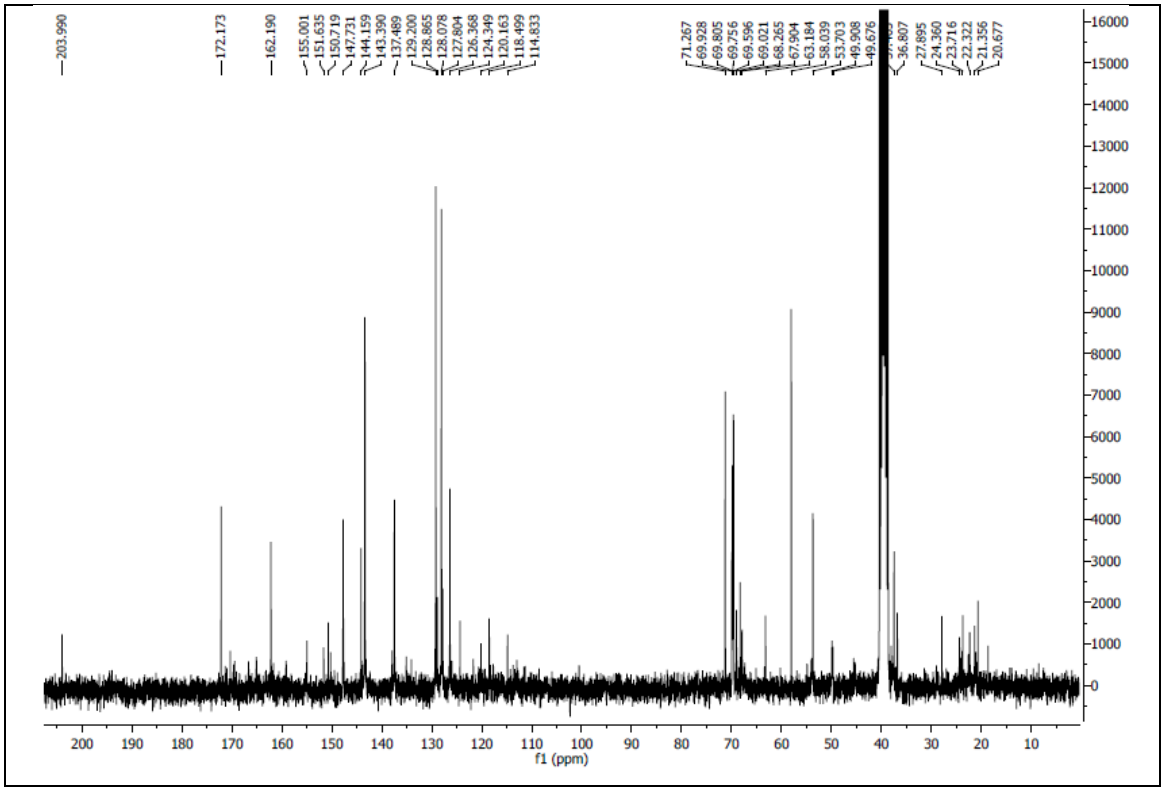

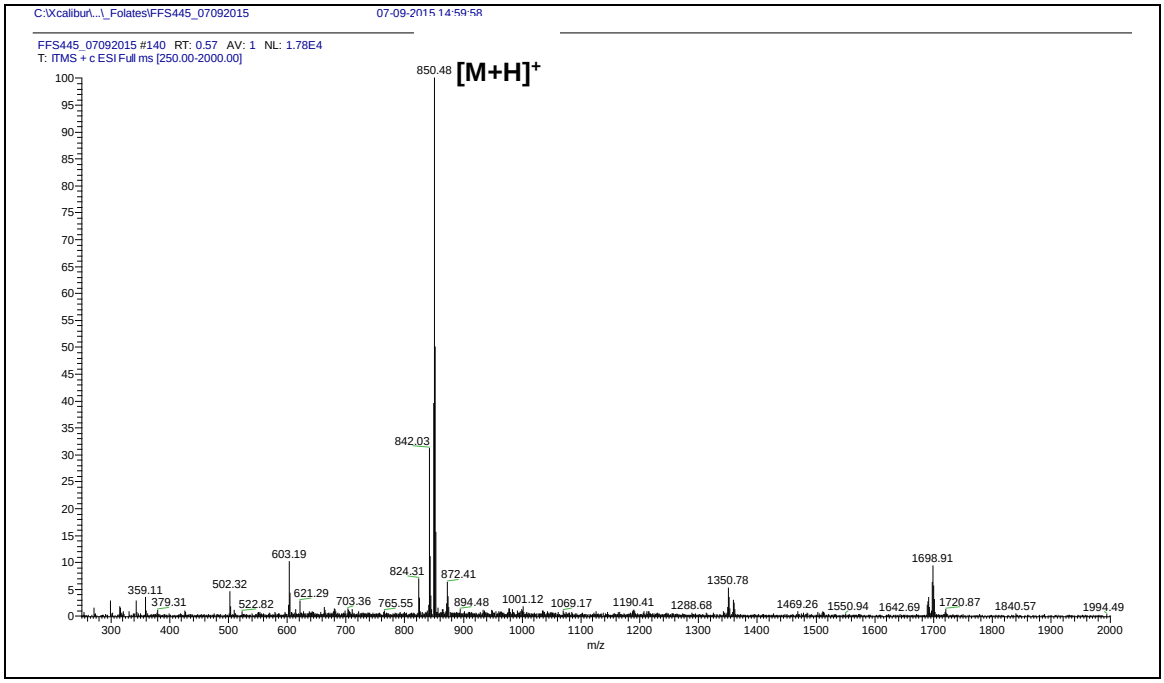
C:\Xcalibur\..._Folates\FFS445_07092015
07-09-2015 14:59:58
FFS445_07092015 #140 RT: 0.57 AV: 1 NL: 1.78E4
T: ITMS + c ESI Full ms [250.00-2000.00]
850.48 [M+H]+
842.03
603.19
824.31
872.41
359.11
379.31
502.32
522.82
621.29
703.36
765.55
894.48
1001.12
1069.17
1190.41
1288.68
1350.78
1469.26
1550.94
1642.69
1698.91
1720.87
1840.57
1994.49
m/z

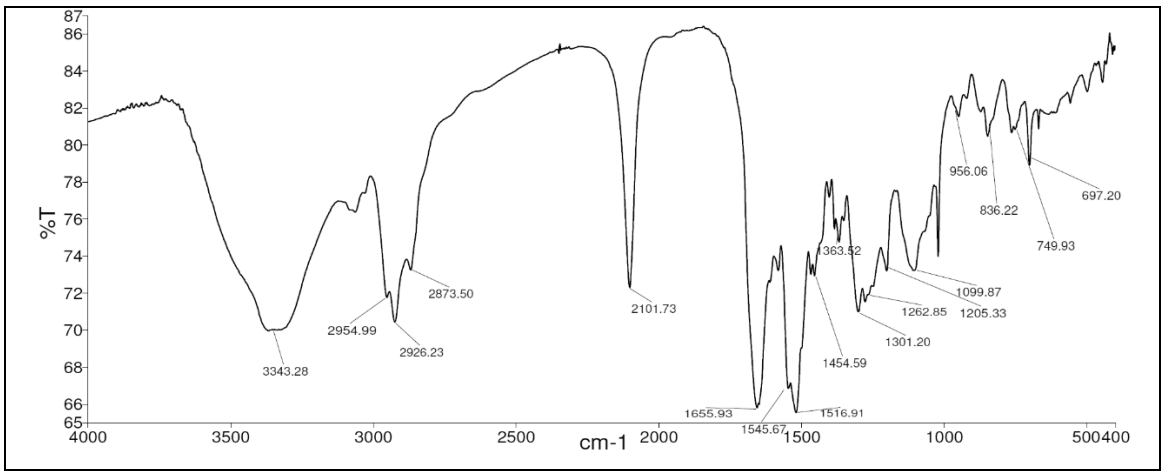
%T
cm-1
3343.28
2954.99
2926.23
2873.50
2101.73
1655.93
1545.67
1516.91
1454.59
1363.52
1301.20
1262.85
1205.33
1099.87
956.06
836.22
749.93
697.20

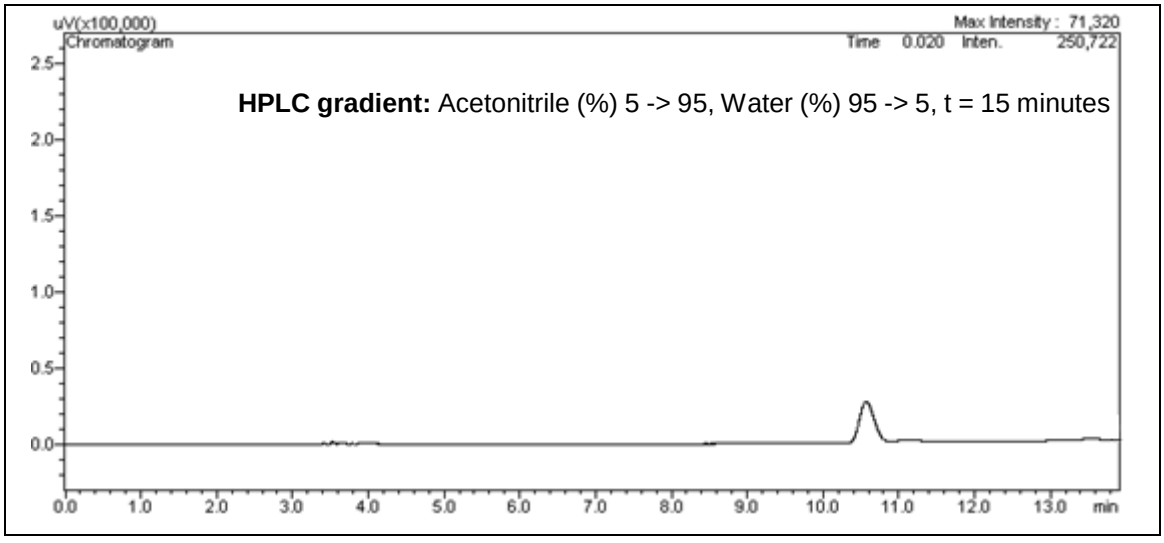
uV(x100,000)
Chromatogram
Max Intensity : 71,320
Time 0.020 Inten. 250,722
HPLC gradient: Acetonitrile (%) 5 -> 95, Water (%) 95 -> 5, t = 15 minutes
min

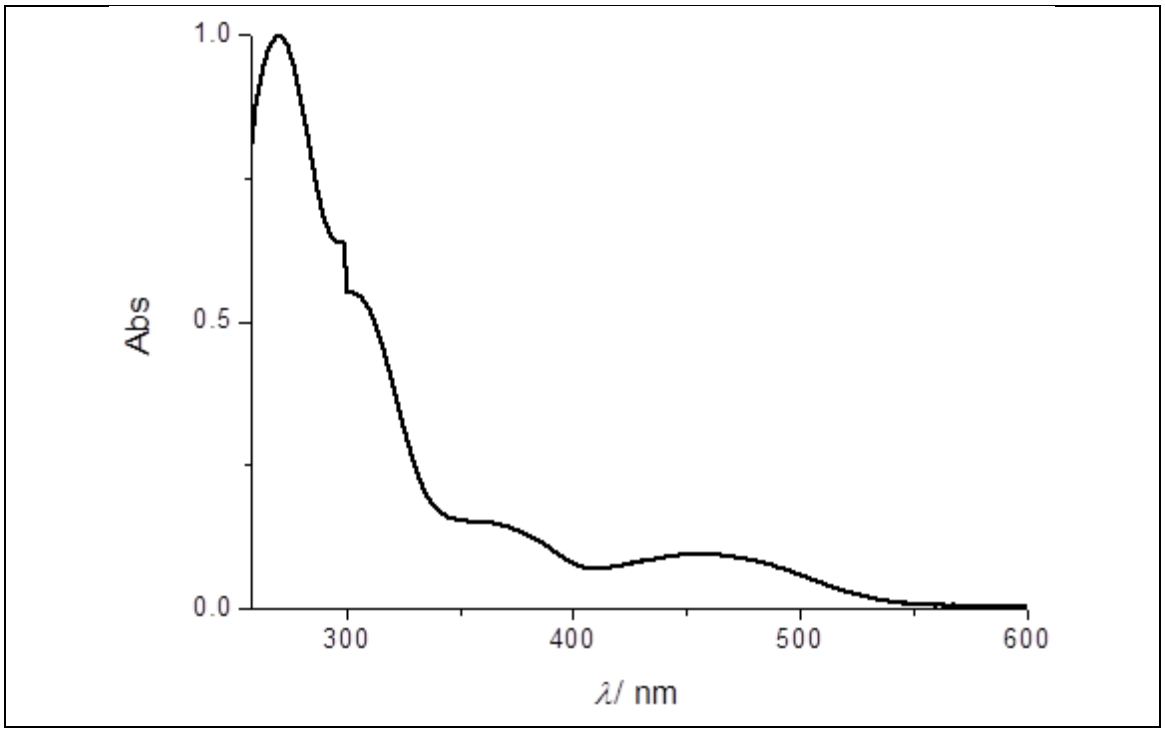

- **SMDC 63**

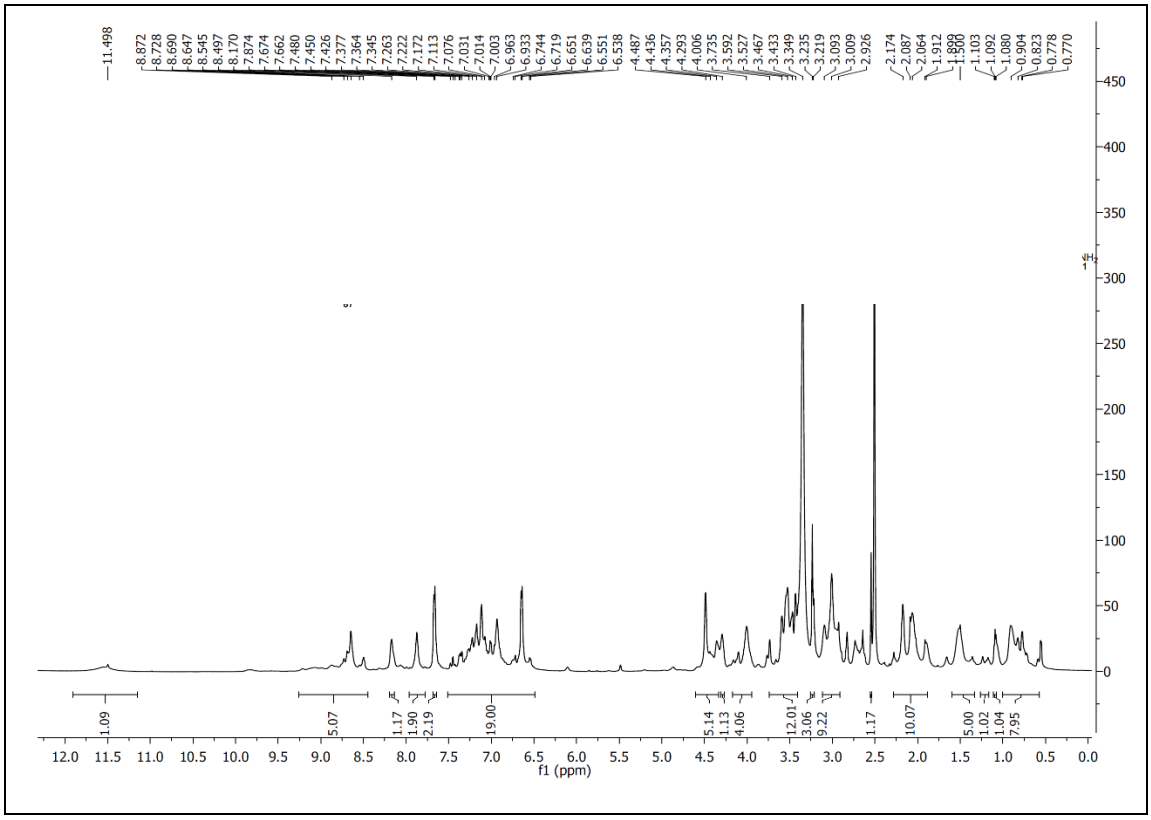

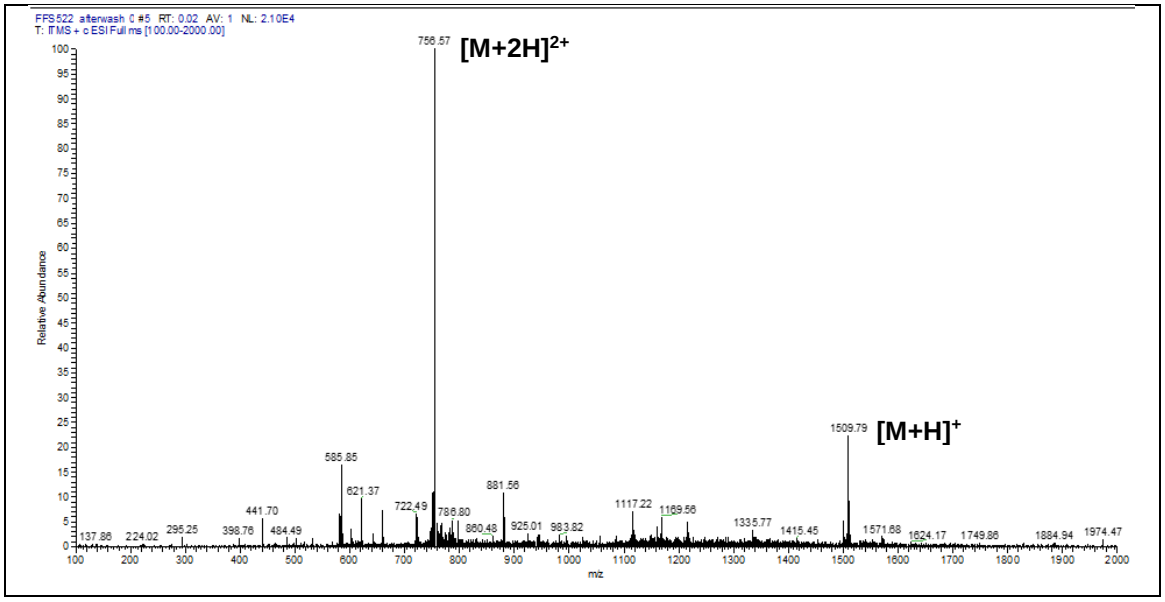
FPS522 afterwash 0 #5 RT: 0.02 AV: 1 NL: 2.10E4
T: ITMS + c ESI Full ms [100.00-2000.00]
[M+2H]2+
[M+H]+
Relative Abundance
m/z

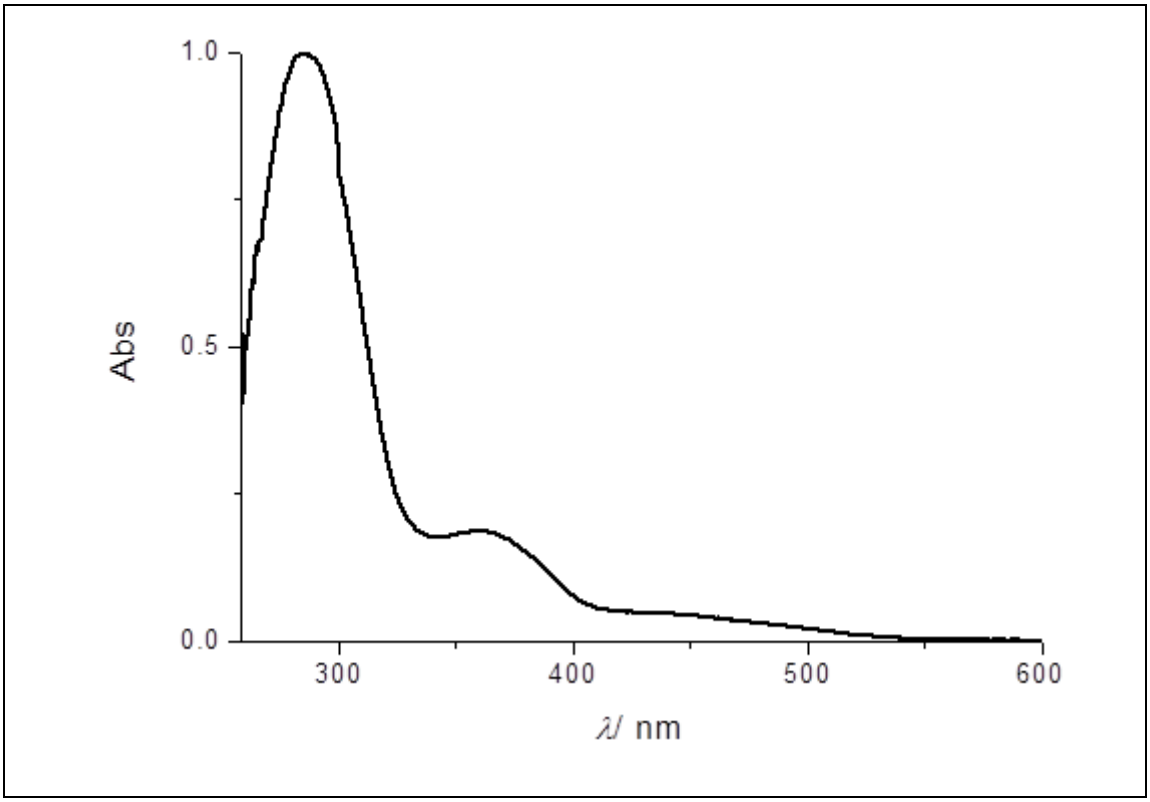
Abs
λ/ nm

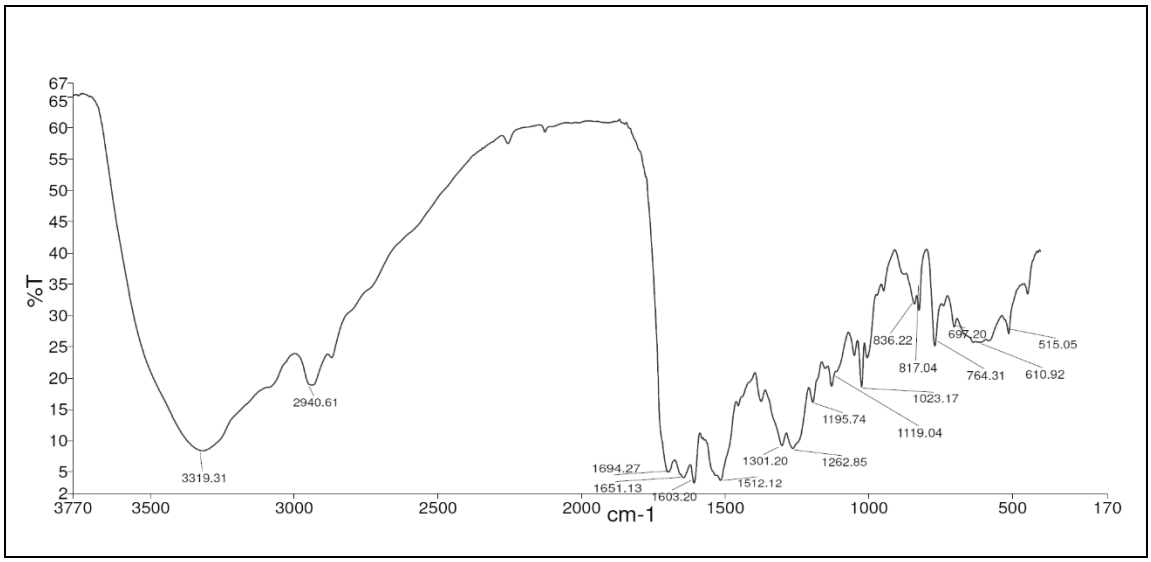

- **Building block 64**

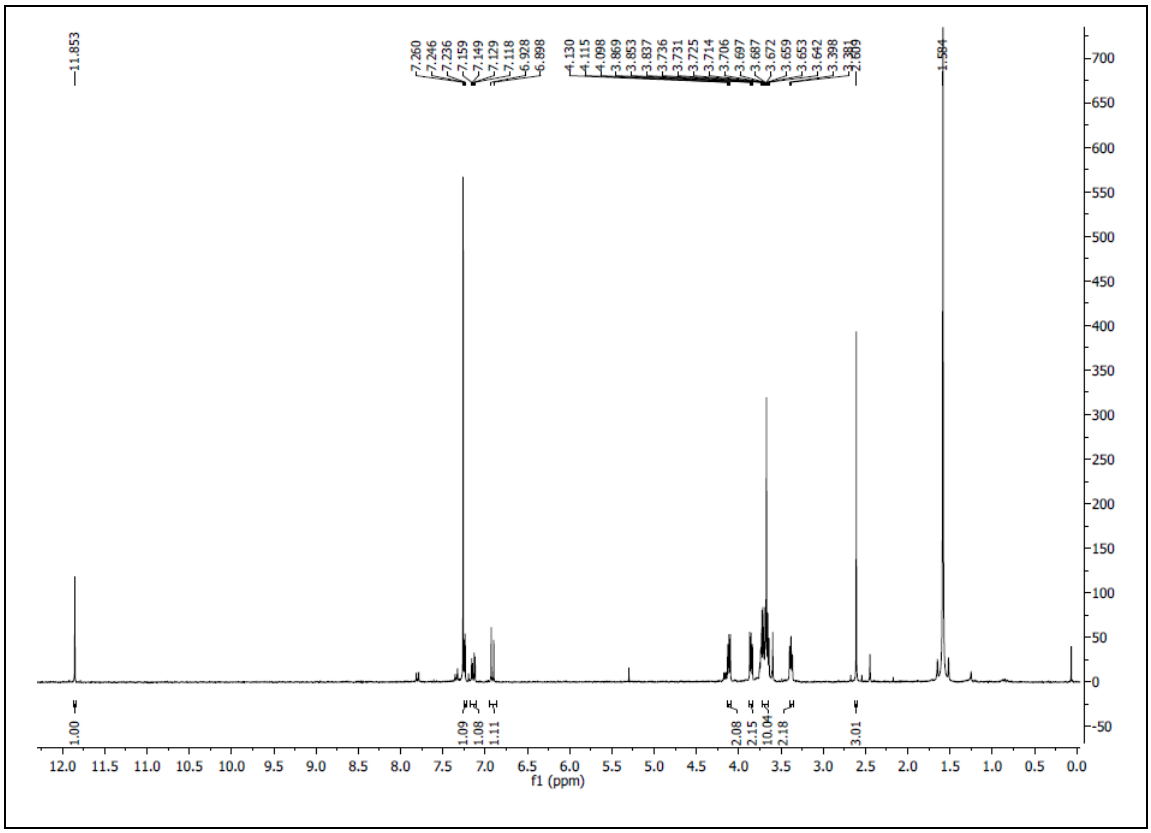

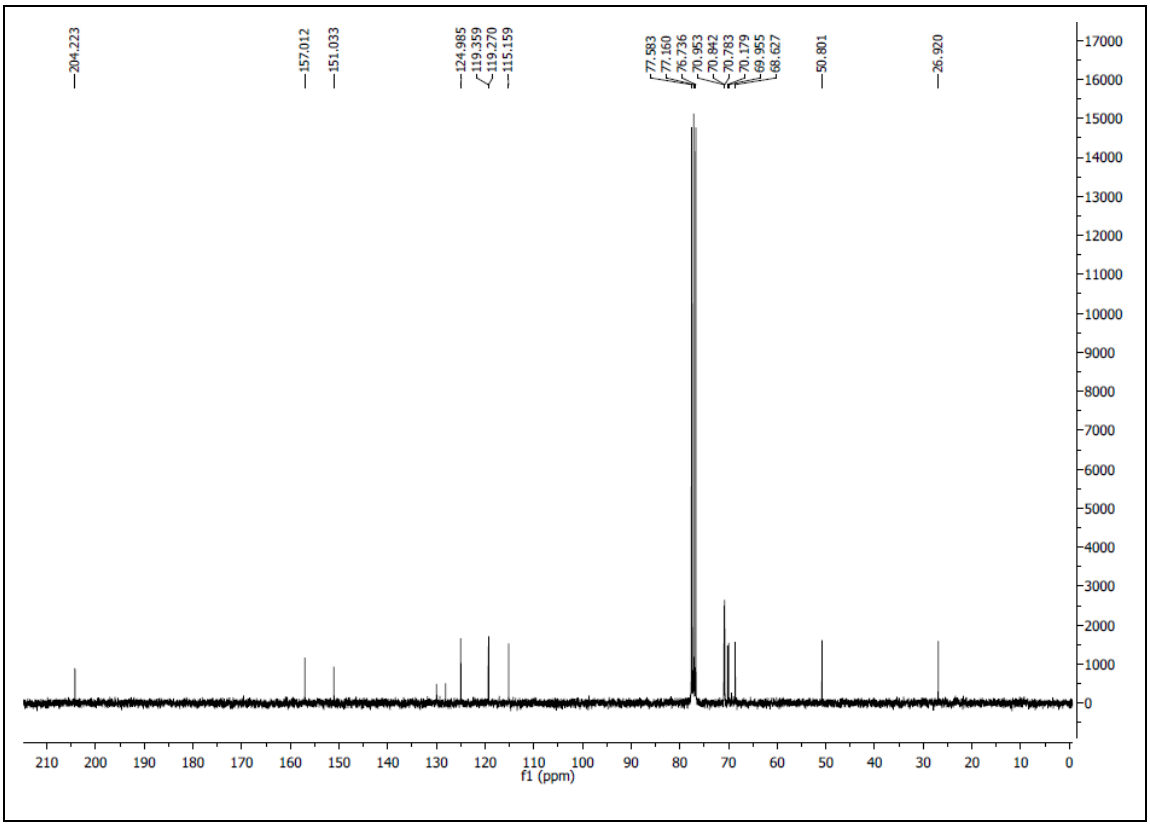
204.223
157.012
151.033
124.985
119.359
119.270
115.159
77.583
77.160
76.736
70.953
70.842
70.783
70.179
69.955
68.627
50.801
26.920
f1 (ppm)

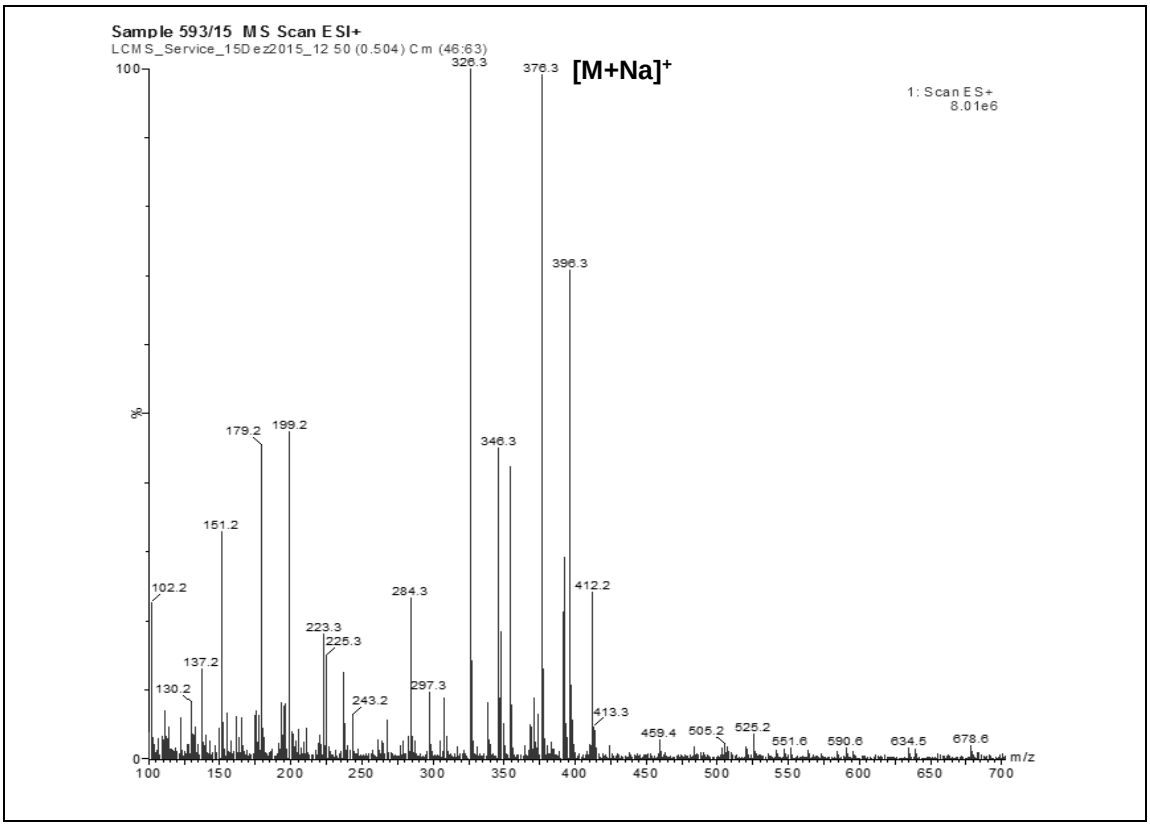
Sample 593/15 MS Scan ESI+
LCMS_Service_15Dez2015_12 50 (0.504) Cm (46:63)
[M+Na]+
1: Scan ES+
8.01e6
326.3
376.3
396.3
346.3
179.2
199.2
151.2
102.2
284.3
412.2
223.3
225.3
137.2
130.2
297.3
243.2
413.3
459.4
505.2
525.2
551.6
590.6
634.5
678.6
m/z

- **Building block 65**

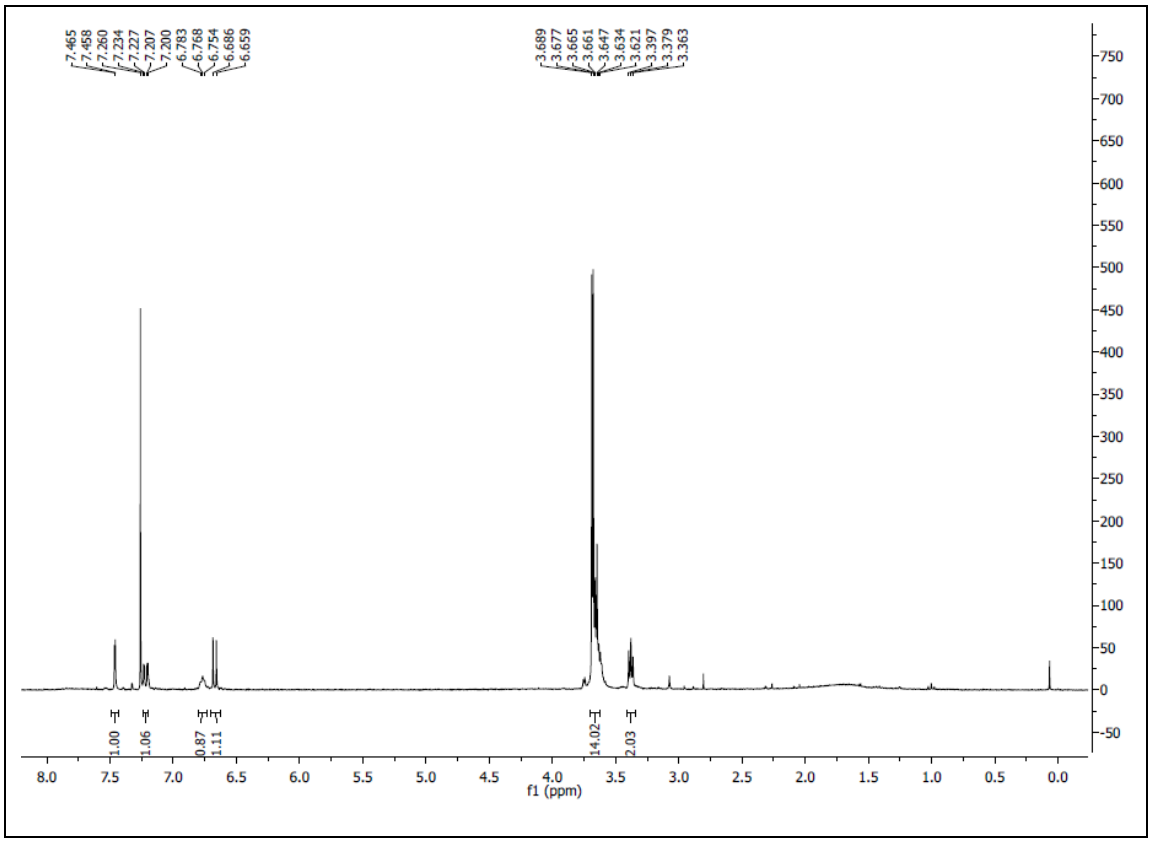

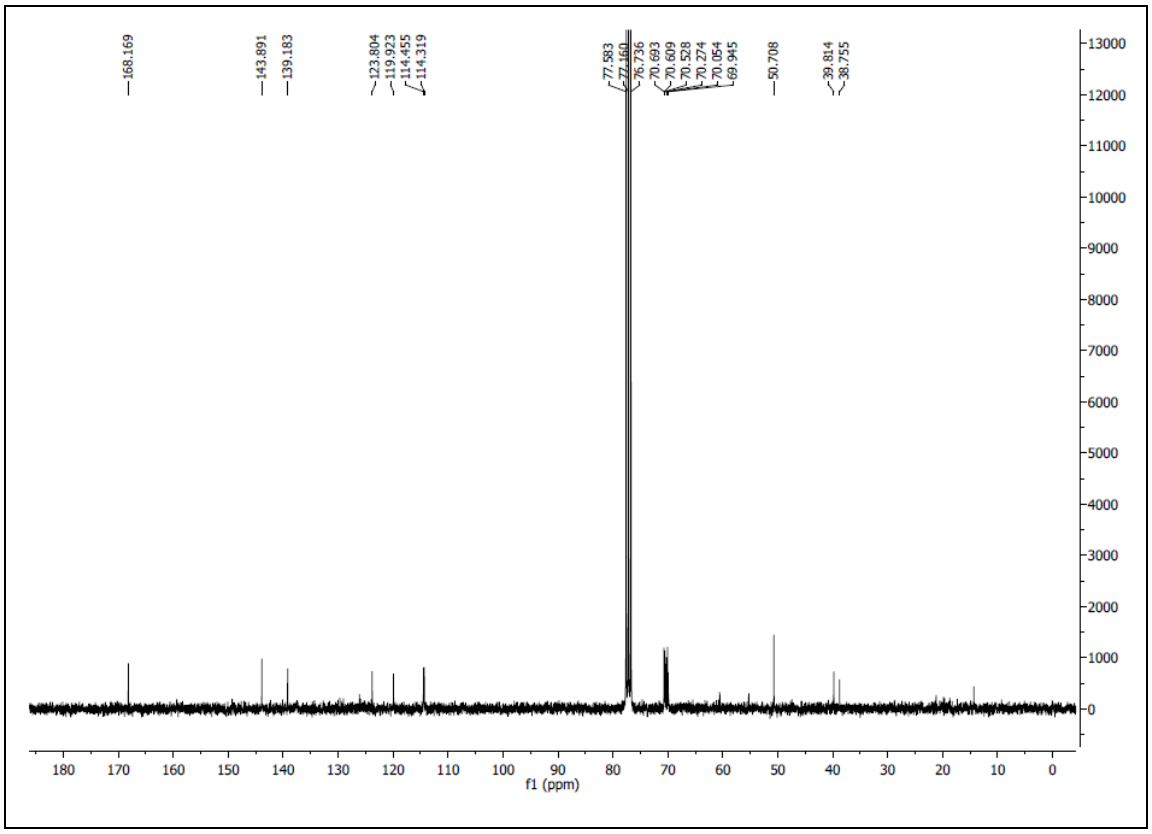

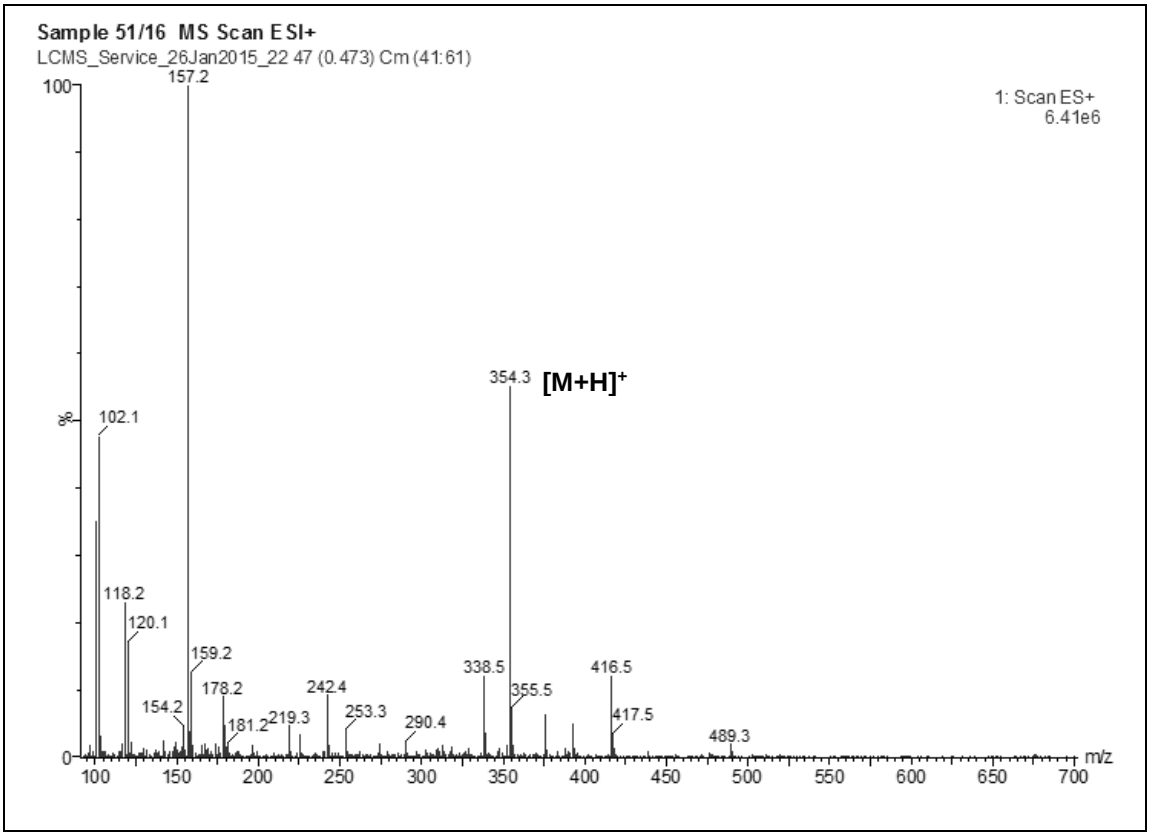
Sample 51/16 MS Scan ESI+
LCMS_Service_26Jan2015_22 47 (0.473) Cm (41:61)
1: Scan ES+
6.41e6
157.2
354.3
[M+H]+
102.1
118.2
120.1
159.2
178.2
154.2
181.2
219.3
242.4
253.3
290.4
338.5
355.5
416.5
417.5
489.3
%
m/z

- **B-complex 66**

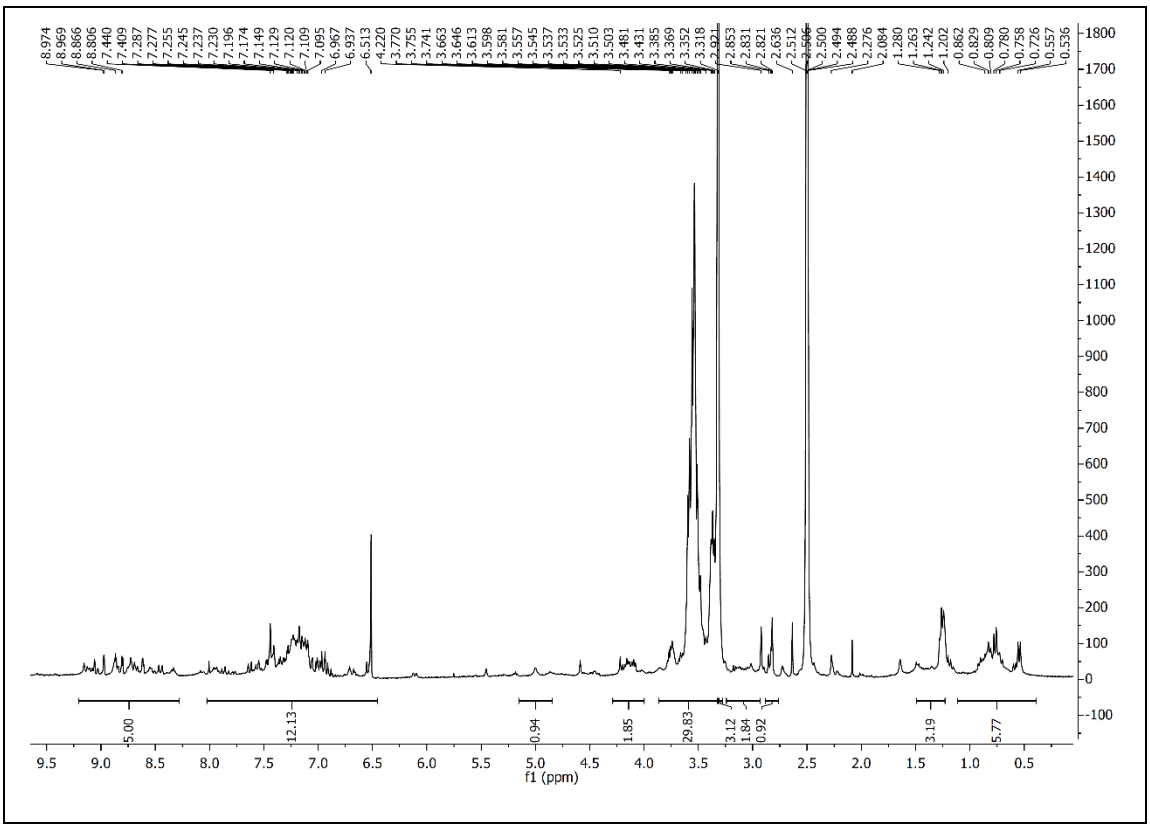
f1 (ppm)

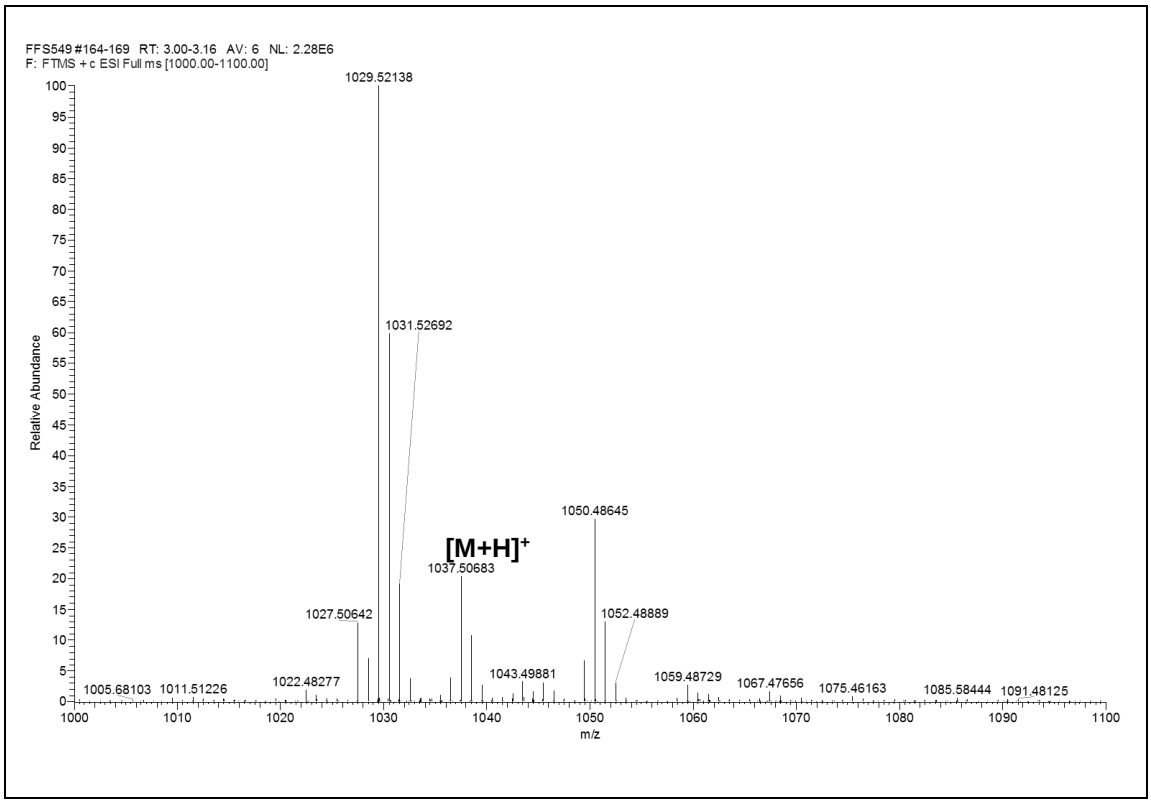
FFS549 #164-169 RT: 3.00-3.16 AV: 6 NL: 2.28E6
F: FTMS + c ESI Full ms [1000.00-1100.00]
Relative Abundance
m/z
1029.52138
1031.52692
1050.48645
[M+H]+
1037.50683
1027.50642
1052.48889
1043.49881
1005.68103
1011.51226
1022.48277
1059.48729
1067.47656
1075.46163
1085.58444
1091.48125

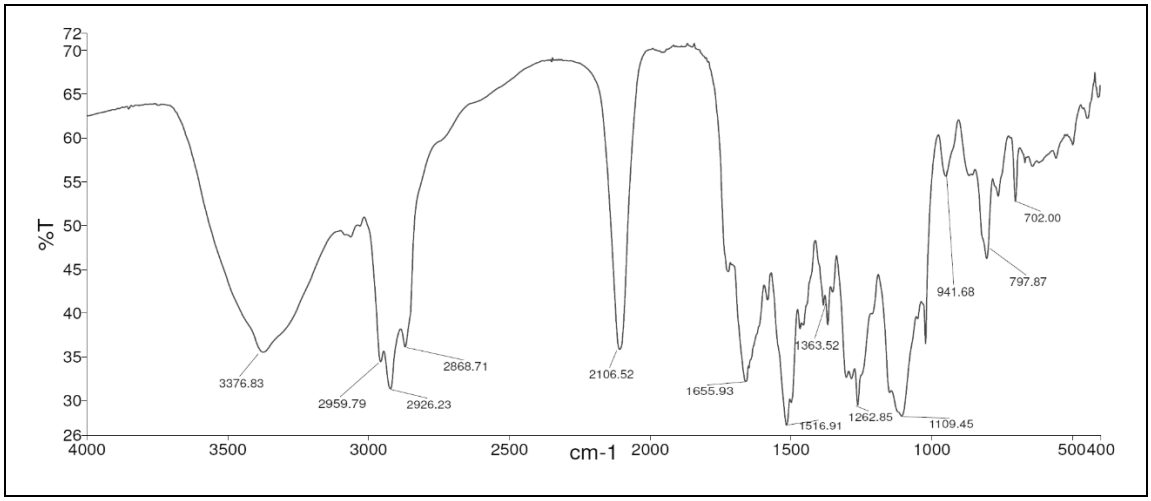
%T
cm-1
3376.83
2959.79
2926.23
2868.71
2106.52
1655.93
1516.91
1363.52
1262.85
1109.45
941.68
797.87
702.00

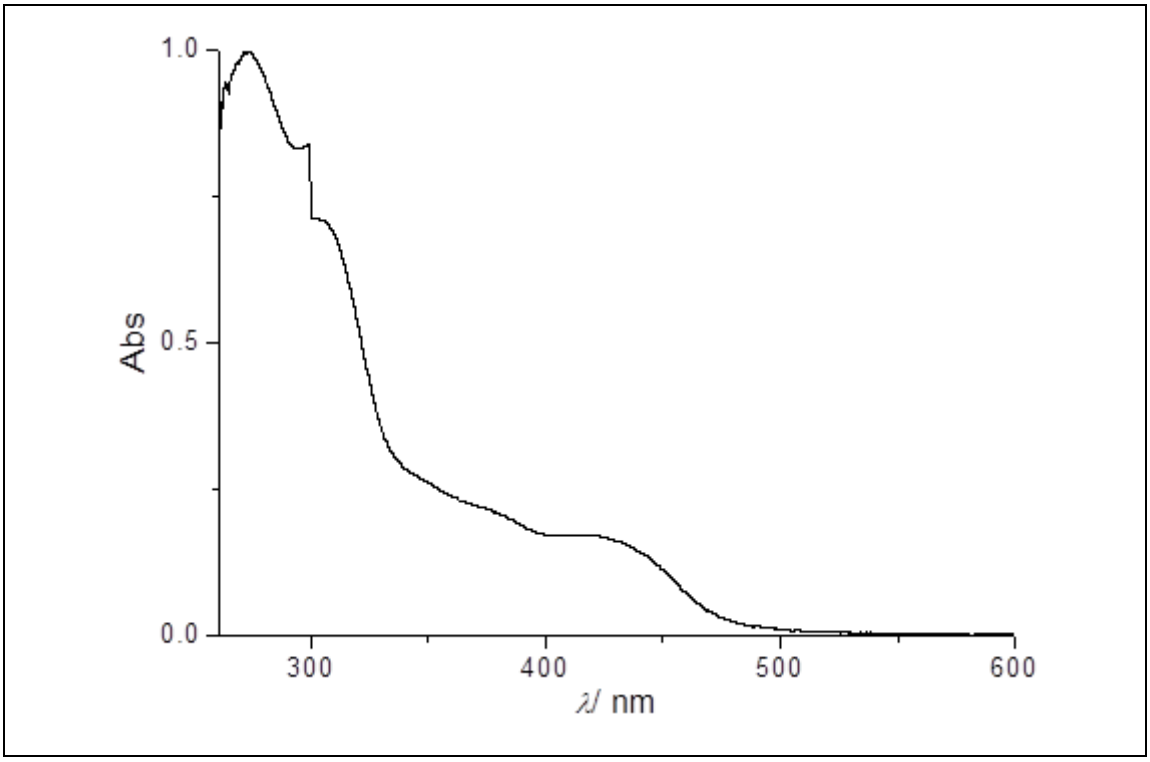
1.0
0.5
0.0
Abs
300
400
500
600
λ/ nm

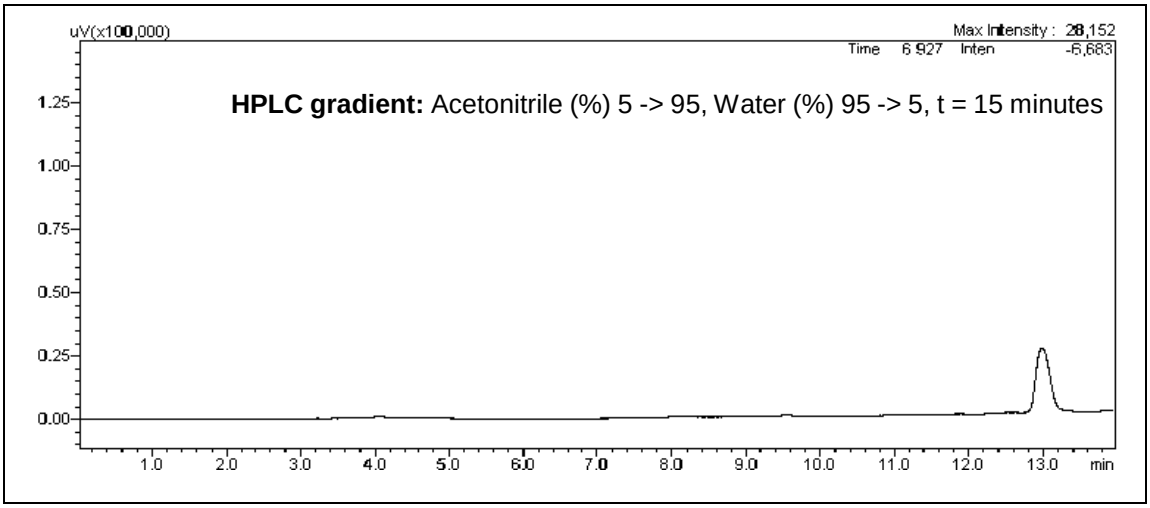
uV(x100,000)
Max Intensity : 28,152
Time 6.927 Inten -6,683
HPLC gradient: Acetonitrile (%) 5 -> 95, Water (%) 95 -> 5, t = 15 minutes
1.25
1.00
0.75
0.50
0.25
0.00
1.0
2.0
3.0
4.0
5.0
6.0
7.0
8.0
9.0
10.0
11.0
12.0
13.0
min

- **SMDC 67**

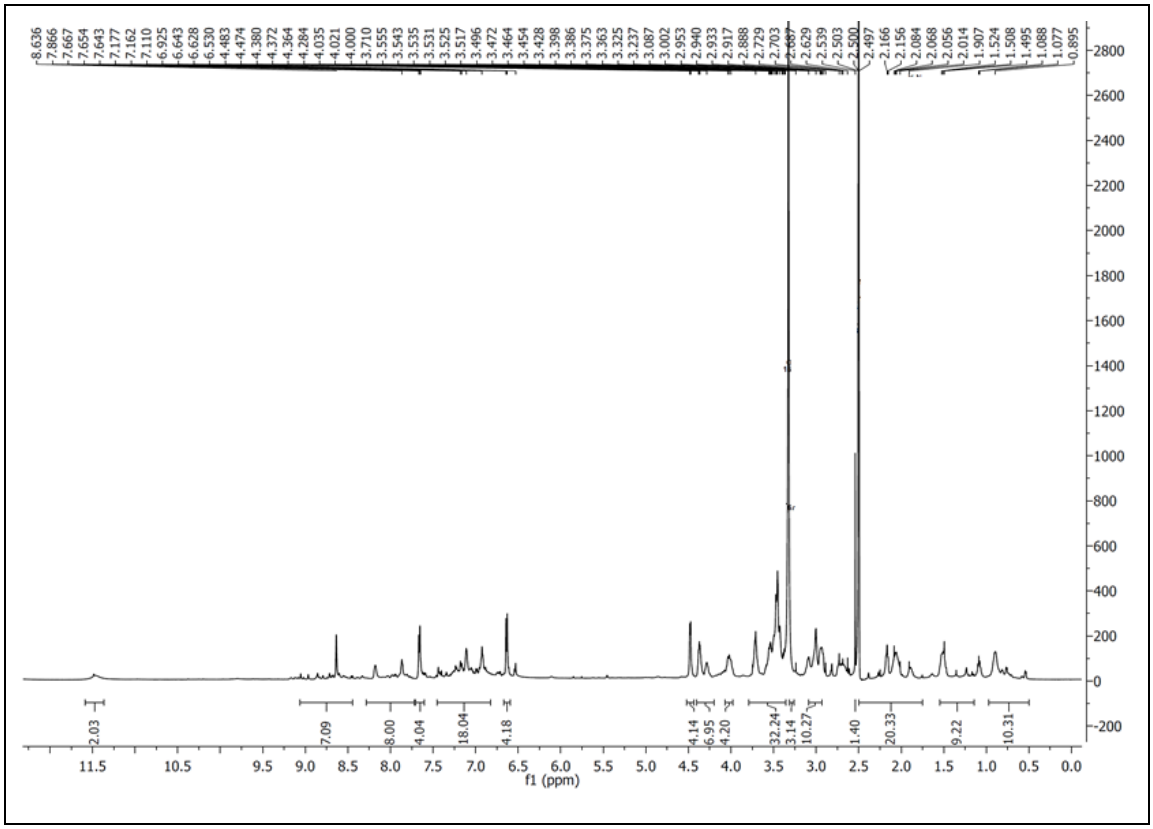
f1 (ppm)

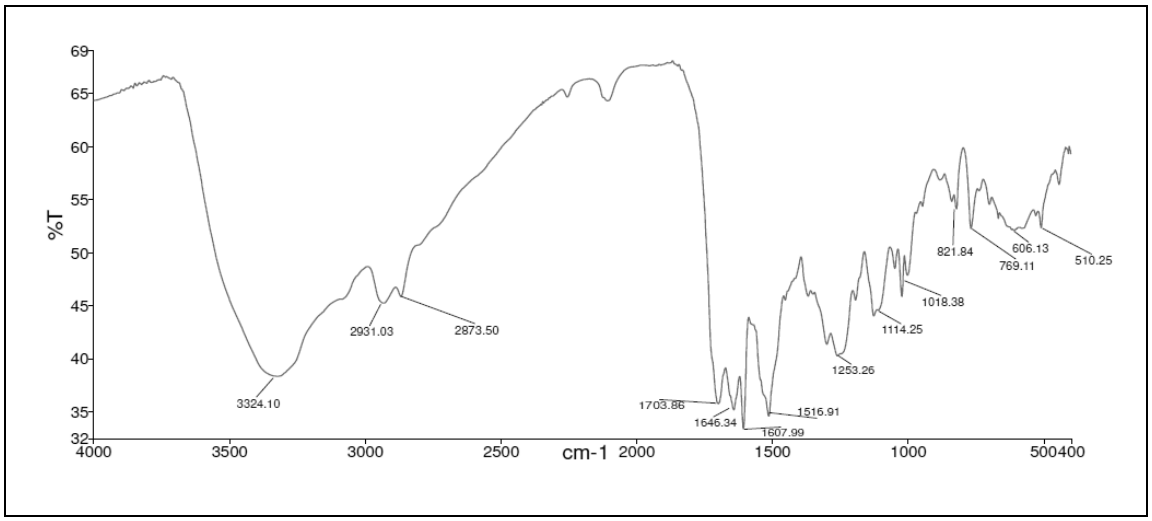
%T
cm-1
3324.10
2931.03
2873.50
1703.86
1646.34
1607.99
1516.91
1253.26
1114.25
1018.38
821.84
769.11
606.13
510.25

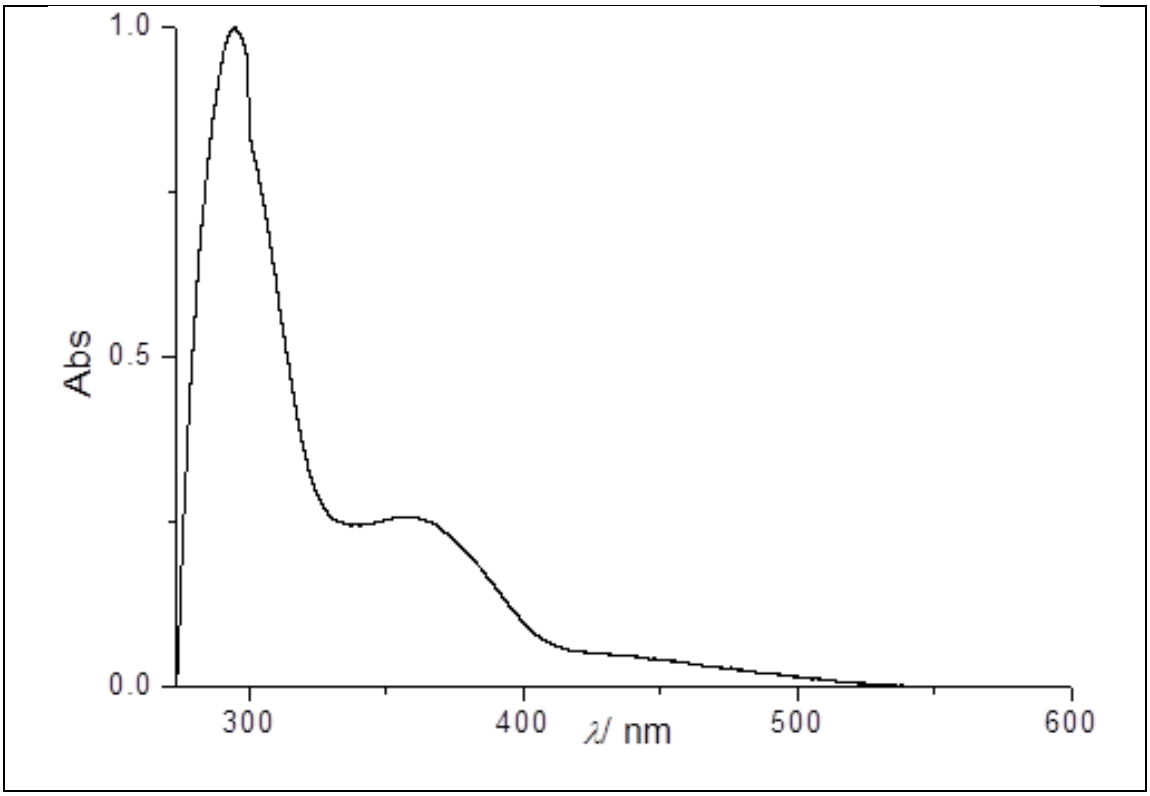
1.0
0.5
0.0
Abs
300
400
500
600
λ/ nm

- **B-complex 68’**

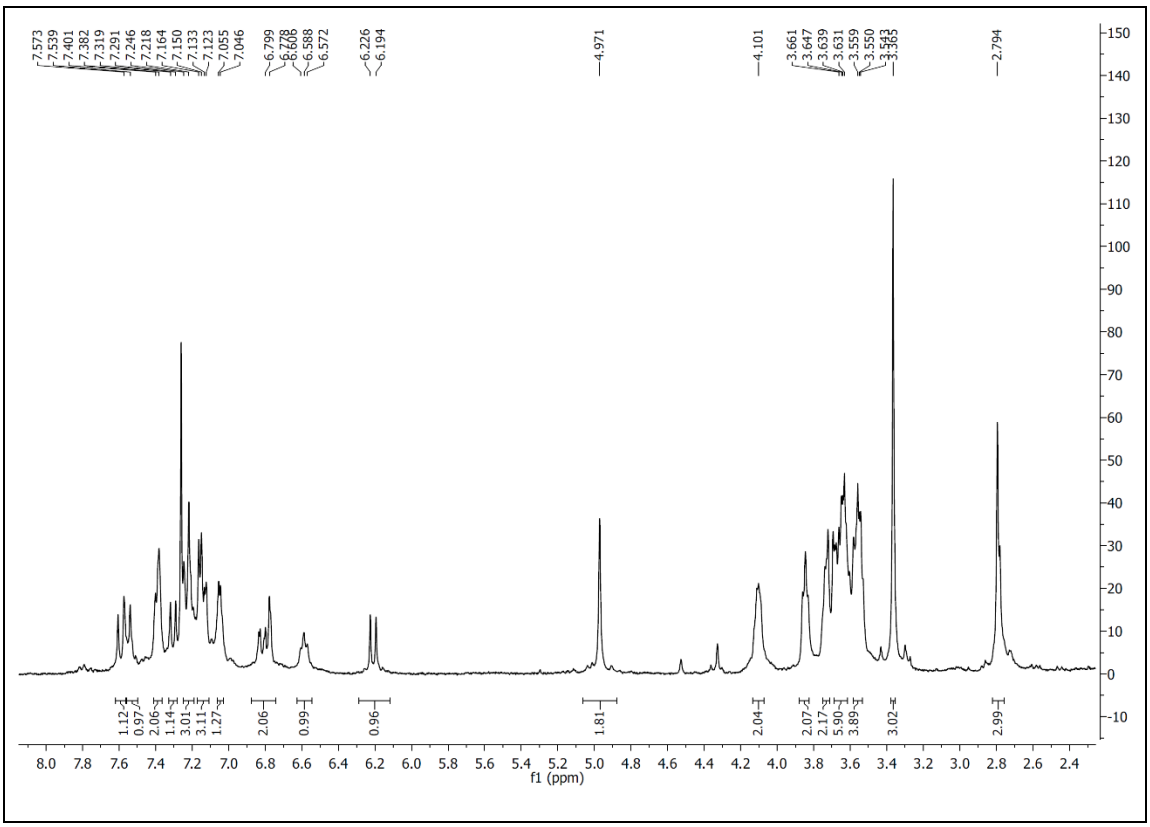
7.573
7.539
7.401
7.382
7.319
7.291
7.246
7.218
7.164
7.150
7.133
7.123
7.055
7.046
6.799
6.588
6.572
6.226
6.194
4.971
4.101
3.661
3.647
3.639
3.631
3.559
3.550
2.794
1.12
0.97
2.06
1.14
3.01
3.11
1.27
2.06
0.99
0.96
1.81
2.04
2.07
2.17
5.90
3.89
3.02
2.99
f1 (ppm)

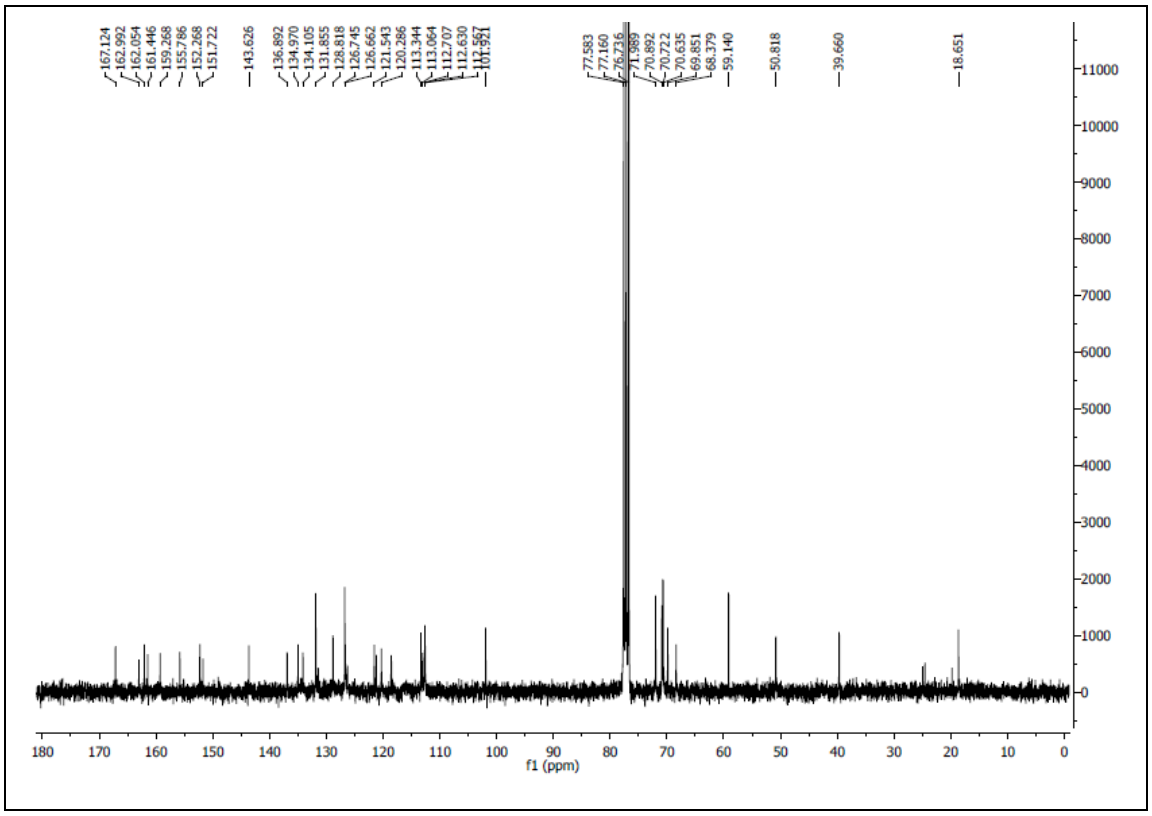
167.124
162.992
162.054
161.446
159.288
155.786
152.268
151.722
143.626
136.892
134.970
134.105
131.855
128.818
126.745
126.662
121.543
120.286
113.344
113.064
112.707
112.630
101.921
77.583
77.160
76.736
71.989
70.892
70.722
70.635
69.851
68.379
59.140
50.818
39.660
18.651
f1 (ppm)

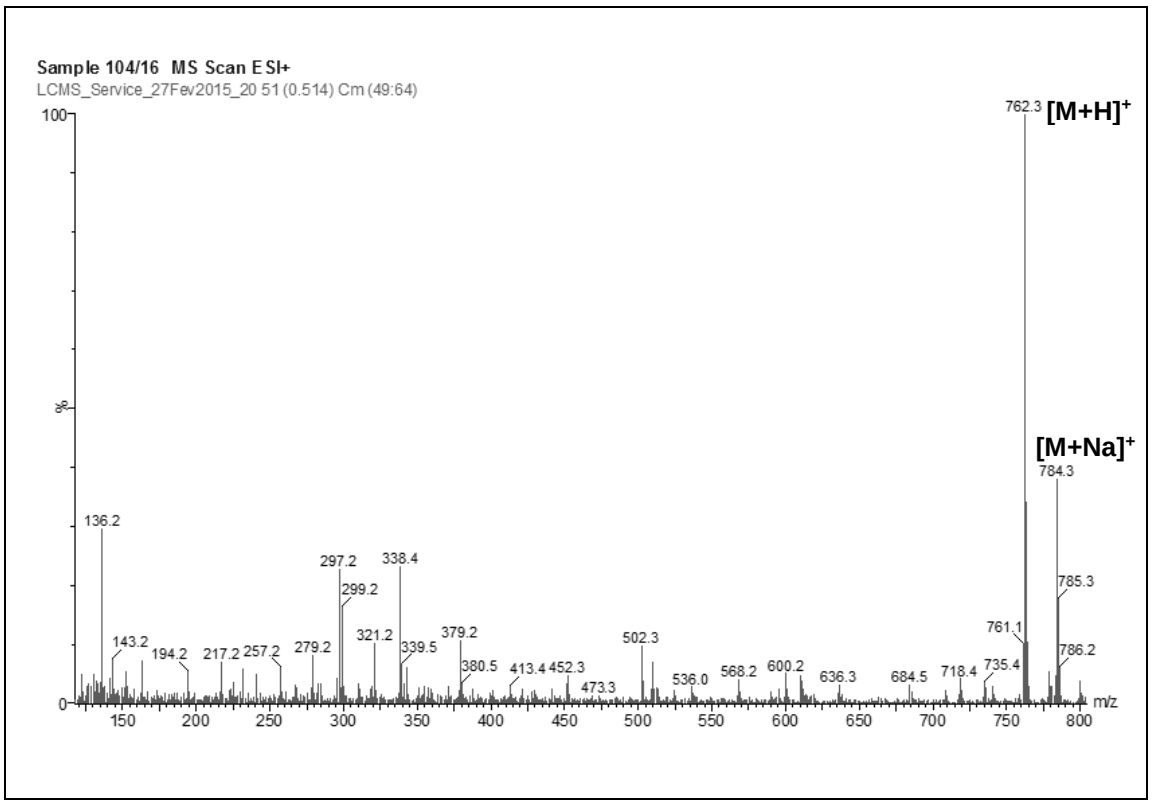
Sample 104/16 MS Scan ESI+
LCMS_Service_27Fev2015_20 51 (0.514) Cm (49:64)
762.3 [M+H]+
[M+Na]+
784.3
136.2
297.2
338.4
299.2
785.3
761.1
143.2
194.2
217.2
257.2
279.2
321.2
339.5
379.2
502.3
786.2
380.5
413.4
452.3
473.3
536.0
568.2
600.2
636.3
684.5
718.4
735.4
%
m/z

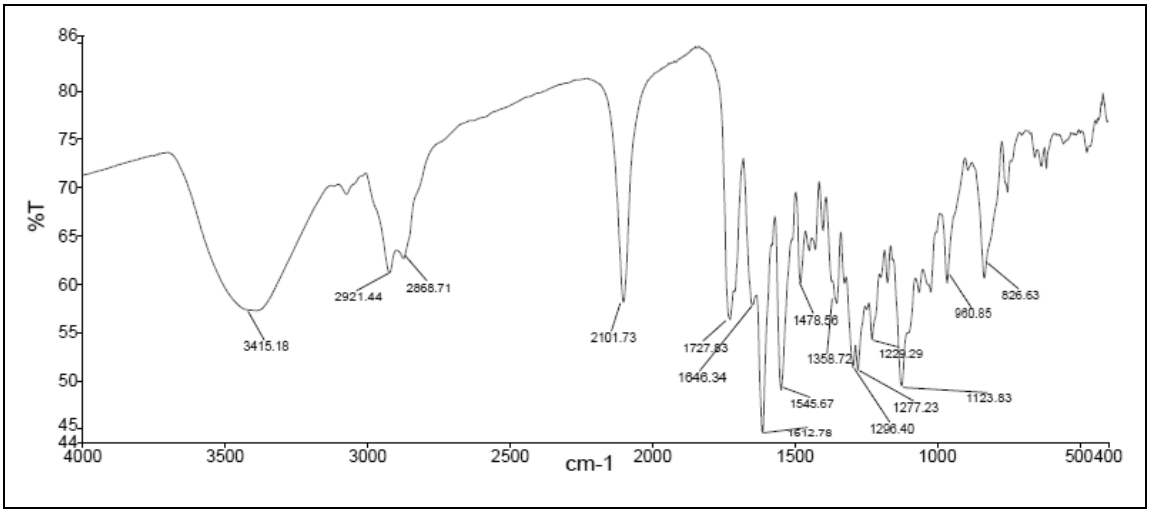
%T
cm-1
3415.18
2921.44
2868.71
2101.73
1727.83
1646.34
1545.67
1612.78
1478.56
1358.72
1296.40
1277.23
1229.29
1123.83
960.85
826.63

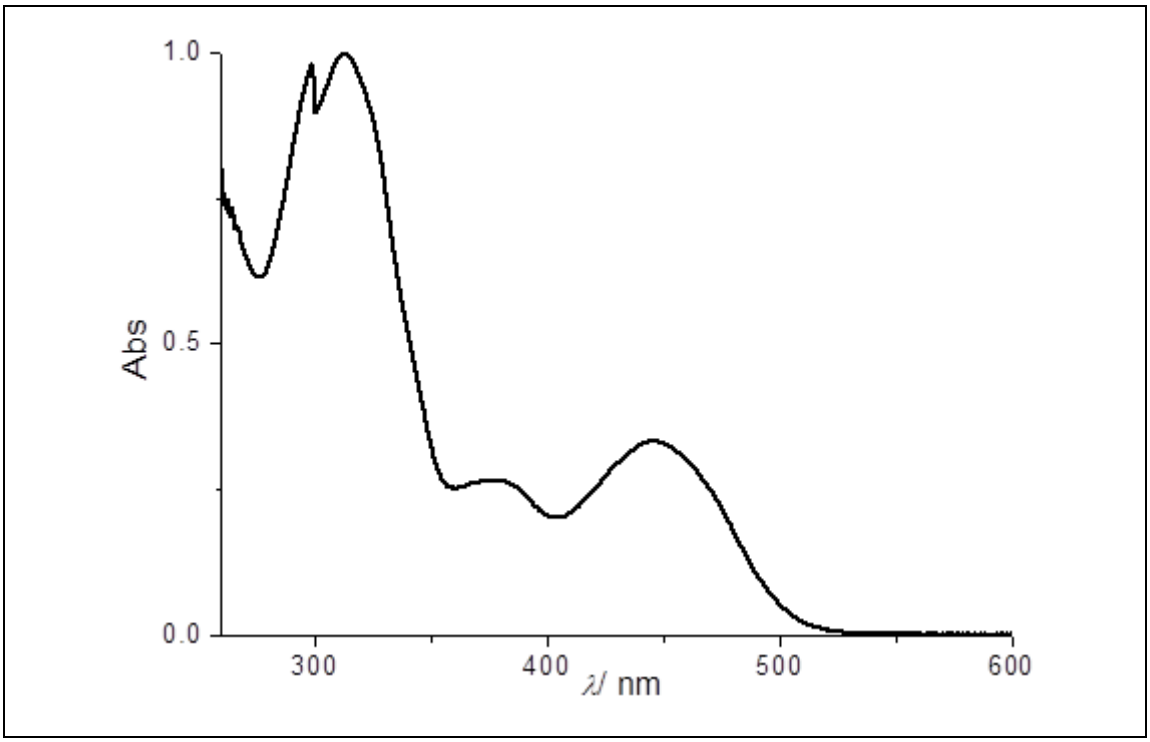
Abs
λ/ nm

- **Conjugate 68**

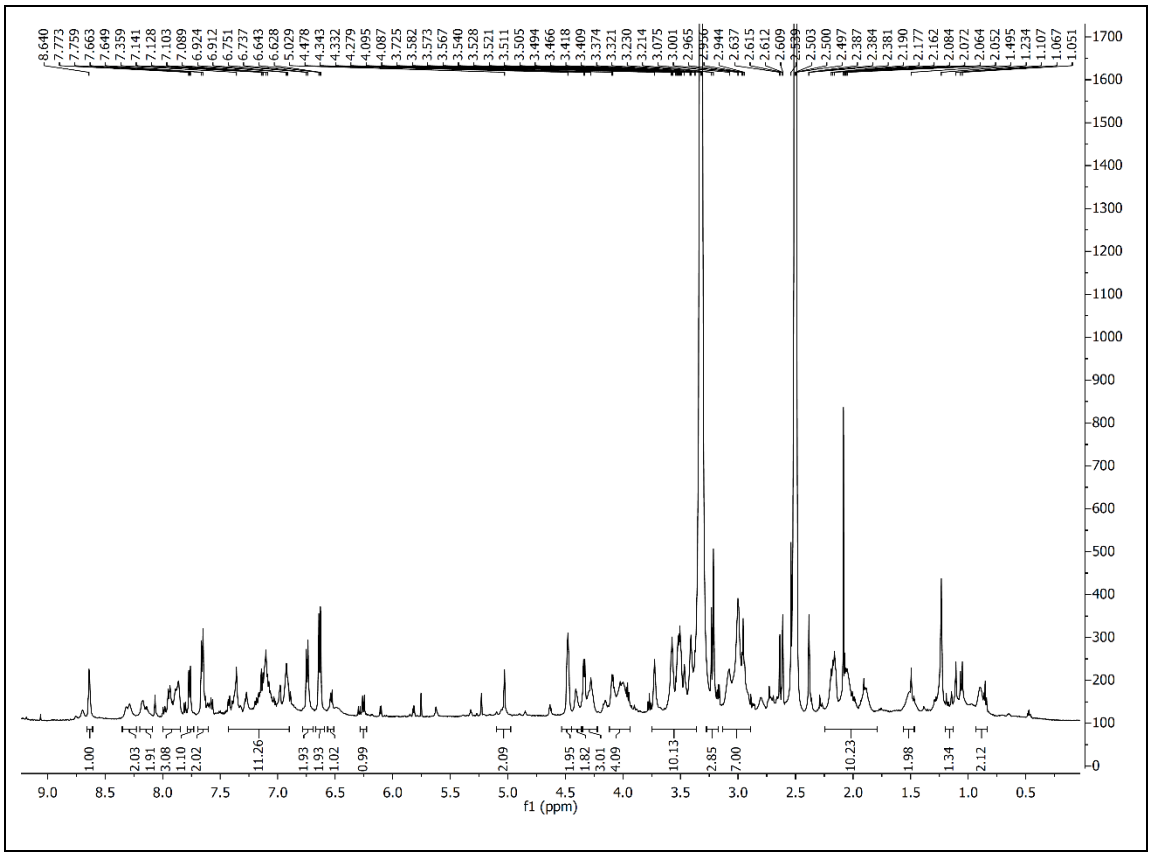

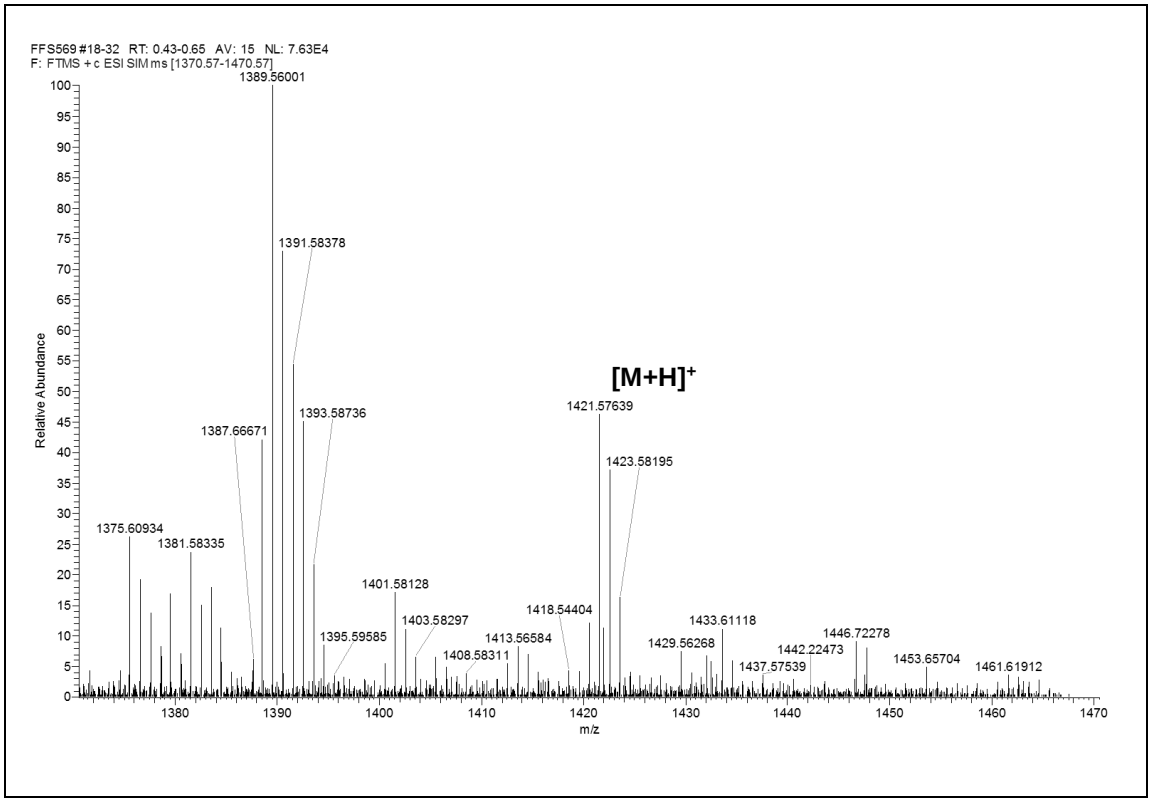

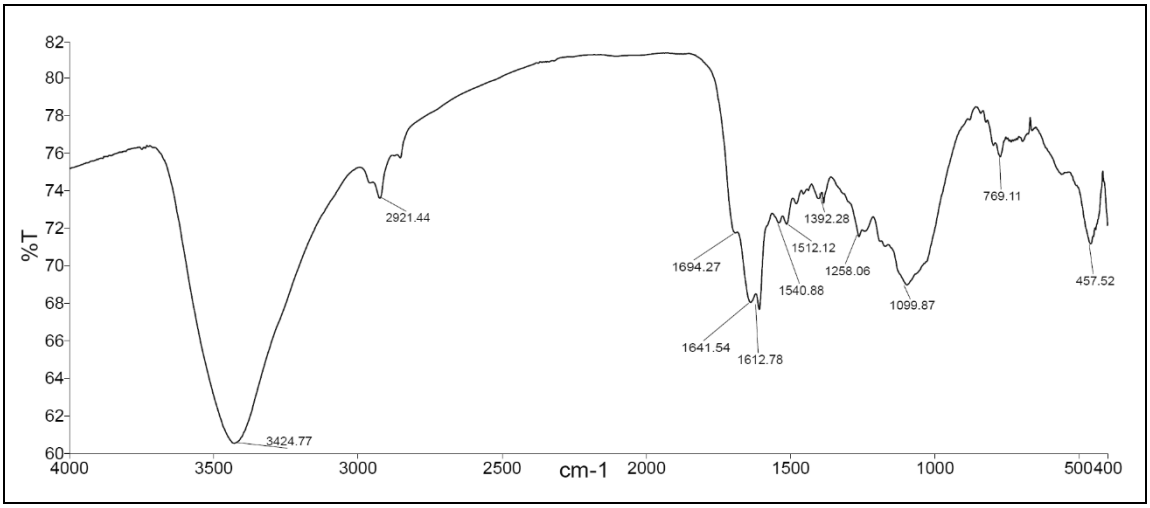
%T
cm-1
3424.77
2921.44
1694.27
1641.54
1612.78
1540.88
1512.12
1392.28
1258.06
1099.87
769.11
457.52

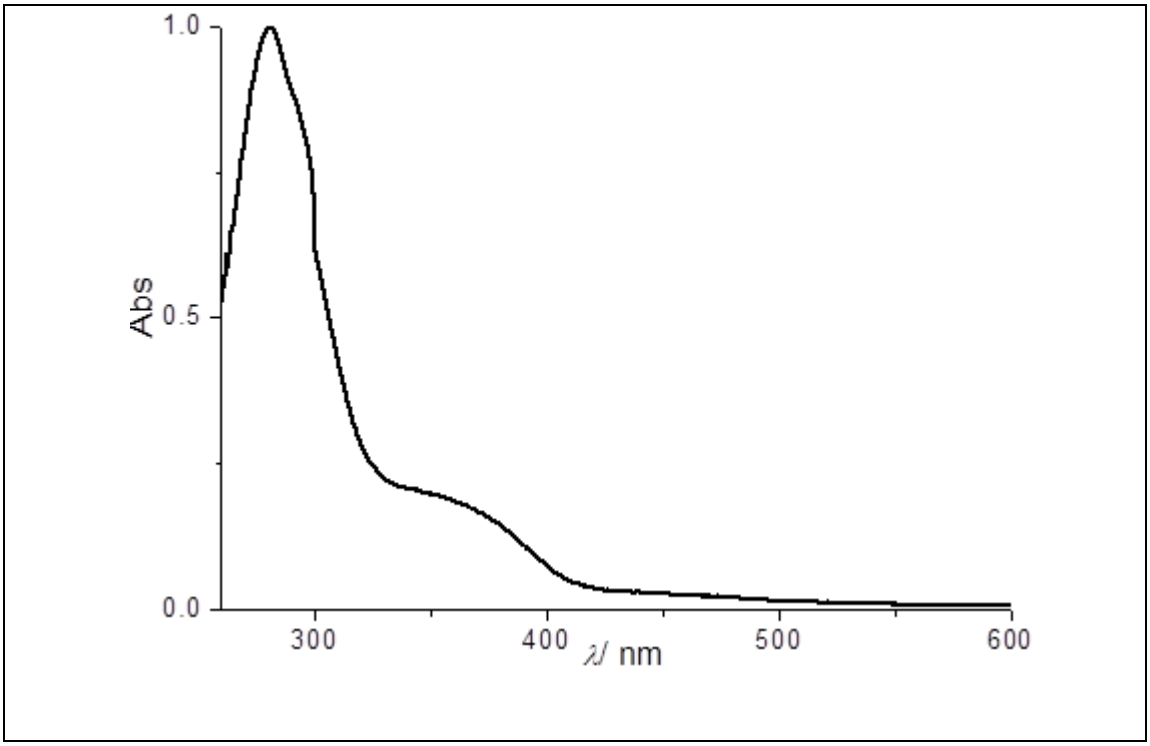
Abs
λ/ nm

- **B-complex 72**

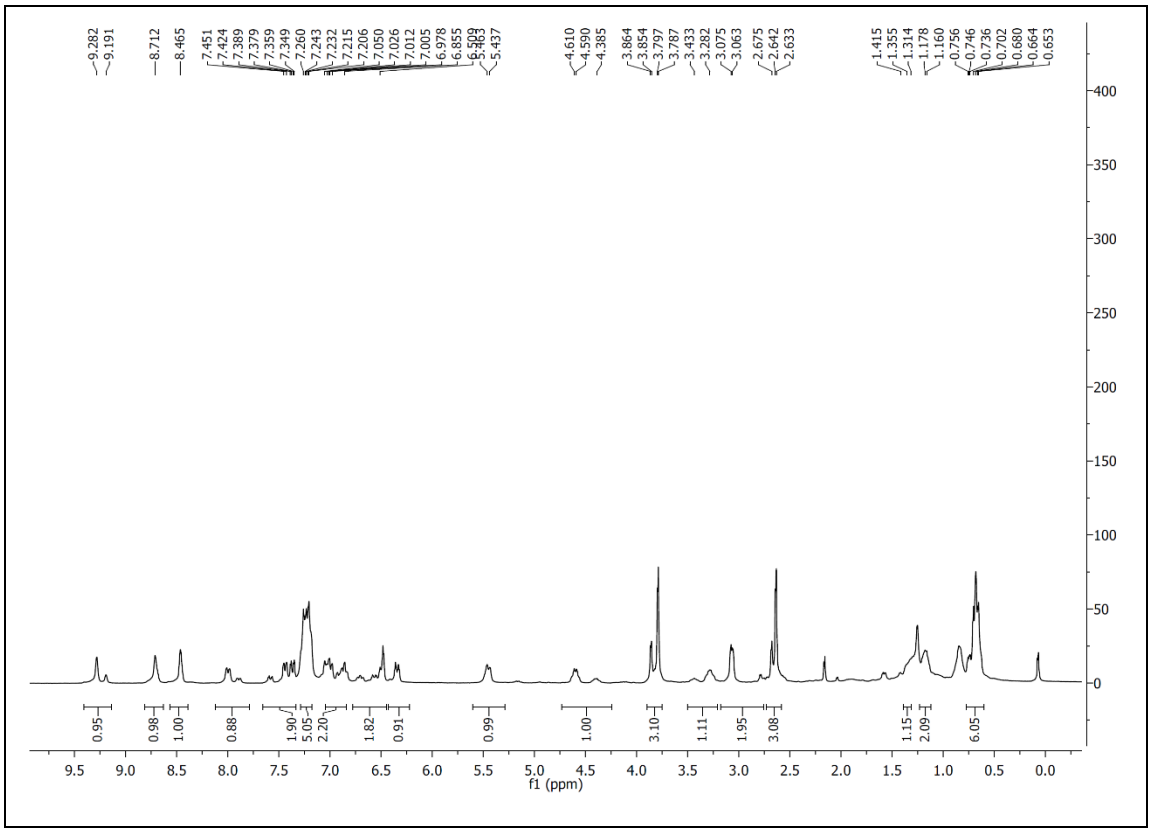
9.282
9.191
8.712
8.465
7.451
7.424
7.389
7.379
7.359
7.349
7.260
7.243
7.232
7.215
7.206
7.050
7.026
7.012
7.005
6.978
6.855
5.437
4.610
4.590
4.385
3.864
3.854
3.797
3.787
3.433
3.282
3.075
3.063
2.675
2.642
2.633
1.415
1.355
1.314
1.178
1.160
0.756
0.746
0.736
0.702
0.680
0.664
0.653
0.95
0.98
1.00
0.88
1.90
5.05
2.20
1.82
0.91
0.99
1.00
3.10
1.11
1.95
3.08
1.15
2.09
6.05
f1 (ppm)

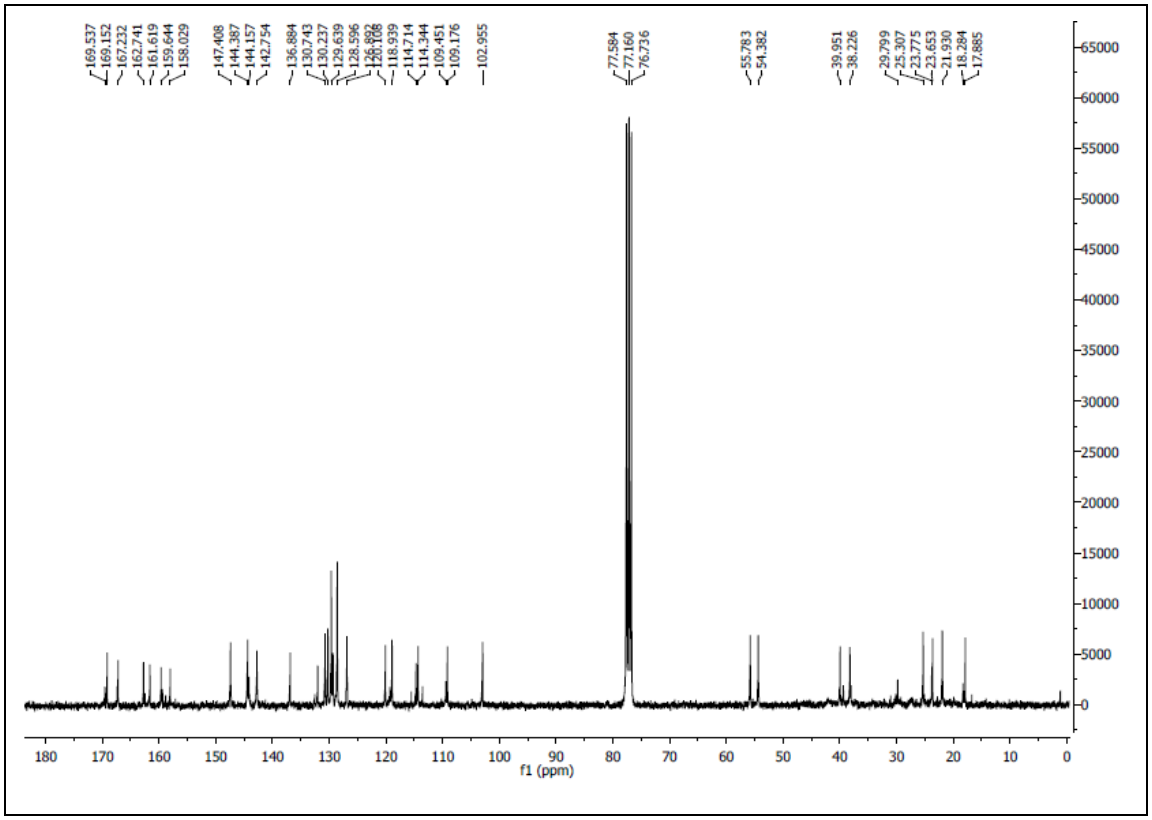
169.537
169.152
167.232
162.741
161.619
159.644
158.029
147.408
144.387
144.157
142.754
136.884
130.743
130.237
129.639
128.596
126.892
120.108
118.939
114.714
114.344
109.451
109.176
102.955
77.584
77.160
76.736
55.783
54.382
39.951
38.226
29.799
25.307
23.775
23.653
21.930
18.284
17.885
f1 (ppm)

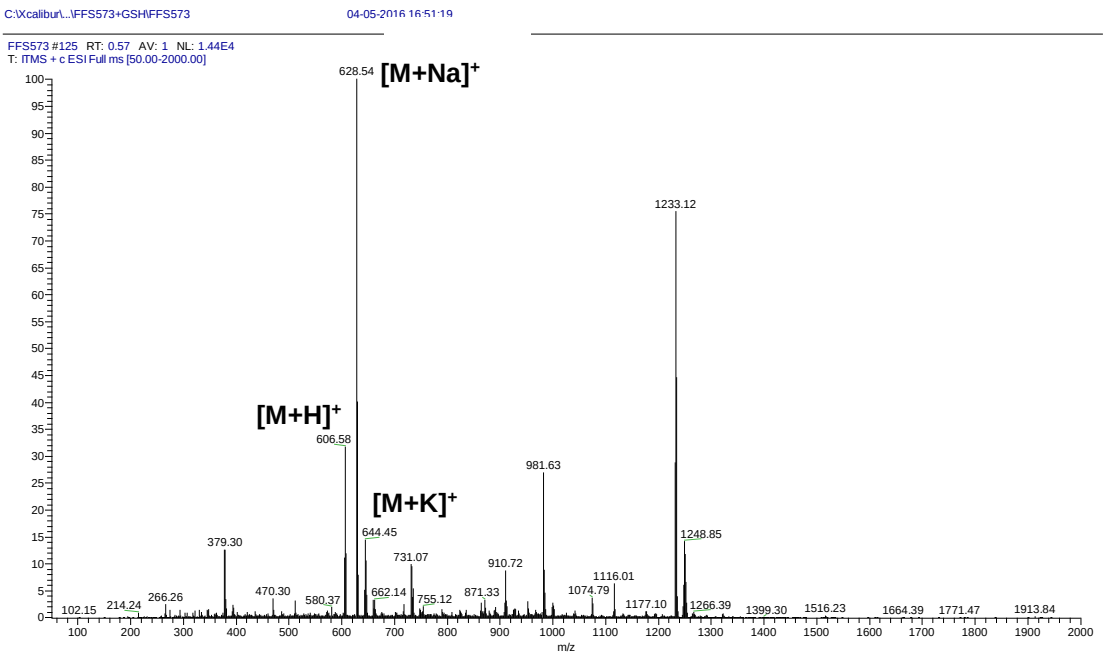

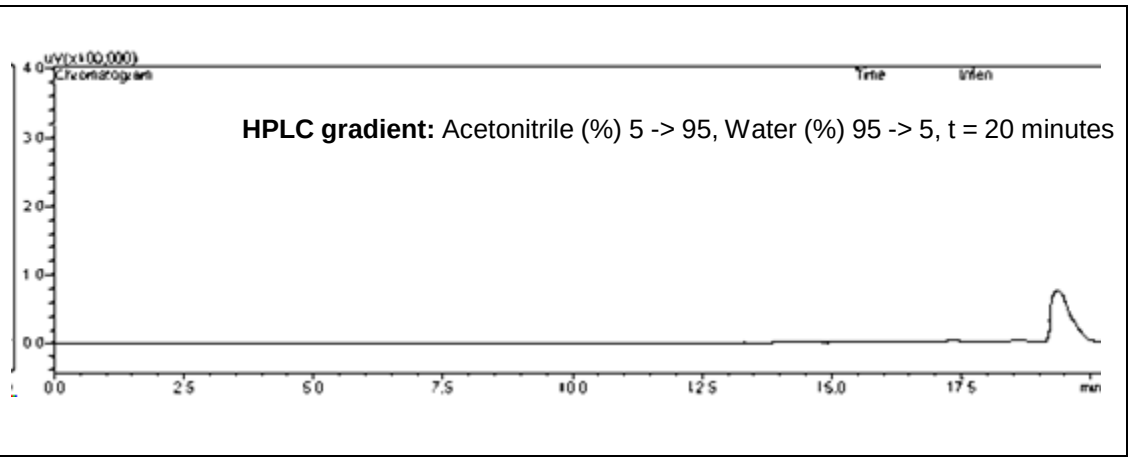

HPLC gradient: Acetonitrile (%) 5 -> 95, Water (%) 95 -> 5, t = 20 minutes

- **Folic acid-cyclooctyne 61**

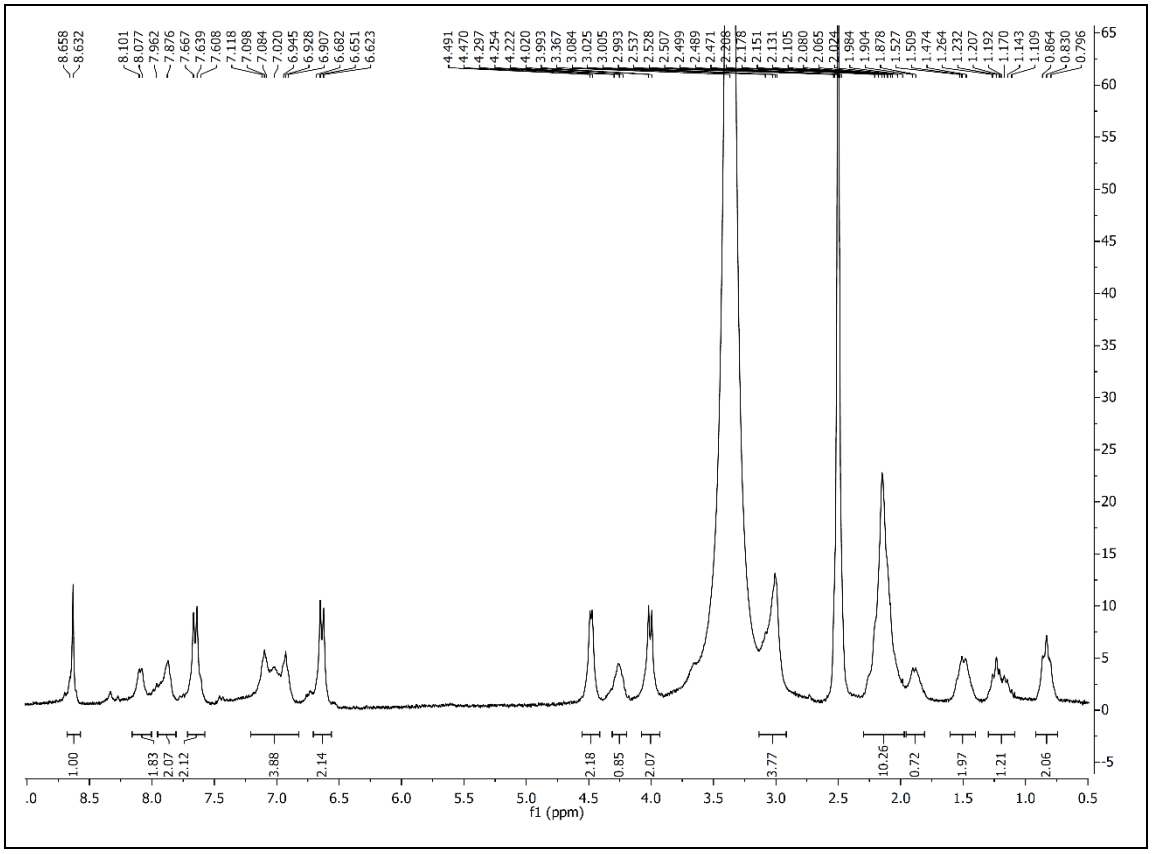

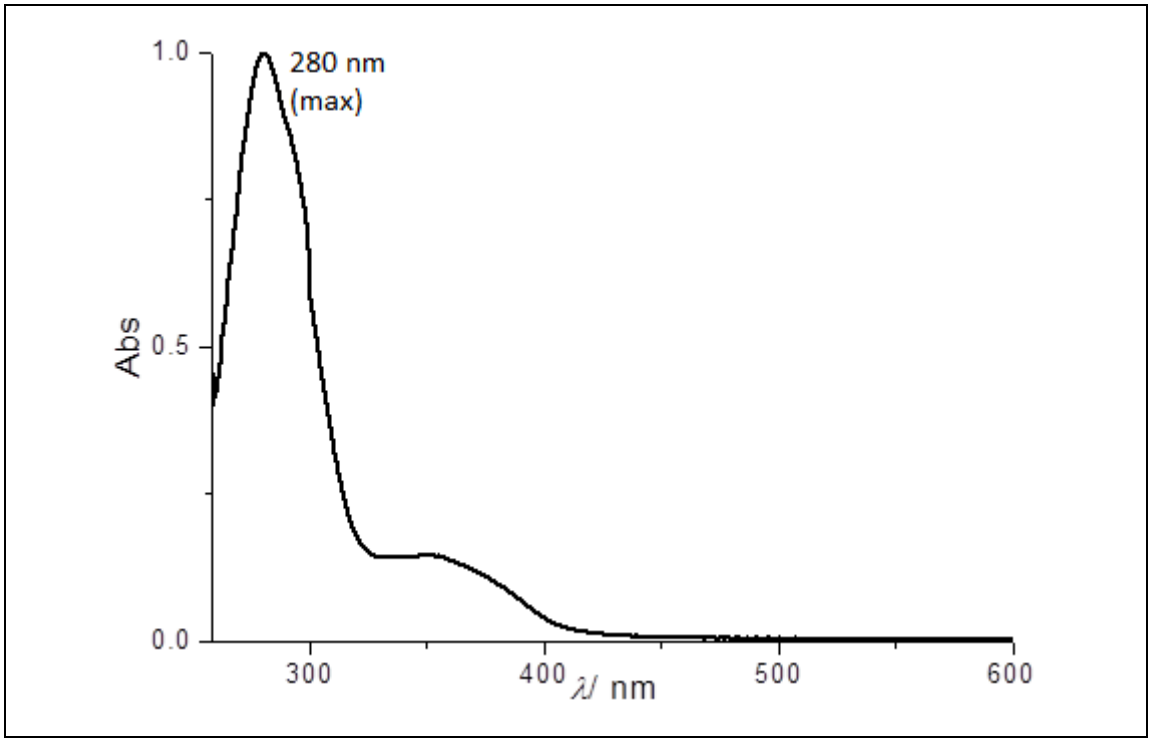

- **Bortezomib**

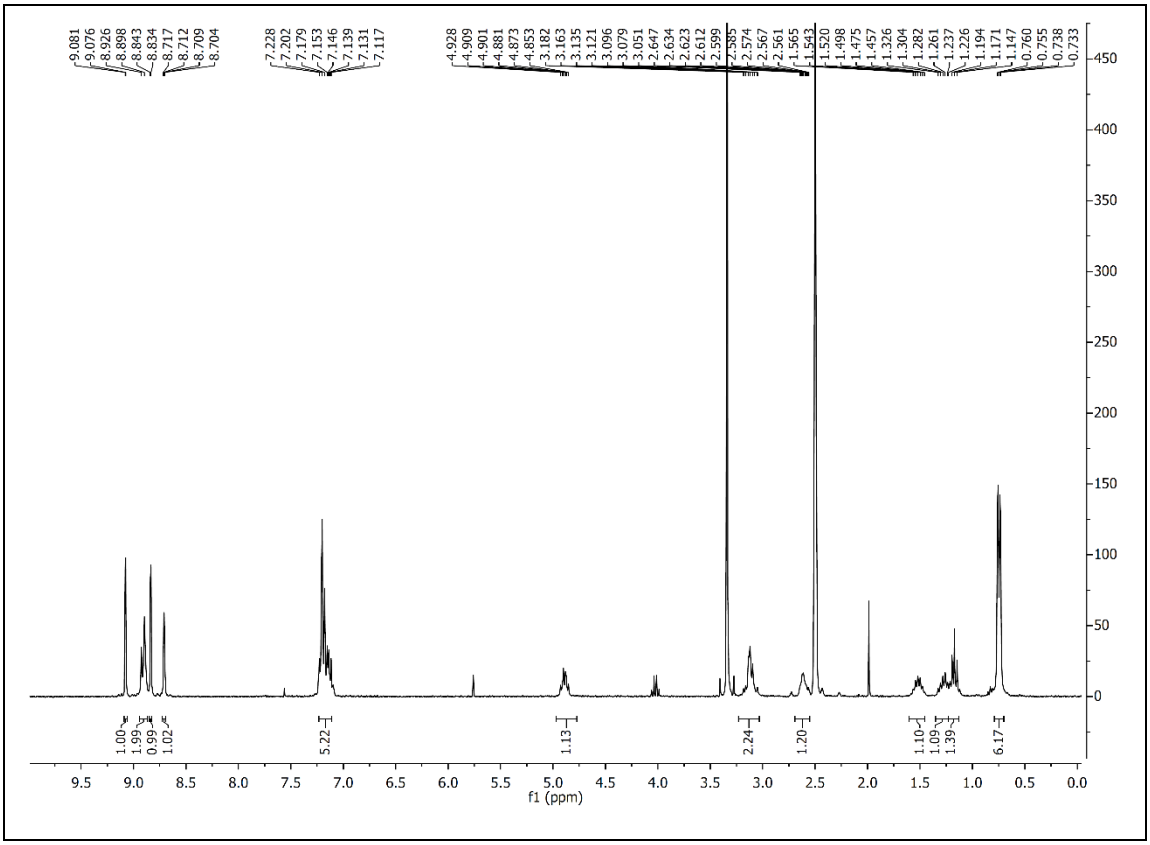

- **Salicylhydrazone 76a**

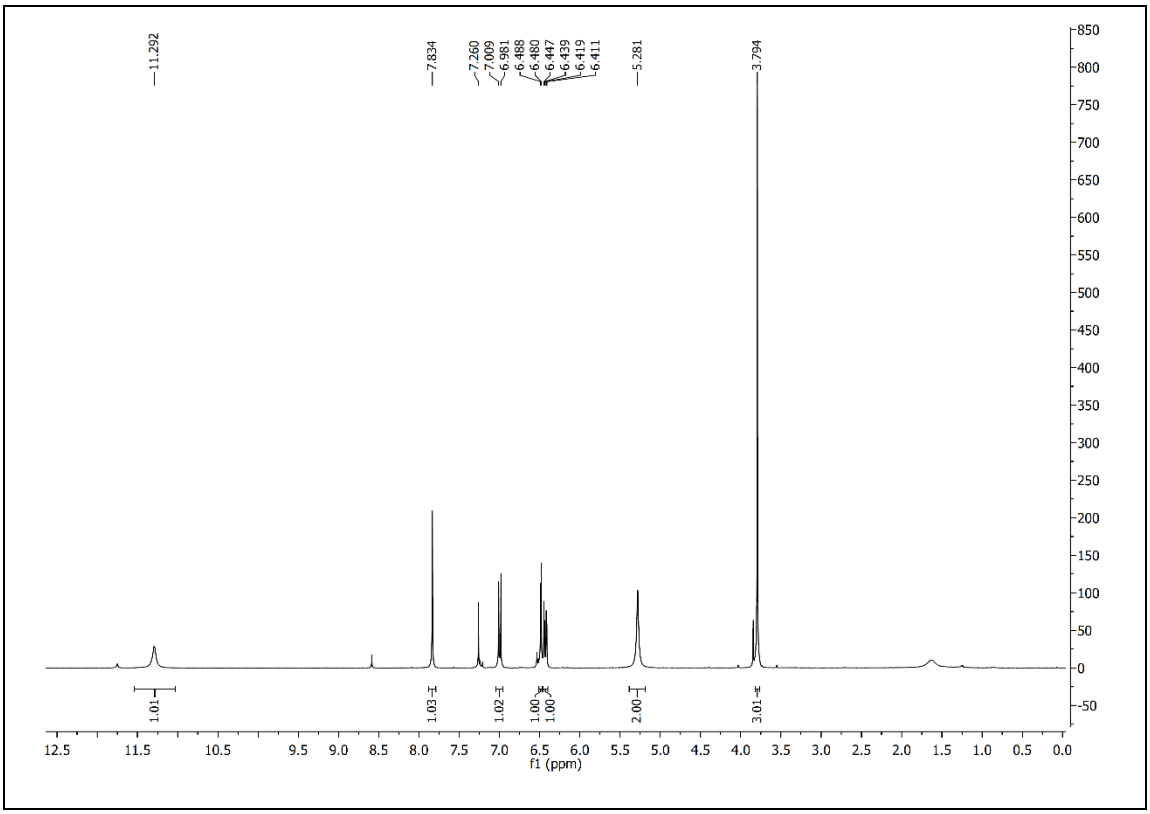

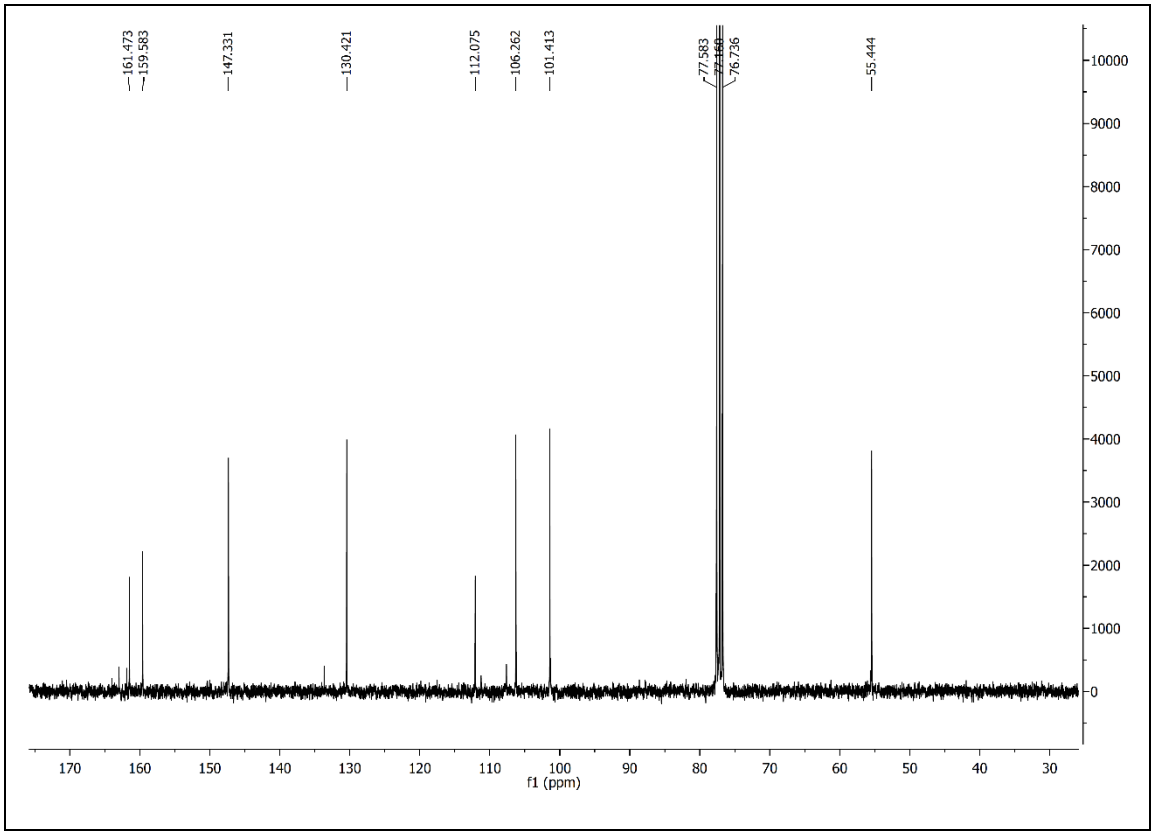
161.473
159.583
147.331
130.421
112.075
106.262
101.413
77.583
77.160
76.736
55.444
10000
9000
8000
7000
6000
5000
4000
3000
2000
1000
0
170 160 150 140 130 120 110 100 90 80 70 60 50 40 30
f1 (ppm)

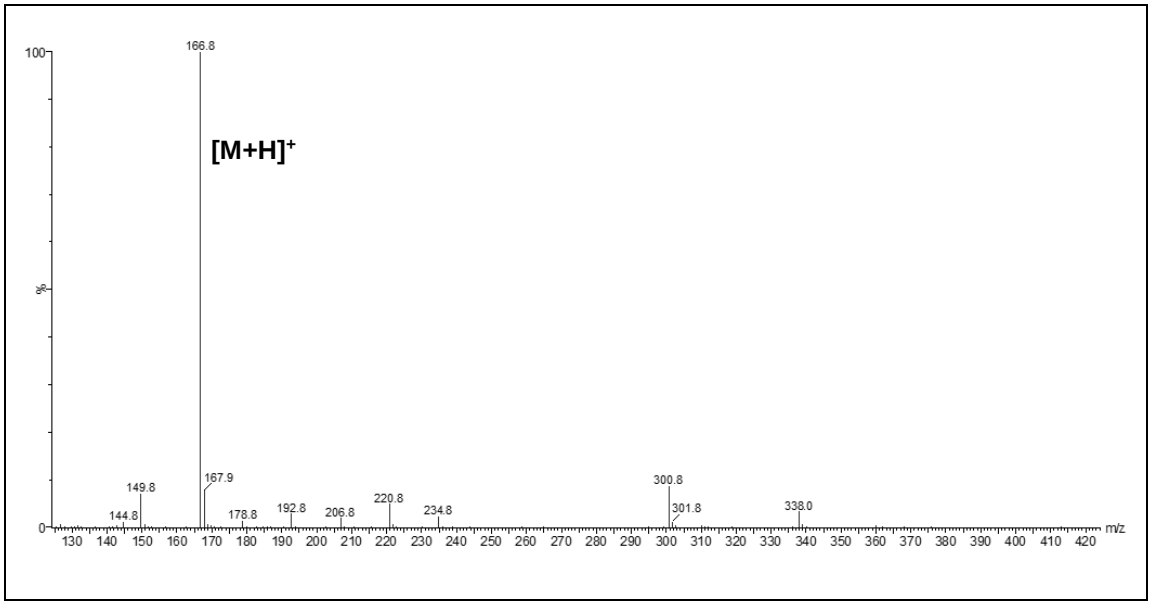
166.8
[M+H]+
100
%
0
149.8
144.8
167.9
178.8
192.8
206.8
220.8
234.8
300.8
301.8
338.0
130 140 150 160 170 180 190 200 210 220 230 240 250 260 270 280 290 300 310 320 330 340 350 360 370 380 390 400 410 420
m/z

- **Salicylhydrazone 76b**

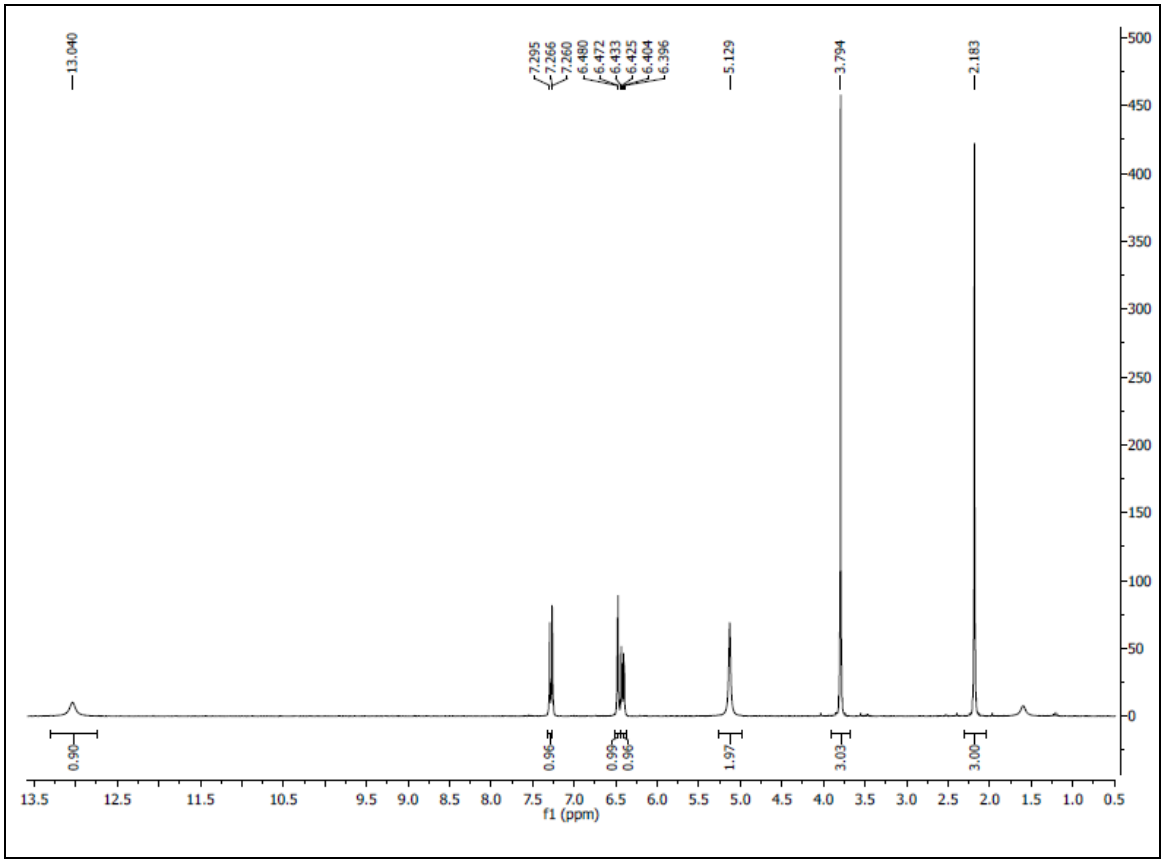

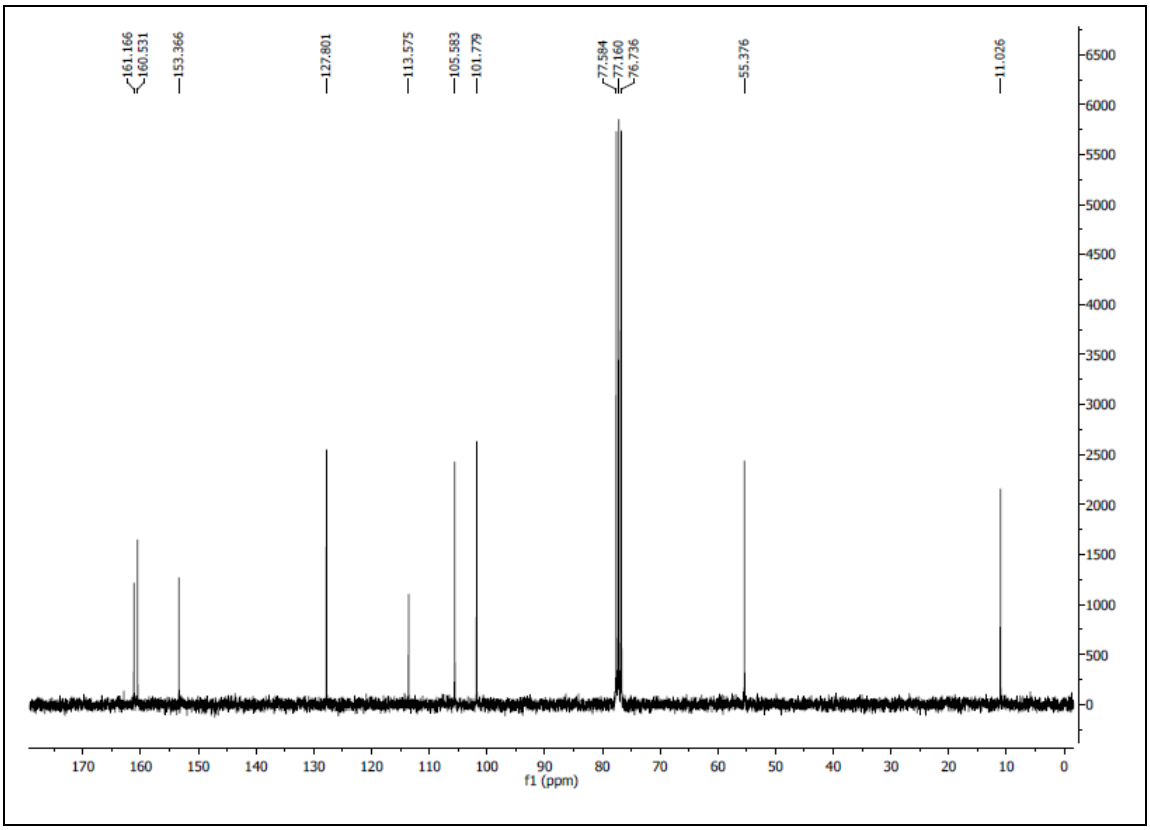

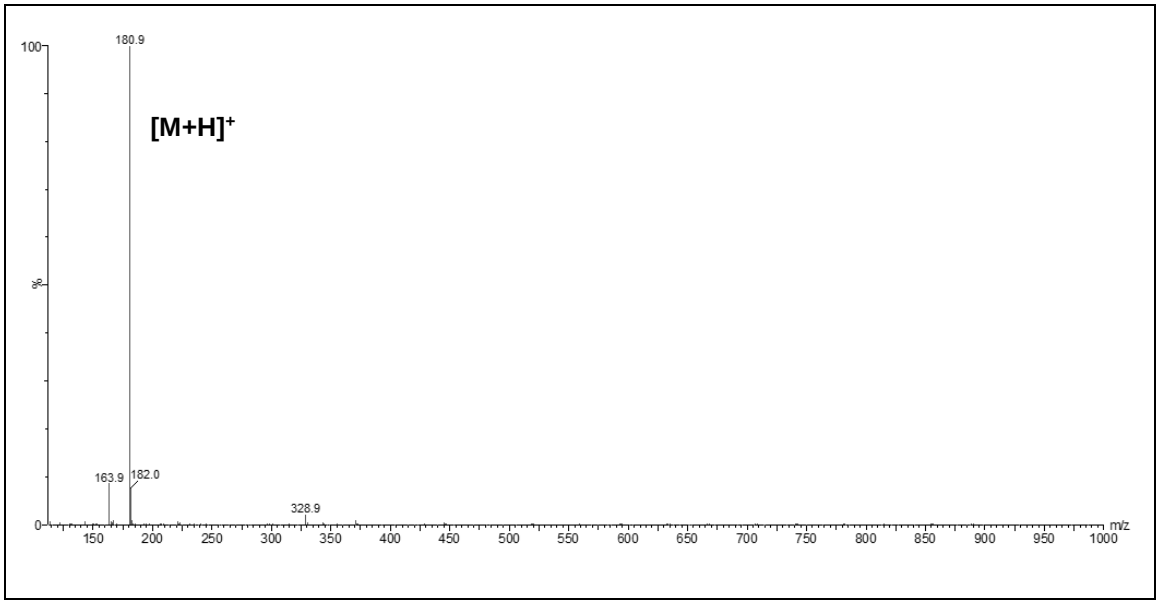

- **Salicylhydrazone 76c**

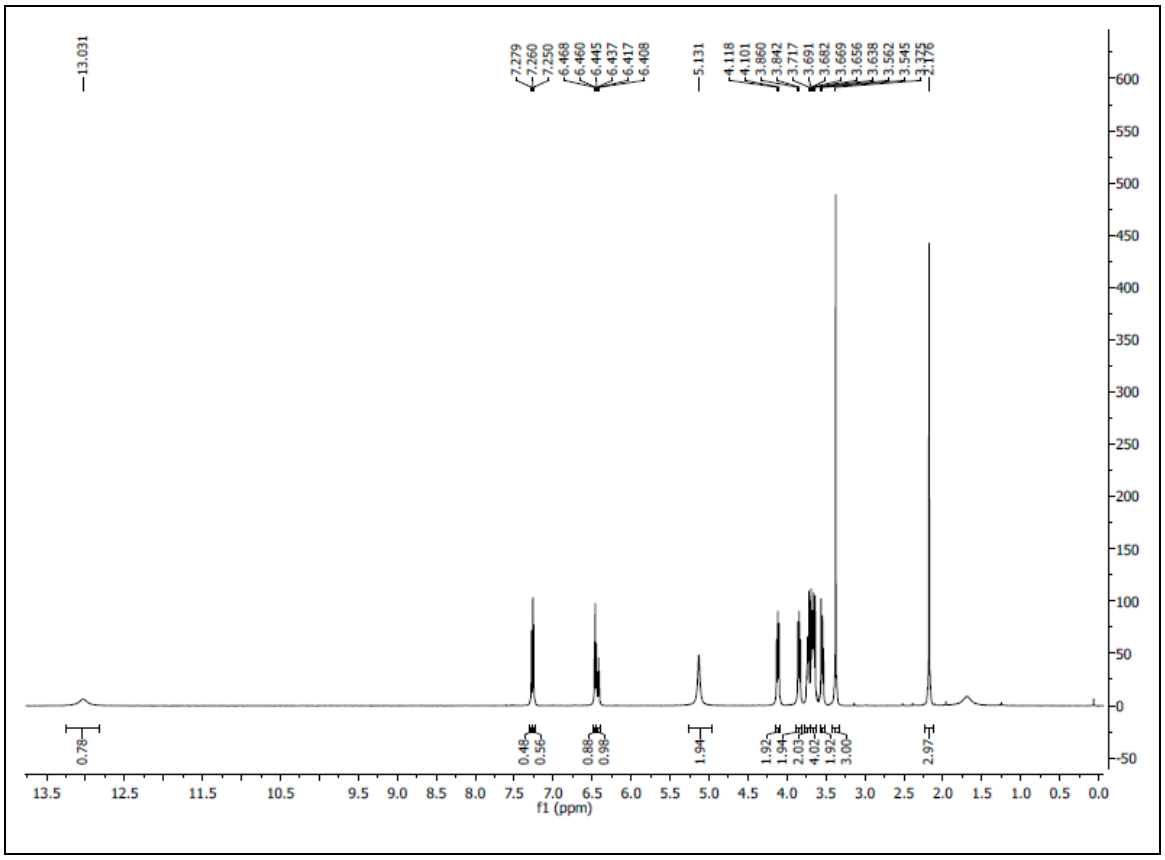

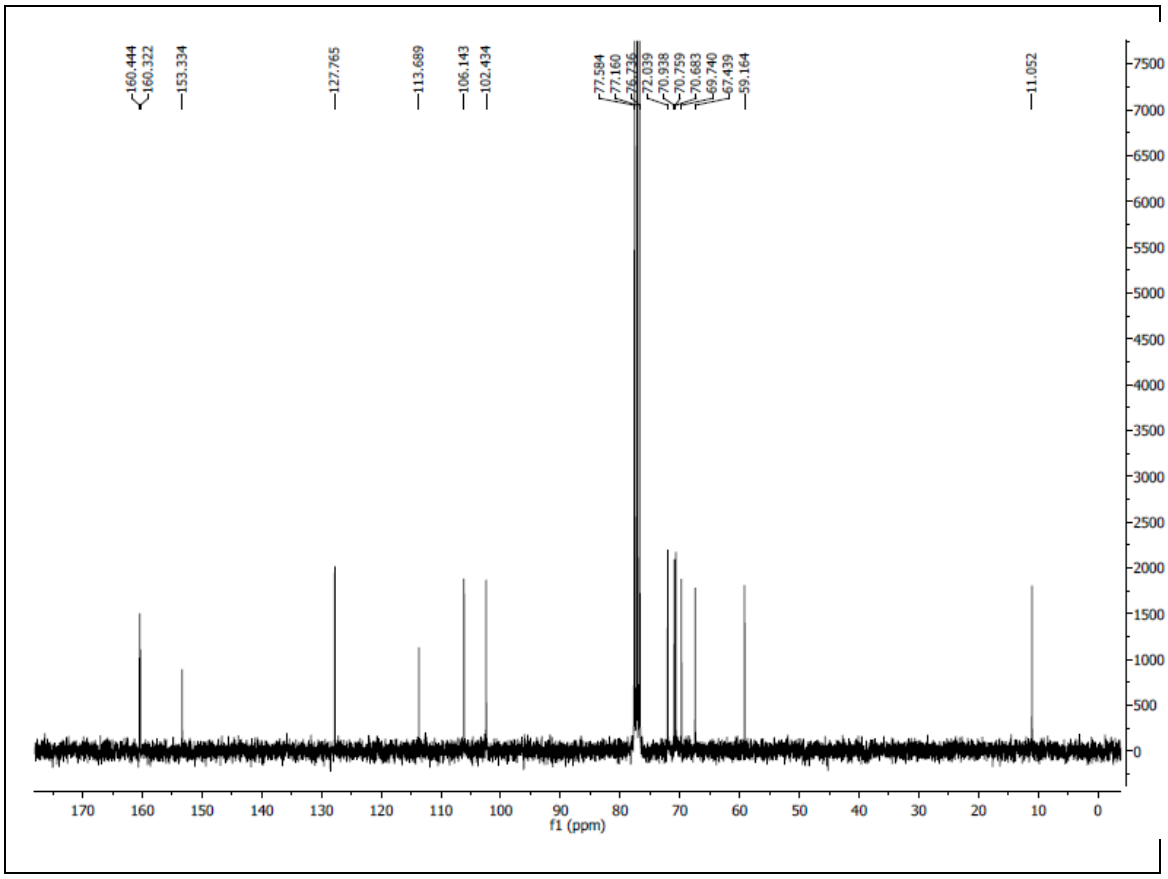
160.444
160.322
153.334
127.765
113.689
106.143
102.434
77.584
77.160
76.736
72.039
70.938
70.759
70.683
69.740
67.439
59.164
11.052
f1 (ppm)

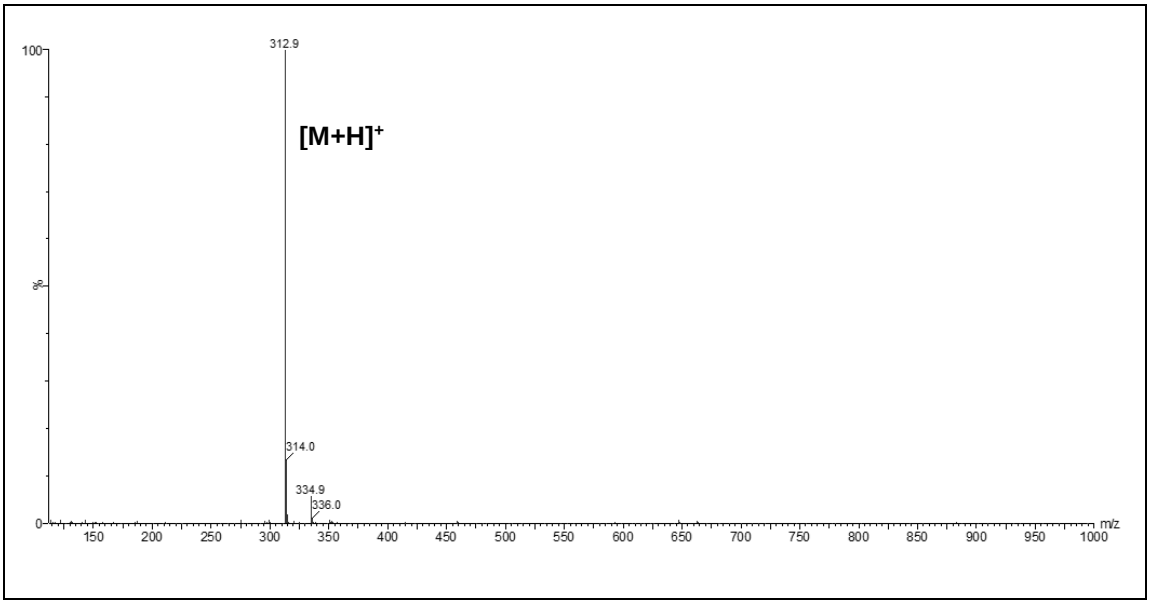
312.9
[M+H]+
314.0
334.9
336.0
%
m/z

- **BASHY 78a**

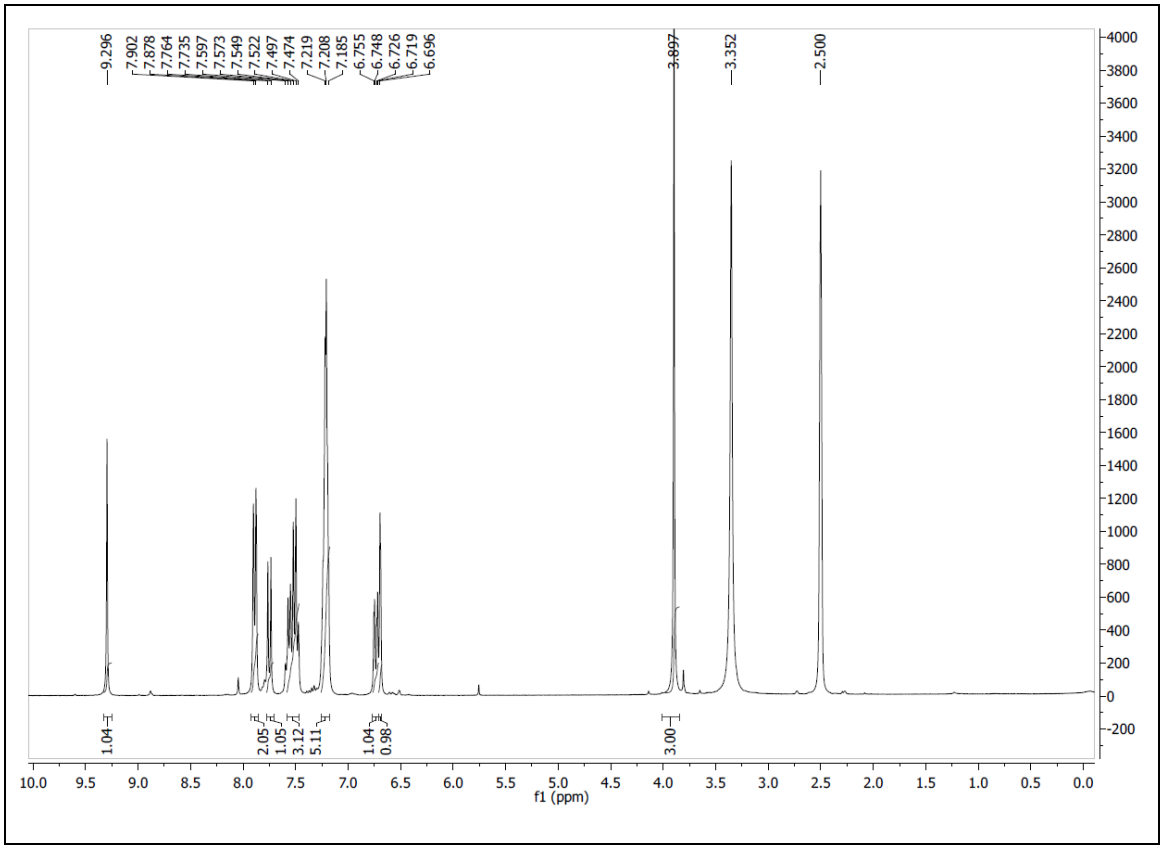
9.296
7.902
7.878
7.764
7.735
7.597
7.573
7.549
7.522
7.497
7.474
7.219
7.208
7.185
6.755
6.748
6.726
6.719
6.696
3.897
3.352
2.500
1.04
2.05
1.05
3.12
5.11
1.04
0.98
3.00
f1 (ppm)

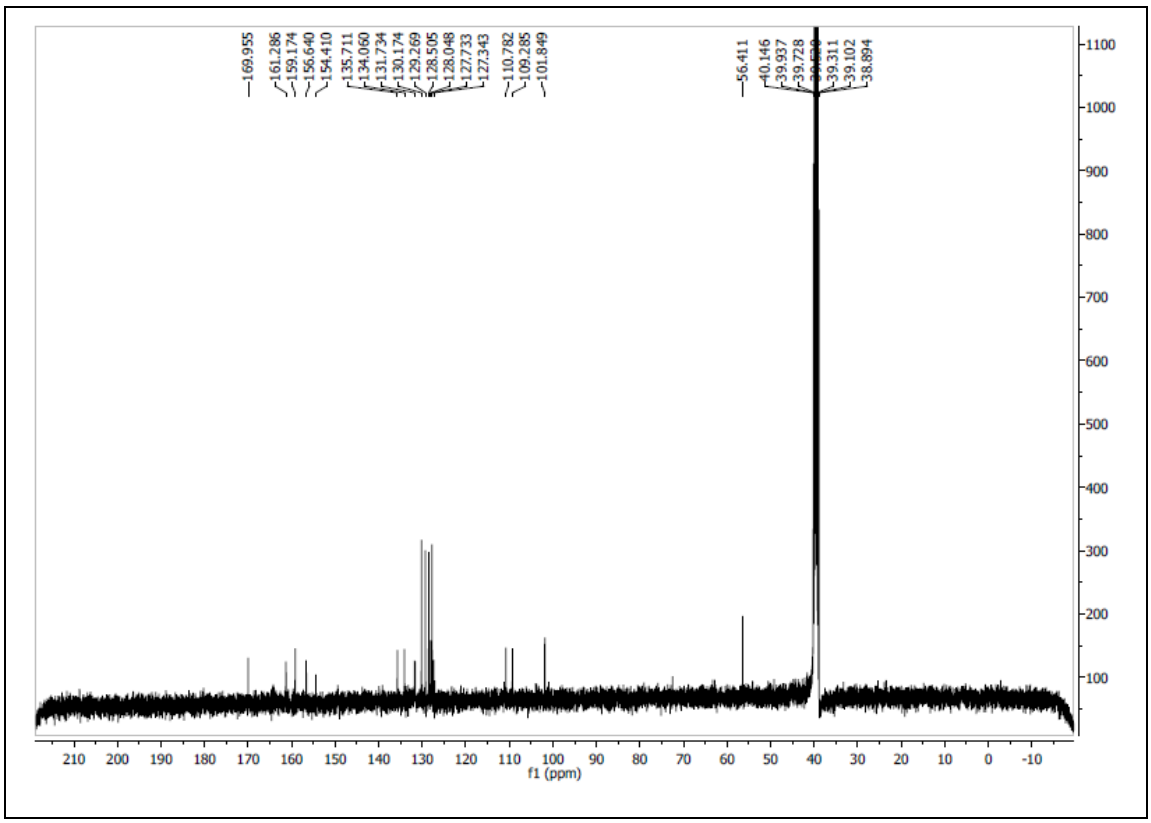
169.955
161.286
159.174
156.640
154.410
135.711
134.060
131.734
130.174
129.269
128.505
128.048
127.733
127.343
110.782
109.285
101.849
56.411
40.146
39.937
39.728
39.311
39.102
38.894
f1 (ppm)

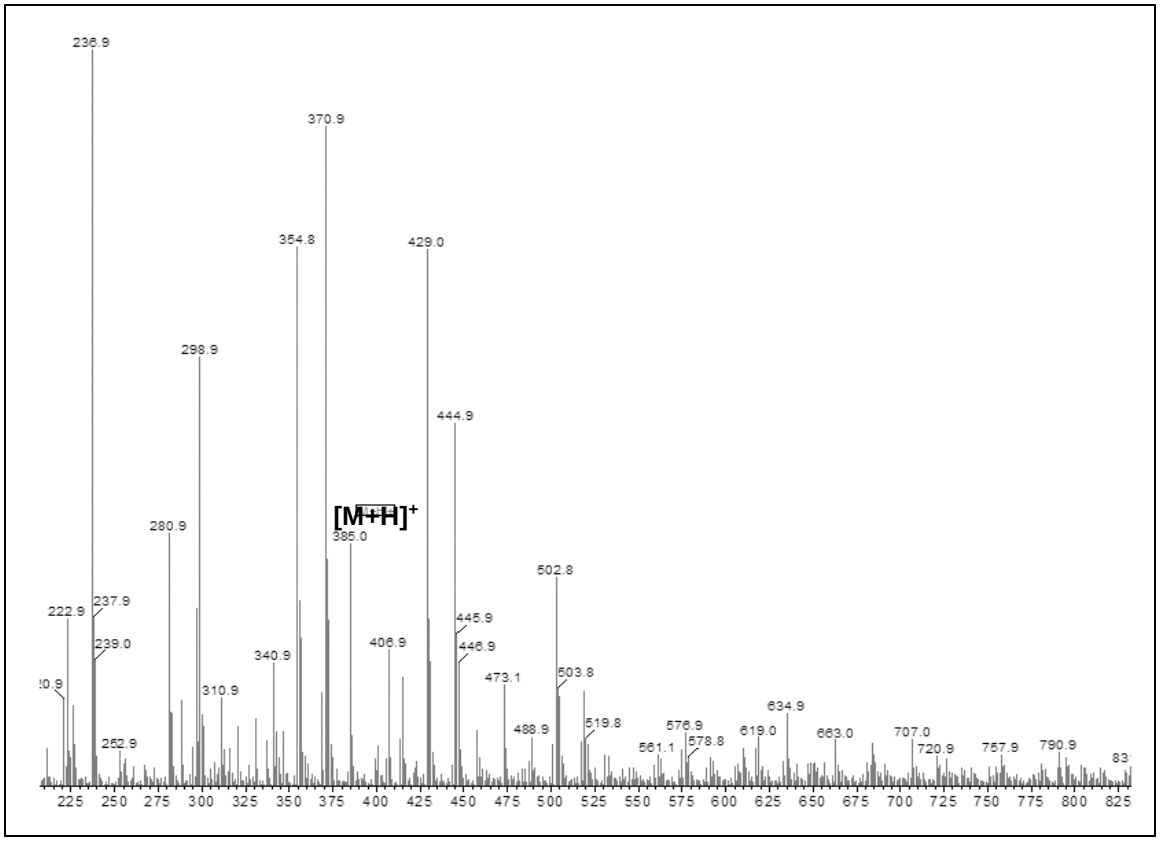
236.9
370.9
354.8
429.0
298.9
444.9
[M+H]+
280.9
385.0
502.8
222.9
237.9
445.9
239.0
406.9
446.9
340.9
473.1
503.8
310.9
634.9
488.9
519.8
576.9
619.0
663.0
707.0
561.1
578.8
720.9
757.9
790.9
252.9
225 250 275 300 325 350 375 400 425 450 475 500 525 550 575 600 625 650 675 700 725 750 775 800 825

- **BASHY 78b**

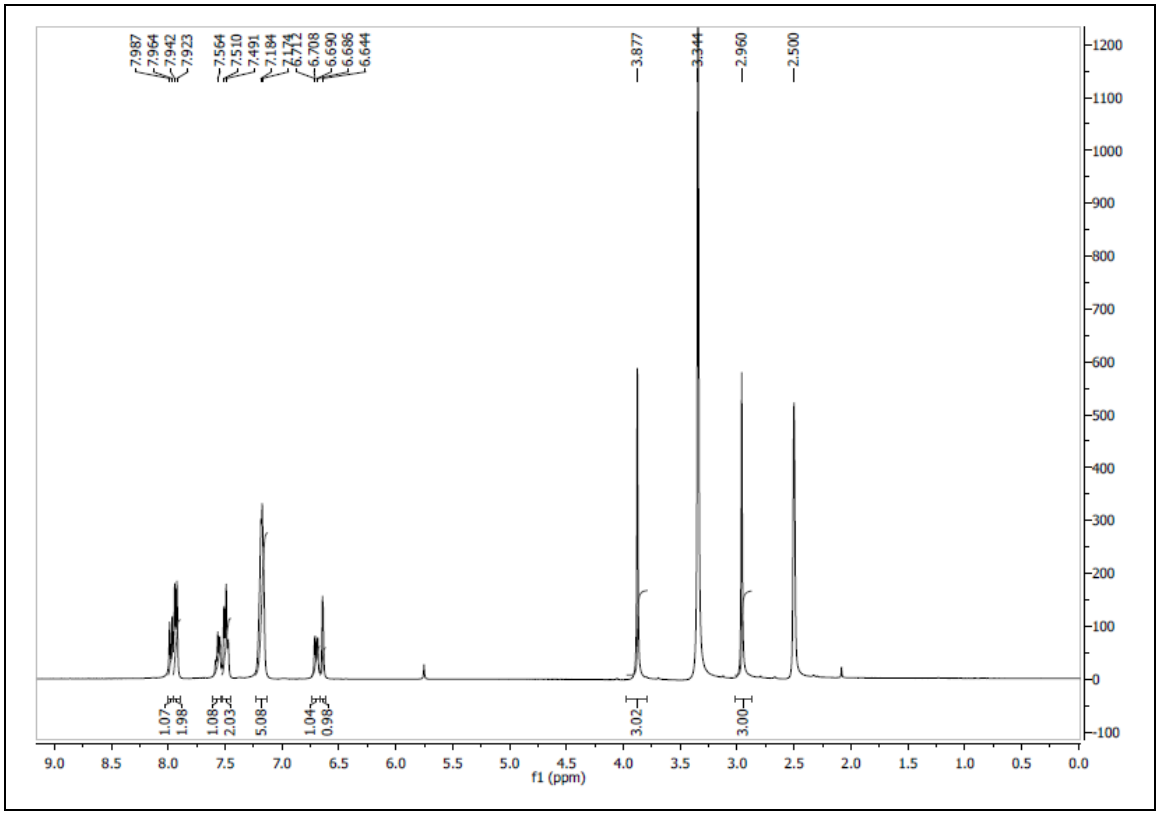
7.987
7.964
7.942
7.923
7.564
7.510
7.491
7.184
6.713
6.708
6.690
6.686
6.644
3.877
3.344
2.960
2.500
1.07
1.98
1.08
2.03
5.08
1.04
0.98
3.02
3.00
9.0 8.5 8.0 7.5 7.0 6.5 6.0 5.5 5.0 4.5 4.0 3.5 3.0 2.5 2.0 1.5 1.0 0.5 0.0
f1 (ppm)
1200 1100 1000 900 800 700 600 500 400 300 200 100 0 -100

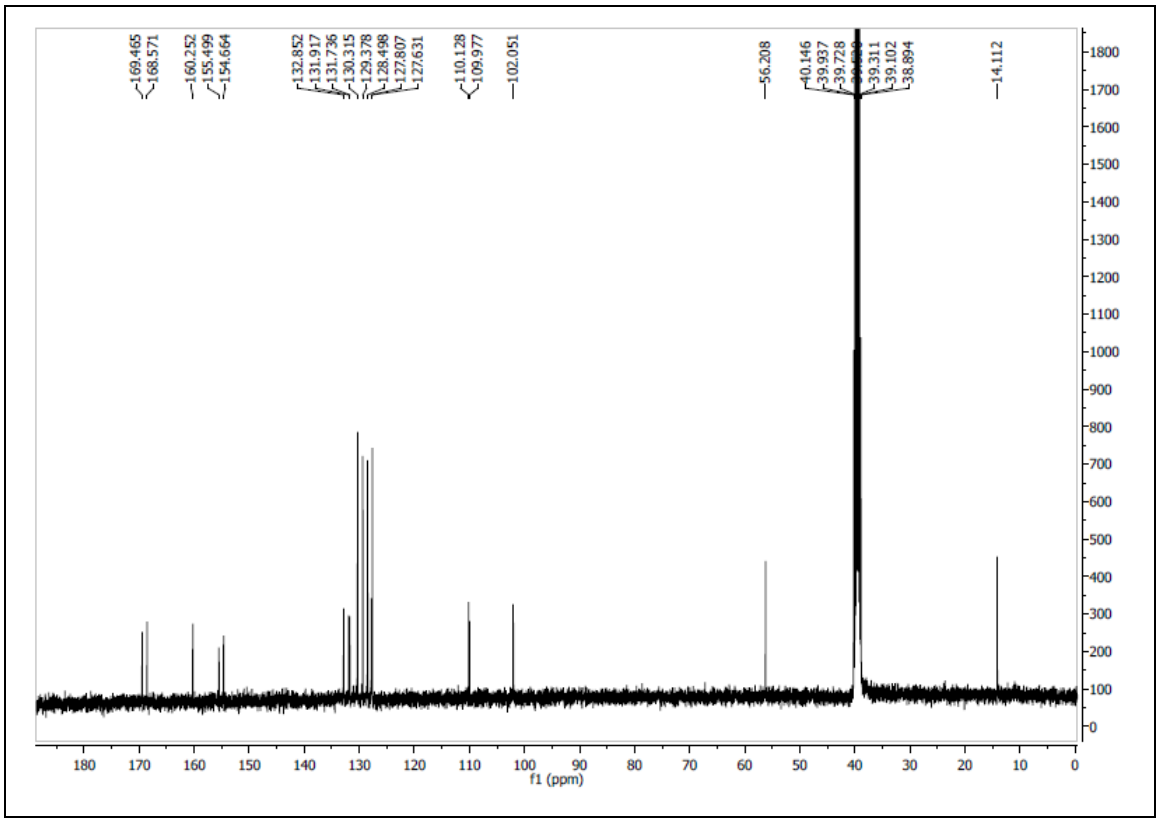
169.465
168.571
160.252
155.499
154.664
132.852
131.917
131.736
130.315
129.378
128.498
127.807
127.631
110.128
109.977
102.051
56.208
40.146
39.937
39.728
39.311
39.102
38.894
14.112
f1 (ppm)

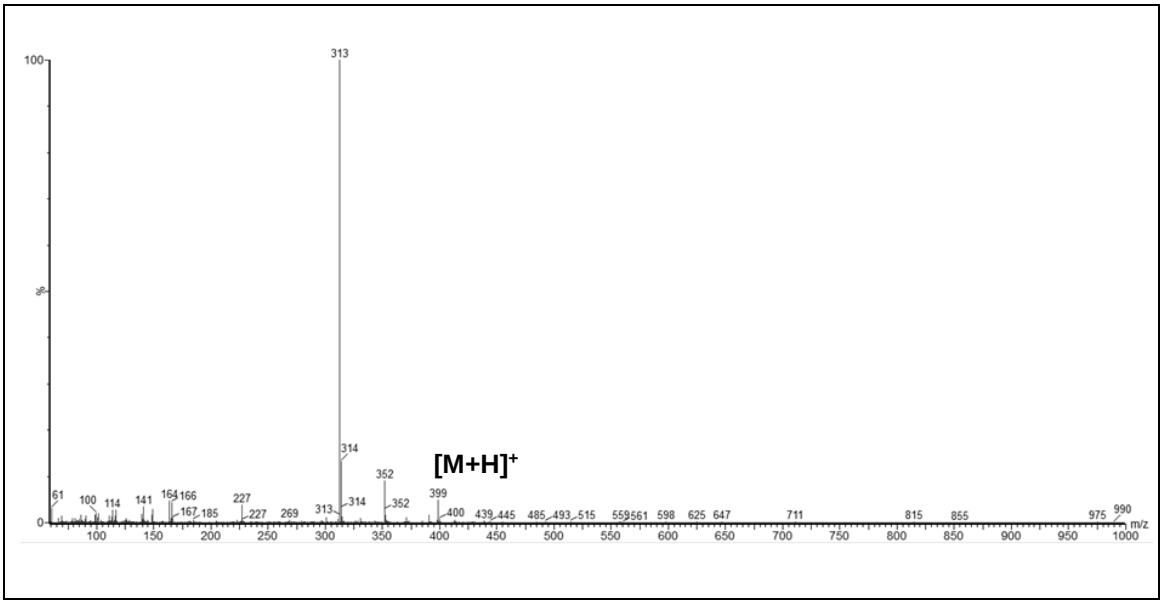
313
314
352
399
[M+H]+
m/z

- **BASHY 78c**

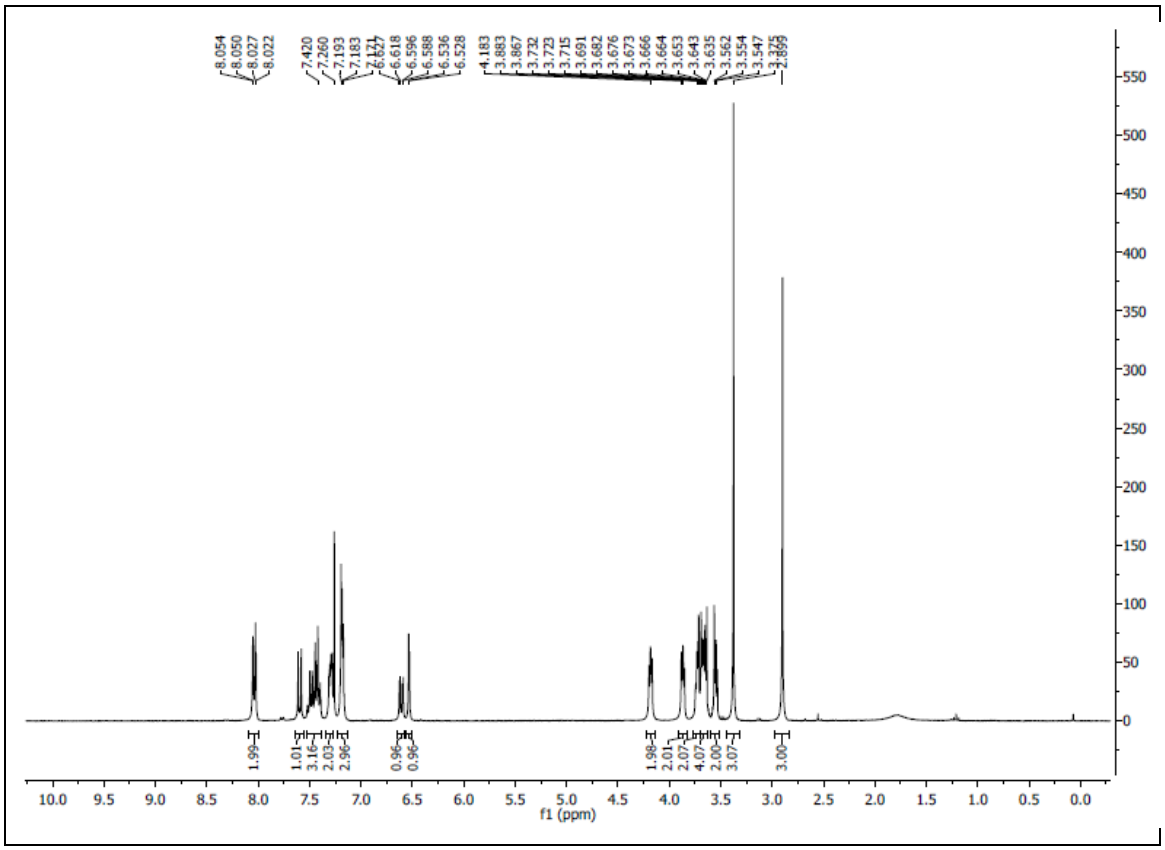
8.054
8.050
8.027
8.022
7.420
7.260
7.193
7.183
7.171
6.627
6.618
6.596
6.588
6.536
6.528
4.183
3.883
3.867
3.732
3.723
3.715
3.691
3.682
3.676
3.673
3.666
3.664
3.653
3.643
3.635
3.562
3.554
3.547
3.375
2.899
1.99
1.01
3.16
2.03
2.96
0.96
0.96
1.98
2.01
2.07
4.07
2.00
3.07
3.00
f1 (ppm)

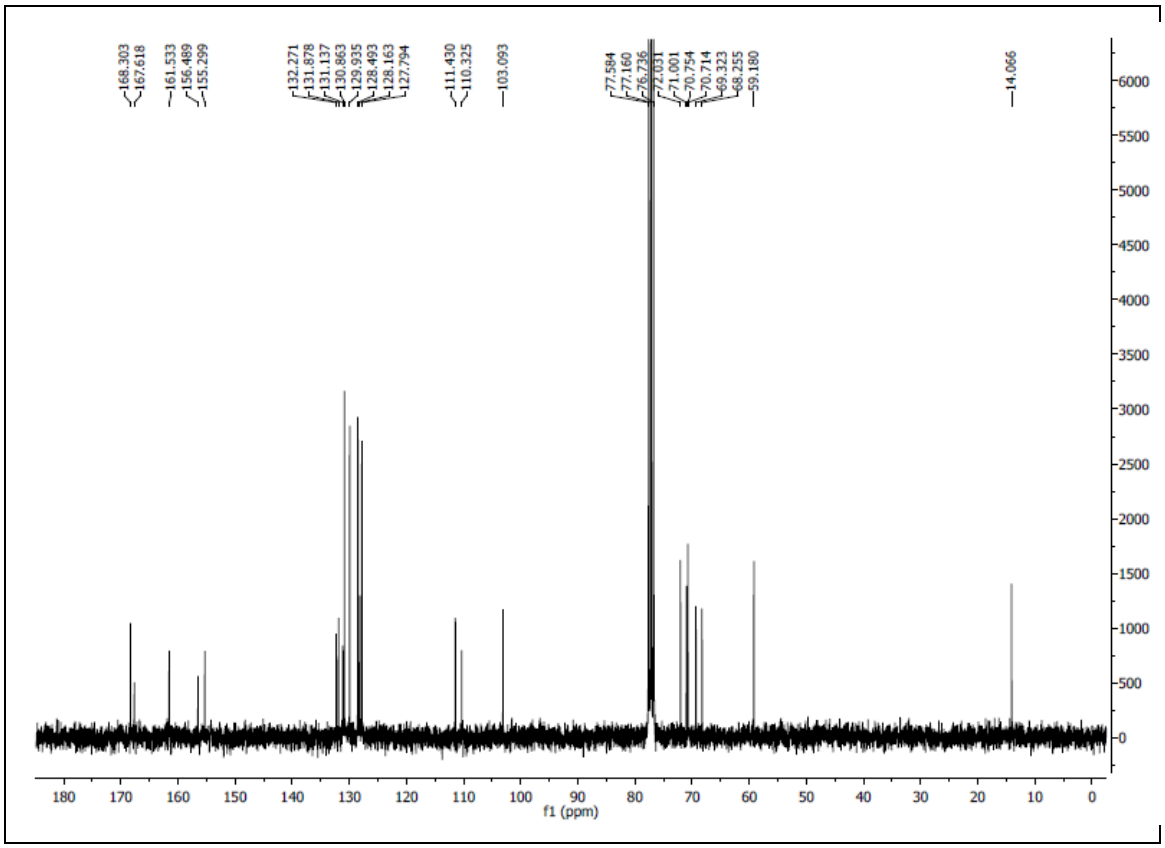
168.303
167.618
161.533
156.489
155.299
132.271
131.878
131.137
130.863
129.935
128.493
128.163
127.794
111.430
110.325
103.093
77.584
77.160
76.736
72.031
71.001
70.754
70.714
69.323
68.255
59.180
14.066
f1 (ppm)

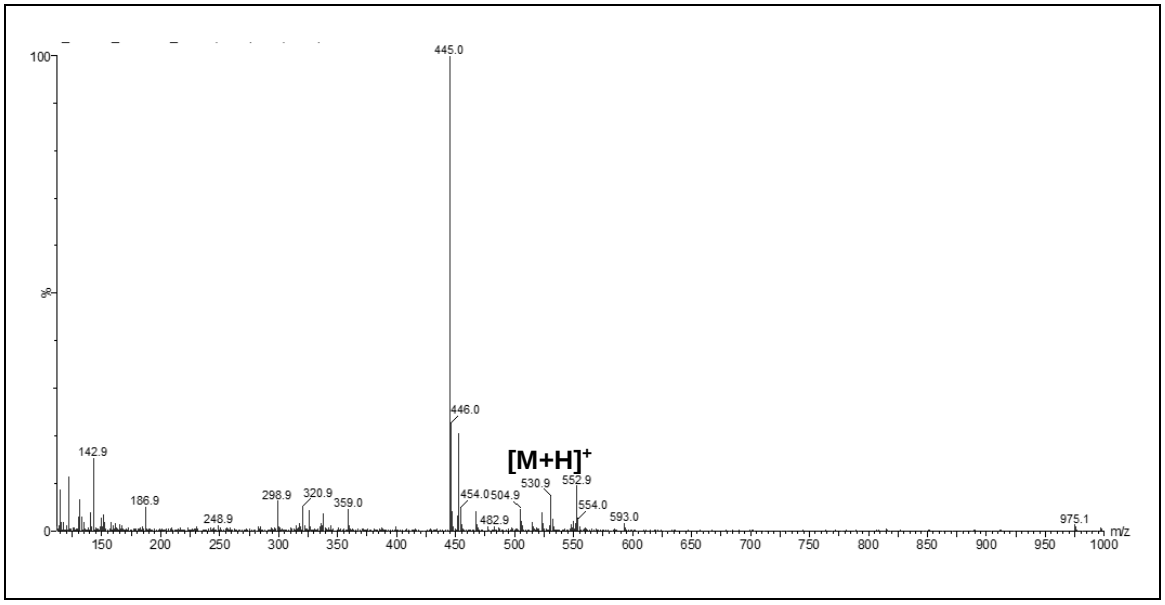
445.0
446.0
[M+H]+
142.9
186.9
248.9
298.9
320.9
359.0
454.0
504.9
530.9
552.9
554.0
482.9
593.0
975.1
%
m/z

- **Ligand 80a**

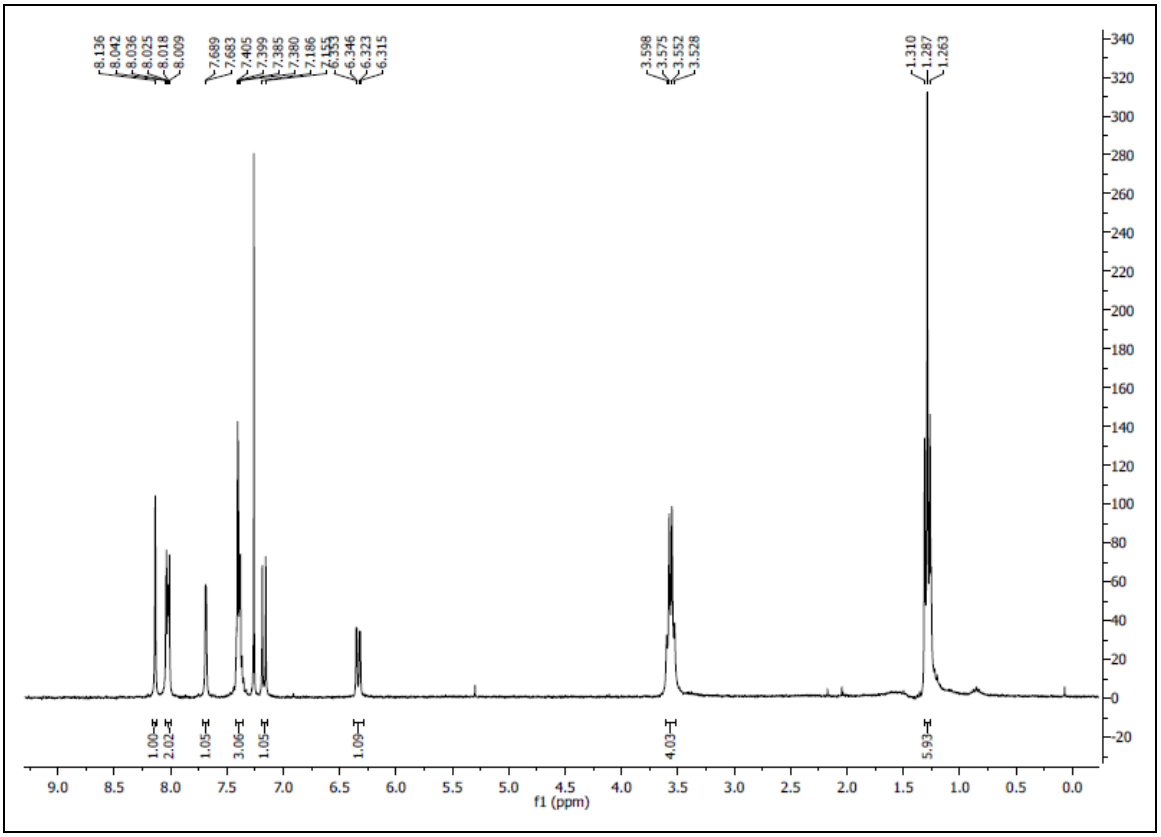
8.136
8.042
8.036
8.025
8.018
8.009
7.689
7.683
7.405
7.399
7.385
7.380
7.186
6.346
6.323
6.315
3.598
3.575
3.552
3.528
1.310
1.287
1.263
1.00
2.02
1.05
3.06
1.05
1.09
4.03
5.93
f1 (ppm)

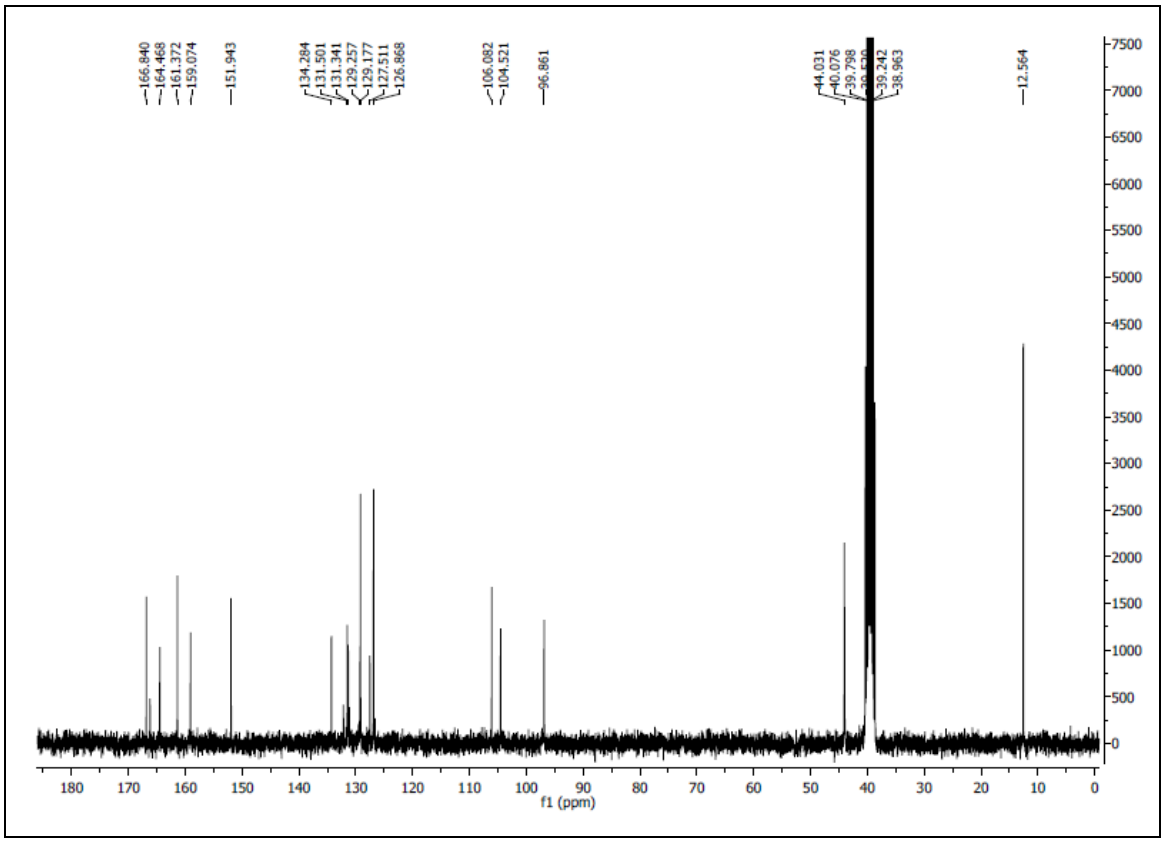
166.840
164.468
161.372
159.074
151.943
134.284
131.501
131.341
129.257
129.177
127.511
126.868
106.082
104.521
96.861
44.031
40.076
39.798
39.520
39.242
38.963
12.564
f1 (ppm)

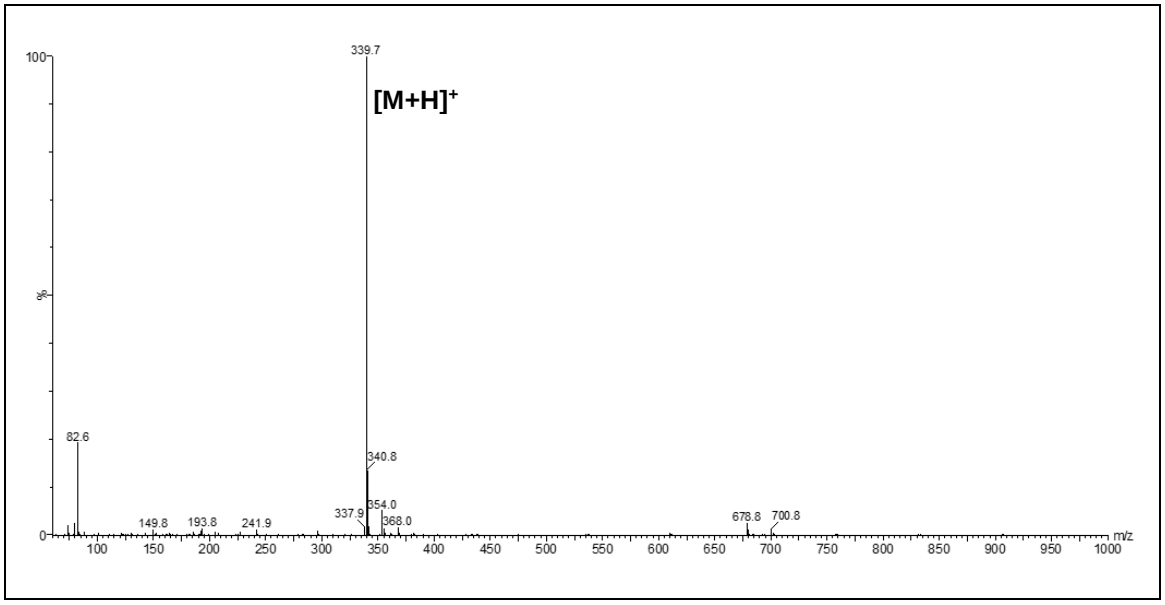
339.7
[M+H]+
%
82.6
340.8
354.0
337.9
368.0
149.8
193.8
241.9
678.8
700.8
m/z

- **Ligand 80b**

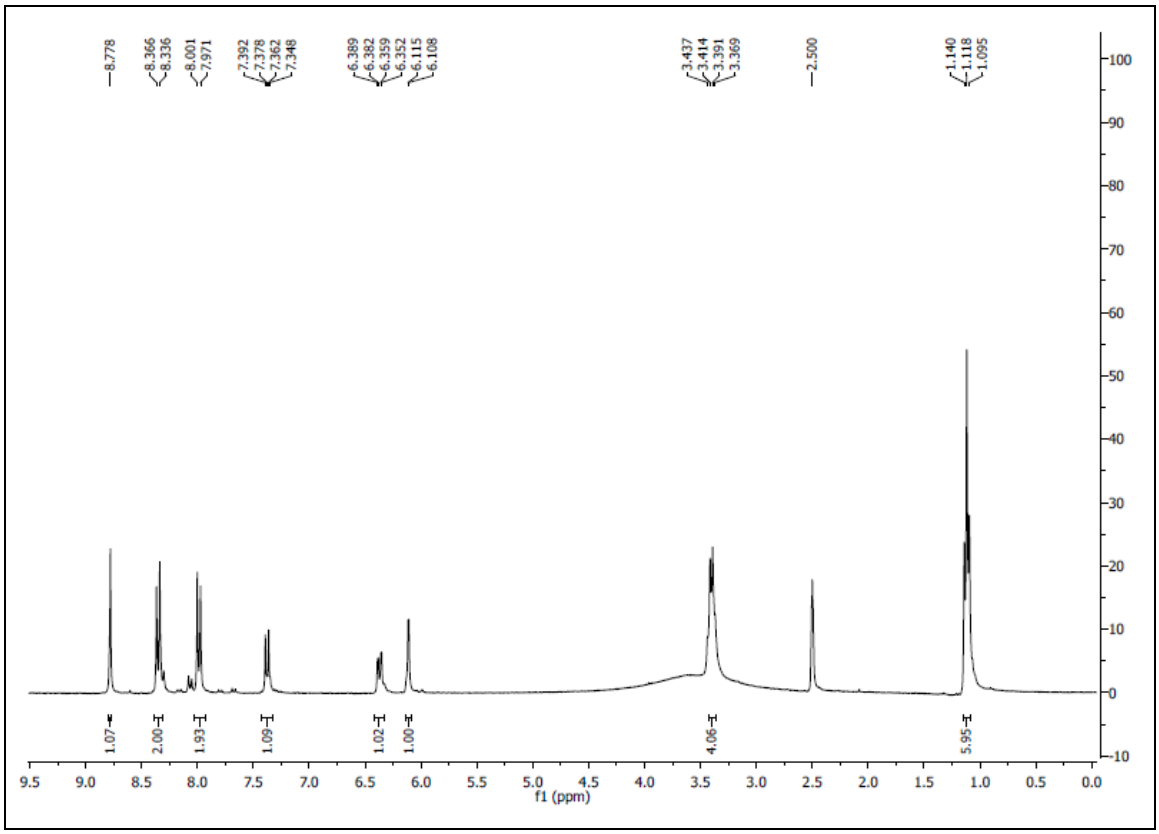
8.778
8.366
8.336
8.001
7.971
7.392
7.378
7.362
7.348
6.389
6.382
6.359
6.352
6.115
6.108
3.437
3.414
3.391
3.369
2.500
1.140
1.118
1.095
1.07
2.00
1.93
1.09
1.02
1.00
4.06
5.95
f1 (ppm)

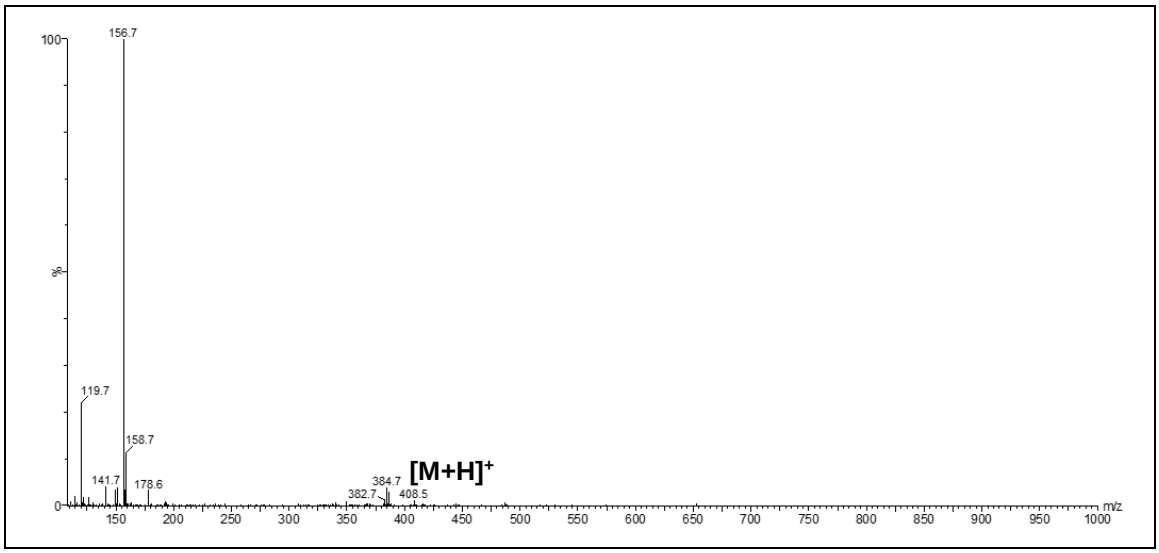
156.7
119.7
158.7
141.7
178.6
382.7
384.7
408.5
[M+H]+
%
m/z

- **Ligand 80c**

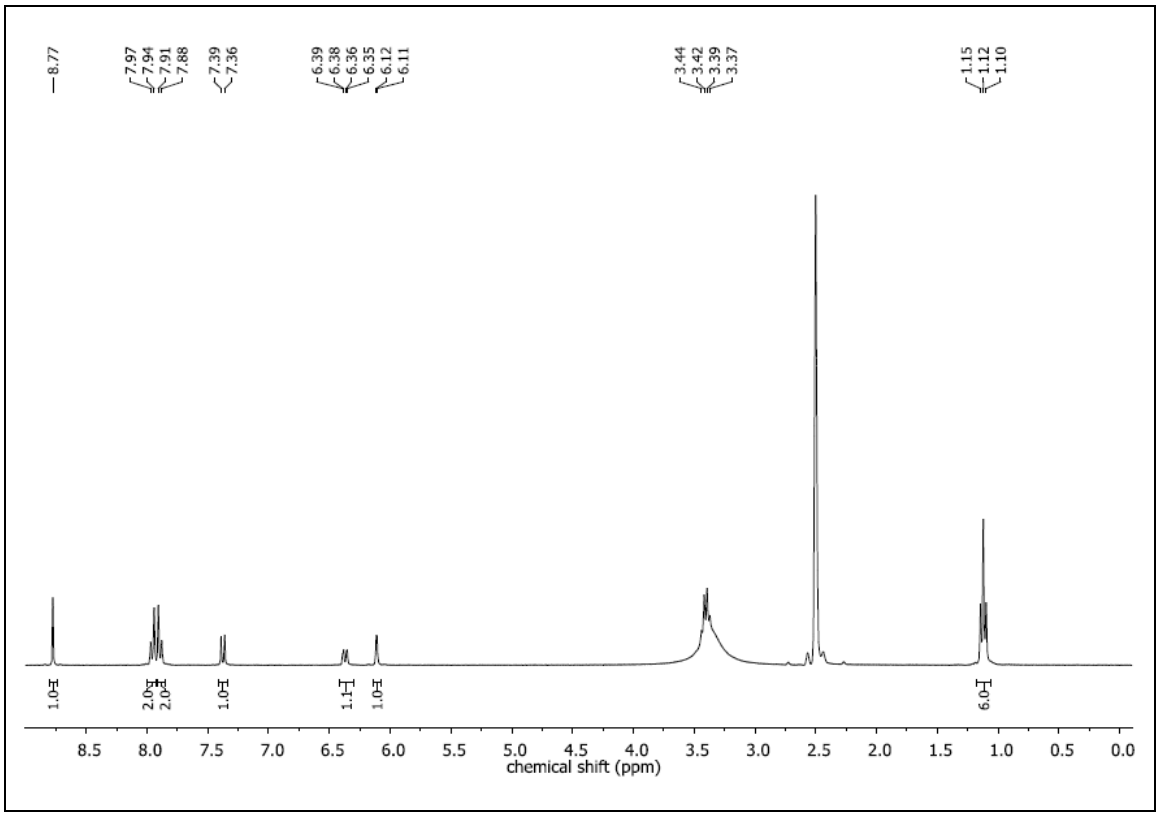
8.77
7.97
7.94
7.91
7.88
7.39
7.36
6.39
6.38
6.36
6.35
6.12
6.11
3.44
3.42
3.39
3.37
1.15
1.12
1.10
1.0
2.0
2.0
1.0
1.1
1.0
6.0
chemical shift (ppm)

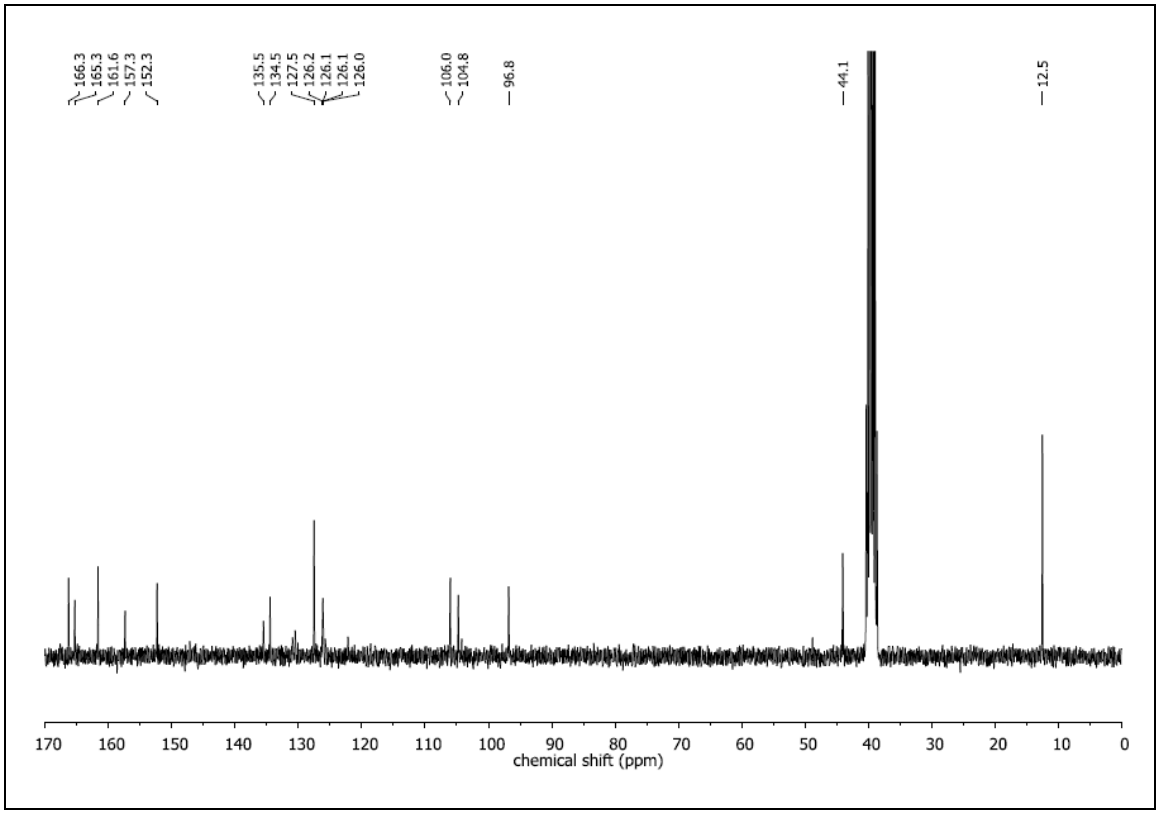
166.3
165.3
161.6
157.3
152.3
135.5
134.5
127.5
126.2
126.1
126.1
126.0
106.0
104.8
96.8
44.1
12.5
chemical shift (ppm)

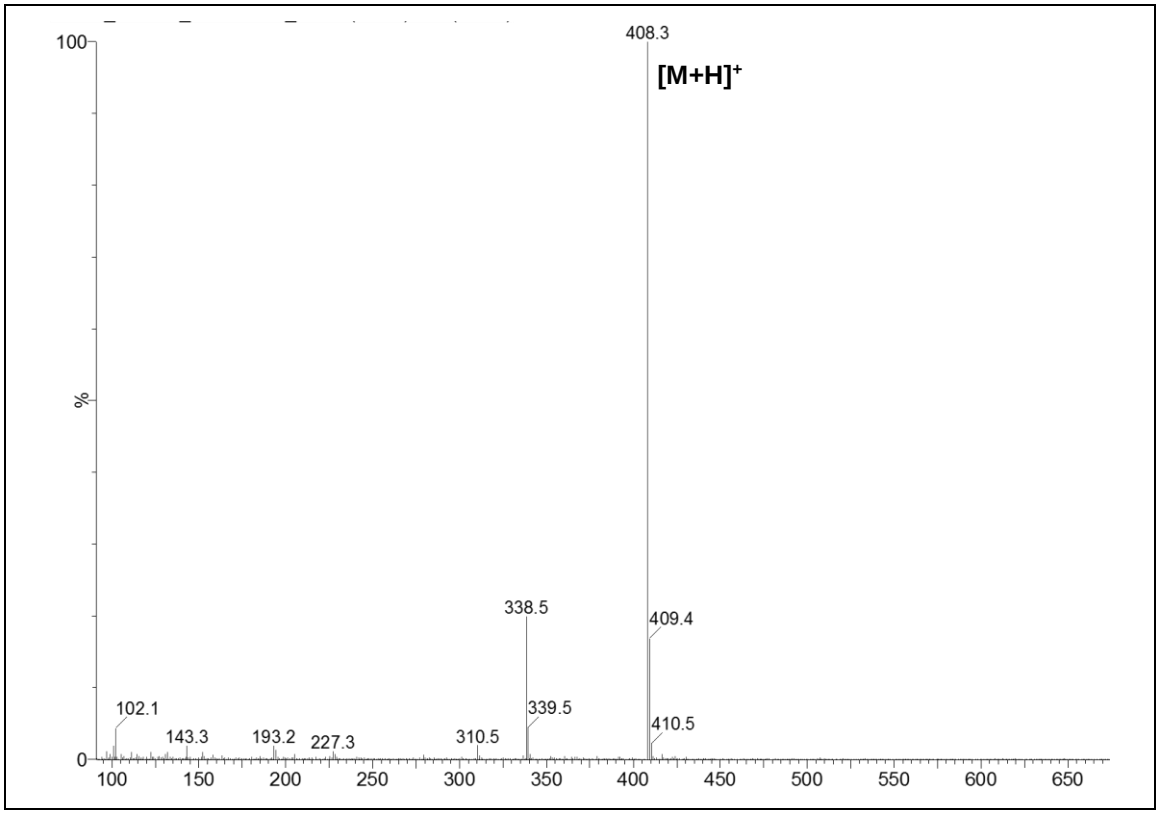
100
%
0
408.3
[M+H]+
338.5
409.4
102.1
339.5
143.3
193.2
227.3
310.5
410.5
100
150
200
250
300
350
400
450
500
550
600
650

- **Ligand 80d**

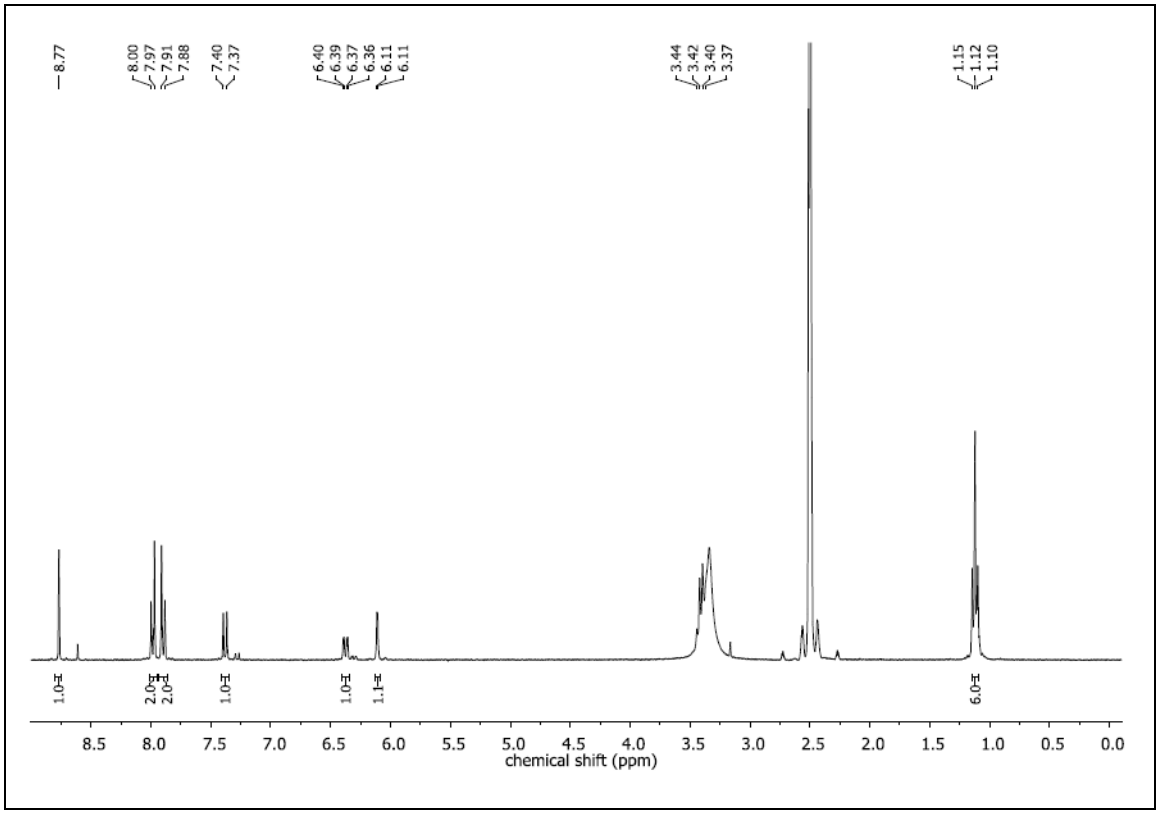
8.77
8.00
7.97
7.91
7.88
7.40
7.37
6.40
6.39
6.37
6.36
6.11
6.11
3.44
3.42
3.40
3.37
1.15
1.12
1.10
1.0
2.0
2.0
1.0
1.0
1.1
6.0
8.5
8.0
7.5
7.0
6.5
6.0
5.5
5.0
4.5
4.0
3.5
3.0
2.5
2.0
1.5
1.0
0.5
0.0
chemical shift (ppm)

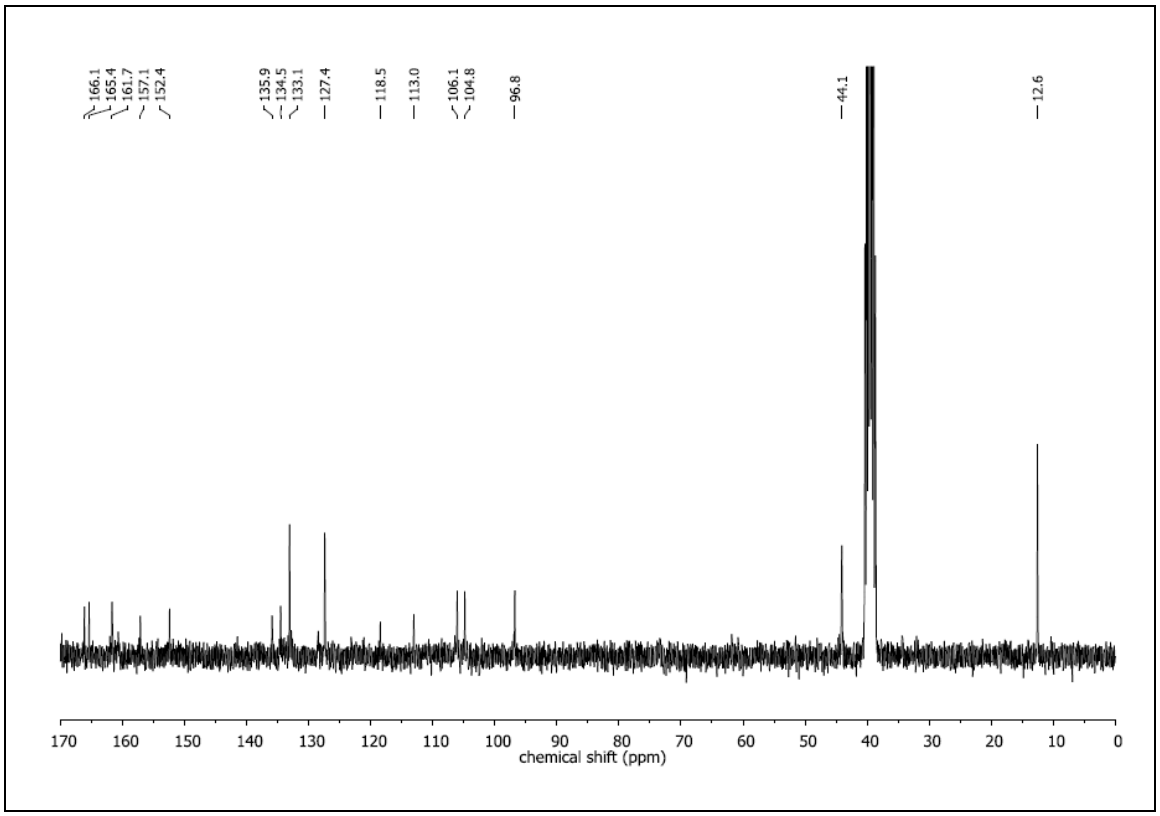
166.1
165.4
161.7
157.1
152.4
135.9
134.5
133.1
127.4
118.5
113.0
106.1
104.8
96.8
44.1
12.6
170 160 150 140 130 120 110 100 90 80 70 60 50 40 30 20 10 0
chemical shift (ppm)

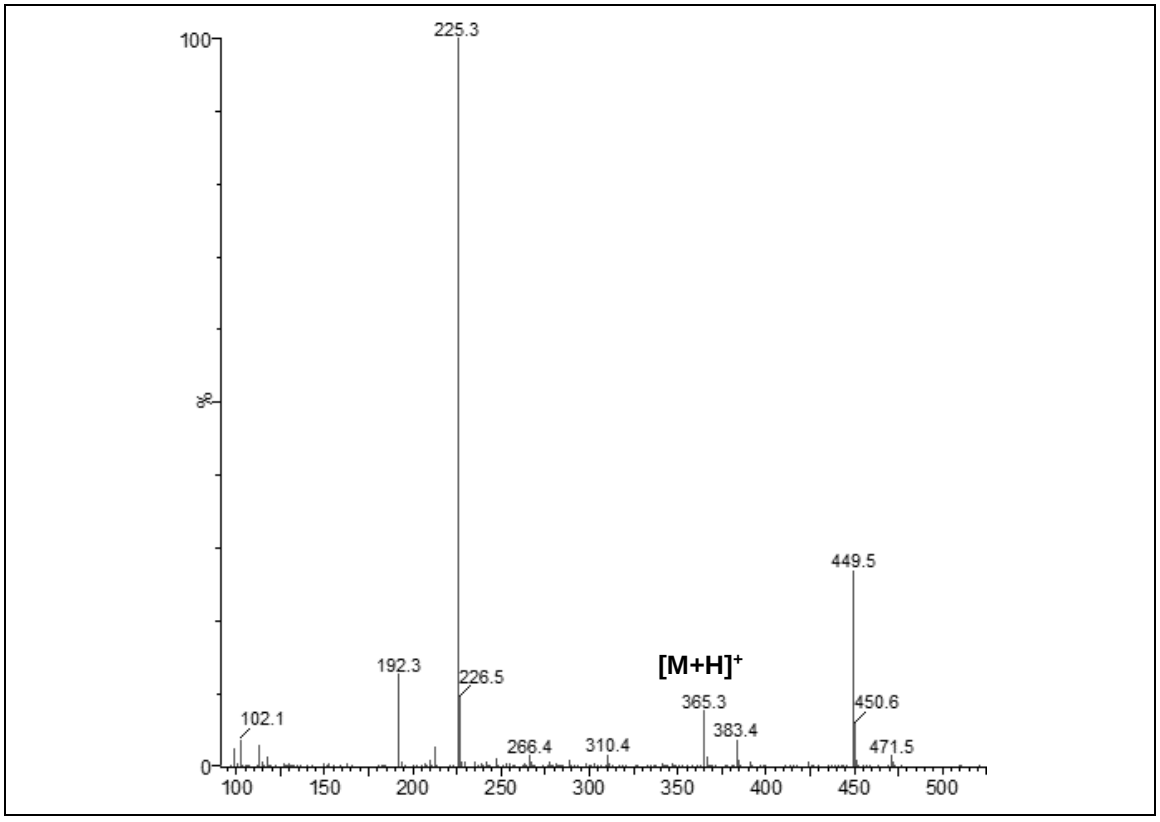
100
%
0
225.3
449.5
192.3
226.5
[M+H]+
365.3
450.6
102.1
383.4
266.4
310.4
471.5
100 150 200 250 300 350 400 450 500

- **BASHY 81a**

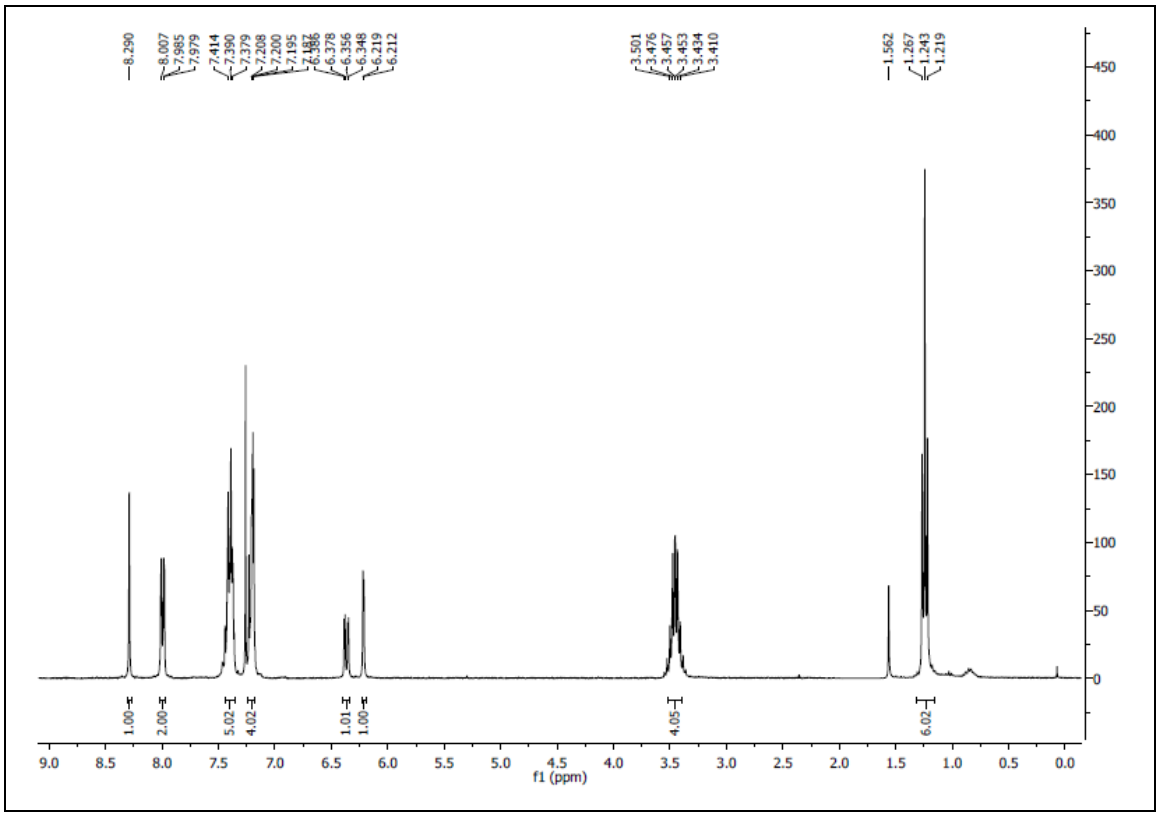
8.290
8.007
7.985
7.979
7.414
7.390
7.379
7.208
7.200
7.195
7.182
6.386
6.378
6.356
6.348
6.219
6.212
3.501
3.476
3.457
3.453
3.434
3.410
1.562
1.267
1.243
1.219
1.00
2.00
5.02
4.02
1.01
1.00
4.05
6.02
f1 (ppm)

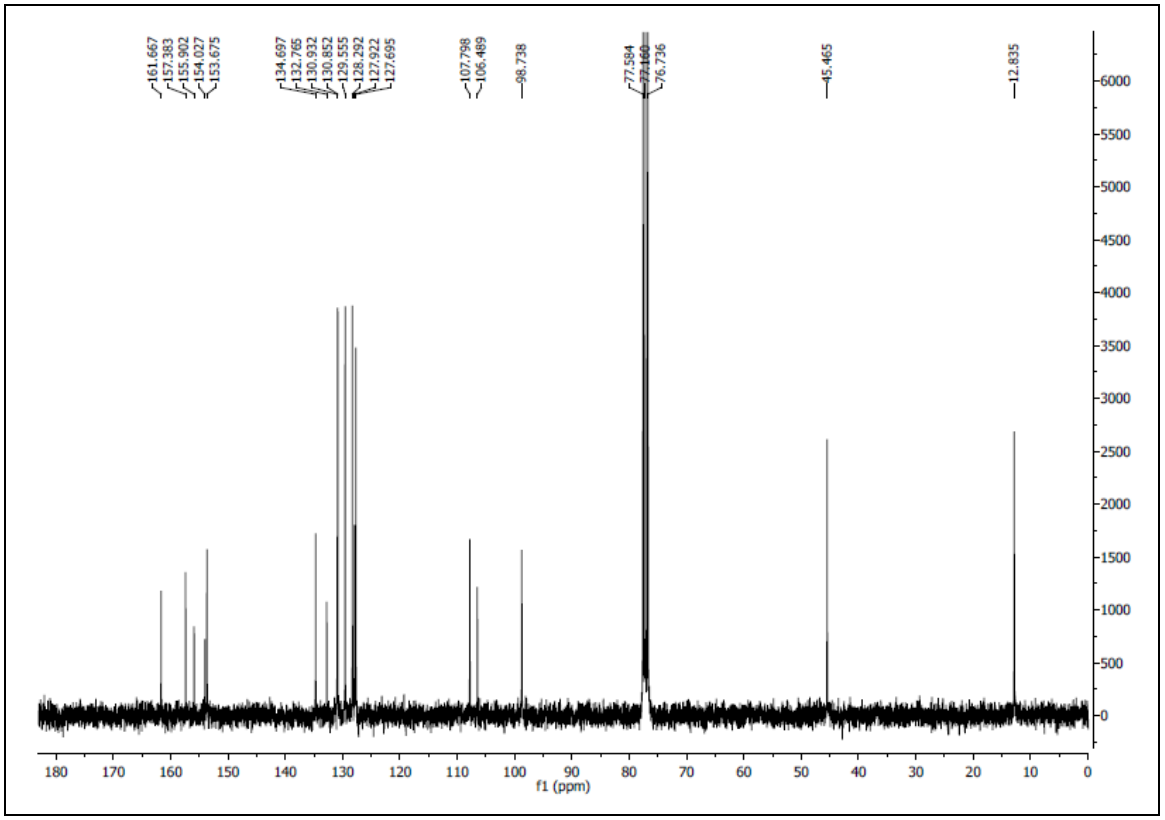
161.667
157.383
155.902
154.027
153.675
134.697
132.765
130.932
130.852
129.555
128.292
127.922
127.695
107.798
106.489
98.738
77.584
77.160
76.736
45.465
12.835
f1 (ppm)

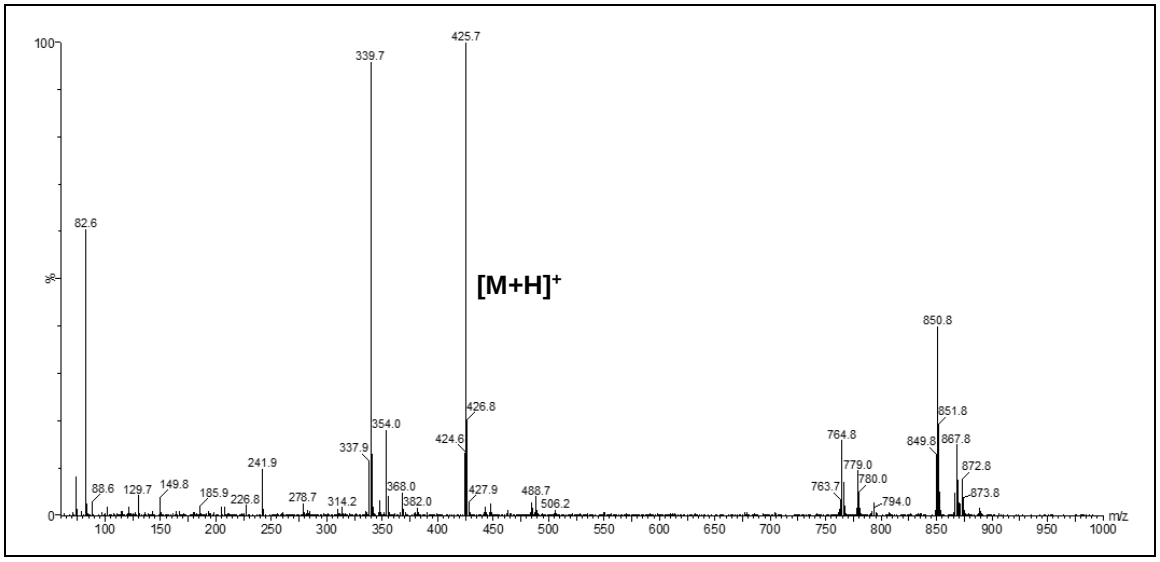
100
%
0
425.7
339.7
82.6
[M+H]+
850.8
426.8
354.0
851.8
764.8
424.6
337.9
849.8
867.8
779.0
872.8
241.9
780.0
763.7
88.6
129.7
149.8
185.9
226.8
278.7
314.2
368.0
382.0
427.9
488.7
506.2
794.0
873.8
m/z
100
150
200
250
300
350
400
450
500
550
600
650
700
750
800
850
900
950
1000

- **BASHY 81b**

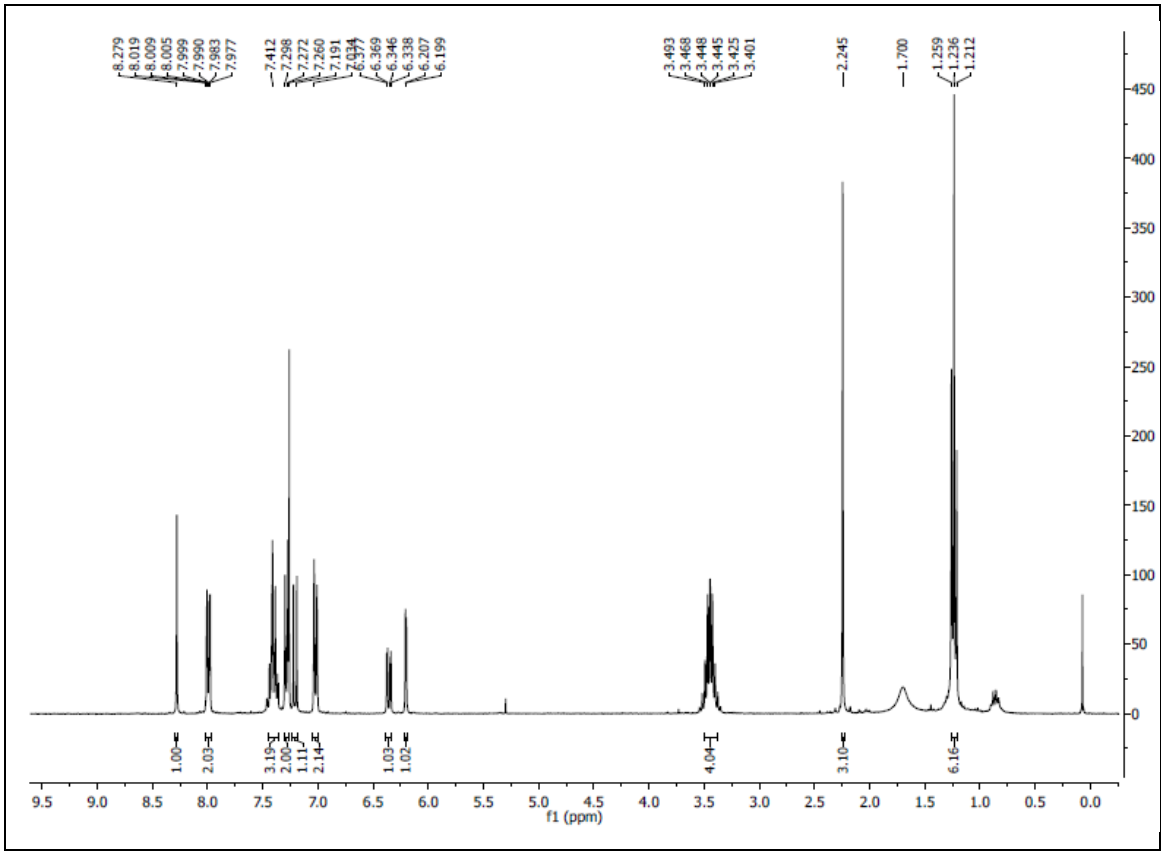
8.279
8.019
8.009
8.005
7.999
7.990
7.983
7.977
7.412
7.298
7.272
7.260
7.191
7.034
6.377
6.369
6.346
6.338
6.207
6.199
3.493
3.468
3.448
3.445
3.425
3.401
2.245
1.700
1.259
1.236
1.212
1.00
2.03
3.19
2.00
1.11
2.14
1.03
1.02
4.04
3.10
6.16
f1 (ppm)

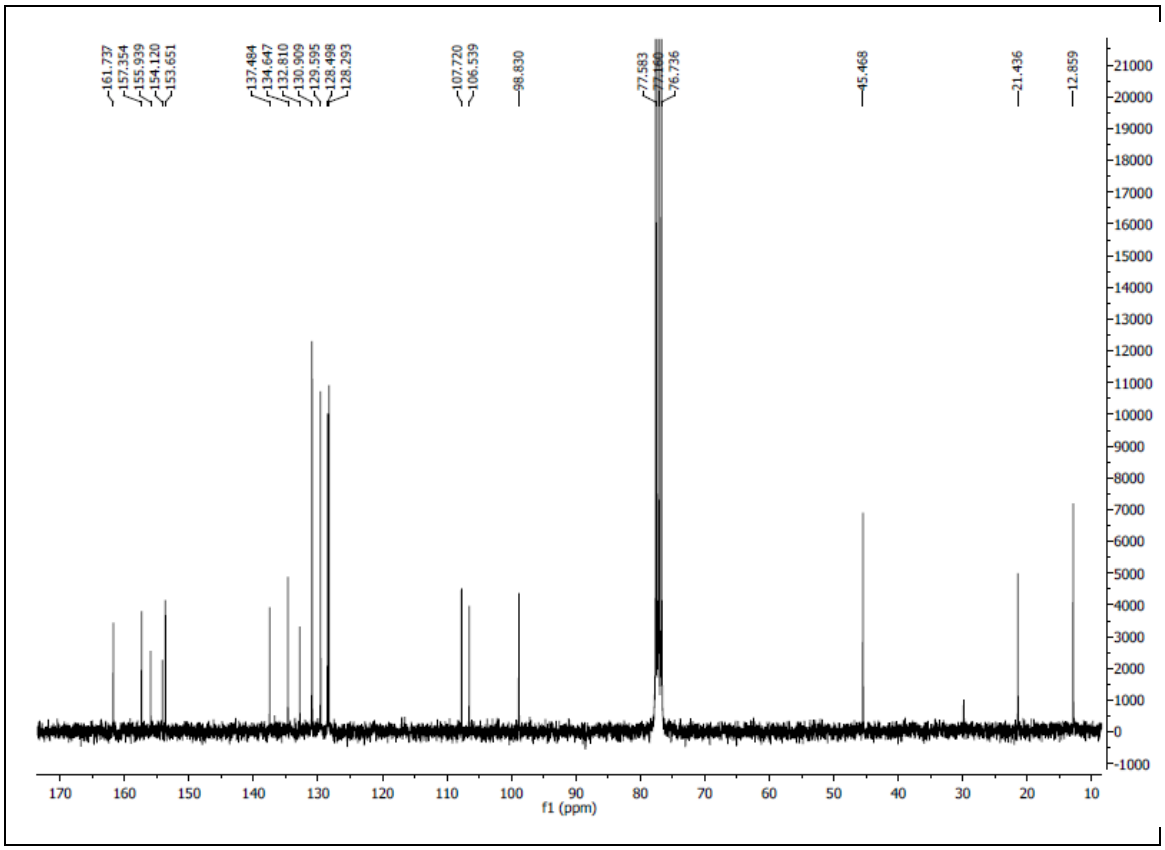
161.737
157.354
155.939
154.120
153.651
137.484
134.647
132.810
130.909
129.595
128.498
128.293
107.720
106.539
98.830
77.583
77.160
76.736
45.468
21.436
12.859
f1 (ppm)

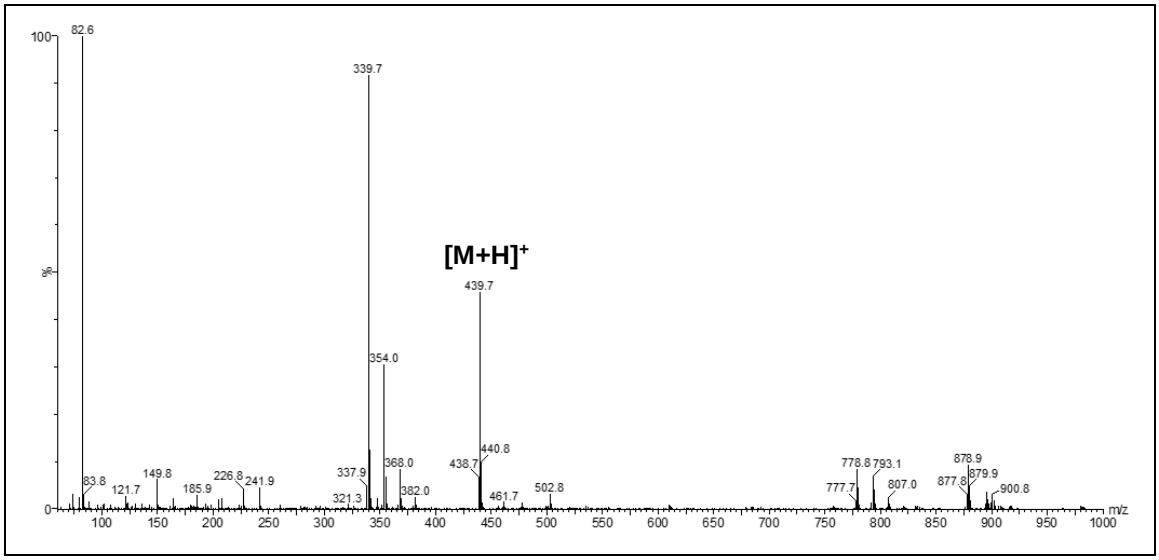
[M+H]+
82.6
339.7
439.7
354.0
440.8
83.8
121.7
149.8
185.9
226.8
241.9
337.9
321.3
368.0
382.0
438.7
461.7
502.8
778.8
793.1
777.7
807.0
878.9
877.8
879.9
900.8
%
m/z

- **BASHY 81c**

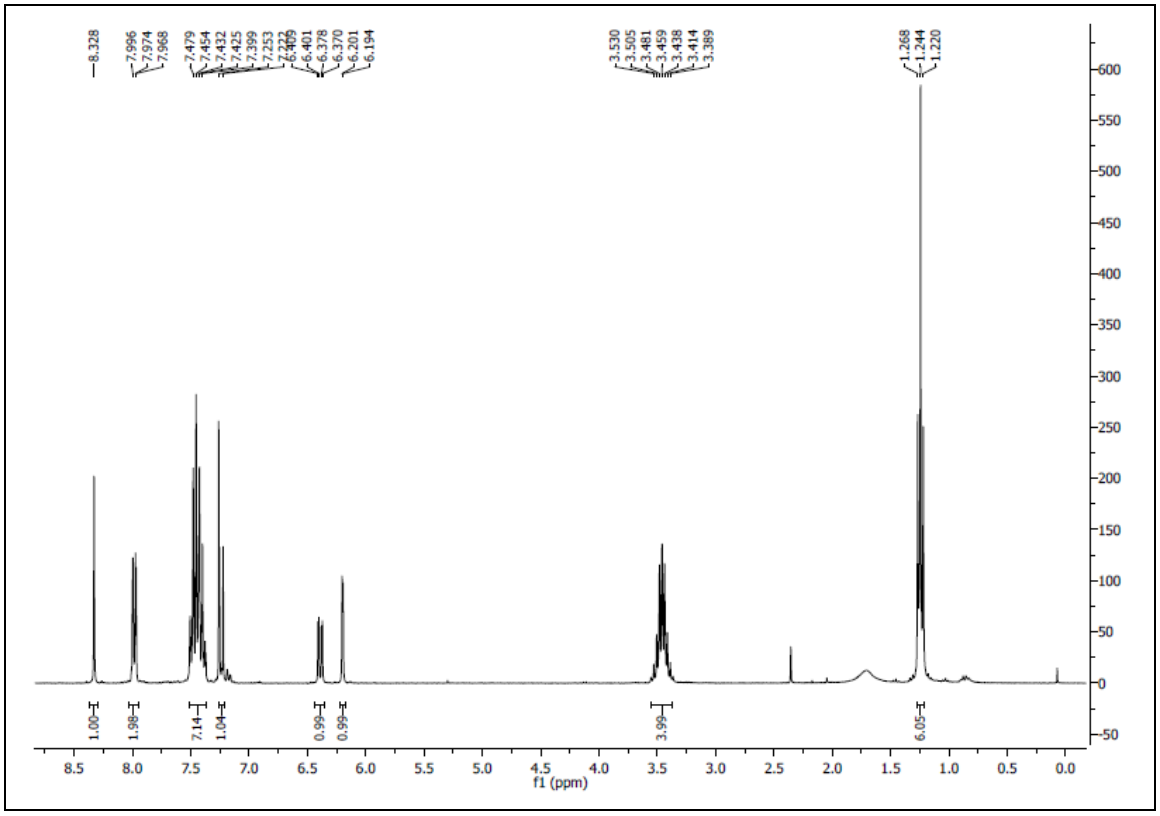
8.328
7.996
7.974
7.968
7.479
7.454
7.432
7.425
7.399
7.253
7.222
6.409
6.401
6.378
6.370
6.201
6.194
3.530
3.505
3.481
3.459
3.438
3.414
3.389
1.268
1.244
1.220
1.00
1.98
7.14
1.04
0.99
0.99
3.99
6.05
f1 (ppm)

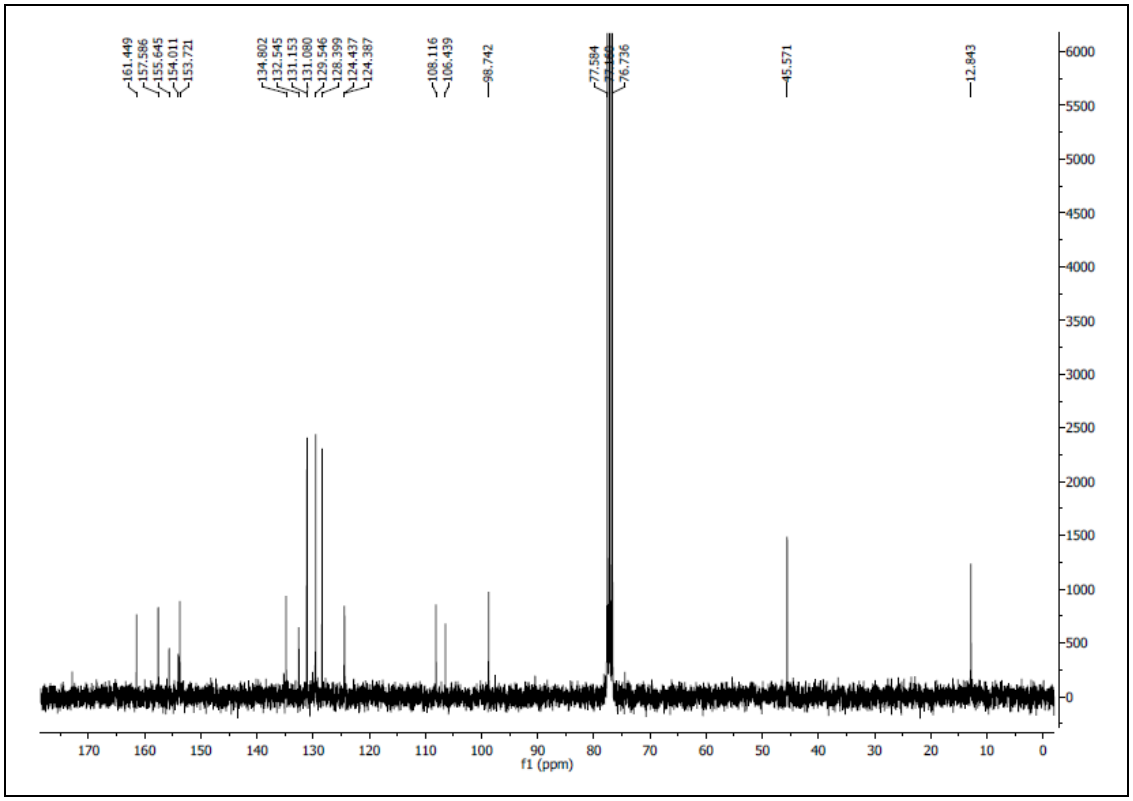
161.449
157.586
155.645
154.011
153.721
134.802
132.545
131.153
131.080
129.546
128.399
124.437
124.387
108.116
106.439
98.742
77.584
77.368
76.736
45.571
12.843
f1 (ppm)

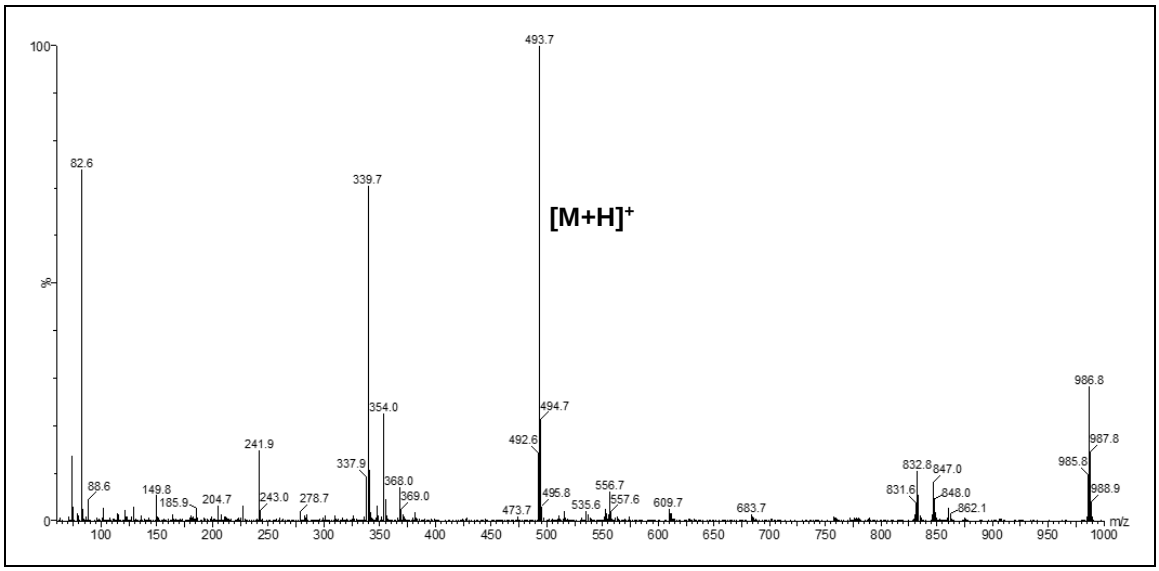
493.7
[M+H]+
82.6
339.7
354.0
494.7
492.6
241.9
337.9
368.0
369.0
88.6
149.8
185.9
204.7
243.0
278.7
473.7
495.8
535.6
556.7
557.6
609.7
683.7
831.6
832.8
847.0
848.0
862.1
985.8
986.8
987.8
988.9
%
m/z

- **BASHY 81d**

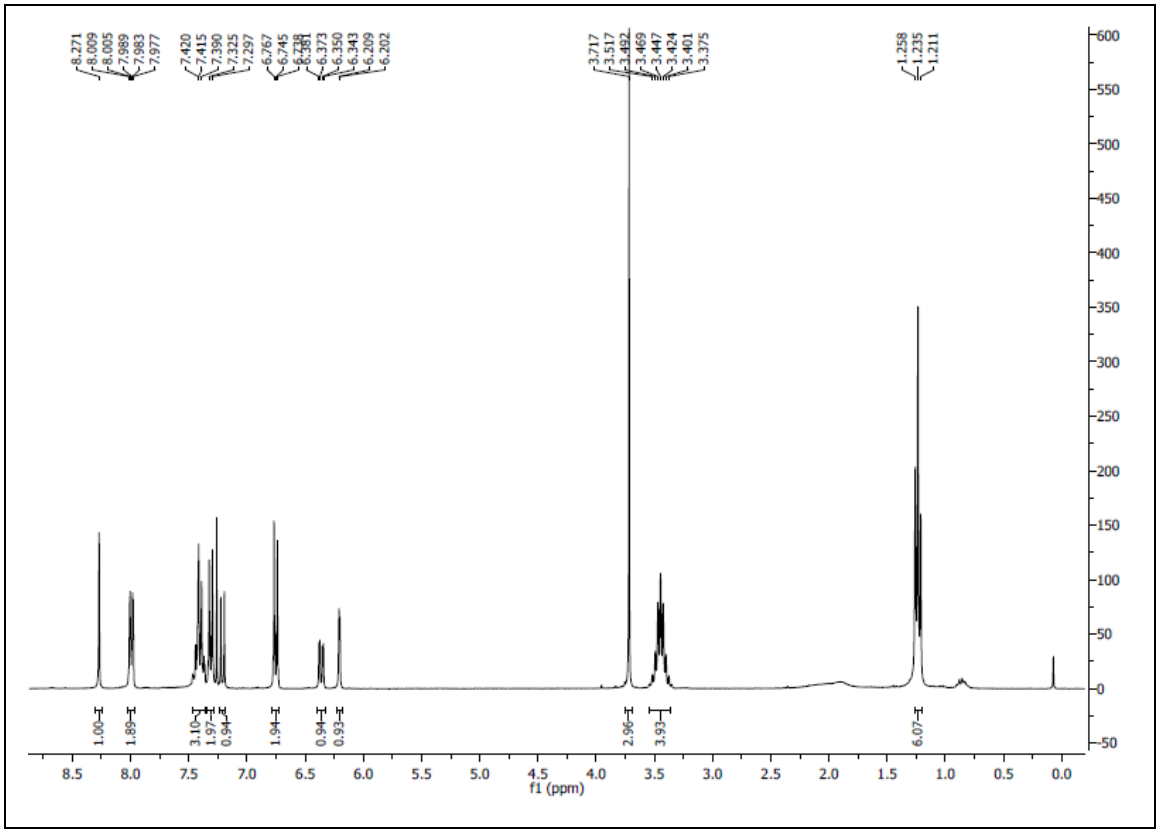
8.271
8.609
8.005
7.989
7.983
7.977
7.420
7.415
7.390
7.325
7.297
6.767
6.745
6.373
6.350
6.343
6.209
6.202
3.717
3.517
3.492
3.469
3.447
3.424
3.401
3.375
1.258
1.235
1.211
1.00
1.89
3.10
1.97
0.94
1.94
0.94
0.93
2.96
3.93
6.07
f1 (ppm)

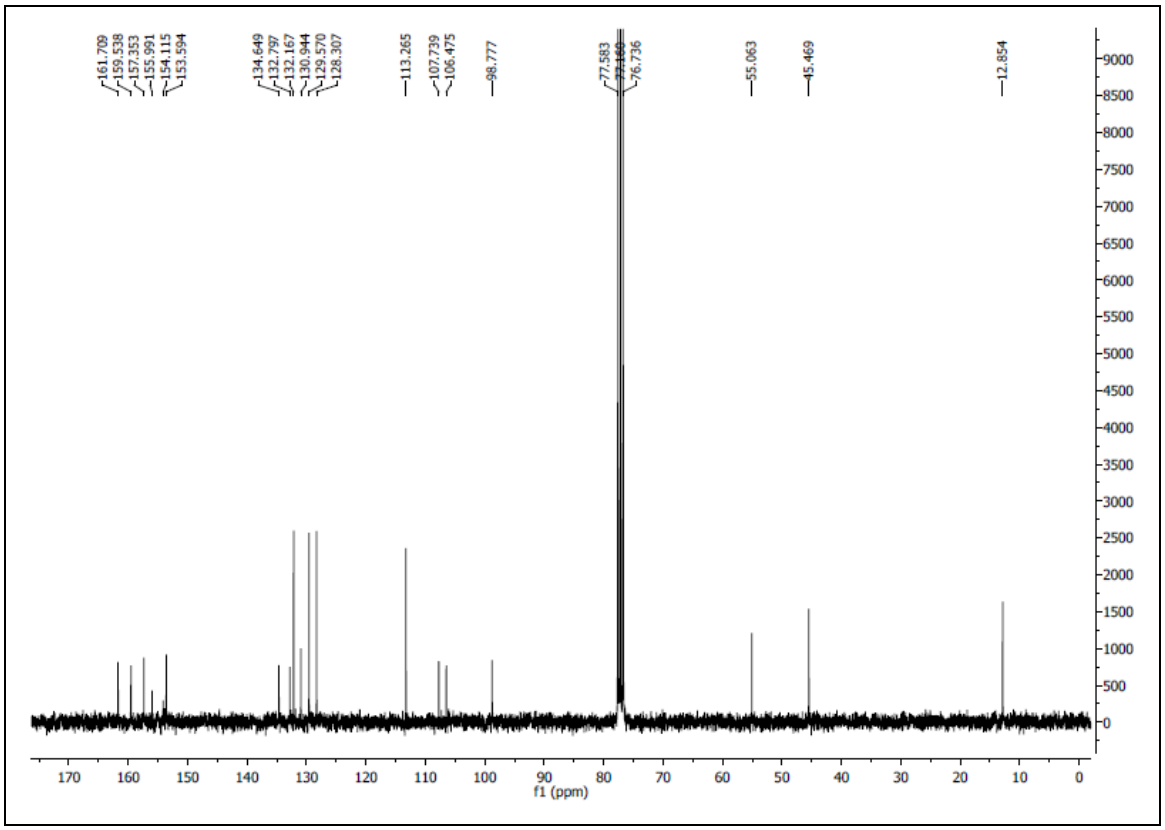
161.709
159.538
157.353
155.991
154.115
153.594
134.649
132.797
132.167
130.944
129.570
128.307
113.265
107.739
106.475
98.777
77.583
77.160
76.736
55.063
45.469
12.854
f1 (ppm)

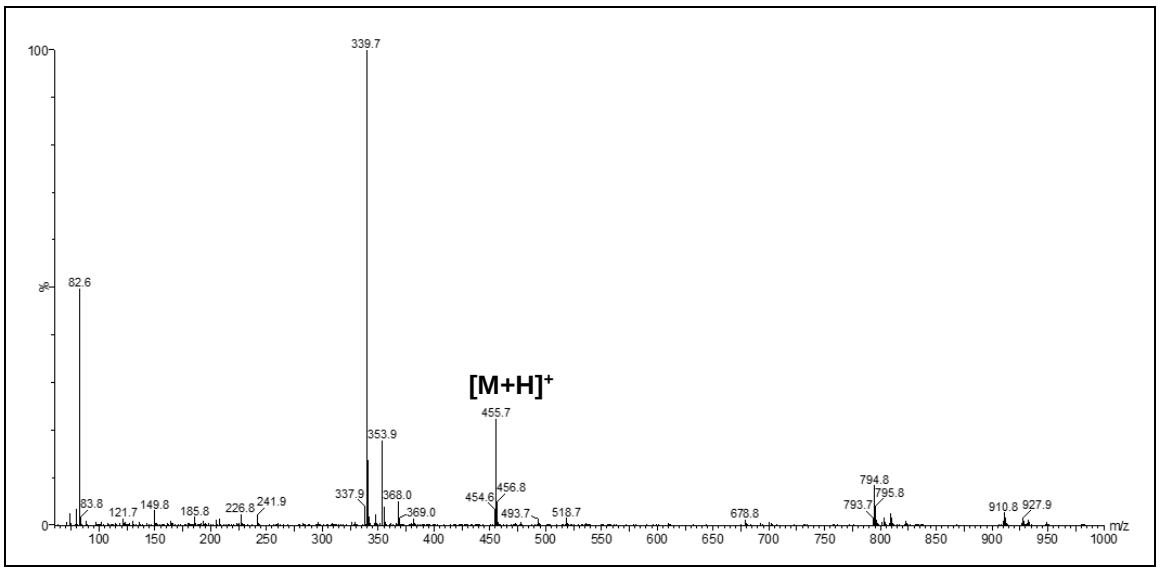
339.7
82.6
[M+H]+
455.7
353.9
456.8
794.8
795.8
83.8
121.7
149.8
185.8
226.8
241.9
337.9
368.0
369.0
454.6
493.7
518.7
678.8
793.7
910.8
927.9
%
m/z

- **BASHY 81e**

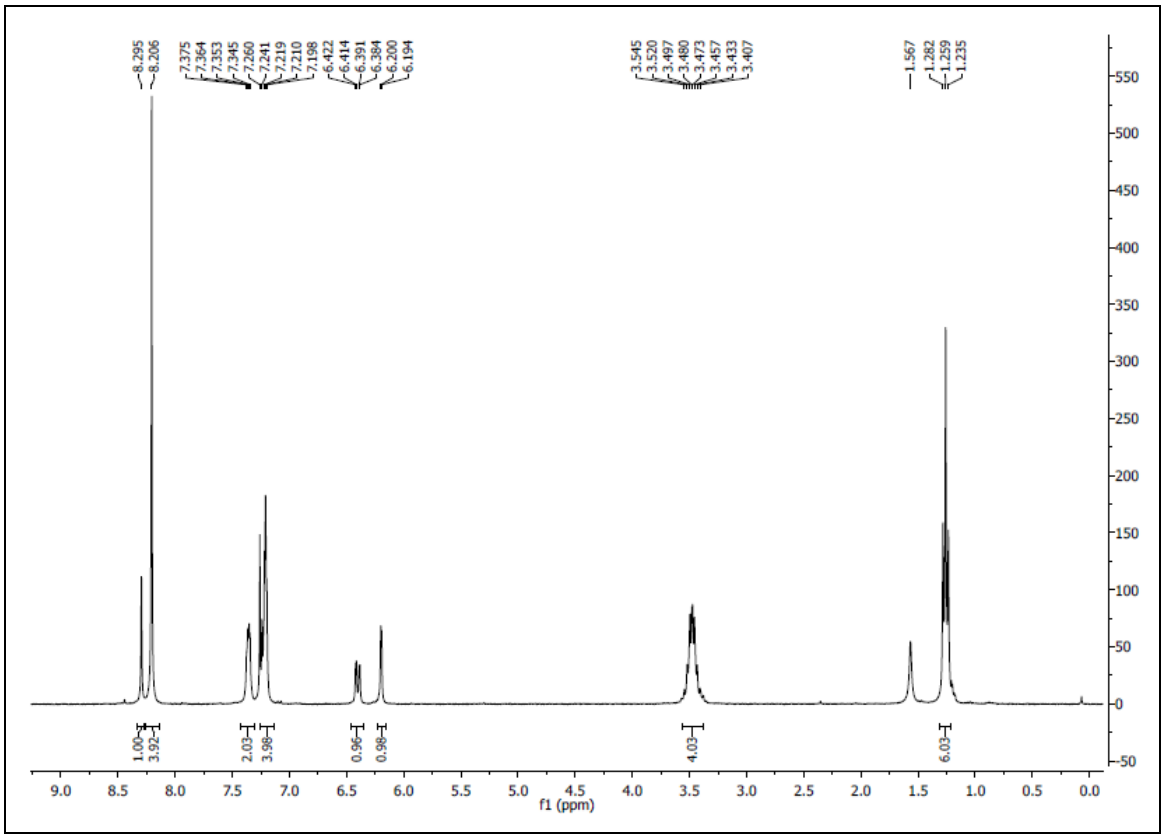
8.295
8.206
7.375
7.364
7.353
7.345
7.260
7.241
7.219
7.210
7.198
6.422
6.414
6.391
6.384
6.200
6.194
3.545
3.520
3.497
3.480
3.473
3.457
3.433
3.407
1.567
1.282
1.259
1.235
1.00
3.92
2.03
3.98
0.96
0.98
4.03
6.03
f1 (ppm)

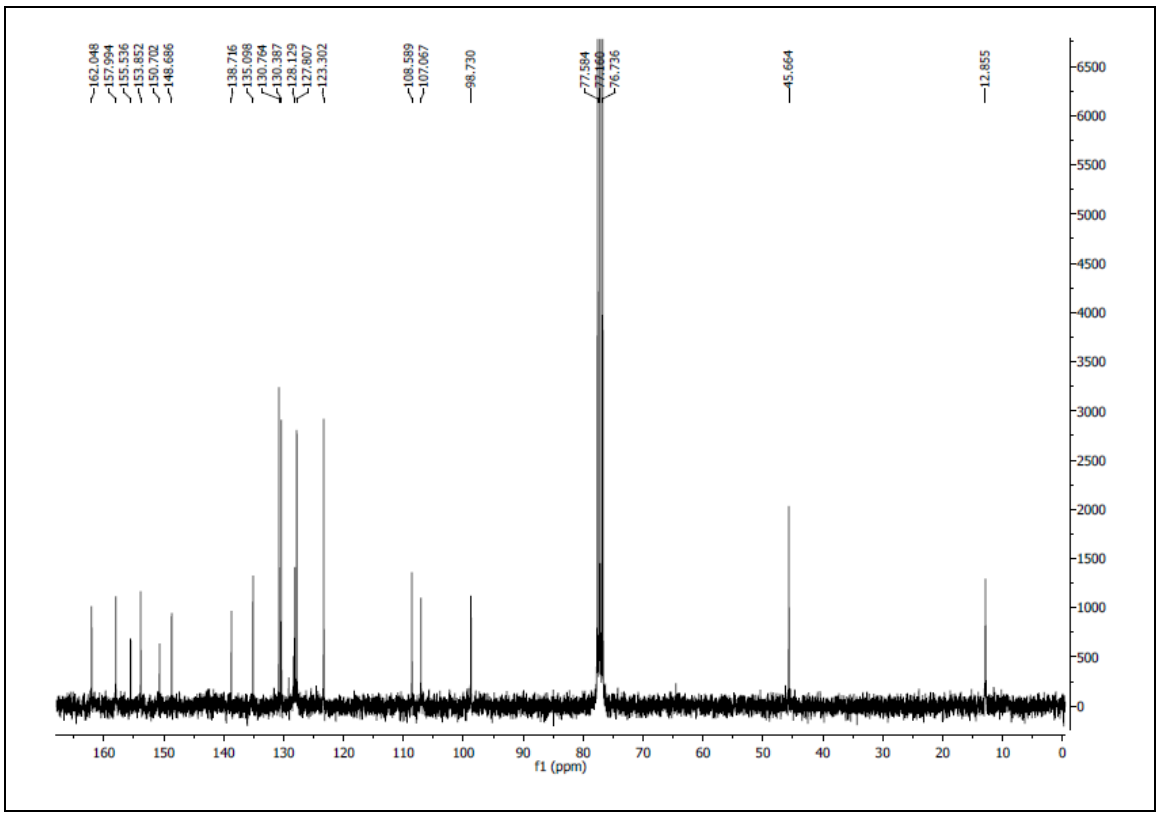
162.048
157.994
155.536
153.852
150.702
148.686
138.716
135.098
130.764
130.387
128.129
127.807
123.302
108.589
107.067
98.730
77.584
77.160
76.736
45.664
12.855
f1 (ppm)

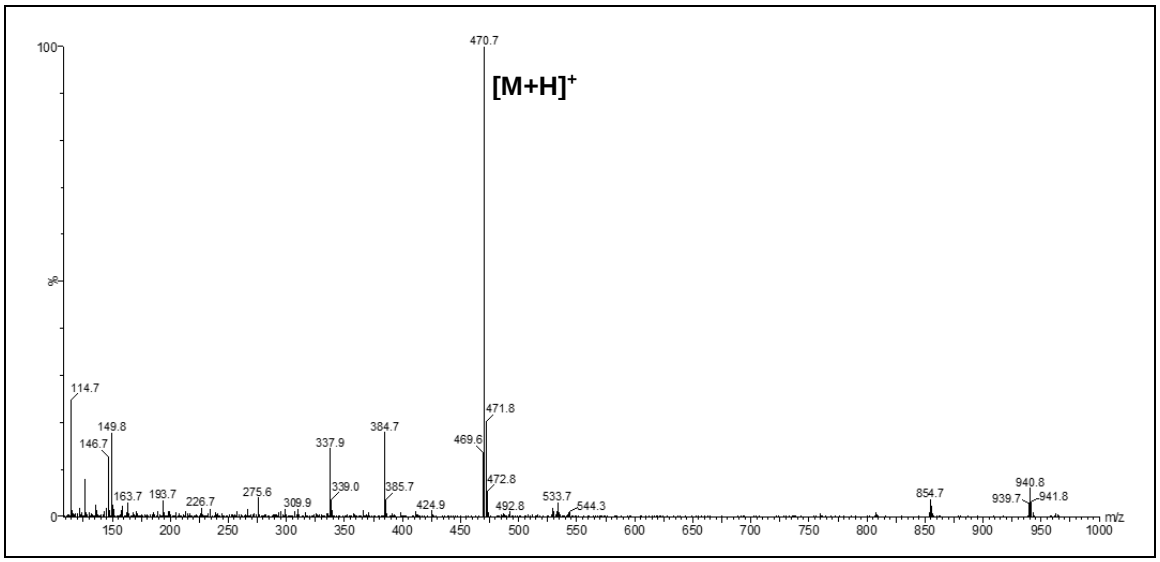
[M+H]+
470.7
100
%
0
114.7
149.8
146.7
163.7
193.7
226.7
275.6
309.9
337.9
339.0
384.7
385.7
424.9
469.6
471.8
472.8
492.8
533.7
544.3
854.7
939.7
940.8
941.8
m/z
150
200
250
300
350
400
450
500
550
600
650
700
750
800
850
900
950
1000

- **BASHY 81f**

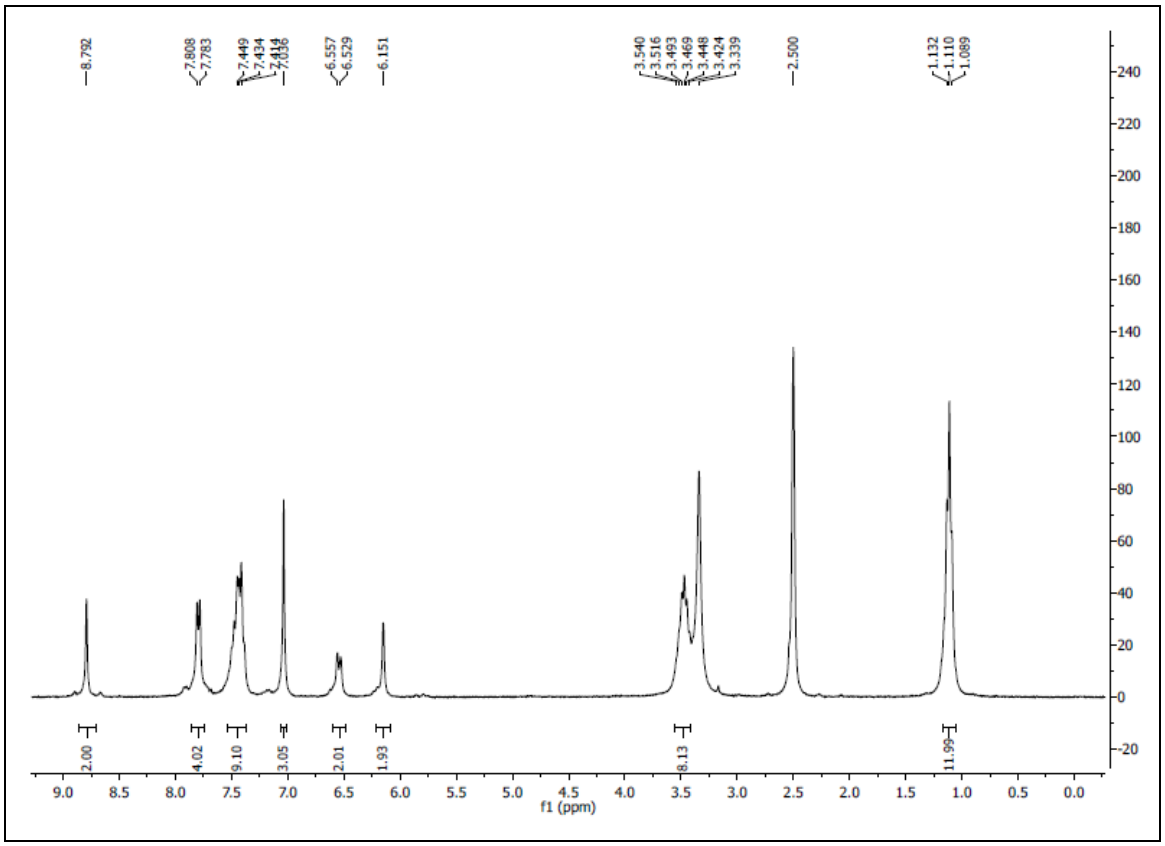
8.792
7.808
7.783
7.449
7.434
7.414
7.408
6.557
6.529
6.151
3.540
3.516
3.493
3.469
3.448
3.424
3.339
2.500
1.132
1.110
1.089
2.00
4.02
9.10
3.05
2.01
1.93
8.13
11.99
f1 (ppm)

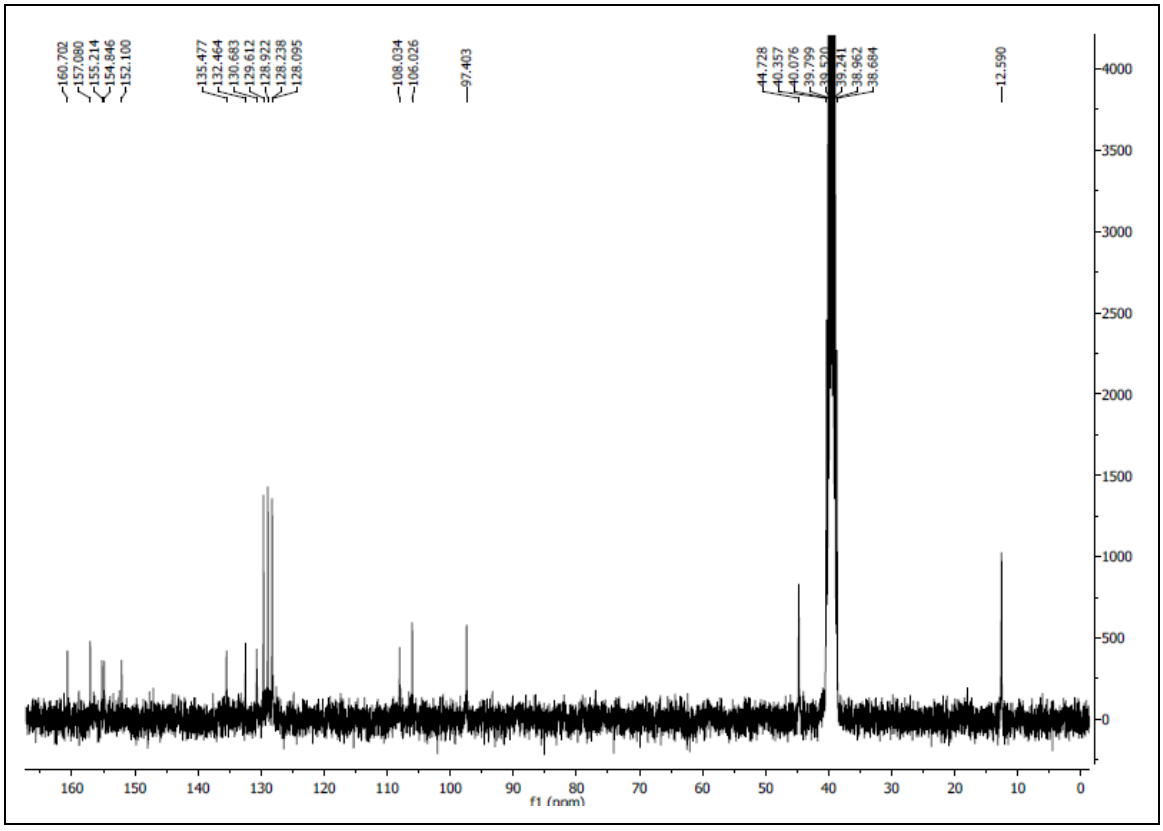
160.702
157.080
155.214
154.846
152.100
135.477
132.464
130.683
129.612
128.922
128.238
128.095
108.034
106.026
97.403
44.728
40.357
40.076
39.799
39.520
39.241
38.962
38.684
12.590
4000
3500
3000
2500
2000
1500
1000
500
0
160
150
140
130
120
110
100
90
80
70
60
50
40
30
20
10
0
f1 (ppm)

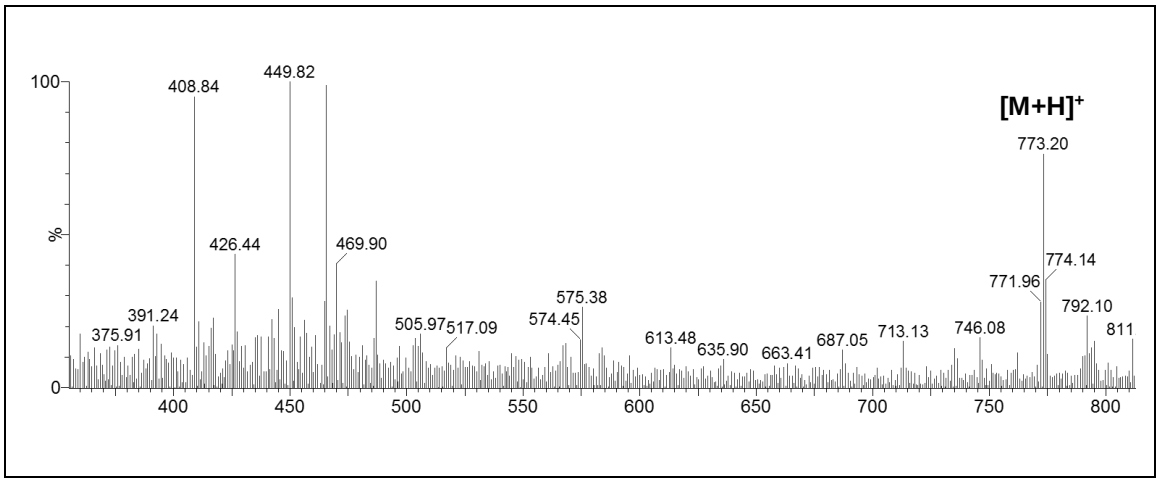
100
%
0
408.84
449.82
426.44
469.90
391.24
375.91
505.97
517.09
575.38
574.45
613.48
635.90
663.41
687.05
713.13
746.08
[M+H]+
773.20
774.14
771.96
792.10
811
400
450
500
550
600
650
700
750
800

- **BASHY 82a**

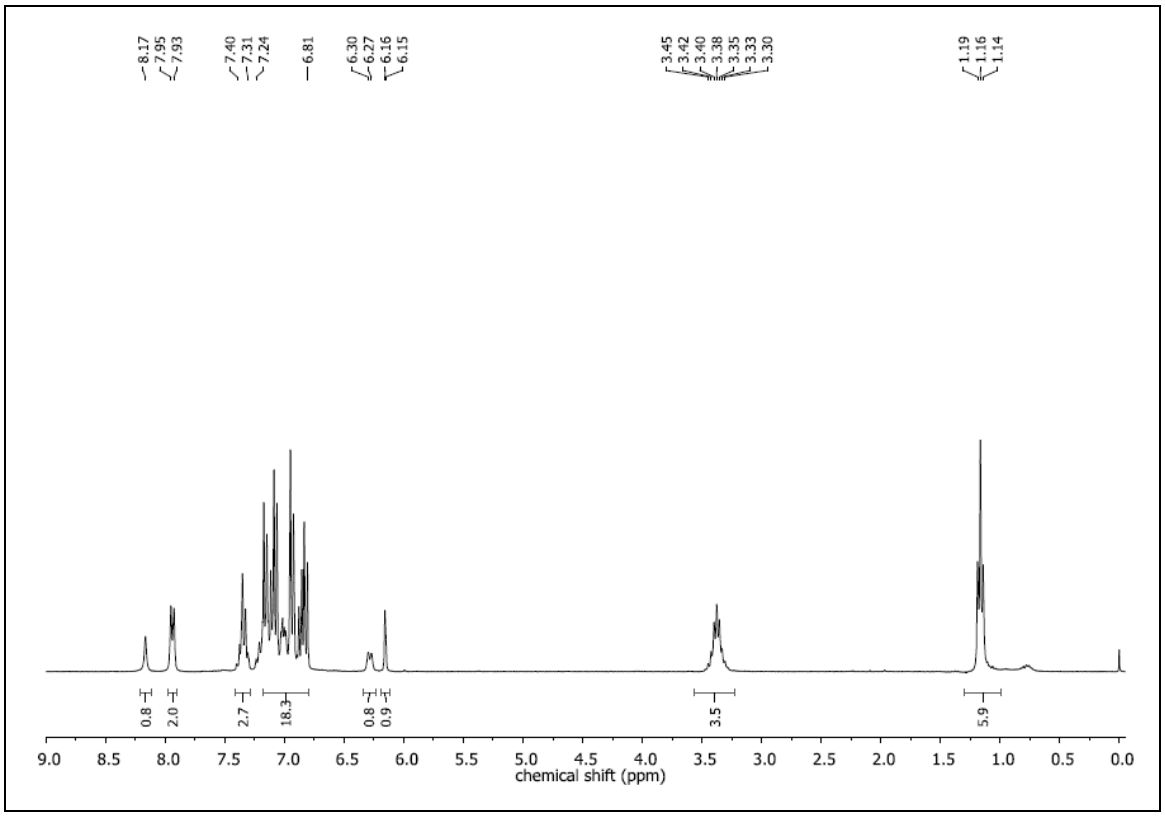
8.17
7.95
7.93
7.40
7.31
7.24
6.81
6.30
6.27
6.16
6.15
3.45
3.42
3.40
3.38
3.35
3.33
3.30
1.19
1.16
1.14
0.8
2.0
2.7
18.3
0.8
0.9
3.5
5.9
chemical shift (ppm)

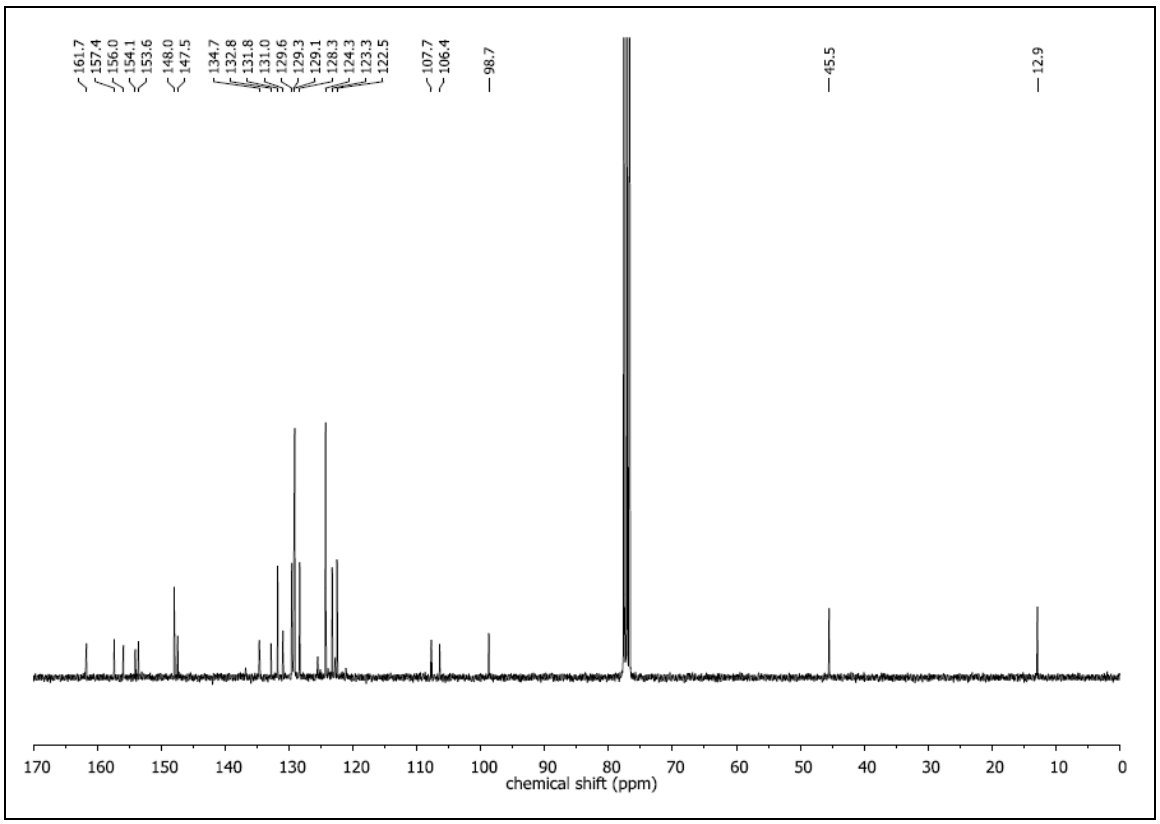
161.7
157.4
156.0
154.1
153.6
148.0
147.5
134.7
132.8
131.8
131.0
129.6
129.3
129.1
128.3
124.3
123.3
122.5
107.7
106.4
98.7
45.5
12.9
chemical shift (ppm)

Boron NMR

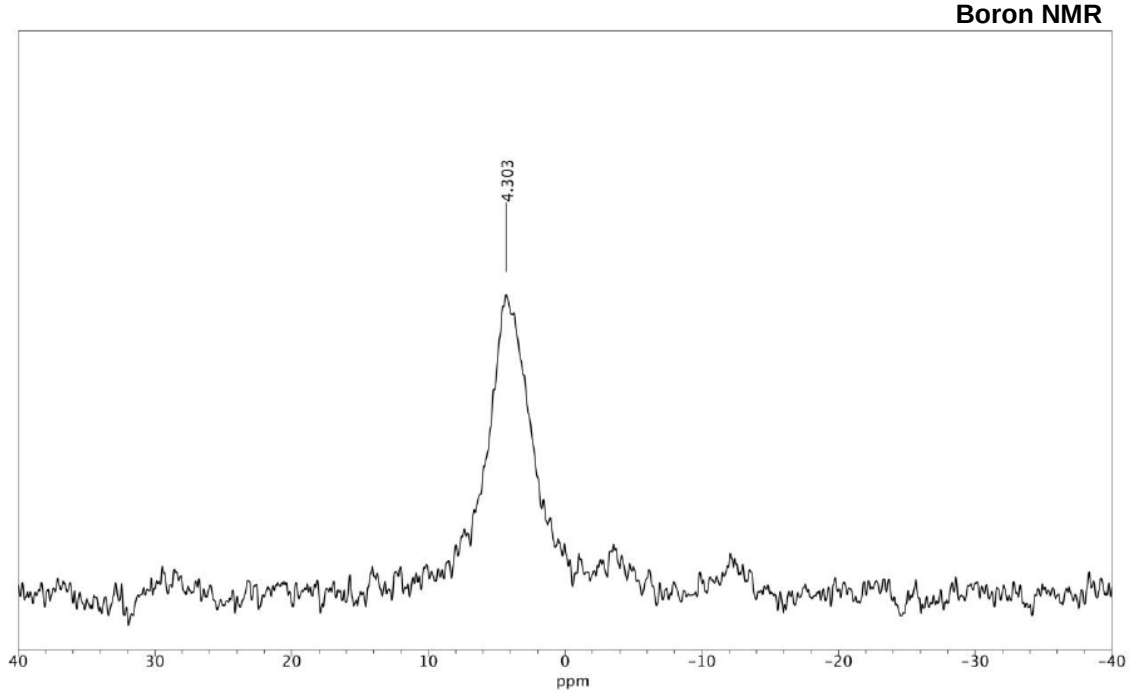
4.303
40
30
20
10
0
-10
-20
-30
-40
ppm

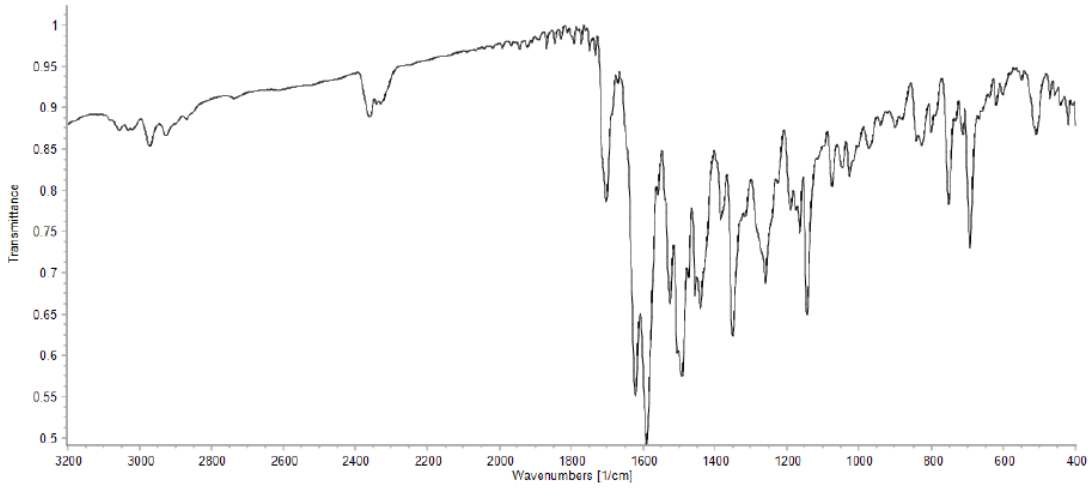
Transmittance
1
0.95
0.9
0.85
0.8
0.75
0.7
0.65
0.6
0.55
0.5
3200
3000
2800
2600
2400
2200
2000
1800
1600
1400
1200
1000
800
600
400
Wavenumbers [1/cm]

- **BASHY 82b**

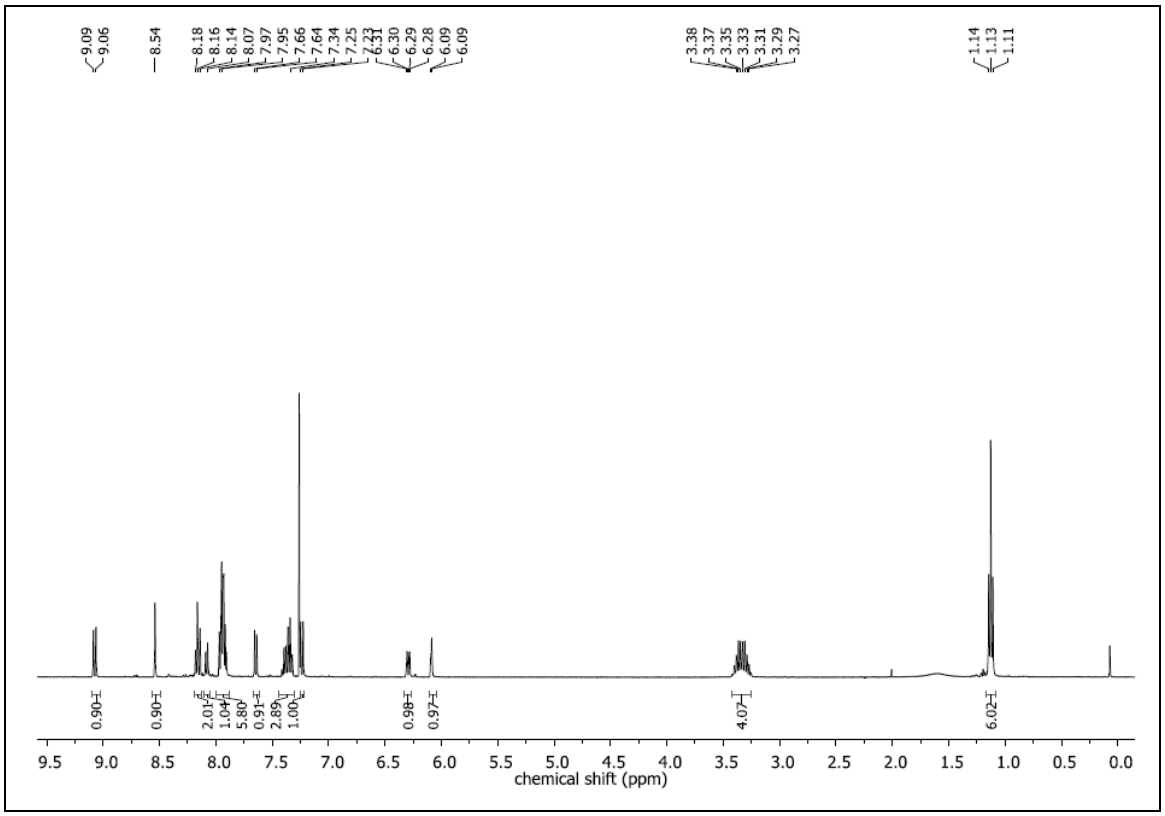
9.09
9.06
8.54
8.18
8.16
8.14
8.07
7.97
7.95
7.66
7.64
7.34
7.25
7.23
6.31
6.30
6.29
6.28
6.09
6.09
3.38
3.37
3.35
3.33
3.31
3.29
3.27
1.14
1.13
1.11
0.90
0.90
2.01
1.04
5.80
0.91
2.89
1.00
0.98
0.97
4.07
6.02
chemical shift (ppm)

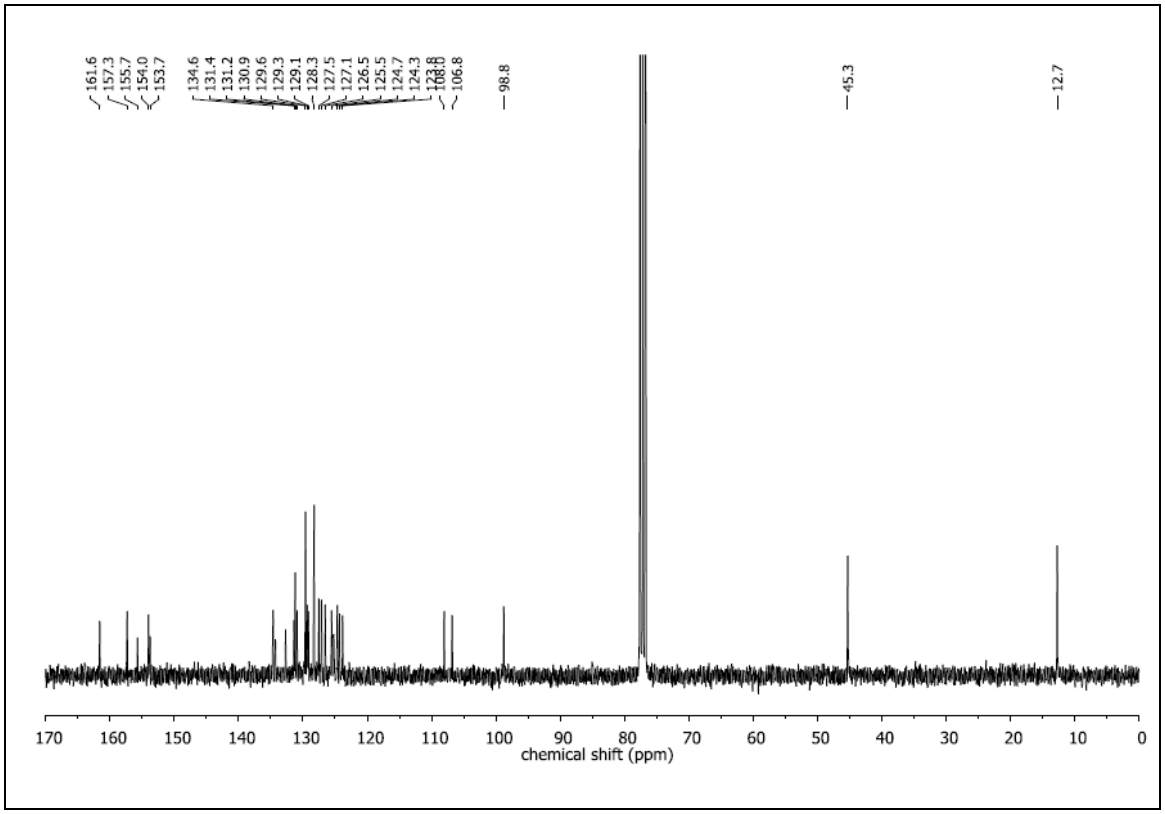
161.6
157.3
155.7
154.0
153.7
134.6
131.4
131.2
130.9
129.6
129.3
129.1
128.3
127.5
127.1
126.5
125.5
124.7
124.3
106.8
98.8
45.3
12.7
chemical shift (ppm)

Boron NMR

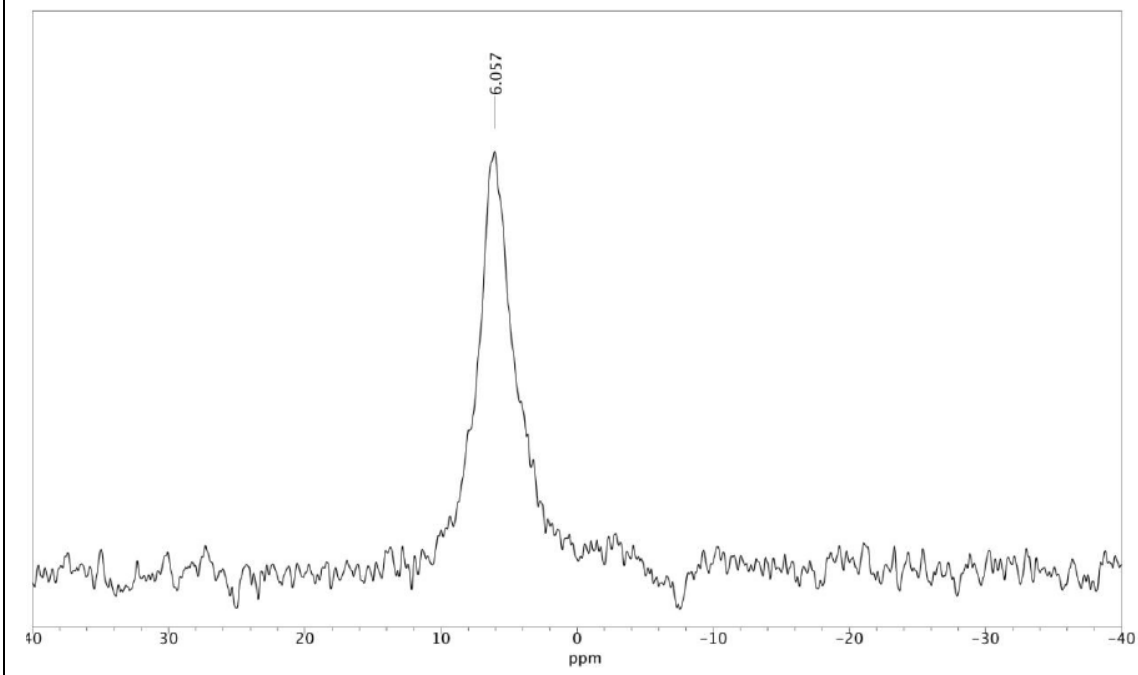
6.057
40
30
20
10
0
-10
-20
-30
-40
ppm

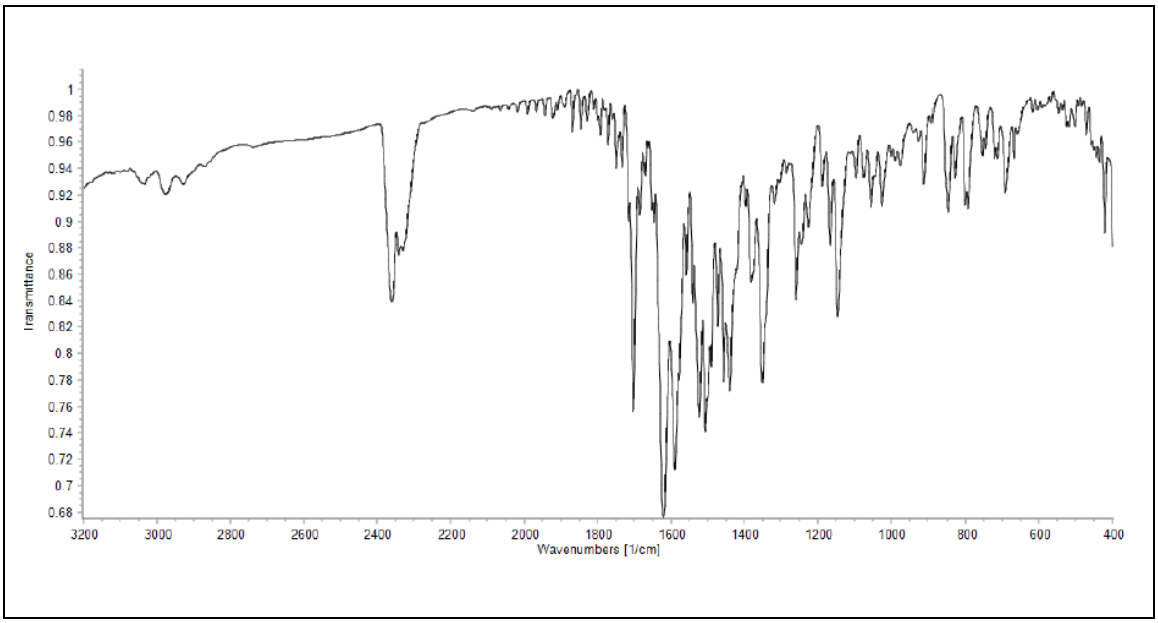
Transmittance
1
0.98
0.96
0.94
0.92
0.9
0.88
0.86
0.84
0.82
0.8
0.78
0.76
0.74
0.72
0.7
0.68
3200
3000
2800
2600
2400
2200
2000
1800
1600
1400
1200
1000
800
600
400
Wavenumbers [1/cm]

- **BASHY 82c**

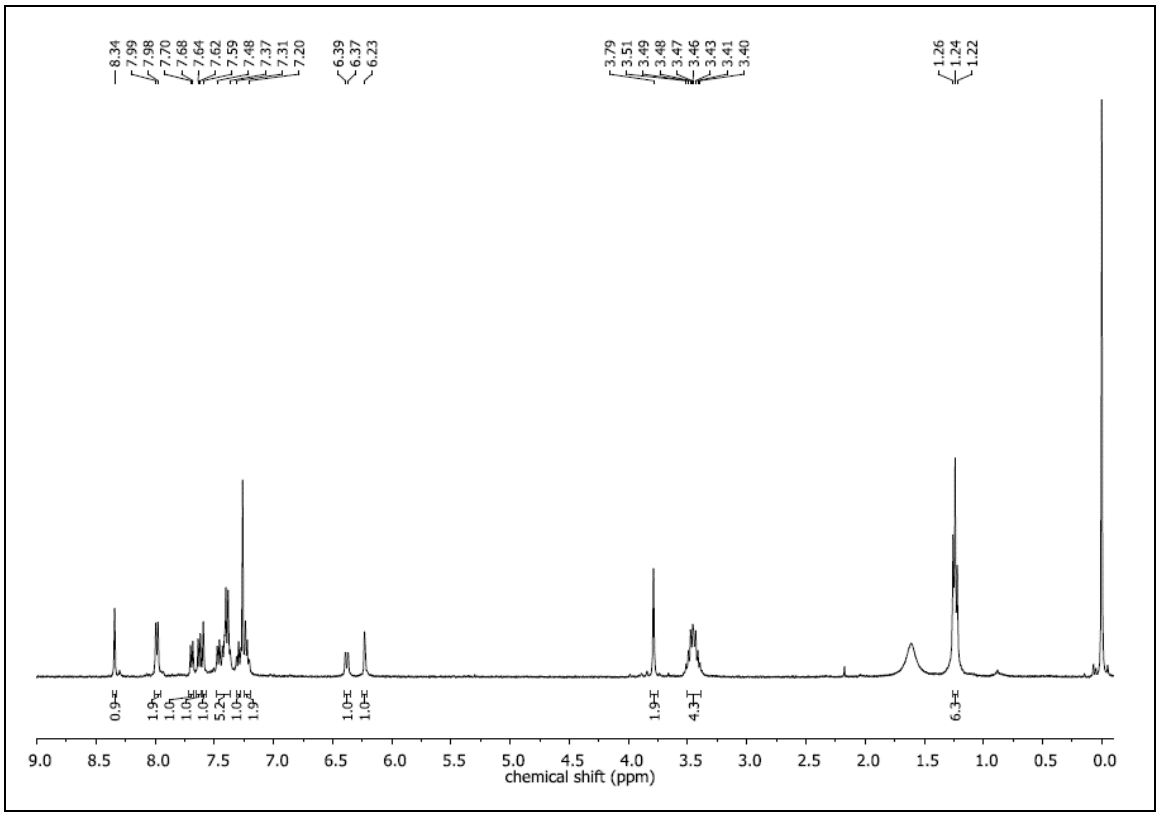
8.34
7.99
7.98
7.70
7.68
7.64
7.62
7.59
7.48
7.37
7.31
7.20
6.39
6.37
6.23
3.79
3.51
3.49
3.48
3.47
3.46
3.43
3.41
3.40
1.26
1.24
1.22
0.9
1.9
1.0
1.0
1.0
5.2
1.0
1.9
1.0
1.0
1.9
4.3
6.3
chemical shift (ppm)

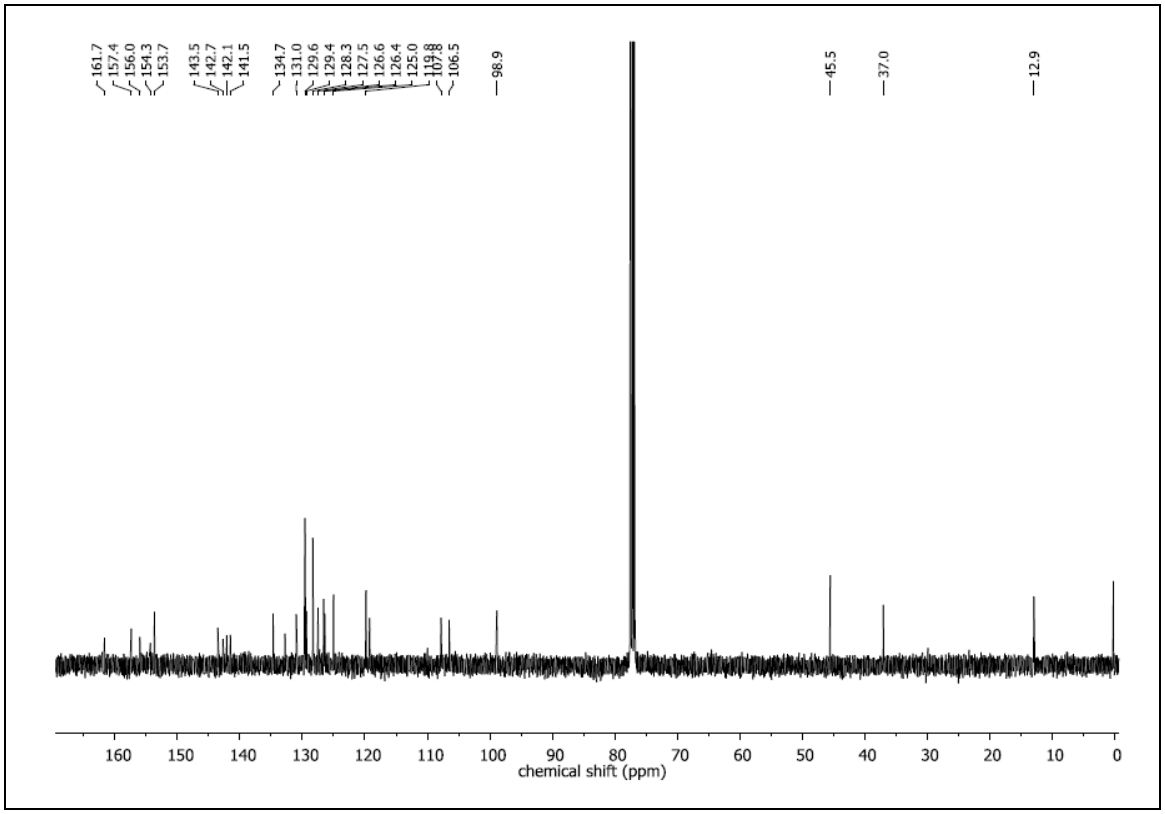
161.7
157.4
156.0
154.3
153.7
143.5
142.7
142.1
141.5
134.7
131.0
129.6
129.4
128.3
127.5
126.6
126.4
125.0
106.5
98.9
45.5
37.0
12.9
chemical shift (ppm)

Boron NMR

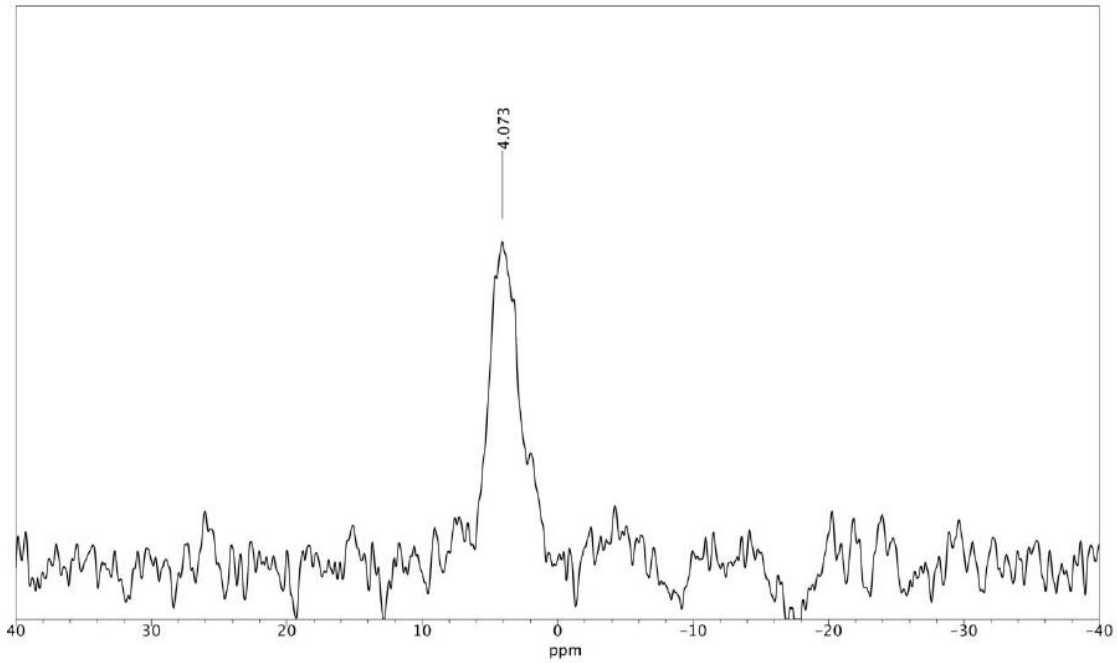
4.073
40
30
20
10
0
-10
-20
-30
-40
ppm

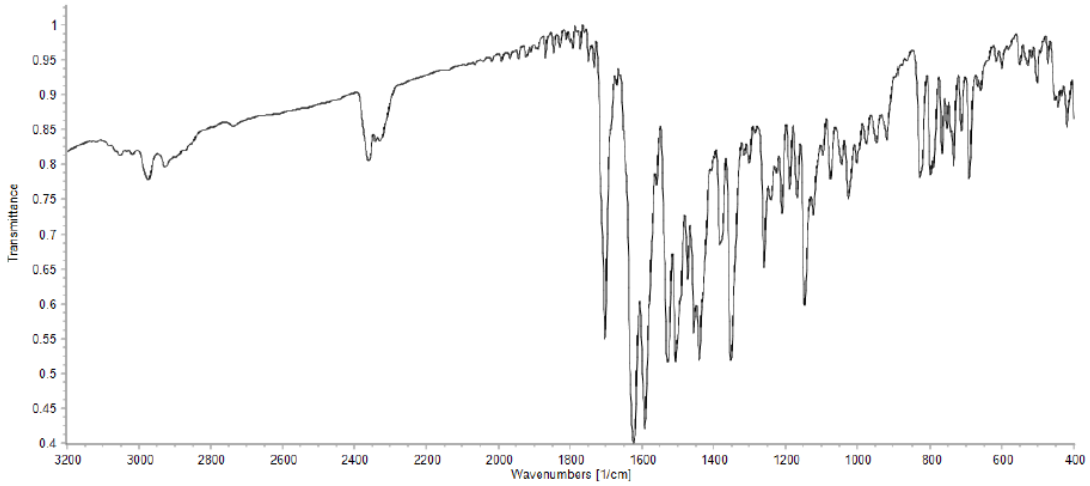
Transmittance
1
0.95
0.9
0.85
0.8
0.75
0.7
0.65
0.6
0.55
0.5
0.45
0.4
3200
3000
2800
2600
2400
2200
2000
1800
1600
1400
1200
1000
800
600
400
Wavenumbers [1/cm]

- **BASHY 82d**

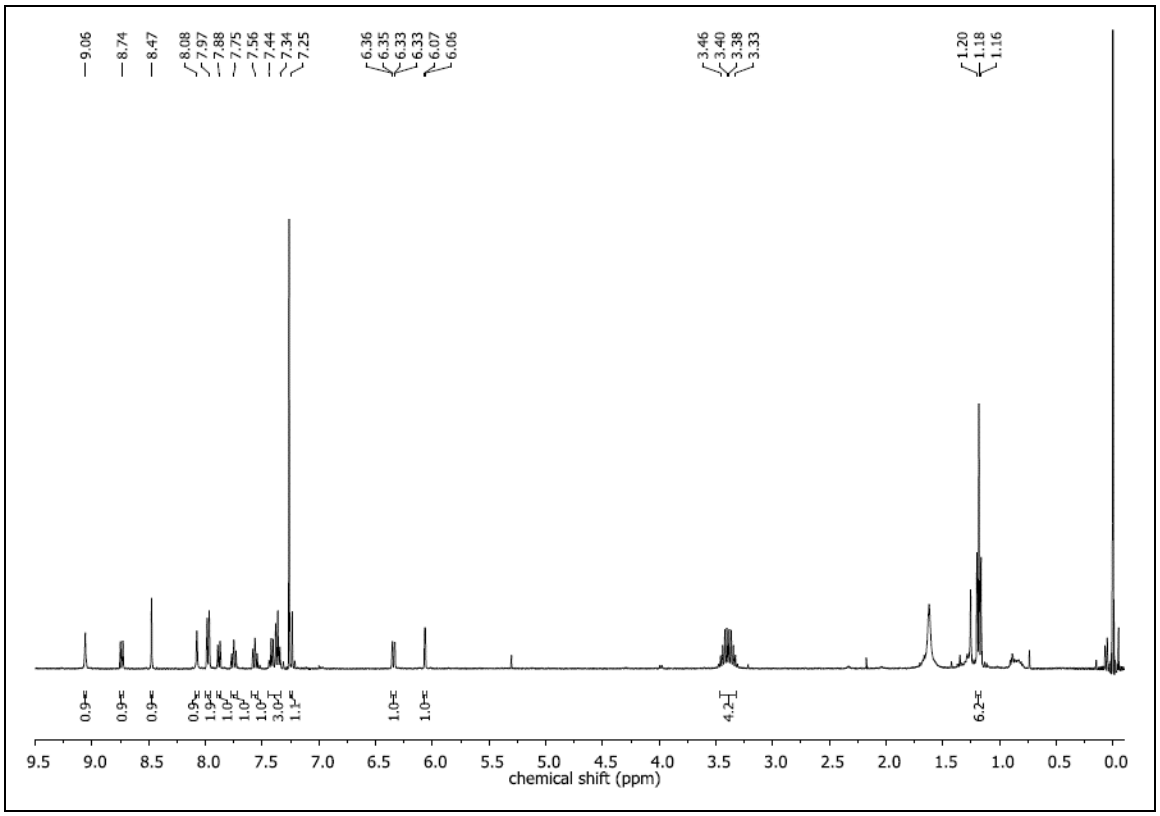
9.06
8.74
8.47
8.08
7.97
7.88
7.75
7.56
7.44
7.34
7.25
6.36
6.35
6.33
6.33
6.07
6.06
3.46
3.40
3.38
3.33
1.20
1.18
1.16
0.9
0.9
0.9
0.9
1.9
1.0
1.0
1.0
3.0
1.1
1.0
1.0
4.2
6.2
chemical shift (ppm)

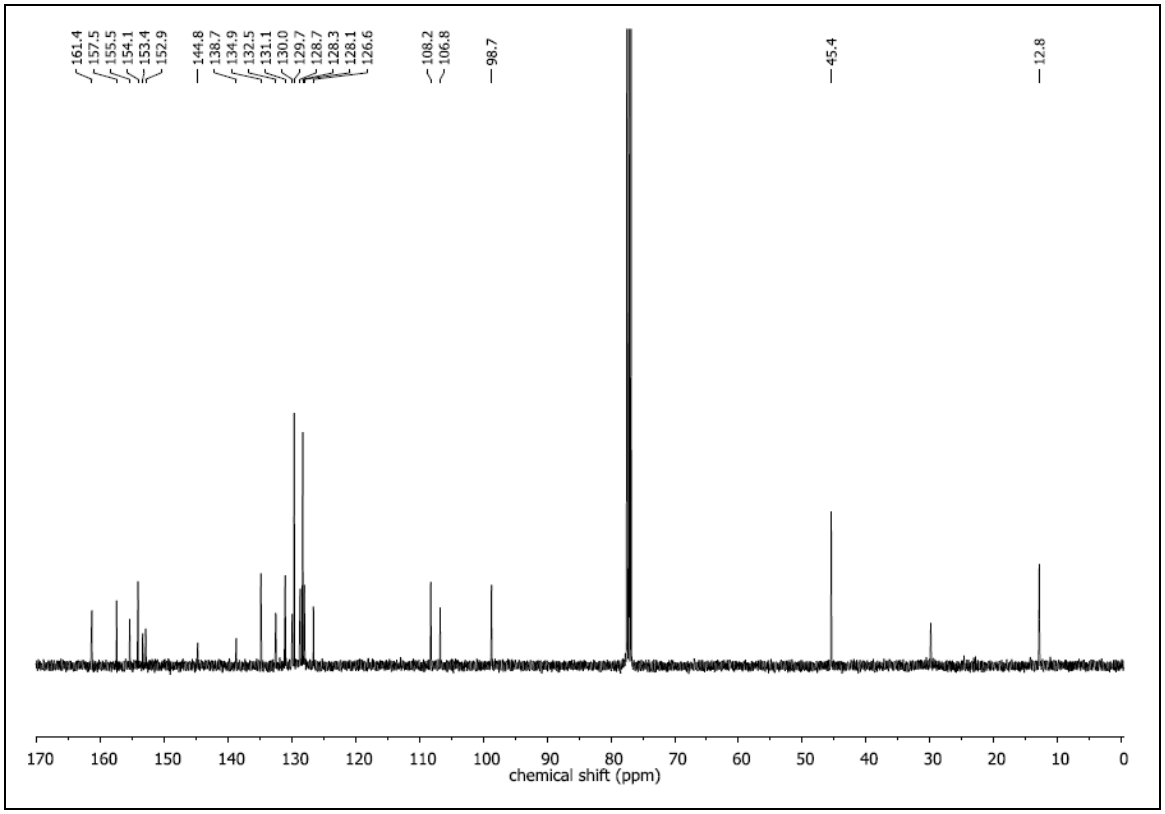
161.4
157.5
155.5
154.1
153.4
152.9
144.8
138.7
134.9
132.5
131.1
130.0
129.7
128.7
128.3
128.1
126.6
108.2
106.8
98.7
45.4
12.8
chemical shift (ppm)

Boron NMR

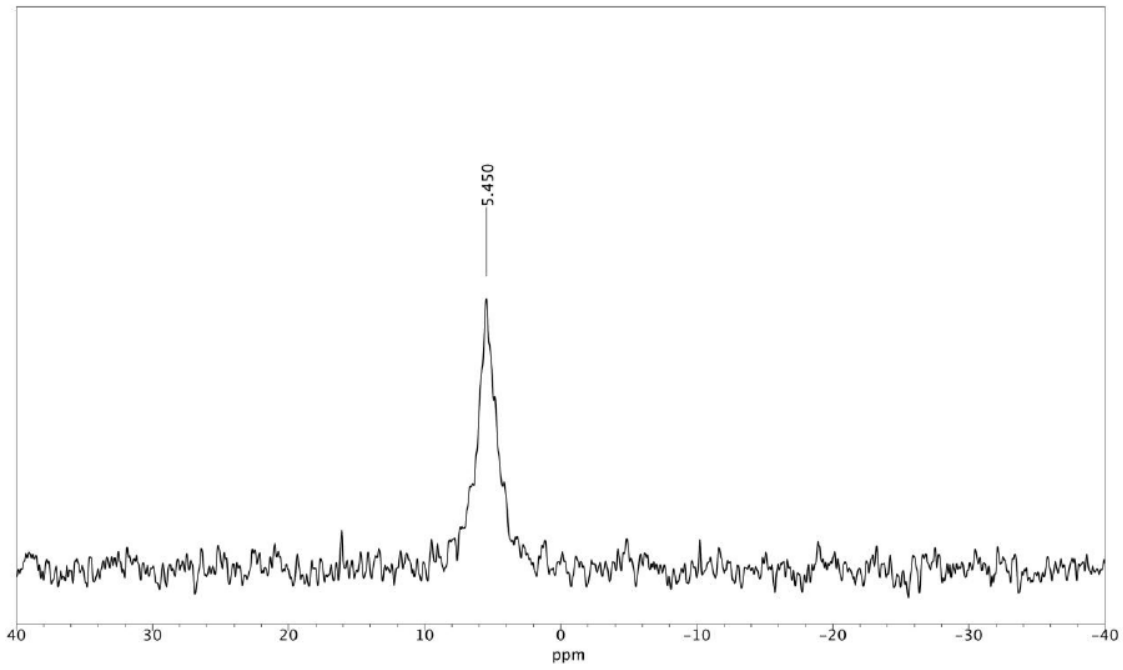
5.450
40
30
20
10
0
-10
-20
-30
-40
ppm

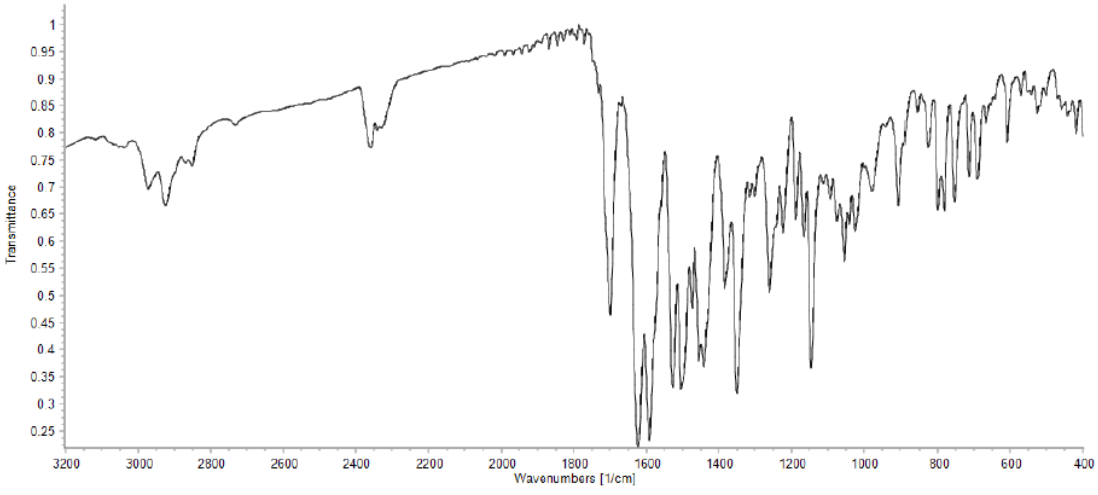
Transmittance
1
0.95
0.9
0.85
0.8
0.75
0.7
0.65
0.6
0.55
0.5
0.45
0.4
0.35
0.3
0.25
3200
3000
2800
2600
2400
2200
2000
1800
1600
1400
1200
1000
800
600
400
Wavenumbers [1/cm]

- **BASHY 82e**

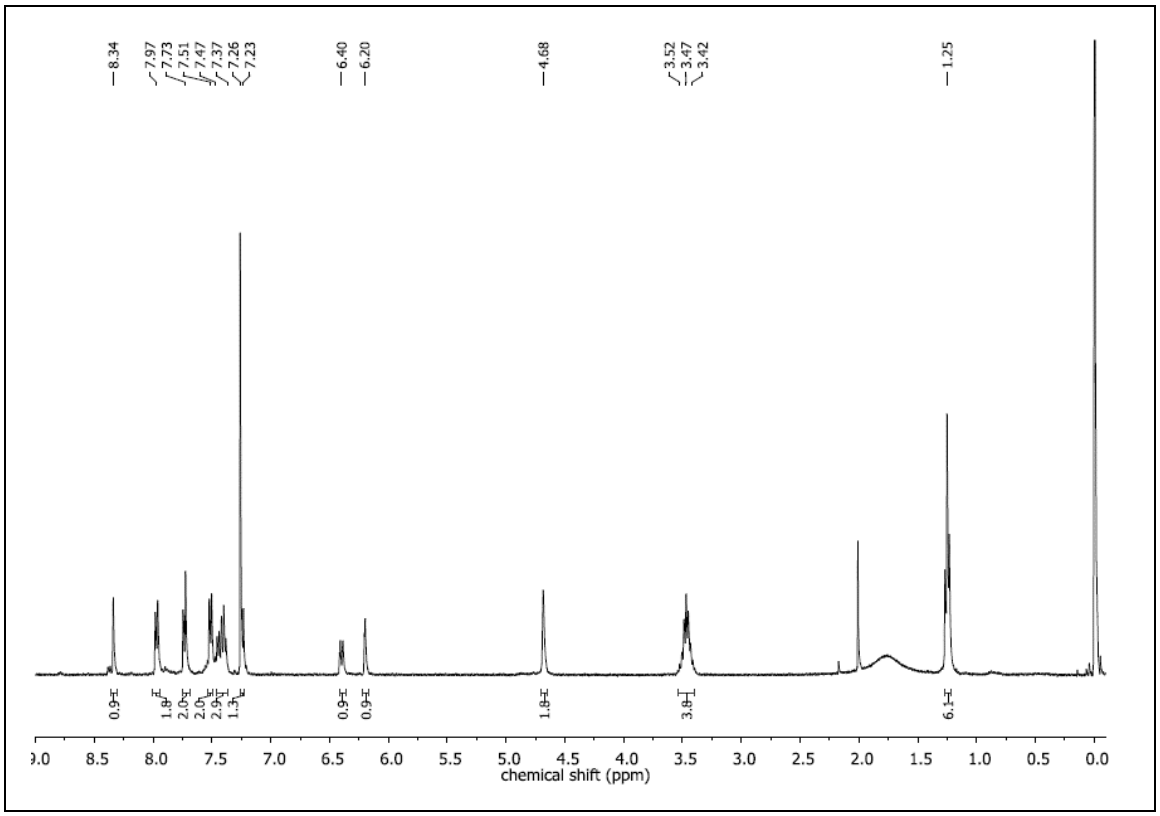
8.34
7.97
7.73
7.51
7.47
7.37
7.26
7.23
6.40
6.20
4.68
3.52
3.47
3.42
1.25
0.9
1.8
2.0
2.0
2.0
1.3
0.9
0.9
1.8
3.8
6.1
chemical shift (ppm)

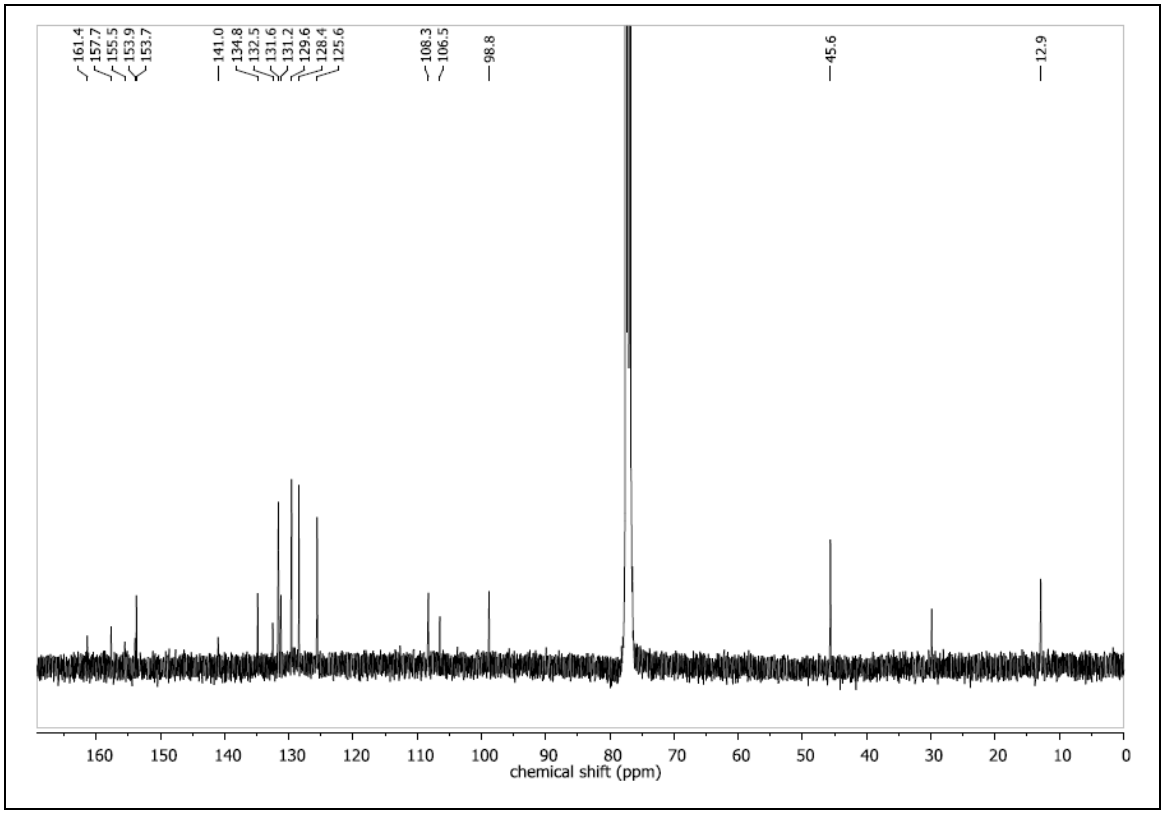
161.4
157.7
155.5
153.9
153.7
141.0
134.8
132.5
131.6
131.2
129.6
128.4
125.6
108.3
106.5
98.8
45.6
12.9
chemical shift (ppm)

Boron NMR

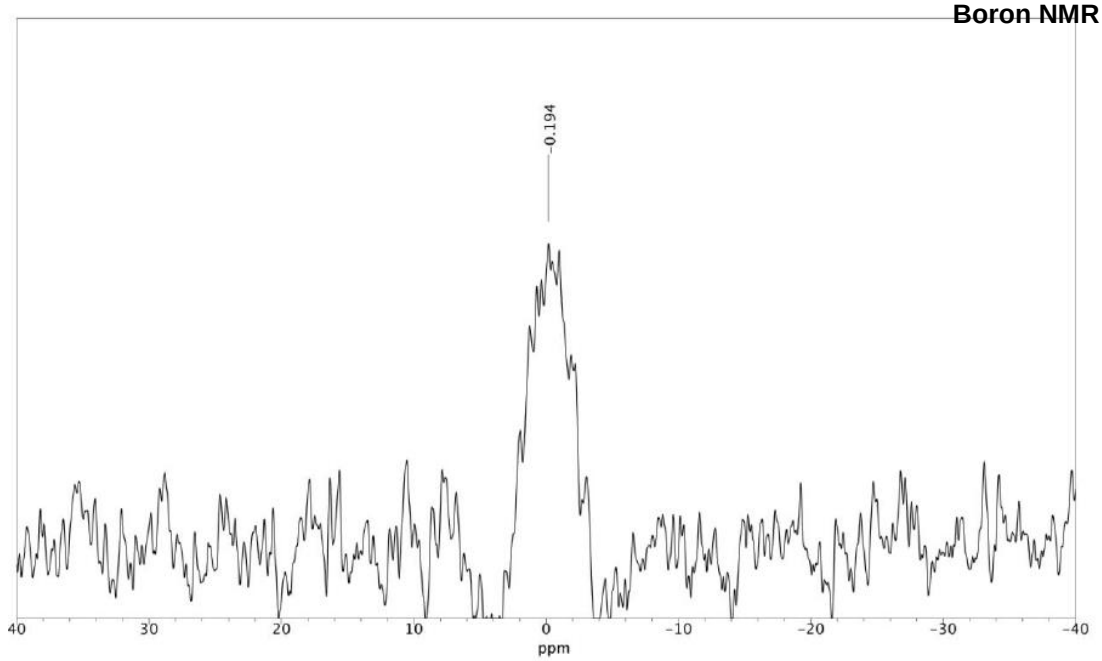
0.194
40
30
20
10
0
-10
-20
-30
-40
ppm

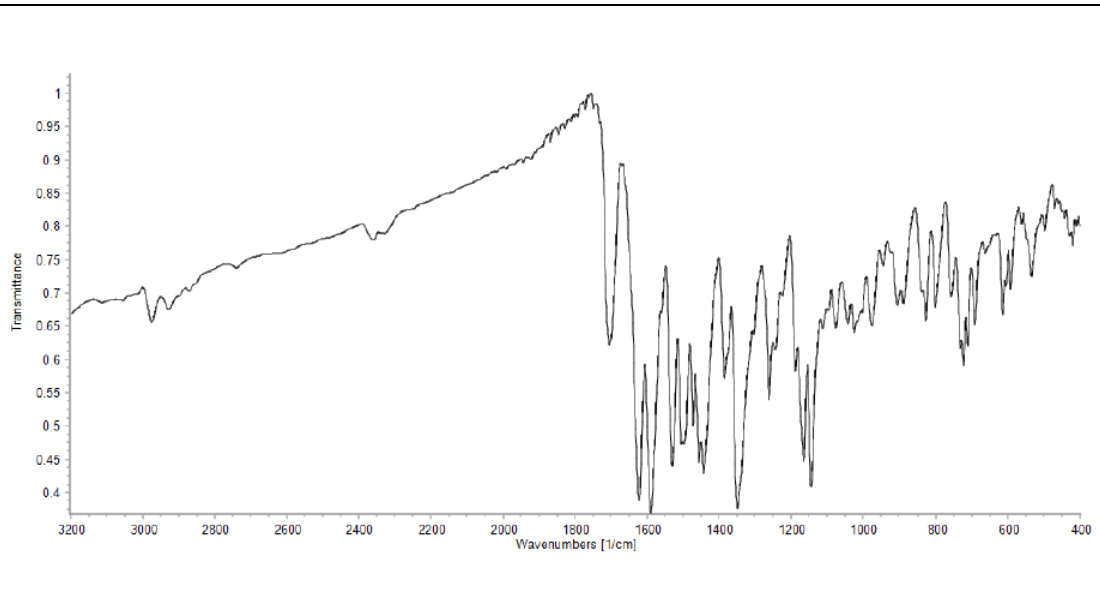
Transmittance
1
0.95
0.9
0.85
0.8
0.75
0.7
0.65
0.6
0.55
0.5
0.45
0.4
3200
3000
2800
2600
2400
2200
2000
1800
1600
1400
1200
1000
800
600
400
Wavenumbers [1/cm]

- **BASHY 82f**

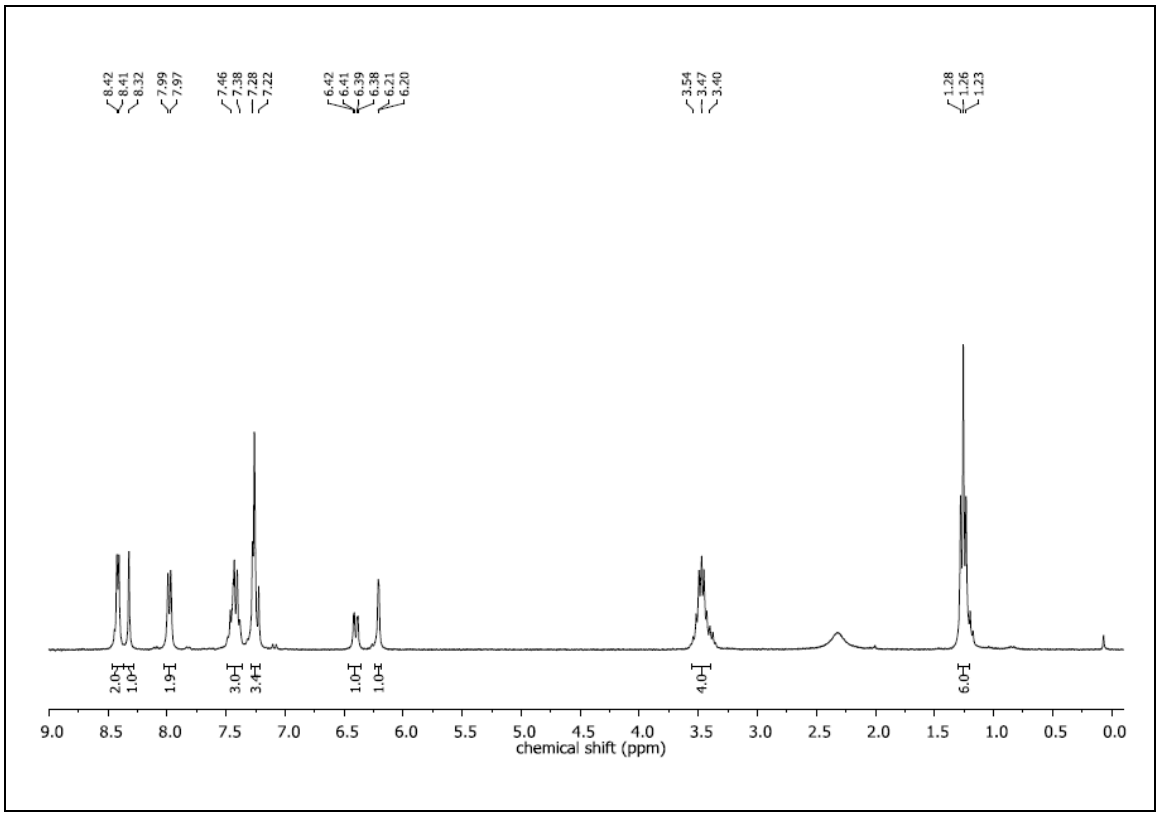
8.42
8.41
8.32
7.99
7.97
7.46
7.38
7.28
7.22
6.42
6.41
6.39
6.38
6.21
6.20
3.54
3.47
3.40
1.28
1.26
1.23
2.0
1.0
1.9
3.0
3.4
1.0
1.0
4.0
6.0
chemical shift (ppm)

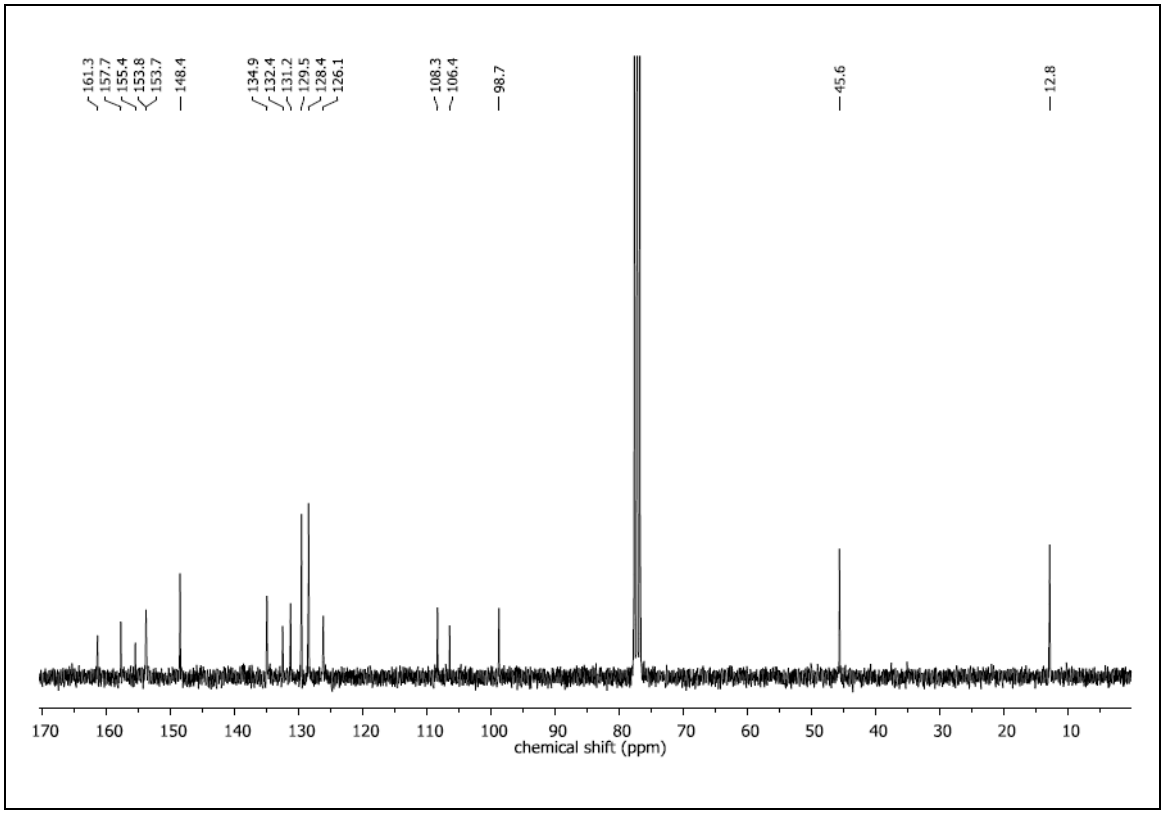
161.3
157.7
155.4
153.8
153.7
148.4
134.9
132.4
131.2
129.5
128.4
126.1
108.3
106.4
98.7
45.6
12.8
chemical shift (ppm)

Boron NMR

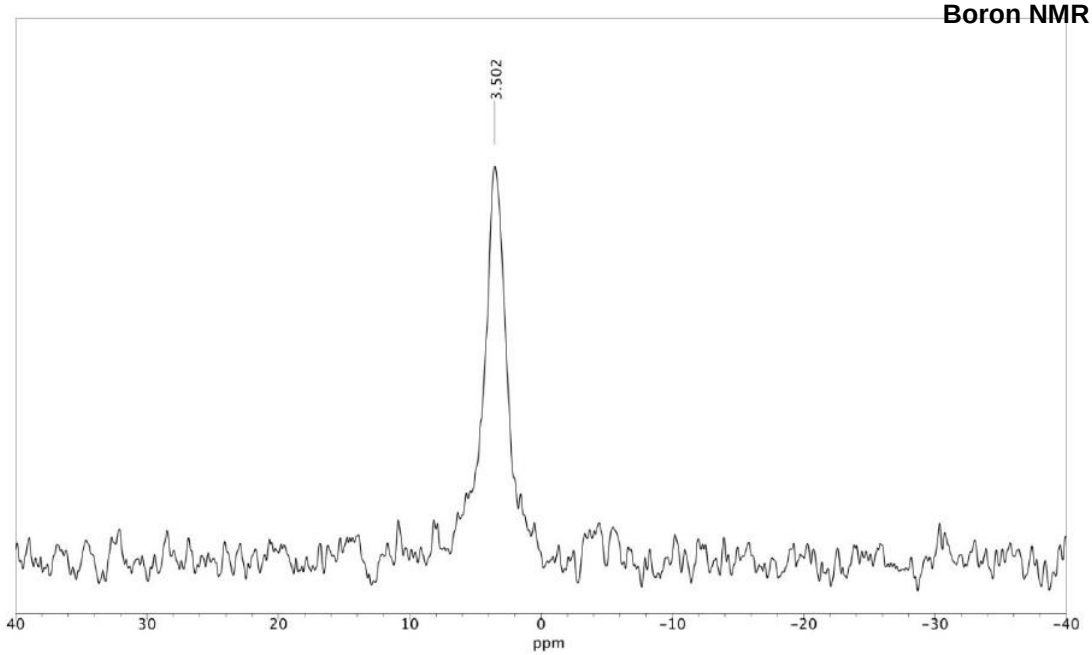
3.502
40
30
20
10
0
-10
-20
-30
-40
ppm

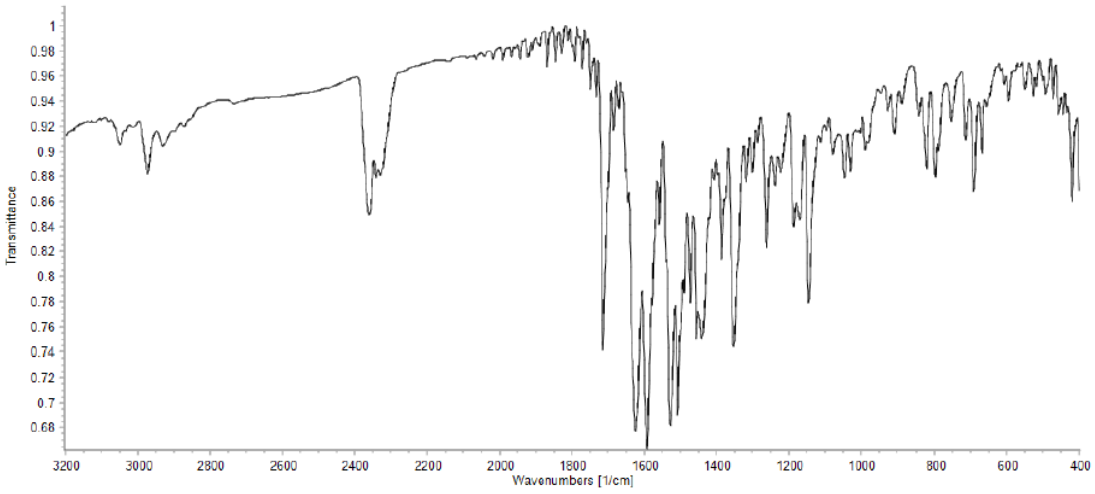
Transmittance
1
0.98
0.96
0.94
0.92
0.9
0.88
0.86
0.84
0.82
0.8
0.78
0.76
0.74
0.72
0.7
0.68
3200
3000
2800
2600
2400
2200
2000
1800
1600
1400
1200
1000
800
600
400
Wavenumbers [1/cm]

- **BASHY 82g**

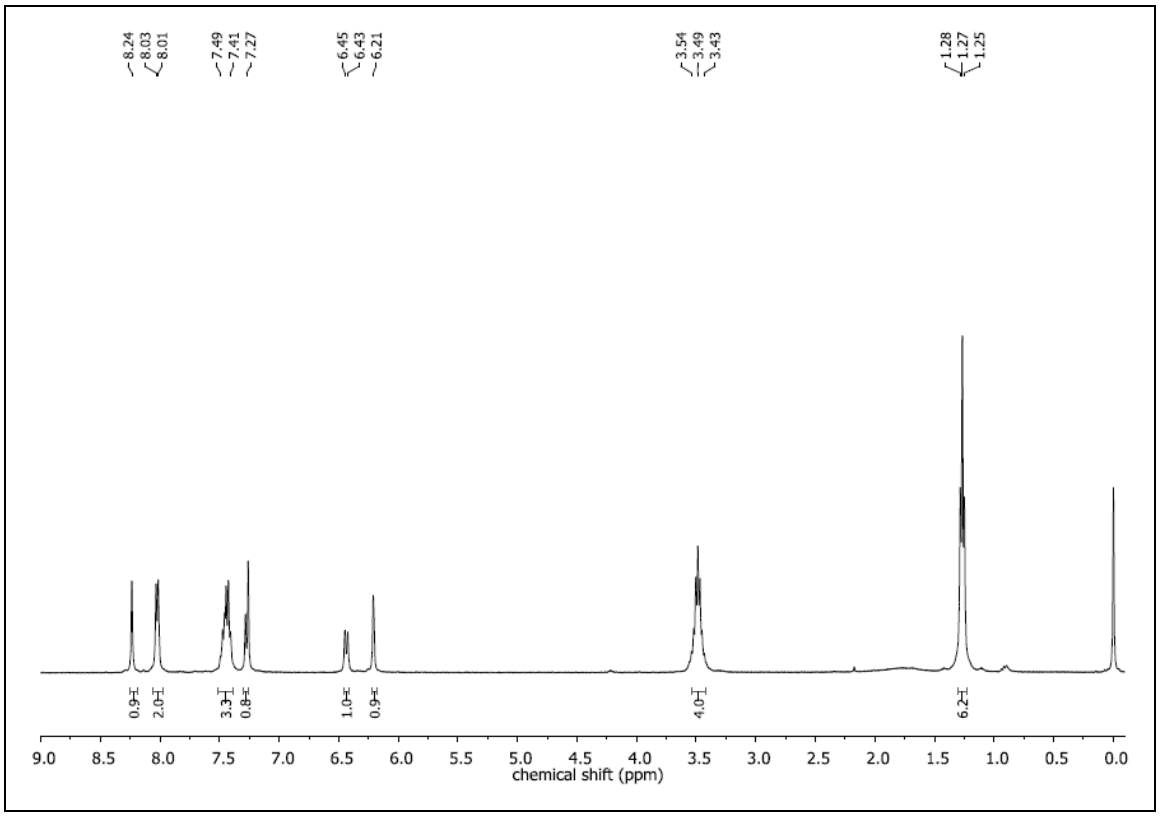
8.24
8.03
8.01
7.49
7.41
7.27
6.45
6.43
6.21
3.54
3.49
3.43
1.28
1.27
1.25
0.9
2.0
3.3
0.8
1.0
0.9
4.0
6.2
chemical shift (ppm)

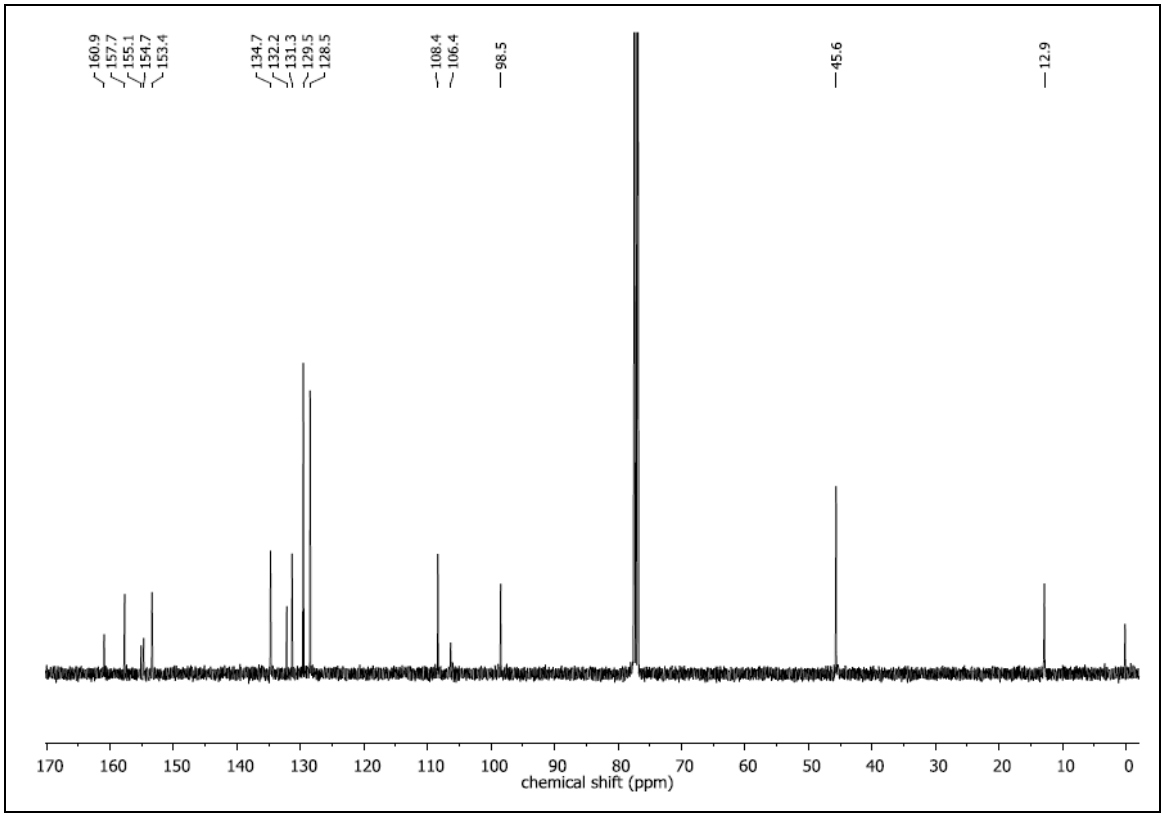
160.9
157.7
155.1
154.7
153.4
134.7
132.2
131.3
129.5
128.5
108.4
106.4
98.5
45.6
12.9
chemical shift (ppm)

Boron NMR

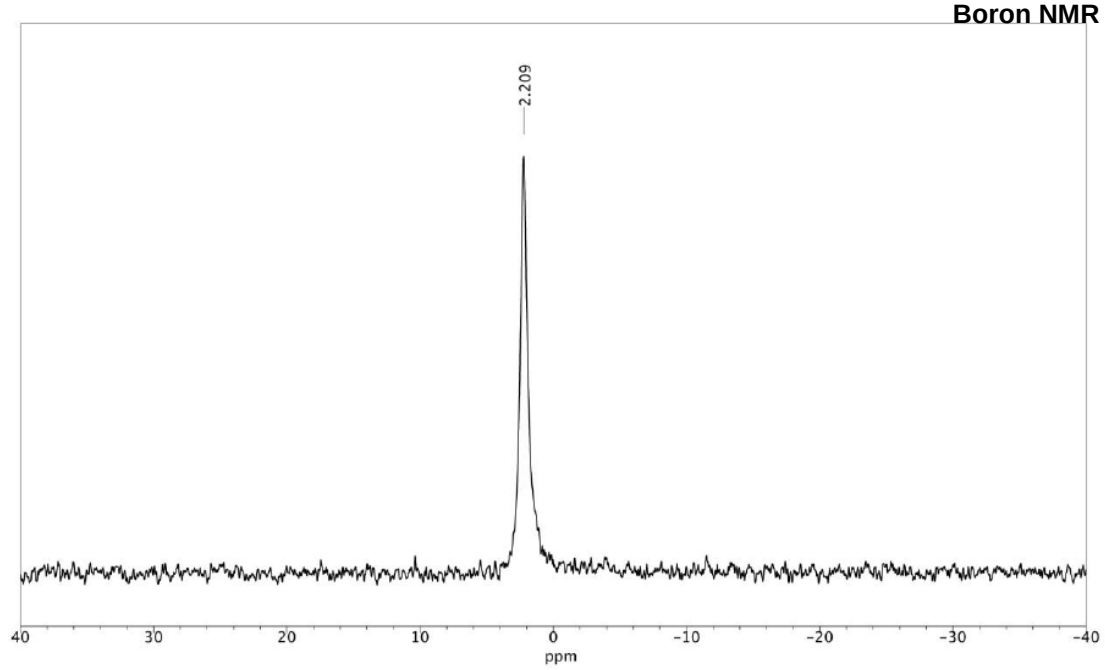
2.209
40
30
20
10
0
-10
-20
-30
-40
ppm

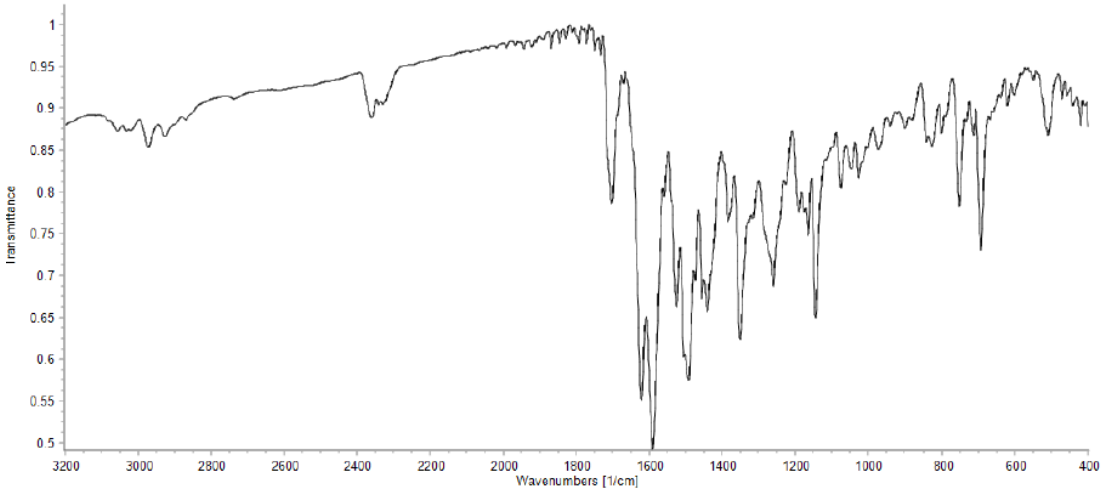
Transmittance
1
0.95
0.9
0.85
0.8
0.75
0.7
0.65
0.6
0.55
0.5
3200
3000
2800
2600
2400
2200
2000
1800
1600
1400
1200
1000
800
600
400
Wavenumbers [1/cm]

- **BASHY 82h**

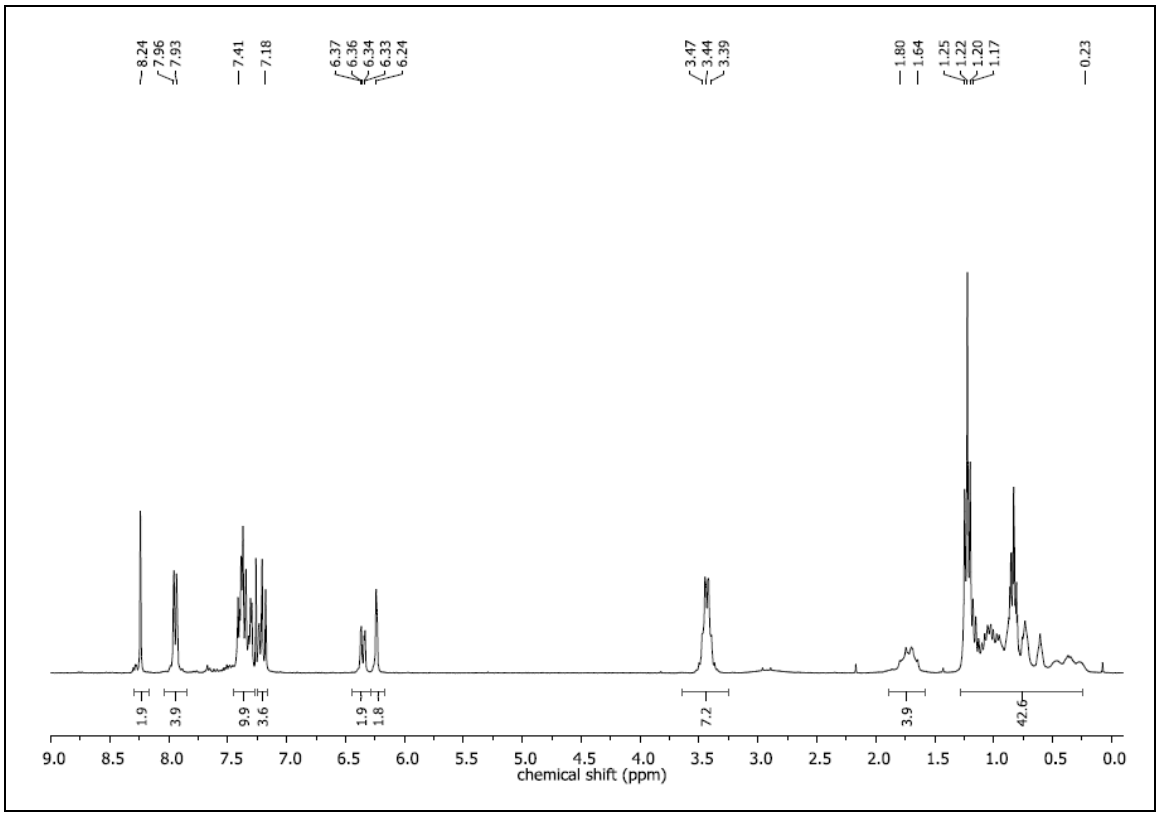
8.24
7.96
7.93
7.41
7.18
6.37
6.36
6.34
6.33
6.24
3.47
3.44
3.39
1.80
1.64
1.25
1.22
1.20
1.17
0.23
1.9
3.9
9.9
3.6
1.9
1.8
7.2
3.9
42.6
chemical shift (ppm)

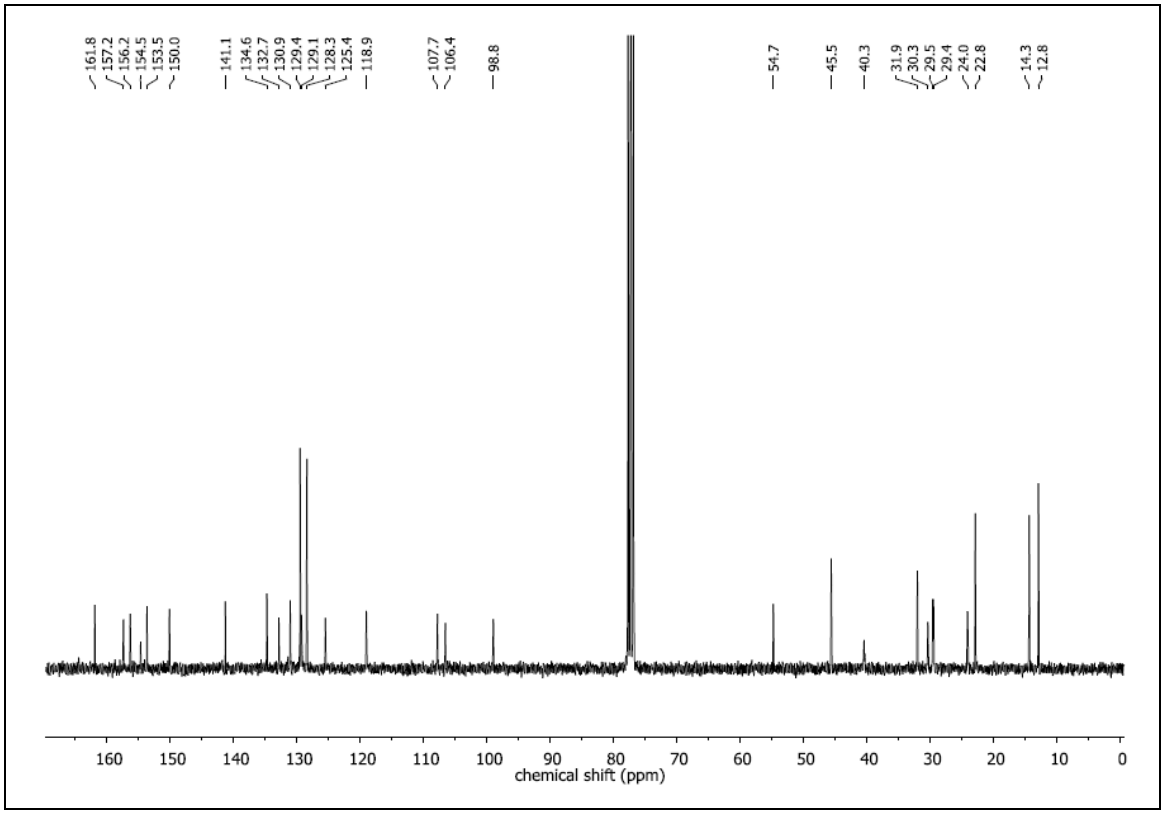
161.8
157.2
156.2
154.5
153.5
150.0
141.1
134.6
132.7
130.9
129.4
129.1
128.3
125.4
118.9
107.7
106.4
98.8
54.7
45.5
40.3
31.9
30.3
29.5
29.4
24.0
22.8
14.3
12.8
chemical shift (ppm)

Boron NMR

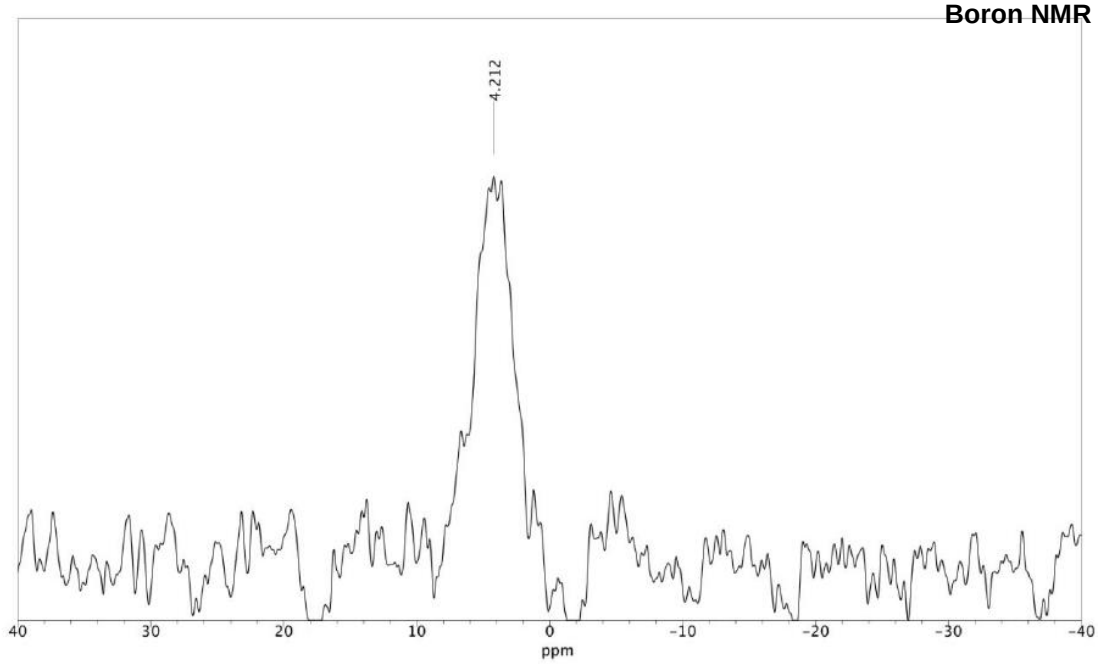
4.212
40
30
20
10
0
-10
-20
-30
-40
ppm

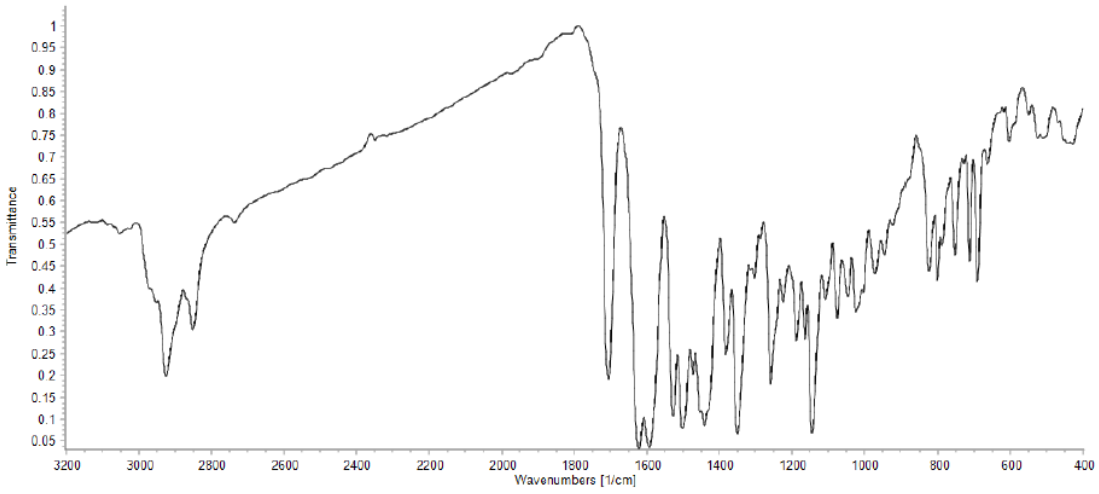
Transmittance
1
0.95
0.9
0.85
0.8
0.75
0.7
0.65
0.6
0.55
0.5
0.45
0.4
0.35
0.3
0.25
0.2
0.15
0.1
0.05
3200
3000
2800
2600
2400
2200
2000
1800
1600
1400
1200
1000
800
600
400
Wavenumbers [1/cm]

- **BASHY 83a**

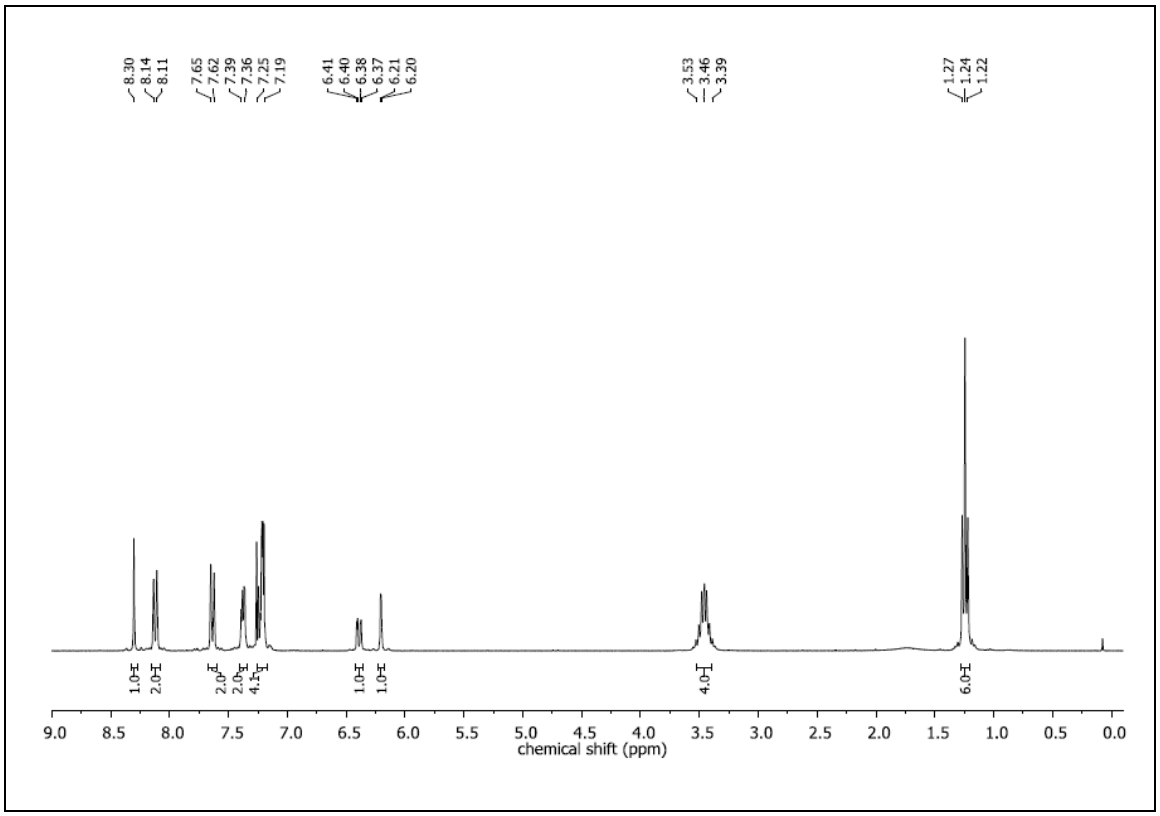
8.30
8.14
8.11
7.65
7.62
7.39
7.36
7.25
7.19
6.41
6.40
6.38
6.37
6.21
6.20
3.53
3.46
3.39
1.27
1.24
1.22
1.0
2.0
2.0
2.0
4.1
1.0
1.0
4.0
6.0
chemical shift (ppm)

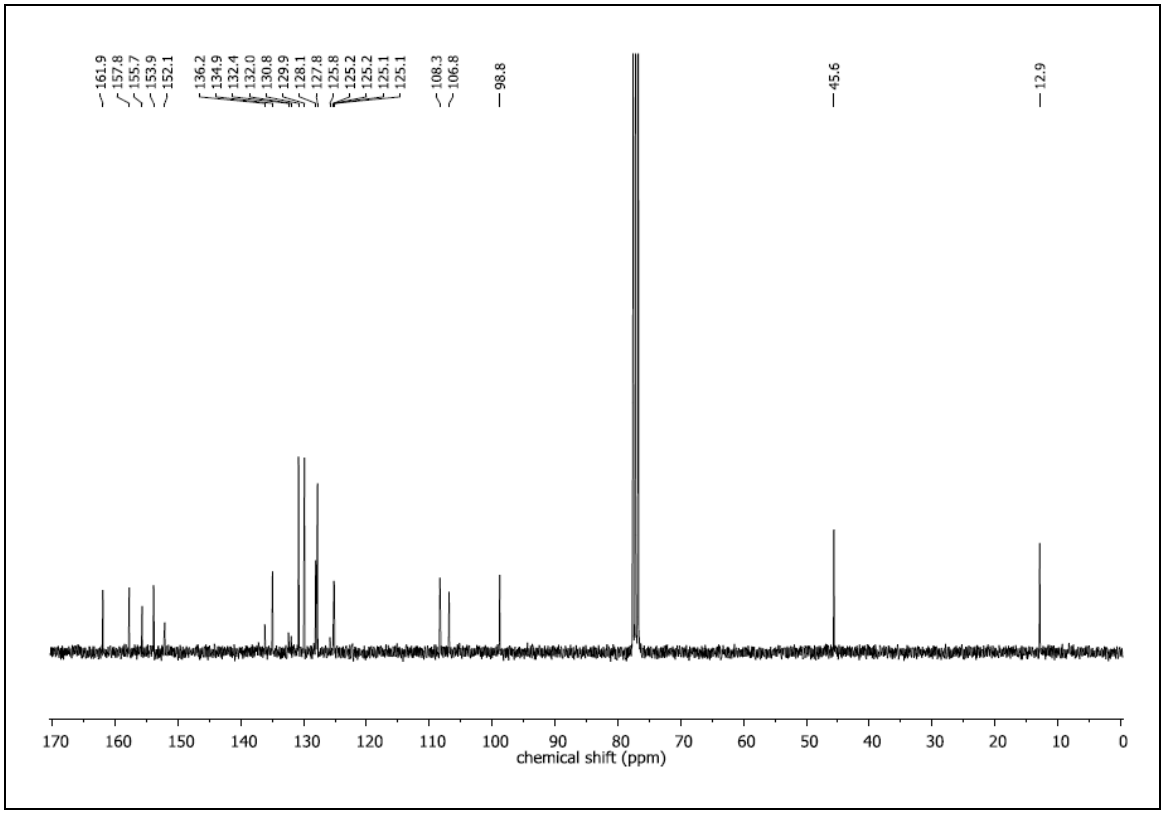
161.9
157.8
155.7
153.9
152.1
136.2
134.9
132.4
132.0
130.8
129.9
128.1
127.8
125.8
125.2
125.2
125.1
125.1
108.3
106.8
98.8
45.6
12.9
chemical shift (ppm)

Boron NMR

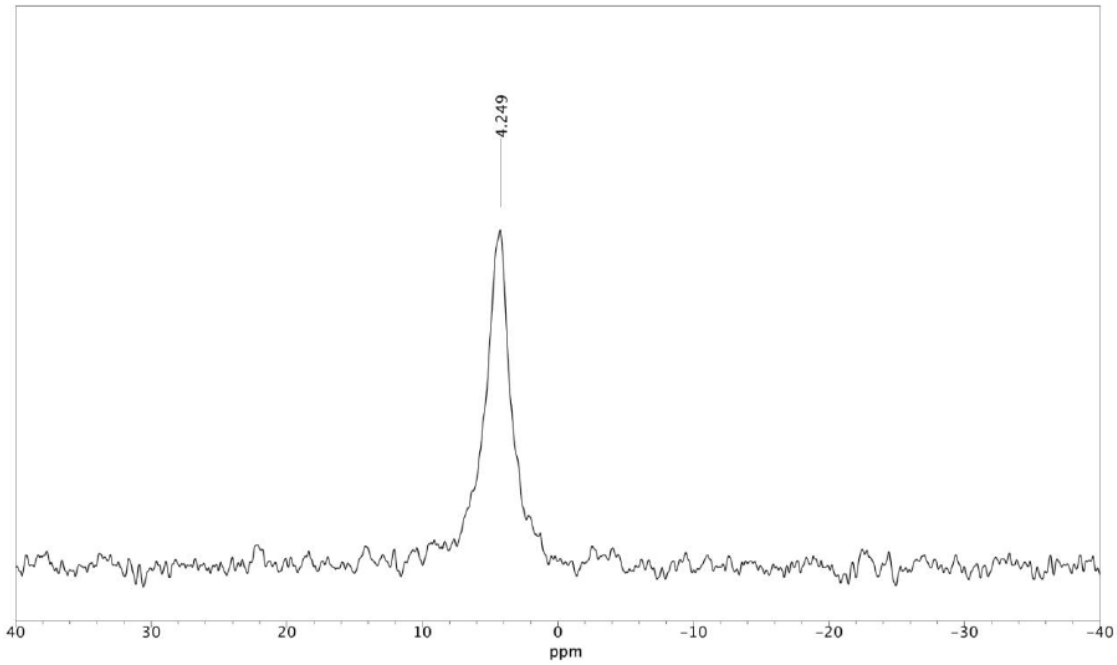
4.249
40
30
20
10
0
-10
-20
-30
-40
ppm

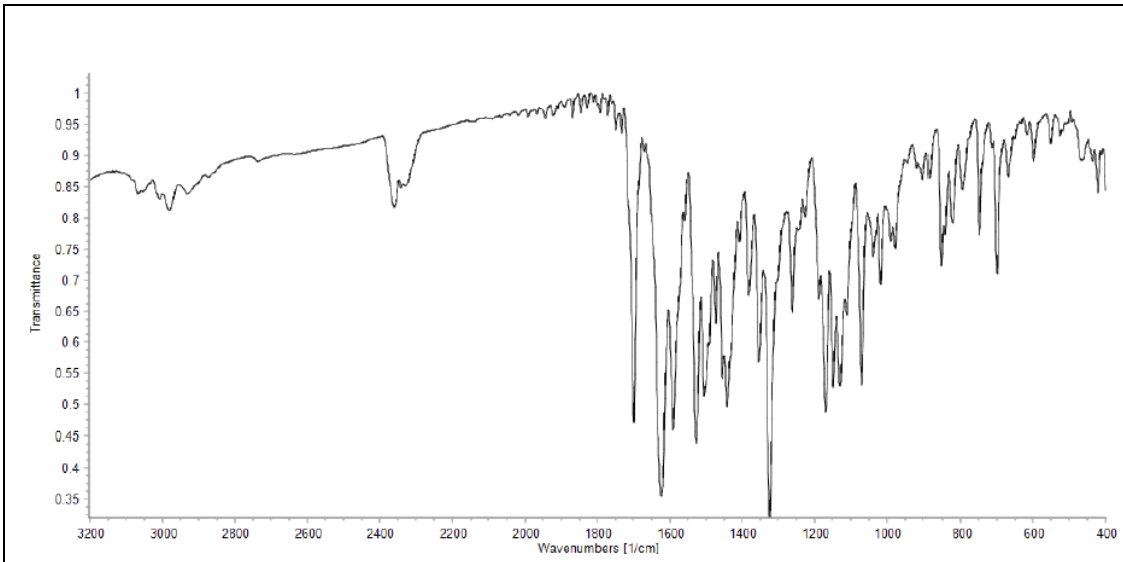
Transmittance
1
0.95
0.9
0.85
0.8
0.75
0.7
0.65
0.6
0.55
0.5
0.45
0.4
0.35
3200
3000
2800
2600
2400
2200
2000
1800
1600
1400
1200
1000
800
600
400
Wavenumbers [1/cm]

- **BASHY 83b**

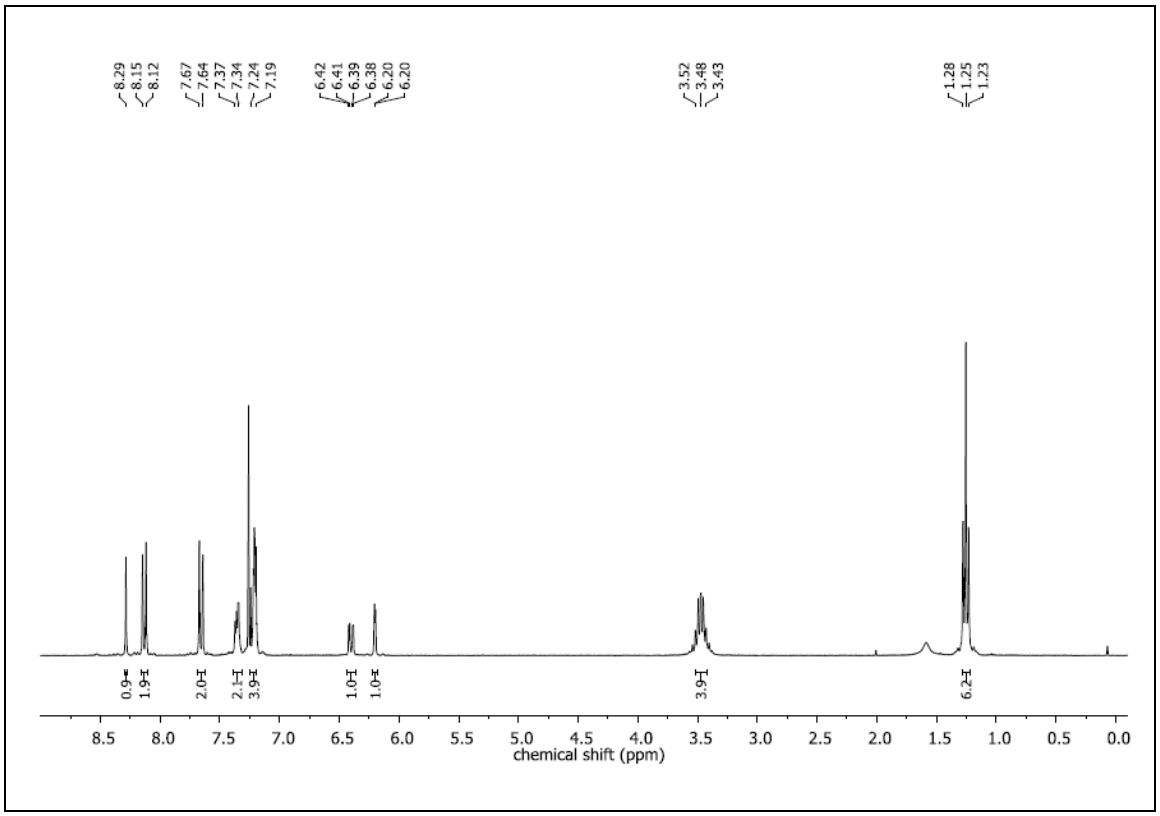
8.29
8.15
8.12
7.67
7.64
7.37
7.34
7.24
7.19
6.42
6.41
6.39
6.38
6.20
6.20
3.52
3.48
3.43
1.28
1.25
1.23
0.9
1.9
2.0
2.1
3.9
1.0
1.0
3.9
6.2
chemical shift (ppm)

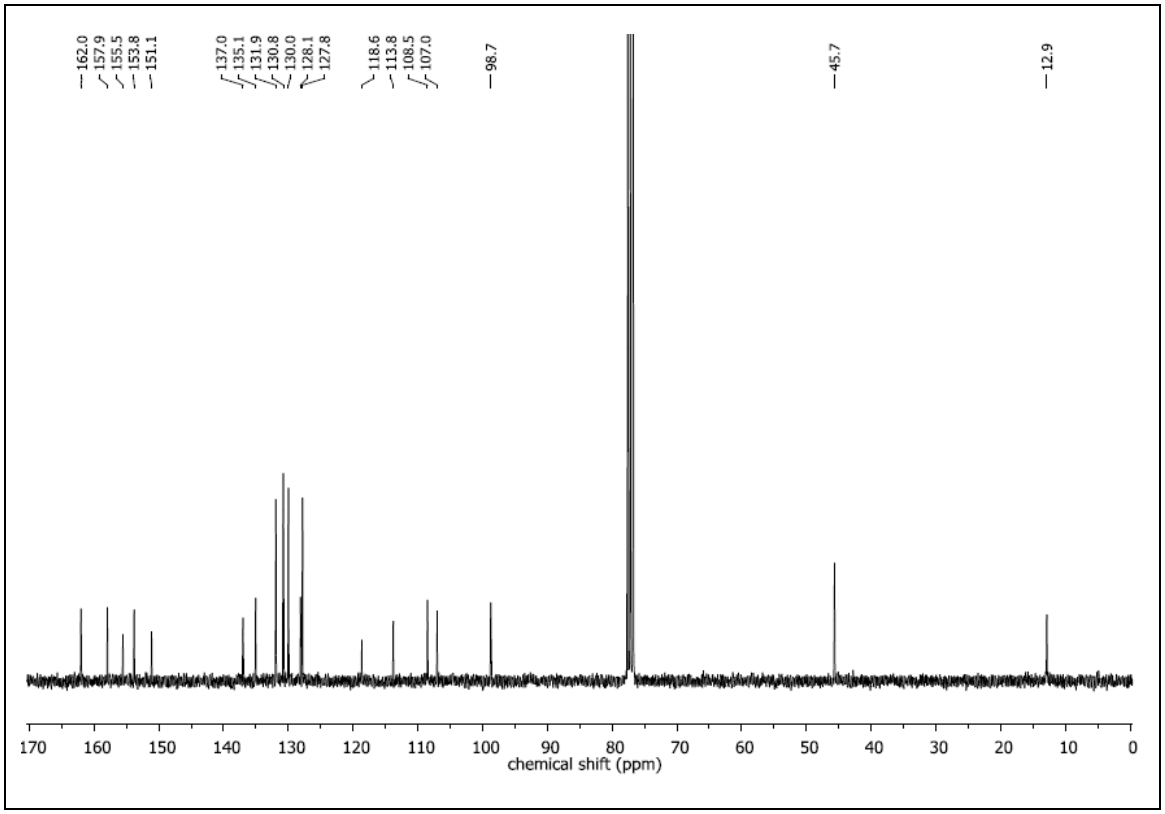
162.0
157.9
155.5
153.8
151.1
137.0
135.1
131.9
130.8
130.0
128.1
127.8
118.6
113.8
108.5
107.0
98.7
45.7
12.9
chemical shift (ppm)

Boron NMR

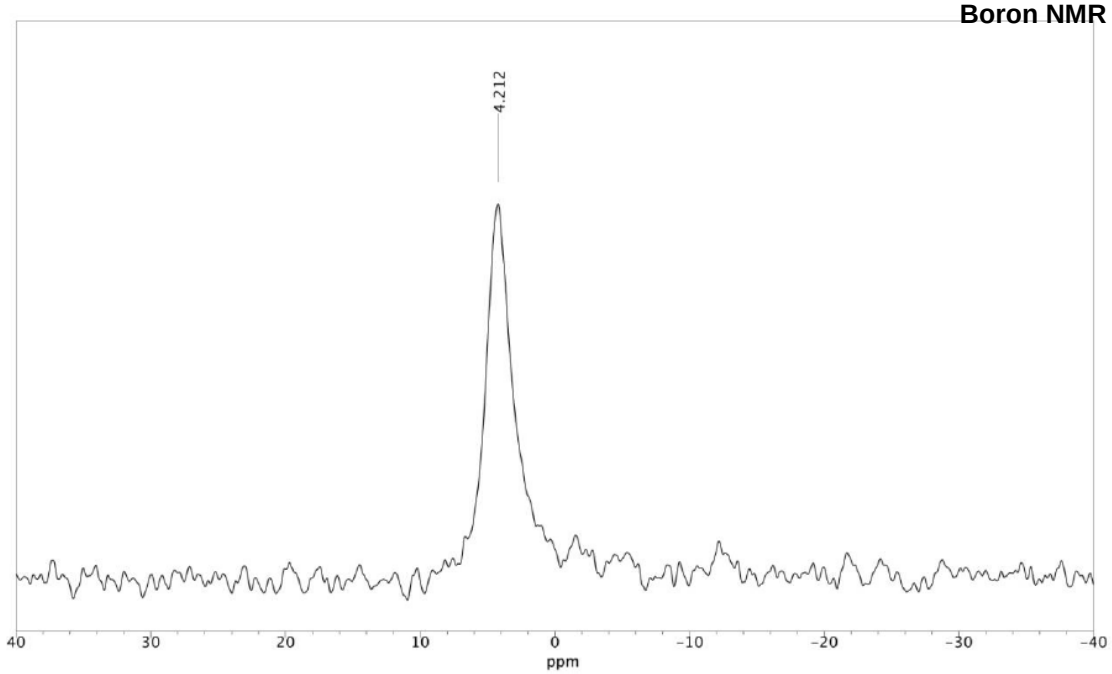
4.212
40
30
20
10
0
-10
-20
-30
-40
ppm

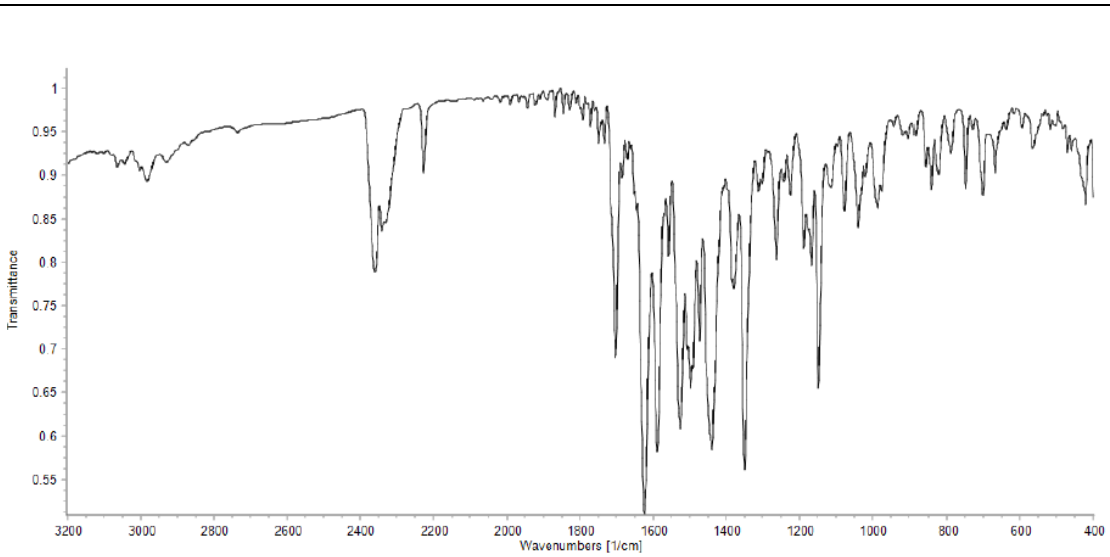
Transmittance
1
0.95
0.9
0.85
0.8
0.75
0.7
0.65
0.6
0.55
3200
3000
2800
2600
2400
2200
2000
1800
1600
1400
1200
1000
800
600
400
Wavenumbers [1/cm]

- **BASHY-Bodipy 85**

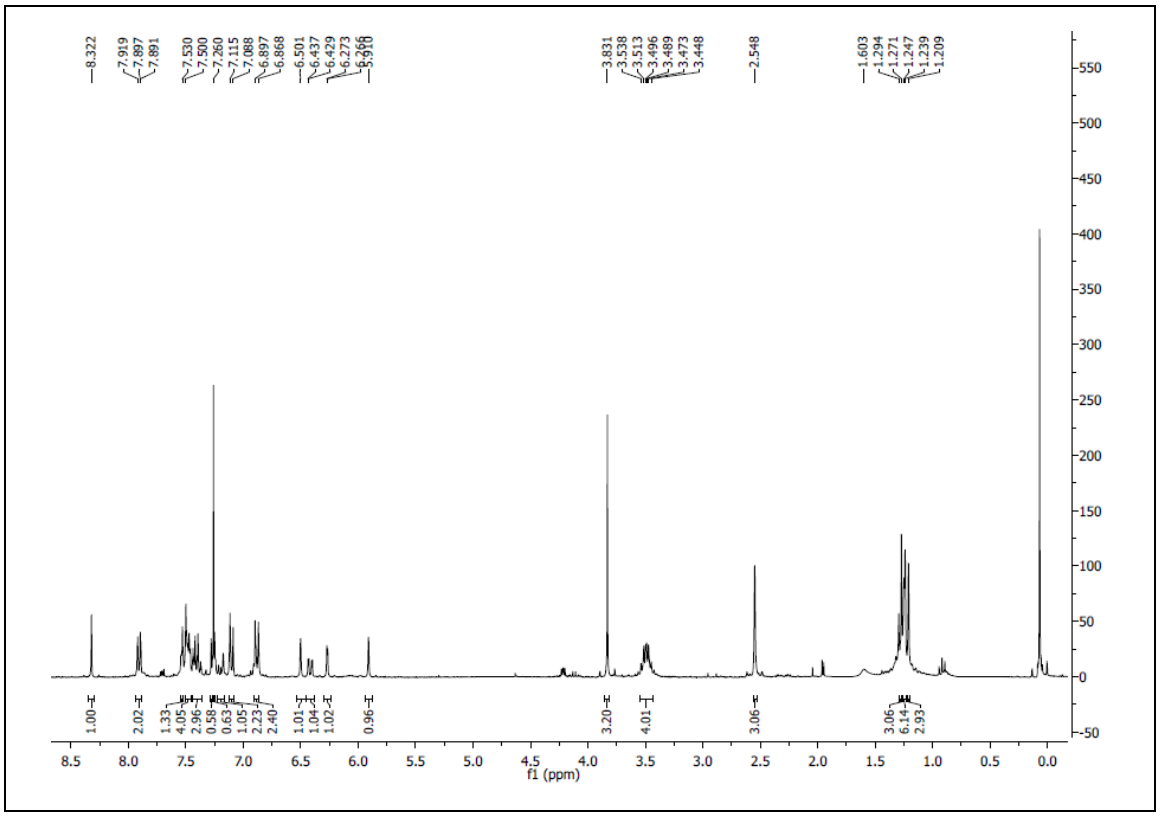

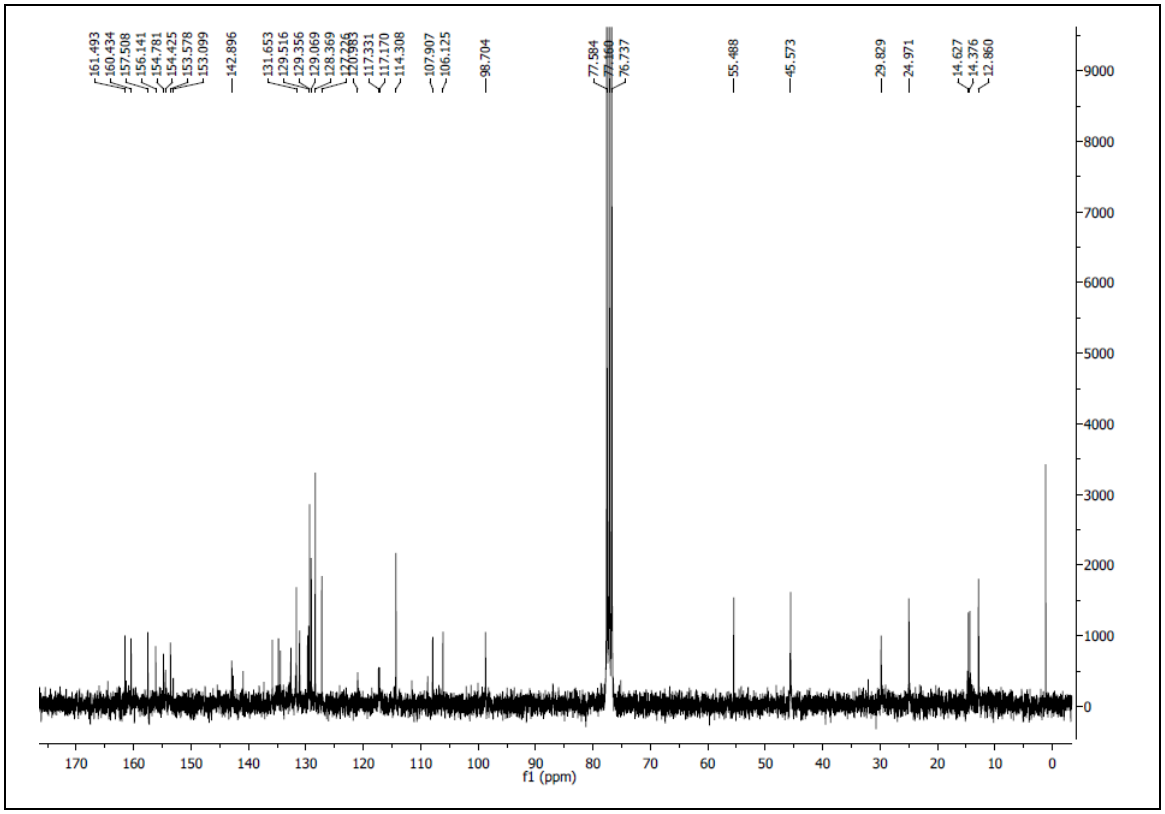

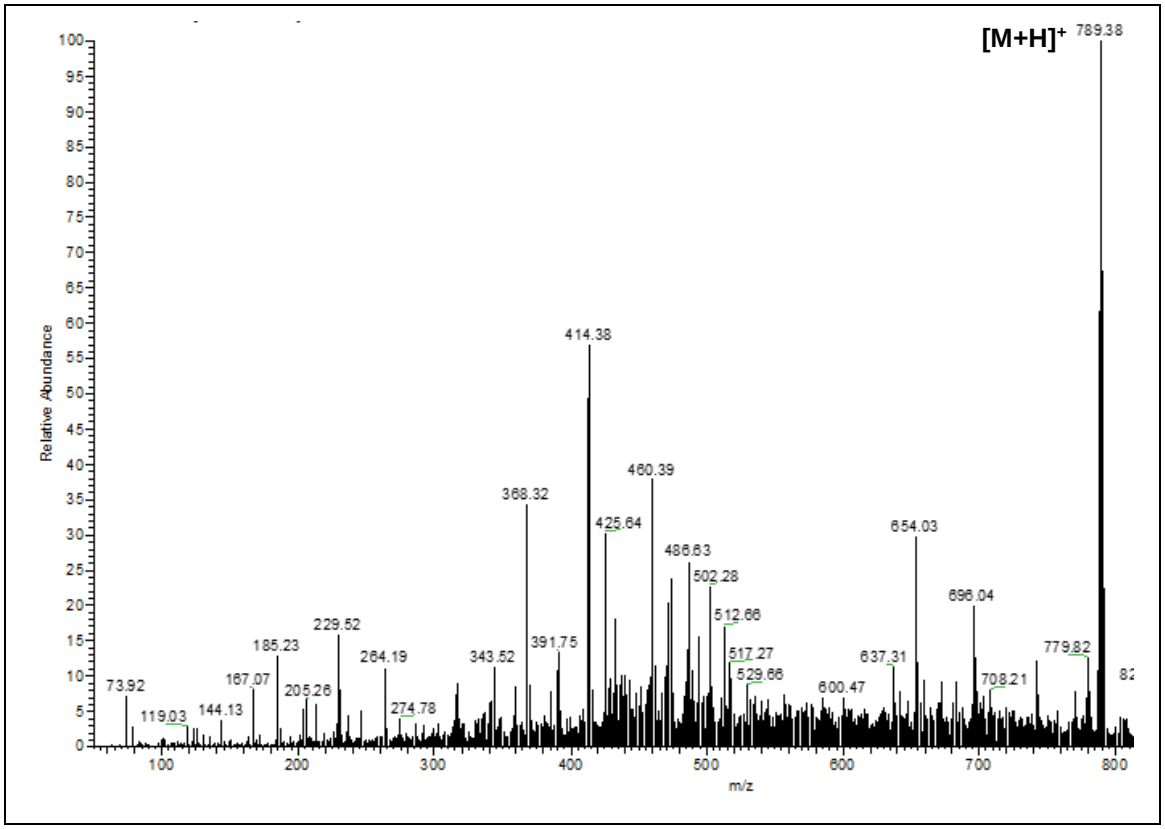

- **BASHY-coumarin 87**

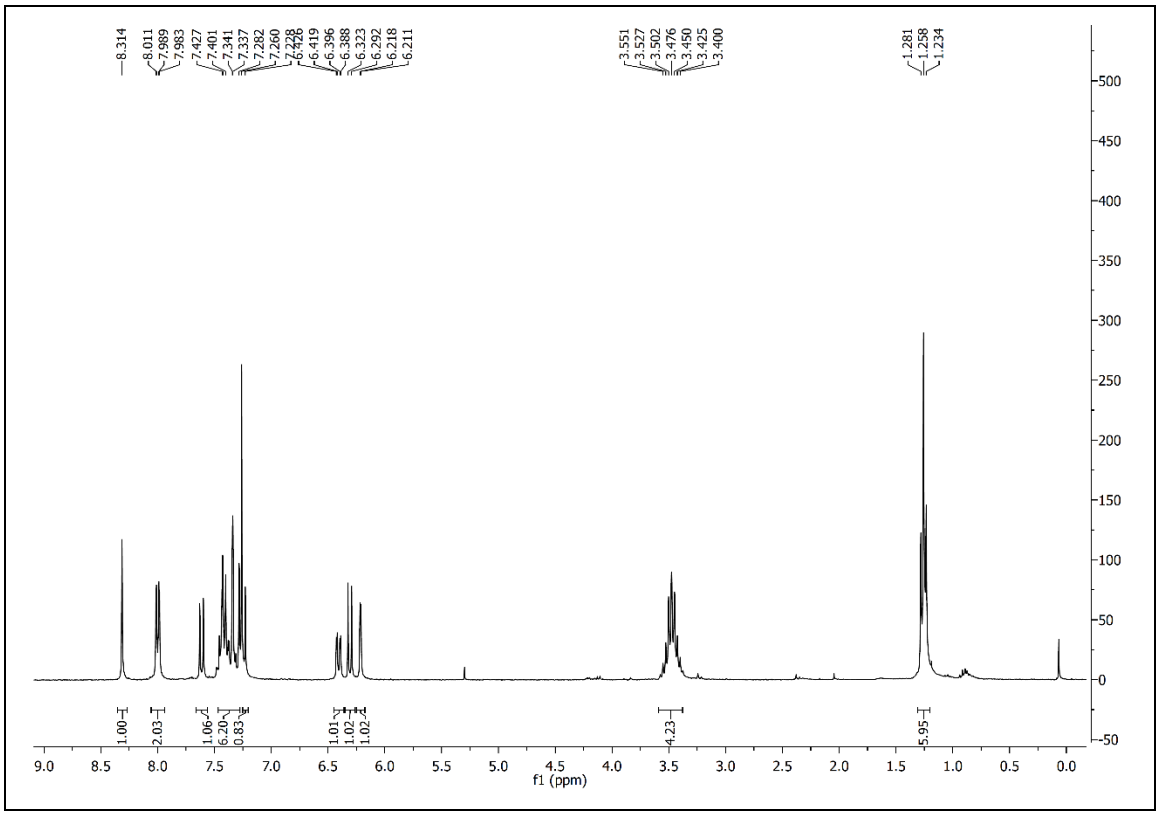

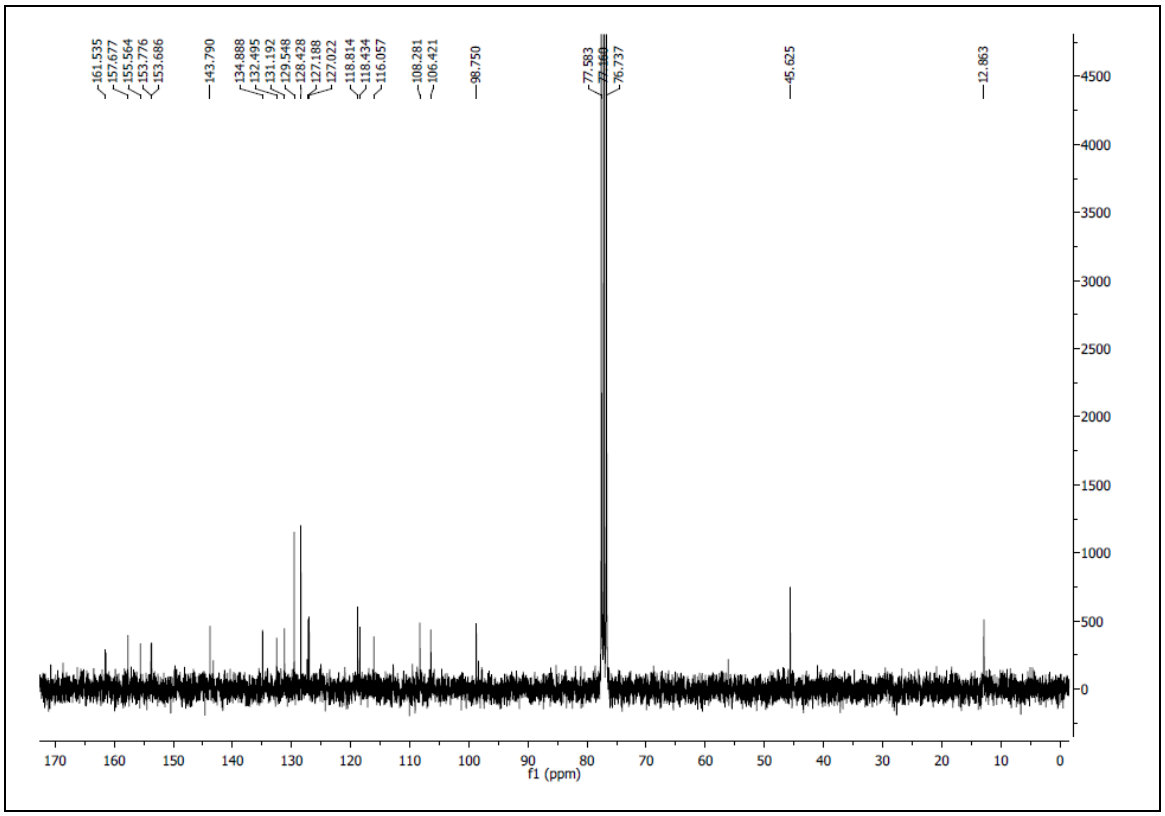
161.535
157.677
155.564
153.776
153.686
143.790
134.888
132.495
131.192
129.548
128.428
127.188
127.022
118.814
118.434
116.057
108.281
106.421
98.750
77.583
77.160
76.737
45.625
12.863
f1 (ppm)

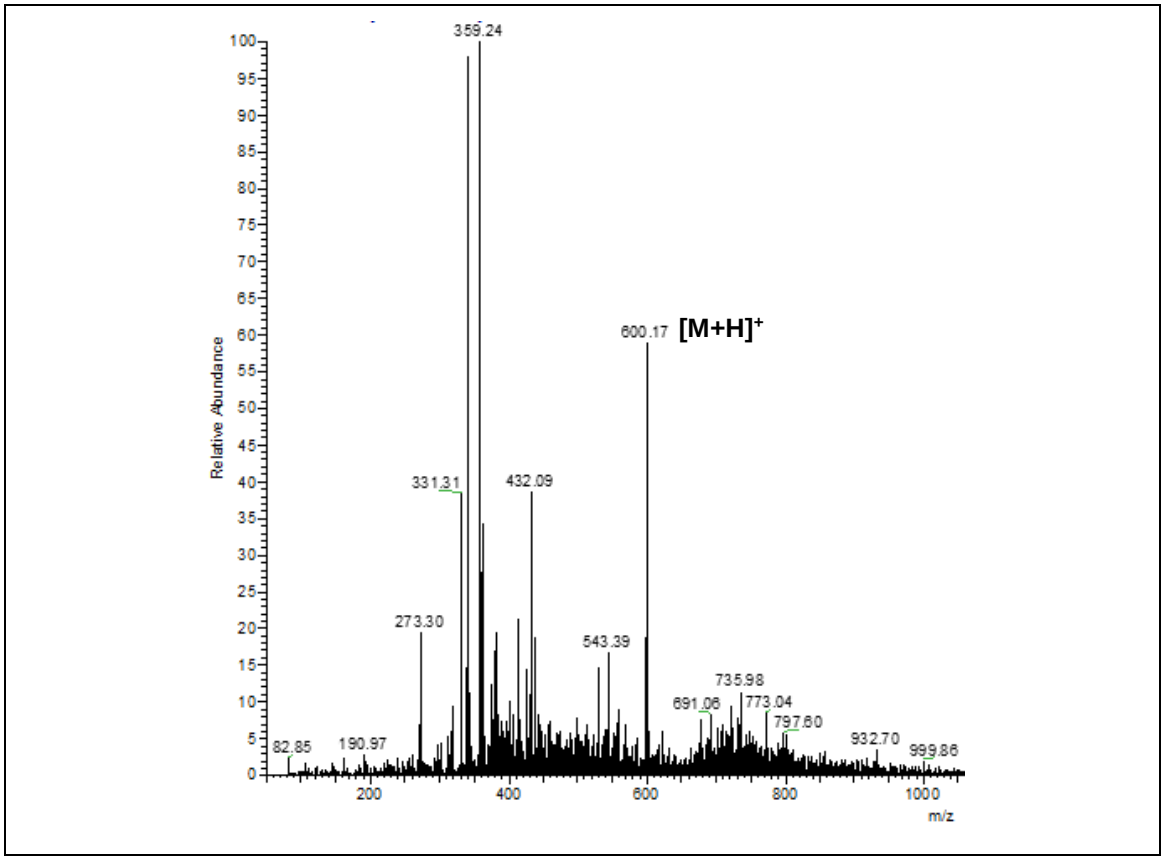
Relative Abundance
m/z
359.24
600.17 [M+H]+
331.31
432.09
273.30
543.39
735.98
691.06
773.04
797.80
932.70
999.86
82.85
190.97

- **BASHY 88**

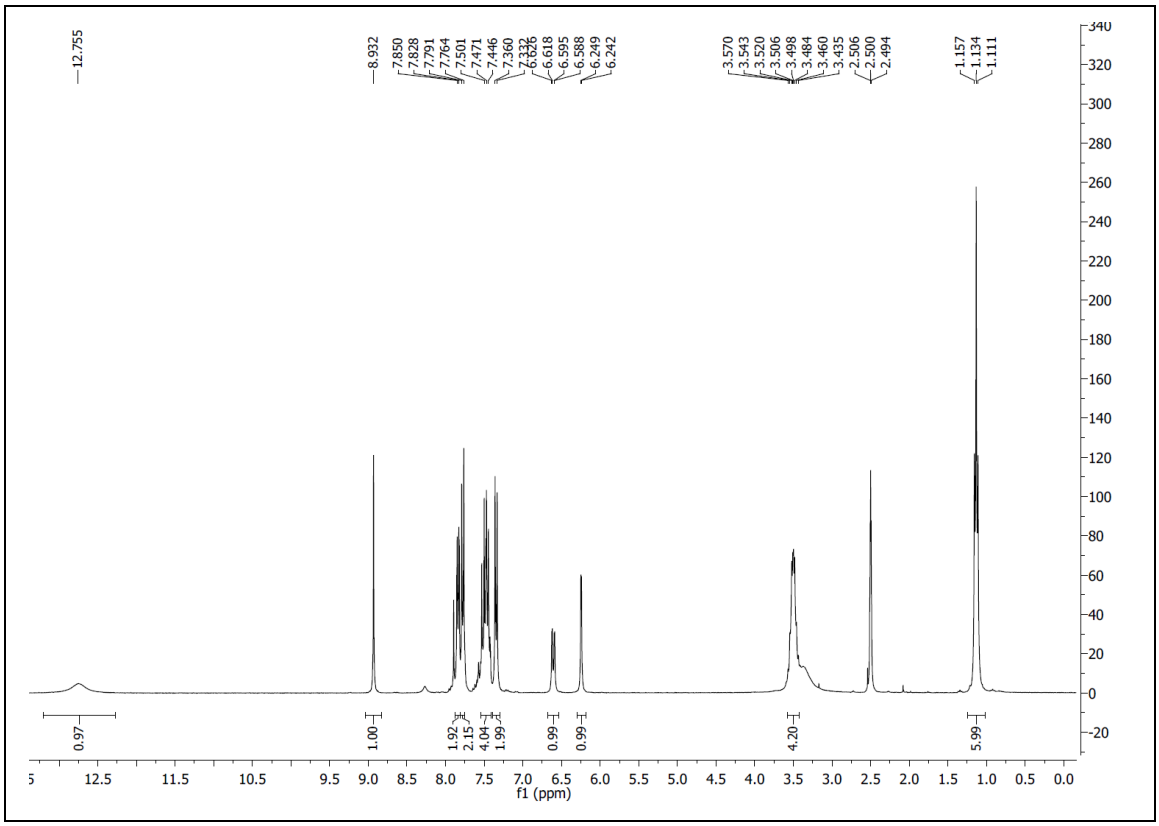
12.755
8.932
7.850
7.828
7.791
7.764
7.501
7.471
7.446
7.360
7.332
6.618
6.595
6.588
6.249
6.242
3.570
3.543
3.520
3.506
3.498
3.484
3.460
3.435
2.506
2.500
2.494
1.157
1.134
1.111
0.97
1.00
1.92
2.15
4.04
1.99
0.99
0.99
4.20
5.99
f1 (ppm)

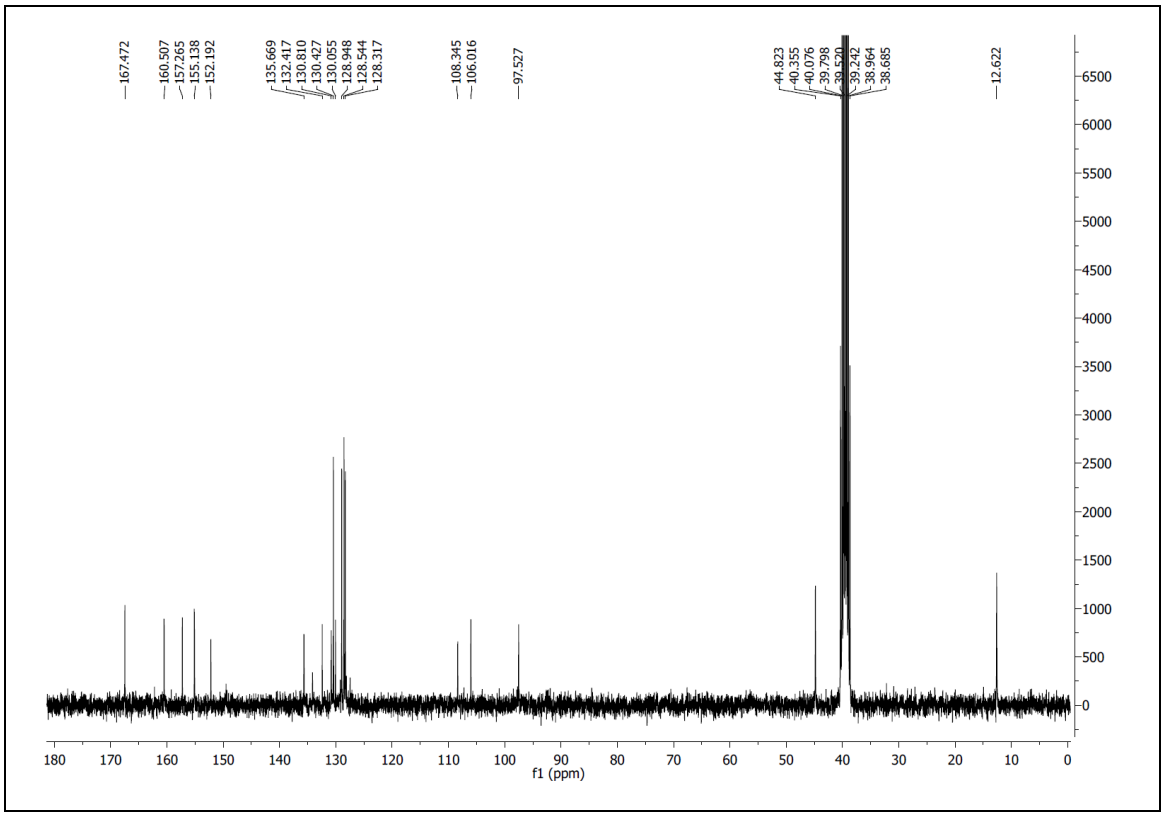
167.472
160.507
157.265
155.138
152.192
135.669
132.417
130.810
130.427
130.055
128.948
128.544
128.317
108.345
106.016
97.527
44.823
40.355
40.076
39.798
39.520
39.242
38.964
38.685
12.622
f1 (ppm)

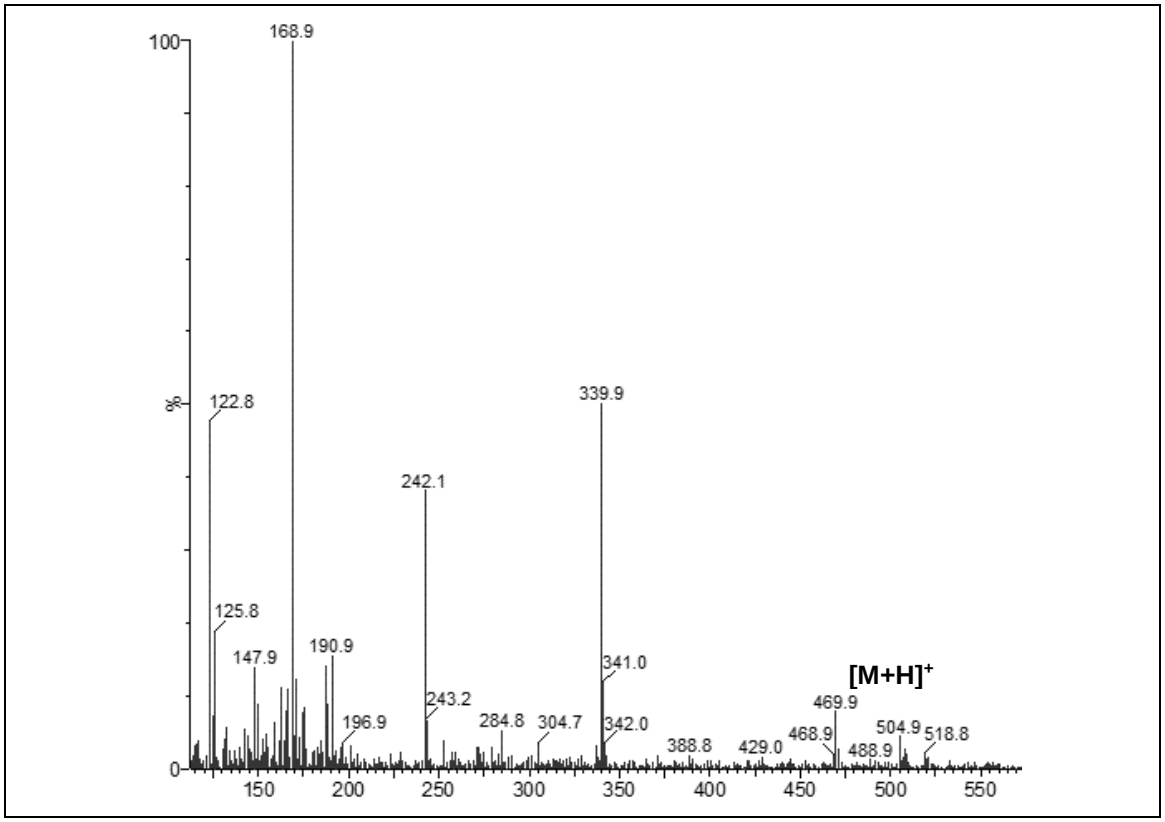
100
%
0
168.9
122.8
339.9
242.1
125.8
147.9
190.9
341.0
243.2
196.9
284.8
304.7
342.0
388.8
429.0
468.9
469.9
488.9
504.9
518.8
[M+H]+
150
200
250
300
350
400
450
500
550

- **BASHY 89**

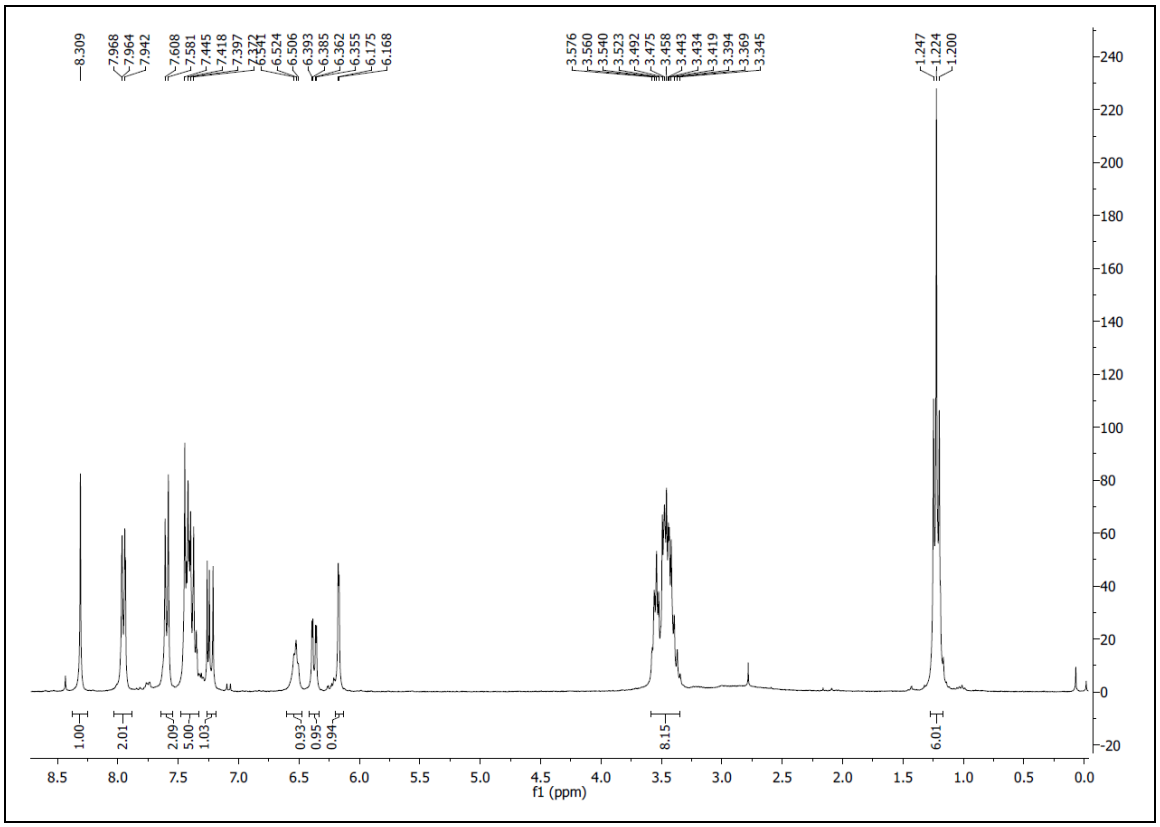
8.309
7.968
7.964
7.942
7.608
7.581
7.445
7.418
7.397
7.332
6.541
6.524
6.506
6.393
6.385
6.362
6.355
6.175
6.168
3.576
3.560
3.540
3.523
3.492
3.475
3.458
3.443
3.434
3.419
3.394
3.369
3.345
1.247
1.224
1.200
1.00
2.01
2.09
5.00
1.03
0.93
0.95
0.94
8.15
6.01
f1 (ppm)

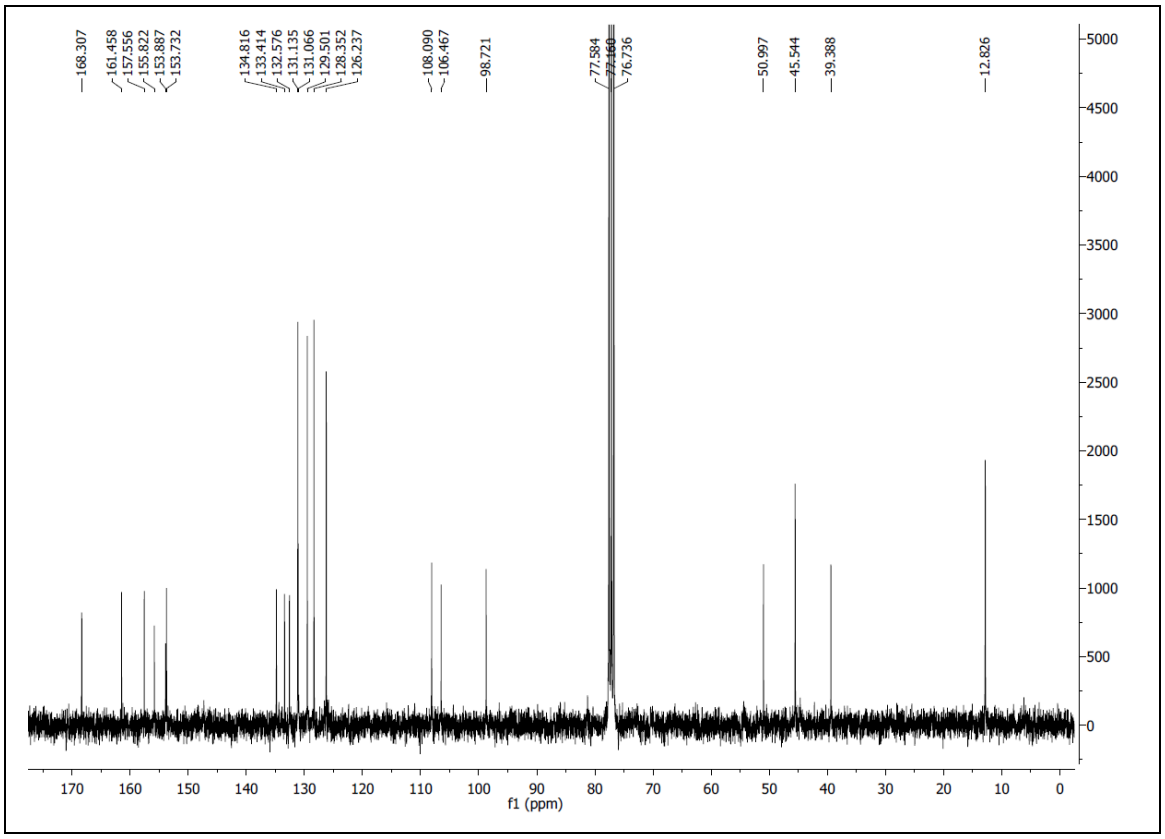
168.307
161.458
157.556
155.822
153.887
153.732
134.816
133.414
132.576
131.135
131.066
129.501
128.352
126.237
108.090
106.467
98.721
77.584
77.160
76.736
50.997
45.544
39.388
12.826
f1 (ppm)

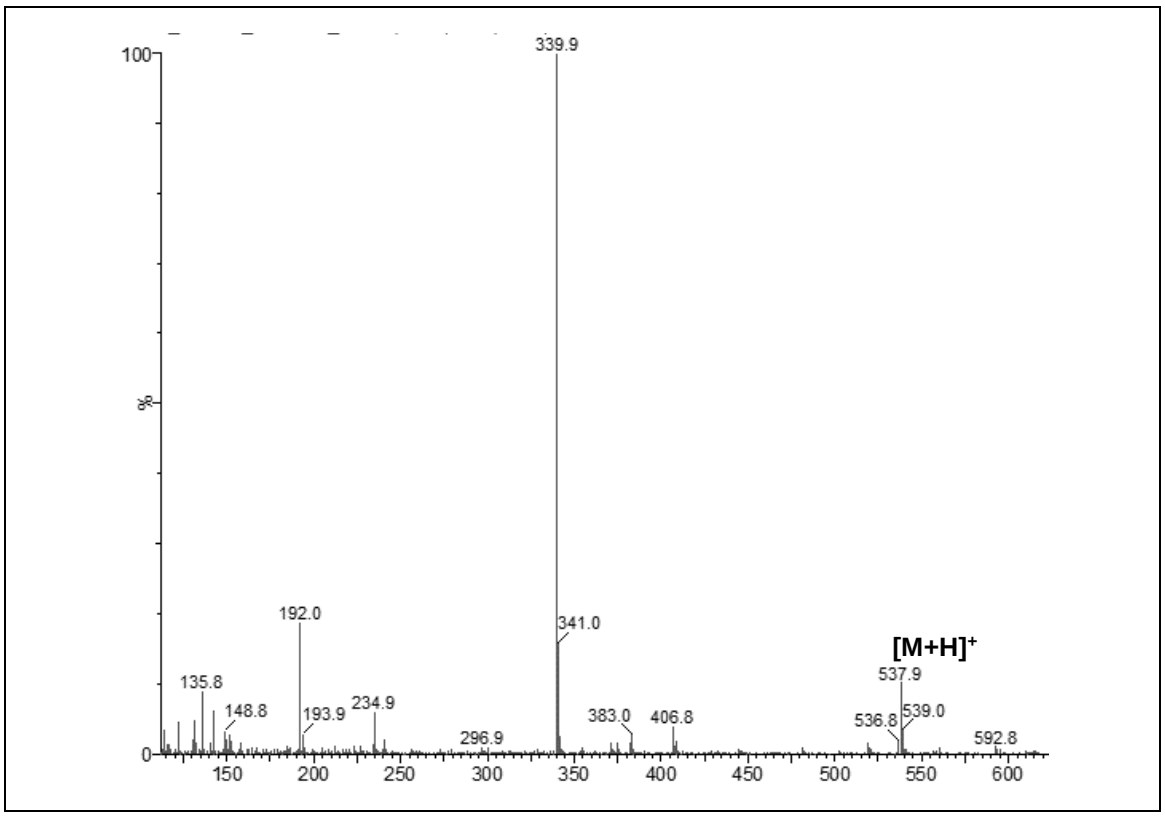
339.9
192.0
341.0
[M+H]+
135.8
148.8
193.9
234.9
296.9
383.0
406.8
537.9
536.8
539.0
592.8
%